RATIONAL DESIGN OF NOVEL TUBULIN BINDING ANTICANCER AGENTS BASED ON CHEMOINFORMATICS EVALUATION OF NOSCAPINOIDS, THEIR CHEMICAL SYNTHESIS AND EXPERIMENTAL VALIDATION

A Dissertation Submitted to the Sambalpur University in Partial Fulfilment of the Requirements for the Degree of

DOCTOR OF PHILOSOPHY

IN

BIOTECHNOLOGY

by

RAJESH KUMAR MEHER

Regd. No. 237/2016/Biotechnology

DEPARTMENT OF BIOTECHNOLOGY & BIOINFORMATICS,
SAMBALPUR UNIVERSITY, JYOTIVIHAR, BURLA,
SAMBALPUR- 768019, ODISHA

February, 2022

RATIONAL DESIGN OF NOVEL TUBULIN BINDING ANTICANCER AGENTS BASED ON CHEMOINFORMATICS EVALUATION OF NOSCAPINOIDS, THEIR CHEMICAL SYNTHESIS AND EXPERIMENTAL VALIDATION

A Dissertation Submitted to the Sambalpur University in Partial Fulfilment of the Requirements for the Degree of

DOCTOR OF PHILOSOPHY
IN
BIOTECHNOLOGY

by

RAJESH KUMAR MEHER
Regd. No. 237/2016/Biotechnology

Under the Joint Supervision of

Supervisor: *Dr. Pradeep K. Naik, Professor, Department of Biotechnology & Bioinformatics, Sambalpur University*

Co-supervisor: *Dr. Manu Lopus, Reader, School of Biological Sciences, UM-DAE Center for Excellence in Basic Sciences, Mumbai*

DEPARTMENT OF BIOTECHNOLOGY & BIOINFORMATICS, SAMBALPUR UNIVERSITY, JYOTIVIHAR, BURLA, SAMBALPUR- 768019, ODISHA

April, 2022

Contents

Contentsof Table

List of Figures

ABSTRACT OF THE DISSERTATION

Microtubules are important cytoskeletal structures that preserve genetic stability during cell division. The dynamics of these polymers, which may be defined as their growth rate at the plus ends, catastrophic shortening, frequency of transition between the two phases, pause between the two phases, release from the microtubule organising centre, and so on, are all critical for this

function. Interfering with microtubule dynamics results in programmed cell death. Therefore microtubule-binding agents such as paclitaxel, docetaxel, and the vinca alkaloids are utilised in clinics to treat a variety of cancers. However, because of their non-selective action, these drugs are associated with severe toxicity (especially peripheral neuropathies, gastrointestinal damage, myelosuppression, and immunosuppression) mainly by overpolymerizing (by taxanes) or depolymerizing (by vincas) the microtubules. In a quest to find new tubulin-binding compounds for the treatment of cancer, noscapine, an opium alkaloid was discovered. It was found to binds stoichiometrically to tubulin, alter its conformation upon binding, and arrest mammalian cells in mitosis. Even at high doses, noscapine, unlike many other microtubule inhibitors, does not appreciably enhance or inhibit microtubule polymer mass. Instead, it alters the steady-state dynamics of microtubule assembly, principally by increasing the amount of time that microtubules spend in an attenuated (halt) state, in which neither microtubule growth nor shortening can be detected. Owing to the compromised cell cycle check points, cancer cells are preferentially destroyed by noscapine and its derivatives (together known as noscapinoids) without affecting normal cells. In addition, as a lead molecule, noscapine has the following advantages: (1) it retains activity against paclitaxel-resistant cell lines (1A9/PTX10, 1A9/PTX22) and epothilone-resistant cell lines (1A9/A8); (2) it has a favourable pharmacokinetics (clearance in 6-10 hours); (3) it is a poor substrate for drug-pumps (polyglycoproteins and MDR-related proteins. Despite the fact that noscapine is cytotoxic in a wide range of cancer cell lines (NCI 60 cell lines panel), the IC_{50} values (between 21.1 and 100 μM) are still in the high micromolar range. Research is focusing on rational design and chemical synthesis of noscapine derivatives to improve therapeutic outcomes. In persistence of our endeavours to create novel derivatives of noscapine with improved binding affinity with tubulin, we have designed five new classes of noscapinoids: (1) 1,3-diynyl-noscapinoids, (2) 9-arylimino noscapinoids, (3) N-arylalkylamino-noscapinoids, (4) N-imidazopyridine-noscapinoids and (5) 9-Urea noscapinoids.

A class of 9-arylimino noscapinoids was developed that binds to tubulin and displayed anticancer activity against a panel of breast cancer cells. These compounds were rationally designed by coupling of Schiff base containing imine groups at position C-9 of the isoquinoline ring of noscapine. Based on a combination of Glide docking and free energy of binding (FEB) calculation a panel of three 9-arylimino noscapinoids were screened out with improved binding affinity with tubulin compared to noscapine. These novel derivatives were strategically synthesized and validated their anticancer activity based on cellular studies using two human breast adenocarcinoma, MCF-7 and MDAMB-231, as well as with a panel of primary breast tumor cells isolated from patients. Interestingly, all these derivatives inhibited cellular proliferation in all the cancer cells that ranged between 3.6 to 26.4 μM, which is 11.02 to 2.03 fold lower than that of noscapine. Unlike previously reported derivatives of noscapine that arrest cells in the S-phase, these

novel derivatives effectively inhibit the proliferation of cancer cells, arrest the cell cycle in the G2/M-phase and induce apoptosis.

In our next attempt, the scaffold structure of noscapine was modified by inducting N-aryl methyl pharmacophore at C-9 position of the isoquinoline ring to rationally design and screened out three novel 9-(N-arylmethylamino) noscapinoids, with robust binding affinity with tubulin. The selected 9-(N-arylmethylamino) noscapinoids revealed improved predicted binding energy in comparison to the lead molecule. These derivatives were chemically synthesized and validated their anticancer activity based on cellular studies using two human breast adenocarcinoma, MCF-7 and MDA-MB-231, as well as with a panel of primary breast tumor cells. These derivatives inhibited cellular proliferation in all the cancer cells that ranged between 3.2 to 32.2 μM, which is 11.9 to 1.8 fold lower than that of noscapine. These novel derivatives effectively arrest the cell cycle in the G2/M-phase followed by apoptosis and the appearance of apoptotic cells.

In our furher attempt, 1,3-diynyl derivatives of noscapine were developed through *in silico* combinatorial approach and screened out a panel of promising derivatives that bind tubulin and display anticancer activity. The selected derivatives revealed improved predicted binding energy in comparison to noscapine. These 1,3-diynyl derivatives were strategically synthesized in high yields by regioselective modification of noscapine scaffold and HPLC purified (purity is > 96%). The decrease in intrinsic fluorescence of purified compared to control suggests their binding capability to tubulin. Their cytotoxicity activity was validated based on cellular studies using two human breast adenocarcinoma (MCF-7 and MDA-MB-231), a panel of primary breast tumor cells and one normal human embryonic kidney cell (293T). The 1,3-diynyl noscapinoids, inhibited cellular proliferation in all the cancer cells that ranged between 6.2 and 38.9 μM, without affecting the normal healthy cells (cytotoxicity is < 5% at 100 μM). Further, these novel derivatives arrest cell cycle in the G2/M-phase, followed by induction of apoptosis to cancer cells.

Additionally, a panel of urea-noscapine conjugates was developed to increase the anticancer potential of noscapine. These compounds were chemically synthesized and their antiproliferation activity was evaluated using human breast cancer cell lines (MCF-7 and MDA-MB-239), primary breast tumour cells and normal healthy cells using an MTT assay. All the urea-noscapine conjugates developed were inhibited the proliferation of breast cancer cell lines (MCF-7 and MDA-MB-231) without affecting the normal healthy cell. The most potent compound inhibited cell proliferation of MCF-7 (IC_{50} of 4.8 μM), and MDA-MB-231 (IC_{50} of 8.1 μM), primary breast tumour cells from different patients

(IC_{50} ranges from 6.2 to 10.9 μM) and colony formation (IC_{50} 1.6 ± 0.35 μM) by arresting the cells at G2/M phase of the cell cycle. Further, it was found to effectively induce apoptosis which is facilitated by the elevated level of ROS. The compound was also found to significantly reduce the implanted tumour in the xenograft mice model without any toxicity to vital organs.

In our last attempt, another class of noscapinoids, N-imidazopyridine-noscapinoids was developed by coupling the imidazo[1,2-*a*] pyridine pharmacophore with noscapine scaffold. These novel derivatives were chemically synthesized and validated their anticancer activity based on cellular studies using two human breast adenocarcinoma, MCF-7 and MDAMB-231, as well as with a panel of primary breast cancer cells isolated from patients. Interestingly, all these derivatives inhibited cellular proliferation in all the cancer cells that ranged between 3.7 to 15.8 μM, which is 11.8 to 2.7 fold lower than that of noscapine. These novel derivatives effectively inhibit the proliferation of cancer cells, arrest the cell cycle in the G2/M-phase followed by apoptosis.

In conclusion, five different classes of noscapinoids were developed by coupling active pharmacophore such as urea and imidazo[1,2-*a*] pyridine with noscapine scaffold based on in silico combinatorial approach. We have primarily focused on these functional groups because they are recognized as a key pharmacophore in several anticancer drugs utilized in the clinic. All the noscapinoids developed were found to enhance the anticancer activity to several folds. Thus, these noscapinoids have great potential to be a novel therapeutic agent for breast cancers.

CHAPTER-1

Introduction and review of literature

1. Introduction

1.1 Cancer and it's scenario

Cancer is a broad word that encompasses a wide range of disorders that may affect any organ in the body. Malignant tumours and neoplasms are also the terminologies used. One of the hallmarks of cancer is the fast emergence of aberrant cells that expand beyond their normal bounds and spread to other regions of the body, a process known as metastasis. The leading cause of cancer-related mortality is metastasis. Cancer is a prominent cause of death and a significant impediment to extending life expectancy in every country of the world (WHO, 2020; Bray et al., 2021). In 2020, there were an estimated 19.3 million new cancer cases and 10 million cancer deaths globally. Out of new cancer cases in 2020, the most prevalent were 2.26 million instances of breast cancer; 2.21 million cases of lung cancer; 1.93 million cases of colon and rectum cancer; 1.41 million cases of prostate cancer; 1.20 million cases of skin cancer (non-melanoma); and 1.20 million cases of stomach cancer (1.09 million cases). Out of death cases in 2020, 1.80 million deaths were due to lungs cancer, 9,35,000 deaths in colon and rectum cancer, 8,30,000 deaths in liver cancer, 7,69,000 deaths in stomach cancer and 6,85,000 deaths in breast cancer. The global burden of cancer incidence and death is rapidly increasing, reflecting both population aging and growth, as well as changes in the prevalence and distribution of the key cancer risk factors, many of which are linked to socioeconomic development (Sung et al., 2021).

1.2 Breast cancer and its scenario:

With an expected 2.3 million new cases in 2020, female breast cancer has surpassed lung cancer as the main cause of worldwide cancer incidence, accounting for 11.7 percent of all cancer cases. With 6,85,000 fatalities globally, it is the seventh-highest cause of cancer death. Breast cancer is the most common cancer in women, accounting for one out of every four cases and one out of every six deaths, and it is the most common disease in the great majority of countries (Sung et al., 2021).

1.3 Cancer treatment:

Chemotherapy is still a common treatment, recurrence prevention, and palliative care option for a range of cancer types including breast cancer. The chemical agents used in chemotherapeutics belong to different categories based on their therapeutic targets (Table 1.1). The major limitations of many of the chemotherapeutics used in clinics do not particularly target the cancer cells exclusively and can equally be cytotoxic to normal healthy dividing cells leading to severe side effects to cancer patients. Therefore, there is a quest to develop new chemical agents that are having no severe side effects on patients.

Table 1.1. Drugs currently used for cancer treatment(Zorn et al., 2007; Medeiros et al., 2009; Luh et al., 2006; Gerber et al., 2008).

Mode of inhibition	Drugs and their targets
DNA integrity and metabolism	***Folic acid metabolism*:** Dihydrofolate reductase inhibitor (Aminopterin, Methotrexate, Pemetrexed); Thymidylate synthase inhibitor (Raltitrexed, Pemetrexed). ***Purine metabolism*:** Adenosine deaminase inhibitor (Pentostatin); Halogenated/ribonucleotide reductase inhibitors (Cladribine, Clofarabine, Fludarabine); Thiopurine (Thioguanine, Mercaptopurine). ***Pyrimidine metabolism*:** Thymidylate synthase inhibitor (Fluorouracil, Capecitabine, Tegafur, Carmofur, Floxuridine); DNA polymerase inhibitor (Cytarabine); Ribonucleotide reductase inhibitor (Gemcitabine); Hypomethylating agent (Azacitidine, Decitabine). ***Deoxyribonucleotides metabolism*:** Ribonucleotide reductase inhibitor (Hydroxyurea). ***Topoisomerase I inhibitor*:** Camptotheca (Camptothecin, Topotecan, Irinotecan, Rubitecan, Belotecan). ***Topoisomerase II inhibitor***: Podophyllum (Etoposide, Teniposide). ***TopoisomeraseII+ intercalation***: Anthracyclines (Aclarubicin, Daunorubicin, Doxorubicin, Epirubicin, Idarubicin, Amrubicin, Pirarubicin, Valrubicin, Zorubicin); Anthracenediones (Mitoxantrone, Pixantrone). ***Crosslinkers*:** *Nitrogen mustards*: Mechlorethamine; Cyclophosphamide (Ifosfamide, Trofosfamide); Chlorambucil (Melphalan, Prednimustine); Bendamustine; Uramustine; Estramustine. ***Nitrosoureas**:* Carmustine; Lomustine (Semustine); Fotemustine; Nimustine; Ranimustine; Streptozocin. ***Alkyl sulfonates**:* Busulfan (Mannosulfan, Treosulfan). ***Aziridines**:* Carboquone; ThioTEPA; Triaziquone; Triethylenemelamine; Platinum (Carboplatin, Cisplatin, Nedaplatin, Oxaliplatin, Triplatin tetranitrate, Satraplatin); Hydrazines (Procarbazine); Triazenes (Dacarbazine, Temozolomide); Altretamine; Mitobronitol; Streptomyces (Actinomycin, Bleomycin, Mitomycin,).
Radiation and photosensitizers	***Radiation therapy***: High-energy radiation from x-rays, gamma rays, neutrons, protons, and other sources. ***Photosensitizers*:** Aminolevulinic acid/Methyl aminolevulinate; Efaproxiral; Porphyrin derivatives (Porfimer sodium, Talaporfin, Temoporfin, Verteporfin).
Signal Transduction	***Receptor tyrosine kinase inhibitors*:** *ErbB*: HER1/EGFR (Erlotinib, Gefitinib, Lapatinib, Vandetanib, Neratinib); HER2/neu (Lapatinib, Neratinib) *RTK class III:* C-kit (Axitinib, Sunitinib, Sorafenib); FLT3 (Lestaurtinib); PDGFR (Axitinib, Sunitinib, Sorafenib); VEGFR (Vandetanib, Semaxanib, Cediranib, Axitinib, Sunitinib, Sorafenib). ***Non recptor tyrosine kinase inhibitors*:** bcr-abl (Imatinib, Nilotinib, Dasatinib), Src (Bosutinib), Janus kinase 2 (Lestaurtinib). ***Enzyme inhibitors***: Farnesyl transferase FI (Tipifarnib); CDK inhibitors (Alvocidib, Seliciclib); proteosome inhibitor PrI (Bortezomib); PDE II inhibitor PhI (Anagrelide); Imp dehydrogenase inhibitor IMPDI (Tiazofurine); Lipoxygenase inhibitor LI (Masoprocol).

	***Receptor antagonists/hormones*:** Endothelial receptor antagonist ERA (Atrasentan); retinoid X receptor (Bexarotene); sex steroid (Testolactone).
Monoclonal antibodies	***Receptor tyrosine kinase*:** *ErbB*: HER1/EGFR (Cetuximab, Panitumumab); HER2/neu (Trastuzumab). *Solid tumors*: EpCAM (Catumaxomab, Edrecolomab); VEGF-A (Bevacizumab). Leukemia/lymphoma. *Lymphoid*: CD20 (Rituximab, Tositumomab, Ibritumomab). *Myeloid*: CD52 (Alemtuzumab). *Lymphoid+Myeloid*: CD33 (Gemtuzumab). ***Others*:** Afutuzumab, Alemtuzumab, Bevacizumab/Ranibizumab, Bivatuzumab mertansine, Cantuzumab mertansine, Citatuzumab bogatox, Dacetuzumab, Etaracizumab, Farletuzumab, Gemtuzumab ozogamicin, Inotuzumab ozogamicin, Labetuzumab, Lintuzumab, , Milatuzumab, Nimotuzumab, Oportuzumab monatox, Pertuzumab, Sibrotuzumab, Sontuzumab, Tacatuzumab tetraxetan, Tigatuzumab.
Tubulin binding drugs	***Inhibit microtubule assembly*:**Vinca alkaloids (Vinblastine, Vincristine, Vinflunine, Vindesine, Vinorelbine) ***Promote microtubule assembly***:Taxanes (Paclitaxel, Docetaxel, Larotaxel, Ortataxel, Tesetaxel); Epothilones (Ixabepilone)
Miscellaneous	Amsacrine; Trabectedin; Retinoids (Alitretinoin, Tretinoin); Arsenic trioxide; Asparagine depleter (Asparaginase/Pegaspargase); Celecoxib; Demecolcine; Elesclomol; Elsamitrucin; Etoglucid; Lonidamine; Lucanthone; Mitoguazone; Mitotane; Oblimersen; Temsirolimus; Vorinostat

1.4 Microtubule structure and function in cell division:

Microtubules are the major cytoskeletal protein in eukaryotic cells that play a significant role in cell growth, division, motility, signaling, and the development and maintenance of cell shape (Dustin, 1984). It is a heterodimeric polymer composed of α- and β- tubulin subunits, which are assembled into tubular structures that have inherent structural and kinetic polarity (Gelfand and Bershadky, 1991. Microtubule assembly is initiated at a critical subunit concentration, and elongation proceeds by the reversible addition of tubulin dimers to microtubule ends. The addition of tubulin subunits to microtubule ends is known as polymerization, whereas the loss of subunits is known as depolymerization. One end of a microtubule grows and shortens faster than the other end and hence it is called the plus end to distinguish it from the slower minus end (Nogales, 2001; Valiron, et al., 2001). A single microtubule contains 13 linear protofilaments which form the hollow tubular structure of approximately 25 nm in diameter. The α and β tubulin subunits are around 50% similar in amino acid sequence and each of the subunits is around 50,000 Da. (Jordan et al., 1998). The dimension of the microtubule heterodimer is 4nm x 5nm x 8nm x 100000 Daltons in mass and they are arranged in a form of a slender tube of many micrometers long (**Figure 1.1**). Each subunit of tubulin consists of three domains,

amino-terminal domain which contains the nucleotide binding site, an intermediate domain and carboxyl terminal domain which regulates the interaction of drugs like colchicine and vinblastine (Rai, et al., 1998; Bhattacharya, et al., 2008).

The assembly of microtubules depends on several parameters including (1) polymerization rate, (2) depolymerization rate, (3) rescue rate (disassembly to assembly transition), and (4) catastrophe rate (assembly to disassembly rate) (Mitchison and Kirschner, 1984). In addition to the net addition and loss of tubulin dimers from microtubule ends, GTP binds exchangeably to tubulin and is irreversibly hydrolyzed during tubulin dimer addition to microtubule ends. The energy input from GTP hydrolysis allows for nonequilibrium polymerization dynamics creating behavior in which individual microtubule ends alternate stochastically between prolonged phases of polymerization and depolymerisation (Mitchison and Kirschner, 1984). The rates at which these events occur (1-4 above) and the hydrolysis of GTP accounts for the dynamic instability seen in microtubules. These behaviours are collectively referred to as microtubule dynamics (**Figure 1.2**), which play a major role in a variety of cellular processes such as cell motility, ntracellular transport, maintenance of cellular morphology, and cell division (Andre and Meille, 2006; Margolis and Wilson,1998; Rowinsky et al., 1993). Thus, any agent that changes the assembly or disassembly of microtubules can potentially prevent cell division by interfering with essential cellular functions.

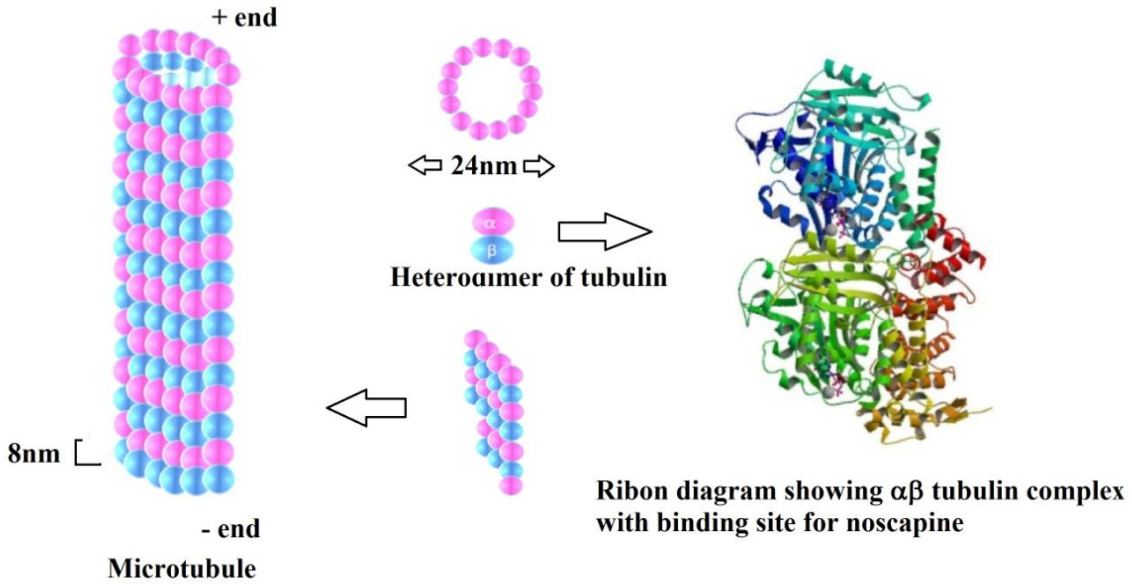

Figure 1.1. Microtubules are composed of 13 distinct linear protofilaments each composed of alternating α- and β- tubulin heterodimers. Heterodimers assemble into parallel rows called protofilaments. The assembly of tubulin heterodimers forms a polar structure with a kinetically distinct plus and minus end. The plus end adds heterodimers at a faster rate and also shrinks by losing heterodimers at a slower rate than the minus end.

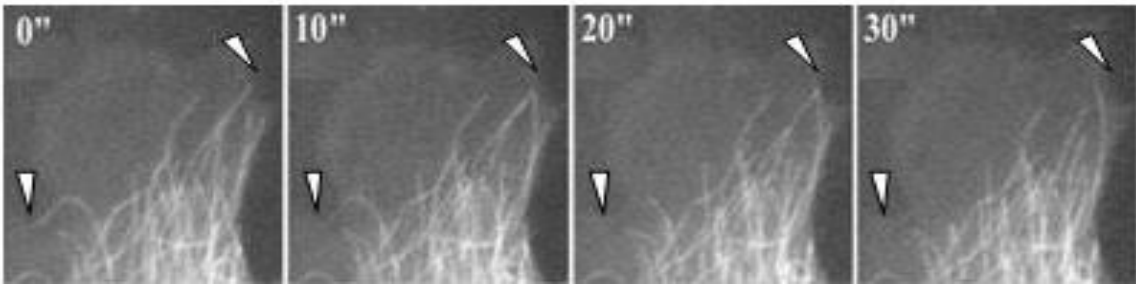

(B) Dynamic Parameters of Microtubule

Growth Phase		Average Pause Duration (sec)	22.54 ± 0.18
Rate (µm/min)	9.89 ± 0.78	% of Time per Phase (Growth/Shrink/Pause)	22.7/ 16.8/ 60.5
Distance (mm)	1.16 ± 0.09		
Duration (sec)	9.62 ± 0.95	Rescue Frequency (sec^{-1})	0.147 ± 0.02
Shrink Phase		Catastrophe Frequency (sec^{-1})	0.029 ± 0.004
Rate (µm/min)	11.39 ± 0.81	Dynamicity (µm/min)	102.7 ± 2.94
Distance (mm)	1.60 ± 0.30		
Duration (sec)	8.75 ± 0.26		

Figure 1.2. Noscapine increases the average time cellular microtubules remain inactive (pause duration). (A) A gallery of video frames, 10 seconds apart, showing the plus ends of several microtubules in control and a noscapine-treated PTK-2 cell. As expected in control cells, microtubules alternated between phases of growth and shortening; thus, the position of their plus ends changed significantly over 30 seconds (fixed pixel locations marked with arrowheads). In contrast, noscapine markedly suppressed microtubule dynamics in cells as indicated by the unaltered position of their plus ends (Bar=0.5 µm). Quantitative parameters of microtubule dynamics are listed in (B). Values are mean ± SEM. Dynamicity represents the sum of changes in length (growth or shrinkage) over the lifetime of a microtubule. (Landen et al., 2002)

The polar nature of the microtubule polymer and the hydrolysis of GTP that occurs during microtubule polymerization create two unusual forms of dynamic behaviors in cells both *in vitro* and *in vivo* (Mitchison and Kirschner, 1984; Cassimeris et al., 1988). One form is dynamic instability in which microtubule ends stochastically switch between growth and shortening phases (Mitchison and Kirschner, 1984). The transition from growth to shortening phase is called catastrophe and the transition from a shortening phase to growth state is called rescue. There is a pause state between these two states which is also called attenuated dynamics (Mitchison et al., 1984; Margolis and 1998 Wilson, 1998). The other form, treadmilling, consists of the net addition of tubulin at one microtubule end. Both dynamic processes are critical for mitotic spindle assembly and chromosome movement (Margolis and Wilson, 1998). The dynamics of microtubules are coordinated with the actions of molecular motors to precisely position chromosomes from the two daughter cells on the metaphase plate by the mitotic spindle (**Figure 1.3**). Microtubules

emanating from each spindle pole, undergo extensive growth and shortening events exploring the cytoplasm until they attach to the kinetechore of the chromosome during prometaphase. During metaphase, chromosomes, now under considerable tension, oscillate back and forth from the centrosome. This is a result of microtubule treadmilling where tubulin is added to the microtubule plus ends and lost from the microtubule minus ends at the mitotic spindle poles (Mitchison and Kirschner, 1984; Gorbsky and Borisy; 1989). Our growing knowledge of microtubule dynamics suggests that an agent capable of suppressing dynamics without substantially altering microtubule polymer mass and hence microtubule arrays could be sufficient to sustain mitotic block. This is because the proper assembly and function of the mitotic spindle depend on precise microtubule dynamics.

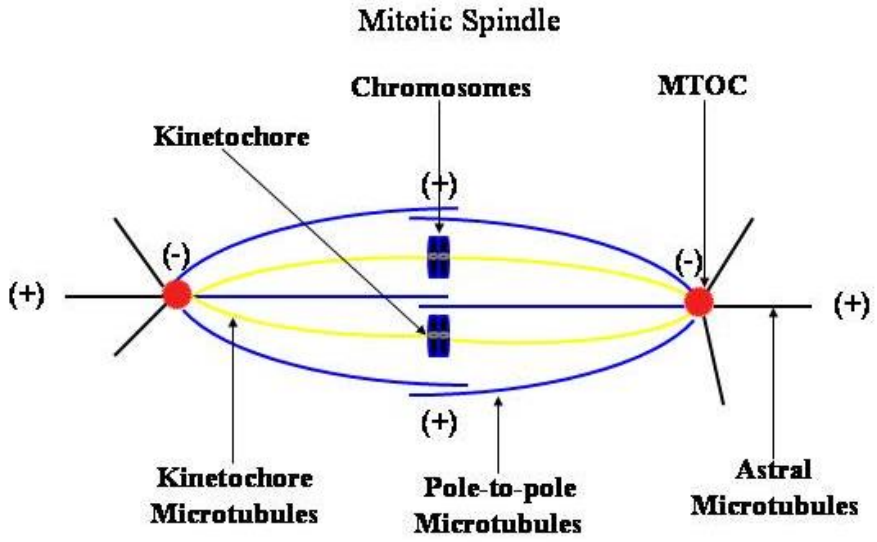

Figure 1.3. The mitotic spindle apparatus. The assembly of the mitotic spindle is the result of microtubule precision. There are three classes of microtubules that compose the mitotic spindle: astral, kinetochore, and polar. Polar microtubules overlap at the spindle midline and are responsible for separating the centromeres and then, during anaphase polar microtubules function to elongate the spindle. Kinetochore microtubules are responsible for capturing chromosomes. Kinetochore microtubules are thought to be responsible for the tension exerted on chromosomes to accurately align sister chromatids on the metaphase plate and to pull the two sister chromatids apart during anaphase. Astral microtubules radiate in all directions and are believed to separate the poles and orient them for the rest of the cell.

Several natural products are known to bind to tubulin or microtubules in the mitotic spindle and block mitosis (Johnson et al, 1963; Fuchs et al., 1978). These agents, most notably, colchicine, colcemid, nocodazole, paclitaxel, and the Vinca alkaloids have played seminal roles in probing the basic mechanisms of mitosis (Reviewed in Jordan and Wilson, 1999). Microtubule interacting drugs either cause microtubule depolymerization or promote excessive stability of microtubules resulting in the formation of microtubule bundles (the aggregation of tubulin into relatively large paracrystalline arrays (Bollag et al., 1995). The action of microtubule agents on microtubule polymerization and dynamics

have been determined to be highly dependent upon drug concentration and have been shown to inhibit cell proliferation at a range of doses in a variety of cell types (Jordan and Wilson, 1999).

It appears that microtubule drugs inhibit cell proliferation and induce cell death by slowing or blocking cell progression through mitosis (Jordan et al., 1993; Reider et al., 1994). It is now becoming clear that the characteristic block of cell proliferation for up to twelve hours during mitosis by microtubule interacting agents such as members of the Vinca alkaloid and taxane families appears to be attributable to a specific action on the mitotic spindle microtubules. High vinblastine concentrations inhibit spindle microtubule polymerization in vivo and in reconstituted microtubule systems prepared from sea urchin sperm axonemes (Kruczynski et al., 1998; Binet et al., 1990; Jordan et al., 1991). High paclitaxel concentrations enhance microtubule polymerization creating extensive bundles of microtubules and increasing the mass of microtubules both in reconstituted systems and in living cells (Horwitz, 1992; Jordan et al., 1993). This is opposite to the effects seen following high vinblastine exposure which results in depolymerization of spindle microtubules and induction of paracrystalline tubulin arrays in reconstituted systems and living cells (Dustin, 1984; Binet et al., 1990; Jordan et al., 1991; Kruczynski et al., 1998). However, identical to vinblastine, paclitaxel also substantially disrupts microtubule arrays including those forming the mitotic spindle (Jordan et al., 1993; Derry et al., 1995). Low concentrations of both vinblastine and paclitaxel (nM concentrations) have been shown to cause mitotic block at the transition from the metaphase to anaphase boundary (Jordan et al., 1993). This effect is accompanied by the suppression of microtubule dynamics at the plus ends of microtubules with little or marginal alterations in polymer mass (Jordan et al., 1993; Derry et al., 1995). This growing body of evidence suggests that low concentrations of microtubule agents can inhibit microtubule dynamics at concentrations below those that inhibit microtubule polymerization (Jordan et al., 1992; Dhamodharan et al., 1995. These data provide evidence showing that the potent antimitotic and antiproliferative effects of the Vinca alkaloid and taxane families involve the suppression of microtubule dynamics at the plus end of mitotic spindle microtubules.

1.5 Cell Cycle and Cell Cycle Checkpoints

The fundamental task of the cell cycle is to ensure that DNA is precisely replicated once during S-phase and that identical duplicated chromosome copies are segregated equally into identical daughter cells during M-phase (mitosis). The mammalian cell cycle is divided into four discrete phases: Gap1 (G1), Synthesis (S-phase), Gap2 (G2), and mitosis (M-phase). Collectively G1, S, and G2 are known as interphase to distinguish it

from the dramatic cell division that occurs during mitosis (Norbury and Nurse, 1992) (**Figure 1.4**). G1 phase is the interval between mitosis and S-phase that allows time for growth, ensures that 2N DNA content is present and undamaged, and determines whether the DNA replication machinery is prepared for replication. DNA replication is completed during synthesis or S-phase. G2 phase is the interval following S-phase and before mitosis. G2 provides time to ensure that DNA replication is complete prior to mitosis. Finally, during M-phase, the nuclear envelope breaks down and the nucleus condenses (prophase), microtubules form the mitotic spindle to separate sister chromatids that align on the metaphase plate (metaphase), sister chromatids separate and move to opposite poles of the spindle where they de-condense (anaphase), and the cell undergoes cytokinesis (telophase)(Grana and reddy, 1995) (**Figure 1.5**).

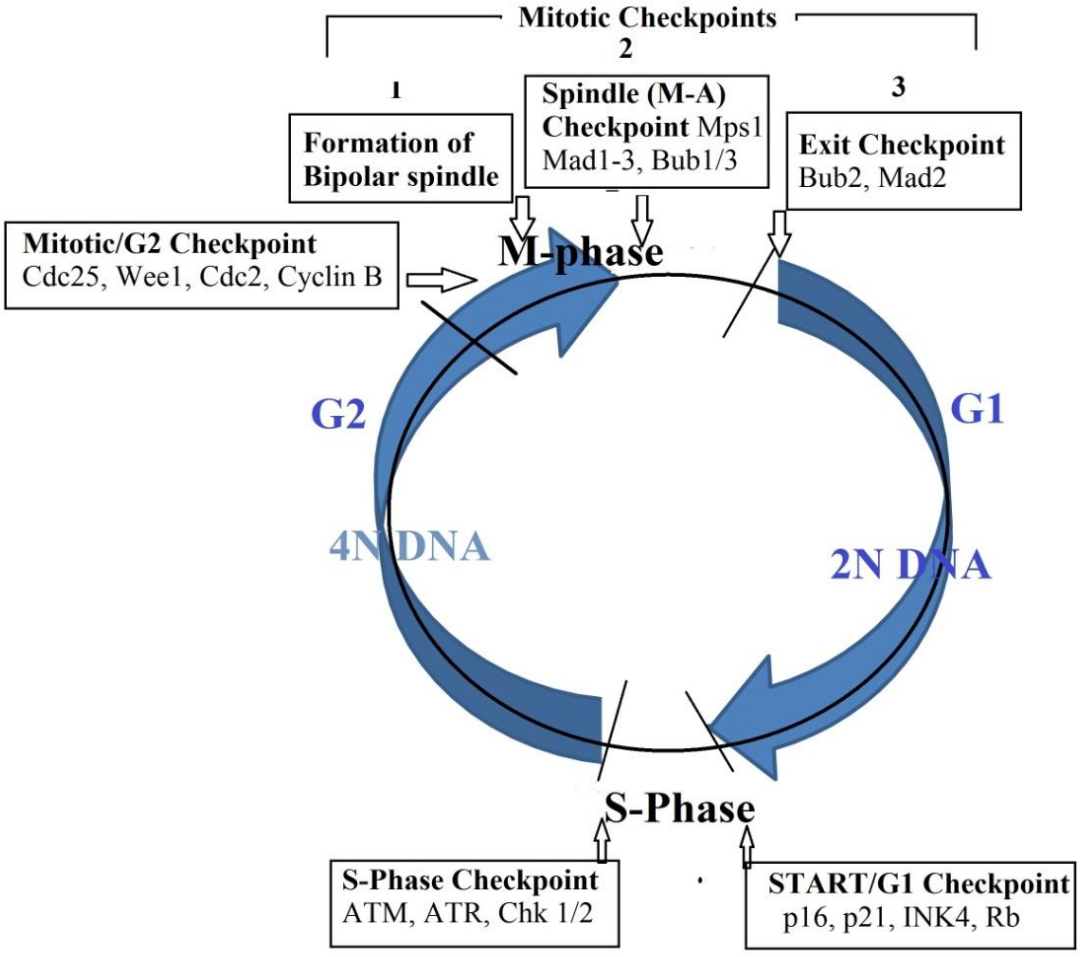

Figure 1.4. Cell cycle. There are 4 successive distinct stages of the cell cycle. G1, S, and G2 are collectively known as interphase in which the cell grows continuously preparing for the fourth phase, mitosis, the process of nuclear division. A cell cycle control system or checkpoints determine whether or not the cell is prepared to proceed to the next phase of the cell cycle. If DNA is damaged, the replication machinery is not assembled, or if the cell is not of proper size, the checkpoints will halt the cell at that point in the cell cycle.

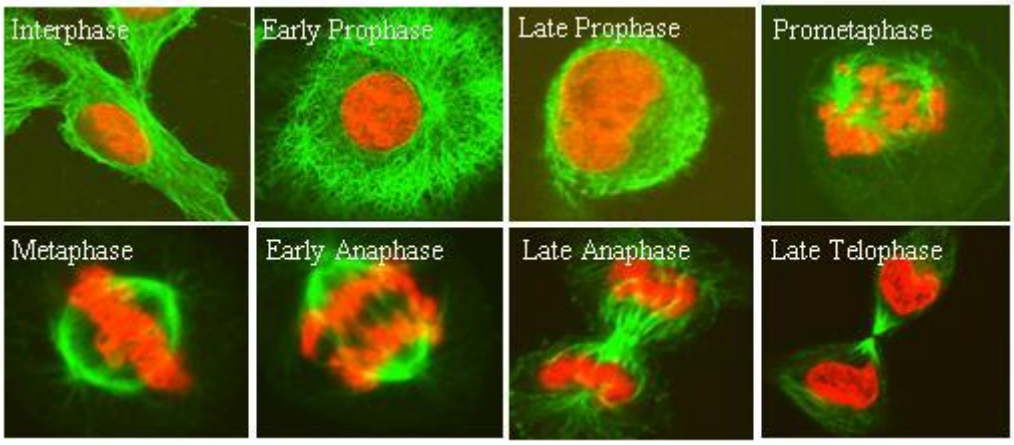

Figure 1.5. Mitosis in eukaryotes. Immunoflorescent cells were stained for tubulin (green) and DNA with propidum iodide (red) and imaged using confocal microscopy. During interphase, cells contain 2N DNA content and microtuble arrays are abundant. Early prophase marks the period when chromatin begins to condense. During late prophase, the centrosome divides and the two microtuble asters begin to separate. Nuclear envelope breakdown occurs during prometaphase and during metaphase the bipolar mitotic spindle is clearly visible. Identical sister chromatids separate during early anaphase as they are pulled to opposite poles by microtubules. Chromosomes are fully separated by late anaphase and cytokinesis occurs during telophase resulting in identical daughter cells.

The mammalian cell cycle is exquisitely controlled by checkpoint mechanisms led by cyclin-dependent kinases (Cdks) that are responsible for regulating cell cycle progression. Cdks govern the initiation, progression, and completion of cell cycle events. The active form of Cdks is thought to consist of a complex of at least two proteins, a catalytic subunit such as cdc2, and a regulatory subunit, such as cyclin B. Cdk regulation occurs by their association with regulated cyclins, kinase phosphorylation state, Cdk inhibitors, and by ubiquitin-mediated proteolysis. Each of these factors is thought to be partially responsible for mediating cell cycle progression (Hartwell and Kastan, 1994; Sampath and Plunkett, 2001). The Kip and INK family of proteins are generally believed to function as Cdk inhibitors and loss of regulation of members of these protein families is strongly implicated in the deregulation of cell cycle control and carcinogenesis (Vidal and Koff, 2000). The transition from one phase of the cell cycle to the next is controlled by checkpoints, a quality control mechanism typically consisting of a signal transduction cascade, that monitors cell growth, DNA integrity, and replication status before cells commit to proceed through the cell cycle. Although not fully understood, it is currently thought that upon checkpoint activation, sensor molecules interact with cyclin-Cdk complexes to halt cell cycle progression. Eukaryotes have an evolutionarily conserved set of checkpoint proteins that arrest cells during the cell cycle to prevent DNA replication during S-phase or chromosome segregation during mitosis of improperly replicated DNA. Many cancer cells are defective in at least one checkpoint pathway (Cahill et al., 1998;

Zou et al., 1999). Pharmacologic agents that exploit our knowledge of the cell cycle checkpoints, may offer promise for cancer therapy because they could serve as tools to halt cancer cell division at specified points during the cell cycle.

Figure 1.4 depicts the checkpoints and molecules involved in cell cycle progression. The G1 checkpoint ensures that 2N DNA is undamaged and that the DNA replication machinery is prepared for synthesis. Multiple regulatory pathways control the transition from G1 to S-phase which is also known as the START checkpoint (Dustin, 1984). The functions of the p16, cyclin D, Cdk4, Cdk6, pRb-E2F pathway (collectively known as the retinoblasoma pathway) play a key role in the G1/S transition (Bruce et al., 2000). It is conceivable that cells with a faulty G1 checkpoint can undergo multiple rounds of S-phase reentry following DNA damage resulting in a multinuclear phenotype (Lanni and Jacks, 1998). The S-phase checkpoint arrests cell progression in S-phase if replication is blocked or DNA synthesis is incomplete. It also blocks further replication of DNA if cells are arrested in mitosis for a prolonged period and then come out of mitosis without productive cytokinesis in a G1-like state, but with abnormal DNA content (Lanni and Jacks, 1998). The S-phase checkpoint is controlled by ATM (Ataxia Telangiectasia Mutated) protein and related kinases such as ATR (Ataxia telangiectasia and rad 3 related) protein. These proteins are members of the PIK (phosphatidylinositol kinase)-related kinase family. This family consists of high molecular weight kinases involved in cell cycle progression that activate the checkpoint kinases Chk1/2 (Falck et al., 2001). The G2 checkpoint is activated in response to DNA damage that prevents mitosis of damaged cells. G2 checkpoint control is thought to be mediated by both p53 and ATM phosphorylation of Chk1/2. In normal cells, negative regulation of cyclin B-Cdc2 by phosphorylation on threonine-14 and tyrosine-15 prevents premature mitotic entry before completion of S-phase (Sampath and Plunkett, 2001). The dephosphorylation of Cdc2, which is necessary for entry into mitosis, is controlled by Cdc25. DNA damage induces the ATM-mediated phosphorylation of Chk1/2 both of which phosphorylate Cdc25. As a consequence Cdc25 cannot dephosphorylate Cdc2 which remains in an inactive state resulting in G2 arrest (Sharpiro et al., 1999). P53 is also believed to be essential for the G2 checkpoint due to evidence suggesting that in cells lacking p53, disruption of Cdc25 results in entry to mitosis of cells with DNA damage or cells may re-enter S phase without completing mitosis; such endoreduplication is typically followed by apoptosis (Waldman et al., 1996). Clearly, there are multiple checkpoint genes and proteins that are required to precisely regulate the cell cycle.

In addition to the checkpoints regulating the phases of the cell cycle, there is evidence suggesting that there are three additional checkpoints controlling mitosis (mitotic checkpoints). Condensed sister chromatids are attached to the mitotic spindle apparatus by their kinetochores in prometaphase and metaphase. Sister chromatids are pulled to opposite poles during anaphase with high fidelity. Missegregation of sister chromatids leads to aneuploidy; thus, this process is tightly regulated by checkpoints that monitor the (1) centrosome separation required for bipolar spindle formation (2) attachment of all kinetochores to microtubules before anaphase (Metaphase-to Anaphase Checkpoint) and (3) completion of chromosome separation before exits from mitosis (Bub-2 dependent checkpoint pathway) (Wassmann and Benezra, 2001). Inactivation or mutation of each of the checkpoint genes and/or proteins discussed above is known to predispose cells to malignancy (Sherr, 1996). Taking advantage of known checkpoint defects that are present in cancer cells, but that are intact in normal cells may offer insight for the development of novel chemotherapeutic agents. Considerable advances have been made over the last five years in understanding checkpoint mechanisms using tubulin-binding drugs as tools to study cell cycle progression. However, novel agents that affect microtubules in new ways may be useful in order to fully elucidate the role that checkpoints play in the transformation of cancer cells and may be capable of interfering with those checkpoints to treat human cancers.

Mutations that inactivate checkpoints have recently been defined in several human tumors of neuroectodermal origin including glioblastoma (Van Meir et al., 1994; Labuhn et al., 2001) and melanoma (Halachmi and Gilchrest, 2001). In fact, the p53 tumor suppressor gene was inactivated in cells in nearly half of the human glioma cells examined due to a lack of expression or by mutation (Asai et al., 1994). p16INK4a, p14ARF, and PTEN were also found to be frequently mutated alone or in combination in approximately 70% of human glioma cells analyzed (Ishii et al., 1994). Reduced, or lack of expression of p16 has also been found in one third of melanomas (Walker et al., 1998; Greene, 1999). In addition, melanomas with p16 deficiencies have been correlated with a poorer prognosis (Reed et al., 1995; Straume et al., 2000). Given the volume of checkpoint mutations identified in cancer cells to date, the loss of checkpoints in tumor cells might be a very common occurrence associated with a variety of neoplasms.

1.6 Microtubule interacting agents

A large number of chemically diverse microtubule binding agents are available which directly bind to microtubule or bind to soluble tubulin. Most of the compounds act on dynamic polymerization of spindle microtubules and inhibit the proliferation of the

cell. These tubulin targeted drugs can be divided into two main classes, the first one is microtubule destabilizing agents and the second one is microtubule stabilizing agents. Microtubule stabilizing agents are those which inhibit microtubule polymerization at a high concentration such as Vinca alkaloids, cryptophycins, estramustin, halicordins, colchicine, and combrestatatin. Some of them are already in use in the clinics and some of them are under clinical trial for the treatment of cancer. In addition, there are large numbers of compounds that are not yet clinically tried for cancer therapy such as noscapine, maytansin, rhizoxin, podophylotoxin, spongistatin, steganacins and curacins. The second group is microtubule stabilizing agent which promotes polymerization of microtubule such as paclitaxel, docetaxel, epothilones, discodrmolide, eleutherobins, sarodictyins, laulimalides, rhazinalam, some steroids and polyisprenyl benzophenones agents.

1.7 Paclitaxel as anticancer drug

Paclitaxel (**Figure 1.6**) was derived from the plant *Taxus brevifolia.* It is a widely used tubulin-targeted chemotherapeutic agent for the treatment of various types of cancer including lungs cancer, ovarian cancer and breast cancer. The drug was first approved by US –FDA in 1992. It has been used in a single and combinational form for the treatment of various types of cancer. It is also considered as first microtubule agent ever isolated and studied its anticancer activity in 1958. Paclitaxel bind to β-tubulin of microtubule at N-terminal domain. After binding, it stimulates the microtubule polymerization by phosphorylation of β-tubulin which leads to arrest of dividing cell at G2/M stage of cell cycle and causes cell death. To enhance prolonged drug release as well as cellular uptake several liposome formulations of paclitaxel have been developed and approved for the clinical trial. As an example, LEP-ETU, liposome-encapsulated paclitaxel has been developed by Neo Pharm and Endo TAG-1 cationic liposome-coated paclitaxel developed by Medigene are under clinical trial. Besides these, some nanospheres carriers have been developed to enhance drug delivery as the nanospheres are biocompatible and biodegradable. These nanospheres are made up of nanoparticles composed of polyD L-lactic-co-glycolic acid (PLGA) and poly D L-lactic acid. Some emulsifying agents such as TOCOSOL-Paclitaxel (a vitamin E-based emulsifying agent) have been developed to solubilize paclitaxel and reduce its toxicity. (Nagel et al.,1995).

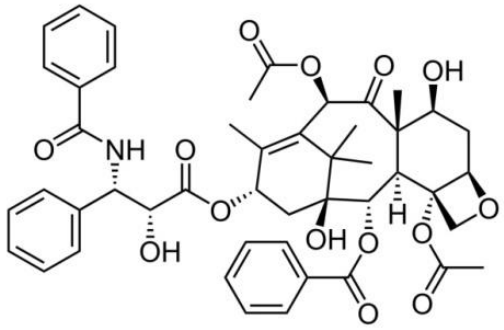

Figure 1.6: Molecular structure of paclitaxel

1.8 Vinca alkaloids as tubulin targeted drug

Vinca alkaloids (**Figure 1.7**) are widely used in clinics as the antineoplastic agent. Particularly two of its derivatives, vinblastine and vincristine are widely used in the treatment of different types of cancer. The vinca alkaloids are isolated from the periwinkle plant *Catharanthus roseus,* also commonly known as *Vinca rosea*, *Lochnera rosea*, and *Ammocallis rosea* (S. S. Rai and J. Wolff, 1996). Vinblastin and vincristine bind to β tubulin, block microtubule polymerization and arrest mitosis at prometaphase. (Jordan et al., 1998; Ngan et al., 2000; Gerwick and Yoo,1995).

It has also been found that they bind stoichiometrically to tubulin and prevent the formation of the heterodimer and prevent polymerization of the tubulin .(Gerwick and Yoo,1995). Another compound vindesine has been produced by modifying the functional group which works on the same principle as vinblastin and vincristin.

Vindesine **Vincristine** **Vinblastine**

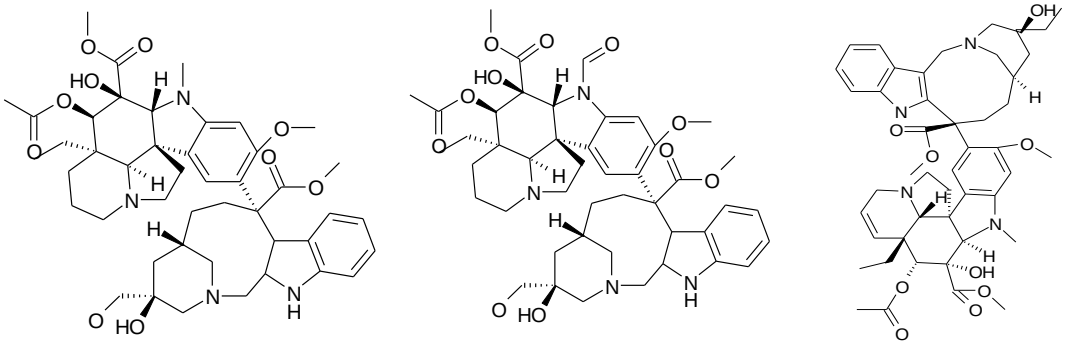

Figure 1.7. Molecular structure of vinca alkaloids.

1.9 Epothilones

It is the most effective cytotoxic antimitotic agent discovered in the early 1990s and was extracted from the mycobacterium *S. cellulosum*. Unlike taxol and Vinca alkaloids, it also binds to the microtubule at β-tubulin and alters its dynamic structure by polymerizing the tubulin. Eribulin, an epothilone has been clinically approved to treat various types of cancer. Ixabepilone, the most potent analogue of Epothilone (**Figure 1.8**) has been reported to effectively kill cancer cells (Bollag et al., 1995; Larkin and Kaye, 2006; Dobbelstein and Moll, 2014).

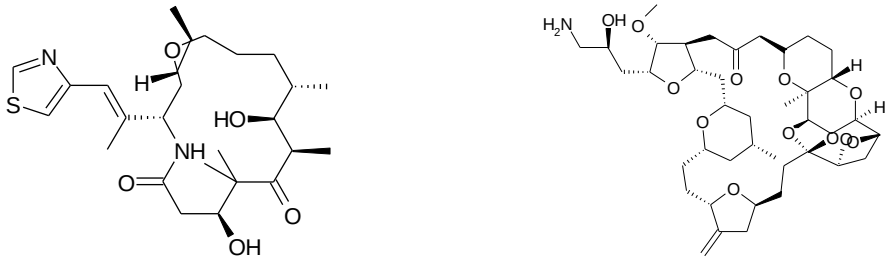

Ixabepilone **Eribulin**

Figure 1.8. Molecular structure of derivatives of epothilone.

1.10 Limitation of currently available microtubule interacting anticancer drug

Despite the initial effective response of microtubule targeting drugs such as taxen and vinca alkaloid, their effectivity becomes limited due to evolving of drug resistant tumor types (Dobbelstein and Moll, 2014; Perez et al., 2009). Many reports suggested that cancer cells have a multidrug resistance phenotype (MDR) due to drug efflux pumps. Another problem associated with the currently available microtubule targeted drug is that they show toxicity to both cancer cells as well as normal cells. As a result, they possess severe side effects such as gastrointestinal disorders like diarrhea, vomiting, nausea, peripheral neuropathy, immunosuppressive, hair fall, anemic, etc. (Pettit,1996) Therefore, it is needed to find a new drug with no toxicity, well-tolerated, and batter pharmacologic properties.

1.11 Noscapine as antimitotic agent:

Noscapine (**Figure 1.9**), an opium alkaloid was discovered in 1817 by Pierre-Jean Robiquet, from Derosne's salt (Rowinsky et al.,1993). Noscapine contains two stereogenic centres, therefore consists of four possible stereoisomers. Out of the stereo-isomers, the naturally occurring *L*-(*S*,*R*)-noscapine isomer has been exploited for the majority of activities in terms of aptitude to arrest mutagenic mammalian cells in mitosis. It is generally used as an anti-cough drug. It is also used as an antimalarial drug by Indians in

the 19th century. Cytotoxicity effect of the compound was first discovered in 1954. Similar studies were also reported by National Cancer Institute, United States in 1958. However, further studies failed to show significant antitumor activities *in vivo*. However, it was rediscovered by the Dr. Joshi group at Emory University School of Medicine, Georgia, Atlanta (Ye et al, 1998) as an anticancer agent. *In vivo* studies in mice xenograft with human breast cancer revealed a significant reduction in tumor size without any toxicity to vital organs or tissue (Aneja et al., 2006; Joshi et al., 2010). The pharmacological usefulness of noscapine since it was discovered is collated in **Figure 1.10.**

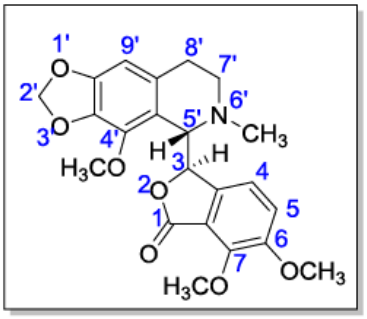

Figure 1.9. Natural α-noscapine Chemical structure and numbering system for *L*-(*S*,*R*)-noscapine (**1**) illustrating the tetrahydroisoquinoline moiety (top) and phthalide moiety (bottom).

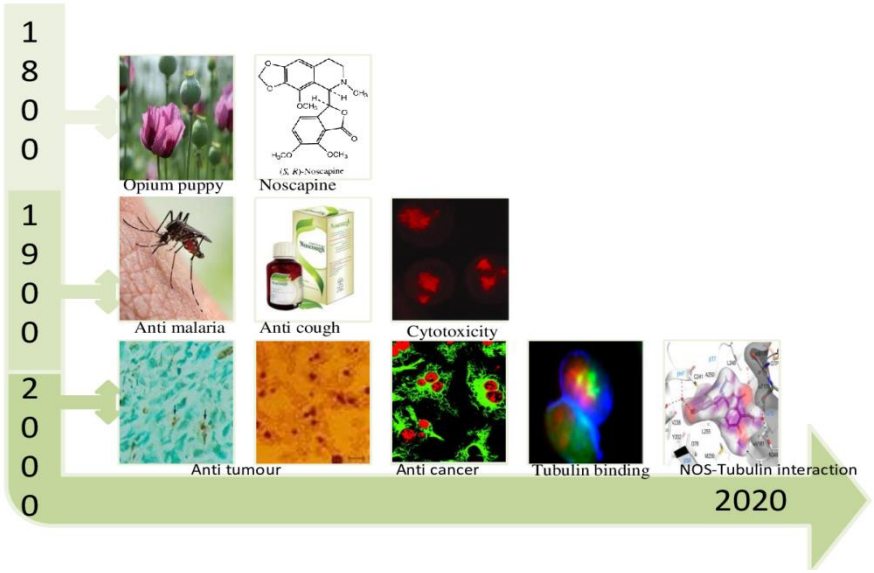

Figure 1.10. Time Scale of pharmacological usefulness of Noscapine.

1.12 Biochemical basis of action of noscapine

It was demonstrated that noscapine binds to microtubule in 1:1 proportion (Ye et al., 1998). Upon binding to microtubule it interfere with the cell cycle progression and induces apoptosis to cancer cells, mainly because the cancer cells are compromised with cell cycle check points. Instead of influencing microtubule polymerization, noscapine alters microtubule assembly steady-state dynamics, increasing the duration spent in an

attenuated state. (Zhou et al., 2002). Noscapine has different modes of action for the activation of apoptosis (**Figure 1.11**). One of them is the activation of cyclin-dependent kinase p^{cdc2}. The induction of apoptosis by activating $p34^{cdc2}$ has been reported in murine cell carcinoma. The role of $p34^{cdc2}$ in the cell cycle has been studied by Ye et al. and found that prolonged activation of the kinase mitotically arrests the cell (Ye et al., 1995). It was reported that noscapine induced apoptosis to cancer cell by cyclin-dependent kinase p^{cdc2} (Rowinsky et al. 1993). The JNK pathway (also known as c-Jun-N-terminal kinase pathway), activates several cellular responses including stress-induced apoptosis. Activation of JNK during apoptosis by microtubule targeted drug has been reported in paclitaxel resistance cancer cell line. The induction of apoptosis by noscapine is reported to be mediated by JNK pathway (Zhou J et al., 2002). Tumor cells are hypoxic in nature which expresses HIF-1α, a transcription factor activated by hypoxia. Studies reported that dimer of HIF-1α and HIF-β induces angiogenesis. HIF-1α induce the expression of angiogenetic promoter like vascular endothelial growth factor (VEGF). Suppression of HIF-1α and subsequent inactivation of VEGF by noscapine have also been reported (Yoo and Gerwick, 1995). Another angiogenetic promoter is NF-κB. Sung et al reported that noscapine induced inactivation of NF-κB signaling along with TNF, IKK, VEGF as well as MMP-9 (Bardelmeijer, 2004). The antagonistic effect of noscapine in fibrosis of human lungs fibroblast culture cells has been reported recently by Kach et al. (Kach et al., 2014)

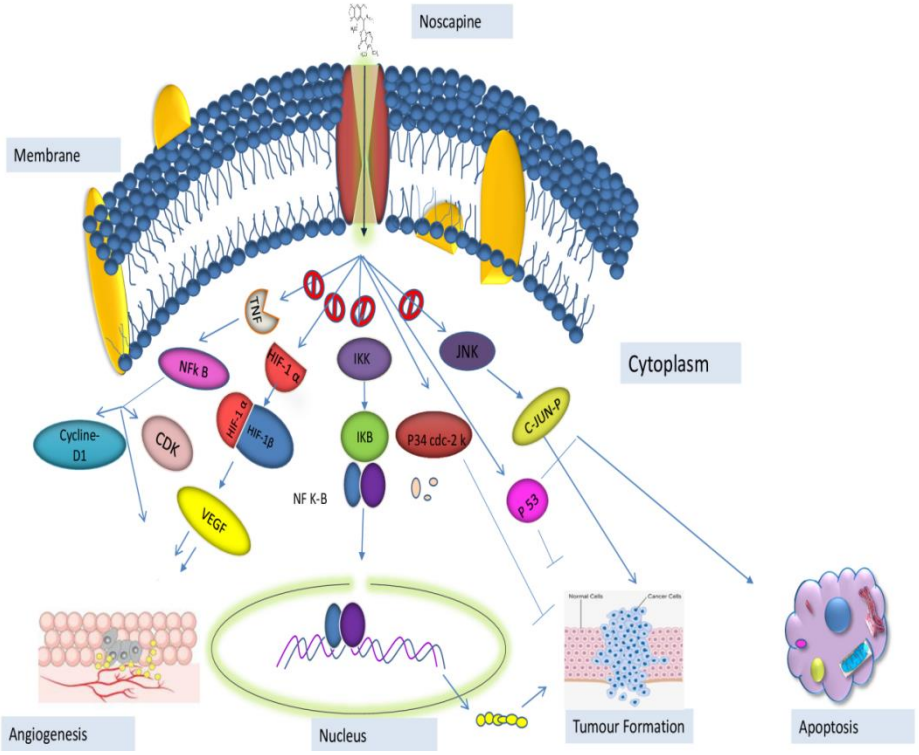

Figure 1.11. Biochemical mechanism of induction of apoptosis and antiangiogenesis by noscapine in cancer cells (Rida et al., 2015).

1.13 Noscapine in the clinic:

Noscapine has been used as a potent anti-tussive agent due to its antagonized effect on bradykinine. (Mooraki et al., 2000). Particularly noscapine is very effective in suppressing cough caused by angiotensin-converting enzyme inhibitors. The efficacy of noscapine as an antineoplastic treatment for a wide spectrum of malignancies has been demonstrated in several investigations, and the drug is now undergoing Phase I/II clinical trials. Noscapine causes apoptosis by arresting cells in mitotic division at doses greater than those employed to control cough. (Ye et al.,1998). As a result of triggering apoptosis, it inhibits the development of murine and human breast cancers implanted in mice. (Ye et al.,1998). To study in vitro cell proliferation effect, MCF-7, a hormone receptor-positive human breast cancer cell line was used, after being injected into athymic mice, noscapine induced 80 percent regression of human breast cancers. Breast cancer cells that are hormone-insensitive and triple-negative are also susceptible to Noscapine. It significantly reduces the size of xenograft tumors using MDAMB-231 (Chougule et al., 2011). Noscapine has also shown a tremendous effect on MDAMB-231 triple negative breast cancer in combination with doxorubicin. Because of these encouraging preclinical results, clinical studies with triple-negative breast cancer patients, for whom treatment choices are currently restricted, should be explored using noscapine in combination with doxorubicin, even if hormone receptor-positive cases may also benefit from noscapine.

1.14 The pharmacology of noscapine

As a result of its rapid and efficient absorption, noscapine is commonly supplied orally to patients. It has been observed that, after 1 hour, the plasma concentration reaches a maximum level. There was bi-exponential kinetics in healthy human volunteers, regardless of gender. According to Dahlstrom et al. (1982) found that an intravenously administered dose of 66 mg of noscapine was fully utilized, whereas 150 mg tablet was quickly dissolved in the mouth. It was observed that after intravenous injection, the average plasma distribution half-life was 13 minutes, with a range of 7 to 22 minutes, and the average plasma elimination half-life was 156 minutes, with a range of 96 to 236 minutes. The total plasma clearance was found to be 22 mL/min/kg and the volume of distribution was 4.7 liters/kilograms. The absolute oral bioavailability was determined to be 30 percent with a 3.6-fold variance across individuals (Dahlstrom et al.,1982). Fang et al. (2012) have mapped noscapine's metabolism and examined its bioactivation to better understand how it works. Noscapine was given to mice orally and different metabolites were identified such as Demethylated, 2-hydroxylatable and bismethylatable compounds

(Fang et al., 2012). Glucuronides, flavin-containing monooxygenase 1, and UDP-glucuronosyltransferases were also detected. No hepatotoxicity was seen in animals with altered glutathione levels in the liver and serum biochemistry, proving that noscapine does not cause hepatotoxicity through bioactivation (Fang et al., 2012).

1.15 Noscapine is safe as a drug:

Several experiments have shown that noscapine is not harmful to organs and tissues. Only a tiny number of individuals have experienced nausea and stomach pain at very high dosages. Patients with terminal cancer received noscapine up to 3000 mg daily as part of Dr. Lasagna's 1961 research at Johns Hopkins University. Only 20% of patients had side effects that included minor drowsiness and stomach pain (Lasagna et.al., 1961) The noscapine is used in combination with morphine which increases the drugs' sedative and pain-relieving effect by up to three times. Some clinicians are now combining the two drugs so that they may be administered in conjunction with morphine, which is safer and has a greater impact (Li et al., 2010).

1.16 Advantage of Noscapine

Noscapien has several advantages as mentioned below as an anticancer agent.

- It arrests mitosis in a variety of cancer cell lines including drug resistance variants and induced apoptosis (Zhou, et al 2002; Mahmoudian. et al, 2009).
- It is a poor substance for drug efflux pumps like polyglycoproteins and MDR-related proteins (Landen et al., 2002).
- It inhibits progression of various tumor types including murine melanoma, Lymphoma glycoblastoma and human breast tumours implanted in nude mice without cytotoxic effect in normal dividing cells and post-mitotic cell such as neurons (Mahmoudian et al., 2009; Landen et al., 2002; Ke et al., 2000; Aneja et al., 2004; Landen et al, 2002).
- It doesn't inhibit primary humoral and cellular response in mice (Landen et al., 2002)
- It doesn't show any immunological and neurological toxicity.
- It is orally available (Mahmoudian et al., 2009).
- It is a most favorable pharmacokinetics clearance in 6-10 hours (Aneja et al 2007)

Despite the above advantages to noscapine, its IC_{50} value ranges from 21 µM to 100 µM. To enhance its activity in lower concentration further efforts have been focused on rational drug design and synthesis of the new generation of noscapine derivatives for better therapeutic outcomes.

1.17 Analogues of noscapine

The analogues of noscapine are also called noscapinoids. The derivatives have been classified based on the site of modification (**Figure 1.12**). Currently, more than three generations of noscapinoids (**Figure 1.13**) have been developed and their anticancer activity have been evaluated based on in silico, in vitro, and in vivo study (Zhou et al., 2003; Zhou et al., 2004; Zhou et al., 2005; Aneja et al., 2006; Santoshi et al., 2011; Naik et al., 2011; Lopus et al., 2011; Mishra et al., 2011; Manchukonda et al., 2013). The first generation of noscapinoids was developed by structural modification of parent noscapine at point modification point 'A' which contains isoquinoline ring and modification point 'B' which contains isobenzofuranone ring system. Different functional groups like nitro, azido, amino and halogenated groups (F, Cl, Br, I) were attached at diversity point A, except these, reduced oxygen at diversity point B of halogenated noscapinoids also comes under first-generation noscapinoids (Zhou et al., 2004; Aneja et al., 2006; Santoshi et al., 2011; Naik et al., 2011). The first-generation noscapinoids were found to be more effective than the parent one. The 2nd generation noscapine analogues were O-alkylated and asylated which were developed by chemical alteration at diversity point 'C' of parent noscapine. These analogues were also found to be better than the parent compound (Manchukonda et al., 2013). The 2nd generation noscapinoids include, benzofuranone derivatives of noscapine, was synthesized by Mishra et al. via modifying the benzofuranone ring structure of noscapine at position-7 (Mishra et al., 2011). The 3rd generation, noscapinoids were developed by manipulation in the isoquinoline ring system at diversity point 'D' (Manchukonda et al., 2013). All these noscapinoids were superior to the parent noscapine based on affectivity (Zhou et al., 2003). Subsequently, several derivatives of O-alkylated noscapine have been synthesized by Andorson et.al. (2005). Furthermore, some noscapinoids like S-benzyl derivatives have been synthesized by same group. One of the derivatives such as 3,4,5-trimethoxybenzyl noscapinoids developed by Aderson group was found to be the most potent which arrest the cell cycle at S-Phase. Usually, all these derivatives of noscapine were chemically synthesised from the natural lead molecule, noscapine. As an example, 9-Br Noscapine and its reduced form were synthesized by derivatizations at C-9 position of noscapine scaffold as mentioned in synthetic scheme 1 (**Figure 1.14**). The reaction scheme was developed by Joshi et al. (2003). Both the derivatives showed improved anticancer activity compared to noscapine. The other halogen derivatives such as 9-Cl Noscapine, 9-I Noscapine and 9-F Noscapine were synthesised by Aneja et al. (Aneja et al., 2006) by the synthetic scheme 2 (**Figure 1.15**) and studied their antiproliferative activity using a panel of cancer cell lines.

Simillarly, cyclic ether halogenated derivatives of noscapine were synthesized from the halogenated derivatives of noscapine (Mishra et al., 2011)

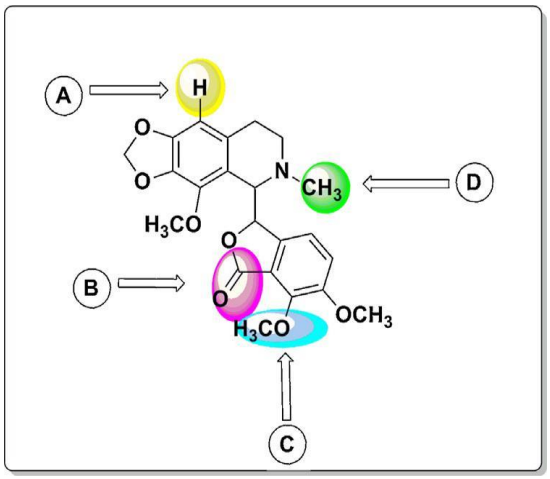

Figure 1.12: Chemical structure of noscapine with modifications points A,B,C and D.

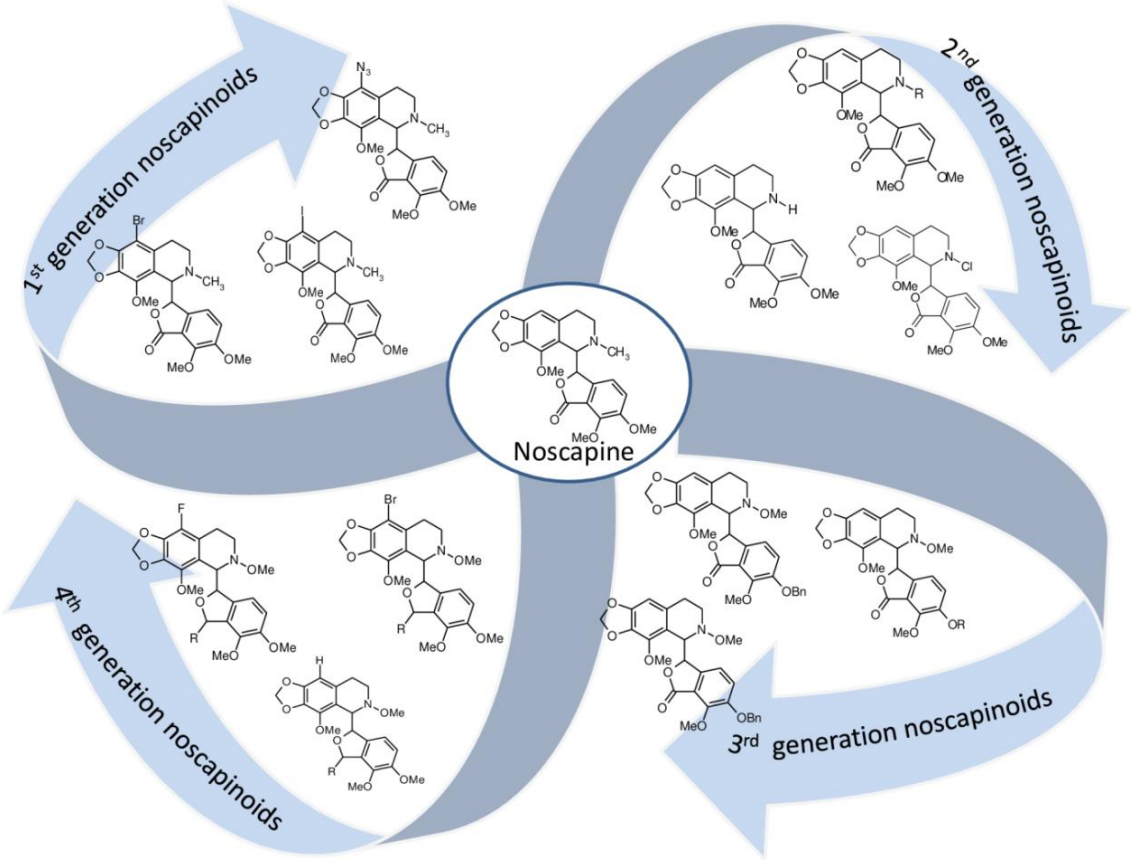

Figure 1.13. Structure of all four generation of noscapine derivatives.

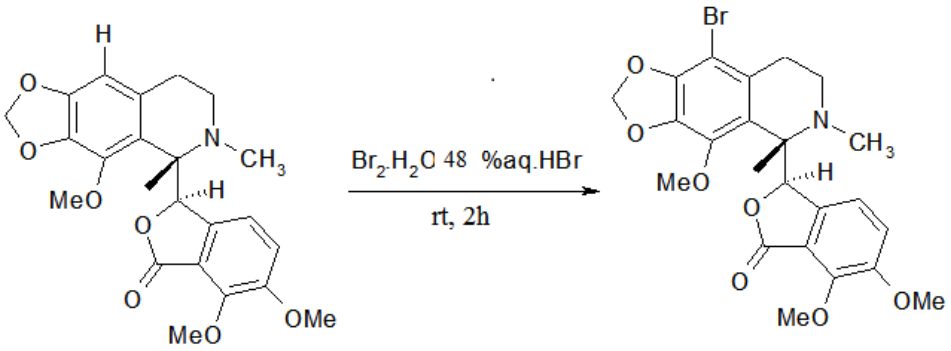

Figure 1.14. Synthetic scheme 1 for synthesis of 9-Br Noscapine from Noscapine.

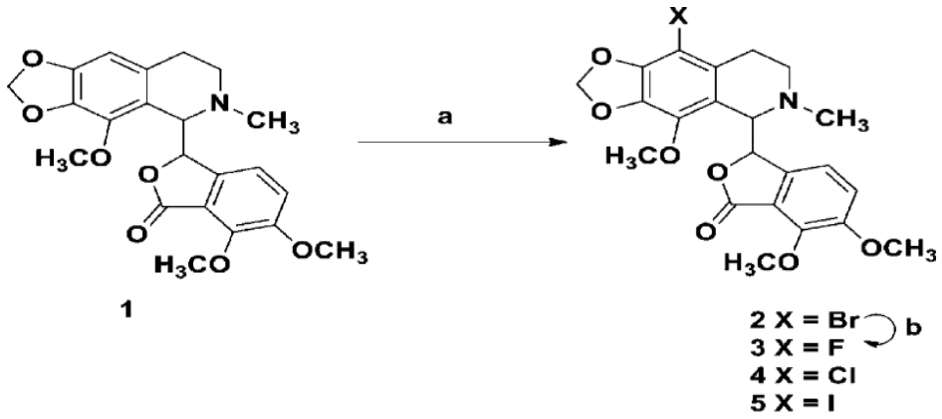

Figure 1.15. Halogenated noscapinoids: 'a' represents bromine water and hydrogen bromide for bromo noscapine; sulfuryl chloride and chloroform for chloro noscapine; fluorine, Amberlyst-A (a slightly basic resin with alkyl amine functionality), and tetrahydrofuran for fluoro noscapine; and pyridine–iodine chloride and acetonitrile for iodo noscapine (Aneja R. et al, 2006).

Aneja et al (2006) strategically sythesized cyclic ether halogenated derivatives of noscapine (**Figure 1.16**) that showed robust anticancer activity against human breast cancer cell lines MCF-7 and MDAMB-231.

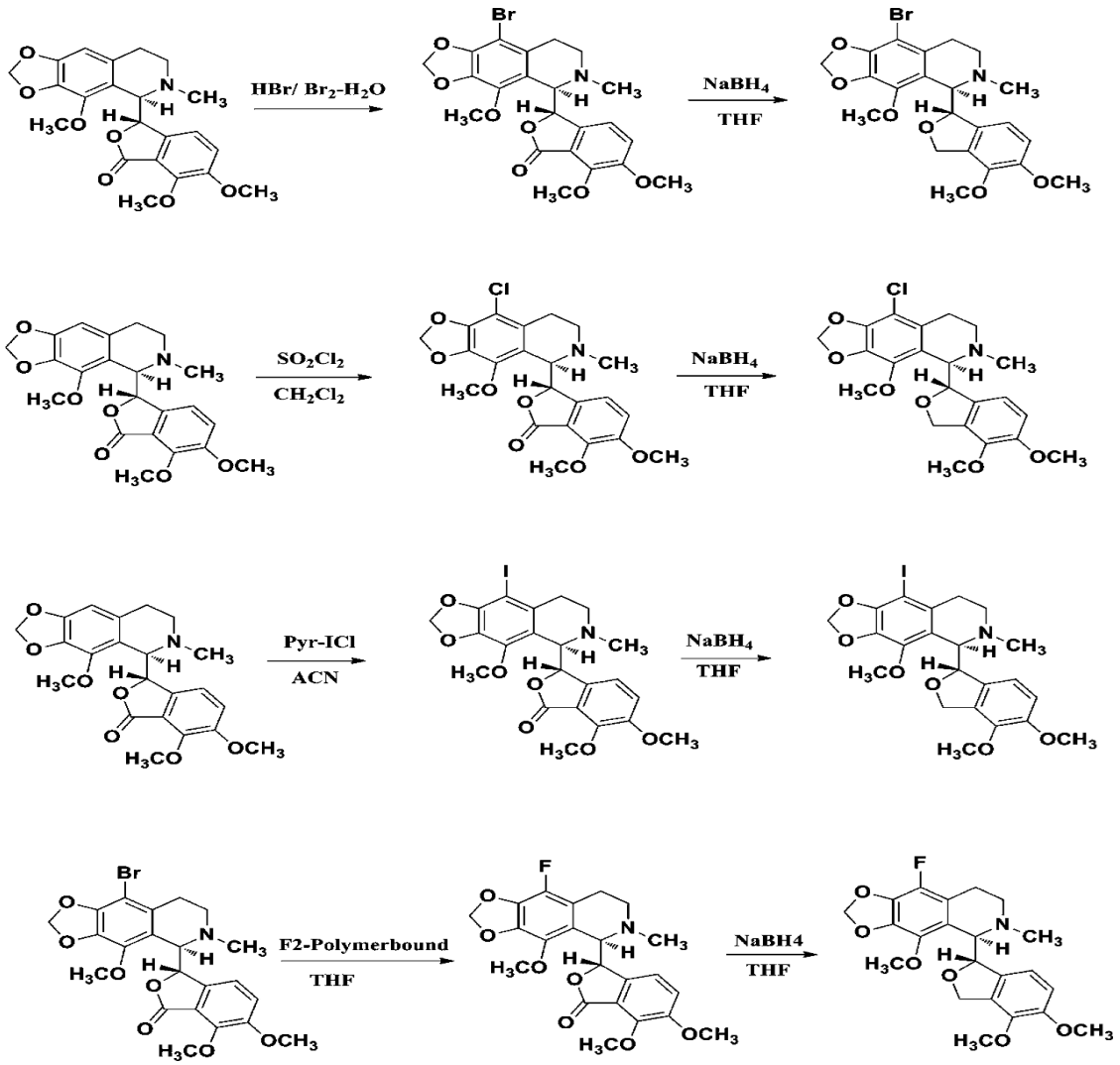

Figure 1.16. Cyclic ether halogenated derivatives (viz. reduced 9-fluoronoscapine (Rd-9-F-nos); reduced 9-chloronoscapine (Rd-9-Cl-nos); reduced 9-bromonoscapine (Rd-9-Br-nos) and reduced 9-iodonoscapine (Rd-9-I-nos)) of noscapine. These derivatives were synthesized from the halogenated derivatives (Aneja et al., 2006).

Naik et al (2011) designed 9-amino noscapine based on computational techniques to be a promising derivative of noscapine and chemically synthesised from natural noscapine (**Figure 1.17**). The 9-amino noscapine was found to be most promising amongst all the previously synthesised noscapinoids as tubulin binding anticancer agent.

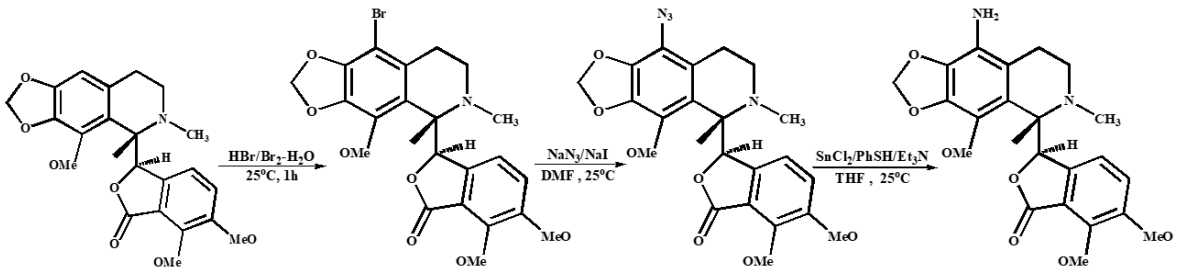

Figure 1.17. Reaction scheme to synthesise 9-amino noscapine.

The benzofuranone ring of noscapine was modified at diversity point C to produce the second generation of noscapinoids **(Fig.1.18)** (Mishra et al., 2011). These compounds have been reported to be effective at inhibiting the growth of lymphoma cells as well as lung, breast, prostate, and pancreatic cancer cell lines in a concentration-dependent way. By inducing structural alteration at the diversity point D of noscapine, a third generation of noscapinoids was developed computationally by Manchakunda et al (2013) (**Fig.1.19)**. The third-generation noscapinoids, like their predecessors, fit exceedingly well into the binding cavity on tubulin, with equivalent or enhanced binding affinities. Furthermore, the congeners of noscapine showed a high level of cytotoxicity against a range of cancer cell types. These derivatives promoted apoptotic cell death in cancer cells by delaying cell cycle progression during the G2/M phase. This class of noscapinoid have significantly greater apoptotic indices than its parent molecule, noscapine.

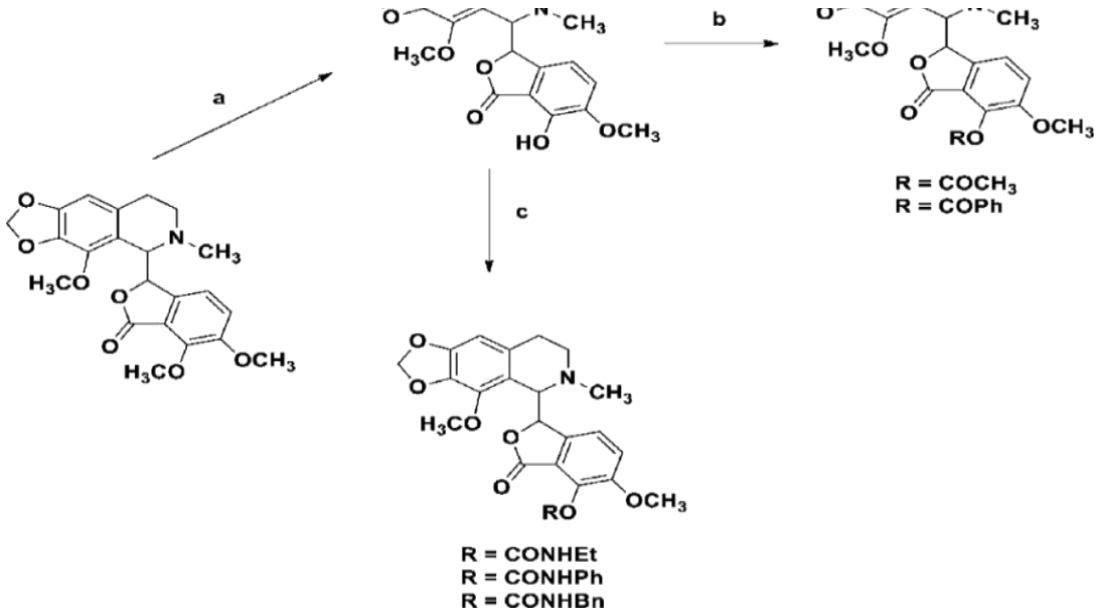

Fig.1.18. Benzofuranone derivatives of noscapine, the second generation of noscapinoids a represents sodium azide/sodium iodide, dimethylformamide (DMF) at 140 8C, 4 h b, dimethylamino pyridine, acetic anhydride, acetonitrile, 50 8C, 6 h for compound 3; potassium carbonate, dimethylformamide, and bezoyl chloride at 80 8C for 8 h for compound 4. c, Dimethylamino pyridine, dichloromethane, and isocyanate at room temperature for 6–8 h for compounds 5, 6, and 7 (Mishra et al., 2011).

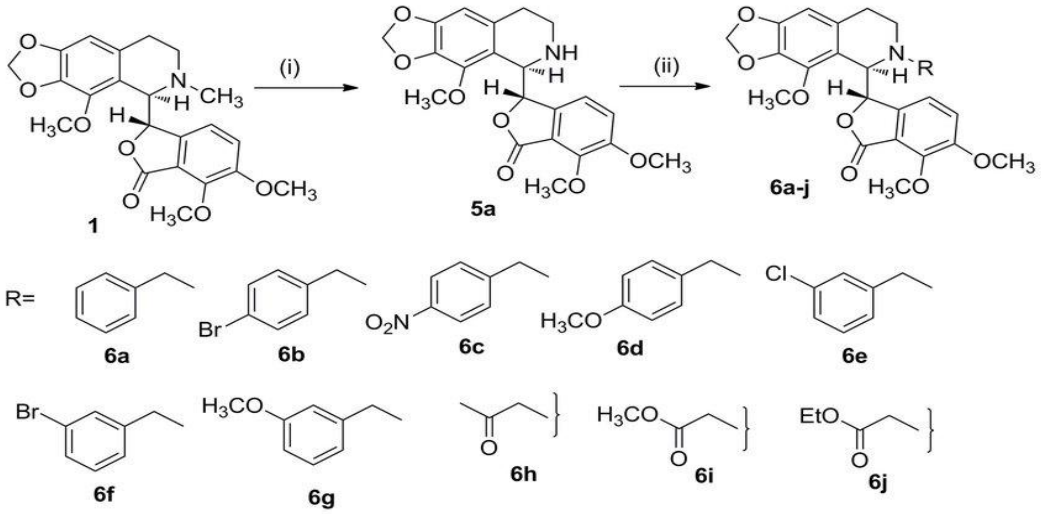

Fig.1.19. Chemical synthesis of third generation noscapinoids from noscapine as starting material. (i) a, meta-chloroperoxybenzoic acid and dichloromethane; b, 2N hydrochloric acid; c, Iron(II) SulfateHeptahydrate; (ii) Bromo methane, potassium iodide, K_2Cr_3, and Acetone (Manchakunda et al., 2013).

1.18 Current status, challenges and future prospects:

After the discovery of noscapine as tubulin binding anticancer agent in 1998, much progress has been made towards finding a new class of tubulin binding drugs that neither overpolymerize nor depolymerize tubulin but subtle interfere with the tubulin dynamics. Although it kills cancer cells of different tissue origin, its effective concentration was found to be very high. Therefore, several synthetic derivatives were developed to improve its anticancer activity. Another unique edge of noscapine over the currently-available antimitotics lies in its oral bioavailability and the ease of oral administration. Although noscapine can inhibit tumor growth and cause regression of localized breast tumor xenografts to a fair degree of extent in preclinical mice models, a complete obliteration of the disease has not been achieved even on increasing noscapine dosage as high as 600 mg/kg, possibly due to saturation of its uptake by cancer cells. From an ongoing quest to improve our therapeutic arsenal, we have developed several Noscapinoids and demonstrated that they are devoid of debilitating toxicities even at very high doses. In this study, we are approaching optimization of the natural lead compound for breast cancer therapy by developing extremely promising and novel Noscapinoids that are strong enough to kill human breast cancer cells, are non-toxic or tolerably toxic to normal tissues by derivatisation. The study will also focus on understanding the mechanism of action and anticancer potential (preclinical evaluation in breast cancer cell lines and mouse models), and assessment of side effects (in animal models), of the novel agents.

1.19 Objective of the study

1. To develop 3D pharmacophore and predictive QSAR model for anti-cancer activity of noscapinoids. This pharmacophore as well as the QSAR model will be helpful not only to design new derivatives of noscapine and to understand their mechanism of action but also to predict potential reactive sites that may lead to off-target effects.

2. To design novel and potent derivatives of noscapine *in silico* followed by theoretical evaluation of their binding affinity onto α- and β-tubulin complex utilizing molecular docking, MM-GBSA and linear interaction energy methodwith a surface generalized Born (LIE-SGB) continuum solvation model.

3. To systematically synthesize designed potent novel noscapinoids with high yield, to purify them (column chromatography and HPLC analysis) and to do their structural characterization (1D NMR, IR, MALDI, etc.).

4. To experimentally evaluate the anti-cancer activity of designed noscapinoidsusing tubulin binding assays, cell proliferation assay using cancer cells of different tissue origins, flow cytometry analysis to measure the perturbation in cell cycle progression, apoptosis assays, tumor regression using xenograft animal modeland toxicity analysis,etc.

1.20 Organization of the Thesis Works

We have developed various theoretical prediction models that were used in designing more potent noscapinoids followed by chemical synthesis and experimental evaluation of anti-cancer drugs. The anticancer activities of the compounds were tested using breast cancer cell line, MCF-7 and MDA-MB-231 as well as primary cells derived from patient. The thesis includes six different chapters, Chapter-1 describe a general introduction and review of literature, current scenario of cancer including breast cancer, microtubule targeted chemotherapeutic drugs for the treatment of cancer and their limitation. It also includes a brief discussion on noscapine as anticancer drug and its benefit over currently available microtubule targeted chemotherapeutic agents as well as different generations of noscapine derivatives. Chapter-2 includes in silico design of new tubulin binding 9-arylimino derivatives of noscapine, their chemical synthesis, and cellular evaluation as effective anticancer drugs against breast cancer. Rational design of new N-alkyl amine analogues of noscapine, chemical synthesis and experimental evaluation as powerful anticancer drugs is presented in Chapter-3. The development of 1,3-diynyl derivatives of noscapine as effective tubulin binding anticancer drugs for the treatment of breast cancer is covered in Chapter 4. Urea congeners of noscapine as effective anticancer agents: chemical production and biological assessment utilising in vitro breast cancer cells and an in vivo xenograft animal model are discussed in Chapter 5. Finally, Chapter 6 discusses the chemical synthesis and cellular assessment of N-imidazopyridine derivatives of noscapine as effective tubulin binding anticancer agents.

CHAPTER-2

In silico design of novel tubulin binding 9-arylimino derivatives of noscapine, their chemical synthesis and cellular activity as potent anticancer agents against breast cancer

Abstract:

A series of 9-arylimino derivatives of noscapine (an antitussive plant alkaloid) was developed that binds to tubulin and displaying anticancer activity against a panel of breast cancer cells. These compounds were rationally designed by coupling of Schiff base containing imine groups at position C-9 of the isoquinoline ring of noscapine. Based on a combination of Glide docking and free energy of binding (FEB) calculation a panel of three 9-compounds, **12-14** were screened out with improved binding affinity with tubulin compared to noscapine. The predicted free energy of binding is -6.166 kcal/mol for **12**, -6.411 kcal/mol for **13** and -7.512 kcal/mol for **14.** In contrast, the predicted FEB of noscapine is -5.135 kcal/mol. These novel derivatives were strategically synthesized and validated their anticancer activity based on cellular studies using two human breast adenocarcinoma, MCF-7 and MDAMB-231, as well as with a panel of primary breast tumor cells isolated from patients. Interestingly, all these derivatives inhibited cellular proliferation in all the cancer cells that ranged between 3.6 to 26.4 μM, which is 11.02 to 2.03 fold lower than that of noscapine. Unlike previously reported derivatives of noscapine that arrest cells in the S-phase, these novel derivatives effectively inhibit the proliferation of cancer cells, arrest the cell cycle in the G2/M-phase and induce apoptosis. Thus, we conclude that 9-arylimino derivatives of noscapine have great potential to be a novel therapeutic agent for breast cancer.

Key words: Noscapine, 9-arylimino noscapinoids, tubulin binding, anticancer agents, breast cancer.

2.1. Introduction

Chemotherapy remains the current method of therapy for metastatic cancer, in that, along with DNA binding drugs, microtubule-interacting drugs, for example, taxanes, vinca alkaloids, estramustine, halaven and ixempra are utilized for the treatment of localized and metastatic breast cancers. However, these medications possess severe toxicities such as leucocytopenias, diarrhea, alopecia, peripheral neuropathies, etc. resulting in poor quality of life (Kavanagh and Kudelka, 1993; Rowinsky and Donehower, 1991). The wonderful promise of taxol in managing breast cancers justifies the further effort to discover novel mitotic inhibitors that may have less side effects and that can be easily administered.

In a quest of finding such molecule, by the rational screening of natural compounds, noscapine (an opium alkaloid, non-narcotic, orally available, safe antitussive drug for over 40 years) was discovered. It binds to tubulin heterodimer with a 1:1 stoichiometry, alters the secondary structure of tubulin and arrests the dividing cells at mitosis (Ye et al., 1998). However, the cancer cells selectively undergo apoptosis because of the compromised cell cycle check points, without hampering the normal dividing cells. The careful real time observation of individual polymerizing microtubules (MTs) *in vitro* and tracking the plus end growth over time revealed that noscapine affected MT-dynamics primarily by enhancing the time period that MTs spend in an attenuated pause state rather than engaging in active depolymerization and repolymerization (Zhou et al., 2002). Because noscapine only affects MT dynamics, cellular functions that do not require exquisite control of MT dynamics may not be interrupted. Noscapine, therefore has no detectable neurotoxic effect on the histologies of peripheral nerves (Landen et al., 2004). It has favourable pharmacokinetics *in vivo* (clearance within ~10 h) (Jordan and Wilson, 1999) and has no significant side effects (Landen et al 2002; Ke et al 2000). *In vitro* as well as mouse xenograft models have shown that noscapine and its analogues are useful in the treatment of cancer of different tissues origin (Ye et al., 1998, Ke et al., 2000, Zhou et al., 2003). These properties enable its therapeutic use at high concentrations (~150–300 mg/kg body weight) in murine models of human cancer (Zhou et al., 2003; Landen et al., 2002). It is found to inhibit proliferation and induce apoptosis in human ovarian carcinoma cell lines that are sensitive or resistant to paclitaxel (Zhou et al., 2002). The oral bioavailability of noscapine offers further support for its clinical advancement as a novel chemotherapeutic agent (Dahlström et al., 1982). Therefore, noscapine is a promising anticancer drug with minimum toxicity and side effects.

From an ongoing quest to improve our therapeutic arsenal, we have developed a battery of derivatives by modification of its scaffolds and demonstrated to have high

tubulin binding and anti-tumor activity compared to noscpine without any debilitating toxicities (Manchukonda et al., 2012; Manchukonda et al., 2013; Santoshi et al., 2011; Santoshi et al., 2015; Naik et al., 2011; Naik et al., 2012). While several synthesized derivatives of noscapine showed promising *in vitro* activity against a panel of breast tumor cell lines, the antiproliferative activity comes to be in higher concentration (IC_{50} > 20 µM). Therefore, there is an urgent need to take up further optimization of noscapine towards the development of novel and more promising derivatives. In this study, we approach to develop 9-arylimino congeners of noscapine by strategically modifying its scaffold structure; followed by the screening of a panel of most potent derivatives based on our *in silico* efforts. The screened out derivatives were then chemically synthesized and validated for their anticancer activity based on a cellular study using two human breast cancer cell lines MCF-7 and MDAMB-231, as well as a panel of primary breast cancer cells directly obtained from breast cancer patients. The novel derivatives were found to bind tubulin heterodimer with increased binding affinity, effectively inhibiting cancer cell proliferation, selectively arresting cancer cells at G2/M phase and inducing apoptosis.

2.2. Materials and methods

2.2.1. Protein preparation

The crystal structure of amino noscapine-tubulin complex (PDB ID: 6Y6D, resolution 2.20 Å, Oliva et al., 2020) was downloaded from the PDB databank and used for structure based designing of novel derivatives of noscapine. It was then prepared using protein preparation wizard workflow (Schrödinger, LLC, New York). Further, an all atom molecular dynamics (MD) simulation of 100 ns in explicit water was performed to refine the structure using GROMACS (version 4.5.4, University of Groningen, Netherlands) software (Berendson et al, 1995) and the GROMOS96 force field with similar parameters as reported earlier (Santoshi and Naik, 2014). Finally, the last 2000 frames from the MD trajectory were used to generate an average structure of the tubulin.

2.2.2. Rational design of 9-arylimino congeners of noscapine

We envisaged developing 9-arylimino derivatives of noscapine by hybridizing with arylimino groups (Schiff bases). It is because; Schiff base analogs have been used in the pharma industry to develop potential analogs for anticancer activity. As an example, Schiff bases obtained from coumarin and pyrazole aldehyde have been tested against cancer cell lines that showed mild anticancer activities (Ali et al., 2013). Furthermore, mono and bis-Schiff bases have been reported efficacious against five cancer cell lines (Sondhi et al., 2012). Towards designing the 9-arylimino noscapinoids, we approached to

strategically appending the Schiff bases containing imino group at the C-9 position of the noscapine scaffold by *in silico* combinatorial chemistry to develop a library as depicted in Figure 2.1. The library was then used to screen out a panel of the most potent compounds using molecular docking and predictive binding free energy.

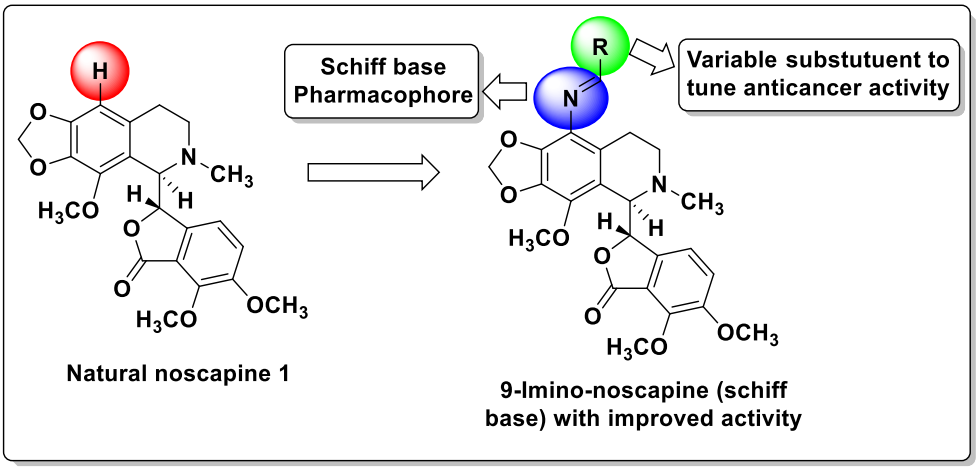

Figure 2.1. Strategic development of 9-arylimino noscapinoids by hybridizing Schiff base with natural noscapine.

2.2.3. Preparation of molecular structure

Molecular structures of noscapinoids (Figure 2.2) that have been previously reported (Aneja et al, 2006a; Naik et al, 2011; Santoshi et al, 2011; Manchukonda et al, 2013; Santoshi et al, 2015) and the newly designed 9-arylimino noscapinoids (Figure 2.1) were built using ChemDraw (version 8.00). These structures were imported into Maestro (Schrödinger, LLC, New York) and were energy minimized using Macromodel (Schrödinger, LLC, New York) and OPLS 2005 force field with PRCG algorithm (energy gradient of 0.001). The molecular structures were further refined through density functional theory (DFT) calculations using hybrid density functional theory with Becke's three-parameter exchange potential and the Lee-Yang-Parr correlation functional (B3LYP) with basis set 6-31G** using Jaguar (Schrödinger, LLC, New York). Further, the structural parameters (bond lengths and bond angles) obtained from the DFT calculations for the newly designed compounds were compared with the crystal structure of the noscapine to validate their structure. The structural parameters of the core structure of newly designed molecules and the crystal structure of noscapine were almost similar. The appropriate bond order for each structure was defined and their various conformations were generated using Ligprep (Schrödinger, LLC, New York).

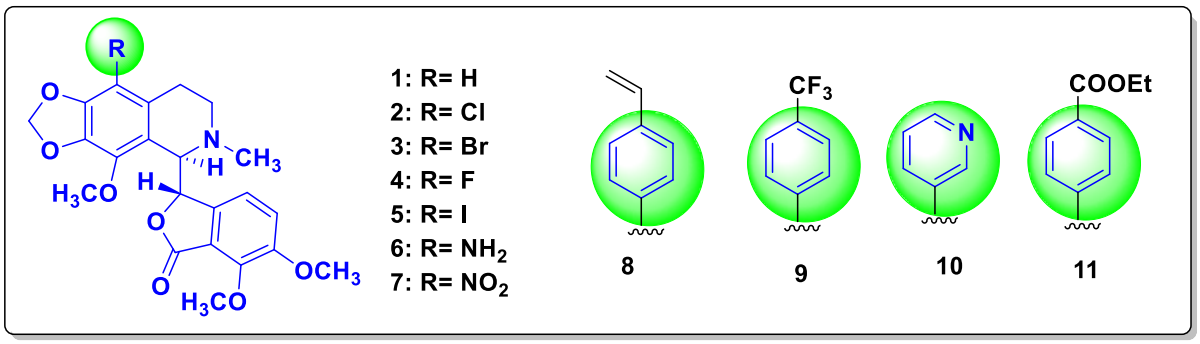

Figure 2.2. The molecular structure of noscapine and its previously reported derivatives **2-11** used as training set for the molecular modelling study.

2.2.4. Molecular docking

Molecular docking of noscapinoids with αβ-tubulin heterodimer was performed using Glide (Schrödinger, LLC, New York) as reported previously (Naik et al, 2011). Briefly, a grid box of size 12Å x 12Å x 12Å was defined at the centroid of the noscapine binding site (Naik et al, 2011) using Glide grid-receptor generation program. All the noscapinoids were docked using Glide XP (extra precision) and evaluated using a Glide XP_{Score} function. The single best conformation for each ligand was considered for further analysis.

2.2.5. LIE-SGB model building

A predictive model was developed based on a linear interaction energy model (LIE) with a surface generalized Born (SGB) continuum solvation model (Zhou et al., 2001) to calculate the free energy of binding ($\Delta G_{bind,pred}$) of the newly designed 9-arylimino noscapinoids with tubulin. The training data set of noscapinoids (Figure 2.2) with known experimental free energy of binding ($\Delta G_{bind,expt}$) was used and mapped with various predicted energy parameters such as van der Waals (U_{vdw}), coulumbic (U_{coul}), reaction field (U_{rxn}) and cavity energy (U_{cav}) based on LIE model to develop the empirical prediction model. The $\Delta G_{bind,expt}$ of noscapinoids with tubulin was calculated from their respective dissociation constant (K_d) values using the relation:

$$\Delta G_{bind,expt} = RT \ln K_d$$

where R is the gaseous constant (0.001986 kcal/mol) and T is the temperature (298 K). Liaison programme (Schrödinger, LLC, New York) was used to estimate the above energy parameters from the docked complexes of the noscapinoids based on Hybrid Monte Carlo simulation technique as reported previously (Naik et al., 2011).

$$\Delta G_{bind,pred} = \alpha\left(\langle U^b_{vdw}\rangle - \langle U^f_{vdw}\rangle\right) + \beta\left(\langle U^b_{coul}\rangle - \langle U^f_{coul}\rangle\right) + \gamma\left(\langle U^b_{rxn}\rangle - \langle U^f_{rxn}\rangle\right) + \delta\left(\langle U^b_{cav}\rangle - \langle U^f_{cav}\rangle\right)$$

Here $\langle\ \rangle$ represents the ensemble average, *b* represents the bound form of the ligand, *f* represents the free form of the ligand, and α, β, γ and δ are the coefficients of various energy terms, determined using Minitab statistical package (Minitab Inc.) Finally based on the docking score and the predictive free energy of binding, we have screened out three most potent 9-arylimino noscapinoids, **12-14** (Figure 2.3) having enhanced binding affinity with tubulin compared to noscapine for chemical synthesis and cellular evaluation to determine their anticancer potential.

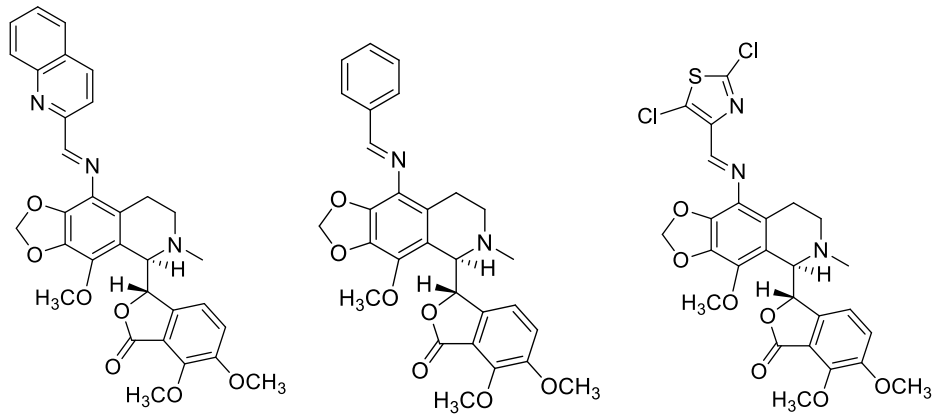

Figure 2.3. A panel of 9-arylimino noscapinoids, **12-14** that are rationally designed and screened out to have higher binding affinity with tubulin for chemical synthesis and experimental evaluation.

2.2.6. General procedure for chemical synthesis of 9-arylimino noscapinoids, 12-14

The natural α-noscapine was used as a starting material to produce 9-aminonoscapine **6** via a two reaction step involving bromination of noscapine using aqueous HBr/Br_2-H_2O followed by amination using CuI, NaN_3 and L-Proline in DMSO as reported earlier (Manchukonda et al., 2012). A solution of 9-aminonoscapine **6** (1.0 mmol), in ethanol (15 mL), was refluxed with substituted aryl/heteroaryl aldehydes (2,5-difluorobenzaldehyde or 5-bromothiophenecarboxaldehyde or p-bromo benzaldehyde, 1.0 mmol), for 12 h. After the starting material was completely consumed in the reaction (judged by TLC), the solvent was evaporated under a vacuum. The crude residue was extracted into dichloromethane (2 x 15 mL) and washed with brine solution. The organic layer was collected and passed through a Na_2SO_4 bed and later on removed under reduced pressure. The crude residue was chromatographed over a triethylamine silica bed, using pet.ether/ethyl acetate (7:3) as eluents, to produce 9-arylimino noscapinoids, **12-14** as solid products in very good yield (Figure 2.4). Structural characterization of all the intermediates and final products **12-14** were done using NMR (^1H and ^{13}C), IR spectroscopy and mass (HRMS) spectrometry techniques.

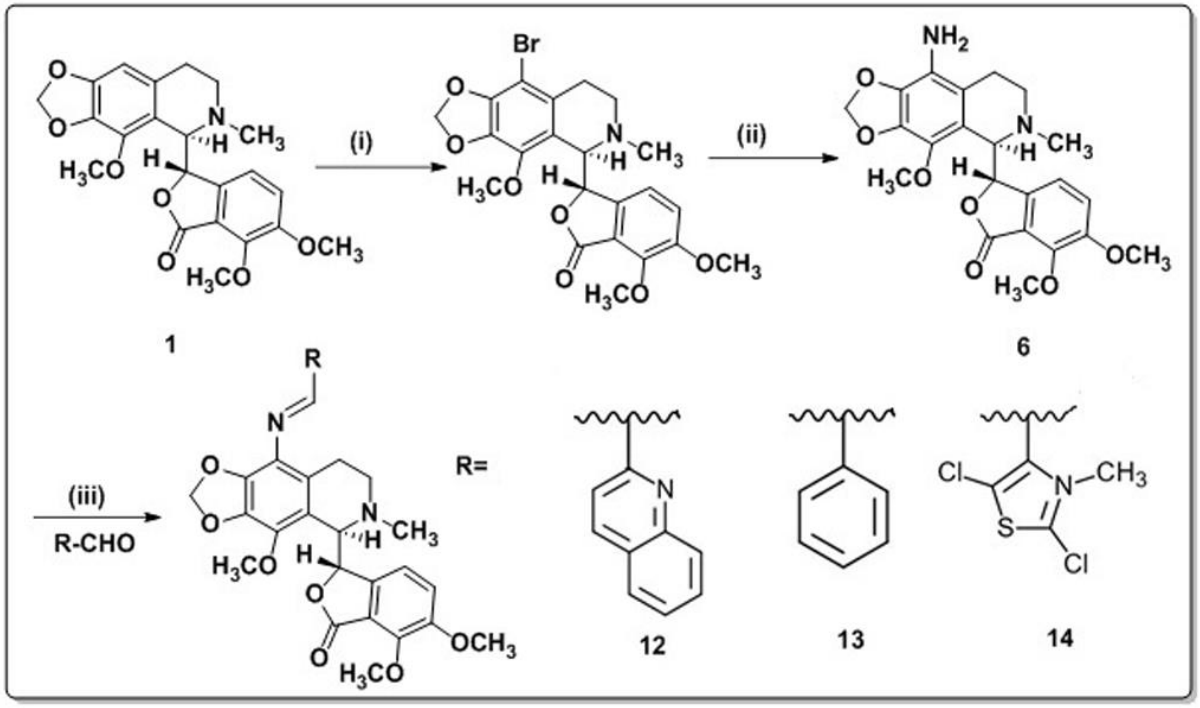

Figure 2.4. General chemical reaction for chemical synthesis of 9-imine-noscapinoids, **12-14** rationally design in the study.

2.2.7. Structural characterization of 9-arylimino noscapinoids, 12-14.

(*S*)-6,7-dimethoxy-3-((*R*)-4-methoxy-6-methyl-9-((*E*)-(quinolin-3-ylmethylene)amino)-5,6,7,8-tetrahydro-[1,3]dioxolo[4,5-*g*]isoquinolin-5-yl)isobenzofuran-1(3*H*)-one (12):

Nature: White solid. TLC (Hexane: Ethylacetate 3:1; Rf: 0.21) M.P: 120-122 ^{o}C. IR (KBr): 3446, 2929, 2794, 1757, 1626, 1498, 1443, 1382, 1268, 1036, 1007, 970, 763 cm^{-1}. ^{1}H NMR (400 MHz, $CDCl_3$): δ 9.22 (s, 1H, N=C*H*), 8.35 (d, *J* = 8.5 Hz, 1H, Ar-H), 8.23-8.15 (m, 2H, Ar-H), 7.86 (d, *J* = 7.9 Hz, 1H, Ar-H), 7.79-7.74 (m, 1H, Ar-H), 7.62-7.57 (m, 1H, Ar-H), 7.00 (d, *J* = 8.3 Hz, 1H, Ar-H), 6.31 (d, *J* = 8.3Hz, 1H, Ar-H), 6.04 (d, *J* = 0.9, 17.7 Hz, 2H, O-C*H*$_2$-O), 5.59 (d, *J* = 4.4 Hz, 1H, Ar-H, (C3-phthalide)), 4.42 (d, *J* = 4.4 Hz, 1H, Ar-H, (C5'-isoquinoline)), 4.10 (s, 3H), 4.07 (s, 3H), 3.85 (s, 3H), 3.16-3.06 (m, 1H, -C*H*H-N-CH_3 (C7'-isoquinoline)), 2.78-2.70 (m, 1H, -CH*H*-N-CH_3 (C7'-isoquinoline)), 2.57 (s, 3H, -N-C*H*$_3$), 2.49-2.40 (m, 1H, Ar-C*H*H (C8'-isoquinoline)), 2.14-2.03 (m, 1H, Ar-CH*H* (C8'-isoquinoline)). ^{13}C NMR (75 MHz, $CDCl_3$) : δ 168.0(C=O), 161.8(Ar-C), 155.8(Ar-CH=N-), 152.1(Ar-C), 147.9(Ar-C), 147.6(Ar-C), 141.2(Ar-C), 139.77(Ar-C), 139.72(Ar-C), 136.3(Ar-C), 134.4(Ar-C), 130.1(Ar-C), 129.7(Ar-C), 129.5(Ar-C), 128.7(Ar-C), 127.6(Ar-C), 127.4(Ar-C), 124.5(Ar-C), 119.8(Ar-C), 118.2(Ar-C), 118.0(Ar-C), 117.7(Ar-C), 117.6(Ar-C), 101.1(-O-CH_2-O-), 81.7(C-phthalide), 62.2(C- isoquinoline), 60.8(-O-CH_3), 59.4(-O-CH_3), 56.7(-O-CH_3), 49.4(-CH_2-), 45.9(N-CH_3), 22.9(-CH_2-). MS (ESI-MS) *m/z*: 568 [M+H]+ HRMS (ESI): Calculated for $C_{32}H_{30}N_3O_7$ [M+H]+: 568.20783, found: 568.20704.

(*S*)-3-((*R*)-9-((*E*)-benzylideneamino)-4-methoxy-6-methyl-5,6,7,8-tetrahydro [1,3]dioxolo [4,5-*g*]isoquinolin-5-yl)-6,7-dimethoxyisobenzofuran-1(3*H*)-one (13):

Nature: White solid. TLC (Hexane: Ethylacetate 3:1; Rf: 0.24) M.P: 88-90 ^{o}C. IR (KBr) : 3426, 2937, 1759, 1627, 1497, 1385, 1266, 1123, 1034, 756, 693 cm^{-1}. ^{1}H NMR (500 MHz, $CDCl_3$) : δ 8.85 (s, 1H, N=C*H*), 7.89 (d, *J* = 3.6 Hz, 2H, Ar-H), 7.50-7.42 (m, 3H, Ar-H), 6.99 (d, *J* = 8.2 Hz, 1H, Ar-H), 6.31 (d, *J* = 8.2 Hz, 1H, Ar-H), 5.99 (d, *J* = 20.44Hz, 2H, O-C*H*2-O), 5.58 (d, *J* = 4.2 Hz, 1H, Ar-CH, (C3-phthalide)), 4.40 (d, *J* = 4.2 Hz, 1H, Ar-CH, (C5'-isoquinoline)), 4.10 (s, 3H, -OCH3), 4.04 (s, 3H, -OCH3), 3.85 (s, 3H, -OCH_3), 3.02-2.94 (m, 1H, -C*H*H-*N*-CH_3 (C7'-isoquinoline)), 2.72-2.65 (m, 1H, -CH*H*-*N*-CH_3 (C7'-isoquinoline)), 2.55 (s, 3H, *N*-C*H*$_3$), 2.44-2.36 (m, 1H, Ar-C*H*H (C8'-isoquinoline)), 2.06- 1.97 (m, 1H, Ar-CH*H* (C8'-isoquinoline)). ^{13}C NMR (100 MHz, $CDCl_3$): δ 168.1(C=O), 161.8(Ar-C), 152.1(Ar-CH=N-), 147.6(Ar-C), 141.3(Ar-C), 141.1(Ar-C), 139.0(Ar-C), 138.7(Ar-C), 136.9(Ar-C), 134.5(Ar-C), 131.1(Ar-C), 129.0(Ar-C), 128.6(Ar-C), 128.3(Ar-C), 125.7(Ar-C), 119.8 (Ar-C), 118.3(Ar-C), 117.7(Ar-C), 117.6(Ar-C), 100.8(-O-CH_2-O-), 81.8(C-phthalide), 62.2(C-isoquinoline), 60.9(-O-CH_3), 59.5(-O-CH_3), 56.7(-O-CH_3), 49.4(-CH_2-), 45.9(N-CH_3), 22.7(-CH_2-). MS (ESI-MS) *m/z*: 517 [M+H]+ HRMS (ESI) : Calculated for $C_{29}H_{29}N_2O_7$ [M+H]+: 517.19693, found: 519.19596.

(*S*)-3-((*R*)-9-((*E*)-((2,4-dichlorothiazol-5-yl)methylene)amino)-4-methoxy-6-methyl-5,6,7,8-tetrahydro[1,3]dioxolo[4,5-*g*]isoquinolin-5-yl)-6,7-dimethoxyisobenzofuran-1(3*H*)-one(14):

Nature : White solid. TLC (Hexane: Ethylacetate 3:1; Rf: 0.26) M.P: 107-109 ^{o}C. IR (KBr): 3451, 2932, 1758, 1622, 1499, 1404, 1267, 1066, 1033, 897, 735 cm^{-1}. ^{1}H NMR (500 MHz, $CDCl_3$) : δ 8.97 (s, 1H, N=CH), 7.02 (d, *J* = 8.2 Hz, 1H, Ar-H), 6.39 (d, *J* = 8.2 Hz, 1H, Ar-H), 6.04 (dd, *J* = 1.0, 16.3 Hz, 2H, O-C*H*$_2$-O), 5.53 (d, *J* = 4.4 Hz, 1H, Ar-CH, (C3-phthalide)), 4.36 (d, *J* = 4.4 Hz, 1H, Ar-CH, (C5'- isoquinoline)), 4.10 (s, 3H, -OCH_3), 4.02 (s, 3H, -OCH_3), 3.87 (s, 3H, -OCH_3), 2.96-2.89 (m, 1H, - C*H*H-*N*-CH_3 (C7'-isoquinoline)), 2.80-2.73 (m, 1H, - CH*H*-*N*-CH3 (C7'-isoquinoline)), 2.53 (s, 3H, NC*H*3), 2.47-2.39 (m, 1H, Ar-C*H*H (C8'-isoquinoline)), 2.09-2.01 (m, 1H, Ar-CH*H* (C8'-isoquinoline)). ^{13}C NMR (100 MHz, $CDCl_3$) : δ 167.9(C=O), 154.2(Ar-C), 152.2(Ar-CH=N-), 149.2(Ar-C), 147.6(Ar-C), 141.3(Ar-C), 140.1(Ar-C), 139.8(Ar-C), 138.0(Ar-C), 134.8(Ar-C), 134.2(Ar-C), 130.2(Ar-C), 123.6C(Ar-C), 119.6(Ar-C), 118.4(Ar-C), 117.8(Ar-C), 117.5(Ar-C), 101.2(-O-CH_2-O-), 81.5(C-phthalide), 62.2(C-isoquinoline), 60.8(-OCH_3), 59.4(-OCH_3), 56.7(-OCH_3), 48.9(-CH_2-), 45.5(N-CH_3), 22.3(-CH_2-). MS (ESI-MS) *m/z*: 592 [M+H]+ HRMS (ESI): Calculated for $C_{26}H_{24}Cl_2N_3O_7$ [M+H]+: 592.07065, found: 592.07031.

2.2.8. Cell culture and reagents

Noscapine was obtained from Sigma. All the chemical reagents and media for cell culture were obtained from Sigma. Human breast cancer cell lines, MCF-7 and MDAMB-231 were obtained from the cell repository of the National Centre for Cell Science Pune, Maharashtra, India. Primary breast cancer cells were isolated from the patient's samples. Stock solution (100 mM) of the newly synthesized 9-arylimino noscapinoids, **12-14** was prepared with dimethyl sulfoxide (DMSO) and stored at 4 ^{o}C until use. The cells were allowed to grow at a temperature of 37 °C in a 5% CO_2 and 95% humidity in Dulbecco's modified Eagle medium (DMEM), supplemented with 10% fetal bovine serum (FBS) and antibiotics. Cells with a 70-80% confluence were sub-cultured for bioassays using trypsin-EDTA (0.25 %).

2.2.9. *In vitro* cell proliferation assay using MCF-7 and MDAMB-231 cell lines

Antiproliferation activity of 9-arylimino noscapinoids, **12-14** was performed in 96-well plates as described previously (Naik et al, 2011) using two human breast cancer cell lines, MCF-7 and MDAMB-231. In brief, cells were grown in DMEM culture medium supplemented with 10% FBS, 1% penicillin/streptomycin and 2 mM l-glutamine at 37 °C in a humidified atmosphere with 5% CO_2. Cells were plated at a density of $5x10^3$ cells per well and were treated with gradient concentrations (5 to 100 µM) of noscapine and its derivatives, 9-arylimino noscapinoids, **12-14** for 72h. The cells were then fixed with 50% trichloroacetic acid and stained with 0.4% sulforhodamine B. The unbound dye was removed by washing. The protein bound dye was then extracted with 10 mM Tris base and measured the optical density at 564 nm using a SPECTRAmax PLUS 384 microplate spectrophotometer. The IC_{50} value that stands for the drug concentration required to achieve a cell kill of 50% was determined using the online tool Quest GraphTM IC_{50} Calculator (AAT Bioquest, Inc., Sunnyvale, CA, USA, https://www.aatbio.com/tools/ic50-calculator). The experiment was repeated for three times.

2.2.10. Primary breast cancer cells (PBCs) culture and *in vitro* cell proliferation assay

Primary breast cancer cells were isolated from the patient's samples (8 nos.) with different stages of breast cancer before drug treatment in aseptic condition. The tumour tissues were treated with 0.25% trypsin and filtered with 70 micron filter followed by centrifugation at 2000 rpm for 3 minutes with serum free medium. The filtered cells were collected and plated in T25 flask and incubated with a complete DMEM culture medium, supplemented with 10% FBS and 1% pentrip (mixture of penicillin and streptomycin) at

37 °C under 5% CO_2. Fresh media was replaced every 3-4 days, and subsequent passages were performed under the same conditions as mentioned above. The cultured were maintained for homogeneous cell type at sub-confluence between 3-8 passages. Cells were allowed to reach 80-90% confluence before experimental treatments. After the confluence reached, the primary cells were plated at 2000 cells/well in 96 wells plate with culture media. The cells were maintained at 37 °C in a humidified atmosphere with 5% CO_2 and were treated with gradient concentrations (5 to 100 µM) of noscapine and 9-arylimino noscapinoids, **12-14** for 72 h. Measurement of cell proliferation was performed by sulforhodamine B (SRB) assay, using the CellTiter96 AQueous One Solution Reagent (Sigma). Cells were stained with SRB for 30 minutes. The unbound dye was removed by washing. The bound dye was extracted with 1mM tris and absorbance was measured using a SPECTRAmax PLUS 384 microplate spectrophotometer at 564 nm. The percentage of cell survival as a function of drug concentration was plotted and the IC_{50} value was determined using the online tool, AAT Bioquest. The experiment was repeated for three times.

2.2.11. Flow cytometry analysis of cell cycle progression

Inhibition of cell cycle progression with the treatment of 9-arylimino noscapinoids was investigated using MDAMB-231 cells. The cells were maintained in DMEM culture media with 4.5 g/L glucose and L-glutamine supplemented with 10% FBS and 1% penicillin/streptomycin, at 37 ^{0}C in a 5% CO_2 atmosphere. After reaching the 80-90% confluence, cells were treated with noscapine and 9-arylimino noscapinoids, **12-14** dissolved in 1% phosphate buffer saline (PBS). After 72 h of treatment, cells were harvested and analysed using flow cytometry. Briefly, 2 x 10^6 cells were centrifuged, washed twice with ice-cold PBS and fixed in 70% ethanol at -20 ^{o}C for 24 h. The cells were centrifuged at 1000 x g for 10 minutes and the supernatant was discarded. The pellet was resuspended in 30 µl of phosphate/citrate buffer (0.2 M Na_2HPO_4/0.1 M citric acid, pH 7.5) at room temperature for 30 minutes. The cells were washed with 5 ml of PBS, incubated with 0.5 ml of propidium iodide (20 µg/ml in 0.6% Triton-X in PBS) and 0.5 ml of RNase A (20 µg/ml in PBS) for 45 minutes. in dark. Samples were analysed on a flow cytometer (BD FACS Aria-III) and the progress in the cell cycle was determined.

2.2.12. Flow cytometry analysis for apoptosis assay

Apoptosis in cancer cells was detected by Annexin-V-FITC apoptosis detection method by using the Apoptosis detection kit (Sigma–Aldrich, USA) based on the instruction provided by the manufacture. For experimental purposes, 3x10^4 cells per well

were seeded on 12 well culture plate and incubated for 24 h with a complete medium. The cells were treated with IC_{50} concentration of noscapine and 9-arylimino noscapinoids, **12-14** and were harvested at 72 h. Cells were typsinized and stained with surface marker antibodies (biotin-conjugated Annexin V, FITC-conjugated streptavidin) and propidium iodide (PI). Cells were allowed to suspend in 1X binding buffer and incubated with Annexin V FITC conjugate for 20 minutes in dark conditions at room temperature. Flow cytometer data with 488 nm excitation for PI and emission at 530 nm were collected. Viable cells (Annexin V^- / PI^-), early apoptotic cells (Annexin V^+ / PI^-), late apoptotic/necrotic cells (Annexin V^+ / PI^+) and late necrotic cells (Annexin V^- / PI^+) were identified and determined their percentage.

2.3. Results and Discussion

After the establishment of anticancer activity of the lead molecule, noscapine, several derivatives have been developed by various groups in order to increase its therapeutic outcome. Many of these derivatives were demonstrated to have higher binding affinity with tubulin, antiproliferative activity and induction of apoptosis. As an example the tubulin binding affinity and antiproliferative activity have been increased to 20 to 80 folds by developing halogenated, nitro, amino and biaryl noscapinoids by modification at C-9 position of the scaffold (Naik et al., 2012; Aneja et al., 2006a; Aneja et al., 2006b; Santoshi et al., 2015) as well as by functionalization of 'N' in isoquinoline unit of natural α-noscapine (Jain et al., 2011). Structure activity data of these derivatives of noscapine led us to develop a reasonable predictive model for predicting the free energy of binding of newly designed derivatives and screening of promising derivatives. We are reporting in this study a panel of 9-arylimino noscapinoids, **12-14** as potent anticancer agents.

2.3.1. Docking score of designed noscapinoids with tubulin

The molecular interaction and binding affinities of designed noscapinods, **12-14** onto tubulin were calculated applying molecular docking in combination with LIE-SGB empirical modeling. Noscapinoids, previously reported (Figure 2.2) and newly designed in this study (Figure 2.3) were docked into the noscapinoids binding site (Oliva et al., 2020; Naik et al., 2011) using Glide XP (extra precision) and evaluated using a Glide XP_{score} function (Friesner et al., 2004; Halgren et al., 2004). The three 9-arylimino noscapinoids, **12-14,** which revealed better docking scores ranging from -8.466 kcal/mol to -6.085 kcal/mol than the parent compound, noscapine (-5.505 kcal/mol) were finally screened out. All the three noscapinoids docked well at the interface of α- and β- tubulin (Figure 2.5). Their mode of interaction with the binding site amino acids is depicted as ligplot

(Figure 2.5). The ligplot explains the formation of different hydrogen bonds and hydrophobic interactions between the ligands and the binding site amino acids.

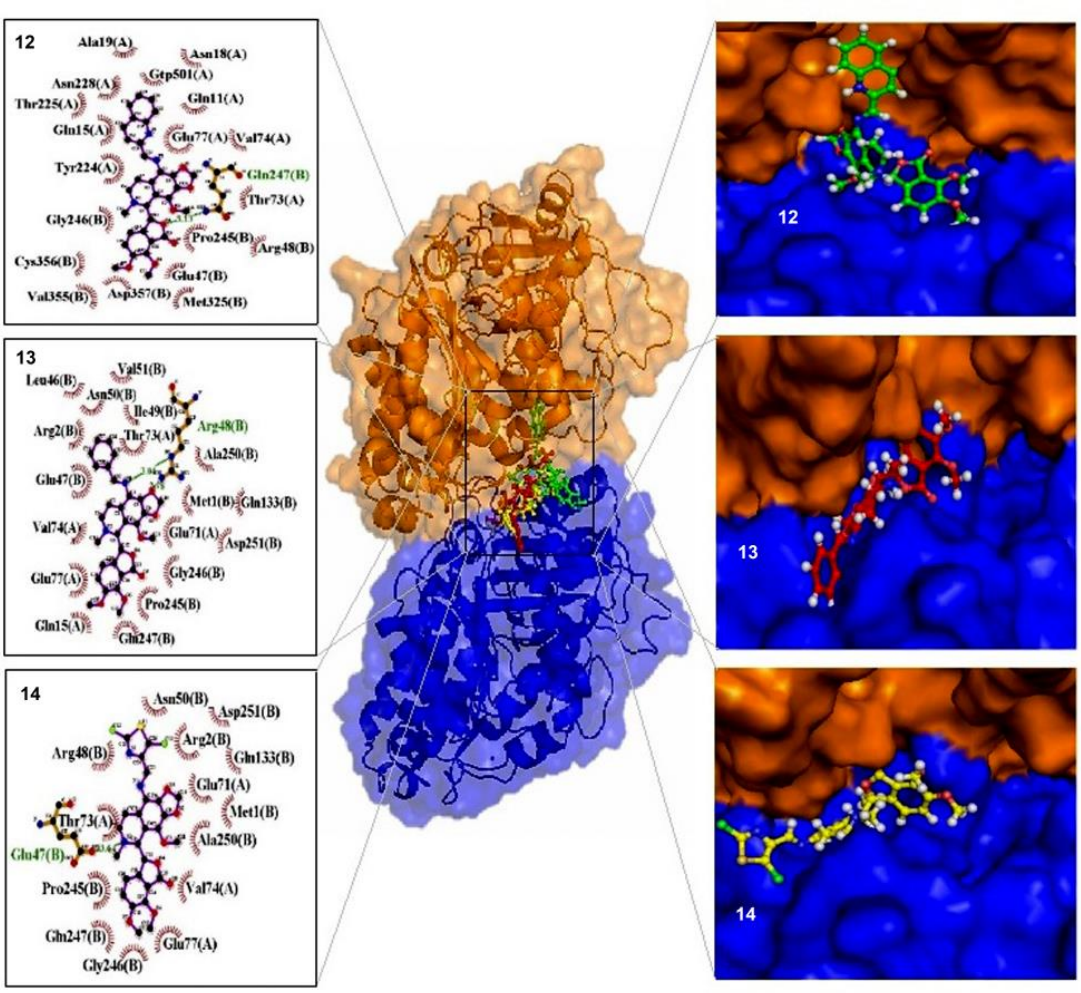

Figure 2.5. The newly designed 9-arylimino noscapinoids **12-14** are well accomodated inside the noscapine binding site at the interface of α- and β- tubulin. The binding site is represented as macromodel surface according to α- and β- tubulin (α-tubulin is represented in blue colour and β-tubulin is represented in brown colour). The ligplot analysis showed the interaction of binding site amino acids with the 9-arylimino noscapinoids **12-14**. The binding site residues involved in the interactions are slightly different mainly because of the variation in functional groups. The hydrogen bonds formed (if any) are represented as dotted lines.

2.3.2. Predictive binding affinity of 9-arylimino noscapinoids, 12-14 with tubulin (LIE-SGB calculation)

The binding affinity ($\Delta G_{bind,pred}$) of 9-arylimino noscapinoids, **12-14** with tubulin was predicted based on computationally developed linear interaction energy model (LIE), utilizing the experimental activity of training set molecules (Table 2.1). Since the molecular docking predicts accurate binding pose for the ligands onto the receptor, we have used the docking complexes of noscapinoids with tubulin and performed hybrid Monte Carlo simulation with generalized Born (SGB) continum solvation model to calculate the various interaction energy terms (van der Waals energy (U_{vdw}), Columbic

energy (U_{coul}), reaction energy (U_{rxn}) and cavity energy (U_{cav})) using liaison (Schrodinger). These energy parameters of the training set molecules (Table 2.1) were mapped with their $\Delta G_{bind,expt}$ based on LIE model to develop the robust prediction model for predicting the $\Delta G_{bind,pred}$ of the noscapinoids with tubulin. The values obtained for the four fitting parameters, α, β, γ and δ are 0.08446, -0.00223, -0.000872 and -0.45601, respectively. The $\Delta G_{bind,pred}$ of the training set molecules based on LIE-SGB model is very close to the $\Delta G_{bind,expt}$ (root mean square error was 0.243 kcal/mol) (Table 2.1). The quality of the fit can also be judged by the value of the squared correlation coefficient (R^2) and analysis of variance (F-value).

$$\Delta G_{bind,pred} = 0.08446\langle U_{vdw}\rangle - 0.00223\langle U_{coul}\rangle - 0.00872\langle U_{rxn}\rangle - 0.45601\langle U_{cav}\rangle$$

$$(n = 11, R^2 = 0.998, s = 0.243, F = 3742.6, P \leq 0.001)$$

Because of high predictability, the LIE-SGB model was used to predict the $\Delta G_{bind,pred}$ of the newly designed 9-arylimino noscapinoids, **12-14,** which revealed improved predicted binding energy of -6.166 kcal/mol for **12**, -6.411 kcal/mol for **13** and -7.512 kcal/mol for **14**, respectively in comparison to the lead molecule (-5.135 kcal/mol) were chemically synthesised for experimental evaluation.

Table 2.1. Results of molecular docking and calculated energies of noscapine and its derivatives: van der Waals energy (U_{vdw}), Columbic energy (U_{coul}), reaction energy (U_{rxn}) and cavity energy (U_{cav}) and predicted binding free energy ($\Delta G_{bind,pred}$) based on LIE-SGB prediction model and experimental binding free energy ($\Delta G_{bind,expt}$). The newly designed 9-arylimino noscapinoids, **12-14** revealed improved $\Delta G_{bind,pred}$ compared to the lead molecule, noscapine.

Ligand	Glide XP_{score} (kcal/mol)	$\langle U_{vdw}\rangle$ (kcal/mol)	$\langle U_{coul}\rangle$ (kcal/mol)	$\langle U_{rxn}\rangle$ (kcal/mol)	$\langle U_{cav}\rangle$ (kcal/mol)	Experimental ΔG_{bind} (kcal/mol)	Predicted ΔG_{bind} (kcal/mol)
1	-1.927	-45.14	-330.8	135.5	2.097	-5.246	-5.212
2	-2.038	-49.00	-210.2	116.0	3.283	-6.006	-6.178
3	-2.766	-42.50	-362.1	155.9	4.208	-5.827	-6.060
4	-2.940	-48.06	-355.8	168.7	2.548	-5.587	-5.899
5	-3.263	-47.69	-285.7	135.5	3.103	-6.360	-5.987
6	-4.492	-47.44	-77.3	118.2	3.954	-6.628	-6.668
7	-2.605	-33.39	-331.9	176.7	4.465	-5.551	-5.657
8	-2.287	-45.57	-277.9	112.3	3.285	-5.665	-5.706
9	-2.350	-33.47	-324.5	152.5	3.766	-5.783	-5.151
10	-3.679	-45.41	-471.2	152.8	3.669	-5.673	-5.790
11	-4.687	-42.69	-267.6	129.9	3.465	-5.518	-5.722
12	-6.031	-42.73	-373.1	180.6	3.976	-	-6.166
13	-2.862	-45.81	-317.4	150.1	4.602	-	-6.411
14	-3.001	-47.26	-277.2	169.3	6.092	-	-7.512

$\langle U_{vdw}\rangle$, $\langle U_{coul}\rangle$, $\langle U_{rxn}\rangle$ and $\langle U_{cav}\rangle$ energy terms represents the ensemble average energy terms calculated as the difference between bound and free state of the ligands and its environment.

2.3.3. 9-Arylimino noscapinoids, 12-14 inhibits proliferation of cancer cell lines

Based on our *in silico* results, we focused at the cellular level to determine if the 9-arylimino noscapinoids, **12-14,** affected cancer cell proliferation. All the 3 compounds including the parent compound, noscapine were analyzed for their anti-proliferative activity in two human breast cancer cell lines, MCF-7 (estrogen- and progesterone-receptor positive) and MDAMB-231 (estrogen- and progesterone- receptor negative). The IC_{50} values for the compounds for both the cell lines are collated in Table 2.2. The 9-arylimino noscapinoids, **12-14** exhibited potent cytotoxic activity in comparison to noscapine using both the cell lines (Figure 2.6). The IC_{50} value amounted to 44.5 µM, 16.0 µM, 7.1 µM and 3.6 µM for noscapine, 1**2, 13** and **14**, respectively for MCF-7 cells, which reflects a modest antiproliferative activity. Parenthetically, a similar modest IC_{50} value of 53.1 µM, 20.5 µM, 11.2 µM and 6.0 µM was measured for noscapine, **12, 13** and **14**, respectively for MDAMB-231 cells. The differences in IC_{50} values obtained using MCF-7 and MDAMB-231 for these 9-arylimino noscapinoids were cell-type dependent. Although a significant correlation on the sensitivity of cancer cells to these analogues cannot yet be established at this stage, it is evident, that tubulin represents a potential target for these compounds.

Table 2.2. IC_{50} values of novel 9-arylimino noscapinoids, **12-14** using two human breast adenocarcinoma cell lines, MCF-7 and MDAMB-231. All the novel derivatives were found to have improved antiproliferative activity compared to noscapine.

	IC_{50} (µM)			
	Noscapine	**12**	**13**	**14**
MCF-7	44.5±4.8	16.0±2.7	7.1±1.3	3.6±0.8
MDA-MB-231	53.1±4.5	20.5±2.9	11.2±1.6	6.0±1.2

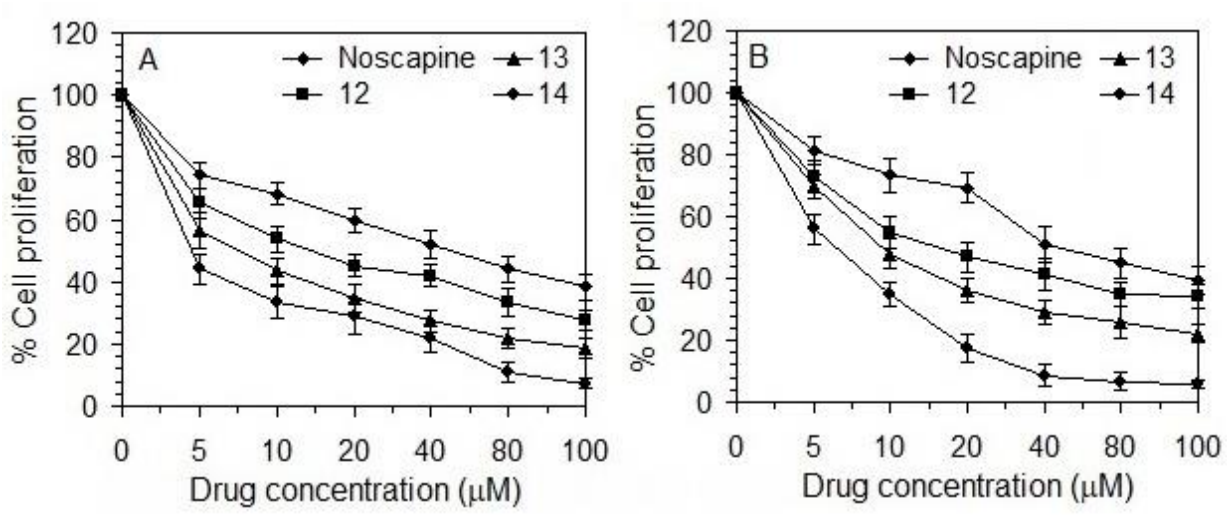

Fig 2.6. The 9-arylimino noscapinoids **12-14** are more active compared to noscapine in inhibiting the proliferation of human breast cancer cells. Both (A) MCF-7 and (B) MDAMB-231cells were treated with noscapine and 9-arylimino noscapinoids, **12-14** for 72h. Each value represents the average of 3 independent experiments.

2.3.4. 9-Arylimino noscapinoids, 12-14 inhibits proliferation of primary breast tumor cells

Further, we tested the antiproliferation activity of 9-arylimino noscapinoids, **12-14** using a panel of primary breast tumor cells. We have obtained the surgically removed breast tumor samples from 08 different patients with different stages of breast cancer and processed the samples to isolate the primary tumor cells. All these primary breast tumor cells were treated with increasing concentrations of the noscapinoids to determine their IC_{50} value. The IC_{50} values for the test compounds are collated in Table 2.3. The IC_{50} value ranges from 39.7 to 53.8 µM for noscapine, 17.2 to 26.4 µM for **12**, 9.7 to 16.4 µM for **13** and 4.4 to 9.5 µM for **14** using a panel of primary breast cancer cells (Table 2.3). All the 9-arylimino noscapinoids developed exhibited potent cytotoxic activity in comparison to noscapine using all the primary breast cancer cells (Figure 2.7).

Table 2.3. IC_{50} values of novel 9-arylimino noscapinoids, **12-14** using primary breast cancer cells isolated from breast tumor tissue of different patients. All the novel derivatives were found to have improved antiproliferative activity compared to noscapine.

	IC_{50} (µM)			
Patients No.	**Noscapine**	**12**	**13**	**14**
1	53.8±5.3	24.4±2.9	14.9±2.4	9.5±0.7
2	47.1±5.7	26.4±2.6	15.6±1.8	7.5±0.5
3	43.8±4.8	24.3±2.7	16.4±2.3	7.3±0.8
4	39.7±4.3	18.6±2.3	10.2±1.3	4.4±0.4
5	44.6±4.9	17.2±2.2	9.9±1.5	5.9±0.6
6	47.0±4.5	21.9±3.1	11.0±1.7	5.3±0.3
7	46.9±4.8	25.9±3.5	9.7±0.8	6.4±0.5
8	46.3±5.2	21.7±2.6	11.1±0.6	6.4±0.4

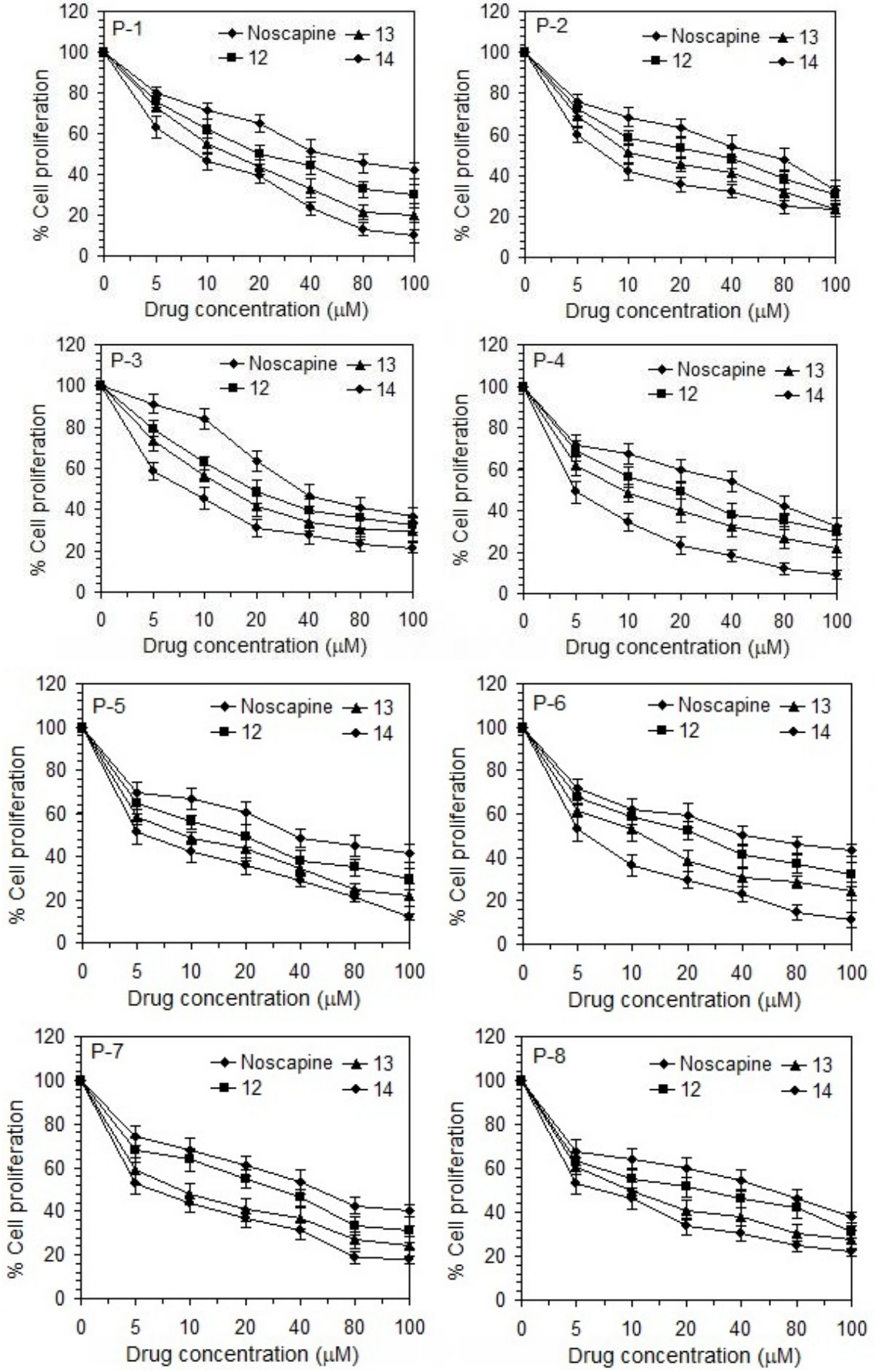

Fiure 2.7. The 9-arylimino noscapinoids, **12-14** are more active compared to noscapine in inhibiting the proliferation of a panel of human primary breast cancer cells. All the cells treated with 9-arylimino noscapinoids, **12-14** for 72 h. Each value represents the average of 3 independent experiments.

2.3.5. 9-Arylimino noscapinoids, 12-14 induced apoptosis to cancer cells

We approached to determine the induction of apoptotic cell death to breast cancer cell by the newly developed 9-arylimino noscapinoids, **12-14**. Biochemically the apoptotic process is characterized by alterations of the lipid composition of cell membrane—phosphatidylserine which is normally on the inner leaflet of the cell membrane, translocates to the outer leaflet, which can be measured fluorescently by annexin V binding. In contrast, a cell-impermeant DNA-binding fluorescent dye, propodium iodide can only enter the cells when it is at the stage of late apoptosis when membrane permeability is compromised. The apoptotic cells can be quantified to a large extent by FACS analysis. The percentage of early apoptotic and late apoptotic cells using MDAMB-231 cell lines for the treatment of noscapine and its 9-arylimino noscapinoids, **12-14** with a concentration of 25 µM for 72 h is collated in Table 2.4. Representative figures of flow cytometry analysis with the treatment of noscapine and its 9-arylimino noscapinoids, **12-14** are included in Figure 2.8. After 72 h of culture, the control untreated cell culture contained only very few early apoptotic (2.5%) and late apoptotic cells (1.0%), which were considered as the background cell death due to regular trauma during cell culture (Table 2.4). In contrast, the percentage of early apoptotic cells of 15%, 45%, 56%, and 5% as well as late apoptotic cells of 30%, 3%, 4% and 35% with treatments of noscapine and its 9-arylimino noscapinoids, **12-14**, respectively was found to be significantly high compared to controlled untreated cells (Table 2.4).

Table 2.4. Percentage of viable (Q3), early apoptotic (Q1), late apoptotic (Q2) and necrotic (Q4) cell measured by flow cytometry

Viability/Apoptotic	Control	Noscapine	12	13	14
Q1	2.5%	15%	45%	56%	5%
Q2	1%	30%	3%	4%	35%
Q3	94%	50%	50%	35%	15
Q4	0.5%	1%	2%	3%	45%

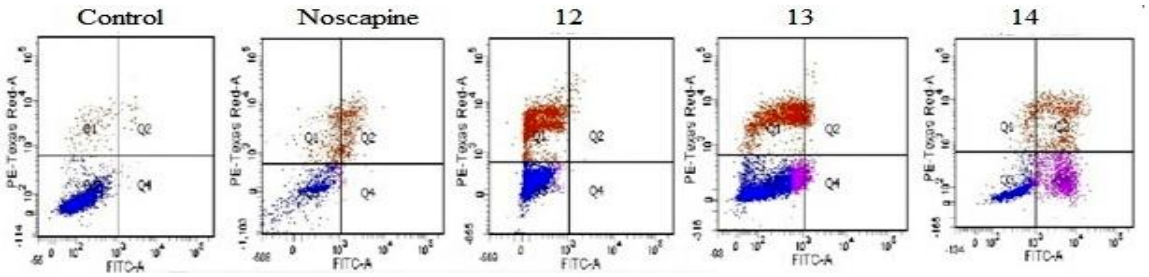

Fig 2.8. Flow cytometry analysis of phosphatidylserine (PS) exposure in MDAMB-231 cells treated with noscapine and its 9-arylimino noscapinoids, **12-14** with 25 µM for 72 hours and compared with non treated control cells. Annexin-V and propidium iodide (PI) were used to distinguish among three sub-populations of cells: PI- and AnnexinV- cells represent viable cells with intact membrane and preserved amino-phospholipid

asymmetry, PI- and Annexin V+ cells represent early apoptotic cells with intact cellular membrane exposing phosphatidylserine, whereas PI+ and Annexin V+ cells represent late apoptotic cells with compromised asymmetry and membrane permeability. Representative results of three independent experiments.

2.3.6. Cell cycle profile and mitotic arrest of cancer cells at G_2/M phase with treatment of noscapinoids

To ensure the induction of cell death, we examined the effect of noscapine and 9-arylimino noscapinoids, **12-14** (25 µM concentration) on the cell cycle profile of MDAMB-231 based on FACS analysis and represented in Figure 2.9. Fluorescently labelled DNA accumulation is a good pointer of cell cycle profile and cell death. Cells with 2N DNA represents the G1 phase, while cells with duplicated 4N DNA represents G2 and M phases. Cells in the process of DNA duplication with 2N and 4N peaks represents S phase when DNA is being synthesized. Less than 2N DNA appears in populations of dying cells that degrade their DNA to different extents. Treatment of MDAMB-231 cells for 72 h with the test compounds led to significant perturbations of the cell cycle profile at 25 µM. FACS analysis revealed high accumulation of cells in the G2M phase at 72 h of treatment of noscapine and its 9-arylimino derivatives compared to untreated cells (Table 2.5). In contrast to G2M block, a characteristic hypodiploid DNA content peak (sub-G1) was seen to rise at 72 h of treatment. The progressive generation of cells having hypodiploid DNA content reflects fragmented DNA, indicating dying cells.

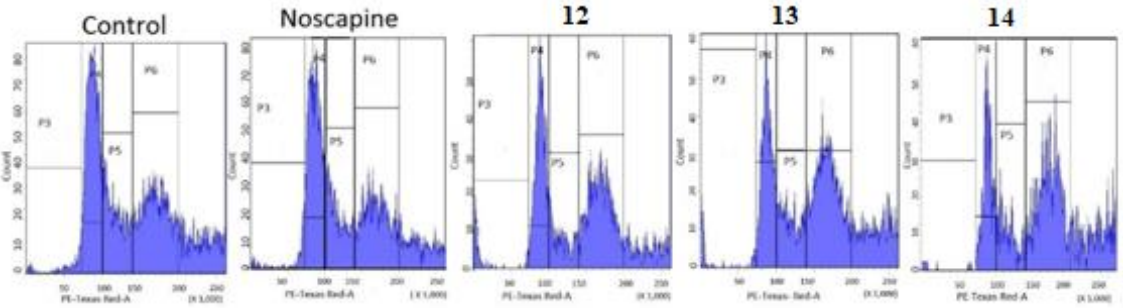

Fig 2.9. Noscapine and its 9-arylimino derivatives inhibit cell cycle progression at mitosis followed by the appearance of a characteristic hypodiploid (sub-G1) DNA peak, indicative of apoptosis. Panels A-E depict analyses of cell cycle profile, determined by flow cytometry using MDAMB-231 cells treated with 25 µM concentration of noscapine and its derivatives at 72 hours of treatment.

Table 2.5. Effect of noscapine and its 9-arylimino noscapinoids, **12-14** on cell cycle profile of MDAMB-231 cells treated with 25 µM solution for 72 hour.

	72 hours			
	Sub-G_1	**G_0/G_1**	**S**	**G_2/M**
Control	0.9	9	14	7.2
Noscapine	3.2	11.8	9.7	13.8
12	5.3	13.2	8.2	19.7
13	7.5	12.7	11.2	32.6

14	8.9	14.2	10.1	37.3

2.4. Conclusion

In conclusion, we have strategically designed a panel of 9-imine-noscapinoids of the natural lead molecule, noscapine in quest of accelerating its anticancer activity. We have also provided the simplest methods for the direct and regioselective modification of noscapine scaffold to produce the 9-arylimino derivatives in high yields. All the three 9-arylimino noscapinoids, **12-14** developed have shown increased antiproliferative activity to cancer cells based on our extensive molecular modelling and cellular study using two human breast cancer cell lines, MCF-7 and MDAMB-231 as well as a panel of primary breast cancer cells. Therefore, these novel compounds may prove efficacious not only in the treatment of breast carcinoma, but also for other types of cancers. Our results compel us to continue to examine the effects of these novel compounds on *in vivo* animal experiments with the final goal of taking it to the human clinical study.

Supporting Information

S1: Comparison of the X-crystallography structure of the lead molecule, Noscapine with the DFT optimized structure of **12**. Only the x-ray crystallography core structure of the noscapine and the newly designed molecule was compared.

Crystal structure of Noscapine				DFT optimized structure of **12**			
Bonds	Length (Å)	Bond angles	Degree	Bonds	Length (Å)	Bond angles	Degree
C1-C3	1.39	C1-C3-C4	121.3	C1-C3	1.40	C1-C3-C4	122.1
C1-C10	1.37	C1-C10-C9	122.5	C1-C10	1.38	C1-C10-C9	122.8
C2-C4	1.41	C1-C10-O11	127.8	C2-C4	1.41	C1-C10-O11	128.3
C2-C9	1.37	C1-C3-C8	120.6	C2-C9	1.38	C1-C3-C8	120.6
C2-O14	1.37	C2-C4-C3	120.6	C2-O14	1.38	C2-C4-C3	121.5
C3-C4	1.39	C2-O14-C15	118.2	C3-C4	1.38	C2-O14-C15	118.4
C3-C8	1.50	C2-C9-C10	121.3	C3-C8	1.50	C2-C9-C10	122.3
C4-C5	1.51	C2-C4-C5	118.0	C4-C5	1.51	C2-C4-C5	119.7
C5-N6	1.47	C4-C2-C9	117.0	C5-N6	1.47	C4-C2-C9	119.2
C5-C16	1.55	C2-C9-O13	129.5	C5-C16	1.56	C2-C9-O13	128.9
C7-N6	1.46	C3-C4-C5	121.3	C7-N6	1.46	C3-C4-C5	122.1
C7-C8	1.51	C3-C8-C7	109.3	C7-C8	1.52	C3-C8-C7	109.6
C9-C10	1.39	C4-C5-N6	115.1	C9-C10	1.38	C4-C5-N6	114.6
C9-O13	1.39	C4-C5-C16	107.5	C9-O13	1.38	C4-C5-C16	107.8
C10-O11	1.38	C4-C3-C8	118.1	C10-O11	1.37	C4-C3-C8	117.2
C12-O11	1.42	C5-N6-C19	111.6	C12-O11	1.43	C5-N6-C19	111.8
C12-O13	1.43	C8-C7-N6	110.3	C12-O13	1.42	C8-C7-N6	112.1
C15-O14	1.42	C9-O13-C12	104.8	C15-O14	1.43	C9-O13-C12	116.1
C16-C20	1.50	C9-C10-O11	109.7	C16-C20	1.50	C9-C10-O11	108.6
C16-O17	1.45	O11-C12-O13	107.9	C16-O17	1.44	O11-C12-O13	108.3
O17-C18	1.37	C16-C20-C25	131.5	O17-C18	1.36	C16-C20-C25	131.3
C19-N6	1.46	C16-C20-C21	108.4	C19-N6	1.45	C16-C20-C21	108.3
C18=O26	1.20	C16-O17-C18	111.6	C18-O26	1.19	C16-O17-C18	112.2
C18-C21	1.47	C18-C21-C22	108.7	C18-C21	1.48	C18-C21-C22	106.8
C20-C21	1.39	C19-N6-C7	110.2	C20-C21	1.39	C19-N6-C7	111.2
C20-C25	1.38	C20-C21-C22	122.0	C20-C25	1.38	C20-C21-C22	121.4
C21-C22	1.39	C20-C25-C24	119.0	C21-C22	1.39	C20-C25-C24	118.2
C23-C24	1.39	C20-C16-C5	116.7	C23-C24	1.39	C20-C16-C5	115.0
C22-C23	1.40	C21-C18-O26	131.9	C22-C23	1.40	C21-C18-O26	132.1
C24-C25	1.39	C21-C22-O27	120.8	C24-C25	1.39	C21-C22-O27	120.7
C30-O27	1.43	C22-C23-C24	120.3	C30-O27	1.43	C22-C23-C24	121.3
C22-O27	1.37	C22-C23-O28	124.1	C22-O27	1.38	C22-C23-O28	124.1
C23-O28	1.37	C25-C20-C21	120.0	C23-O28	1.36	C25-C20-C21	120.4
C29-O28	1.42	C25-C24-C23	121.0	C29-O28	1.42	C25-C24-C23	121.6
		O28-C23-C22	115.4	C1-N31	1.38	O28-C23-C22	116.4
		O27-C22-C23	121.5	C32-N31	1.27	O27-C22-C23	122.4
		C21-C22-C23	117.6	C32-C33	1.47	C21-C22-C23	118.3
		C22-C21-C18	129.2	C33-C34	1.40	C22-C21-C18	130.2
		O26-C18-O17	120.8	C34-C35	1.38	O26-C18-O17	121.3

		O17-C18-C21	107.3	C35-C36	1.39	O17-C18-C21	108.4
		C7-N6-C5	115.0	C36-C37	1.39	C7-N6-C5	116.1
		C10-O11-C12	105.3	C37-C38	1.39	C10-O11-C12	105.1
		C23-O28-C29	116.5	C38-C33	1.39	C16-C5-N6	117.2
		C22-O27-C30	114.8			C22-O27-C30	115.2
		C10-C1-C3	117.2			C10-C1-C3	118.2
		O13-C9-C5	109.2			O13-C9-C5	110.3
		O14-C2-C7	125.7			O14-C2-C7	126.2
		O14-C2-C4	117.2			O14-C2-C4	118.2
		N6-C5-C16	110.0			N6-C5-C16	111.4
		O17-C16-C20	103.9			O17-C16-C20	104.5
		O17-C16-C5	109.2			O17-C16-C5	110.2
						C1-N31-C32	127.5
						C32-C33-C34	121.6
						C33-C38-C37	120.6
						C36-C37-C38	120.1
						C35-C36-C37	119.7
						C34-C35-C36	120.2
						C33-C34-C35	120.6
						C34-C33-C38	120.7
						N31-C32-C33	119.0

S2: Comparison of the X-crystallography structure of the lead molecule, Noscapine with the DFT optimized structure of **13**. Only the x-ray crystallography core structure of the noscapine and the newly designed molecule was compared.

Crystal structure of Noscapine				DFT optimized structure of **13**			
Bonds	Length (Å)	Bond angles	Degree	Bonds	Length (Å)	Bond angles	Degree
C1-C3	1.39	C1-C3-C4	121.3	C1-C3	1.40	C1-C3-C4	121.6
C1-C10	1.37	C1-C10-C9	122.5	C1-C10	1.38	C1-C10-C9	123.4
C2-C4	1.41	C1-C10-O11	127.8	C2-C4	1.40	C1-C10-O11	127.4
C2-C9	1.37	C1-C3-C8	120.6	C2-C9	1.38	C1-C3-C8	121.9
C2-O14	1.37	C2-C4-C3	120.6	C2-O14	1.36	C2-C4-C3	121.9
C3-C4	1.39	C2-O14-C15	118.2	C3-C4	1.40	C2-O14-C15	117.2
C3-C8	1.50	C2-C9-C10	121.3	C3-C8	1.51	C2-C9-C10	122.2
C4-C5	1.51	C2-C4-C5	118.0	C4-C5	1.51	C2-C4-C5	118.4
C5-N6	1.47	C4-C2-C9	117.0	C5-N6	1.47	C4-C2-C9	116.7
C5-C16	1.55	C2-C9-O13	129.5	C5-C16	1.55	C2-C9-O13	129.6
C7-N6	1.46	C3-C4-C5	121.3	C7-N6	1.46	C3-C4-C5	120.3
C7-C8	1.51	C3-C8-C7	109.3	C7-C8	1.50	C3-C8-C7	110.4
C9-C10	1.39	C4-C5-N6	115.1	C9-C10	1.39	C4-C5-N6	114.9
C9-O13	1.39	C4-C5-C16	107.5	C9-O13	1.38	C4-C5-C16	109.8
C10-O11	1.38	C4-C3-C8	118.1	C10-O11	1.38	C4-C3-C8	117.3
C12-O11	1.42	C5-N6-C19	111.6	C12-O11	1.42	C5-N6-C19	111.7
C12-O13	1.43	C8-C7-N6	110.3	C12-O13	1.42	C8-C7-N6	112.4
C15-O14	1.42	C9-O13-C12	104.8	C15-O14	1.43	C9-O13-C12	104.3
C16-C20	1.50	C9-C10-O11	109.7	C16-C20	1.50	C9-C10-O11	109.0
C16-O17	1.45	O11-C12-O13	107.9	C16-O17	1.44	O11-C12-O13	108.4
O17-C18	1.37	C16-C20-C25	131.5	O17-C18	1.37	C16-C20-C25	132.4
C19-N6	1.46	C16-C20-C21	108.4	C19-N6	1.48	C16-C20-C21	107.3
C18=O26	1.20	C16-O17-C18	111.6	C18-O26	1.21	C16-O17-C18	112.1
C18-C21	1.47	C18-C21-C22	108.7	C18-C21	1.47	C18-C21-C22	109.6

C20-C21	1.39	C19-N6-C7	110.2	C20-C21	1.39	C19-N6-C7	111.0
C20-C25	1.38	C20-C21-C22	122.0	C20-C25	1.38	C20-C21-C22	121.9
C21-C22	1.39	C20-C25-C24	119.0	C21-C22	1.39	C20-C25-C24	118.4
C23-C24	1.39	C20-C16-C5	116.7	C23-C24	1.39	C20-C16-C5	115.3
C22-C23	1.40	C21-C18-O26	131.9	C22-C23	1.41	C21-C18-O26	132.4
C24-C25	1.39	C21-C22-O27	120.8	C24-C25	1.39	C21-C22-O27	119.8
C30-O27	1.43	C22-C23-C24	120.3	C30-O27	1.43	C22-C23-C24	121.3
C22-O27	1.37	C22-C23-O28	124.1	C22-O27	1.37	C22-C23-O28	125.6
C23-O28	1.37	C25-C20-C21	120.0	C23-O28	1.38	C25-C20-C21	121.3
C29-O28	1.42	C25-C24-C23	121.0	C29-O28	1.41	C25-C24-C23	120.8
		O28-C23-C22	115.4	C1-N31	1.39	O28-C23-C22	116.8
		O27-C22-C23	121.5	N31-C32	1.28	027-C22-C23	122.4
		C21-C22-C23	117.6	C32-C33	1.51	C21-C22-C23	118.3
		C22-C21-C18	129.2	C33=N34	1.31	C22-C21-C18	131.1
		O26-C18-O17	120.8	C33-C36	1.42	O26-C18-O17	121.3
		O17-C18-C21	107.3	C35-C36	1.36	O17-C18-C21	107.6
		C7-N6-C5	115.0	C35-C37	1.41	C7-N6-C5	116.1
		C10-O11-C12	105.3	C37-C38	1.42	C10-O11-C12	105.8
		C23-O28-C29	116.5	C38-C39	1.41	C23-O28-C29	116.9
		C22-O27-C30	114.8	C39-C40	1.37	C22-O27-C30	115.2
		C10-C1-C3	117.2	C40-C41	1.41	C10-C1-C3	117.9
		O13-C9-C5	109.2	C41-C42	1.37	O13-C9-C5	109.5
		O14-C2-C7	125.7	C42-C37	1.41	O14-C2-C7	125.3
		O14-C2-C4	117.2			O14-C2-C4	117.8
		N6-C5-C16	110.0			N6-C5-C16	111.4
		O17-C16-C20	103.9			O17-C16-C20	103.4
		O17-C16-C5	109.2			O17-C16-C5	110.2
						C1-N31-C32	122.4
						C3-C1-C31	112.6
						C10-C1-N31	104.3
						C32-C33-N34	116.1
						C33-N34-C38	119.3
						C33-C32-N31	110.5
						C33-C36-C35	119.2
						C35-C37-C38	117.1
						C35-C37-C42	123.5
						C36-C35-C37	121.5
						C37-C38-N34	119.5
						C37-C38-C39	119.0
						C37-C42-C41	120.4
						C38-C39-C40	120.3
						C39-C40-C41	120.6
						C40-C41-C42	120.2

S3. Comparison of the X-crystallography structure of the lead molecule, Noscapine with the DFT optimized structure of **14**. Only the x-ray crystallography core structure of the noscapine and the newly designed molecule was compared.

Crystal structure of Noscapine				DFT optimized structure of **14**			
Bonds	Length (Å)	Bond angles	Degree	Bonds	Length (Å)	Bond angles	Degree
C1-C3	1.39	C1-C3-C4	121.3	C1-C3	1.41	C1-C3-C4	121.7
C1-C10	1.37	C1-C10-C9	122.5	C1-C10	1.38	C1-C10-C9	123.5
C2-C4	1.41	C1-C10-O11	127.8	C2-C4	1.41	C1-C10-O11	120.7

C2-C9	1.37	C1-C3-C8	120.6	C2-C9	1.38	C1-C3-C8	121.4
C2-O14	1.37	C2-C4-C3	120.6	C2-O14	1.36	C2-C4-C3	121.6
C3-C4	1.39	C2-O14-C15	118.2	C3-C4	1.39	C2-O14-C15	112.2
C3-C8	1.50	C2-C9-C10	121.3	C3-C8	1.50	C2-C9-C10	120.1
C4-C5	1.51	C2-C4-C5	118.0	C4-C5	1.51	C2-C4-C5	115.2
C5-N6	1.47	C4-C2-C9	117.0	C5-N6	1.47	C4-C2-C9	117.2
C5-C16	1.55	C2-C9-O13	129.5	C5-C16	1.55	C2-C9-O13	128.8
C7-N6	1.46	C3-C4-C5	121.3	C7-N6	1.46	C3-C4-C5	120.7
C7-C8	1.51	C3-C8-C7	109.3	C7-C8	1.52	C3-C8-C7	108.9
C9-C10	1.39	C4-C5-N6	115.1	C9-C10	1.37	C4-C5-N6	116.2
C9-O13	1.39	C4-C5-C16	107.5	C9-O13	1.39	C4-C5-C16	109.7
C10-O11	1.38	C4-C3-C8	118.1	C10-O11	1.39	C4-C3-C8	119.4
C12-O11	1.42	C5-N6-C19	111.6	C12-O11	1.42	C5-N6-C19	112.5
C12-O13	1.43	C8-C7-N6	110.3	C12-O13	1.44	C8-C7-N6	111.5
C15-O14	1.42	C9-O13-C12	104.8	C15-O14	1.43	C9-O13-C12	105.2
C16-C20	1.50	C9-C10-O11	109.7	C16-C20	1.50	C9-C10-O11	110.2
C16-O17	1.45	O11-C12-O13	107.9	C16-O17	1.45	O11-C12-O13	108.2
O17-C18	1.37	C16-C20-C25	131.5	O17-C18	1.37	C16-C20-C25	131.8
C19-N6	1.46	C16-C20-C21	108.4	C19-N6	1.45	C16-C20-C21	108.1
C18=O26	1.20	C16-O17-C18	111.6	C18-O26	1.19	C16-O17-C18	111.4
C18-C21	1.47	C18-C21-C22	108.7	C18-C21	1.48	C18-C21-C22	108.6
C20-C21	1.39	C19-N6-C7	110.2	C20-C21	1.39	C19-N6-C7	111.4
C20-C25	1.38	C20-C21-C22	122.0	C20-C25	1.38	C20-C21-C22	121.9
C21-C22	1.39	C20-C25-C24	119.0	C21-C22	1.39	C20-C25-C24	118.7
C23-C24	1.39	C20-C16-C5	116.7	C23-C24	1.39	C20-C16-C5	116.5
C22-C23	1.40	C21-C18-O26	131.9	C22-C23	1.41	C21-C18-O26	130.8
C24-C25	1.39	C21-C22-O27	120.8	C24-C25	1.39	C21-C22-O27	121.2
C30-O27	1.43	C22-C23-C24	120.3	C30-O27	1.43	C22-C23-C24	120.9
C22-O27	1.37	C22-C23-O28	124.1	C22-O27	1.38	C22-C23-O28	123.7
C23-O28	1.37	C25-C20-C21	120.0	C23-O28	1.36	C25-C20-C21	119.6
C29-O28	1.42	C25-C24-C23	121.0	C29-O28	1.42	C25-C24-C23	121.4
		O28-C23-C22	115.4	C1-N31	1.39	O28-C23-C22	116.3
		O27-C22-C23	121.5	C32-N31	1.28	O27-C22-C23	122.4
		C21-C22-C23	117.6	C32-C33	1.45	C21-C22-C23	118.2
		C22-C21-C18	129.2	C33-C34	1.43	C22-C21-C18	130.1
		O26-C18-O17	120.8	C33-C37	1.37	O26-C18-O17	121.4
		O17-C18-C21	107.3	C34-C35	1.35	O17-C18-C21	108.2
		C7-N6-C5	115.0	C35-Cl38	1.73	C7-N6-C5	115.2
		C10-O11-C12	105.3	C35-S36	1.75	C10-O11-C12	106.3
		C23-O28-C29	116.5	C37-Cl39	1.73	C23-O28-C29	118.9
		C22-O27-C30	114.8			C22-O27-C30	116.9
		C10-C1-C3	117.2			C10-C1-C3	119.4
		O13-C9-C5	109.2			O13-C9-C5	110.2
		O14-C2-C7	125.7			O14-C2-C7	126.3
		O14-C2-C4	117.2			O14-C2-C4	118.3
		N6-C5-C16	110.0			N6-C5-C16	111.4
		O17-C16-C20	103.9			O17-C16-C20	104.7
		O17-C16-C5	109.2			O17-C16-C5	110.3
						C1-N31-C32	119.8
						C32-C33-C37	122.7
						C3-C1-N31	107.3
						C10-C1-N31	104.5
						C32-C33-C34	124.9

						C33-C34-C35	112.8
						C33-C37-Cl39	127.4
						C33-C32-N31	122.2
						C34-C35-S36	112.8
						C34-C35-Cl38	127.4
						C35-S36-C37	89.8

S4: ^{1}H NMR of 12

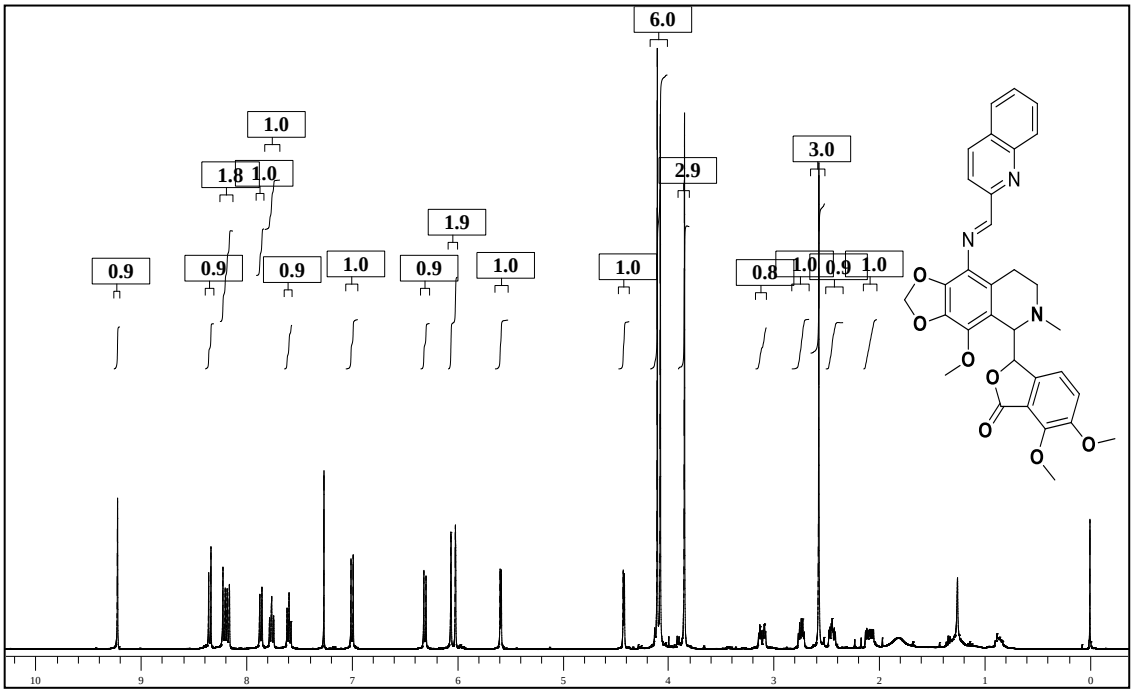

S5: ^{13}C NMR of 12

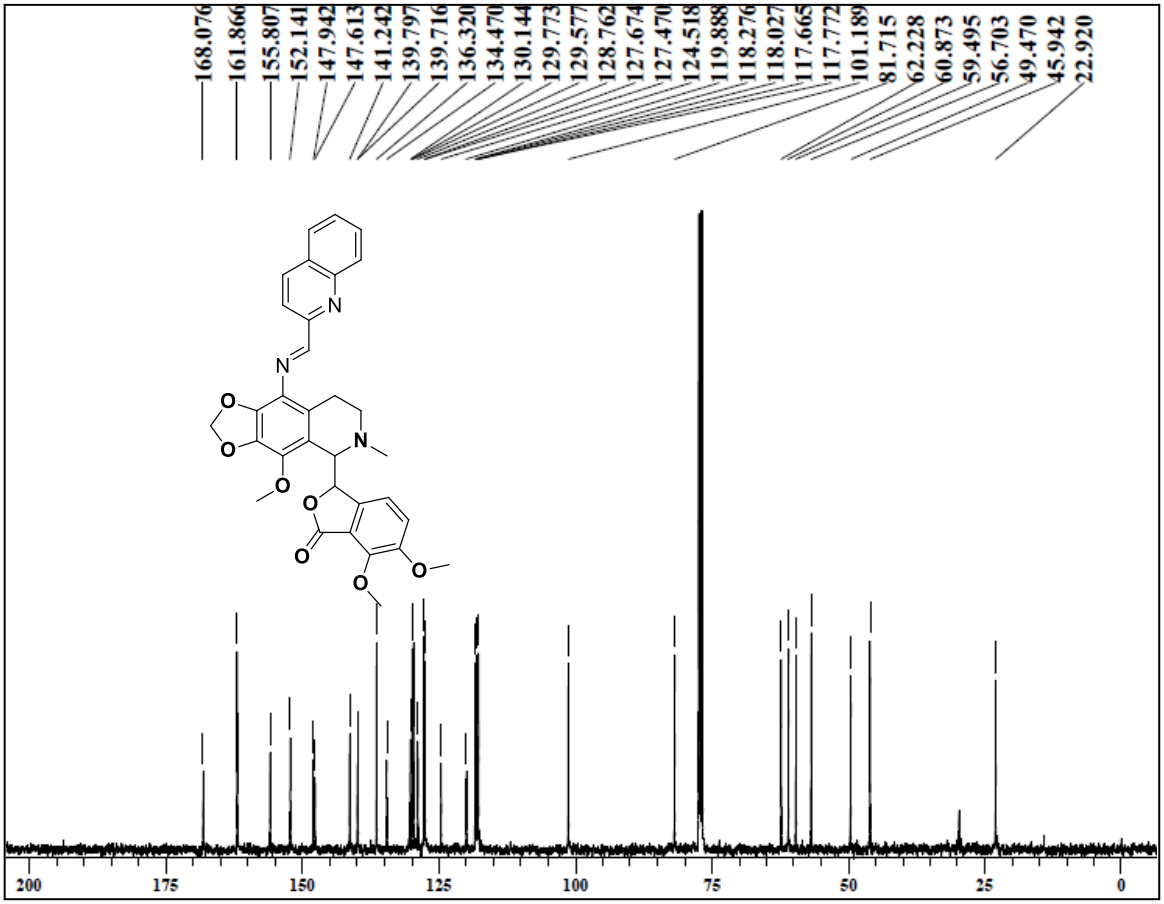

S6: HRMS of 12

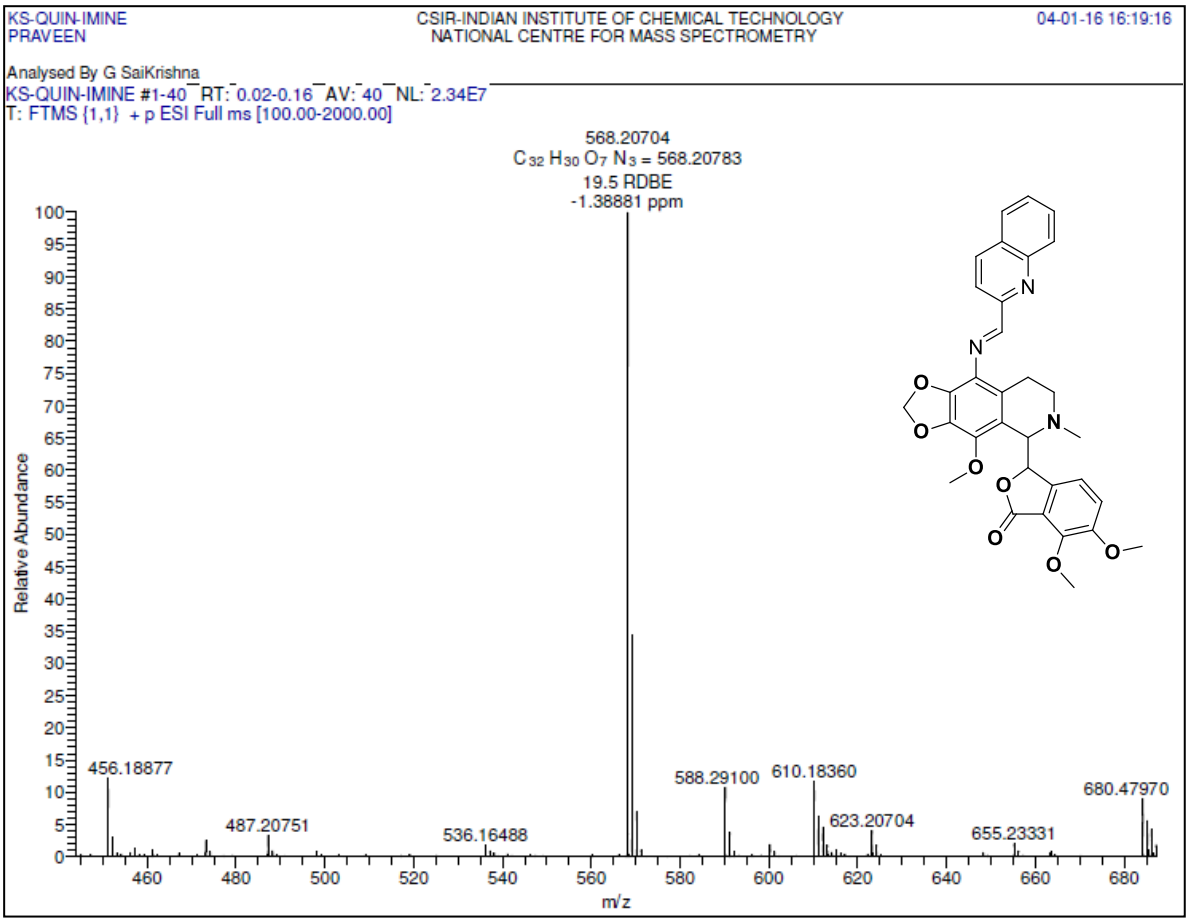

S7: ^{1}H NMR of 13

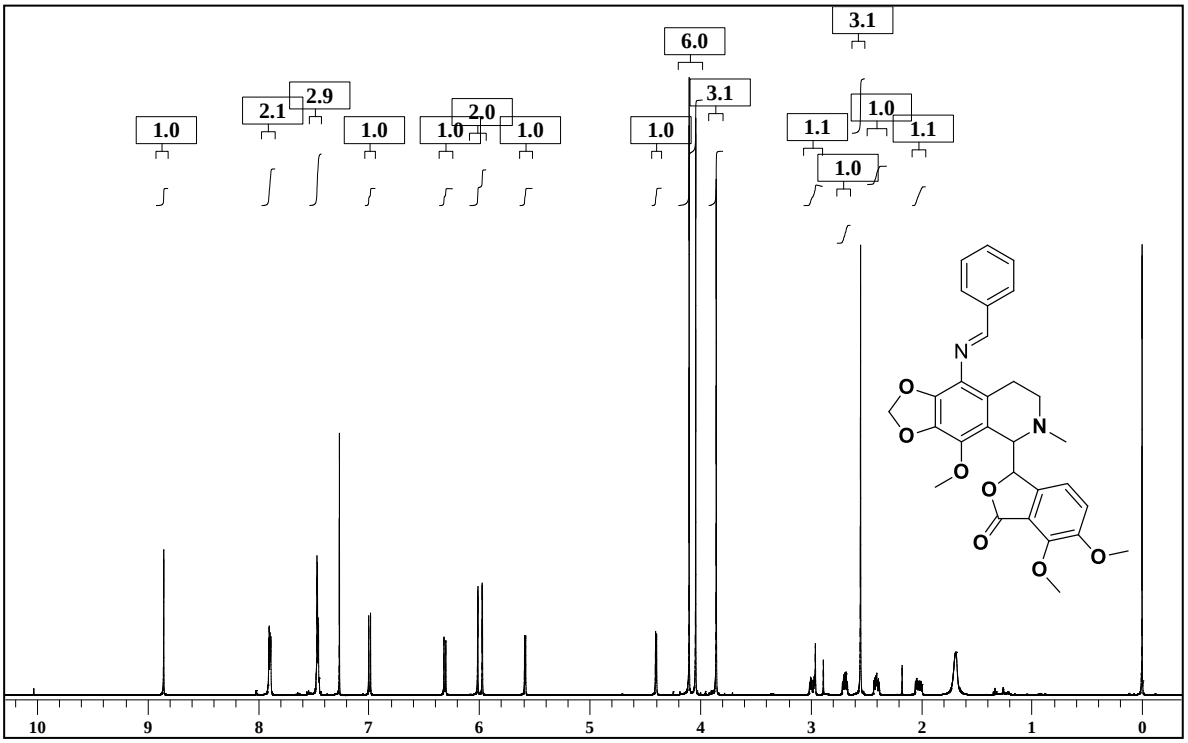

S8: ^{13}C NMR of 13

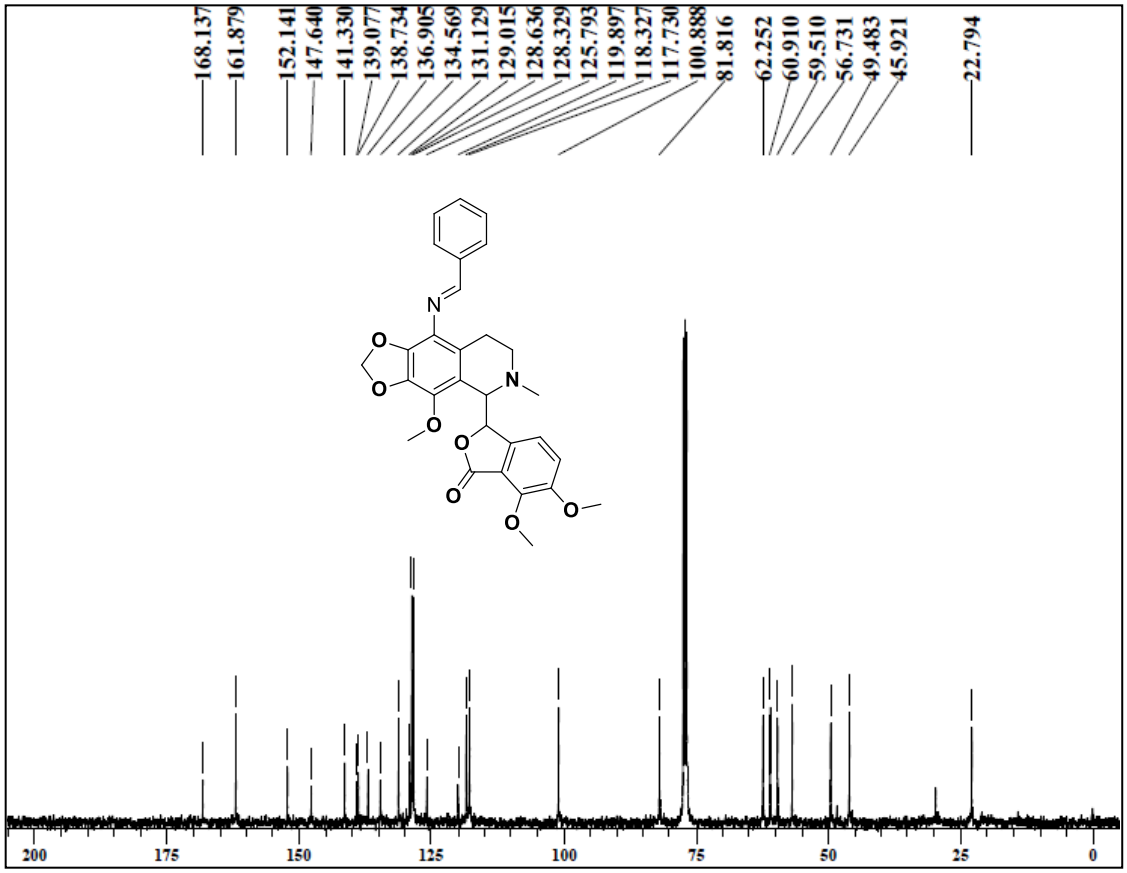

S9: HRMS of 13

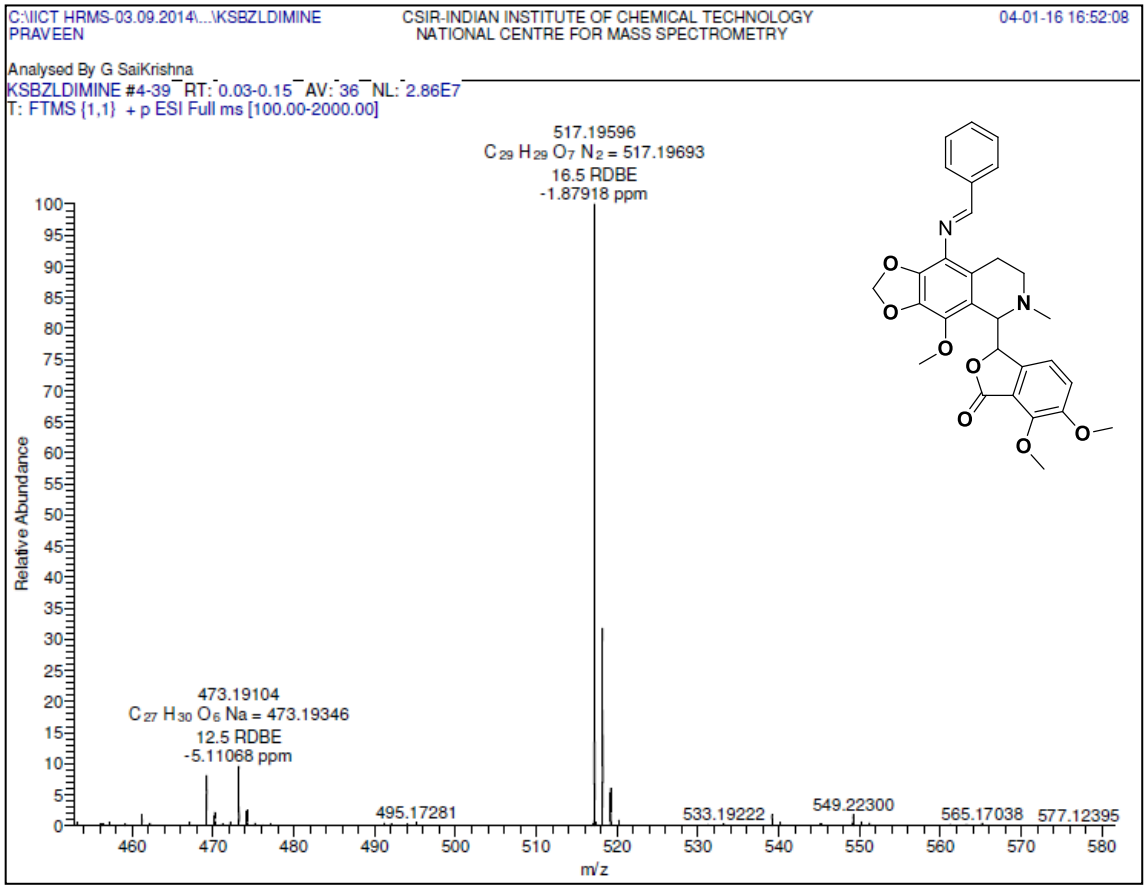

S10: ^{1}H NMR of 14

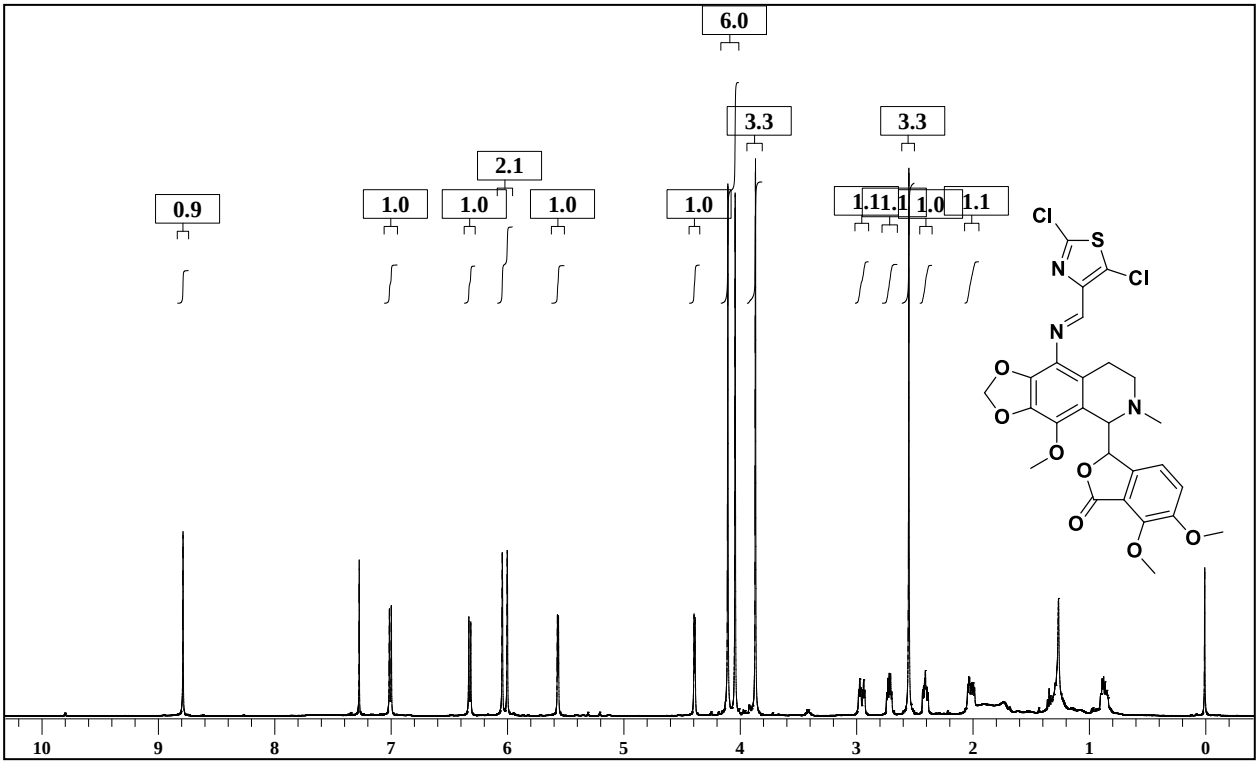

S11: ^{13}C NMR of 14

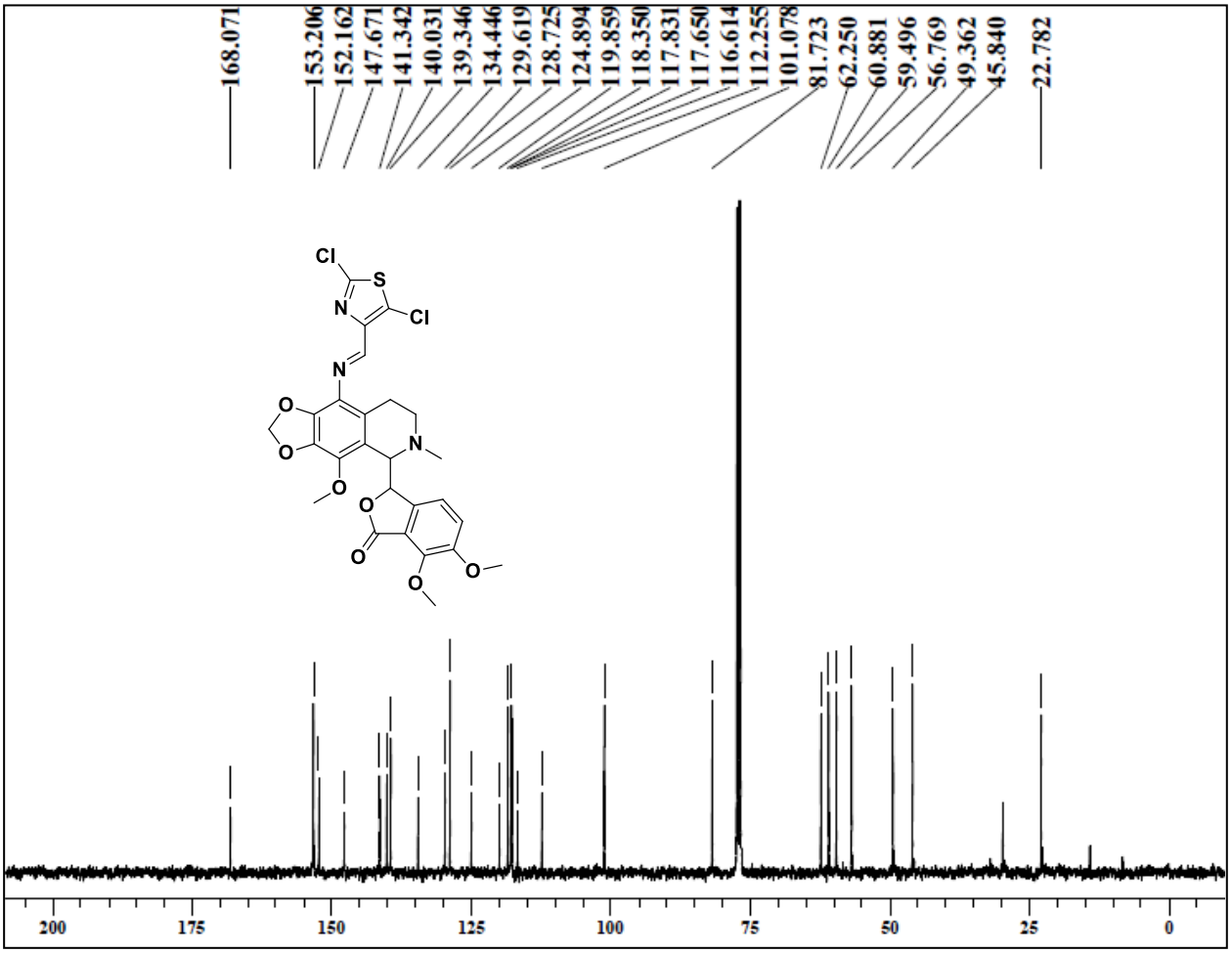

S12: HRMS of 14

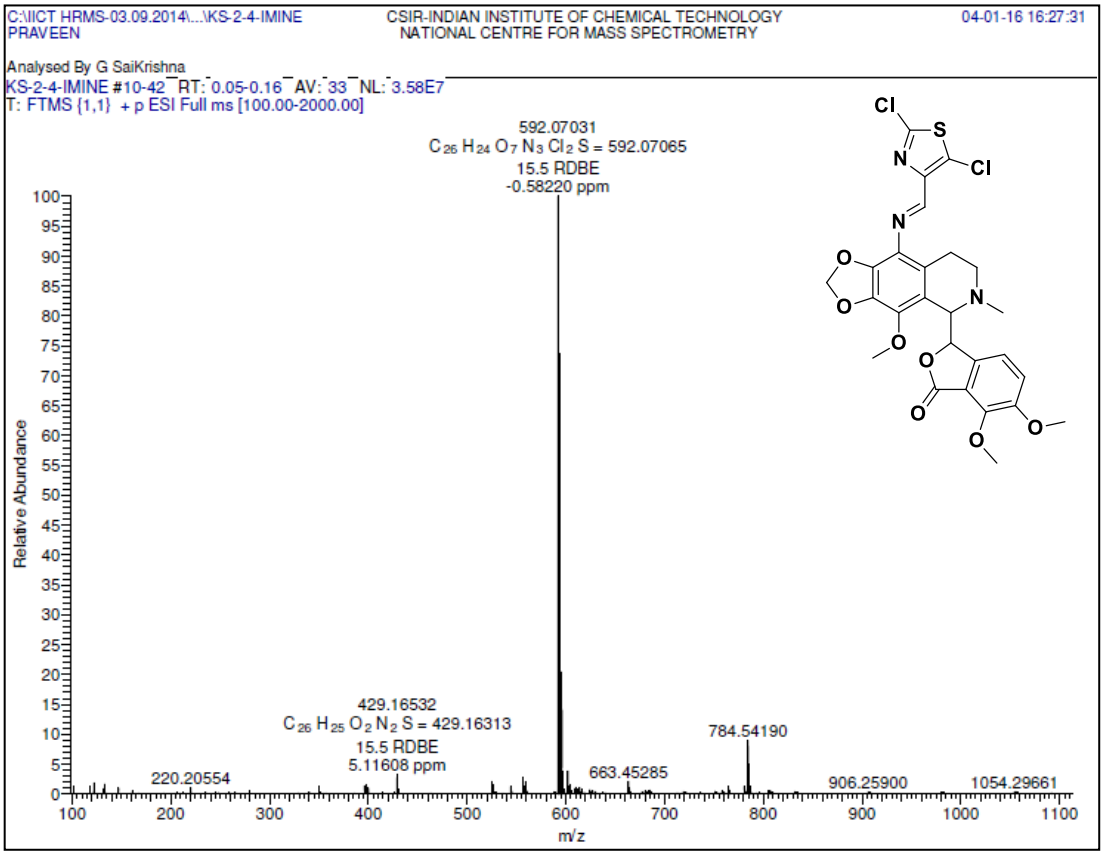
C:\IICT HRMS-03.09.2014\...\KS-2-4-IMINE
PRAVEEN
CSIR-INDIAN INSTITUTE OF CHEMICAL TECHNOLOGY
NATIONAL CENTRE FOR MASS SPECTROMETRY
04-01-16 16:27:31
Analysed By G SaiKrishna
KS-2-4-IMINE #10-42 RT: 0.05-0.16 AV: 33 NL: 3.58E7
T: FTMS {1,1} + p ESI Full ms [100.00-2000.00]
592.07031
C26 H24 O7 N3 Cl2 S = 592.07065
15.5 RDBE
-0.58220 ppm
429.16532
C26 H25 O2 N2 S = 429.16313
15.5 RDBE
5.11608 ppm
220.20554
663.45285
784.54190
906.25900
1054.29661
Relative Abundance
m/z

CHAPTER-3

Rational design of novel N-alkyl amine analogues of noscapine, their chemical synthesis and cellular activity as potent anticancer agents

Abstract:

The scaffold structure of noscapine (an antitussive plant alkaloid) was modified by inducting N-aryl methyl pharmacophore at C-9 position of the isoquinoline ring to rationally design and screened three novel 9-(N-arylmethylamino) noscapinoids, **15-17** with robust binding affinity with tubulin. The selected 9-(N-arylmethylamino) noscapinoids revealed improved predicted binding energy of -6.694 kcal/mol for **15**, -7.118 kcal/mol for **16** and -7.732 kcal/mol for **17**, respectively in comparison to the lead molecule (-5.135 kcal/mol). These novel derivatives were chemically synthesized and validated their anticancer activity based on cellular studies using two human breast adenocarcinoma, MCF-7 and MDA-MB-231, as well as with a panel of primary breast tumor cells. These derivatives inhibited cellular proliferation in all the cancer cells that ranged between 3.2 to 32.2 µM, which is 11.9 to 1.8 fold lower than that of noscapine. These novel derivatives effectively arrest the cell cycle in the G2/M-phase followed by apoptosis and the appearance of apoptotic cells. Thus, we conclude that 9-(N-arylmethyl amino) noscapinoids, **15-17** have a high probability to be a novel therapeutic agent for breast cancers.

Key words: Noscapine; N-arylmethylamino-noscapinoids; tubulin binding; anticancer agents; breast cancer.

3.1.Introduction

Noscapine is an opium alkaloid. It is non-narcotic, non-sedative and does not produce elation or addiction (Martindale, 1977). In the clinic, it has been used as an orally available, safe antitussive drug for over 40 years. The ability of noscapine to bind microtubule, suppressing its dynamic instability and thereby inhibiting cell proliferation as well as induction of apoptosis encouraged several investigators to examine its anticancer potential (Ye et al., 1998; Landen et al., 2002; Zhou et al., 2002a; Jordan and Wilson, 2004).Towards increment of its anticancer potential, several synthetic derivatives were synthesized and evaluated (Ye et al., 1998; Landen et al., 2002; Zhou et al., 2002b; 2003; Landen et al., 2004). Interestingly, unlike the classic microtubule-targeted agents, taxanes (that over polymerizes microtubules and bundles them) and vincas (that depolymerizes microtubules), noscapine and its derivatives do not significantly alter the polymer and monomer ratio of microtubules and were known as a "kindler" microtubule poison. From a clinical perspective, noscapine is also very unique from many other microtubule-targeted agents in the sense that it is lacking substantial cytotoxicity to normal cells. It is also demonstrated to have very little or no toxicity to healthy volunteers (Dahlstrom et al., 1982; Karlsson et al., 1990; Jensen et al., 1992). It also possesses a very good pharmacokinetic and ADME profile (Aneja et al, 2007)and does not produce any major organ toxicities. To enhance its anticancer activity, several derivatives have been developed (called noscapinoids) without inducing considerable toxic effects to normal cells. The first-generation, halogenated (fluoro, chloro, bromo, and iodo-noscapine), nitro, amino, and azido derivatives of noscapine analogues were developed by modification on the C-9 position of isoquinoline ring system of noscapine scaffold (Aneja et al, 2006a; Naik et al, 2011; Santoshi et al, 2011; Aneja et al, 2006b). These derivatives were demonstrated to have more anticancer activity compared to noscapine. The second-generation derivatives were developed by alteration of the benzofuranone ring system of noscapine, giving rise to O-alkylated and acylated noscapinoids (Mishra et al, 2011). These derivatives revealed better activity compared to noscapine. The third-generation derivatives were generated through manipulation in the isoquinoline ring system by functionalization of 'N' (Manchukonda et al, 2013). Many of these derivatives exhibited substantial antiproliferative activity with a panel of cancer cells of different tissue origins. We have also recently developed a panel of hybrid analogs of noscapine (biaryl-noscapinoids) by coupling the biaryl pharmacophore (Santoshi et al, 2015) with improved cytotoxic activity. All the noscapinoids bind at the interface of α- and β- tubulin, near to colchicine binding site thereby inhibits the progression of the cell cycle at G2/M phase and induced apoptotic cell death in cancer cells.

In this study, we approach to develop a panel of N-arylmethylamino derivatives of noscapine **15-17** by strategically modifying its scaffold structure. These derivatives were then chemically synthesized and demonstrated their anticancer activity based on a cellular study using two human breast cancer cell lines (MCF-7 and MDA-MB-231) and a panel of primary breast tumor cells. The novel derivatives, **15-17** were found to bind tubulin heterodimer with increased binding affinity, effectively inhibit cancer cell proliferation, arrest cancer cells in the G2/M phase and effectively induce apoptosis to cancer cells.

3.2. Materials and methods

3.2.1. Protein preparation

The PDB structure (PDB ID: 6Y6D, resolution 2.20 Å, Oliva et al., 2020) of tubulin heterodimer was used for the *in silico* study. Although the crystal structure was obtained at high resolution, the missing hydrogen atoms were added and the structure was prepared using the multistep procedure of protein preparation wizard (Schrodinger). The structure was refined by energy minimization using Macromodel (Schrodinger). OPLS 2005 force field was used with Polak-Ribiere Conjugate Gradient (PRCG) algorithm and energy gradient of 0.01 kcal/mol.The structure was further refined by performing an all-atom molecular dynamics (MD) simulation of 100 ns in explicit water using GROMACS 4.5.4 software (Berendson et al., 1995) and the GROMOS96 force field as reported earlier (Santoshi and Naik, 2014). Thetopmost 5 structures with the lowest minimum total energy from the MD trajectory were used to generate the average structure of the tubulin.

3.2.2. Rational design of N-alkyl amine derivatives of noscapine

From the literature, it is evident that modification on the C-9 position of the isoquinoline ring system of noscapine scaffold with halogens (fluoro, chloro, bromo, and iodo-noscapine), nitro, amino, and azido groups exerted to have enhanced anticancer activity compared to the parent compound, noscapine. Among these derivatives, 9-aminonoscapine is the most prominent one. Later studies predicted that further functionalization of groups at the C-9 position of the isoquinoline ring system could be the choice to tune the anticancer activity profile of noscapine. In this direction, we envisaged functionalizingthe 9-amino group of noscapine with alkyl or arylalkyl units to examine their anticancer potential. Initially, we have developed a library of N-arylalkylamino-noscapinoids by *in silico*combinatorial approach as depicted in Figure 3.1 followed by the screening of a panel of most potent compounds using a combination of both molecular docking and predictive binding free energy.

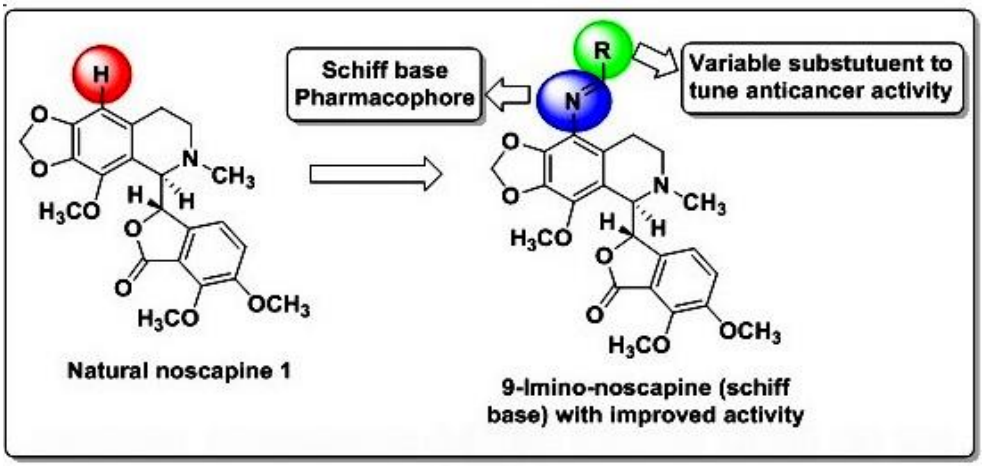

Figure 3.1. Strategic design of 9-(N-arylalkylamino) noscapinoids. The 9-amino group of noscapine was functionalize with alkyl or arylalkyl units to developed a library of 9-(N-arylalkylamino) noscapinoids.

3.2.3. Preparation of molecular structure of noscapinoids

Molecular structures of noscapinoids (Figure 3.2) that had been reported earlier (Aneja et al., 2006a; Naik et al., 2011; Santoshi et al., 2011; Manchukonda et al., 2013; Santoshi et al., 2015) and the newly designed N-arylalkylamino-noscapinoids (Figure 3.1) were built using ChemDraw and imported into Maestro (Schrödinger package). The molecular structures were energy minimized using Macromodel (Schrödinger package) and OPLS 2005 force field with PRCG algorithm (energy gradient of 0.001). The structures were further refined by geometric optimization using hybrid density functional theory with Becke's three-parameter exchange potential and the Lee-Yang-Parr correlation functional (B3LYP) with basis set 3-21G* using Jaguar (Schrödinger, package). Further, the various conformations of each molecule were generated using Ligprep (Schrödinger package).

3.2.4. Molecular docking of noscapinoids

The prepared molecular structures of noscapinoids were docked onto the αβ-tubulin heterodimer using Glide (Schrödinger package) as reported previously (Naik et al., 2011). Briefly, an inner grid box of size 12Å x 12Å x 12Å was defined at the centroid of the binding site(Oliva et al., 2020) by selecting the co-complex ligand, amino-noscapine using Glide grid-receptor generation program.This box defines the search space in which the diameter midpoint of each docked ligand is required to be present. Further, an outer grid box was also defined with a size of ≤ 24 Å of the co-complexed ligand, amino noscapine in the crystal structure. It defines the volume within which all ligand atoms of a valid pose must be located. All the noscapinoids were docked using Glide XP (extra

precision) algorithm and evaluated their binding poses using Glide XP_{Score} function (Friesner et al., 2004; Halgren et al., 2004). The single best conformation for each ligand was used for further analysis.

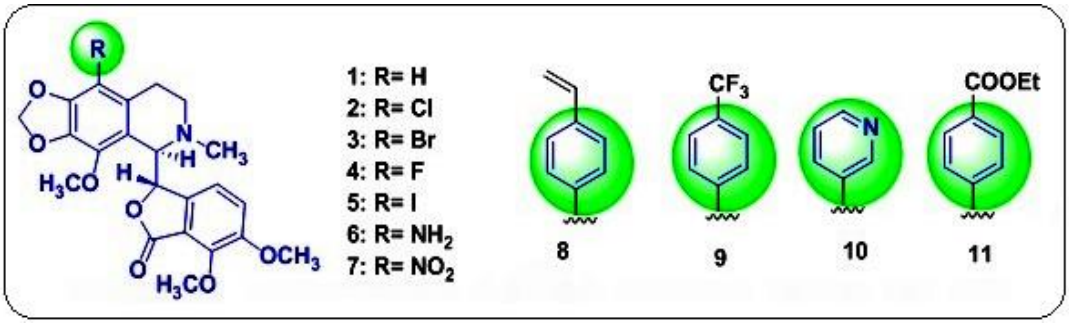

Figure 3.2. Molecular structures of previously reported noscapine derivatives that have experimentally proven to bind tubulin with known binding free energy (Table 1) and used as training test molecules for LIE-SGB building.

3.2.5. LIE-SGB model building

A robust predictive model was developed based on linear interaction energy model (LIE) with a surface generalized Born (SGB) continuum solvation model (Zhou et al., 2001) to determine the free energy of binding ($\Delta G_{bind,pred}$) of the newly designed N-arylalkylamino-noscapinoids with tubulin. A training data set of noscapinoids (Figure 3.2) with known experimental binding free energy, $\Delta G_{bind,expt}$ was used and mapped with various predicted energy parameters such as van der Waals (U_{vdw}), coulumbic (U_{coul}), reaction field (U_{rxn}) and cavity energy (U_{cav}) based on LIE model to develop the empirical prediction model. $\Delta G_{bind,expt}$ of noscapinoids with tubulin was determined from their respective dissociation constant (K_d) values using the relation:

$$\Delta G_{bind,expt} = RT \ln K_d$$

where R is gaseous constant (0.001986 kcal/mol) and T is the temperature (298 K). Liaison programme (Schrödinger package) was used with the parameters set up as reported previously (Santoshi et al, 2015) to estimate the above energy parameters from the docked complexes of the noscapinoids based on Hybrid Monte Carlo simulation technique.

$$\Delta G_{bind,pred} = \alpha\left(\langle U^b_{vdw}\rangle - \langle U^f_{vdw}\rangle\right) + \beta\left(\langle U^b_{coul}\rangle - \langle U^f_{coul}\rangle\right) + \gamma\left(\langle U^b_{rxn}\rangle - \langle U^f_{rxn}\rangle\right) + \delta\left(\langle U^b_{cav}\rangle - \langle U^f_{cav}\rangle\right)$$

Here $\langle\ \rangle$ represents the ensemble average, *b* represents the bound form of the ligand, *f* represents the free form of the ligand, and α, β, γ and δ are the coefficients of the energy parameters. Finally based on the docking score and the predictive binding free energy, we have screened out the following three 9-(N-arylmethylamino) noscapinoids, **15-**

17(Figure3.3) having enhanced binding affinity with tubulin compared to noscapine for chemical synthesis and cellular evaluation to determine their anticancer potential.

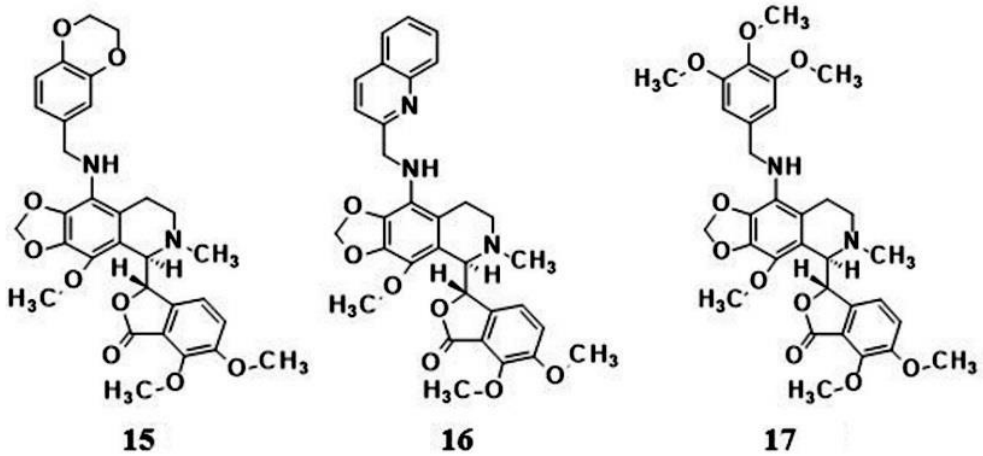

Figure 3.3. A panel of 9-(N-arylmethylamino) noscapinoids, **15-17**that are rationally designed and screened out to have higher binding affinity with tubulin for chemical synthesis and experimental evaluation.

3.2.6. Molecular dynamics simulation

Molecular dynamics (MD) simulation of 100 ns was performed using GROMACS 2019.2 package (Abraham et al., 2015)for the docked complexes of tubulin and 9-(N-arylmethylamino) noscapinoids, **15-17.** The protein was processed by Gromacs with AMBER999SB force field (Hornak et al., 2006) to generate coordinates and topology files. The ligands parameters were defined using a general amber force field (GAFF) (Wang et al., 2004) implemented in the Antechamber program of Amber18. All atomic point charges were calculated using the AM1-BCC charge model (Jakalian et al., 2002; Jakalian et al., 2000). Topologies and internal coordinates of the complex were generated using the tleap program of Amber18 and ACPYPE software (Da Silva and Vranken, 2012).The molecular system was neutralized by adding counter-ions and solvation using the TIP3P water model in a truncated octahedron. The molecular system was relaxed and the bad contacts were removed by performing three rounds of minimization. Position restraints of 10 kcal/Å^2 and 2 kcal/Å^2 were imposed on the molecular system for the first and the second round respectively, whereas no restraints were imposed in the third round. The molecular systems were equilibrated at 300 K and 1 atm for 500 ps. The equilibrated systems were then run for 100 ns each with a time step of 2 fm. Throughout simulations, the cut-off for non-bonded interaction was 10 Å, electrostatics were calculated using Particle Mesh Ewald (PME) (Essmann et al., 1995) and bonds were constrained using shake algorithm (Darden et al., 1993). Langevin thermostat was used to regulate the temperature of simulations. Co-ordinates were written every 20 ps to write 5000 frames

for each molecular system. CPPTAJ implemented in Ambertools was used to analyze trajectories for root mean square deviation analyses.

3.2.7. Predictive binding affinity

Predicted binding affinity ($\Delta G_{bind,pred}$) of 9-(N-arylmethylamino) noscapinoids, **15-17** with tubulin was calculated using Molecular Mechanics Poisson-Boltzmann Surface Area (MM-PBSA). From the last 20 ns of MD trajectory, a total of 1000 snapshots were extracted with a time step of 20 ps and the ensemble average of the $\Delta G_{bind,pred}$ was determined as reported earlier (Kollman et al., 2000).

$$\Delta G_{bind,pred} = \Delta G_{complex} - [\Delta G_{Rec} + \Delta G_{lig}]$$

$$G = E_{gas} + G_{sol} - TS.$$

$$E_{gas} = E_{int} + E_{ele} + E_{vdw}$$

$$G_{sol} = G_{PB(GB)} + G_{sol-np}$$

$$G_{sol-np} = \gamma SAS$$

Where G is Gibbs free energy, E_{gas} is the gas phase energy calculated as the sum of internal energy (E_{int}), energy generated as a result of the electrostatic interaction (E_{ele}) and the van der Waals interaction (E_{vdw}). G_{sol} is the solvation free energy calculated as the sum of polar (G_{PB}) and nonpolar contributions (G_{sol-np}). Polar interaction contribution (G_{PB}) was calculated as the summation of electrostatic contribution (E_{ele}) and polar solvation contribution (G_{PB}). The nonpolar solvation contribution (G_{sol-np}) is approximated as linearly dependent on the solvent accessible surface area (SAS) and γ is the surface tension constant that was set to 0.0072 kcal mol^{-1} $Å^{-2}$.

3.2.8. Chemical synthesis of 9-(N-arylmethylamino)noscapinoids, 15-17

The natural α-noscapine was used as a starting material to produce 9-amino-noscapine via two reaction steps involving bromination of noscapine using aqueous HBr/Br_2-H_2O followed by amination using CuI, NaN_3 and L-Proline in DMSO as reported earlier (Manchukonda et al., 2014). A solution of 9-aminonoscapine **6**(1.0 mmol), in ethanol (15 mL), was refluxed with various substituted aromatic aldehydes (1.0 mmol), for 24 h. After the compound was completely utilized in the reaction (judged by TLC), the solvent was evaporated under a vacuum. The crude residue was extracted into dichloromethane (2 x 15 mL) and washed with brine solution. The organic layer was collected and passed through a Na_2SO_4 bed. The crude residue was chromatographed over a triethylamine silica bed, using petroleum ether/ethyl acetate (7:3) as eluents, to produce 9-(arylimino) noscapinoids **12-14** as solid products in very good yields. The synthesized

12-14 (1.0 mmol) were reduced to their respective 9-(N-arylmethylamino) noscapinoids, **15-17**by reacting them with sodium cyanoborohydride (1.2 mmol), in methanol (10 mL), for 4h at room temperature (Figure 3.4). Structural characterization of all the intermediates and final products were done using NMR (^{1}H and ^{13}C), IR spectroscopy and mass (HRMS) spectrometry techniques. The NMR (^{1}H and ^{13}C) and mass (HRMS) spectra of the 9-(N-arylmethylamino) noscapinoids, **15-17** were included in the supplementary material (Page 31-39). All the synthesized compounds are HPLC purified using the C18 column (acetonitrile:water, 90:10) and were found to be > 96.5% pure.

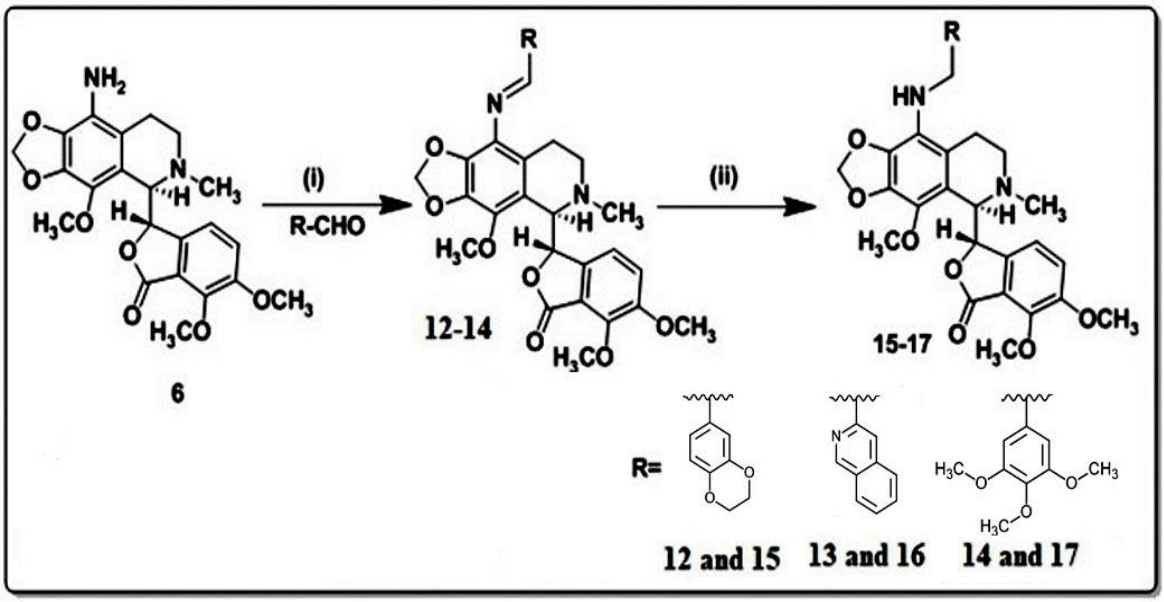

Figure 3.4. Synthesis of 9-(N-arylmethylamino) noscapinoids, **15-17**. Reaction conditions: (i)RCHO, EtOH, Reflux, 24h. (ii) $NaCNBH_3$, Methanol, RT, 4h. The 9-amino-noscapine was converted to 9-(arylimino) noscapinoids12-14, whichwere then reduced to their respective 9-(N-arylmethylamino) noscapinoids.

3.2.9. Structural characterization of 9-(arylimino) noscapinoids, 12-14 and 9-(N-arylmethylamino) noscapinoids, 15-17

(S)-6,7-dimethoxy-3-((R)-4-methoxy-6-methyl-9-((E)-(3,4,5-trimethoxybenzylidene) amino)-5,6,7,8-tetrahydro-[1,3]dioxolo[4,5-g]isoquinolin-5-yl)isobenzofuran-1(3H)-one (12):

Nature : White solid. M.P: 124-126 °C. IR (KBr) : 3493, 2952, 2899, 2843, 2794, 1758, 1628, 1580, 1499, 1459, 1390, 1275, 1122, 1037, 1006, 975, 846, 798, 727 cm^{-1}. ^{1}H NMR (400 MHz, $CDCl_3$) : δ 8.73 (s, 1H, N=CH), 7.15 (s, 2H, Ar-H), 7.01 (d, *J* = 8.3 Hz, 1H, Ar-H), 6.35 (d, *J* = 8.3 Hz, 1H, Ar-H), 5.99 (dd, *J* = 1.3, 16.0 Hz, 2H, O-CH_2-O), 5.58 (d, *J* = 4.4 Hz, 1H, Ar-CH, (C3-phthalide)), 4.39 (d, *J* = 4.4 Hz, 1H, Ar-CH, (C5'-isoquinoline)), 4.10 (s, 3H, - OCH_3), 4.03 (s, 3H, -OCH_3), 3.94 (s, 6H, 2 x -OCH_3), 3.91 (s, 3H, -OCH_3), 3.86 (s, 3H, -OCH_3),3.01-2.91 (m, 1H, -C*H*H-*N*-CH_3 (C7'- isoquinoline)),

2.75-2.67 (m, 1H, -CH*H*-*N*-CH_3 (C7'- isoquinoline)), 2.55 (s, 3H, *N*-CH_3), 2.47-2.39 (m, 1H, Ar-C*H*H (C8'-isoquinoline)), 2.09-2.00 (m, 1H, Ar-CH*H* (C8'-isoquinoline)). ^{13}C NMR (100 MHz, $CDCl_3$) : δ 168.1, 161.4, 153.4, 152.1, 147.6, 141.4, 140.8, 138.9, 138.6, 134.5, 132.3, 128.6, 125.8, 119.8, 118.4, 117.7, 105.3, 100.8, 81.7, 62.2, 60.9, 59.5, 56.7, 56.1, 54.8, 49.3, 45.8, 22.6. MS (ESI-MS) *m/z*: 607 [M+H]+ HRMS (ESI) : Calcd for $C_{32}H_{35}N_2O_{10}$ [M+H]+: 607.22862, found: 607.22803.

(S)-6,7-dimethoxy-3-((R)-4-methoxy-6-methyl-9-((E)-(quinolin-3-ylmethylene)amino)-5,6,7,8-tetrahydro-[1,3]dioxolo[4,5-g]isoquinolin-5-yl)isobenzofuran-1(3H)-one (13):

Nature: White solid. M.P: 120-122 ºC. IR (KBr): 3446, 2929, 2794, 1757, 1626, 1498, 1443, 1382, 1268, 1036, 1007, 970, 763 cm^{-1}. ^{1}H NMR (400 MHz, $CDCl_3$): δ 9.22 (s, 1H, N=C*H*), 8.35 (d, *J* = 8.5 Hz, 1H, Ar-H), 8.23-8.15 (m, 2H, Ar-H), 7.86 (d, *J* = 7.9 Hz, 1H, Ar- H), 7.79-7.74 (m, 1H, Ar-H), 7.62-7.57 (m, 1H, Ar- H), 7.00 (d, *J* = 8.3 Hz, 1H, Ar-H), 6.31 (d, *J* = 8.3 Hz, 1H, Ar-H), 6.04 (d, *J* = 0.9, 17.7 Hz, 2H, O-C*H*2- O), 5.59 (d, *J* = 4.4 Hz, 1H, Ar-H, (C3-phthalide)), 4.42 (d, *J* = 4.4 Hz, 1H, Ar-H, (C5'-isoquinoline)), 4.10 (s, 3H), 4.07 (s, 3H), 3.85 (s, 3H), 3.16-3.06 (m,1H, -C*H*H-N-CH_3 (C7'-isoquinoline)), 2.78-2.70 (m, 1H, -CH*H*-N-CH_3 (C7'-isoquinoline)), 2.57 (s, 3H, - N-CH_3), 2.49-2.40 (m, 1H, Ar-C*H*H (C8'- isoquinoline)), 2.14-2.03 (m, 1H, Ar-CH*H* (C8'-isoquinoline)). ^{13}C NMR (75 MHz, $CDCl_3$) δ 168.0, 161.8, 155.8, 152.1, 147.9, 147.6, 141.2, 139.77, 139.72, 136.3, 134.4, 130.1, 129.7, 129.5, 128.7, 127.6, 127.4, 124.5, 119.8, 118.2, 118.0, 117.7, 117.6, 101.1, 81.7, 62.2, 60.8, 59.4, 56.7, 49.4, 45.9, 22.9. MS (ESI-MS) *m/z* : 568 [M+H]+ HRMS (ESI) : Calcd for $C_{32}H_{30}N_3O_7$ [M+H]+: 568.20783, found: 568.20704.

(S)-3-((R)-9-((E)-((2,3-dihydrobenzo[b][1,4]dioxin-6-yl)methylene)amino)-4-methoxy-6-methyl-5,6,7,8-tetrahydro-[1,3]dioxolo[4,5-g]isoquinolin-5-yl)-6,7-dimethoxyisobenzo furan-1(3H)-one (14):

Nature: White solid. M.P: 155-157 ºC. IR (KBr) : 3423, 2928, 2796, 1759, 1629, 1578, 1430, 1383, 1294, 1268, 1068, 1034, 1007, 971, 885 cm^{-1}. ^{1}H NMR (400 MHz, $CDCl_3$) : δ 8.71 (s, 1H, N=CH), 7.46 (d, *J* = 1.9 Hz, 1H, Ar-H), 7.36 (dd, *J* = 1.9, 8.4 Hz, 1H, Ar-H), 6.98 (d, *J* = 8.1Hz, 1H, Ar-H), 6.93 (d, *J* = 8.3 Hz, 1H, Ar-H), 6.27 (d, *J* = 8.1 Hz, 1H, Ar-H), 5.98 (dd, *J* = 1.3, 15.5 Hz, 2H, O-CH_2-O), 5.58 (d, *J* = 4.2 Hz, 1H, Ar-CH, (C3-phthalide)), 4.39 (d, *J* = 4.2 Hz, 1H, Ar-CH, (C5'- isoquinoline)), 4.34-4.28 (m, 4H, O-CH_2-CH_2-O), 4.10 (s, 3H, -OCH_3), 4.03 (s, 3H, -OCH_3), 3.86 (s, 3H, -OCH_3), 2.99-2.90 (m, 1H, -C*H*H-*N*-CH_3 (C7'- isoquinoline)), 2.70-2.62 (m, 1H, -CH*H*-*N*-CH_3 (C7'-isoquinoline)), 2.54 (s, 3H, *N*-CH_3), 2.42-2.33 (m, 1H, Ar-C*H*H (C8'-isoquinoline)), 2.02-1.92 (m, 1H, Ar-CH*H* (C8'-isoquinoline)). ^{13}C NMR (100 MHz, $CDCl_3$) : δ 168.1, 161.0,

152.1, 147.6, 146.4, 143.7, 141.3, 138.9, 138.4, 134.6, 130.8, 128.8, 125.9, 122.4, 119.9, 118.2, 117.7, 117.6, 117.4, 116.6, 100.8, 81.8, 64.5, 64.1, 62.2, 60.9, 59.5, 56.7, 49.5, 45.9, 22.8. MS (ESI-MS) *m/z*: 575 [M+H]+ HRMS (ESI) : Calcd for $C_{31}H_{31}N_2O_9$ [M+H]+: 575.20241, found: 575.20129.

(S)-6,7-dimethoxy-3-((R)-4-methoxy-6-methyl-9-((3,4,5-trimethoxybenzyl)amino)-5,6,7,8-tetrahydro-[1,3]dioxolo[4,5-g]isoquinolin-5-yl)isobenzofuran-1(3H)-one (15):

Nature: White solid. M.P: 160-162 ^oC. IR (KBr) : 3406, 2943, 1749, 1591, 1504, 1460, 1432, 1318, 1269, 1123, 1037, 1009, 848 cm^{-1}. ^1H NMR (500 MHz, $CDCl_3$) : δ 6.86 (d, *J* = 8.2 Hz, 1H, Ar-H), 6.56 (s, 2H, Ar-H), 6.02 (d, *J* = 8.2 Hz, 1H, Ar-H), 5.96 (dd, *J* = 1.2, 15.8 Hz, 2H, O-CH_2-O), 5.56 (d, *J* = 4.1 Hz, 1H, Ar-CH, (C3-phthalide)), 4.40 (d, *J* = 4.1 Hz, 1H, Ar-CH, (C5'- isoquinoline)), 4.29 (dd, *J* = 13.8, 51.5 Hz, 2H, *N*CH_2), 4.08 (s, 3H, -OCH_3), 3.94 (s, 3H, - OCH_3), 3.84 (s, 12H, 4 x -OCH_3), 2.64-2.57 (m, 1H, -C*H*H-*N*-CH_3 (C7'-isoquinoline)), 2.52 (s, 3H, *N*-C*H*$_3$), 2.39-2.30 (m, 2H, -CH*H*-*N*-CH_3 (C7'-isoquinoline), Ar-C*H*H (C8'-isoquinoline)), 1.71-1.63 (m, 1H, Ar-CH*H* (C8'-isoquinoline)). ^{13}C NMR (100MHz, $CDCl_3$) : δ 168.0, 153.2, 152.1, 147.5, 140.9, 137.4, 137.1, 135.9, 135.3, 134.8, 124.2, 121.0, 119.9, 118.1, 117.6, 104.6, 100.6, 81.8, 62.2, 60.9, 60.7, 59.6, 56.7, 56.0, 51.4, 49.2, 45.8, 22.5. MS (ESI-MS) *m/z*: 609 [M+H]+ HRMS (ESI): Calcd for $C_{32}H_{37}N_2O_9$ [M+H]+: 609.24427, found: 609.24513.

(S)-6,7-dimethoxy-3-((R)-4-methoxy-6-methyl-9-((quinolin-2-ylmethyl)amino)-5,6,7,8-tetrahydro-[1,3]dioxolo[4,5-g]isoquinolin-5-yl)isobenzofuran-1(3H)-one (16):

Nature: White solid. M.P: 96-98 ^oC. IR (KBr): 3380, 2928, 1757, 1623, 1498, 1443, 1268, 1035, 967, 885, 821, 753, 474 cm^{-1}. ^1H NMR (400 MHz, $CDCl_3$) : δ 8.35 (d, *J* = 8.5 Hz, 1H, Ar-H), 8.21 (d, *J* = 8.5 Hz, 1H, Ar-H), 8.17 (d, *J* = 8.5 Hz, 1H, Ar-H), 7.86 (d, *J* = 8.0 Hz, 1H, Ar-H), 7.78-7.73 (m, 1H, Ar-H), 7.62-7.57 (m, 1H, Ar-H), 7.03 (d, *J* = 8.3 Hz, 1H, Ar-H) 6.44 (d, *J*= 8.3 Hz, 1H, Ar-H), 6.03 (d, *J* = 19.0 Hz, 2H, O-C*H*$_2$-O), 5.93 (bs, 1H, -*NH*), 5.66 (d, *J* = 4.1 Hz, 1H, Ar-CH, (C3-phthalide)), 4.50 (d, *J*= 4.1 Hz, 1H, Ar-CH, (C5'-isoquinoline)), 4.11-4.06 (m, 4H, -*N*C*H*H, -OCH_3), 4.00 (s, 3H, -OCH_3), 3.87-3.83 (m, 4H, -*N*-CH*H*, -OCH_3), 3.16-3.08 (m, 1H, -C*H*H-*N*CH_3 (C7'-isoquinoline)), 2.91-2.81 (m, 1H, -CH*H*-N CH_3 (C7'-isoquinoline)), 2.63-2.52 (m, 4H, Ar-C*H*H (C8'-isoquinoline), *N*-C*H*$_3$), 2.28-2.16 (m, 1H, Ar-CH*H* (C8'-isoquinoline)). ^{13}C NMR (100 MHz, $CDCl_3$) : δ 168.0, 161.9, 155.8, 152.2, 147.9, 147.6, 141.1, 140.0, 139.6, 137.8, 136.3, 134.4, 129.8, 129.6, 128.8, 127.7, 127.5, 124.5, 118.4, 118.0, 117.8, 116.7, 101.2, 81.5, 62.2, 60.9, 59.3, 56.7, 48.9, 47.6, 45.1, 22.4. MS (ESI-MS) *m/z*: 570 [M+H]+

(S)-3-((R)-9-(((2,3-dihydrobenzo[b][1,4]dioxin-6-yl)methyl)amino)-4-methoxy-6-methyl-5,6,7,8-tetrahydro-[1,3]dioxolo[4,5-g]isoquinolin-5-yl)-6,7dimethoxyisobenzofuran-1(3H)-one (17):

Nature: White solid. M.P: 73-75 ^{o}C. IR (KBr): 3392, 2930, 1756, 1592, 1501, 1432, 1386, 1266, 1122, 1036, 921, 882, 812, 740 cm-1. ^{1}H NMR (400 MHz, $CDCl_3$) : δ 6.91-6.76 (m, 4H, Ar-H), 5.98-5.92 (m, 3H, Ar-H, O-C*H*$_2$-O), 5.56 (d, *J* = 4.1 Hz, 1H, Ar-CH, (C3-phthalide)), 4.41 (d, *J* = 4.1 Hz, 1H, Ar-CH, (C5'-isoquinoline)), 4.32 (d, *J* = 13.9 Hz, 1H, *N*-CH_2*H*), 4.24 (s, 4H, O-C*H*$_2$-C*H*$_2$-O), 4.17 (d, *J* = 13.9 Hz, 1H, *N*-CH_2*H*), 4.08 (s, 3H, -OCH_3), 3.95 (s, 3H, -OCH_3), 3.84 (s, 3H, -OCH_3), 2.59-2.49 (m, 4H, -C*H*H-*N*-CH_3 (C7'-isoquinoline), *N*-C*H*$_3$), 2.36-2.25 (m, 2H, -CH*H*-N-CH_3 (C7'-isoquinoline), Ar-C*H*H (C8'-isoquinoline)), 1.65-1.53 (m, 1H, Ar-CH*H* (C8'- isoquinoline)). ^{13}C NMR (100 MHz, $CDCl_3$) : δ 168.0, 152.0, 147.4, 143.3, 142.6, 140.8, 137.1, 135.4, 134.5, 133.7, 124.2, 120.9, 120.5, 120.0, 117.9, 117.7, 117.6, 117.1, 116.4, 100.5, 81.9, 64.2 (x2), 62.1, 60.8, 59.6, 56.6, 50.3, 49.4, 46.0, 22.6. MS (ESI-MS) *m/z*: 576 [M+H]+ HRMS (ESI) : Calcd for $C_{31}H_{33}N_2O_9$ [M+H]+: 576.21806, found: 576.21835.

3.2.10. Cell culture and reagents

All the chemical reagents and media were obtained from Sigma. Human breast cancer cell line, MCF7 and MDA-MB-231 were obtained from the cell repository of the National Center for Cell Science Pune, Maharashtra, India. The primary breast cancer cells were isolated from the surgically removed tumor tissues of patients. The approval from the Institutional ethical committee of King George's Medical University, Lucknow, Uttar Pradesh, India and the consent from the patients was taken for the use of samples. Stock solution (100 mM) of the newly synthesized 9-(N-arylmethylamino) noscapinoids, **15-17** was prepared with dimethyl sulfoxide (DMSO) and stored at 4˚C. The cells were grown at a temperature of 37 °C in a 5% CO_2 and 95% humidity in Dulbecco's modified Eagle medium (DMEM, Sigma), supplemented with 10% fetal bovine serum (FBS) and antibiotics. Cells with a 70-80% confluence were subcultured for bioassays using trypsin-EDTA (0.25%).

3.2.11. *In vitro* cell proliferation assay using MCF-7 and MDA-MB-231 breast cancer cell lines

The cell proliferation assay was performed using MCF7 and MDA-MB-231 human breast cancer cell lines as reported earlier (Naik et al, 2011). In brief, cells were grown in a culture medium (MEM, DMEM) supplemented with 10% FBS, 1% penicillin/streptomycin, 2 mM l-glutamine at 37 °C and 5% CO_2. In a 96-well plate cells were plated at a density of $5x10^3$ cells per well and were treated with increasing

concentrations (5 µM to 100 µM) of noscapine and 9-(N-arylmethylamino) noscapinoids, **15-17**for 72h. The cells were then stained with 0.4% sulforhodamine B (dissolved in 1% acetic acid). The unbound dye was removed by washing with 1% acetic acid. The protein-bound dye was then extracted with 10 mM Tris base and the absorbance was measured at 564 nm wavelength using a SPECTRAmax PLUS 384 microplate spectrophotometer. The IC_{50} values (the drug concentration required to achieve a cell kill of 50%)of the compounds were determined using the online tool Quest GraphTM IC_{50} Calculator (AAT Bioquest, Inc., Sunnyvale, CA, USA, https://www.aatbio.com/tools/ic50-calculator).

3.2.12. Culture of primary breast tumor cells and in vitro cell proliferation assay

Primary breast tumor cells were isolated from the surgically removed breast tumor tissue of patients (8 nos.) with different stages of breast cancer before drug treatment in aseptic condition. The tumor tissues were treated with 0.25% trypsin and filtered with 70-micron filter followed by centrifugation at 2000 rpm for 3 minutes with serum-free medium. The filtered cells were collected and plated in T25 flask and incubated with complete DMEM medium, supplemented with 10% FBS and 1% pentrip (mixture of penicillin and streptomycin) at 37 °C under 5% CO_2. Fresh media was replaced every 3-4 days, and subsequent passages were performed under the same conditions as mentioned above. The cultured were maintained for homogeneous cell type at sub-confluence between 3-8 passages. After the confluence (70 to 80%) was reached, the tumor cells were plated at 2000 cells/well in 96 wells plate with standard growth media, DMEM (low glucose). The cells were maintained at 37 °C in a humidified atmosphere with 5% CO_2 and were treated with gradient concentrations (5 µM to 100 µM) of noscapine and 9-(N-arylmethylamino) noscapinoids, **15-17**for 72h. Quantification of cells was performed by sulforhodamine B assay, using the CellTiter96 AQueous One Solution Reagent (Sigma). Cells were treated with sulforhodamine B for 30 minutes, the unbound dye was removed by washing and the bound dye was extracted with 1mM tris. The absorbance was measured using a SPECTRAmax PLUS 384 microplate spectrophotometer at a wavelength of 564 nm. The percentage of cell survival as a function of drug concentration was plotted and theIC_{50} value was determined using the online tool, AAT Bioquest.

3.2.13. Flow cytometry analysis of cell cycle progression

MDA-MB-231 cells were grown in DMEM with 4.5 g/L glucose and L-glutamine supplemented with 10% FBS and 1% penicillin/streptomycin at 37 ^{0}C in 5% CO_2. Cells were treated with IC_{50} concentration of noscapine and 9-(N-arylmethylamino) noscapinoids, **15-17,** dissolved in 1% phosphate buffer saline (PBS) for 72h. For the flow

cytometer analysis, $2x10^6$ cells were harvested and centrifuged;the pellets were washed with ice-cold PBS, and then fixed in 70% ethanol. The cell pellets were centrifuged at 1000 x g for 10 min and the pellets were resuspended in 30 µL of phosphate/citrate buffer (0.2 M Na_2HPO_4/0.1 M citric acid, pH 7.5) at room temperature. After 30 min the cell pellets were washed with 5 mL of PBS and incubated with 0.5 mL of propidium iodide (20 µg/mL in 0.6% Triton-X in PBS) and 0.5 mL of RNase A (20 µg/ml in PBS) for 45 min. in dark. Samples were analysed on a flow cytometer (BD FACS Aria-III) and the progress in the cell cycle was determined.

3.2.14. Flow cytometry analysis for apoptosis assay

Apoptosis in cancer cells was detected by Annexin-V-FITC detection method by using an apoptosis detection kit (Sigma). For experimental purposes $3x10^4$ cells per well were seeded on 12 well culture plate and incubated for 24h with complete medium. The cells were treated with IC_{50} concentration of noscapine and 9-(N-arylmethylamino) noscapinoids, **15-17**for 72h. Cells were trypsinized and stained with surface marker antibodies (biotin-conjugated Annexin V, FITC-conjugated streptavidin) and propidium iodide (PI) in 1X binding buffer for 20 min in dark condition at room temperature. Flow cytometer data with 488 nm excitation for PI and emission at 530 nm were collected. Viable cells (Annexin V^- / PI^-), early apoptotic cells (Annexin V^+ / PI^-), late apoptotic/necrotic cells (Annexin V^+ / PI^+) and late necrotic cells (Annexin V^- / PI^+) were identified and determined their percentage.

3.2.15. DAPI staining

Apoptotic cells with the treatment of test compounds were visualized by inverted fluorescence microscopy following DAPI staining. MDA-MB-231 cells were grown on poly-L-lysine coated coverslips in 6-well plates and were treated with noscapine and 9-(N-arylmethylamino) noscapinoids, **15-17**at IC_{50} concentration for 72h. After incubation, coverslips were fixed in cold methanol and washed with PBS, stained with DAPI, and mounted on slides. Images were captured using an inverted fluorescent microscope (Nikon Eclipse Ts2R-FL). Apoptotic cells were identified by changes in morphology compared to untreated cells.

3.2.16. Acridine Orange (AO)& Ethidium bromide (Etbr) staining

MDA-MB-231 cancer cells were grown in culture plates and treated with noscapine and 9-(N-arylmethylamino) noscapinoids, **15-17**at IC_{50} concentration for 72h. After incubation, coverslips were fixed in cold methanol and washed with PBS. It was stained with acridine orange and ethidium bromide and mounted on slides. Images were

captured using an inverted fluorescent microscope (Nikon Eclipse Ts2R-FL). Apoptotic cells were identified by changes in morphology compared to untreated cells.

3.2.17. Tubulin purification

Tubulin was purified from the goat brain via temperature cycles and GTP-dependent polymerization and depolymerization (Hamel and Lin, 1981; Panda etal., 2000) using PEM buffer (50 mM pipes, 3 mM $MgSO_4$, and 1 mM EGTA, pH 6.8). The amount of tubulin in the extract was estimated by the Bradford method using BSA as the standard (Bradford 1976). The purified tubulin was frozen and stored at -80 °C for further use.

3.2.18. Tubulin binding assay

Tubulin is autofluorescence in nature due to the presence of several tryptophan residues. Therefore, to examine the tubulin-binding of chemical compounds, a fluorescence titration was used to analyse the quenching of the intrinsic fluorescence of tubulin (Dash et al, 2020). The purified tubulin (2 µM) was treated with 9-(N-arylmethylamino) noscapinoids, **15-17**at a concentration of 25 µMin PEM buffer (50 mM pipes, 3 mM MgSO4, 1 mM EGTA, pH 6.8) for 45 min at 35 ˚C. The samples were excited at 295 nm and the emission spectrum was measured at 310-400 nm. For the spectrofluorometric titrations, a FlouroMax ® 4 spectrofluorometer (Horiba Scientifc, Edison, NJ) assisted by Fluor Essence 3.5 software was used. The experiments were repeated twice.

3.3. Results and Discussion

A battery of noscapine derivatives was developed in past decades to increase the efficacy in inhibiting cancer cell proliferation. Many of these derivatives revealed high tubulin binding affinity as indicated by lowering the dissociation constant ($K_d$value) to several folds compared to the lead molecule, noscapine (Naik et al., 2012; Aneja et al., 2006; Aneja et al., 2006; Jain et al., 2011; Santoshi et al., 2015).The available experimental data led us to develop a reasonable predictive model for determining the binding affinity of newly designed 9-(N-arylmethylamino) noscapinoids and screening promising derivatives. We are reporting in this study a panel of three 9-(N-arylmethylamino) noscapinoids, **15-17**as potent anticancer agents.

3.3.1. Molecular docking of designed noscapinoids with tubulin

Noscapinoids, previously reported (Figure 3.2) and newly designed in this study (Figure 3.1)were docked onto the binding pocket of noscapinoids (Oliva et al., 2020) and evaluated using a Glide XP_{score} function (Friesner et al., 2004; Halgren et al., 2004).All the noscapinoids were found to docked well within the binding pocket with improved docking

score (ranged from -2.038 to -4.492 kcal/mol) compared to noscapine (-1.927 kcal/mol) (Table 3.1). Further, the best docked poses of each noscapinoid were considered for determining the binding energy with tubulin based on LIE-SGB calculations.

Table 3.1. Molecular docking results (Glide XP) as well as calculated energies using Liasion programme (Schrodinger package) of noscapine and its derivatives: van der Waals energy (U_{vdw}), Columbic energy (U_{coul}), reaction energy (U_{rxn}) and cavity energy (U_{cav}) as well as predicted binding free energy ($\Delta G_{bind,pred}$) based on LIE-SGB prediction model and experimental binding free energy ($\Delta G_{bind,expt}$). The newly designed 9-(N-arylmethylamino) noscapinoids,**15-17** revealed improved $\Delta G_{bind,pred}$compared to the lead molecule, noscapine.

Ligand	Glide XP_{score} (kcal/mol)	$<U_{vdw}>$ (kcal/mol)	$<U_{coul}>$ (kcal/mol)	$<U_{rxn}>$ (kcal/mol)	$<U_{cav}>$ (kcal/mol)	Experimental ΔG_{bind} (kcal/mol)	Predicted ΔG_{bind} (kcal/mol)
1	-1.927	-45.14	-330.8	135.5	2.097	-5.246	-5.212
2	-2.038	-49.00	-210.2	116.0	3.283	-6.006	-6.178
3	-2.766	-42.50	-362.1	155.9	4.208	-5.827	-6.060
4	-2.940	-48.06	-355.8	168.7	2.548	-5.587	-5.899
5	-3.263	-47.69	-285.7	135.5	3.103	-6.360	-5.987
6	-4.492	-47.44	-77.3	118.2	3.954	-6.628	-6.668
7	-2.605	-33.39	-331.9	176.7	4.465	-5.551	-5.657
8	-2.287	-45.57	-277.9	112.3	3.285	-5.665	-5.706
9	-2.350	-33.47	-324.5	152.5	3.766	-5.783	-5.151
10	-3.679	-45.41	-471.2	152.8	3.669	-5.673	-5.790
11	-4.687	-42.69	-267.6	129.9	3.465	-5.518	-5.722
15	-4.175	-56.30	-268.8	122.9	3.766	Nd	-6.694
16	-4.208	-47.20	-422.3	193.8	5.486	Nd	-7.118
17	-3.941	-58.31	-266.2	137.7	5.473	Nd	-7.732

3.3.2. Predictive binding affinity of 15-17 with tubulin (LIE-SGB calculation)

The predicted binding energy ($\Delta G_{bind,pred}$) of 9-(N-arylmethylamino) noscapinoidswith tubulin was determined based on the LIE-SGB empirical prediction model developed in this study by using the experimental activity of training set molecules (Table 3.1). Different interaction energy terms used in the model were included inTable 3.1.The values of the coefficients α, β, γ and δ for nonbonding interactions terms U_{vdw}, U_{coul}, U_{rxn} and $U_{cav}$are 0.08446, -0.00223, -0.000872 and -0.45601, respectively. The largestcontribution for the binding free energy comes from the van derWaals interactions. The predicted binding energy ($\Delta G_{bind,pred}$) of the training set molecules based on the LIE-SGB model is very close to the experimental binding energy ($\Delta G_{bind,expt}$) (root mean square error was 0.223 kcal/mol).The accuracy of the prediction model is determined from the value of the squared correlation coefficient (R^2 = 0.998) and analysis of variance (F-value = 3742.6).

$$\Delta G_{bind,pred} = 0.08446\langle U_{vdw}\rangle - 0.00223\langle U_{coul}\rangle - 0.00872\langle U_{rxn}\rangle - 0.45601\langle U_{cav}\rangle$$
$$(n = 11, R^2 = 0.998, s = 0.243, F = 3742.6, P \leq 0.001)$$

The LIE-SGB model was used to predict the $\Delta G_{bind,pred}$ of the newly designed 9-(N-arylmethylamino) noscapinoids. The top three 9-(N-arylmethylamino) noscapinoids (Figure 3.3) that revealed improved$\Delta G_{bind,pred}$of -6.694 kcal/mol for **15**, -7.118 kcal/mol for **16**and -7.732 kcal/mol for **17**, compared to noscapine (-5.135 kcal/mol) were screened out for chemical synthesis and experimental evaluation. All the three compounds also have improved docking score (-3.941 kcal/mol for **15**, -4.175 for **16** and -4.208 for **17**).

3.3.3. MD simulations and prediction of predicted binding free energy using MM-PBSA

The docked complexes of 9-(N-arylmethylamino) noscapinoids,**15-17** with tubulin were used to perform MD simulations of 100 ns to observed their stability, followed by MM-PBSA calculation to determine their predicted binding energy ($\Delta G_{bind,pred}$). The convergence of the MD trajectories was monitored by plotting root mean square deviation (RMSD) and radius of gyration (Rg) of the backbone C_α atoms with respect to time. The RMSD and the Rgvalues were very small after ~40 ns suggesting the stability of the system (Figure 3.5 and 3.6). It was also observed that the root mean square fluctuations (RMSF) of most of the residues of tubulin in the bound form with ligands and in the free form were not so much different (within the range of 1 to 2.5 Å) indicating that the residues were more rigid. However, only very few residues showed fluctuation >5 Å, indicating that these residues seem to be more flexible (Figure 3.7).

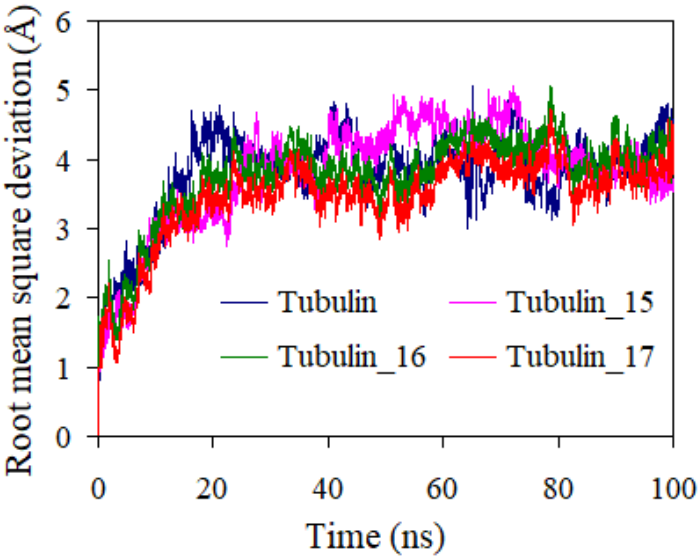

Figure 3.5. Root mean square deviations (RMSD) of Cα carbon atoms of tubulin only and in complex with 9-(N-arylmethylamino) noscapinoids,**15-17**during 100 ns of MD simulation. The relative fluctuation in the RMSD of the Cα atoms is very small after ~ 20 ns of the simulation. The time step of 20ps was used during the simulation that generated 5,000 frames.

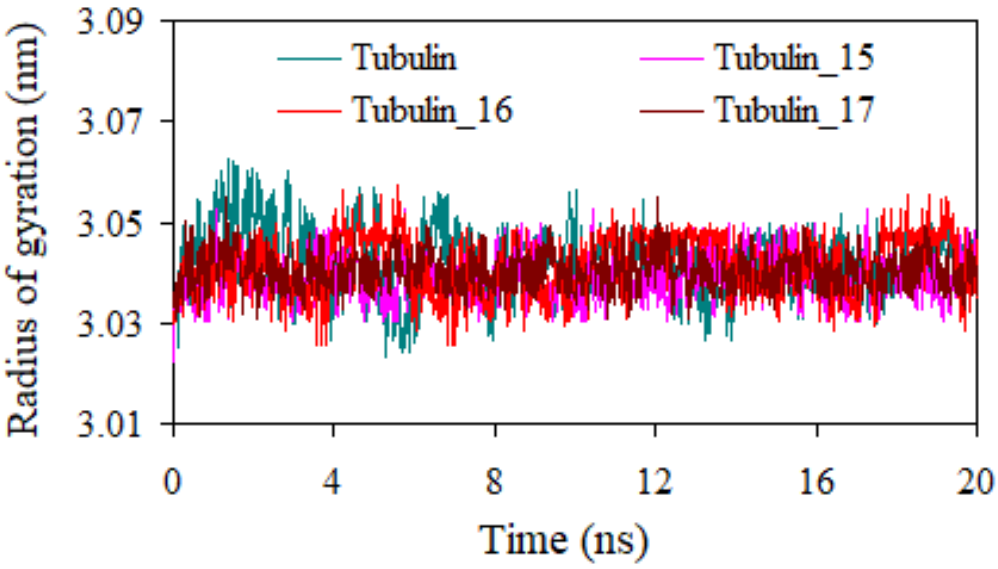

Figure 3.6. Time evolution of radius of gyration of the tubulin and its complex with 9-(N-arylmethylamino) noscapinoids,**15-17**over a period of 100 ns of MD simulation. All the molecular systems were found to be stable after 40 ns of simulation.

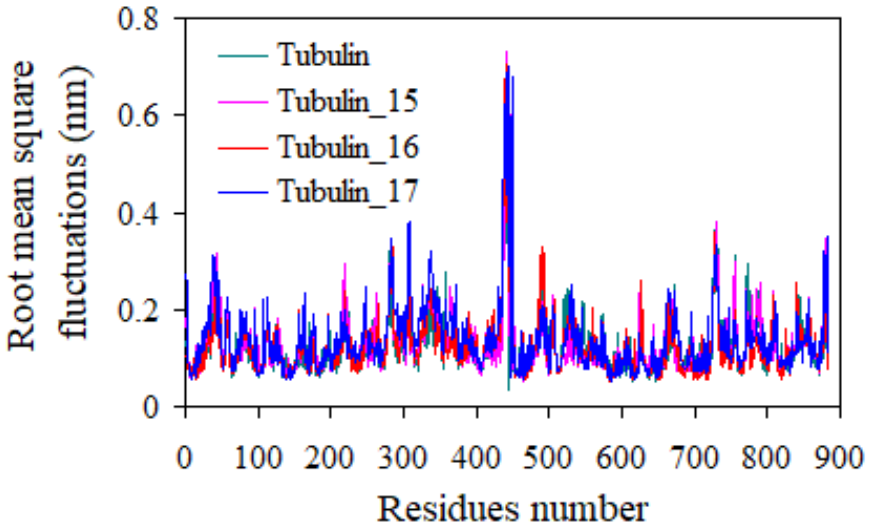

Figure 3.7. Root mean square fluctuation (RMSF) of the residues of tubulin of the docked ligands in the bound form and in the unbound form of tubulin heterodimer. Different levels of flexibility of these residues were noticed in the free and bound form of tubulin with ligands. Only very few residues showed flexibilities > 0.5 nm indicating that most of the residues were rigid both in free and bound form of tubulin.

All the three 9-(N-arylmethylamino) noscapinoids,**15-17**were found to accommodate well inside the binding cavity (Figure 3.8) at the interface between α- and β-tubulin. However, their binding modes inside the binding cavity are distinct as shown in the ligplotmay be due to different functional groups (Figure 3.9). As shown in the figure the most potent 9-(N-arylmethylamino) noscapinoid **17**in terms of binding energy and docking score interacts more intensely with the residues of tubulin compared to the other two derivatives. Its binding involved 4 hydrogen bonds (dashed line). The oxygen atom O10 hydrogen bonded with the side chain nitrogen atom (ND2) of residue AsnA228 (bond

length 3.04 Å), the nitrogen atom (N1) form 03 hydrogen bonds with side-chain oxygen atom (OE_2) of Glu A77 (bond length 4.15 Å), OE1 of Glu A77 (bond length 4.27 Å) and OE1 of Gln A15 (bond length 3.3 Å) (Figure 3.9c). In contrast, the binding of 9-(N-arylmethylamino) noscapinoids, 15 and 16involved only 3 hydrogen bonds with the binding site residues (Figure3.9a,b). In case of molecule **15**,the oxygen atom O8 hydrogen bonded with the side chain nitrogen atom (ND2) of residue Asn A228 (bond length 2.75 Å), the nitrogen atom N1 form two hydrogen bonds with side chain oxygen atoms (OE1) of Glu A77 (bond length 4.93 Å) and Gln A15 (bond length 3.32 Å). Similarly in case of molecule **16**, the oxygen atom (O3) hydrogen bonded with the side chain nitrogen atom (NE2) of Gln B247 (bond length 3.06 Å), the nitrogen atom (N1) form hydrogen bond with the side chain oxygen atom (OE2) of residue Glu B47 (bond length 2.88 Å) and the nitrogen atom (N3) hydrogen bonded with the side chain oxygen atom (OG1) of residue Thr A73 (bond length 4.07Å).Besides, hydrogen bonding, a good number of hydrophobic interactions were involved in the binding of 9-(N-arylmethylamino) noscapinoids **15-17** with binding site residues (Supplementary Table S1-S4). Inspired by our computational findings, we have chemically synthesized the newly designed -(N-arylmethylamino) noscapinoids **15-17** to further evaluate their anticancer potential.

The predictive binding free energy ($\Delta G_{bind,pred}$) of noscapine and its 9-(N-arylmethylamino) noscapinoids,**15-17**based on MM-PBSA is collated in Table 3.2. It is revealed that the 9-(N-arylmethylamino) noscapinoids,**15-17**have high $\Delta G_{bind,pred}$(ranges from -167.4 kcal/mol to -178.6 kcal/mol) compared to noscapine (-156.3 kcal/mol). Both the intermolecular van der Waals (ΔE_{vdw})and the electrostatic (ΔE_{ele}) interactions were found to be significant contributors to the binding energy. Also, the non-polar solvation terms (ΔG_{sol-np}), which define the burial of solvent-accessible surface-area upon binding was somewhat favorable to the binding of ligands. In contrast, the polar solvation terms (ΔG_{PB}) and the electrostatic interaction energy ($\Delta G_{ele,PB}$) were not favorable to the binding of ligands. This might be due to the large desolvation penalty of charged and polar groups. The hydrogen bonding energy contribution of binding site amino acids for the binding of the noscapine and its 9-N-arylmethylamino derivatives is included in Table 3.3. The hydrogen bonding energy contribution was found to be high for 9-N-arylmethylamino noscapinoids, **17** compared to 16 and 15.

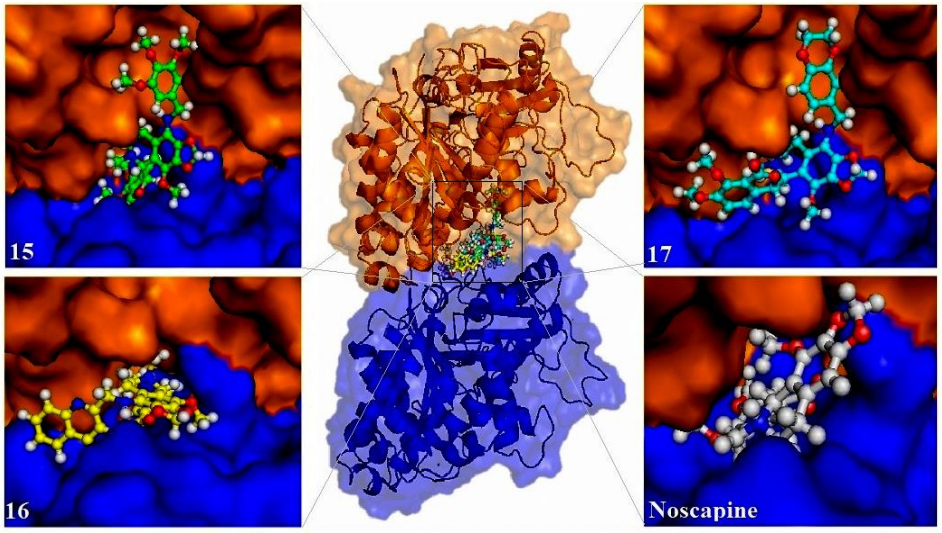

Figure 3.8. The newly designed 9-(N-arylmethylamino) noscapinoids, **15-17** are well accomodated inside the noscapine binding site at the interface of α- and β- tubulin. The binding site is represented as macromodel surface according to α- and β- tubulin (α-tubulin is represented in blue colour and β-tubulin is represented in brown colour).

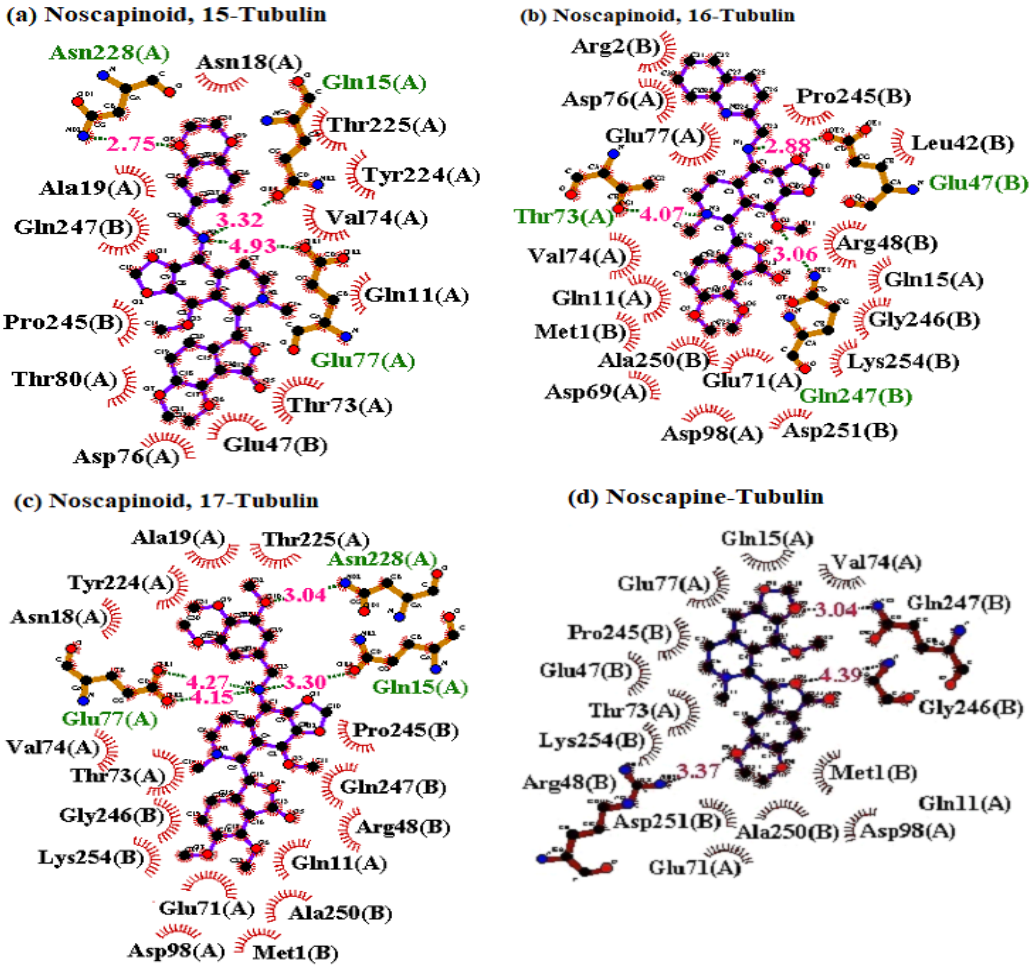

Figure 3.9. Two dimensional representation of interaction observed between the binding site residues of tubulin with 9-(N-arylmethylamino) noscapinoids, **(a) 15, (b) 16, (c) 17** and **(d) Noscapine**. Dashed lines denote hydrogen bonds and numbers indicate hydrogen bond lengths in Å. Hydrophobic interactions are shown as arcs with radial spokes. The figure was made using LIGPLOT. The residues within 5 Å distance from the docked ligands were only shown in the figures.

Table 3.2: Binding free energy and its components (kcal/mol) for noscapine and its 9-N-arylmethylamino derivatives, **15-17** with the receptor αβ tubulin dimmer.

.Energy components (kcal/mol)	Noscapine	15	16	17
ΔE_{vdw}	-56.22	-32.64	-35.91	-57.90
ΔE_{ele}	-202.5	-184.3	-177.3	-190.6
$\Delta G_{solv,PB}$	108.6	52.48	47.45	76.26
ΔG_{sol-np}	-6.19	-4.28	-4.74	-6.38
$\Delta G_{bind,\ PBSA}$	-156.3	-167.4	-170.5	-178.6

Table 3.3: Hydrogen bonding energycontribution of binding site amino acids of αβ tubulin dimmer for the binding of noscapine and its 9-N-arylmethylamino derivatives. The hydrogen bonds with a distance of ≤ 3.6 Å are only considered for the calculation.

Binding site residues	Hydrogen bonding energy contribution (kcal/mol)			
	Noscapine	15	16	17
Gln 247(B)	-0.493	-	-0.462	-
Arg 48(B)	-0.262	-	-	-
Asn 228(A)	-	-0.463	-	-0.482
Gln 15(A)	-	-0.402	-	-0.452
Glu 47(B)	-	-	-0.436	-

3.3.4. N-alkyl amine-noscapinoids15-17inhibits proliferation of MCF-7 and MDA-MB-231

Based on our *in silico* results, we next want to test if the 9-(N-arylmethylamino) noscapinoids,**15-17,** affected proliferation of breast cancer cell lines, MCF-7 and MDA-MB-231. N-arylmethylamino-noscapinoids,**15-17** exhibited potent cytotoxic activity in comparison to noscapine using both the cell lines (Figure 3.10). The IC_{50} values for the test compounds for both the cell lines are collated in Table 3.4.The IC_{50} value amounted to 62.2µM, 11.2 µM, 8.03 µM and 3.8µM for noscapine, **15, 16**and**17**, respectively for MCF-7 cells. Parenthetically, a similar modest IC_{50} value of 59.8µM, 24.4µM, 9.7µM and 6.4µM was measured for noscapine, **15, 16** and **17**, respectively for MDA-MB-231 cells.

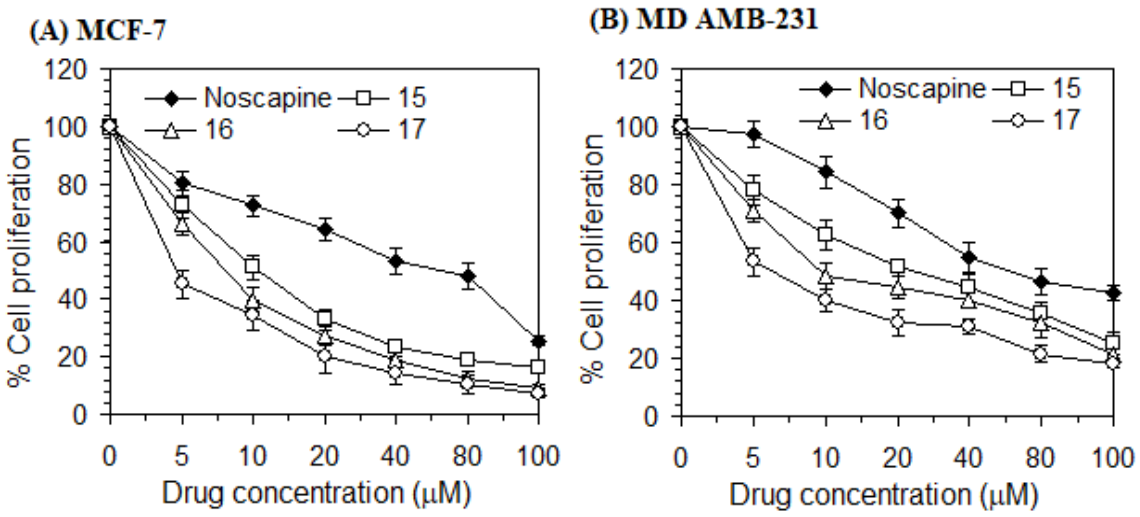

Figure: 3.10. The 9-(N-arylmethylamino) noscapinoids, **15-17**are more active compared to noscapine in inhibiting the proliferation of human breast cancer cells. Both (A) MCF-7 and (B) MDA-MB-231cells were treated with noscapine and its 9-(N-arylmethylamino) noscapinoids, **15-17** for 72h. Each value represents the average of 3 independent experiments.

Table 3.4. IC_{50} values of novel 9-(N-arylmethylamino) noscapinoids,**15-17** using two human breast adenocarcinoma cell lines, MCF-7 and MDA-MB-231. All the novel derivatives were found to have improved antiproliferative activity compared to noscapine.

	IC_{50} (μM)			
	Noscapine	**15**	**16**	**17**
MCF-7	44.3±3.9	11.2±2.5	7.9±1.7	3.9±0.8
MDA-MB-231	58.4±4.8	24.9±2.9	14.8±1.4	5.4±1.2

3.3.5. 9-(N-arylmethylamino) noscapinoids, 15-17 inhibits proliferation of primary breast tumor cells

We next wanted to evaluate whether the newly developed 9-(N-arylmethylamino) noscapinoids, **15-17**also inhibit the proliferation of primary breast tumor cells. We have obtained the surgically removed breast tumor samples from 08 different patients with different stages of breast cancer and isolated the primary cancer cells. The IC_{50} values for the test compounds are collated in Table 3.5. The IC_{50} value ranges from 41.8 to 51.5 μM for noscapine, 21.3 to 32.2 μM for **15**, 9.9 to 16.9 μM for **16** and 3.2 to 8.7 μM for **17** using a panel of primary breast tumor cells (Table 3.5). All the N-arylmethylamino-noscapinoidsdeveloped exhibited potent cytotoxic activity in comparison to noscapine using all the primary breast cancer cells (Figure 3.11).

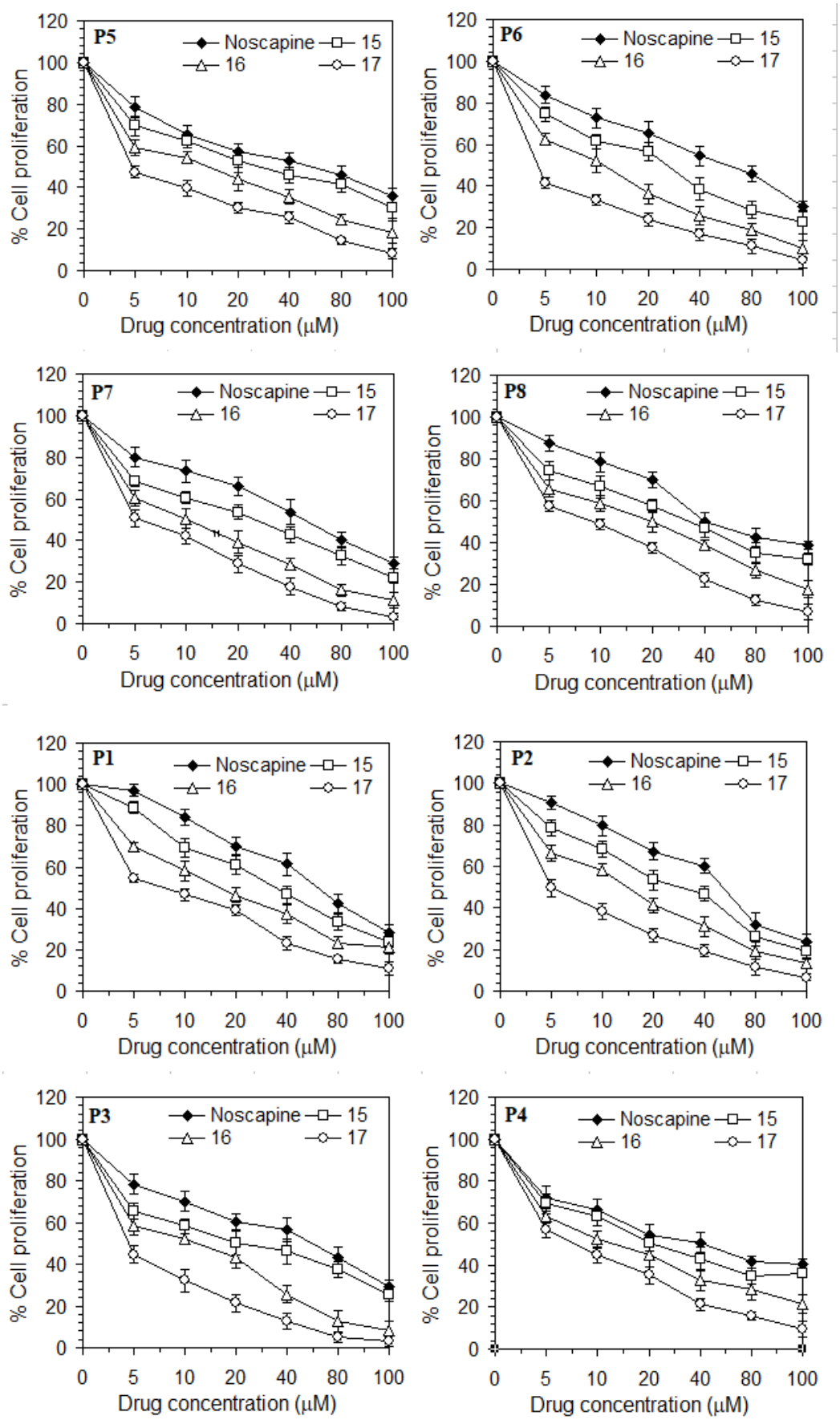

Figure: 3.11. The 9-(N-arylmethylamino) noscapinoids, **15-17** are more active compared to noscapine in inhibiting the proliferation of a panel of human primary breast tumor cells. All the cells treated with **15-17** for 72h. Each value represents the average of 3 independent experiments.

Table 3.5. IC_{50} values of novel 9-(N-arylmethylamino) noscapinoids,**15-17** using primary breast tumorr cells isolated from breast tumor tissue of different patients. All the novel derivatives were found to have improved antiproliferative activity compared to noscapine.

	IC_{50} (µM)			
Primary breast tumor cells.	**Noscapine**	**15**	**16**	**17**
1	51.5±5.7	32.2±4.3	16.5±2.4	7.9±1.2
2	44.2±4.9	25.6±3.9	13.4±2.9	5.1±0.8
3	42.3±5.3	20.9±3.5	10.4±2.3	4.1±0.6
4	38.2±5.5	24.8±4.2	12.5±1.9	7.6±1.3
5	41.8±4.7	27.4±3.4	11.8±3.1	4.7±1.5
6	46.8±4.9	22.3±3.7	10.1±2.8	3.2±0.6
7	43.3±5.3	21.3±2.8	9.9±1.9	6.1±0.5
8	50.4±4.2	30.8±2.6	16.9±1.6	8.7±0.8

3.3.6. N-arylmethylamino-noscapinoids induced apoptosis to cancer cells

The induction of apoptotic cell death to breast cancer cell with the treatment of N-alkyl amine-noscapinoids was investigated by FACS using fluorescent dyes, annexin V and propidium iodide (PI). The phosphatidylserine translocated to outer leaflet of cell membrane during apoptosis is labelled with annexin V. In contrast, the DNA-binding fluorescent dye, propidium iodide intercalates with the DNA when the cells are undergone apoptosis. Thus the apoptotic cells are quantified to large extent using both the dyes by FACS analysis. The percentage of early and late apoptotic cells using MDA-MB-231 cell lines for the treatment of noscapine and its N-alkyl amine-noscapinoids, **15-17** with IC_{50} concentration for 72h is collated in Table 3.6. Representative figures of flow cytometry analysis are included in Figure 3.12. After 72h, the control untreated cell culture contained only very few early apoptotic (3.5%) and late apoptotic cells (2.0%), which were considered as the background cell death due to regular trauma during cell culture (Table 3.6). However, the percentage of early apoptotic cells of20%, 15%, 15%, and 6% as well as late apoptotic cells of 25%, 30%, 40% and 24% with treatments of noscapine and its N-alkyl amine-noscapinoids, **15-17**, respectively were found to be significantly high compared to controlled untreated cells (Table 3.6).

Besides, morphological examination using DAPI, Acridyne orange and Ethidium bromide staining revealed apoptotic cell death of MDA-MB-231 cancer cells characterized by condensed chromatin, formation of membrane blebs and numerous fragmented nuclei (Figure 3.12&3.13).

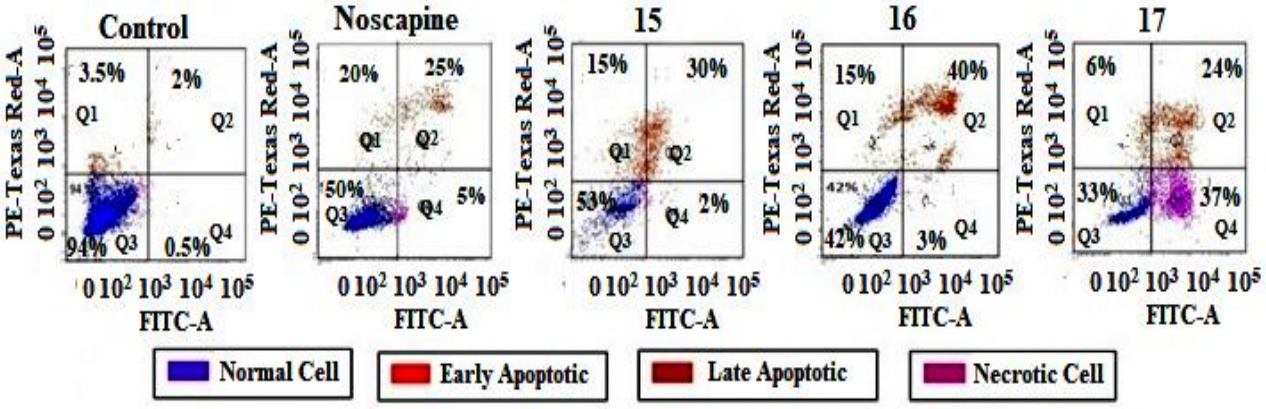

Figure 3.12. Flow cytometry analysis of induction of apoptosis in MDA-MB-231 cells treated with noscapine and its 9-(N-arylmethylamino) noscapinoids, **15-17** with IC_{50} concentration for 72 hours. Cells with PI- and Alexa Fluor 488- indicate viable cells, PI- and Alexa Fluor 488+ indicate early apoptotic cells, PI+, Alexa Fluor 488+ indicate late apoptotic cells.

Table 3.6. Percentage of early apoptotic (Q1), late apoptotic (Q2), viable (Q3) and necrotic (Q4) cells with the treatment of 9-(N-arylmethylamino) noscapinoids,**15-17**measured by flow cytometry.

Viability/Apoptotic	Control	Noscapine	15	16	17
Q1	3.5%	20%	15%	15%	6%
Q2	2%	25%	30%	40%	24%
Q3	94%	50%	53%	42%	32.4%
Q4	0.5%	5%	2%	3%	37%

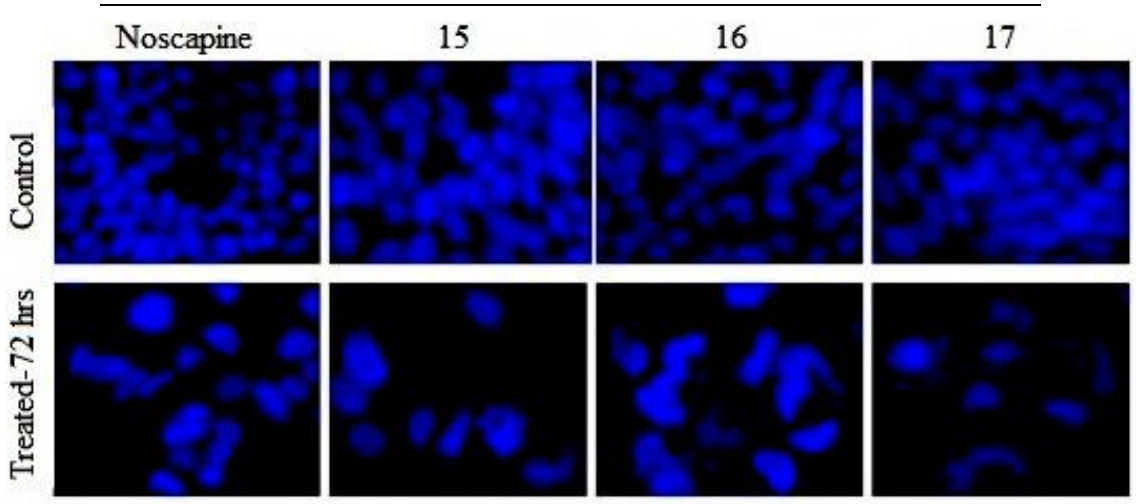

Figure 3.13. The changes in morphological characters such as chromatin condensation, plasma membrane blebbing and appearance of small, apoptotic bodies indicated the apoptotic cells. Panels show morphological features of cells stained with DAPI from control cells (upper panels) and cells treated with IC_{50} concentration of noscapine and 9-(N-arylmethylamino) noscapinoids, **15-17** (lower panels) for 72 hours.

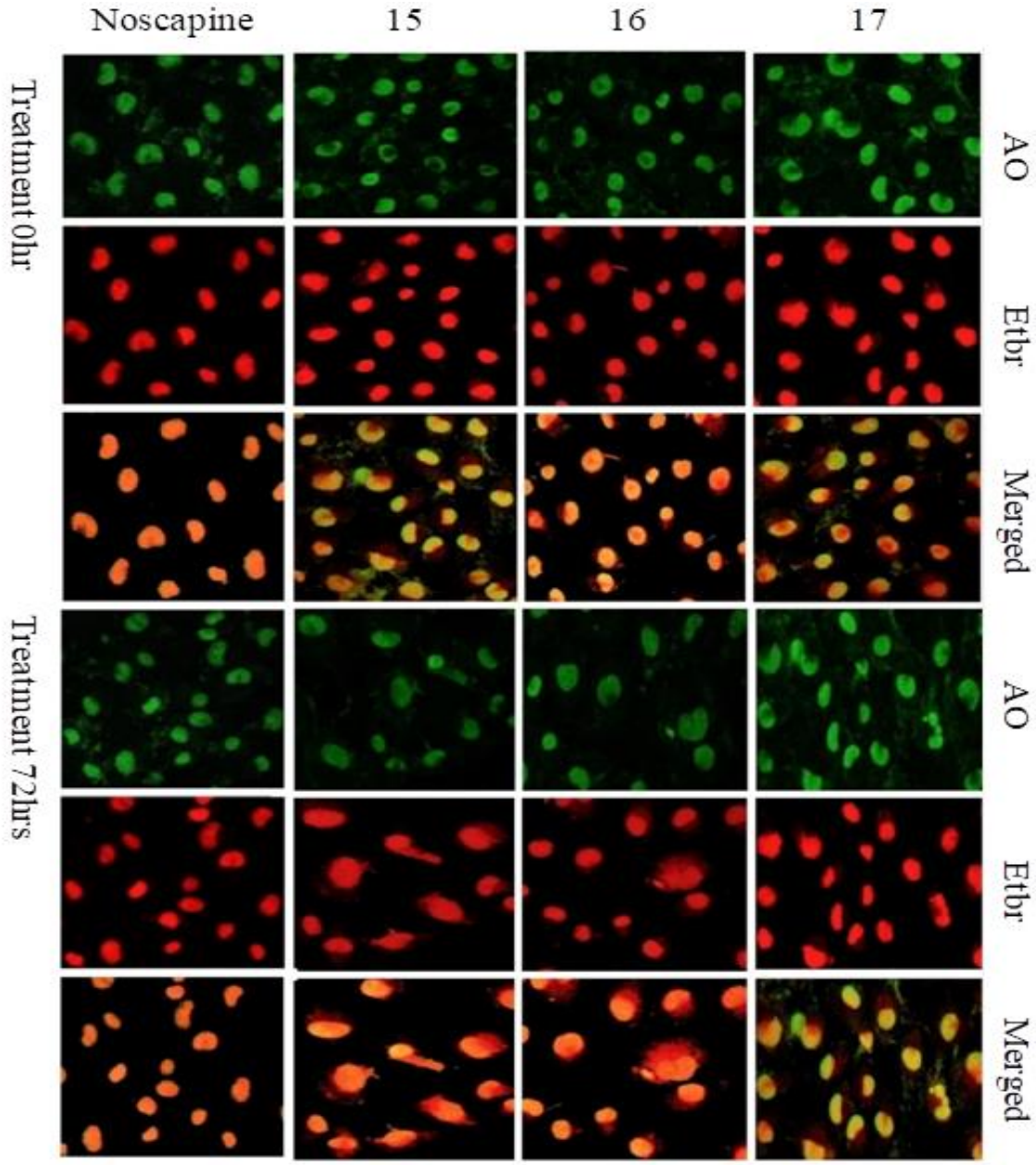

Figure 3.14. The changes in morphological characters such as chromatin condensation, plasma membrane blebbing and appearance of small, apoptotic bodies indicated the apoptotic cells. Panels show morphological features of cells stained with AO, EtBr and merged channel of AO and EtBr from 0h treatment (upper panels) and cells treated with IC_{50} concentration of noscapine and 9-(N-arylmethylamino) noscapinoids, **15-17** (lower panels) for 72 hours using fluorescence microscopy.

3.3.7. Interference in cell cycle progression by 9-(N-arylmethylamino) noscapinoids

The effect of noscapine and 9-(N-arylmethylamino) noscapinoids, **15-17** (25 µM concentration) on the cell cycle progression of MDAMB-231 based on FACS analysisis represented in Figure 3.14. Accumulation of fluorescently labelled DNA in presence of noscapinoid, demonstrates the perturbation of cell cycle and cell death. The presence of 2N DNA indicate that the cells are in the G1 phase, while the accumulation of duplicated 4N DNA indicates that the cells are in G2 and M phases. Accumulation of DNA in between 2N and 4N peaks represents, the cells are in the S phase. In contrast, less than 2N

DNA indicates the apoptotic cells in which the DNA is degraded to different extents. Treatment of MDA-MB-231 cells for 72h with the noscapine and 9-(N-arylmethylamino) noscapinoids, **15-17** led to significant inhibition of the cell cycle profile at IC_{50} concentration. FACS analysis revealed a high accumulation of cells in the G2/M phase at 72h of treatment with the test compounds (Table 3.7). In contrast to G2/M block, a hypodiploid DNA content peak (sub-G1) was seen to rise at 72 hours of drug treatment, indicating dying cells.

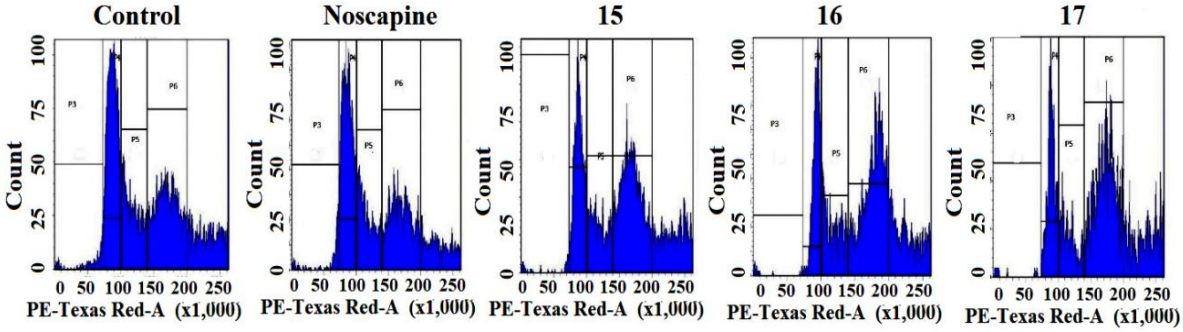

Figure 3.15. Noscapine and its 9-(N-arylmethylamino) noscapinoids, **15-17** perturb cell cycle progression at G2/M phase followed by the appearance of a hypodiploid (sub-G1) DNA peak that indicate apoptotic cells. Panels A-E demonstrated the analyses of cell cycle progression, determined by flow cytometry in MDA-MB-231 cells treated with IC_{50} concentration of noscapine and its N-alkyl-amine derivatives for 72 hours.

Table 3.7. Effect of noscapine and its 9-(N-arylmethylamino) noscapinoids,**15-17**on cell cycle progression of MDA-MB-231 cells treated with IC_{50} concentration for 72 hour before being stained with propidium iodide for cell cycle analysis.

	72 hours			
	Sub-G_1	G_0/G_1	S	G_2/M
Control	0.7	21	23.4	10.4
Noscapine	6.4	17.5	13.4	26.5
15	9.8	15.8	14.2	28.1
16	13.2	17.2	10.1	31.3
17	18.5	15.3	13.4.	32.7

3.3.8. 9-(N-arylmethylamino) noscapinoids, 15-17 binds to tubulin at high affinity

Microtubules are autofluorescent by nature due to the presence of aromatic amino acids, tryptophan which can be selectively measured by exciting at 295 nm. Any chemical compounds that bind with tubulin and alter its conformation lead to a decrease in its intrinsic fluorescence.This is a standard assay to test whether a chemical compound binds to tubulin or not. We have used a similar assay to test whether the 9-(N-arylmethylamino) noscapinoids, **15-17** also bind to tubulin or not. It was revealed that intrinsic fluorescence

of tubulin, decreased in presence of 9-(N-arylmethylamino) noscapinoids, **15-17,** suggests the binding capability of these compounds to tubulin. The relative percentage of decrease in fluorescence intensity was 5.034%, 14.094% and 22.148% respectively in presence of 25 µM concentration of**15-17**(Figure 3.15), compared to control.

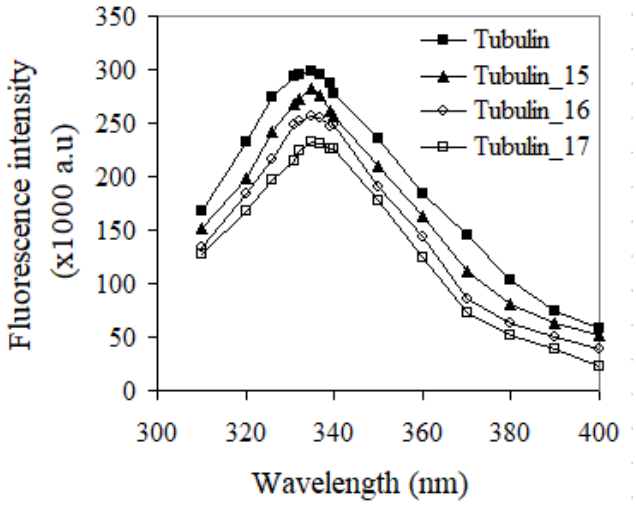

Figure 3.16. Treatmentof purified tubulin with 9-(N-arylmethylamino) noscapinoids, **15-17** at a concentration of 25 µM quenched the intrinsic fluorescence of tubulin significantly compared to untreated tubulin. The relative percentage of decreased in fluorescence intensity was 5.034%, 14.094% and 22.148% respectively in presence of 25 µM concentration of**15-17** compared to control. Emission spectra were collected in a range of 310 nm – 400 nm.

3.4. Discussion

Microtubule-targeting drugs are widely employed in the clinic to treat different types of cancer. Mostly three classes of drugs namely, taxanes, vinca alkaloids and colchicine analogs are well recognized and the sites they positioned on the tubulin, have been well studied (Jordan and Wilson, 2004). Traditionally these classes of drugs either stabilize microtubules, causing over polymerization of microtubules into bundles and sheets, such as the taxane family or destabilizes microtubules resulting in depolymerization of microtubules into soluble tubulin, like the vinca alkaloids. Unfortunately, the clinical success of these drugs has been severely hampered by the emergence of various toxicities, such as gastrointestinal toxicity, alopecia, and peripheral neuropathy. A coupled aspect of the toxicity manifestation is their lack of specificity for dividing cells. Moreover, patients have developed resistance to these drugs. Yet another class of microtubule-binding anticancer agents is based upon noscapine, a non-sedative, naturally occurring opium alkaloid and is known for its antitussive properties for decades Zhou et al., 2005; Ye et al., 1998). Ever since, noscapine has been successfully shown to inhibit various neoplasms *in vitro* as well as *in vivo* such as leukemia and lymphoma (Ye

et al., 1998; Ke et al., 2000; Sung et al., 2010), melanoma (Landen et al., 2002), ovarian Zhou et al., 2002), gliomas Landen et al., 2004), breast (Aneja et al., 2006), lung (Jackson et al., 2008), and colon (Aneja et al., 2007) cancer. It was demonstrated that noscapine and its analogs, collectively referred to as the noscapinoid family, do not impair crucial microtubule functions mainly by maintaining the steady-state equilibrium between the monomeric and polymeric form of tubulin (Karna et al., 2011). As a result, this class of microtubule-interfering agents escapes the severe side effects of currently available tubulin-binding chemotherapeutics. Hence, noscapine derivatives can potentially be exploited for therapeutic usage individually or in combination with existing toxic anti-microtubule drugs.

Ongoing efforts of rational design and chemical synthesis to improve the therapeutic efficacy and pharmacological properties of noscapine have yielded a battery of noscapine derivatives (Aneja et al., 2006a; Aneja et al., 2006b; Aneja et al., 2006c; Aneja et al., 2006d; Manchukonda et al., 2013; Manchukonda et al., 2014; Naik et al., 2011; Santoshi et al., 2015; Meher et al., 2021). These derivatives have been extensively shown to impede cell-cycle progression, inhibit cell proliferation and induce apoptosis in a variety of cancer cells both *in vitro* and in xenograft models of human cancers implanted in nude mice (Aneja et al., 2006e; Aneja et al., 2007; Aneja et al., 2008). From a synthetic perspective, most of these derivatives were generated by the chemical manipulation of the C-9 position on the isoquinoline ring system of noscapine. The C-9 substituted derivatives of noscapine revealed superior activity (Aneja et al., 2006a; Aneja et al., 2006b). In particular the 9-bromo-noscapine is well-studied because of its effectiveness against drug-resistant xenograft tumors without any detectable toxicity (Aneja et al., 2006e; Aneja et al., 2008). This strongly suggested that chemical maneuvering at the C-9 position had a significant impact on the anticancer activity of the parent molecule. Based upon this impetus, we have rationally designed a new series of derivatives of noscapine by substituting alkyl or arylalkyl units at C-9 position to examine their anticancer potential.Finally based on our *in silico* efforts we have screened out three 9-(N-arylmethylamino) noscapinoids, **15-17** based on their lowest negative docking score and predictive binding free energy for chemical synthesis and experimental validation.

All three synthesized 9-(N-arylmethylamino) noscapinoids, **15-17**showed antiproliferative activityat a lower concentration compared to the parent compound against two human breast cancer cell lines, MCF-7 and MDA-MB-231 as well as a panel of primary breast tumor cells. It is also revealed that each compound has a narrow range of antiproliferative activity among these cells. These differences in cellular sensitivities to the

same compound may be due to altered expression of β-tubulin isotypes, or point mutations in tubulin resulting in alterations of expression patterns of post-translational modifications of tubulin regulatory proteins, such as stathmin, microtubule-associated protein (MAP), tau and MAP4 (Burkhart et al., 2001; Cabral et al., 1982). These changes in microtubule accessory proteins have been well recognized to affect microtubule dynamicity and can perhaps contribute to the development of drug resistance (Liu et al., 2001). Furthermore, these derivatives significantly arrest cells at the G2/M phase of the cell cycle followed by apoptotic cell death, as revealed by several prototypic features of apoptosis. Therefore, these novel compounds may prove efficacious not only in the treatment of breast carcinoma but also for other types of cancers. Our results compel us to continue to examine the effects of these novel compounds on *in vivo* animal experiments with the final goal of taking it to the human clinical study.

Supporting Information

Table of contents ----------

Copies of ^{1}H-NMR, ^{13}C-NMR, HRMSSpectra

Table of H-bonding and Hydrophobic interactions

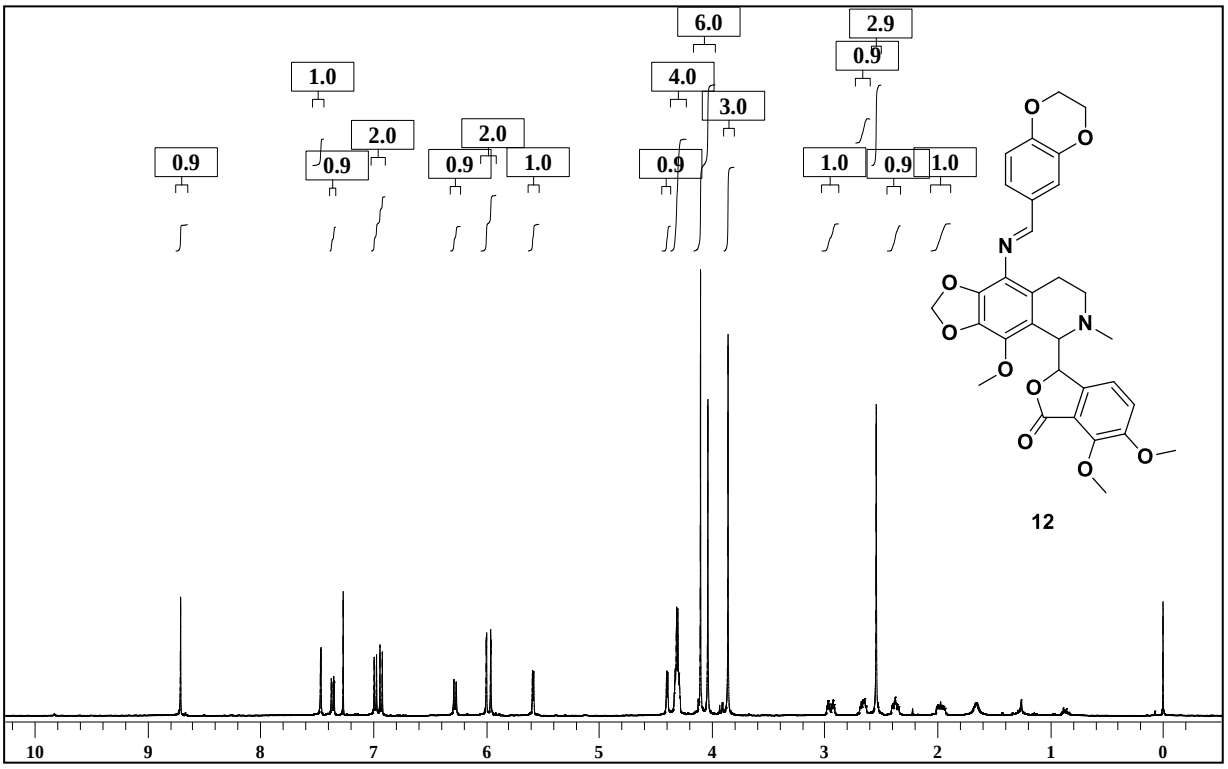

.

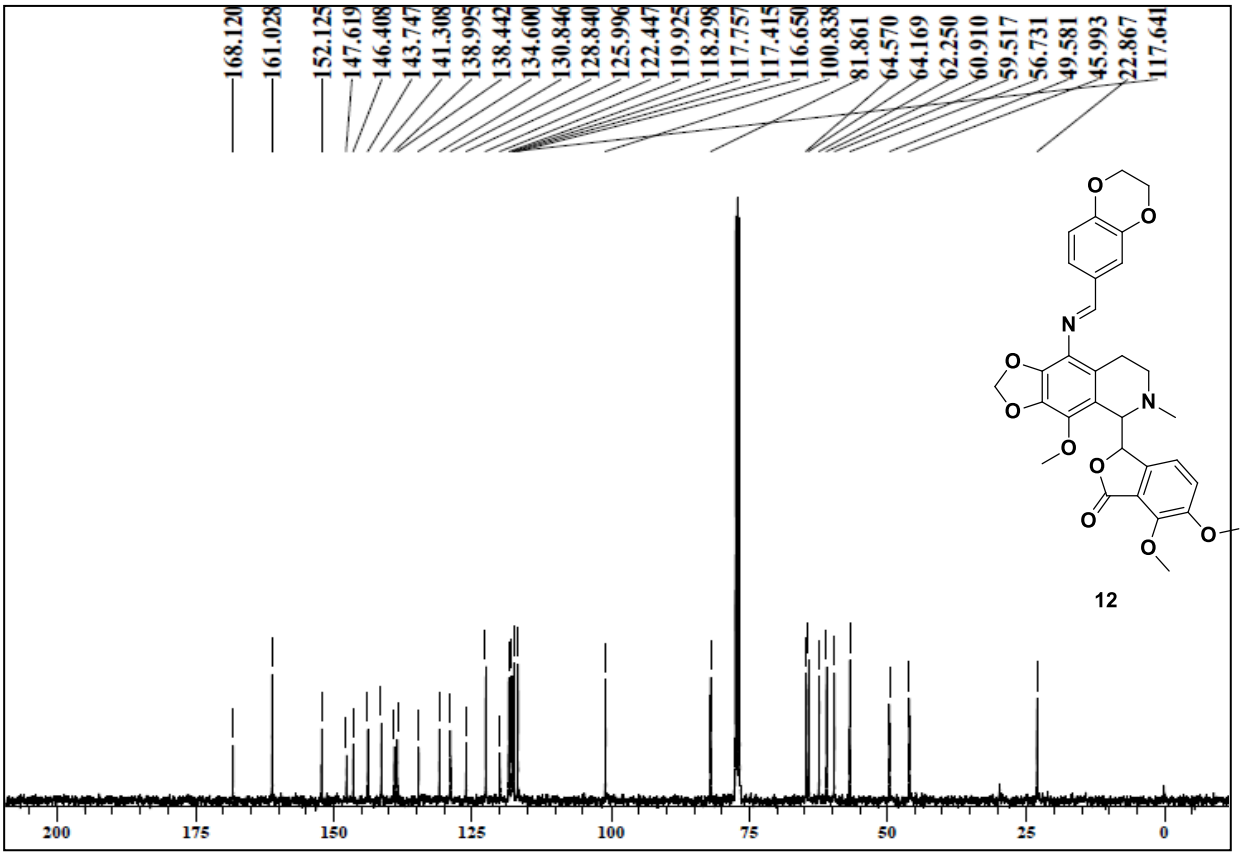

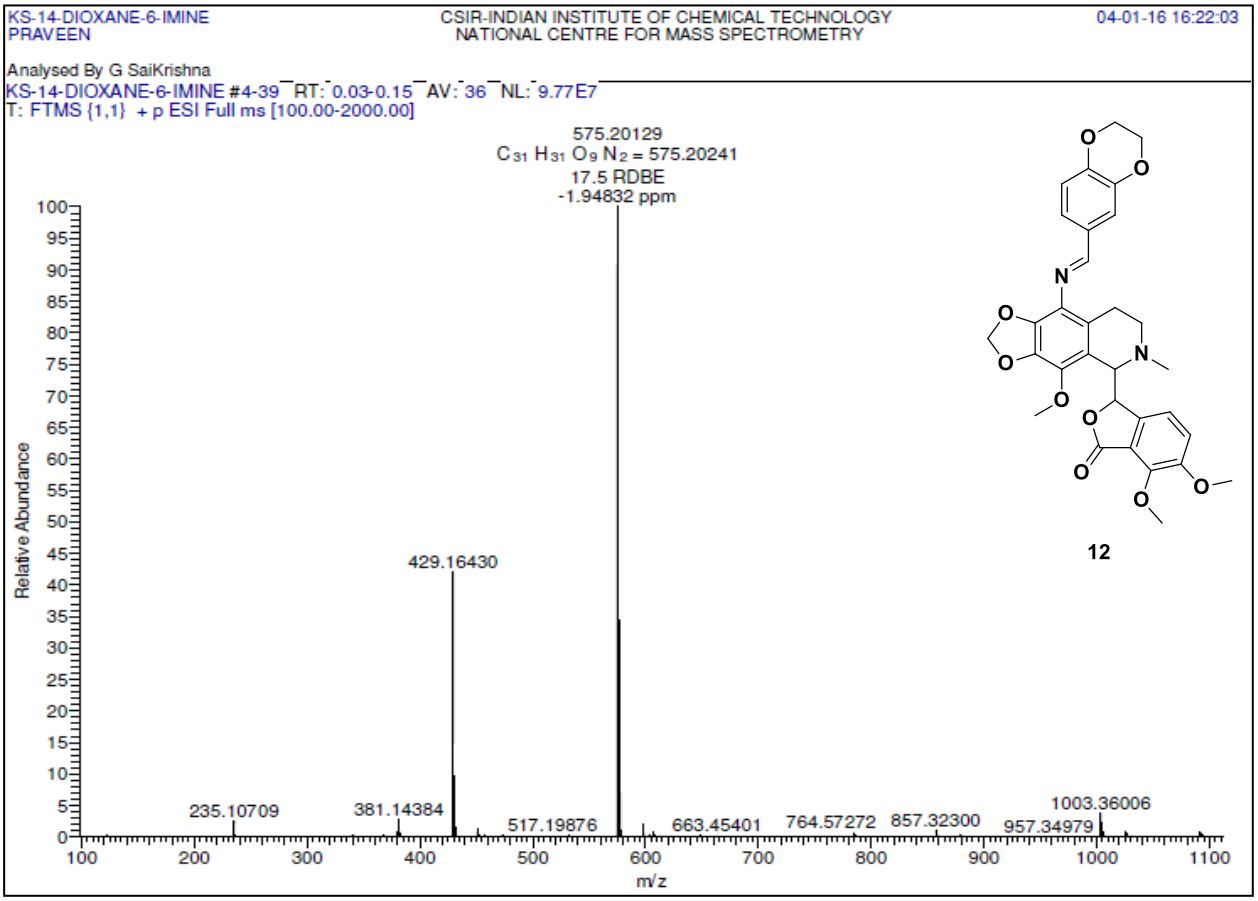
KS-14-DIOXANE-6-IMINE
PRAVEEN
CSIR-INDIAN INSTITUTE OF CHEMICAL TECHNOLOGY
NATIONAL CENTRE FOR MASS SPECTROMETRY
04-01-16 16:22:03
Analysed By G SaiKrishna
KS-14-DIOXANE-6-IMINE #4-39 RT: 0.03-0.15 AV: 36 NL: 9.77E7
T: FTMS {1,1} + p ESI Full ms [100.00-2000.00]
575.20129
C31 H31 O9 N2 = 575.20241
17.5 RDBE
-1.94832 ppm
429.16430
235.10709
381.14384
517.19876
663.45401
764.57272
857.32300
957.34979
1003.36006
Relative Abundance
m/z
12

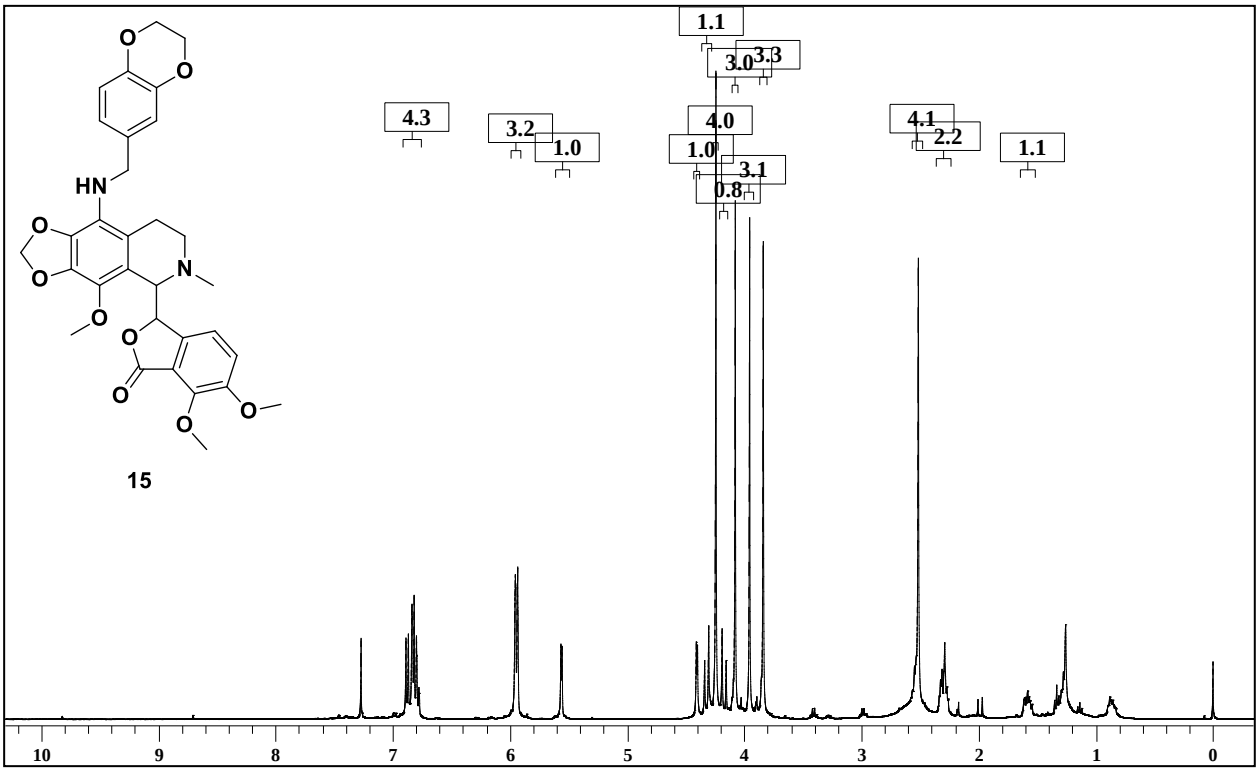
15
4.3
3.2
1.0
1.1
3.0
3.3
4.0
1.0
3.1
0.8
4.1
2.2
1.1
10
9
8
7
6
5
4
3
2
1
0

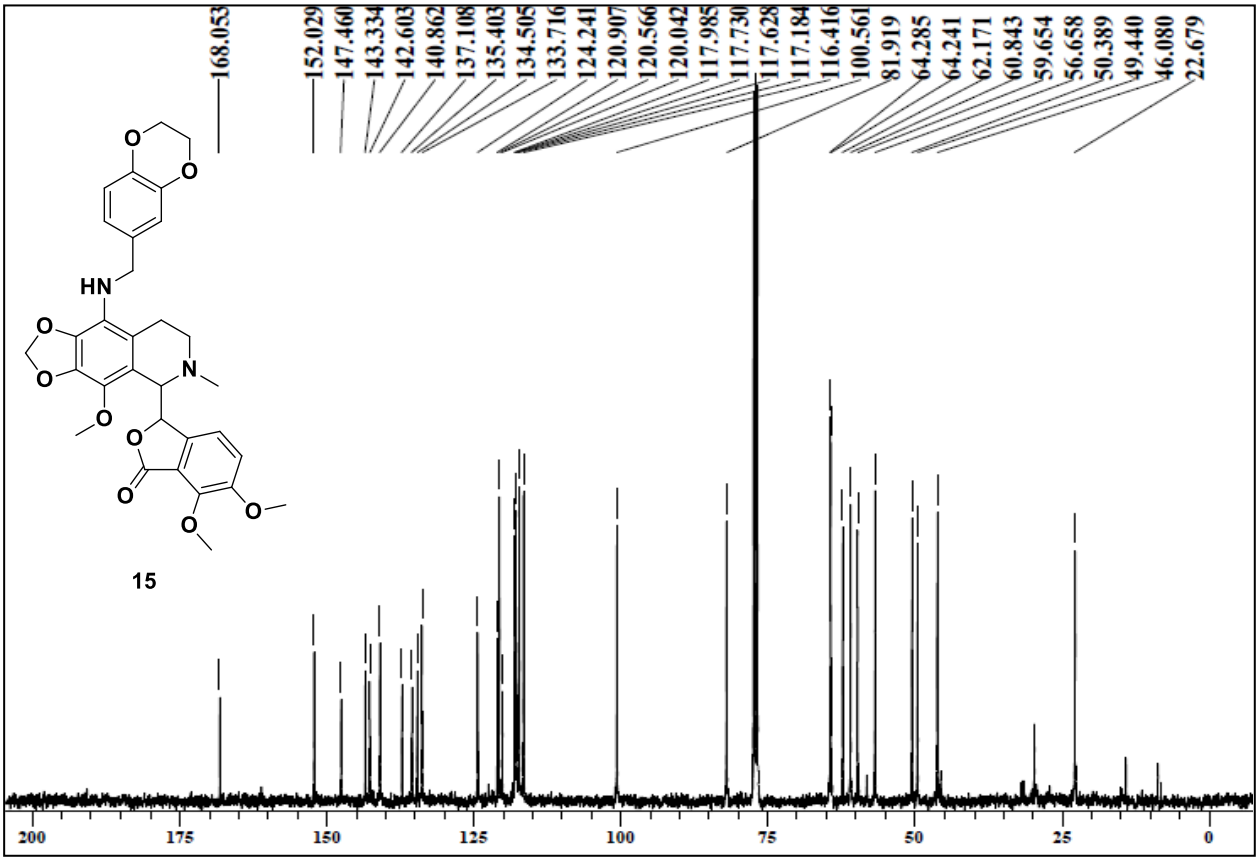
168.053
152.029
147.460
143.334
142.603
140.862
137.108
135.403
134.505
133.716
124.241
120.907
120.566
120.042
117.985
117.730
117.628
117.184
116.416
100.561
81.919
64.285
64.241
62.171
60.843
59.654
56.658
50.389
49.440
46.080
22.679
HN
O
O
O
O
N
O
O
O
O
O
O
200
175
150
125
100
75
50
25
0

15

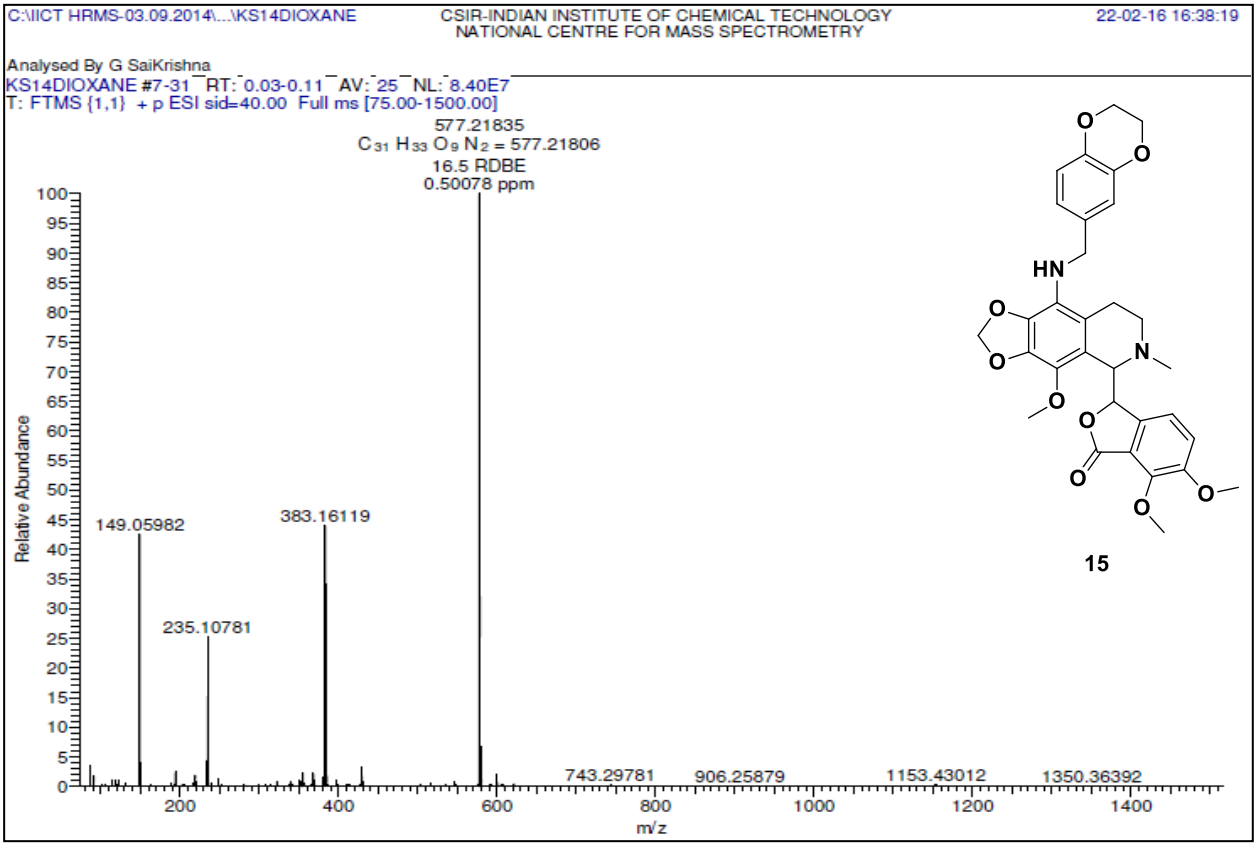
C:\IICT HRMS-03.09.2014\...\KS14DIOXANE
CSIR-INDIAN INSTITUTE OF CHEMICAL TECHNOLOGY
NATIONAL CENTRE FOR MASS SPECTROMETRY
22-02-16 16:38:19
Analysed By G SaiKrishna
KS14DIOXANE #7-31 RT: 0.03-0.11 AV: 25 NL: 8.40E7
T: FTMS {1,1} + p ESI sid=40.00 Full ms [75.00-1500.00]
577.21835
C31 H33 O9 N2 = 577.21806
16.5 RDBE
0.50078 ppm
Relative Abundance
149.05982
235.10781
383.16119
743.29781
906.25879
1153.43012
1350.36392
m/z
HN
O
O
O
O
N
O
O
O
O
O
O

15

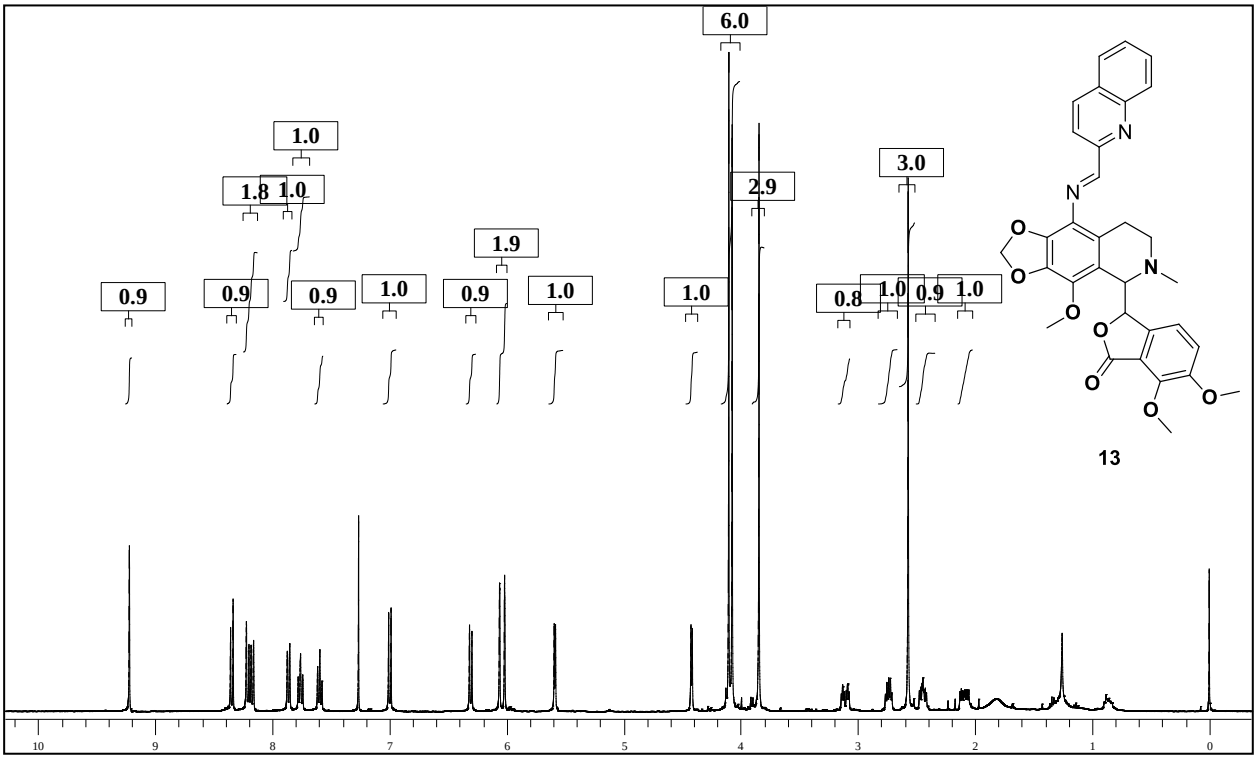
6.0
1.0
1.8
1.0
2.9
3.0
1.9
0.9
0.9
0.9
1.0
0.9
1.0
1.0
0.8
1.0
0.9
1.0
13

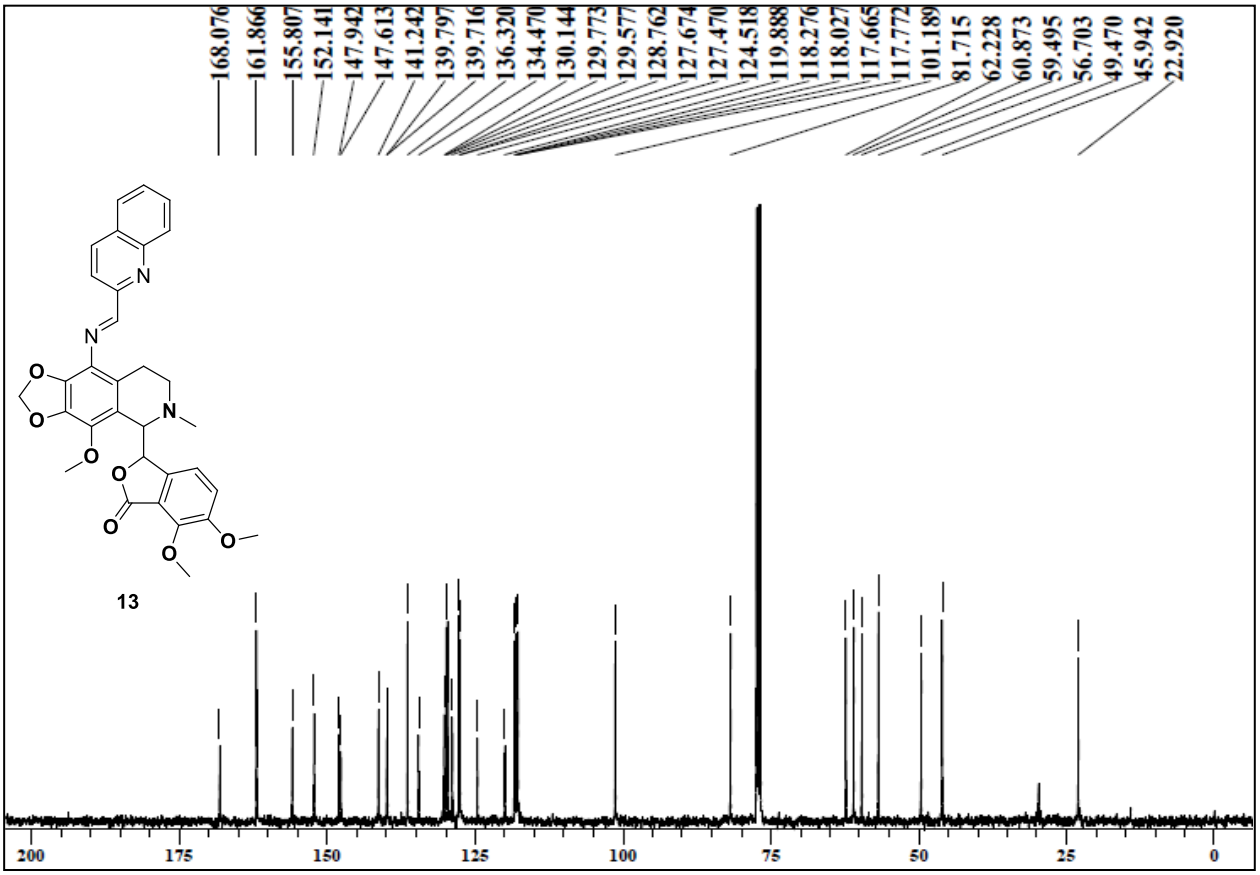
168.076
161.866
155.807
152.141
147.942
147.613
141.242
139.797
139.716
136.320
134.470
130.144
129.773
129.577
128.762
127.674
127.470
124.518
119.888
118.276
118.027
117.665
117.772
101.189
81.715
62.228
60.873
59.495
56.703
49.470
45.942
22.920
13

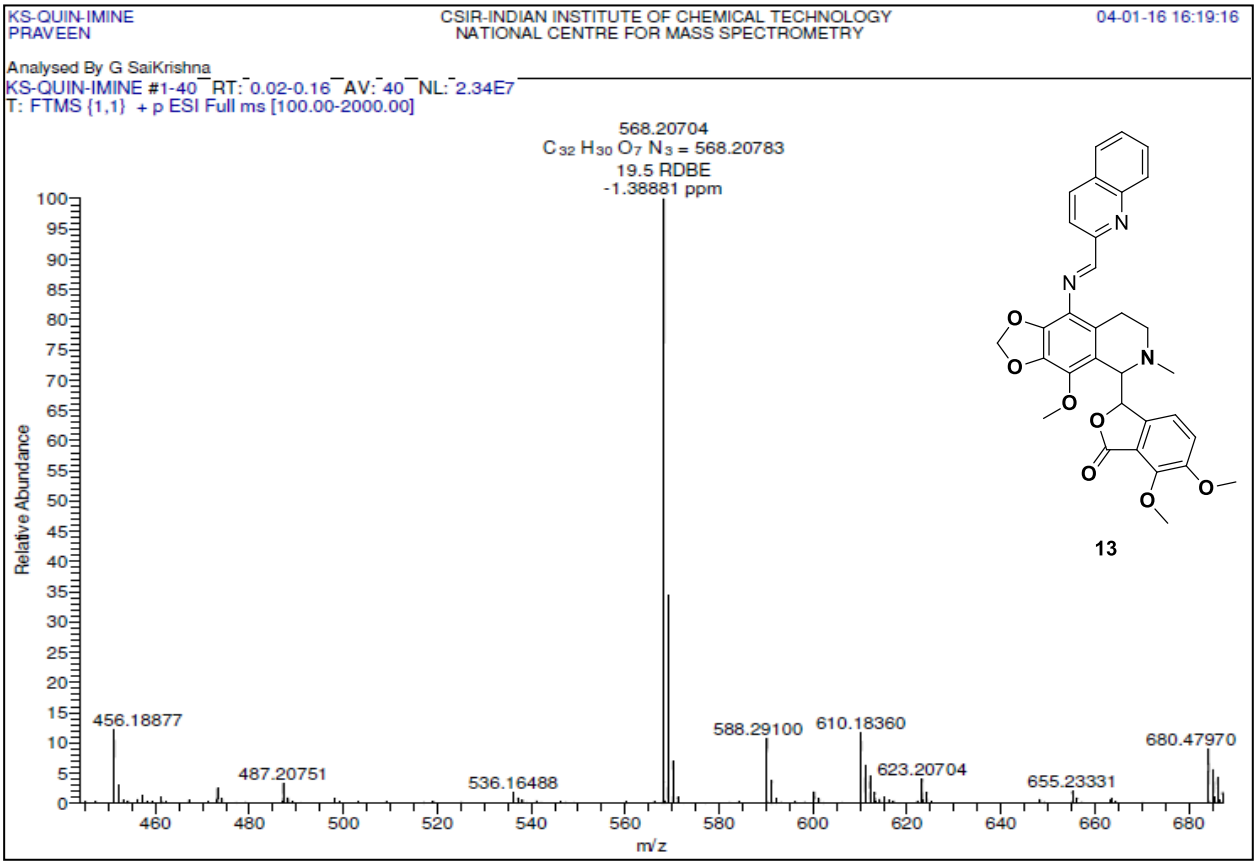
KS-QUIN-IMINE
PRAVEEN
CSIR-INDIAN INSTITUTE OF CHEMICAL TECHNOLOGY
NATIONAL CENTRE FOR MASS SPECTROMETRY
04-01-16 16:19:16
Analysed By G SaiKrishna
KS-QUIN-IMINE #1-40 RT: 0.02-0.16 AV: 40 NL: 2.34E7
T: FTMS {1,1} + p ESI Full ms [100.00-2000.00]
568.20704
C32 H30 O7 N3 = 568.20783
19.5 RDBE
-1.38881 ppm
Relative Abundance
m/z
456.18877
487.20751
536.16488
588.29100
610.18360
623.20704
655.23331
680.47970
13

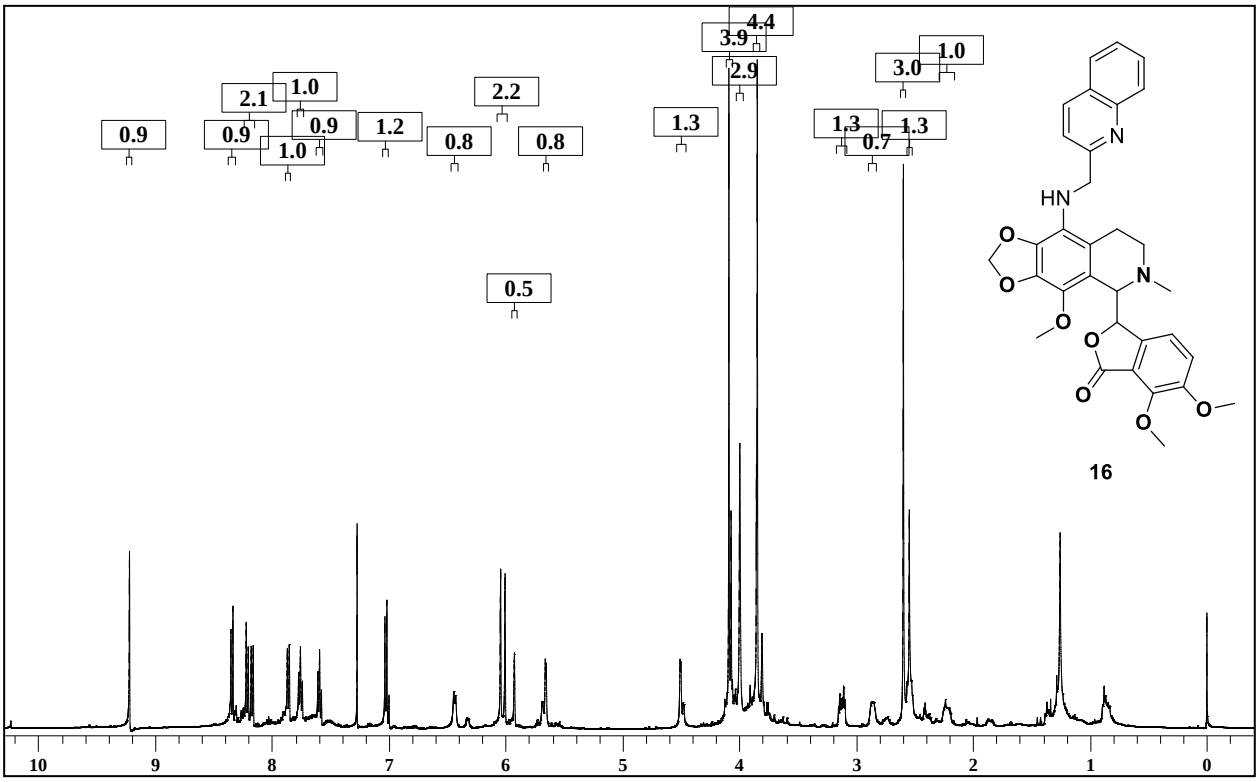
0.9
2.1
1.0
0.9
0.9
1.0
1.2
2.2
0.8
0.8
0.5
1.3
4.4
3.9
2.9
3.0
1.0
1.3
0.7
1.3
HN
16
10
9
8
7
6
5
4
3
2
1
0

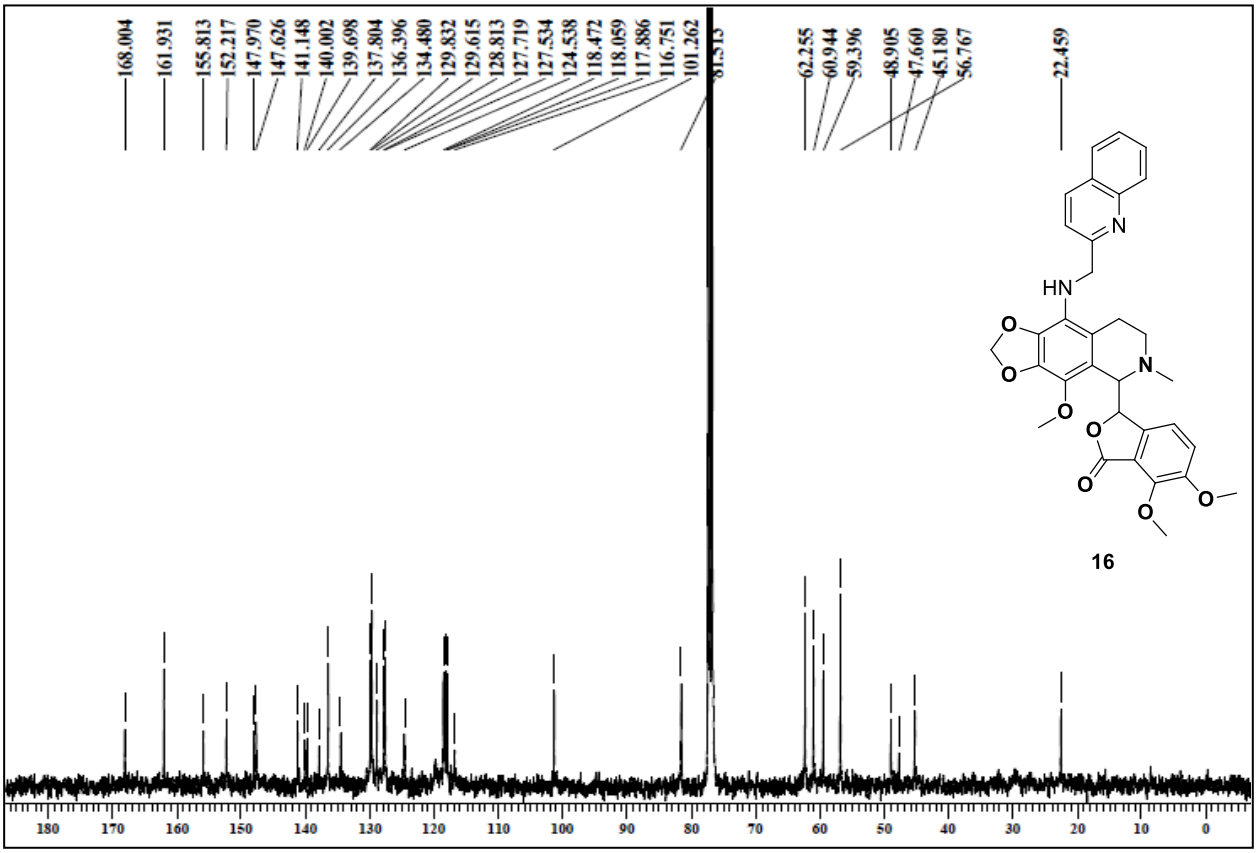

16

KSNQUINEAMINE
DR K SRINIVAS
THERMOFISHER EXACTIVE ORBITRAP
Analysed By G SaiKrishna
7/20/2018 4:09:34 PM
MLP-0002
N PRAVEEN4

CSIR-INDIAN INSTITUTE OF CHEMICAL TECHNOLOGY
ANALYTICAL CHEMISTRY AND MASS SPECTROMETRY

KSNQUINEAMINE #4-34 RT: 0.02-0.12 AV: 31 NL: 1.83E7
T: FTMS {1,1} + p ESI Full ms [80.00-1600.00]

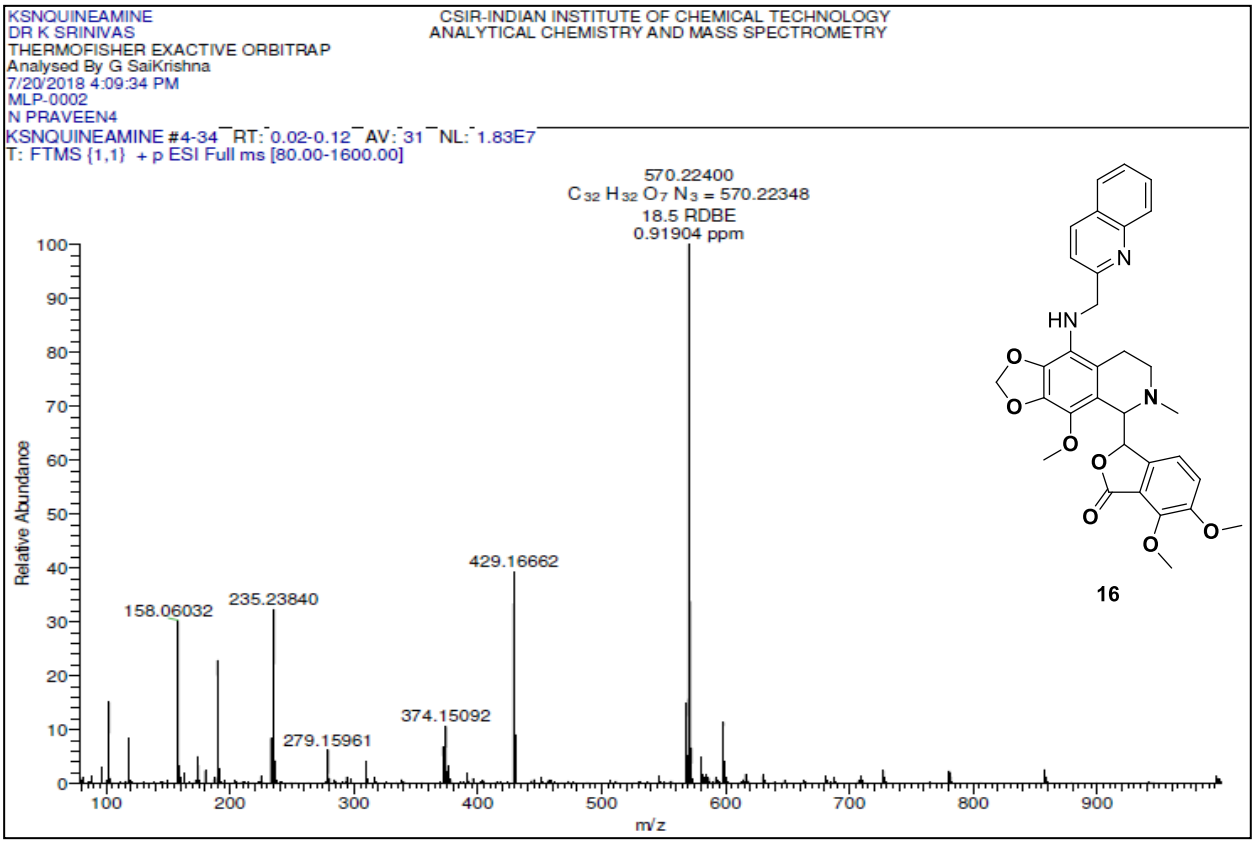

16

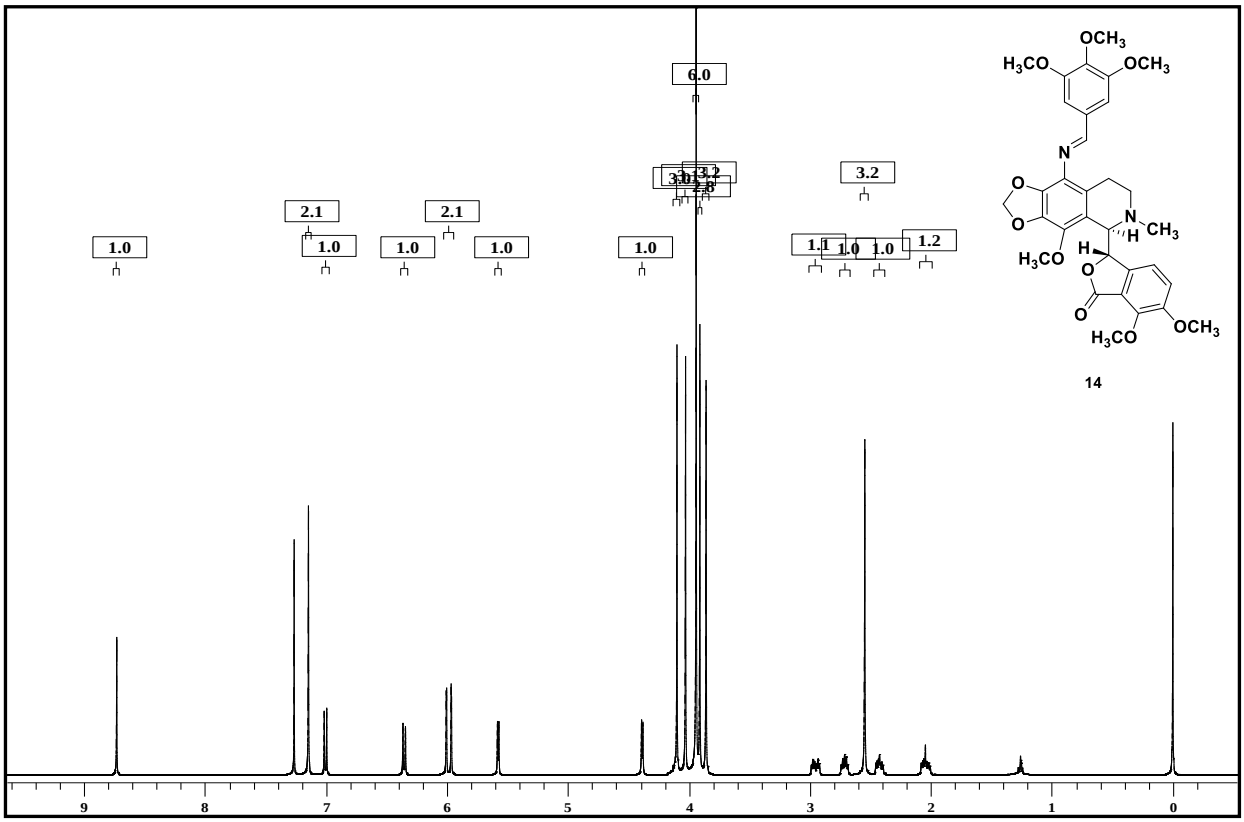
1.0
2.1
1.0
2.1
1.0
1.0
1.0
6.0
3.2
1.1
1.0
1.0
3.2
1.2
14

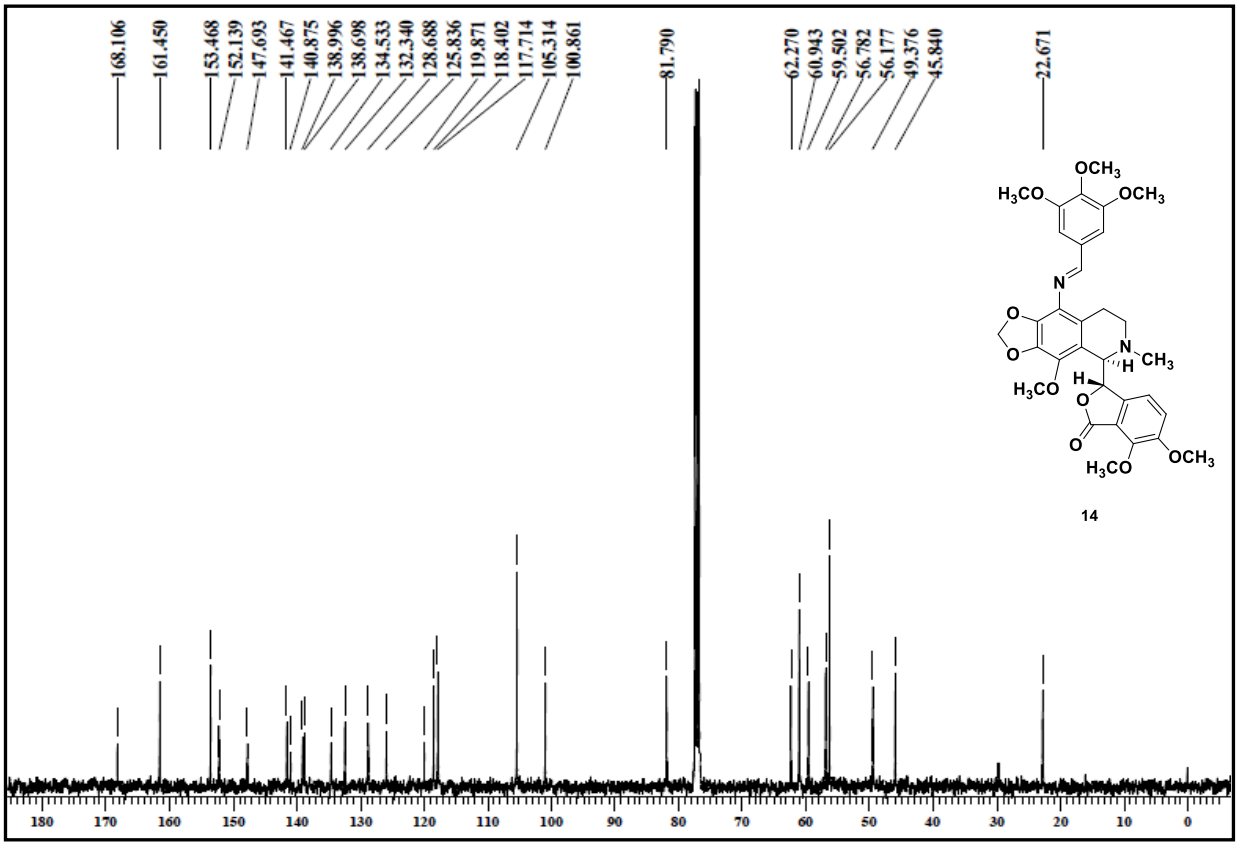
168.106
161.450
153.468
152.139
147.693
141.467
140.875
138.996
138.698
134.533
132.340
128.688
125.836
119.871
118.402
117.714
105.314
100.861
81.790
62.270
60.943
59.502
56.782
56.177
49.376
45.840
22.671
14

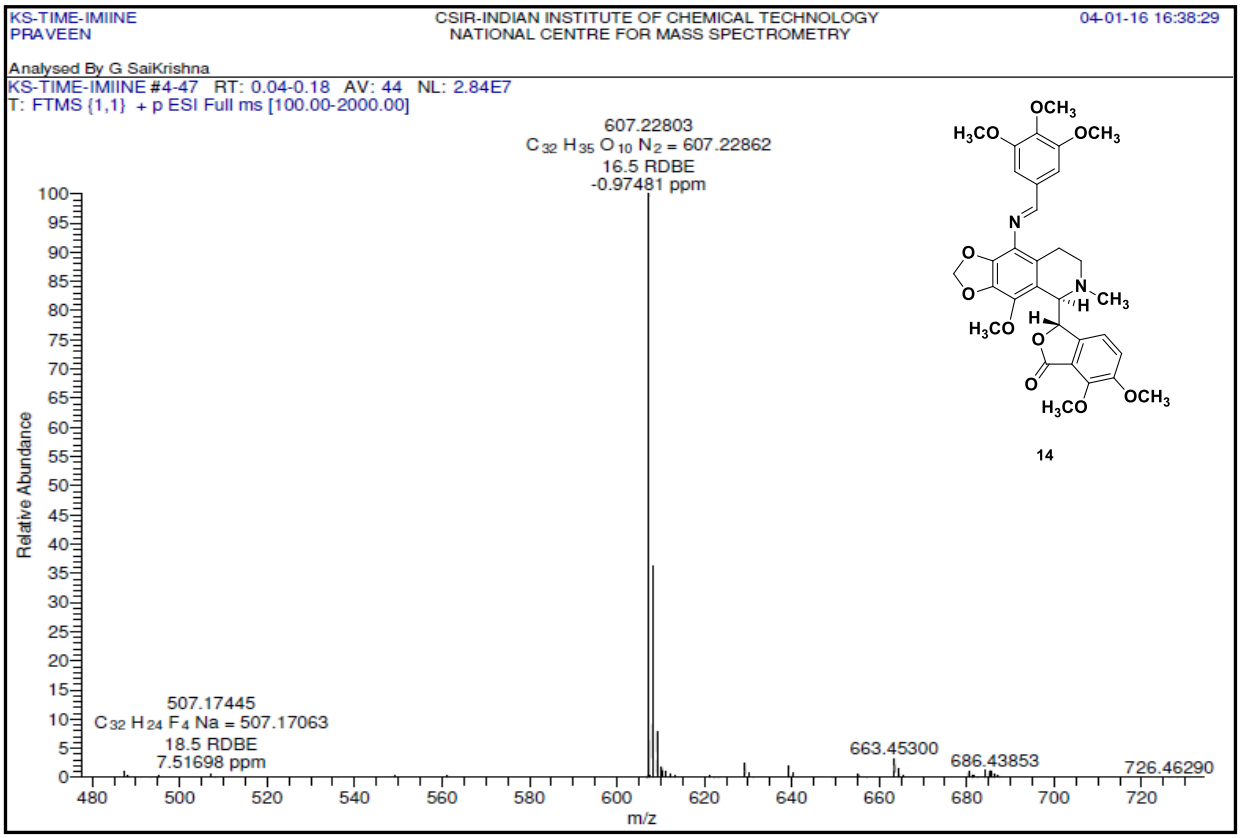
KS-TIME-IMIINE
PRAVEEN
CSIR-INDIAN INSTITUTE OF CHEMICAL TECHNOLOGY
NATIONAL CENTRE FOR MASS SPECTROMETRY
04-01-16 16:38:29
Analysed By G SaiKrishna
KS-TIME-IMIINE #4-47 RT: 0.04-0.18 AV: 44 NL: 2.84E7
T: FTMS {1,1} + p ESI Full ms [100.00-2000.00]
607.22803
C32 H35 O10 N2 = 607.22862
16.5 RDBE
-0.97481 ppm
507.17445
C32 H24 F4 Na = 507.17063
18.5 RDBE
7.51698 ppm
663.45300
686.43853
726.46290
Relative Abundance
m/z
14

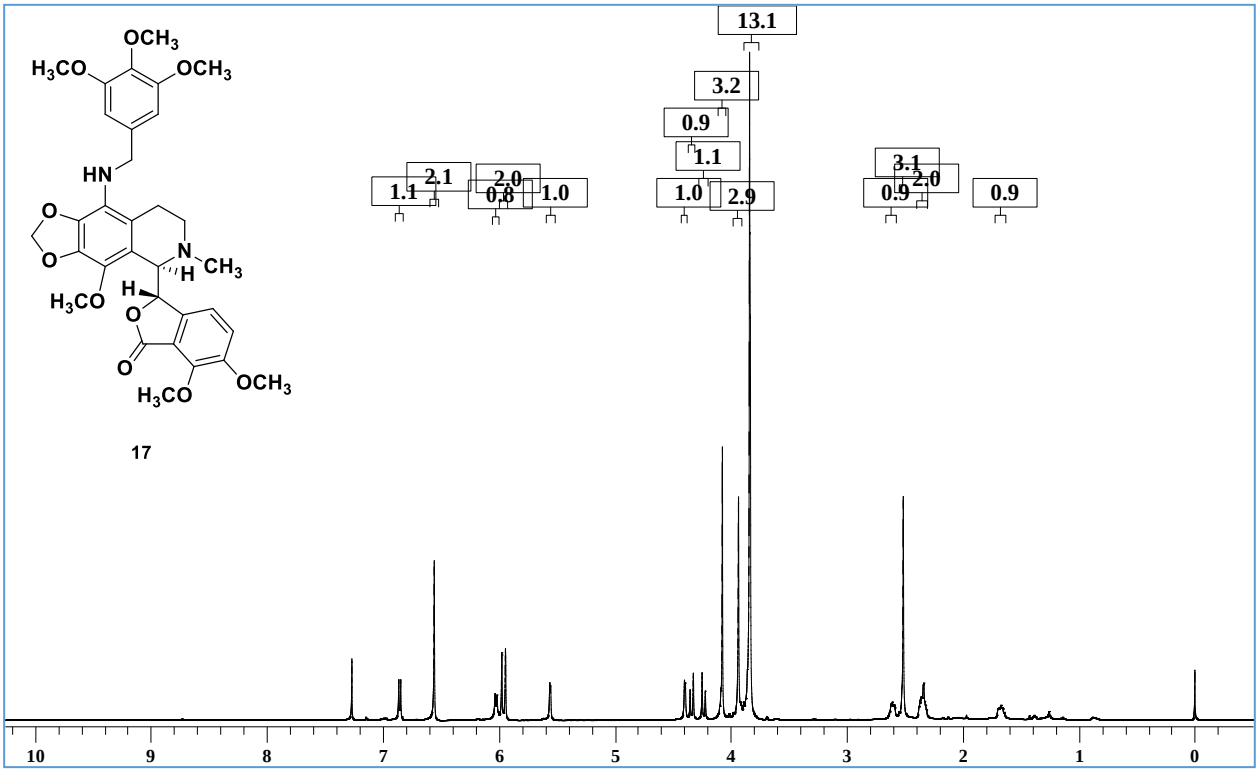
17
13.1
3.2
0.9
1.1
2.1
2.0
0.8
1.0
1.0
2.9
3.1
2.0
0.9
0.9

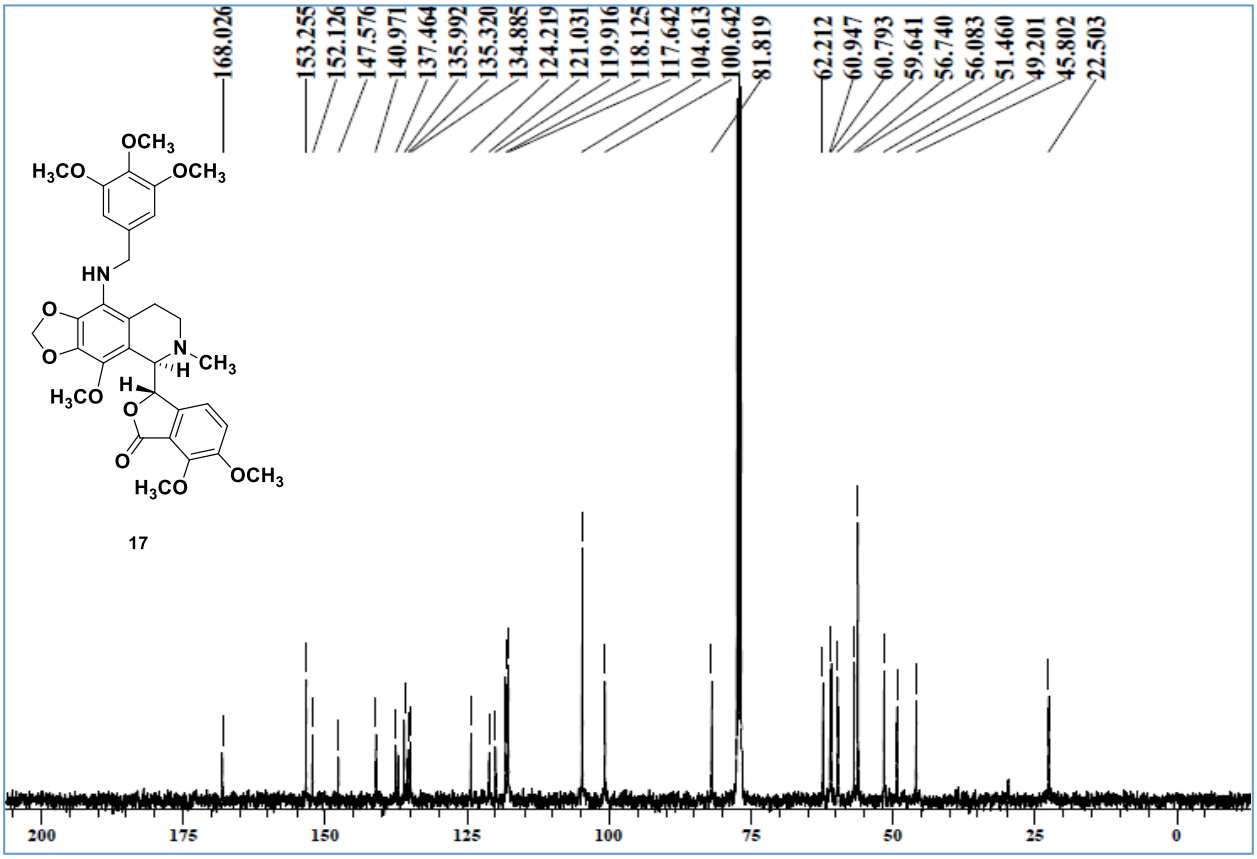
168.026
153.255
152.126
147.576
140.971
137.464
135.992
135.320
134.885
124.219
121.031
119.916
118.125
117.642
104.613
100.642
81.819
62.212
60.947
60.793
59.641
56.740
56.083
51.460
49.201
45.802
22.503
200
175
150
125
100
75
50
25
0

17

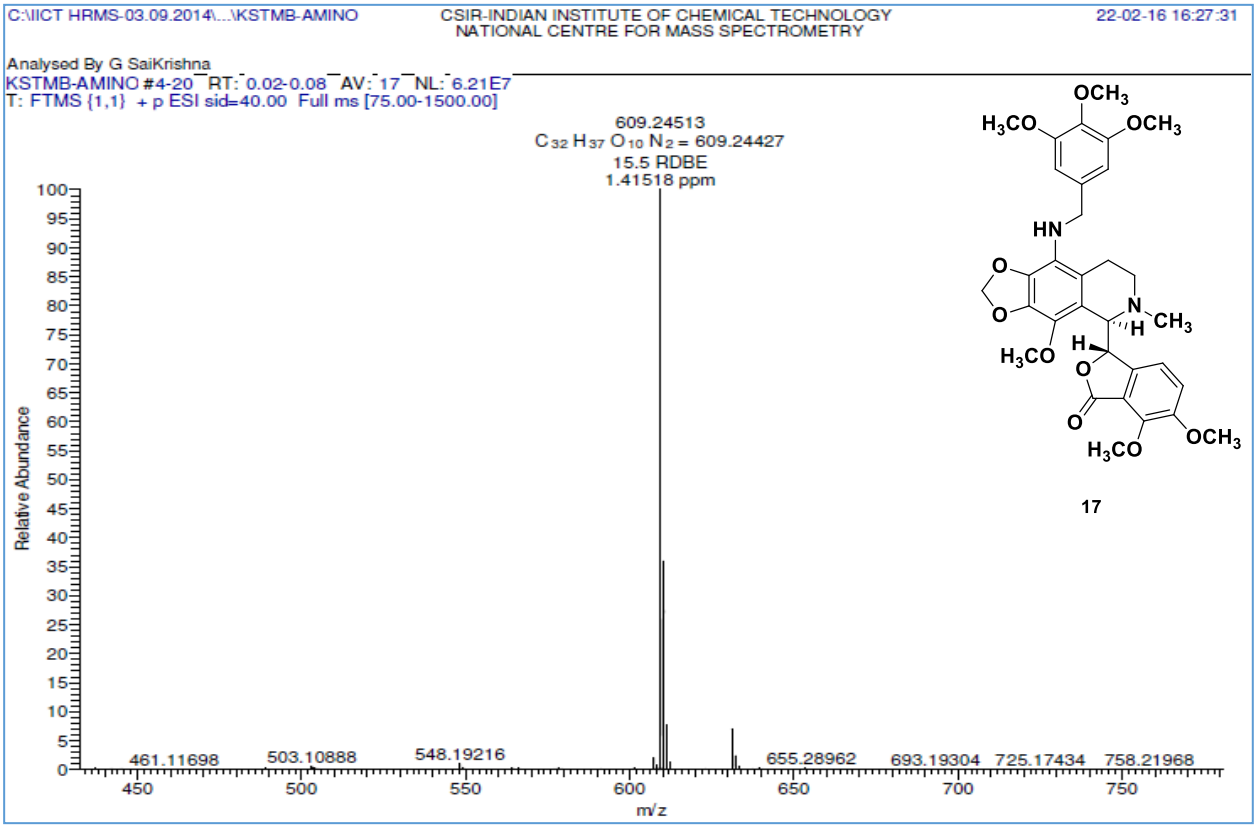
C:\IICT HRMS-03.09.2014\...\KSTMB-AMINO
CSIR-INDIAN INSTITUTE OF CHEMICAL TECHNOLOGY
NATIONAL CENTRE FOR MASS SPECTROMETRY
22-02-16 16:27:31
Analysed By G SaiKrishna
KSTMB-AMINO #4-20 RT: 0.02-0.08 AV: 17 NL: 6.21E7
T: FTMS {1,1} + p ESI sid=40.00 Full ms [75.00-1500.00]
609.24513
C32 H37 O10 N2 = 609.24427
15.5 RDBE
1.41518 ppm
Relative Abundance
m/z
461.11698
503.10888
548.19216
655.28962
693.19304
725.17434
758.21968

17

Table S1-S4: Geometry of hydrogen bonds and hydrophobic interaction of 9-(N-arylmethylamino) noscapinoids, **15-17** and the lead molecule, noscapine with the binding site residues of tubulin.

Table S1			**Table S2**		
(a) 9-(N-arylmethylamino) noscapinoid, 15-Tubulin			**(b) 9-(N-arylmethylamino) noscapinoid, 16-Tubulin**		
Hydrogen bonding			**Hydrogen bonding**		
Hydrogen Donor (D)	**Hydrogen Acceptor (A)**	**Distance (D-A) in Å**	**Hydrogen Donor (D)**	**Hydrogen Acceptor (A)**	**Distance (D-A) in Å**
ASN A 228 ND2	15 O8	2.75	GLN B 247 NE2	16O3	3.06
15 N1	GLU A 77 OE1	4.93	16 N1	GLU B 47 OE2	2.88
15 N1	GLN A 15 OE1	3.32	16 N3	THR A 73 OG1	4.07
Hydrophobic interaction			**Hydrophobic interaction**		
15	**Tubulin**	**Distance**	**16**	**Tubulin**	**Distance**
C23	GLN D 247 NE2	4.93	C21	LYS D 254 NZ	3.46
C10	GLN D 247 NE2	4.84	C19	LYS D 254 NZ	4.01
C9	GLN D 247 NE2	3.55	C18	LYS D 254 NZ	3.93
C8	GLN D 247 NE2	3.81	C21	LYS D 254 CE	4.71
C7	GLN D 247 NE2	4.02	O7	LYS D 254 CE	4.28
C6	GLN D 247 NE2	4.5	O7	LYS D 254 CD	4.75
C5	GLN D 247 NE2	4.92	C22	ASP D 251 OD2	3.9
C4	GLN D 247 NE2	3.87	C22	ASP D 251 CG	4.72
C3	GLN D 247 NE2	3.48	C22	ASP D 251 CB	4.74
C2	GLN D 247 NE2	3.97	C22	ALA D 250 CB	3.71
C1	GLN D 247 NE2	3.36	O7	ALA D 250 CB	4.74
N1	GLN D 247 CD	4.83	O6	ALA D 250 CB	4.19
O1	GLN D 247 CD	4.98	O5	ALA D 250 CB	4.83
C9	GLN D 247 CD	4.68	C20	ALA D 250 CB	4.7
C8	GLN D 247 CD	4.94	C19	ALA D 250 CB	4.47
C3	GLN D 247 CD	4.8	C18	ALA D 250 CB	4.09
C1	GLN D 247 CD	4.59	C17	ALA D 250 CB	3.79
C11	PRO D 245 CB	3.23	C16	ALA D 250 CB	4.03
O3	PRO D 245 CB	3.46	C15	ALA D 250 CB	4.52
C2	PRO D 245 CB	4.82	C13	ALA D 250 CB	4.63
C11	PRO D 245 CG	3.86	C22	ALA D 250 O	4.46
O3	PRO D 245 CG	4.42	C22	ALA D 250 C	4.57
O3	PRO D 245 C	4.82	C22	ALA D 250 CA	4.81
C11	PRO D 245 CA	4.63	C20	GLN D 247 OE1	3.9
O3	PRO D 245 CA	4.55	C19	GLN D 247 OE1	4.72
C20	GLU D 47 OE2	3.64	C15	GLN D 247 OE1	4.84
C19	GLU D 47 OE2	4.05	C20	GLN D 247 NE2	4.06
C18	GLU D 47 OE2	4.44	C15	GLN D 247 NE2	4.39
C17	GLU D 47 OE2	4.37	C14	GLN D 247 NE2	4.3
C16	GLU D 47 OE2	3.9	C12	GLN D 247 NE2	3.91
C15	GLU D 47 OE2	3.5	C11	GLN D 247 NE2	3.82
C13	GLU D 47 OE2	4.31	C5	GLN D 247 NE2	3.48
C12	GLU D 47 OE2	3.88	C4	GLN D 247 NE2	4.26
C11	GLU D 47 OE2	4.28	C2	GLN D 247 NE2	4.07
C20	GLU D 47 CD	4.72	C20	GLN D 247 CD	4.11
C19	GLU D 47 CD	4.92	C15	GLN D 247 CD	4.72
C15	GLU D 47 CD	4.72	C12	GLN D 247 CD	4.56
C20	GLU D 47 CG	4.96	C11	GLN D 247 CD	4.48
C19	GLU D 47 CG	4.81	O3	GLN D 247 CD	4.07
C31	ASN A 228 ND2	4.66	C5	GLN D 247 CD	4.49
C30	ASN A 228 ND2	3.63	C11	GLN D 247 CG	4.23

C29	ASN A 228 ND2	3.71	O3	GLN D 247 CG	4.29
C28	ASN A 228 ND2	4.94	C20	GLN D 247 O	4.72
C25	ASN A 228 ND2	3.93	C19	GLN D 247 O	4.82
C30	ASN A 228 CG	4.33	C20	GLN D 247 CA	4.4
O8	ASN A 228 CG	3.73	C15	GLN D 247 CA	4.83
C29	ASN A 228 CG	4.85	C12	GLN D 247 N	4.96
C30	ASN A 228 CB	3.97	C11	GLN D 247 N	4.3
O8	ASN A 228 CB	3.83	C20	GLY D 246 O	4.03
C30	THR A 225 OG1	4.78	C19	GLY D 246 O	4.81
C29	THR A 225 OG1	3.79	C17	GLY D 246 O	4.88
C28	THR A 225 OG1	4.36	C16	GLY D 246 O	4.07
C27	THR A 225 OG1	4.3	C15	GLY D 246 O	3.65
C26	THR A 225 OG1	4.61	C13	GLY D 246 O	4.27
C25	THR A 225 OG1	3.42	C12	GLY D 246 O	3.71
C24	THR A 225 OG1	3.68	C11	GLY D 246 O	4.47
C23	THR A 225 OG1	4.09	C20	GLY D 246 C	4.9
O8	THR A 225 CB	4.66	C15	GLY D 246 C	4.6
C29	THR A 225 CB	4.62	O4	GLY D 246 C	4.83
C25	THR A 225 CB	4.38	C12	GLY D 246 C	4.41
C24	THR A 225 CB	4.91	C11	GLY D 246 C	4.1
C30	THR A 225 CA	4.56	O3	GLY D 246 C	4.93
O8	THR A 225 CA	4	C11	GLY D 246 CA	4.23
C29	THR A 225 CA	4.32	C12	GLY D 246 N	4.83
C25	THR A 225 CA	4.1	C11	GLY D 246 N	3.82
C24	THR A 225 CA	4.98	O4	PRO D 245 CB	4.88
C29	THR A 225 N	4.51	C11	PRO D 245 CB	3.55
C25	THR A 225 N	3.86	O3	PRO D 245 CB	4.41
C24	THR A 225 N	4.63	O2	PRO D 245 CB	3.65
C23	THR A 225 N	4.66	C10	PRO D 245 CB	3.83
C23	TYR A 224 CD1	4.56	O1	PRO D 245 CB	4.46
N1	TYR A 224 CD1	4.68	C9	PRO D 245 CB	4.23
C23	TYR A 224 CG	4.79	C8	PRO D 245 CB	3.73
C25	TYR A 224 CB	4.09	C4	PRO D 245 CB	4.95
C24	TYR A 224 CB	4.57	C2	PRO D 245 CB	4.14
C23	TYR A 224 CB	4.01	C11	PRO D 245 CG	4.98
N1	TYR A 224 CB	4.81	O2	PRO D 245 CG	4.31
C29	TYR A 224 O	4.86	C10	PRO D 245 CG	3.97
C25	TYR A 224 O	4.46	O1	PRO D 245 CG	4.42
O8	TYR A 224 C	4.46	C9	PRO D 245 CG	4.51
C29	TYR A 224 C	4.77	C8	PRO D 245 CG	4.44
C25	TYR A 224 C	4.08	C11	PRO D 245 O	3.77
C24	TYR A 224 C	4.99	C11	PRO D 245 C	3.6
C23	TYR A 224 C	4.97	O3	PRO D 245 C	4.86
C25	TYR A 224 CA	4.73	O4	PRO D 245 CA	4.76
C23	TYR A 224 CA	4.94	C11	PRO D 245 CA	4.06
C22	THR A 80 CG2	4.1	C8	PRO D 245 CA	4.95
O6	THR A 80 CG2	4.75	C22	ARG D 48 NH2	4.7
C27	GLU A 77 OE2	4.05	C13	ARG D 48 NH2	4.8
C26	GLU A 77 OE2	4.44	C13	ARG D 48 NH1	4.78
C17	GLU A 77 OE2	4.82	O5	ARG D 48 CZ	3.75
C16	GLU A 77 OE2	3.84	C13	ARG D 48 CZ	4.6
C15	GLU A 77 OE2	4.13	C13	ARG D 48 NE	4.78
C14	GLU A 77 OE2	3.77	C25	ARG D 48 CD	4.98
C13	GLU A 77 OE2	3.12	O5	ARG D 48 CD	4.44
C12	GLU A 77 OE2	3.59	C25	ARG D 48 CG	4.46
C7	GLU A 77 OE2	3.09	C26	GLU D 47 OE2	3.14
C6	GLU A 77 OE2	3.4	C25	GLU D 47 OE2	4.09
C5	GLU A 77 OE2	3.42	C24	GLU D 47 OE2	3.82

C4	GLU A 77 OE2	3.63	C23	GLU D 47 OE2	3.77
C3	GLU A 77 OE2	3.41	C10	GLU D 47 OE2	3.74
C2	GLU A 77 OE2	4.75	C9	GLU D 47 OE2	3.32
C1	GLU A 77 OE2	4.27	C8	GLU D 47 OE2	4.34
C28	GLU A 77 OE1	4.44	C3	GLU D 47 OE2	4.63
C27	GLU A 77 OE1	3.54	C1	GLU D 47 OE2	3.44
C26	GLU A 77 OE1	3.39	C10	GLU D 47 OE1	4.28
C24	GLU A 77 OE1	4.66	C9	GLU D 47 OE1	4.89
C14	GLU A 77 OE1	4.97	C26	GLU D 47 CD	3.92
C7	GLU A 77 OE1	3.69	C25	GLU D 47 CD	4.55
C6	GLU A 77 OE1	4.19	C24	GLU D 47 CD	4.75
C3	GLU A 77 OE1	4.56	C23	GLU D 47 CD	4.86
N2	GLU A 77 CD	3.57	N1	GLU D 47 CD	4.09
C27	GLU A 77 CD	4.14	C10	GLU D 47 CD	4.41
C26	GLU A 77 CD	4.18	O1	GLU D 47 CD	3.88
O5	GLU A 77 CD	4.07	C9	GLU D 47 CD	4.44
C16	GLU A 77 CD	4.55	C1	GLU D 47 CD	4.68
C15	GLU A 77 CD	5	C27	GLU D 47 CG	5
C14	GLU A 77 CD	4.2	C26	GLU D 47 CG	3.76
C13	GLU A 77 CD	3.99	C25	GLU D 47 CG	3.9
O4	GLU A 77 CD	4.05	C24	GLU D 47 CG	4.78
C12	GLU A 77 CD	4.7	N1	GLU D 47 CG	4.91
C7	GLU A 77 CD	3.65	C32	GLU D 47 O	4.14
C6	GLU A 77 CD	3.89	C27	GLU D 47 O	4.36
C5	GLU A 77 CD	4.47	C26	GLU D 47 O	4.71
C4	GLU A 77 CD	4.75	C25	GLU D 47 O	3.79
C3	GLU A 77 CD	4.32	C25	GLU D 47 C	4.76
N2	GLU A 77 CG	4.22	C10	LEU D 42 CD2	4.74
C22	GLU A 77 CG	3.96	C31	ARG D 2 NH2	4.15
O6	GLU A 77 CG	4.37	C30	ARG D 2 NH2	4.69
O5	GLU A 77 CG	3.92	C31	ARG D 2 CZ	4.55
C17	GLU A 77 CG	4.53	C32	ARG D 2 NE	4.42
C16	GLU A 77 CG	4.23	C31	ARG D 2 NE	4.04
C15	GLU A 77 CG	4.97	C22	MET D 1 CE	3.3
C14	GLU A 77 CG	4.39	O7	MET D 1 CE	4.74
C13	GLU A 77 CG	3.98	O6	MET D 1 CE	4.38
O4	GLU A 77 CG	4.51	C22	MET D 1 O	4.65
C7	GLU A 77 CG	4.94	C22	ASP A 98 OD2	4.74
C6	GLU A 77 CG	4.82	C21	ASP A 98 OD2	3.3
C22	GLU A 77 CB	4.5	C18	ASP A 98 OD2	4.58
O5	GLU A 77 CB	4.85	C21	ASP A 98 CG	4.48
C22	GLU A 77 CA	3.87	O7	ASP A 98 CG	4.46
O6	GLU A 77 CA	4.83	C21	ASP A 98 CB	4.97
C22	GLU A 77 N	3.59	C23	GLU A 77 OE2	4.34
C21	ASP A 76 OD2	3.49	C14	GLU A 77 OE2	3.57
C21	ASP A 76 CG	4.09	C9	GLU A 77 OE2	4.64
C22	ASP A 76 CB	3.78	C7	GLU A 77 OE2	3.65
C21	ASP A 76 CB	3.74	C6	GLU A 77 OE2	4.46
O7	ASP A 76 CB	4.48	C4	GLU A 77 OE2	4.39
C22	ASP A 76 O	3.42	C3	GLU A 77 OE2	3.77
C22	ASP A 76 C	3.42	C1	GLU A 77 OE2	3.98
O6	ASP A 76 C	4.81	C14	GLU A 77 OE1	4.17
C22	ASP A 76 CA	4.25	C23	GLU A 77 CD	5
N2	VAL A 74 CG2	4.81	C14	GLU A 77 CD	4
C14	VAL A 74 CG2	4.39	C7	GLU A 77 CD	4.34
C7	VAL A 74 CG2	4.77	C6	GLU A 77 CD	4.96
C6	VAL A 74 CG2	3.88	C3	GLU A 77 CD	4.78
C7	VAL A 74 CG1	4.87	C23	GLU A 77 CG	4.6

C6	VAL A 74 CG1	4.63	C7	GLU A 77 CG	4.58
C14	VAL A 74 CB	4.81	C31	ASP A 76 OD2	4.79
C6	VAL A 74 CB	4.48	C30	ASP A 76 OD2	3.47
N2	VAL A 74 CA	4.62	C29	ASP A 76 OD2	3.22
C14	VAL A 74 CA	4.01	C28	ASP A 76 OD2	4.42
C6	VAL A 74 CA	4.31	C30	ASP A 76 CG	4.49
C14	VAL A 74 N	3.76	C29	ASP A 76 CG	4.04
C6	VAL A 74 N	4.71	C30	ASP A 76 CB	4.88
C20	THR A 73 OG1	4.64	C29	ASP A 76 CB	4.03
C19	THR A 73 OG1	4.84	C28	ASP A 76 CB	4.86
C14	THR A 73 OG1	3.17	N2	ASP A 76 CB	4.66
C6	THR A 73 OG1	4.76	N3	VAL A 74 CG2	4.02
C21	THR A 73 CG2	4.26	C21	VAL A 74 CG2	4.5
C20	THR A 73 CG2	4.94	C14	VAL A 74 CG2	3.76
C19	THR A 73 CG2	4.48	C6	VAL A 74 CG2	4.12
C14	THR A 73 CG2	4.86	C14	VAL A 74 CG1	4.43
N2	THR A 73 CB	4.97	N3	VAL A 74 CB	4.96
C21	THR A 73 CB	4.19	C14	VAL A 74 CB	4.38
C20	THR A 73 CB	4.32	C6	VAL A 74 CB	4.87
C19	THR A 73 CB	4.12	N3	VAL A 74 CA	4.86
C18	THR A 73 CB	4.77	C14	VAL A 74 CA	4.36
C14	THR A 73 CB	3.51	C7	VAL A 74 CA	4.93
C22	THR A 73 O	4.17	C6	VAL A 74 CA	4.39
C21	THR A 73 O	4.34	C14	VAL A 74 N	4.85
C20	THR A 73 O	4.69	C7	VAL A 74 N	4.7
C19	THR A 73 O	4.59	C6	VAL A 74 N	4.09
C18	THR A 73 O	4.42	C18	THR A 73 OG1	4.64
C17	THR A 73 O	4.41	C17	THR A 73 OG1	3.93
C16	THR A 73 O	4.57	C16	THR A 73 OG1	3.95
C15	THR A 73 O	4.73	C15	THR A 73 OG1	4.66
C14	THR A 73 O	3.01	C13	THR A 73 OG1	3.94
C6	THR A 73 O	4.69	C7	THR A 73 OG1	3.79
N2	THR A 73 C	4.52	C6	THR A 73 OG1	2.91
C21	THR A 73 C	4.84	C32	THR A 73 CG2	4.29
C14	THR A 73 C	3.29	C31	THR A 73 CG2	4.32
C6	THR A 73 C	4.86	C30	THR A 73 CG2	4.1
C21	THR A 73 CA	4.25	C29	THR A 73 CG2	3.88
C19	THR A 73 CA	4.92	C28	THR A 73 CG2	3.88
C14	THR A 73 CA	4.01	C27	THR A 73 CG2	4.07
C31	ALA A 19 CB	4.25	C25	THR A 73 CG2	4.73
C30	ALA A 19 CB	3.99	N2	THR A 73 CG2	4.42
C31	ALA A 19 CA	4.63	O6	THR A 73 CG2	4.63
C30	ALA A 19 CA	4.82	O5	THR A 73 CG2	4.59
C31	ALA A 19 N	4.32	C6	THR A 73 CG2	4.9
C30	ALA A 19 N	4.89	C30	THR A 73 CB	4.79
C31	ASN A 18 ND2	4.25	C29	THR A 73 CB	4.12
C31	ASN A 18 CG	4.93	C28	THR A 73 CB	3.96
C31	ASN A 18 CB	4.49	C27	THR A 73 CB	4.49
C31	ASN A 18 C	4.8	C26	THR A 73 CB	4.98
C29	GLN A 15 OE1	4.91	C25	THR A 73 CB	4.96
C27	GLN A 15 OE1	4.01	N2	THR A 73 CB	4.01
C26	GLN A 15 OE1	4.61	C24	THR A 73 CB	4.53
C25	GLN A 15 OE1	4.33	O6	THR A 73 CB	4.76
C24	GLN A 15 OE1	3.87	O5	THR A 73 CB	4.68
C23	GLN A 15 OE1	4.07	C13	THR A 73 CB	4.84
C7	GLN A 15 OE1	2.91	C7	THR A 73 CB	4.03
C6	GLN A 15 OE1	3.78	C6	THR A 73 CB	3.65
C3	GLN A 15 OE1	4.06	C29	THR A 73 O	4.79

C1	GLN A 15 OE1	4.15	C28	THR A 73 O	4.7
C29	GLN A 15 NE2	4.4	C24	THR A 73 O	4.55
C27	GLN A 15 NE2	4.64	C23	THR A 73 O	4.43
C25	GLN A 15 NE2	3.68	C14	THR A 73 O	4.98
C24	GLN A 15 NE2	3.86	C7	THR A 73 O	3.66
C23	GLN A 15 NE2	4	C6	THR A 73 O	3.84
C7	GLN A 15 NE2	4.76	N3	THR A 73 C	4.97
O8	GLN A 15 CD	4.99	N2	THR A 73 C	4.65
C29	GLN A 15 CD	4.32	C7	THR A 73 C	4.1
C28	GLN A 15 CD	4.7	C6	THR A 73 C	3.83
C27	GLN A 15 CD	4.19	C30	THR A 73 CA	4.98
C26	GLN A 15 CD	4.6	C29	THR A 73 CA	4.23
C25	GLN A 15 CD	3.85	C28	THR A 73 CA	4.46
C24	GLN A 15 CD	3.81	N2	THR A 73 CA	4.4
C23	GLN A 15 CD	4.22	C7	THR A 73 CA	4.7
N1	GLN A 15 CD	3.85	C6	THR A 73 CA	4.39
C7	GLN A 15 CD	4.08	C22	GLU A 71 OE2	3.56
C1	GLN A 15 CD	4.92	C21	GLU A 71 OE2	4.31
O8	GLN A 15 CG	4.62	C18	GLU A 71 OE2	4.58
C29	GLN A 15 CG	4.16	C17	GLU A 71 OE2	4.14
C28	GLN A 15 CG	4.35	C22	GLU A 71 OE1	4.83
C27	GLN A 15 CG	4.58	C21	GLU A 71 OE1	3.43
C26	GLN A 15 CG	4.52	C18	GLU A 71 OE1	4.32
C25	GLN A 15 CG	4.21	C17	GLU A 71 OE1	4.31
C24	GLN A 15 CG	4.46	C22	GLU A 71 CD	4.14
O9	GLN A 15 CB	4.92	C21	GLU A 71 CD	3.5
C31	GLN A 15 CB	4.64	O7	GLU A 71 CD	3.72
C30	GLN A 15 CB	4.75	O6	GLU A 71 CD	3.6
O8	GLN A 15 CB	3.94	C18	GLU A 71 CD	4.33
C29	GLN A 15 CB	3.96	C17	GLU A 71 CD	4.25
C28	GLN A 15 CB	4.44	C22	GLU A 71 CG	4.65
C25	GLN A 15 CB	4.23	C21	GLU A 71 CG	3.37
C24	GLN A 15 CB	4.93	O7	GLU A 71 CG	3.78
C31	GLN A 15 O	3.19	O6	GLU A 71 CG	4.48
C30	GLN A 15 O	3.23	C18	GLU A 71 CG	4.79
C29	GLN A 15 O	4.27	C21	GLU A 71 CB	4.87
C28	GLN A 15 O	4.65	C21	ASP A 69 OD2	4.85
C31	GLN A 15 C	4.15	C14	GLN A 15 OE1	3.4
C30	GLN A 15 C	4.27	C14	GLN A 15 CD	4.62
O8	GLN A 15 C	4.13	C21	GLN A 11 OE1	4.13
C29	GLN A 15 C	4.81	C20	GLN A 11 OE1	3.3
O9	GLN A 15 CA	4.86	C19	GLN A 11 OE1	3.17
C31	GLN A 15 CA	4.32	C18	GLN A 11 OE1	4.3
C30	GLN A 15 CA	4.74	C15	GLN A 11 OE1	4.51
O8	GLN A 15 CA	4.37	C14	GLN A 11 OE1	4.59
C29	GLN A 15 CA	4.61	C20	GLN A 11 NE2	4.72
C28	GLN A 15 CA	4.82	C19	GLN A 11 NE2	4.98
C6	GLN A 11 OE1	4.9	C20	GLN A 11 CD	4.32
			C19	GLN A 11 CD	4.36
			C14	GLN A 11 CD	4.82

Table S3			**Table S4**		
(c) 9-(N-arylmethylamino) noscapinoid, 17-Tubulin			**(d) Noscapine_Tubulin**		
Hydrogen bonding			**Hydrogen bonding**		
Hydrogen	**Hydrogen**	**Distance**	**Hydrogen**	**Hydrogen**	**Distance**

Donor (D)	Acceptor (A)	(D-A) in Å	Donor (D)	Acceptor (A)	(D-A) in Å
ASN A 228 ND2	17 O10	3.04	GLN D 247 NE2	O2	3.04
17 N1	GLU A 77 OE2	4.15	GLY D 246 N	O3	4.39
17 N1	GLU A 77 OE1	4.27	ARG D 48 NH2	O5	3.37
17 N1	GLN A 15 OE1	3.3			
Hydrophobic interaction			**Hydrophobic interaction**		
17	**Tubulin**	**Distance**	**Noscapine**	**Tubulin**	**Distance**
C21	LYS D 254 NZ	3.08	C20	LYS D 254 NZ	3.42
C19	LYS D 254 NZ	4.62	C16	LYS D 254 NZ	4.9
C18	LYS D 254 NZ	4.58	C20	LYS D 254 CE	3.9
C21	LYS D 254 CE	4.22	C20	LYS D 254 CD	3.94
O7	LYS D 254 CE	4.56	C20	LYS D 254 CG	4.95
C21	LYS D 254 CD	4.74	C20	ASP D 251 OD2	3.2
O7	LYS D 254 CD	4.61	C17	ASP D 251 OD2	4.65
C22	ALA D 250 CB	4.34	C20	ASP D 251 CG	4.32
C21	ALA D 250 CB	4.89	O4	ASP D 251 CG	4.49
O7	ALA D 250 CB	3.55	C20	ASP D 251 CB	5
O6	ALA D 250 CB	3.5	O4	ASP D 251 CB	4.73
C19	ALA D 250 CB	4.41	C20	ALA D 250 CB	3.93
C18	ALA D 250 CB	3.61	O6	ALA D 250 CB	4.52
C17	ALA D 250 CB	3.51	O5	ALA D 250 CB	4.8
C16	ALA D 250 CB	4.3	O4	ALA D 250 CB	3.77
C13	ALA D 250 CB	4.99	C19	ALA D 250 CB	4.48
O6	ALA D 250 C	4.85	C18	ALA D 250 CB	4.05
O6	ALA D 250 CA	4.71	C17	ALA D 250 CB	3.45
C17	ALA D 250 CA	4.92	C16	ALA D 250 CB	3.26
C20	GLN D 247 OE1	3.8	C15	ALA D 250 CB	3.7
C19	GLN D 247 OE1	4.51	C14	ALA D 250 CB	4.32
C15	GLN D 247 OE1	4.74	C13	ALA D 250 CB	4.3
C20	GLN D 247 NE2	3.62	C18	ALA D 250 O	4.52
C19	GLN D 247 NE2	4.86	C17	ALA D 250 O	4.73
C15	GLN D 247 NE2	3.96	O4	ALA D 250 C	4.75
C12	GLN D 247 NE2	3.57	C18	ALA D 250 C	4.98
C11	GLN D 247 NE2	4.02	C17	ALA D 250 C	4.83
C9	GLN D 247 NE2	3.78	O4	ALA D 250 CA	4.92
C8	GLN D 247 NE2	3.61	C17	ALA D 250 CA	4.76
C7	GLN D 247 NE2	4.17	C16	ALA D 250 CA	4.76
C6	GLN D 247 NE2	4.94	C13	GLN D 247 OE1	4.68
C5	GLN D 247 NE2	3.73	C13	GLN D 247 NE2	4.22
C4	GLN D 247 NE2	3.1	C10	GLN D 247 NE2	3.63
C3	GLN D 247 NE2	3.35	C9	GLN D 247 NE2	3.91
C2	GLN D 247 NE2	3.28	C8	GLN D 247 NE2	3.42
C1	GLN D 247 NE2	3.7	C4	GLN D 247 NE2	4.81
C20	GLN D 247 CD	3.85	C2	GLN D 247 NE2	4.78
C19	GLN D 247 CD	4.85	C1	GLN D 247 NE2	3.94
C15	GLN D 247 CD	4.46	O7	GLN D 247 CD	4.87
C12	GLN D 247 CD	4.39	O6	GLN D 247 CD	3.59
C11	GLN D 247 CD	4.73	C13	GLN D 247 CD	4.49
O3	GLN D 247 CD	4.98	O3	GLN D 247 CD	4.71
C9	GLN D 247 CD	4.93	O2	GLN D 247 CD	4.24
C8	GLN D 247 CD	4.75	C10	GLN D 247 CD	4.85
C5	GLN D 247 CD	4.86	C8	GLN D 247 CD	4.69
C4	GLN D 247 CD	4.4	O6	GLN D 247 CG	4.41
C3	GLN D 247 CD	4.66	O6	GLN D 247 CB	4.52
C2	GLN D 247 CD	4.49	O6	GLN D 247 C	4.48
C1	GLN D 247 CD	4.93	O6	GLN D 247 CA	3.65
C20	GLN D 247 CG	4.88	C13	GLN D 247 CA	4.39

C11	GLN D 247 CG	4.44	O3	GLN D 247 CA	4.82
C2	GLN D 247 CG	4.91	C13	GLN D 247 N	4.6
C19	GLN D 247 O	4.84	C16	GLY D 246 O	4.45
C20	GLN D 247 CA	4.44	C15	GLY D 246 O	3.74
C19	GLN D 247 CA	4.89	C14	GLY D 246 O	4.16
C15	GLN D 247 CA	4.82	C13	GLY D 246 O	3.15
C15	GLN D 247 N	4.98	C12	GLY D 246 O	4.08
C11	GLN D 247 N	4.68	O6	GLY D 246 C	4.06
C20	GLY D 246 O	4.03	C15	GLY D 246 C	4.88
C19	GLY D 246 O	4.39	C13	GLY D 246 C	4.09
C18	GLY D 246 O	4.44	O3	GLY D 246 C	4.03
C17	GLY D 246 O	4.04	C12	GLY D 246 C	4.91
C16	GLY D 246 O	3.62	O3	GLY D 246 CA	4.87
C15	GLY D 246 O	3.66	C12	GLY D 246 N	4.63
C13	GLY D 246 O	3.86	N1	PRO D 245 CB	4.9
C12	GLY D 246 O	4.04	C12	PRO D 245 CB	4.89
C11	GLY D 246 O	4.94	C7	PRO D 245 CB	3.79
C20	GLY D 246 C	4.82	C6	PRO D 245 CB	3.58
C16	GLY D 246 C	4.65	C3	PRO D 245 CB	4.63
C15	GLY D 246 C	4.49	C6	PRO D 245 CD	4.92
C13	GLY D 246 C	4.71	C7	PRO D 245 CG	4.07
O4	GLY D 246 C	4.64	C6	PRO D 245 CG	3.73
C12	GLY D 246 C	4.55	C12	PRO D 245 CA	4.74
C11	GLY D 246 C	4.52	C7	PRO D 245 CA	4.82
C11	GLY D 246 CA	4.56	C6	PRO D 245 CA	4.2
C13	GLY D 246 N	4.34	C21	ARG D 48 NH2	4.66
C12	GLY D 246 N	4.82	C19	ARG D 48 NH2	3.73
C11	GLY D 246 N	4.14	C18	ARG D 48 NH2	3.75
O5	PRO D 245 CB	4.76	C17	ARG D 48 NH2	4.76
C13	PRO D 245 CB	4.79	C14	ARG D 48 NH2	4.68
O4	PRO D 245 CB	4.08	C19	ARG D 48 NH1	4.4
C11	PRO D 245 CB	3.54	C18	ARG D 48 NH1	4.94
O3	PRO D 245 CB	3.72	C14	ARG D 48 NH1	4.74
C11	PRO D 245 CG	4.92	O5	ARG D 48 CZ	4.23
O3	PRO D 245 CG	4.89	C19	ARG D 48 CZ	3.85
C11	PRO D 245 O	3.84	C18	ARG D 48 CZ	4.32
O5	PRO D 245 C	4.9	C14	ARG D 48 CZ	4.56
C13	PRO D 245 C	4.87	C19	ARG D 48 NE	4.07
O4	PRO D 245 C	4.49	C18	ARG D 48 NE	4.78
C11	PRO D 245 C	3.78	C14	ARG D 48 NE	4.84
O3	PRO D 245 C	4.6	C11	ARG D 48 NE	4.33
O5	PRO D 245 CA	4.27	C19	ARG D 48 CD	4.88
C13	PRO D 245 CA	4.49	C11	ARG D 48 CD	4.28
O4	PRO D 245 CA	4.16	C6	ARG D 48 CD	4.62
C11	PRO D 245 CA	4.2	C11	ARG D 48 CG	4.55
O3	PRO D 245 CA	4.6	C11	GLU D 47 OE2	4.56
C22	ARG D 48 NH2	4.54	C7	GLU D 47 OE2	3.02
C13	ARG D 48 NH1	4.51	C6	GLU D 47 OE2	3.07
O6	ARG D 48 CZ	4.37	C3	GLU D 47 OE2	4.47
O5	ARG D 48 CZ	3.44	C7	GLU D 47 OE1	4.89
C13	ARG D 48 CZ	4.54	C6	GLU D 47 OE1	4.95
C13	ARG D 48 NE	4.64	C7	GLU D 47 CD	4.17
O5	ARG D 48 CD	3.66	C6	GLU D 47 CD	4.05
C13	ARG D 48 CD	4.78	C6	GLU D 47 CG	4.57
O5	ARG D 48 CG	4.77	C21	MET D 1 CE	3.79
C22	MET D 1 CE	4.22	C20	MET D 1 CE	3.31
C21	MET D 1 CE	4.86	O5	MET D 1 CE	4.27
O7	MET D 1 CE	4.85	O4	MET D 1 CE	3.06

C22	MET D 1 O	4.93	C18	MET D 1 CE	4.78
C32	ASN A 228 ND2	4.01	C17	MET D 1 CE	4.32
C29	ASN A 228 ND2	4.01	C20	MET D 1 SD	4.82
C28	ASN A 228 ND2	3.98	O4	MET D 1 SD	4.79
C32	ASN A 228 CG	4.46	C21	MET D 1 O	3.36
O10	ASN A 228 CG	3.87	C18	MET D 1 O	4.95
C32	ASN A 228 CB	3.82	C21	MET D 1 C	4.4
O10	ASN A 228 CB	3.74	O5	MET D 1 C	4.85
C32	THR A 225 OG1	4.28	C21	MET D 1 N	4.37
C29	THR A 225 OG1	3.18	C20	ASP A 98 OD2	2.95
C28	THR A 225 OG1	3.66	C20	ASP A 98 OD1	4.3
C27	THR A 225 OG1	4.31	C20	ASP A 98 CG	3.93
C26	THR A 225 OG1	4.39	O4	ASP A 98 CG	4.94
C25	THR A 225 OG1	3.9	C10	GLU A 77 OE2	3.79
C24	THR A 225 OG1	3.34	C9	GLU A 77 OE2	3.33
C23	THR A 225 OG1	3.68	C8	GLU A 77 OE2	3.55
C32	THR A 225 CG2	4.15	C4	GLU A 77 OE2	4.39
O10	THR A 225 CG2	4.82	C3	GLU A 77 OE2	4.19
C29	THR A 225 CG2	4.9	C2	GLU A 77 OE2	3.67
C28	THR A 225 CG2	4.77	C1	GLU A 77 OE2	4.1
C32	THR A 225 CB	4.31	C10	GLU A 77 OE1	4.34
O10	THR A 225 CB	4.54	C9	GLU A 77 OE1	4.89
C29	THR A 225 CB	4.14	C8	GLU A 77 OE1	4.73
C28	THR A 225 CB	4.42	O2	GLU A 77 CD	4.63
C24	THR A 225 CB	4.6	C10	GLU A 77 CD	4.46
C23	THR A 225 CB	4.94	O1	GLU A 77 CD	4.65
C32	THR A 225 O	4.03	C9	GLU A 77 CD	4.42
C32	THR A 225 C	4.45	C8	GLU A 77 CD	4.4
O10	THR A 225 C	4.87	C2	GLU A 77 CD	4.89
C32	THR A 225 CA	3.82	C1	GLU A 77 CD	4.88
O10	THR A 225 CA	3.93	C22	VAL A 74 CG2	3.12
C29	THR A 225 CA	3.93	O7	VAL A 74 CG2	3.85
C28	THR A 225 CA	4.21	C1	VAL A 74 CG2	4.88
C24	THR A 225 CA	4.78	C22	VAL A 74 CB	4.27
C32	THR A 225 N	4.8	O7	VAL A 74 CB	4.93
C29	THR A 225 N	3.94	C22	VAL A 74 CA	4.29
C28	THR A 225 N	4.63	C22	VAL A 74 N	4.03
C24	THR A 225 N	4.66	C22	THR A 73 OG1	2.91
C23	THR A 225 N	4.62	C21	THR A 73 OG1	4.34
C29	TYR A 224 CB	4.61	C19	THR A 73 OG1	3.93
C23	TYR A 224 CB	4.41	C18	THR A 73 OG1	4.17
C32	TYR A 224 O	4.82	C17	THR A 73 OG1	4.42
C29	TYR A 224 O	4.59	C16	THR A 73 OG1	4.5
O10	TYR A 224 C	4.66	C15	THR A 73 OG1	4.32
C29	TYR A 224 C	4.28	C14	THR A 73 OG1	3.99
C21	ASP A 98 OD2	3.19	C12	THR A 73 OG1	4.52
C21	ASP A 98 CG	4.42	C11	THR A 73 OG1	4.25
C30	GLU A 77 OE2	4.83	C5	THR A 73 OG1	3.84
C25	GLU A 77 OE2	4.46	C4	THR A 73 OG1	4.68
C14	GLU A 77 OE2	4.61	C1	THR A 73 OG1	4.76
C9	GLU A 77 OE2	4.95	C21	THR A 73 CG2	3.71
C7	GLU A 77 OE2	3.06	O5	THR A 73 CG2	4.51
C6	GLU A 77 OE2	2.87	C19	THR A 73 CG2	4.47
C5	GLU A 77 OE2	4.44	C18	THR A 73 CG2	4.59
C4	GLU A 77 OE2	4.12	C11	THR A 73 CG2	4.2
C3	GLU A 77 OE2	3.51	N1	THR A 73 CB	4.51
C1	GLU A 77 OE2	4.03	C22	THR A 73 CB	4.08
C30	GLU A 77 OE1	3.68	C21	THR A 73 CB	4.68

C27	GLU A 77 OE1	4.97	C19	THR A 73 CB	4.66
C26	GLU A 77 OE1	4.09	C18	THR A 73 CB	4.98
C25	GLU A 77 OE1	3.92	C14	THR A 73 CB	4.94
C24	GLU A 77 OE1	4.62	C11	THR A 73 CB	4.15
C7	GLU A 77 OE1	3.56	C5	THR A 73 CB	4.42
C6	GLU A 77 OE1	3.75	C22	THR A 73 O	4.61
C3	GLU A 77 OE1	4.51	C22	THR A 73 C	4.22
C1	GLU A 77 OE1	4.78	C22	THR A 73 CA	4.74
N2	GLU A 77 CD	4.75	C21	GLU A 71 OE2	2.71
C30	GLU A 77 CD	4.18	C20	GLU A 71 OE2	4.28
O8	GLU A 77 CD	4.62	C19	GLU A 71 OE2	4.72
C26	GLU A 77 CD	4.78	C18	GLU A 71 OE2	3.86
C25	GLU A 77 CD	4.49	C17	GLU A 71 OE2	3.76
N1	GLU A 77 CD	4.64	C16	GLU A 71 OE2	4.61
C7	GLU A 77 CD	3.55	C22	GLU A 71 OE1	4.22
C6	GLU A 77 CD	3.36	C21	GLU A 71 OE1	4.66
C3	GLU A 77 CD	4.35	C20	GLU A 71 OE1	4.98
C1	GLU A 77 CD	4.82	C17	GLU A 71 OE1	4.61
C30	GLU A 77 CG	4.64	C16	GLU A 71 OE1	4.82
C7	GLU A 77 CG	4.83	C21	GLU A 71 CD	3.88
C6	GLU A 77 CG	4.26	C20	GLU A 71 CD	4.32
C30	GLU A 77 CB	3.95	O5	GLU A 71 CD	4.82
C30	GLU A 77 O	4.85	O4	GLU A 71 CD	4
C30	GLU A 77 C	4.99	C18	GLU A 71 CD	4.6
N2	VAL A 74 CG2	4.28	C17	GLU A 71 CD	4.19
C14	VAL A 74 CG2	4.25	C16	GLU A 71 CD	4.72
C7	VAL A 74 CG2	4.61	C21	GLU A 71 CG	4.81
C6	VAL A 74 CG2	4.05	C20	GLU A 71 CG	4.22
C7	VAL A 74 CG1	4.67	O4	GLU A 71 CG	4.31
C6	VAL A 74 CG1	4.61	C17	GLU A 71 CG	4.9
C7	VAL A 74 CB	4.99	C10	GLN A 15 OE1	3.24
C6	VAL A 74 CB	4.47	C9	GLN A 15 OE1	4.95
N2	VAL A 74 CA	4.89	C8	GLN A 15 OE1	4.15
C14	VAL A 74 CA	4.54	C1	GLN A 15 OE1	4.93
C7	VAL A 74 CA	4.97	C10	GLN A 15 NE2	4.39
C6	VAL A 74 CA	4.13	O2	GLN A 15 CD	4.11
C14	VAL A 74 N	4.19	C10	GLN A 15 CD	4.08
C6	VAL A 74 N	4.56	C22	GLN A 11 OE1	4.29
C22	THR A 73 OG1	3.82	C13	GLN A 11 OE1	4.75
C18	THR A 73 OG1	4.61	O7	GLN A 11 CD	4.64
C17	THR A 73 OG1	4.21	O6	GLN A 11 CD	4.79
C16	THR A 73 OG1	4.34	O2	GLN A 11 CD	4.7
C15	THR A 73 OG1	4.82			
C14	THR A 73 OG1	2.84			
C13	THR A 73 OG1	4.76			
C6	THR A 73 OG1	4.82			
C22	THR A 73 CG2	4.37			
C14	THR A 73 CG2	4.8			
C22	THR A 73 CB	4.72			
C14	THR A 73 CB	3.59			
C14	THR A 73 O	3.93			
C6	THR A 73 O	4.34			
N2	THR A 73 C	4.93			
C14	THR A 73 C	3.9			
C6	THR A 73 C	4.63			
C14	THR A 73 CA	4.39			
C22	GLU A 71 OE2	3.09			
C21	GLU A 71 OE2	4.22			

C18	GLU A 71 OE2	4.94			
C17	GLU A 71 OE2	4.92			
C22	GLU A 71 OE1	4.25			
C21	GLU A 71 OE1	3.94			
C18	GLU A 71 OE1	4.81			
C22	GLU A 71 CD	3.77			
C21	GLU A 71 CD	3.76			
O7	GLU A 71 CD	4.41			
O6	GLU A 71 CD	4.96			
C18	GLU A 71 CD	4.86			
C22	GLU A 71 CG	4.71			
C21	GLU A 71 CG	3.77			
O7	GLU A 71 CG	4.72			
C32	ALA A 19 CB	4.16			
C31	ALA A 19 CB	4.39			
O10	ALA A 19 CB	4.68			
C31	ALA A 19 CA	4.5			
C31	ALA A 19 N	4.04			
C31	ASN A 18 ND2	3.46			
C30	ASN A 18 ND2	4.42			
C31	ASN A 18 CG	4.16			
C31	ASN A 18 CB	3.85			
C31	ASN A 18 O	4.9			
C31	ASN A 18 C	4.32			
C31	ASN A 18 CA	4.68			
C29	GLN A 15 OE1	4.76			
C25	GLN A 15 OE1	4.9			
C24	GLN A 15 OE1	4.37			
C23	GLN A 15 OE1	4.2			
C7	GLN A 15 OE1	2.78			
C6	GLN A 15 OE1	3.88			
C3	GLN A 15 OE1	3.77			
C1	GLN A 15 OE1	3.96			
C29	GLN A 15 NE2	4.22			
C24	GLN A 15 NE2	4.41			
C23	GLN A 15 NE2	4.23			
C7	GLN A 15 NE2	4.68			
C1	GLN A 15 NE2	4.91			
C29	GLN A 15 CD	4.29			
C28	GLN A 15 CD	4.98			
C25	GLN A 15 CD	4.99			
C24	GLN A 15 CD	4.28			
C23	GLN A 15 CD	4.31			
N1	GLN A 15 CD	3.8			
C7	GLN A 15 CD	3.96			
C3	GLN A 15 CD	4.8			
C1	GLN A 15 CD	4.72			
C29	GLN A 15 CG	4.46			
C28	GLN A 15 CG	4.71			
C24	GLN A 15 CG	4.7			
N1	GLN A 15 CG	4.84			
C7	GLN A 15 CG	4.97			
C31	GLN A 15 CB	4.98			
O10	GLN A 15 CB	4.39			
C29	GLN A 15 CB	4.41			
C28	GLN A 15 CB	4.44			
C32	GLN A 15 O	4.16			
C31	GLN A 15 O	3.49			

C28	GLN A 15 O	4.28			
C27	GLN A 15 O	4.78			
C31	GLN A 15 C	4.4			
O10	GLN A 15 C	4.32			
C28	GLN A 15 C	4.98			
C31	GLN A 15 CA	4.49			
O10	GLN A 15 CA	4.68			
C28	GLN A 15 CA	4.91			
C21	GLN A 11 OE1	4.6			
C20	GLN A 11 OE1	3.46			
C19	GLN A 11 OE1	3.33			
C18	GLN A 11 OE1	4.57			
C15	GLN A 11 OE1	4.77			
C20	GLN A 11 NE2	4.73			
C20	GLN A 11 CD	4.38			
C19	GLN A 11 CD	4.47			

CHAPTER-4

Development of 1,3-diynyl derivatives of noscapine as potent tubulin binding anticancer agents for the management of breast cancer

Abstract

We developed 1,3-diynyl derivatives of noscapine (an opium alkaloid) through *in silico* combinatorial approach and screened out a panel of promising derivatives that bind tubulin and display anticancer activity. The selected derivatives such as 9-4-^{t}Bu-Ph-Diyne **(20p)**, 9-3,4-Di-Cl-Diyne **(20k)** and 9-3,4-Di-F-Diyne **(22s)** noscapinoids revealed improved predicted binding energy of -6.676 kcal/mol for **20p**, -7.294 kcal/mol for **20k** and -7.750 kcal/mol for **20s** respectively in comparison to noscapine (-5.246 kcal/mol). These 1,3-diynyl derivatives **(20p, 29k** and **20s)** were strategically synthesized in high yields by regioselective modification of noscapine scaffold and HPLC purified (purity is > 96%). The decrease in intrinsic fluorescence of purified tubulin to 8.39%, 17.39% and 25.47% by **20p, 20k** and **20s** respectively, compared to control suggests their binding capability to tubulin. Their cytotoxicity activity was validated based on cellular studies using two human breast adenocarcinoma (MCF-7 and MDA-MB-231), a panel of primary breast tumor cells and one normal human embryonic kidney cell (293T). The 1,3-diynyl noscapinoids, **20p, 20k** and **20s** inhibited cellular proliferation in all the cancer cells that ranged between 6.2 and 38.9 µM, without affecting the normal healthy cells (cytotoxicity is < 5% at 100 µM). Further, these novel derivatives arrest cell cycle in the G2/M-phase, followed by induction of apoptosis to cancer cells. Thus, we conclude that 1,3-diynyl-noscapinoids have great potential to be a novel therapeutic agent for breast cancers.

Key words: Noscapine; 1, 3-diynyl-noscapinoids; tubulin binding; anticancer agents; breast cancer

4.1.Introduction

Currently available breast cancer chemotherapeutic regimens have been plagued with serious toxicity (peripheral neuropathies, gastrointestinal toxicity, myelosuppression, and immunosuppression) owing to their non-selective action and extreme over polymerizing or depolymerizing effects on microtubules (Rowinsky, 1997; Pace et al., 1996; Crown & O' Leary, 2000; Theiss & Meller, 2000; Topp et al., 2000).This unsatisfactory situation has driven intensive research over the last few decades to find novel tubulin binding anticancer agents that are more specific to cancer cells without having severe side effects. Noscapine, a safe anti-tussive drug, is an excellent choice of drug to use and because of the nature of its action; it is not harmful to healthy cells or healthy volunteers including pregnant mothers (Ye et al., 1998; Zhou et al., 2006; Dahlstrom et al., 1982; Karlsson et al., 1990; Jensen et al., 1992). It was found that noscapine binds stoichiometrically to tubulin (one noscapine molecule for each αβ-tubulin dimer), modifies tubulin compliance and arrests mammalian cells at the mitotic phase (Lettre, 1954). However, unlike vinca alkaloids and taxanes, it does not induce over-polymerization, depolymerization or any change in the general interphase microtubule organization. Because of its subtle effect on the kinetic parameters of dynamic instability of microtubules, it inhibits mitosis at prometaphase and induces apoptosis, specifically to cancer cells without affecting normal cells (Warolin, 1999). Further, in comparison to the other microtubule binding drugs such as taxanes and vinca alkaloids, noscapine offers various advantages in cancer treatment. It arrests a variety of mammalian cells including drug resistant variants in mitosis and targets them for apoptosis (Karlsson et al., 1990; Jordan et al., 1993; Wang et al., 2005). It is a poor substrate for drug pumps (poly glycoproteins and MDR-related proteins) which constitute a major cause of drug resistance (Karlsson et al., 1990). It inhibits the progression of murine melanoma, lymphoma, glioblastoma and human breast tumors implanted in nude mice,without any detectable toxicity (Karlsson et al., 1990; Jordan et al., 1993; Wang et al., 2005). It doesn't cause any immunological and neurological toxicity. It is orally administered and hence is devoid of any anaphylactic reactions (Karlsson et al., 1990; Jordan et al., 1993; Wang et al., 2005). It shows a mean bioavailability of ~30-32 % over a dose range of 10 mg/kg to 300 mg/kg in mice (Wang et al., 2005). However, noscapine has low cytotoxicity. The values of IC_{50} remain within the high micromolar ranges (~21.1 to 100 μM) with the cancer cells of different tissue origin (Karlsson et al., 1990; Jordan et al., 1993; Wang et al., 2005; Mahmoudian and Rahimi- Moghaddam, 2009). To further improve its efficacy, efforts were based on rational drug design and synthesis of new generations of noscapine

derivatives for better therapeutic outcomes. We have already developed a battery of noscapinoids based on our *in silico* combinatorial approaches and screening of derivatives as potent tubulin binding agents using molecular docking in combination with molecular dynamics simulations. Some of these derivatives are seen to be 40-80 folds more potent compared to noscapine as anticancer compounds (Mahaddalkar et al., 2017; Santoshi et al., 2015; Manchukonda et al., 2014, 2013; Naik et al., 2012, 2011). For instance, 9-nitronoscapine was found to be active against drug-resistant ovarian cancer and T-cell lymphoma cells (Aneja et al., 2006a) and its reduced congener, 9-aminonoscapine (Naik et al., 2011) as well as biaryl inserted noscapine analogs (Santoshi et al., 2015) have good activity as tubulin binding anticancer agents.

Considering the increased activity of 9'-substituted derivatives compared to its parent molecule noscapine, in this study, we aimed to develop a new series of noscapine derivatives by substituting 1,3-diynyl functional group at the C9'-position (called diynyl derivatives). These derivatives were then chemically synthesized and their anticancer activity was validated, based on a cellular study using established human breast cancer cell lines (MCF-7 and MDAMB-231) and a panel of primary breast tumor cells. The novel derivatives were seen to bind tubulin heterodimer with increased binding affinity, effectively inhibit cancer cell proliferation, cause selective G2/M arrest in cancer cells and induce apoptosis.

4.2. Materials and methods

4.2.1. Protein preparation

The co-crystallized PDB structure of the amino noscapine-tubulin complex (PDB ID: 6Y6D, resolution 2.20 Å) (Oliva et al., 2020) was used for the molecular docking and calculation of the binding affinity of the noscapinoids with tubulin. A complex consisting of both 'A' and 'D' chains of the protein was acquired after a manual inspection and cleaning of the structure. The hydrogen atoms were added and the protein structure was prepared using the protein preparation wizard (Schrodinger software package). All water molecules were removed from the complex. The complex obtained was energy minimized using OPLS 2005 force field with Polack-Ribiere Conjugate Gradient (PRCG) algorithm (Polak & Ribiere, 1969). The minimization was stopped either after 5,000 steps of minimizations or after the energy gradient converged below 0.001 kcal/mol. The structure was further refined by performing an all-atom molecular dynamics (MD) simulation of 100 ns in explicit water using GROMACS 4.5.4 software (Berendsen et al., 1995) and the GROMOS96 force field with similar parameters set up as reported earlier (Santoshi et al., 2014). A time step of 2 fs was used for sampling from the MD trajectory, whereas the five

frames with the lowest minimum total energy from the trajectory were used to generate an average structure of the tubulin.

4.2.2. Rational design of 1,3-diynyl derivatives of noscapine

Several natural products **1-8** (Figure1) which are in the clinics consist of ethyne and 1,3-diynes functionality as an active pharmacophore for their anticancer, anti-HIV, antifungal, antibacterial and antiviral activities (Lehmann et al., 2016; Wang et al., 2014; Fekete & Fekete, 2019; Shi & Lei, 2014; Ma et al., 2017; Liang et al., 2016; Erwin, 2016; Lee et al., 2016; Gubaidullin et al., 2018). Inspired by these pharmacological properties, we rationalized to incorporate 1,3-diynyl structural motif into the natural noscapine to develop a new series of analogs (we called 1,3-diynyl-noscapinoids) (Figure 2). Initially, we have developed a library of 20 derivatives as depicted in Figure 3 by *in silico* combinatorial approach, followed by the screening of a panel of three most potent derivatives using molecular docking for chemical synthesis and experimental evaluation.

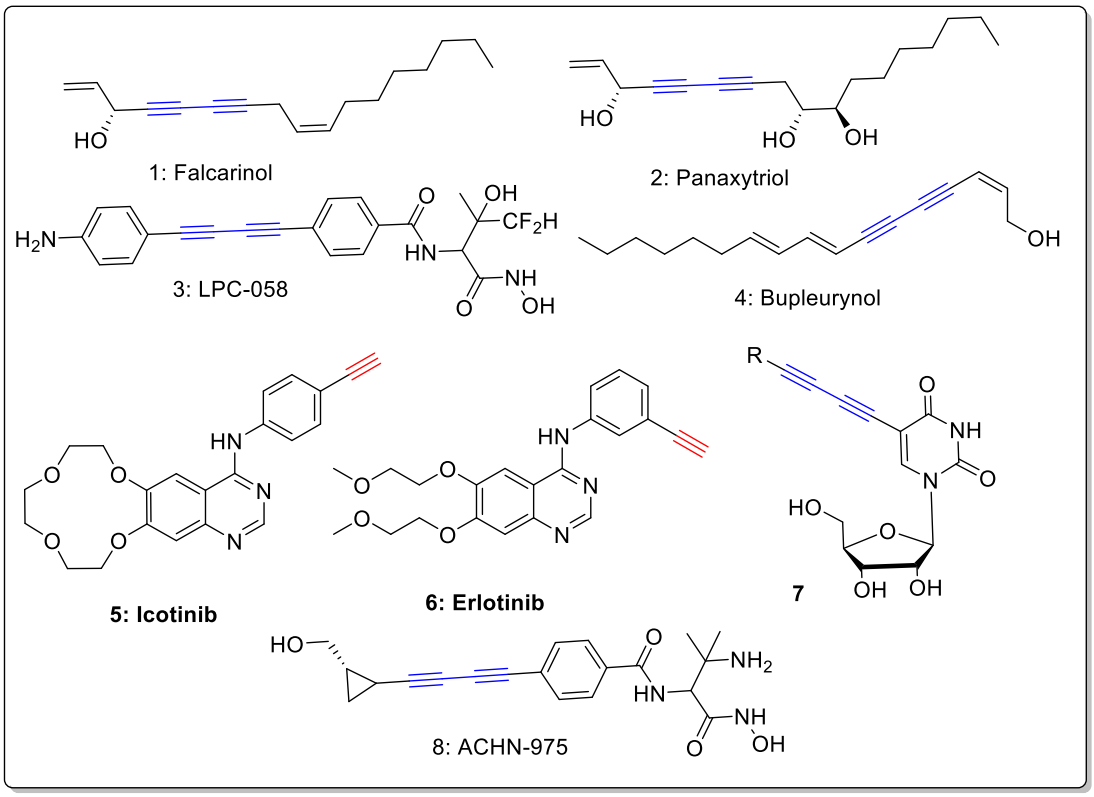

Figure 4.1. Structures of anticancer drugs **1** and **2** containing ethyne group and 1,3-diyne containing bioactive natural and synthetic products**3-8**.

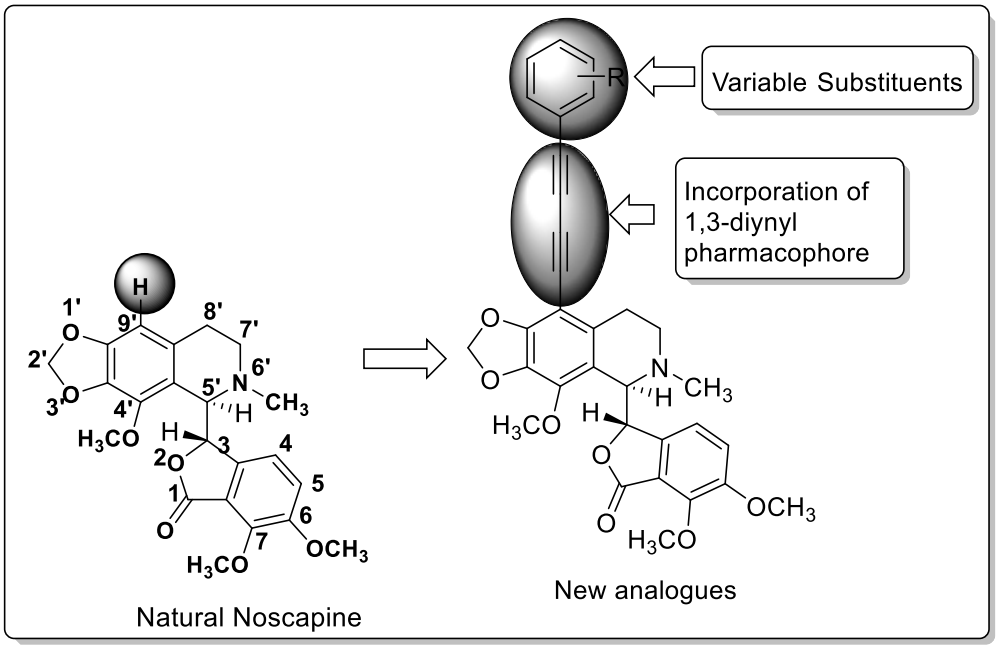

Figure 4.2. Structural representation of the design of 1,3-diynyl noscapinoids by derivatization at the C-9 position of noscapine.

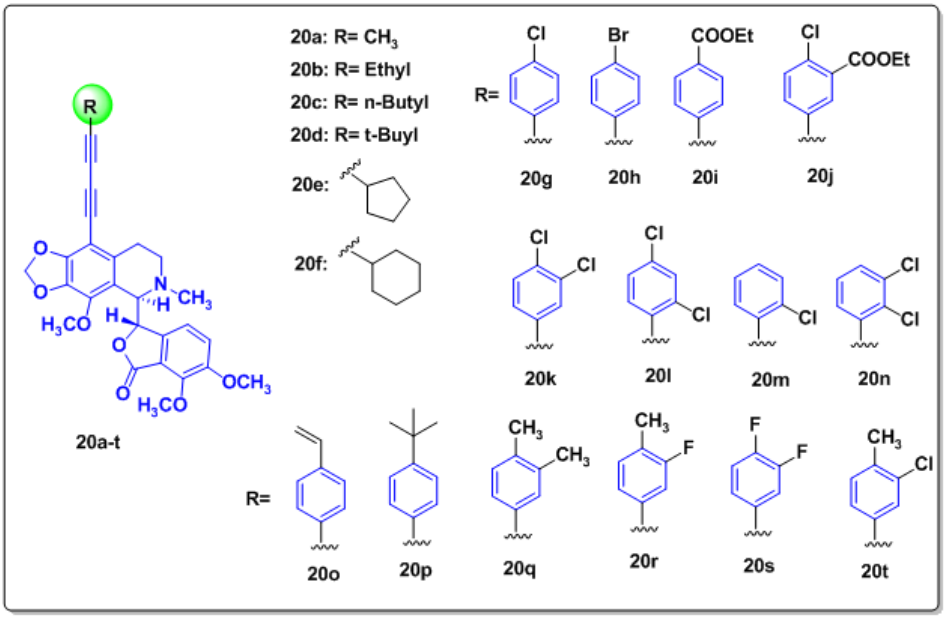

Figure 4. 3. Design of a library of twenty 1,3-diynyl noscapinoids by substitution of different functional groups at 'R' based on *in silico* combinatorial approach.

4.2.3. Preparation of molecular structure

Molecular structures of 1,3-diynyl-noscapinoids (Figure 3) and the previously reported (Figure 4) were built using ISIS draw and converted into 3D structure using Chemsketch. These molecular structures were imported into Maestro (Schrödinger software package) and energy minimized using Macromodel (Schrödinger software package). OPLS 2005 force field with PRCG algorithm (energy gradient of 0.001) was used for energy minimization. Complete geometric optimization of these structures was performed using Jaguar (Schrodinger software package). Hybrid density functional theory

with Becke's three-parameter exchange potential and the Lee-Yang-Parr correlation functional (B3LYP) (Lee et al., 1988; Becke, 1993) and 3-21G* basis set (Binkley et al., 1980; Gordon et al., 1982; Pietro et al., 1982) were used for geometric optimization. Ligprep (Schrödinger software package) was used to define appropriate bond order, ionization states at physiological pH, generation of possible tautomers and minimization of the ring conformations for each structure.

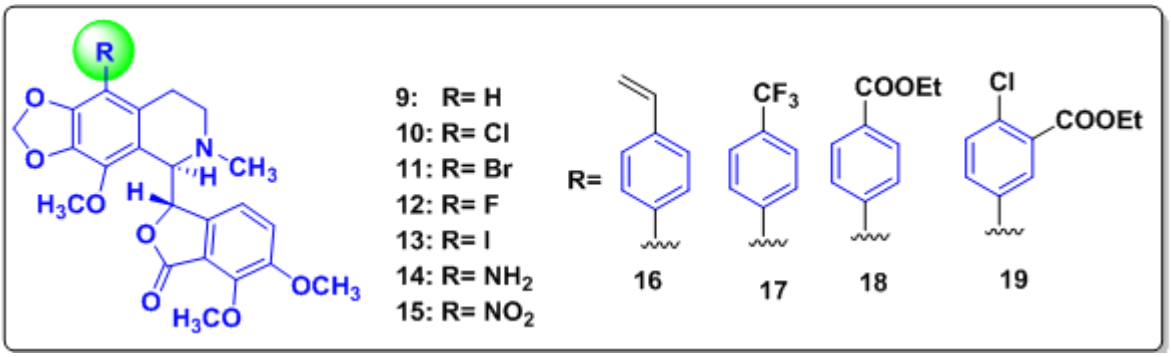

Figure 4.4. Molecular structures of previously reported noscapine derivatives that have experimentally proven to bind tubulin with known binding free energy (Table 1) and used as a training set molecules for LIE-SGB model building.

4.2.4. Molecular docking

Noscapinoids prepared above were docked onto the noscapine binding pocket at the interface of αβ-tubulin (Oliva et al., 2020) using Glide docking (Schrödinger software package). In brief, an inner grid box of size 12Å x 12Å x 12Å was defined at the centroid of the binding site (Oliva et al., 2020) by selecting the co-complex ligand, amino-noscapine using Glide grid-receptor generation program. This box defines the search space in which the diameter midpoint of each docked ligand is required to be present. Further, an outer grid box was also defined with a size of ≤ 24 Å of the co-complexed ligand, amino noscapine. It defines the volume within which all ligand atoms of a valid pose must be located. All the noscapinoids were docked using Glide XP (extra precision) algorithm and their binding pose evaluated, using Glide XP_{Score} function (Friesner et al., 2004; Halgren et al., 2004). A scale factor of 0.4 for van der Waals radii was applied to atoms of protein with absolute partial charges less than or equal to 0.25. The single best conformation for each ligand was used for further analysis. Finally, based on the docking result, we have screened out three 1,3-diynyl-noscapinoids such as 9-4-^{t}Bu-Ph-Diyne **(20p)**, 9-3,4-Di-Cl-Diyne **(20k)** and 9-3,4-Di-F-Diyne **(20s)** (Figure 3) from the library that were having the lowest docking score.

4.2.5. LIE-SGB model building

A predictive model for predicting the binding free energy ($\Delta G_{bind,pred}$) of the 1,3-diynyl-noscapinoids with tubulin was developed based on linear interaction energy model (LIE) with a surface generalized Born (SGB) continuum solvation model (Gordon et al., 1982). A training data set of noscapinoids (Figure 4) with known experimental binding free energy, $\Delta G_{bind,expt}$ was used and mapped with various predicted energy parameters such as van der Waals (U_{vdw}), Coulumbic (U_{coul}), reaction field (U_{rxn}) and cavity energy (U_{cav}) based on the LIE model to develop the empirical prediction model. Liaison programme (Schrödinger software package) was used to estimate the above energy parameters from the docked complexes of the tubulin-noscapinoids based on Hybrid Monte Carlo simulation technique as reported previously (Santoshi et al., 2015). A residue-based cut off of 12 Å was set for the non-bonding interactions.

$$\Delta G_{bind,pred} = \alpha\left(\langle U^b_{vdw}\rangle - \langle U^f_{vdw}\rangle\right) + \beta\left(\langle U^b_{coul}\rangle - \langle U^f_{coul}\rangle\right) + \gamma\left(\langle U^b_{rxn}\rangle - \langle U^f_{rxn}\rangle\right) + \delta\left(\langle U^b_{cav}\rangle - \langle U^f_{cav}\rangle\right)$$

Here $\langle\ \rangle$ represents the ensemble average, *b* represents the bound form of the ligand, *f* represents the free form of the ligand, and α, β, γ and δ are the coefficients determined using Minitab statistical package (Minitab Inc.).

4.2.6. General method of chemical synthesis

Melting points were measured by CINTEX programmable melting point apparatus and are uncorrected. ^{1}H and ^{13}C NMR spectra of samples in $CDCl_3$ were recorded on AVANCE- 300 MHz, 400 MHz and 500 MHz spectrometers. Chemical shifts (δ) are reported relative to TMS (δ = 0.0) as the internal standard. Spin multiplicities are described as s (singlet), brs (broad singlet), d (doublet), t (triplet), q (quartet), or m (multiplet). Coupling constants are reported in hertz (Hz). Mass spectra were recorded in ESI spectrometers. High resolution mass spectra were recorded on QSTAR XL hybrid ms/ms system (Applied Bio systems/MDS Sciex, Foster city, USA), equipped with an ESI source (IICT, Hyderabad). IR was recorded on Thermo Nicolet nexus-670 spectrometer with reference to KBr. TLC was performed on Merck 60 F-254 silica gel plates.

4.2.7. Chemical synthesis of 1,3-diynyl-noscapinoids

The screened out three promising 1,3-diynyl-noscapinoids, **20p, 20k** and **20s** were chemically synthesized by coupling of 1,3-diynyls functionality (Nagireddy et al., 2019) with noscapine scaffold as depicted in Figure 5.

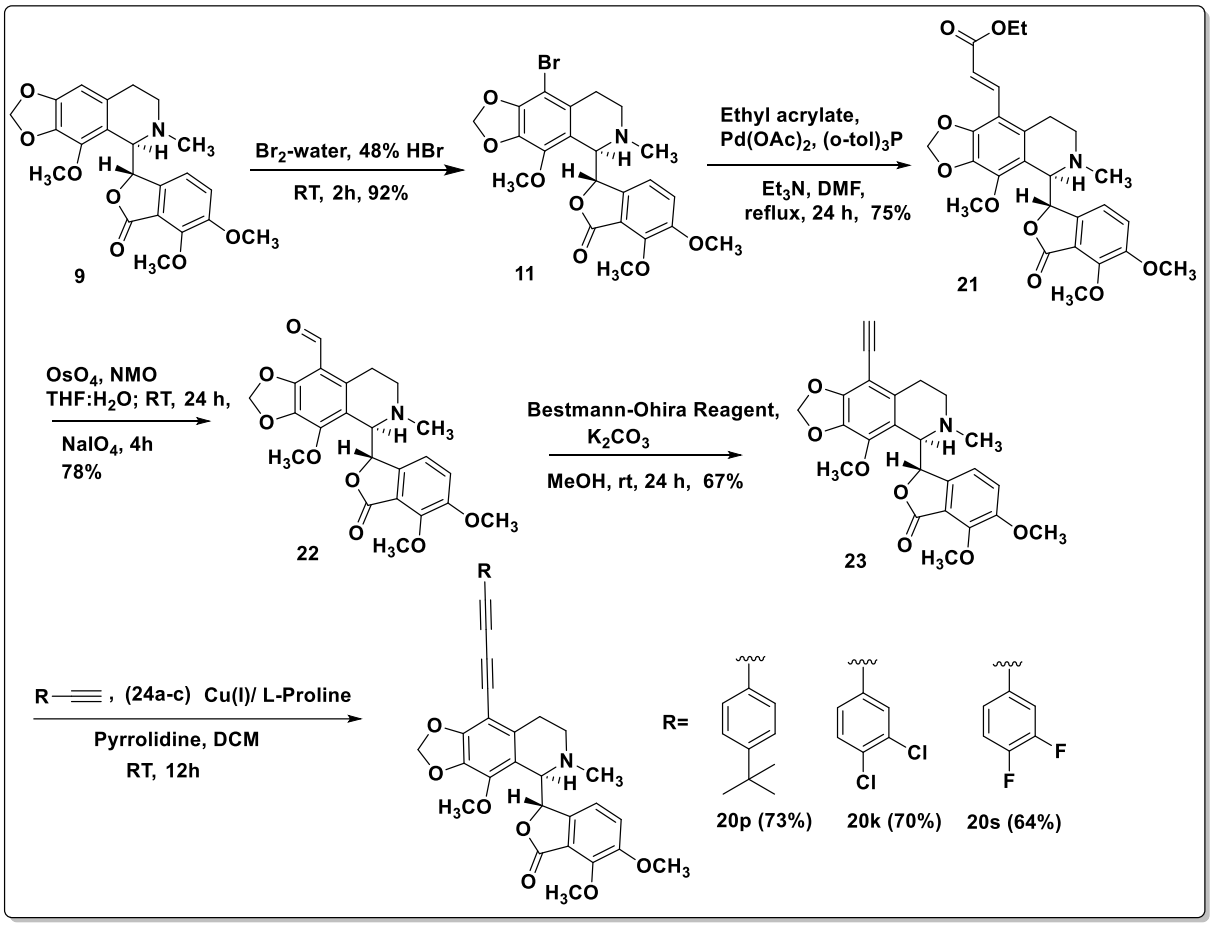

Figure 4.5. Reaction scheme for synthesis of 9-(1,3-diynyl) noscapinoids **20p, 20k and 20s.**

At the starting point of our synthetic strategy, 9-bromo noscapine **11** was developed from the noscapine as starting material using bromine water (48% aq. HBr), as reported earlier (Santoshi et al., 2011) by modifying the reaction conditions. To a solution of 9-bromo noscapine **11** in degassed DMF: Et_3N, was added ethyl acrylate, $Pd(OAc)_2$, and Tri(o-tolyl) phosphine under Argon. The contents were stirred at 130 °C for 24 h; post-completion, the reaction was brought to room temperature and DMF was removed under vacuum. About 20 ml of water was added and extracted with dichloromethane (3 x 20 ml), and the combined organic portions were washed with ice cold water, dried over anhydrous Na_2SO_4 and concentrated to generate the crude residue, which was chromatographed over triethylamine silica bed using 40% EtOAc in *n*-hexane as eluent to form pure compound **21** (7.80 g, 75%). Compound **21** (4.0 g, 7.82 mmol) in THF/H_2O (30mL, 9:1, v/v) and N-methyl morpholine-N-oxide (6.32 g, 47.0 mmol) followed by osmium(IV) oxide (0.08 mL, 1.56 mmol) was added at room temperature. The reaction mixture was stirred for 24 h, and sodium periodate (2.0 g, 9.38 mmol) was added and stirred further for 4 h. The reaction mixture was quenched with sodium sulphite (2.0 g) extracted with chloroform (2 x 20 mL), the combined organic layer was dried over Na_2SO_4 and concentrated. The crude

residue was purified over silica gel column chromatography eluting with hexane/ethyl acetate (70:30) to give compound **22** (2.78 g, 78%). 9-Formylnoscapine **22** (2.0 g, 4.5 mmol) in MeOH (20 mL) and K_2CO_3 (1.25 g, 9.07 mmol) followed by bestmann-ohira reagent (1.13 g, 5.88 mmol) were added and stirred at RT for 24 h. The reaction mixture was quenched with water, extracted with dichloromethane (2 x 10 mL), the organic layer was dried over Na_2SO_4 and concentrated under reduced pressure. The crude residue was purified over silica gel column chromatography eluting with hexane/ethyl acetate (70:30) to give 9-ethynylnoscapine **23** (1.32 g, 67%).

To the solution of 9-ethynylnoscapine **23** (1.0 mmol) in dichloromethane (5 mL), CuI, L-proline, pyrrolidine, and substituted phenyl acetylenes (**24a-c**) (1.2 mmol) were added and stirred at RT for 12 h. The solvent was removed under vacuum, water (5 mL), and dichloromethane (2 x 10 mL) were added, the organic layer was separated, dried over anhydrous Na_2SO_4, and filtered. The crude residue thus obtained was chromatographed over a triethylamine treated silica gel column, eluting with n-hexane/ethyl acetate (7:3) to produce **20p, 20k** and **20s** as solid products in good yields (Figure 5). Purity of the products **20p, 20k and 20s** were assessed by analytical HPLC using C18 column, acetonitrile: water (25:75) as eluents were found be > 96% pure. All the intermediate and final products were structurally characterized by IR, ^{1}H &^{13}C NMR spectroscopy and mass spectrometry techniques and were included in the supporting material (S1-S8).

(*E*)-ethyl-3-((*R*)-5-((*S*)-4,5-dimethoxy-3-oxo-1,3-dihydroisobenzofuran-1-yl)-4-methoxy-6-methyl-5,6,7,8-tetrahydro-[1,3]dioxolo[4,5-*g*]isoquinolin-9-yl)acrylate (21)
M.P: 75 ºC. ^{1}H NMR (500MHz, $CDCl_3$): δ= 7.71 (d, *J*=15.8 Hz, 1H), 6.99 (d, *J*=8.1 Hz, 1H), 6.69 (d, *J*=15.8 Hz, 1H), 6.25 (d, *J*=8.1 Hz, 1H), 6.05 (s, 2H), 5.43 (d, *J*=4.4 Hz, 1H), 4.38 (d, *J*=4.4 Hz, 1H), 4.26 (q, *J*=7.0 Hz, 2H), 4.10 (s, 3H), 4.05 (s, 3H), 3.88 (s, 3H), 2.79-2.68 (m, 2H), 2.53 (s, 3H), 2.46-2.38 (m, 1H), 2.10-2.00 (m, 1H), 1.33 (t, *J*=7.0Hz, 3H). ^{13}C NMR (75 MHz, $CDCl_3$): δ= 167.9, 167.7, 152.1, 148.2, 147.6, 141.6, 141.1, 135.6, 133.6, 131.4, 120.5, 119.6, 118.1, 117.7, 117.3, 109.5, 101.1, 81.4, 62.1, 60.8, 60.3, 59.3, 56.6, 48.8, 45.5, 23.9, 14.2. IR (KBr): 2939, 2800, 1761, 1706, 1616, 1498, 1437, 1270, 1178, 1140, 1034, 887, 732 cm^{-1}. MS (ESI) m/z: 512 $[M+H]^+$; HRMS (ESI): Calcd for $C_{27}H_{30}NO_9$ $[M+H]^+$: 512.19151, found: 512.19203.

(*R*)-5-((*S*)-4,5-dimethoxy-3-oxo-1,3-dihydroisobenzofuran-1-yl)-4-methoxy-6-methyl-5,6,7,8-tetrahydro[1,3]dioxolo[4,5-*g*]isoquinoline-9-carbaldehyde (22)
M.P: 182 °C. ^{1}H NMR (500MHz, $CDCl_3$): δ= 10.25 (s, 1H), 7.26 (d, *J*=8.3 Hz, 1H), 6.51 (d, *J*=8.2 Hz, 1H), 6.08 (s, 2H), 5.44 (d, *J*=4.8 Hz, 1H), 4.30 (d, *J*=4.8 Hz, 1H), 4.09 (s,

3H), 4.08 (s, 3H), 3.89 (s, 3H), 3.20-3.12 (m, 1H), 2.87-2.79 (m, 1H), 2.54-2.46 (m, 4H), 2.46-2.38 (m, 1H). ^{13}C NMR (125 MHz, $CDCl_3$): δ= 185.9, 166.8, 152.4, 146.4, 143.8, 140.3, 132.2, 118.3, 117.7, 116.7, 110.2, 101.2, 80.0, 61.0, 59.8, 58.5, 55.7, 46.8, 44.1, 22.4. IR (KBr): 2949, 2739, 1751, 1677, 1615, 1496, 1447, 1270, 1127, 999, 970, 940, 786, 695, 509 cm^{-1}. MS (ESI): m/z: 442 $[M+H]^+$; HRMS (ESI): Calcd for $C_{23}H_{24}O_8N$ $[M+H]^+$: 442.14964, found: 442.15032.

(*S*)-3-((*R*)-9-ethynyl-4-methoxy-6-methyl-5,6,7,8-tetrahydro-[1,3]dioxolo[4,5-*g*]isoquinolin-5-yl)-6,7dimethoxy isobenzofuran-1(3*H*)-one (23)

mp: 148 °C. ^{1}H NMR (500MHz, $CDCl_3$): δ= 7.02 (d, *J*=8.1 Hz, 1H), 6.28 (d, *J*=8.1 Hz, 1H), 6.02 (s, 2H), 5.52 (d, *J*=4.1 Hz, 1H), 4.33 (d, *J*=4.1 Hz, 1H), 4.09 (s, 3H), 4.03 (s, 3H), 3.88 (s, 3H), 3.42 (s, 1H), 2.80-2.65 (m, 2H), 2.52 (s, 3H), 2.46-2.38 (m, 1H), 2.10-1.99 (m, 1H). ^{13}C NMR (75MHz, $CDCl_3$): δ= 167.9, 152.1, 150.5, 147.6, 141.2, 133.8, 133.1, 119.6, 118.2, 117.4, 101.3, 96.6, 84.3, 81.2, 75.9, 62.1, 60.6, 59.3, 56.7, 48.5, 45.4, 24.7. IR (KBr): 3297, 2948, 2796, 1757, 1626, 1501, 1463, 1440, 1277, 1119, 1033, 1003, 653 cm^{-1}. MS (ESI) m/z: 438 $[M+H]^+$; HRMS (ESI): Calcd for $C_{24}H_{24}O_7N$ $[M+H]^+$: 438.15473, found: 438.15521.

(*S*)-3-((*R*)-9-((4-(tert-butyl)phenyl)buta-1,3-diyn-1-yl)-4-methoxy-6-methyl-5,6,7,8-tetra hydro-[1,3]dioxolo[4,5-*g*]isoquinolin-5-yl)-6,7-dimethoxyisobenzofuran-1(3*H*)-one (20p)

Yield: 73%; White solid; mp: 122-124 °C. ^{1}H NMR (400 MHz, $CDCl_3$): δ = 7.46-7.42 (m, 2H), 7.37-7.33 (m, 2H), 7.04 (d, *J* = 8.31 Hz, 1H), 6.30 (d, *J* = 8.31 Hz, 1H), 6.03 (s, 2H), 5.53 (d, *J* = 4.40 Hz, 1H), 4.34 (d, *J* = 4.40 Hz, 1H), 4.09 (s, 3H), 4.04 (s, 3H), 3.89 (s, 3H), 2.83-2.67 (m, 2H), 2.53 (s, 3H), 2.48-2.41 (m, 1H), 2.15-2.06 (m, 1H), 1.31 (s, 9H). ^{13}C NMR (100 MHz, $CDCl_3$): δ = 167.9, 152.6, 152.2, 151.4, 147.6, 141.4, 141.0, 134.3, 133.2, 132.0, 129.4, 126.2, 125.4, 119.5, 118.4, 118.3, 117.5, 117.2, 101.4, 96.7, 83.2, 81.1, 80.8, 73.5, 73.0, 62.1, 60.7, 59.3, 56.6, 48.2, 45.1, 34.8, 30.9, 24.7. IR (KBr): 3380, 2955, 2923, 2141, 1759, 1625, 1497, 1437, 1265, 1035, 939, 834, 663, 558, 462 cm^{-1}. MS (ESI): *m/z* 594 $[M+H]^+$. HRMS (ESI) *m/z* $[M+H]^+$ Calcd for $C_{36}H_{36}NO_7$: 594.24863; found: 594.25171.

(*S*)-3-((*R*)-9-((3,4-dichlorophenyl)buta-1,3-diyn-1-yl)-4-methoxy-6-methyl-5,6,7,8-tetrahydro -[1,3]dioxolo[4,5-*g*]isoquinolin-5-yl)-6,7-dimethoxyisobenzofuran-1(3*H*)-one (20k)

Yield: 70%; Yellow solid; mp: 170-172 °C. ^{1}H NMR (400 MHz, $CDCl_3$): δ = 7.58 (d, *J* = 1.83 Hz, 1H), 7.41 (d, *J* = 8.31 Hz, 1H), 7.32 (dd, *J* = 1.83, 8.31 Hz, 1H), 7.05 (d, *J* = 8.19 Hz, 1H), 6.40 (d, *J* = 8.19 Hz, 1H), 6.03 (d, *J* = 0.73 Hz, 2H), 5.53 (d, *J* = 3.66 Hz, 1H), 4.35 (d, *J* = 3.66 Hz, 1H), 4.09 (s, 3H), 4.01 (s, 3H), 3.89 (s, 3H), 2.83-2.72 (m, 2H), 2.56-2.48 (m, 4H), 2.23-2.11 (m, 1H).^{13}C NMR (100 MHz, $CDCl_3$): δ = 167.9, 152.2, 151.6, 147.7, 141.8, 141.1, 134.4, 133.7, 133.2, 132.7, 131.3, 130.5, 121.7, 119.5, 118.4, 117.4, 101.5, 96.1, 81.1, 80.3, 80.1, 75.7, 75.3, 62.2, 60.7,59.4, 56.7, 48.1, 45.1, 24.6. IR (KBr): 3421, 2933, 2801, 1759, 1622, 1496, 1436, 1265, 1028, 821 cm^{-1}. MS (ESI): *m/z* 606 $[M+H]^+$. HRMS (ESI): *m/z*$[M+H]^+$ Calcd for $C_{32}H_{26}Cl_2NO_7$: 606.10808; found: 606.10956.

(*S*)-3-((*R*)-9-((3,4-difluorophenyl)buta-1,3-diyn-1-yl)-4-methoxy-6-methyl-5,6,7,8-tetrahydro -[1,3]dioxolo[4,5-*g*]isoquinolin-5-yl)-6,7-dimethoxyisobenzofuran-1(3*H*)-one (20s)

Yield: 64%; White solid; mp: 102-104 °C. ^{1}H NMR (500 MHz, $CDCl_3$): δ = 7.33-7.23 (m, 2H), 7.13 (q, *J* = 8.39 Hz, 1H), 7.06 (d, *J* = 8.24 Hz, 1H), 6.41 (d, *J* = 8.24 Hz, 1H), 6.03 (d, *J* = 1.52 Hz, 2H), 5.54 (d, *J* = 4.12 Hz, 1H), 4.36 (d, *J* = 4.12 Hz, 1H), 4.08 (s, 3H), 4.00 (s, 3H), 3.89 (s, 3H), 2.82-2.74 (m, 2H), 2.55-2.48 (m, 4H), 2.21-2.13 (m, 1H). ^{13}C NMR (125 MHz, $CDCl_3$): δ = 167.9, 152.2, 151.6, 147.7, 143.1 (d, J_{C-F}=470 Hz), 141.7, 141.1, 134.3, 133.2, 129.5, 129.1, 126.2, 121.2 (d, J_{C-F}=18.16 Hz), 119.4, 118.4, 117.7 (d, J_{C-F}=17.25 Hz), 117.5, 117.3, 101.5, 96.2, 81.1, 80.5, 80.1, 74.6, 74.3, 62.2, 60.7, 59.3, 56.7, 48.0, 45.0, 24.5. IR (KBr): 3386, 2924, 2853, 2785, 2214, 1764, 1622, 1597, 1505, 1434, 1271, 1040, 816, 767 cm^{-1}. MS (ESI): *m/z* 574 $[M+H]^+$.HRMS (ESI): *m/z*$[M+H]^+$ Calcd for $C_{32}H_{26}NO_7F_2$: 574.16718; found: 574.16674.

4.2.8. Cell culture and reagents

All the chemical reagents and media used for cell culture were obtained from Sigma. Human breast cancer cell lines, MCF-7 (passage number 9) and MDA-MB-231 (passage number 10) were obtained from the cell repository of the National Centre for Cell Science Pune, Maharashtra, India. The normal human embryonic kidney cell (293T) (passage number 12) was obtained from Dr. S. K. Singh, King George's Medical University, Lucknow, India. Stock solution (100 mM) of the newly synthesized noscapine derivatives, **20p, 20k** and **20s** was prepared with dimethyl sulfoxide (DMSO) and stored at 4°C until use. The cells were allowed to grow at a temperature of 37 °C in 5% CO_2 and 95% humidity in Dulbecco's modified Eagle medium (DMEM), supplemented with 10%

fetal bovine serum (FBS) and antibiotics. Cells with a 70-80% confluence were subcultured for bioassays using trypsin-EDTA (0.25%).

4.2.9. *In vitro* cell proliferation assay using MCF-7 and MDA-MB-231 cell lines

Inhibition of cell proliferation was assessed as described previously (Santoshi et al., 2011) using two human breast cancer cell lines, MCF-7 and MDA-MB-231 as well as a normal human embryonic kidney cell (293T). MCF-7 and MDA-MB-231 cells represent a striking example in that they are both invasive ductal/breast carcinoma cells, yet they have many phenotypic/genotypic differences. MCF-7 cell line is a hormone dependent (both estrogen and progesterone receptor positive (ER and PR positive) while MDA-MB-231 cell line is ER, PR, and E-cadherin negative (triple negative) and expresses mutated p53. Lacking of ER and PR has rendered MDA-MB-231 insensitive to many drugs used for the treatment of breast cancer (Osborne, 1998; Mckeon,1999; Fisher et al., 1998). Further, MCF-7 cells express the epithelial phenotype, while MDA-MB-231 are more mesenchymal (Gjerdrum et al., 2010) and have also been documented for their multidrug resistance (Chen et al., 2011). Briefly, the cells were seeded into 96 well plates at a density of 5 x 10^3 cells per well and were treated with gradient concentrations (5 µM to 100 µM) of noscapine and its 1,3-diynyl derivatives **20p, 20k** and **20s** for 72h. The cells were fixed with 50% trichloroacetic acid and stained with 0.4% sulforhodamine B. The unbound dye was removed by washing with 1% acetic acid, whereas the protein bound dye was extracted with 10 mM Tris base. Optical density was measured at 564 nm using a microplate reader. The IC_{50} value (the drug concentration required to achieve a cell kill of 50%) of the compounds was determined using the online tool Quest GraphTM IC_{50} Calculator (AAT Bioquest, Inc., Sunnyvale, CA, USA, https://www.aatbio.com/tools/ic50-calculator). Student t-test was performed to find out the significant differences in the antiproliferative activity of noscapine and its 1,3-diynyl derivatives between cancer cell lines and normal healthy cells.

4.2.10. Primary breast cancer cells (PBCs) culture and in vitro cell proliferation assay

The tumor tissues from breast cancer patients of different stages were obtained according to the guidelines approved by the King George's Medical University (Lucknow, India) ethics committee (number: 95th ECM II A/P25) and were processed in the laboratory. The tumour tissues were treated with 0.25% trypsin and filtered with 70 micron filter followed by centrifugation at 1073 g for 3 minutes with serum free medium.

The filtered cells were collected and plated in T25 flask and incubated with complete DMEM medium, supplemented with 10% FBS and 1% pentrip (mixture of penicillin and streptomycin) at 37 °C under 5% CO_2. Fresh media was replaced every 3-4 days and subsequent passaging was performed under the same conditions as mentioned above. The cultured were maintained for homogeneous cell type at sub-confluence between 3-8 passages. Cells were allowed to reach 80-90% confluence prior to experimental treatments (Patel et al., 2021; Nushtaeva et al., 2019). After the confluence was reached, the primary cells (passage number 3) were plated at 2000 cells/well in 96 wells plate with standard growth media, DMEM (low glucose). The cells were maintained at 37 °C in a humidified atmosphere with 5% CO_2 and were treated with gradient concentrations (5 to 100µM) of noscapine and its derivatives, **20p, 20k** and **20s** for 72h. Inhibition of cell proliferation was assessed by sulforhodamine B (SRB) assay, using the CellTiter96 AQueous One Solution Reagent (Sigma). Cells were stained with SRB for 30 minutes followed by washing with 1% acetic acid to remove the unbound dye. The protein bound dye was extracted in 1.0 mM tris and absorbance (optical density) was measured using a microplate reader (Molecular Devices, Sunnyvale, CA) at a wavelength of 564 nm. The IC_{50} value of the compounds was then determined, using the online tool AAT Bioquest. One way anova test was performed to find out the significant differences in the antiproliferative activity of 1,3-diynyl derivatives compared to noscapine.

4.2.11. Flow cytometry analysis of cell cycle progression and apoptosis

MDA-MB-231 cells were grown in DMEM with 4.5 g/L glucose and L-glutamine supplemented with 10% FBS and 1% penicillin/streptomycin at 37 ^oC in 5% CO_2. Cells were treated with IC_{50} concentration of noscapine and its 1,3-diynyl derivatives, **20p, 20k** and **20s,** dissolved in 1% phosphate buffer saline (PBS) for 72h. For the flow cytometer analysis, $2x10^6$ cells were harvested and centrifuged. The pellets were washed with ice-cold PBS and then fixed in 70% ethanol. The cell pellets were centrifuged at 1000 x g for 10 minutes and the pellets were resuspended in 30 µL of phosphate/citrate buffer (0.2 M Na_2HPO_4/0.1 M citric acid, pH 7.5) at room temperature. After 30 min, the cell pellets were washed with 5 mL of PBS and incubated with 0.5 mL of propidium iodide (20 µg/mL in 0.6% Triton-X in PBS) and 0.5 mL of RNase A (20 µg/ml in PBS) for 45 minutes in the dark. Samples were analysed on a flow cytometer (BD FACS Aria-III) and the progress in the cell cycle was determined (Verma et al., 2021). Student t-test has been performed to find out the significant differences in the antiproliferative activity of 1,3-diynyl derivatives compared to control using both the cancer cell lines.

Apoptosis in MDA-MB-231cancer cells was detected by Annexin-V-FITC detection method (Rieger et al., 2011) by using an apoptosis detection kit (Sigma). Cells were typsinized and stained with surface marker antibodies (biotin-conjugated Annexin V, FITC-conjugated streptavidin) and propidium iodide (PI) in 1X binding buffer for 20 minutes in dark condition at room temperature. Flow cytometer data with 488 nm excitation for PI and emission at 530 nm were collected. Viable cells (Annexin V^- / PI^-), early apoptotic cells (Annexin V^+ / PI^-), late apoptotic/necrotic cells (Annexin V^+ / PI^+) and late necrotic cells (Annexin V^- / PI^+) were identified and their percentage was determined.

4.2.12. DAPI staining

Apoptotic cells with the treatment of test compounds were visualized following DAPI staining (Saadat et al., 2015). MDA-MB-231 cells were grown on poly-L-lysine coated cover slips in 6-well plates and were treated with noscapine and its 1,3-diynyl derivatives, **20p, 20k** and **20s** at IC_{50} concentration for 72h. After incubation, cover slips were fixed in cold methanol and washed with PBS, stained with DAPI and mounted on slides. Images were captured using an inverted fluorescent microscope (Nikon Eclipse Ts2R-FL). Apoptotic cells were identified by changes in morphology compared to untreated cells.

4.2.13. Acridine orange (AO) & ethidium bromide (Etbr) staining

MDA-MB-231 cancer cells were grown in culture plates and treated with noscapine and 1,3-diynyl noscapinoids, **20p, 20k** and **20s** at IC_{50} concentration for 72h. After incubation, cover slips were fixed in cold methanol and washed with PBS. It was stained with acridine orange and ethidium bromide and mounted on slides. Images were captured using an inverted fluorescent microscope (Nikon Eclipse Ts2R-FL). Apoptotic cells were identified by changes in morphology compared to untreated cells (Kasibhatla et al., 2006).

4.2.14. Colony formation assay

To determine the effect of 1,3-diynyl noscapinoids, **20p, 20k** and **20s** against the colony forming ability of triple negative breast cancer cell line (MDA-MB-231), a clonogenic assay was performed (Verma et al., 2020). Briefly, 1000 MDA-MB-231cells were seeded in a 6-well culture plate and incubated for 24h. After incubation, the cells were treated with 1,3-diynyl derivative, **20s** with 1-230 µM concentration and kept for 12 days by maintaining the culture condition in CO_2 incubator to allow the cancer cells to

form colonies. The number of colonies under each condition was enumerated using Image-J software (National Institute of Health, Bethesda, MD, USA).

4.2.15. Tubulin purification

Tubulin was purified from the goat brain via temperature cycles and GTP-dependent polymerization and depolymerisation (Hamel et al., 1981; Panda et al., 2000) using PEM buffer (50 mM pipes, 3 mM $MgSO_4$, and 1 mM EGTA, pH 6.8). The amount of tubulin in the extract was estimated by the Bradford method using BSA as the standard. The purified tubulin was frozen and stored at -80 °C for further use.

4.2.16. Tubulin binding assay

Tubulin is autofluorescence in nature due to the presence of several tryptophan amino acids. Therefore, to examine the tubulin binding of chemical compounds, a fluorescence titration was used to analyse the quenching of intrinsic fluorescence of tubulin (Chamani et al., 2003). The purified tubulin (2 µM) was treated with 1,3-diynyl derivatives of noscapine **20p, 20k** and **20s** at a concentration of 25 µM in PEM buffer (50 mM pipes, 3 mM MgSO4, 1 mM EGTA, pH 6.8) for 45 minutes at 35 ˚C. The samples were excited at 295 nm and emission spectrum was measured at 310-400 nm. The inner filter effects were corrected using a formula: $F_{corrected} = F_{observed} \times antilog\,[\frac{A_{ex}+A_{em}}{2}]$, where $A_{ex}$and A_{em} are the absorbances at the excitation and emission wavelengths. For the spectrofluorometric titrations, a FlouroMax® 4 spectrofluorometer (Horiba Scientifc, Edison, NJ) assisted by Fluor Essence 3.5 software was used. The experiments were repeated twice.

4.3. Results and Discussion

4.3.1. Docking score of designed 1,3-diynyl noscapinoids with tubulin

The library of newly designed 1,3-diynyl noscapinoids (Figure 3) were docked onto the binding pocket of noscapinoids (Oliva et al., 2020) and evaluated using a Glide XP_{score} function (Friesner et al., 2004; Halgren et al., 2004).Molecular docking provides the best binding poses of the ligand inside the binding pocket of a protein. All the twenty1,3-diynyl noscapinoids generated *in silico* were found to be docked well within the binding pocket with improved docking score (ranged from -2.038 to -5.268 kcal/mol) compared to noscapine (-1.927 kcal/mol). Finally, based on the lowest docking score, a panel of three 1,3-diynyl-noscapinoids **20p, 20k** and **20s** (Figure 3) from the library were screened out for chemical synthesis and *in vitro* experimental evaluation using breast

cancer cells. The other 1,3-diynyl derivatives (with poor docking score) were not being considered for chemical synthesis and experimental evaluation.

All the three 1,3-diynyl derivatives, **20p, 20k** and **20s** were docked well at the interface of α- and β- tubulin (Figure 6) with improved docking scores (ranging from -5.268 kcal/mol to -4.505 kcal/mol) compared to noscapine (-1.927 kcal/mol) (Table 1). However, their binding modes inside the binding pocket are distinct as shown in the ligplot (Figure 7a-d). It may be due to the presence of different functional groups. As shown in the figure, the most potent 9-3,4-Di-F-diyne-noscapinoid **(20s)** in terms of docking score interacts more intensely with the residues of tubulin compared to other two derivatives. Its binding involved 6 hydrogen bonds (dashed line) with the binding site residues. The two nitrogen atoms (NH_2 and NE) of Arg D2 form 2 hydrogen bonds with the oxygen atom (O6) of the isobenzofuranone ring of **20s** with bond length 4.77 Å and 3.20 Å, respectively. The nitrogen atom in the isoquinoline ring of **20s** form 2 hydrogen bonds, one with oxygen atom of the carboxylic group of Gly D246 (bond length 4.33 Å) and the other with the side chain oxygen atom of OH group (OG1) of Thr A73 (bond length 3.64 Å). Both the fluorine atoms of **20s** form 2 hydrogen bonds, one with the nitrogen atom of NH_2 group of Tyr A224 (bond length 4.05 Å) and the other with the nitrogen atom of side chain amino group of Arg A221 (bond length 3.39 Å) (Figure 7d). In contrast, the 9-4-^{t}Bu-Ph-diyne-noscapinoid **(20p)** form 4 hydrogen bonds with the binding site residues: Gln D247, Thr A225, Tyr A224 and Gln A15; while9-3,4-Di-Cl-diyne-noscapinoid **(20k)** from 5 hydrogen bonds with the binding site residues: Gln D247, Gly D246, Tyr A224 and Thr A225 (Figure 7b,c). The lead molecule, noscapine formed only 3 hydrogen bonds with the binding site residues Gln D247, Glu D47 and Arg D47 (Figure 7a). Besides hydrogen bonding, a good number of hydrophobic interactions were involved in the binding of 1,3-diynyl noscapinoids, **20p, 20k** and **20s** with the binding site residues (Supplementary Table S9-S12). Inspired by our computational findings, we have chemically synthesized the newly designed 1,3-diynyl noscapinoids, **20p, 20k** and **20s** to further evaluate their anticancer potential.

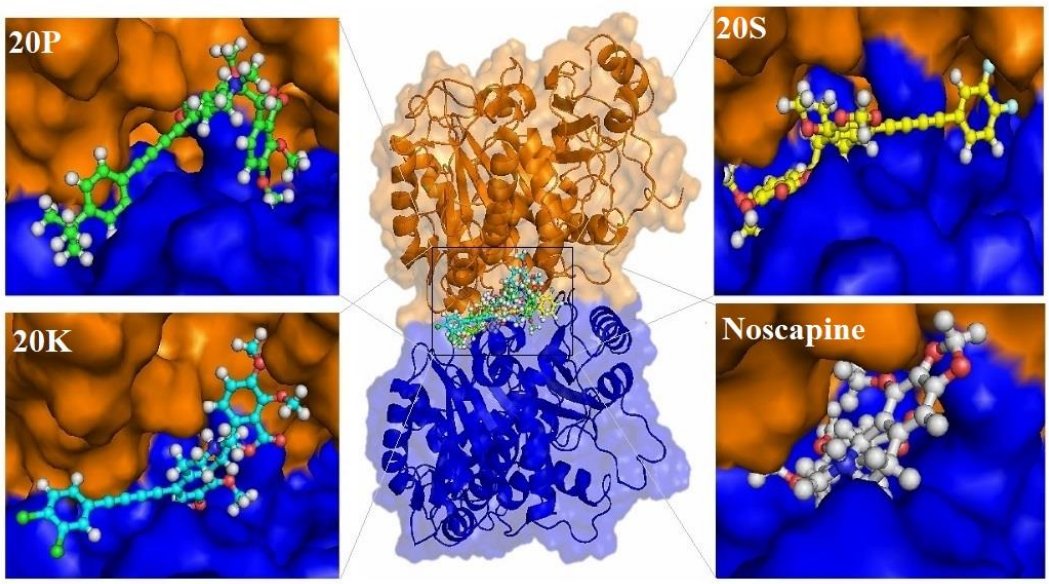

Figure 4.6. The developed 1,3-diynyl-noscapinoids, **20p, 20k** and **20s** are well accomodated inside the noscapine binding site at the interface of α- and β- tubulin. The binding site is represented as macromodel surface according to α- and β- tubulin (α-tubulin is represented in blue colour and β-tubulin is represented in brown colour).

4.3.2. Predictive binding affinity of 20p, 20k and 20s with tubulin (LIE-SGB calculation)

The predicted binding free energy ($\Delta G_{bind,pred}$) of 1,3-diynyl noscapinoids,**20p, 20k** and **20s** with tubulin was determined based on LIE-SGB empirical prediction model developed in this study by using the experimental binding free energy ($\Delta G_{bind,expt}$) of training set molecules (Table 1). Different interaction energy terms used in the model were included in Table 1.The values of the coefficients α, β, γ and δ for nonbonding interactions terms U_{vdw}, U_{coul}, U_{rxn} and U_{cav} are 0.08446, -0.00223, -0.000872 and -0.45601 respectively.The largest contribution for the binding free energy comes from the van der Waals interactions. The $\Delta G_{bind,pred}$ of the training set molecules based on LIE-SGB model is very close to the $\Delta G_{bind,expt}$ (root mean square error was 0.223 kcal/mol). The accuracy of the prediction model is determined from the value of the squared correlation coefficient (R^2 = 0.998) and analysis of variance (F-value = 3742.6).

$$\Delta G_{bind,pred} = 0.08446\langle U_{vdw}\rangle - 0.00223\langle U_{coul}\rangle - 0.00872\langle U_{rxn}\rangle - 0.45601\langle U_{cav}\rangle$$

$$(n = 11, R^2 = 0.998, s = 0.243, F = 3742.6, P \leq 0.001)$$

The LIE-SGB model was used to predict the binding free energy of the 1,3-diynyl-noscapinoids, **20p, 20k** and **20s**. All the three molecules revealed improved $\Delta G_{bind,pred}$ of -6.676 kcal/mol for **20p**, -7.294 kcal/mol for **20k** and -7.750 kcal/mol for **20s** respectively in comparison to the lead molecule, noscapine (-5.212 kcal/mol). Our results compel us to continue to examine the effects of these novel compounds *in vitro* with purified tubulin using fluorescence spectroscopy. Several noscapine derivatives were developed in the past

to increase its anticancer activity. Many of these derivatives revealed high tubulin binding affinity as indicated by lowering the dissociation constant (K_d value) to several folds compared to the lead molecule, noscapine (Beigoli et al., 2019; Manchukonda et al., 2014, Naik et al., 2012; Aneja et al., 2006b; Jain et al., 2011). Many of these derivatives have shown regression of the implanted tumor in xenograft animal models by targeting tubulin and inducing apoptosis to tumor cells. The available K_d value of these derivatives led us to develop a reasonable prediction model for predicting the binding affinity of newly developed 1,3-diynyl-noscapinoids, **20p, 20k** and **20s** with tubulin followed by experimental validation using purified tubulin.

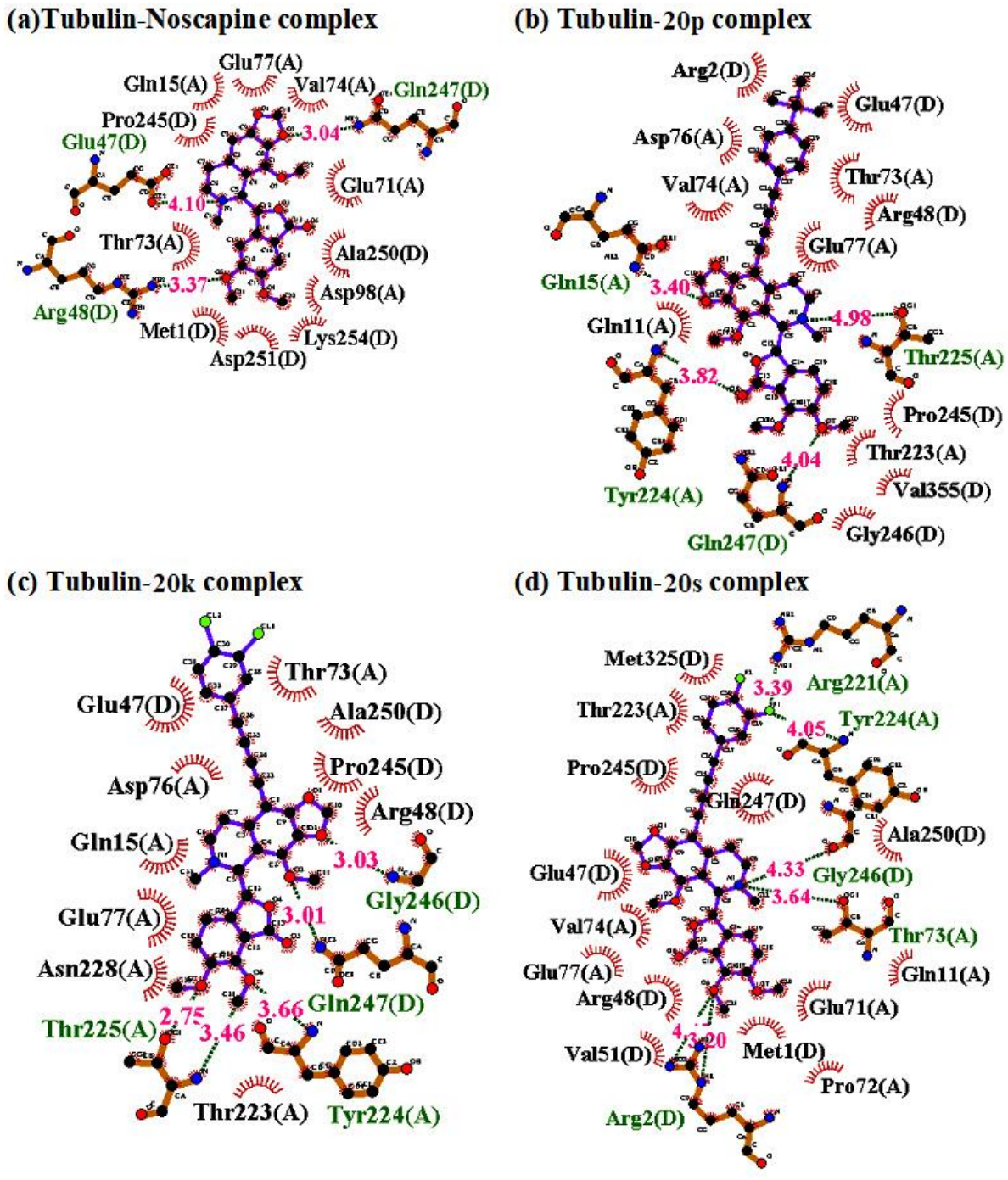

Figure 4.7. Two-dimensional representation of interaction observed between the binding site residues of tubulin with 1,3-diynyl-noscapinoids, (a) **Noscapine**, (b) **20p**, (c) **20k** and (d) **20s**. Dashed lines denote hydrogen bonds and numbers indicate hydrogen bond lengths in Å. Hydrophobic interactions are shown as arcs with radial spokes. The figure was made using LIGPLOT. The residues within 5 Å distance from the docked ligands were only shown in the figures.

Table 4.1. Molecular docking results (Glide XP) as well as calculated energies such as U_{vdw}, U_{coul}, U_{rxn} and U_{cav} using Liasion programme (Schrodinger software package) of noscapine and its 1,3-diynyl derivatives as well as $\Delta G_{bind,pred}$ based on LIE-SGB prediction model and $\Delta G_{bind,expt}$. The 1,3-diynyl-noscapinoids, **20p, 20k** and **20s** revealed improved $\Delta G_{bind,pred}$ compared to the lead molecule, noscapine.

Ligand	Glide XP_{score} (kcal/mol)	$<U_{vdw}>$ (kcal/mol)	$<U_{coul}>$ (kcal/mol)	$<U_{rxn}>$ (kcal/mol)	$<U_{cav}>$ (kcal/mol)	Experimental ΔG_{bind} (kcal/mol)	Predicted ΔG_{bind} (kcal/mol)
9	-1.927	-45.14	-330.8	135.5	2.097	-5.246	-5.212
10	-2.038	-49.00	-210.2	116.0	3.283	-6.006	-6.178
11	-2.766	-42.50	-362.1	155.9	4.208	-5.827	-6.060
12	-2.940	-48.06	-355.8	168.7	2.548	-5.587	-5.899
13	-3.263	-47.69	-285.7	135.5	3.103	-6.360	-5.987
14	-4.492	-47.44	-77.3	118.2	3.954	-6.628	-6.668
15	-2.605	-33.39	-331.9	176.7	4.465	-5.551	-5.657
16	-2.287	-45.57	-277.9	112.3	3.285	-5.665	-5.706
17	-2.350	-33.47	-324.5	152.5	3.766	-5.783	-5.151
18	-3.679	-45.41	-471.2	152.8	3.669	-5.673	-5.790
19	-3.687	-42.69	-267.6	129.9	3.465	-5.518	-5.722
20p	-4.505	-45.14	-330.8	135.5	2.097	-	-6.676
20k	-4.981	-49.00	-210.2	116.0	3.283	-	-7.294
20s	-5.268	-42.50	-362.1	155.9	4.208	-	-7.750

$<U_{vdw}>$, $<U_{coul}>$, $<U_{rxn}>$ and $<U_{cav}>$ energy terms represents the ensemble average energy terms calculated as the difference between bound and free state of the ligands and its environment. The $\Delta G_{bind,expt}$ for the training set noscapinoids was calculated from their respective dissociation constant (K_d) values using the relation: $\Delta G_{bind,expt} = RT \ln K_d$, where R is gaseous constant (0.001986 kcal/mol) and T is temperature (298 K). The K_d values of the noscapinoids used in training set were obtained from earlier published work.

4.3.3. Inhibition of proliferation of cancer cells, MCF-7 and MDA-MB-231

Based on our *in silico* results, we focused at the cellular level to determine if the 1,3-diynyl-noscapinoids, **20p, 20k** and **20s**, affected cancer cell proliferation. All the 3 molecules, **20p, 20k** and **20s** including the parent compound, noscapine were analyzed for their anti-proliferative activity in two human breast adenocarcinoma cells, MCF-7 and

MDA-MB-231. The cancer cell lines, MCF-7 and MDA-MB-231 as well as a normal human embryonic kidney cell (293T) were treated with gradient concentrations ranging from 5 µM to 100 µM of noscapine and its 1,3-diynyl derivatives **20p, 20k** and **20s** for 72 h. The 1,3-diynyl-noscapinoids, **20p, 20k** and **20s** exhibited improved anti-proliferative activity in comparison to noscapine using both the cell lines (Figure 8). The IC_{50} values are collated in Table 2. The IC_{50} value amounted to 44.8 µM, 28.8 µM, 14.7 µM and 10.7 µM with noscapine, **20p, 20k** and **20s** respectively for MCF-7 cells, which reflects a modest antiproliferative activity. Parenthetically, a similar modest IC_{50} value of 57.4 µM, 38.9 µM, 24.6 µM and 17.1 µM were measured for noscapine, **20p, 20k** and **20s** respectively for MDA-MB-231 cells. The IC_{50} value of noscapine and its 1,3-diynyl-noscapinoids for both the cancer cell lines was found to be statistically significant compared to untreated cells ($p < 0.001$). However, the usage concentration of these molecules for regression of the implanted tumor in the animal model may be different. Further, the toxicity if any to the normal healthy cells with the treatment of noscapine and its 1,3-diynyl-derivatives, **20p, 20k** and **20s** was determined using normal human embryonic kidney cells (293T). It was found that noscapine and its 1,3-diynyl derivatives revealed < 5% cell killing to normal cells even at a high concentration of 100 µM (Figure 9), indicating that the molecules are not affecting the normal cells and only selectively inhibiting the proliferation of cancer cells. In contrast, the 1,3-diynyl derivatives, **20p, 20k** and **20s** at relatively low concentrations (5.0 µM) significantly stimulated proliferation of 293T cells, while at higher concentrations (100 µM) inhibited proliferation of 293T cells (< 5%). This biphasic dose-dependent phenomenon demonstrated that 1,3-diynyl derivatives, **20p, 20k** and **20s** exhibited a typical hermetic dose response in normal cells (Calabrese & Baldwin, 2002). In general, the hermetic effect is elaborated as an adaptive mechanism of a cell or an organism to compensate for any imbalance in homeostasis caused by exposure to factors that mediate intermittent stresses (Sertel et al., 2011; Mattson et al., 2006). However, the hermetic response of 1,3-diynyl derivatives, **20p, 20k** and **20s** was not evident with the cancer cell lines used.

Table 4.2. IC_{50} values of novel 1,3-diynyl-noscapinoids, **20p, 20k** and **20s** using two human breast adenocarcinoma cell lines, MCF-7 and MDA-MB-231 as well as a normal healthy cell. All the novel derivatives were found to have improved antiproliferative activity compared to untreated cells. Moreover, the normal healthy cells (293T) is nor being affected by the noscapine and its 1,3-diynyl derivatives. Results were expressed as mean ± standard deviation ***p ≤ 0.01.*

	IC_{50} (µM)			
	Noscapine	**20p**	**20k**	**20s**
MCF-7	44.8±4.3**	28.8±3.2**	14.7±2.8**	10.7±2.5**
MDA-MB-231	57.4±5.3**	38.9±3.6**	24.6±3.4**	17.1±2.7**

293T normal cell	470.5±1.5	380.5±2.5	360.3±3.7	358.5±2.8

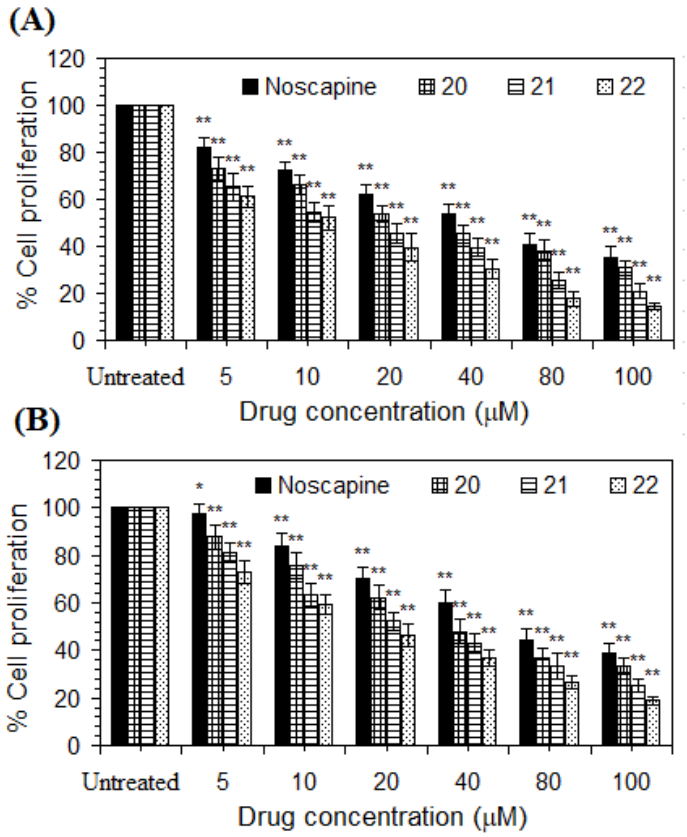

Figure 4.8. Effect of noscapine and its 1,3-diynyl-derivatives **20p, 20k** and **20s** on cell proliferation using MTT assay. The antiproliferative activity of noscapine and its 1,3-diynyl-derivatives was found to be significantly different compared to untreated cells against human breast cancer cells. (A) MCF-7 and (B) MDA-MB-231. Results were expressed as mean ± standard deviation.*$p \leq 0.05$ and **$p \leq 0.01$.

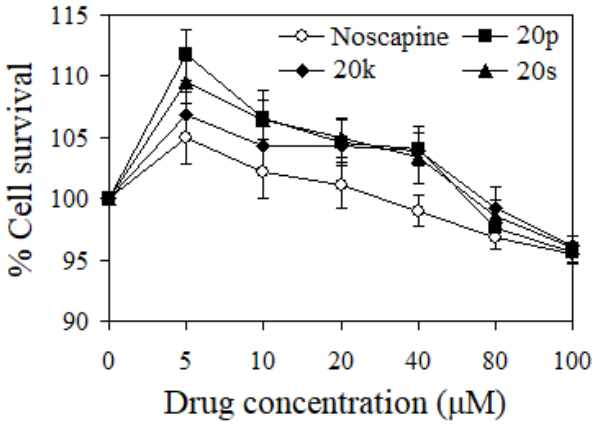

Figure 4.9. Normal human embryonic kidney cells (293T) reveled < 5% cell death with the treatment of noscapine and 1,3-diynyl-noscapinoids, **20p, 20k** and **20s** for 72h. Each value represents the average of 3 independent experiments.

4.3.4. 1,3-diynyl-noscapinoids, 20p, 20k and 20s inhibits proliferation of primary breast cancer cells

We next want to evaluate whether the newly developed 1,3-diynyl-noscapinoids, **20p, 20k** and **20s** could also inhibit the proliferation of primary breast tumor cells isolated

from the surgically removed breast tumor tissue at different stages of breast cancer. All these primary breast cancer cells were treated with increasing concentrations of the noscapinoids to study their antiproliferative activity. The noscapine and its 1,3-diynyl noscapinoids, **20p, 20k** and **20s** exhibited improved anti-proliferative activity compared to untreated cells against a panel of primary breast tumor cells (Figure 10). The IC_{50} values for the test compounds are included in Table 3. It ranges from 41.3 to 58.9 µM for noscapine, 21.8 to 33.4 µM for **20p**, 13.8 to 18.6 µM for **20k** and 6.2 to 10.9 µM for **20s** using a panel of primary breast tumor cells (Table 3).

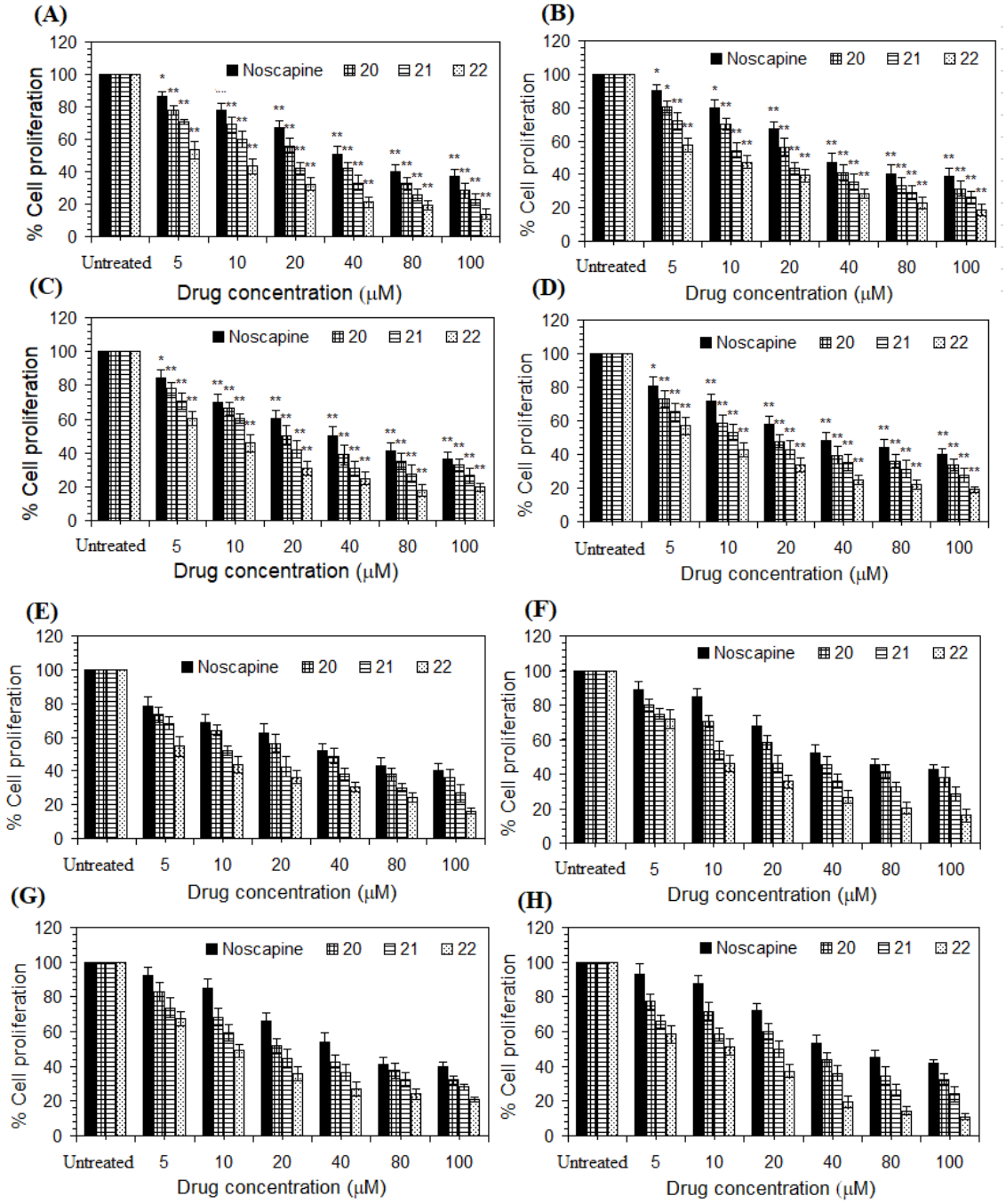

Figure 4.10. The antiproliferative activity of noscapine and its 1,3-diynyl-noscapinoids, **20p, 20k** and **20s** against a panel of human primary breast cancer cells compared to untreated cells. All the cells were treated with varying concentrations of chemical compounds for 72h. Results were expressed as mean ± standard deviation. The

antiproliferative activity of noscapine and its 1,3-diynyl-noscapinoids, **20p, 20k** and **20s** was found to be statistically significant compared to untreated cells at *$p \leq 0.05$ and **$p \leq 0.01$.

Table 4.3. IC_{50} values of noscapine and its 1,3-diynyl-noscapinoids, **20p, 20k** and **20s** using primary breast tumor cells isolated from breast tumor tissue of different patients. All the novel derivatives were found to have improved antiproliferative activity compared to untreated cells. Results were expressed as mean ± standard deviation. **$p \leq 0.01$.

IC50 (μM)				
Patients No.	**Noscapine**	**20p**	**20k**	**20s**
1	47.1±4.3**	27.9±3.9**	15.8±2.5**	6.2±0.5*
2	46.1±4.6**	29.4±2.4**	15.9±1.9**	8.6±0.7**
3	41.3±4.7**	25.6±2.9**	15.8±2.4**	7.8±0.6**
4	42.9±4.6**	21.8±3.3**	13.8±2.3**	6.8±0.9*
5	46.4±3.9**	33.1±3.2**	14.5±1.8**	6.9±0.4**
6	56.9±5.3**	34.3±3.4**	17.6±1.6**	10.9±1.2*
7	51.3±5.4**	29.5±2.5**	18.6±2.3**	10.6±0.8**
8	58.9±5.7**	33.4±3.6**	16.7±1.9**	9.1±0.6**

4.3.5. 1,3-diynyl-noscapinoids, 20p, 20k and 20s inhibits colony formation

We next performed the inhibition to colony formation using the breast cancer cell line, MDA-MB-231 to further establish the anticancer efficacy of the 1,3-diynyl noscapinoids **20p, 20k** and **20s**. The cancer cell was treated with increasing concentration (1-230 μM) of the most potent 1,3-diynyl noscapinoid **20s** and incubated at culture conditions for 10 days for colony formation. The number of colonies formed was determined using image-J software. The inhibition in colony formation was found to be concentration dependent (Figure 11). The number of colonies formed was significantly inhibited by the treated compound compared to untreated cells. The cytotoxicity activity of 1,3-diynyl noscapinoid **20s** expressed in terms of IC_{50} (inhibitory concentration) was found to be 4.5 μM based on the clonogenic assay.

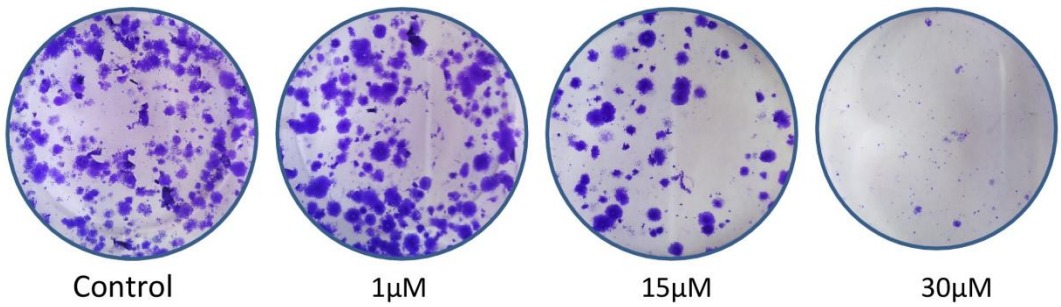

Figure 4. 11. Inhibition in colony formation with the treatment of 1,3-diynyl derivative of noscapine, **20s**. The triple negative cancer cell line MDA-MB-231 was treated with increasing concentration (1 μM, 10 μM and 20 μM) of the compound. The number of colony formation was significantly inhibited by the compound compared to untreated cells.

4.3.6. 1,3-diynyl-noscapinoids, 20p, 20k and 20s induced apoptosis to cancer cells

We aimed to determine the induction of apoptotic cell death to breast cancer cell with the treatment of1,3-diynyl-noscapinoids, **20p, 20k** and **20s**. Biochemically the apoptotic process is characterized by alterations of lipid composition of cell membrane—phosphatidylserine which is normally on the inner leaflet of the cell membrane, translocates to the outer leaflet and is detected by annexin V binding. In contrast, a cell-impermeant DNA-binding fluorescent dye, propidium iodide can only enter the cells when it is at the stage of late apoptosis when membrane permeability is compromised. The apoptotic cells can be quantified to a large extent by FACS analysis. The percentage of early apoptotic and late apoptotic cells using MDA-MB-231 cell line with the treatment of IC_{50} concentration of noscapine and its 1,3-diynyl-noscapinoids, **20p, 20k** and **20s** is collated in Table 4. Representative figures of flow cytometry analysis are included in Figure 12. The control untreated cell culture contained only very few early apoptotic (3%) and late apoptotic cells (2%) which were considered as the background cell death due to regular trauma during cell culture (Table 4). In contrast, the percentage of early apoptotic cells of38%, 30%, 25%, and 56%; late apoptotic cells of 14%, 30%, 20% and 5% as well as necrotic cells of 1%, 0%, 15% and 10% with treatments of noscapine and its 1,3-diynyl-noscapinoids, **20p, 20k** and **20s** respectively were found to be significantly high compared to controlled untreated cells (Table 4).

Table: 4.4. Percentage of viable (Q3), early apoptotic (Q1), late apoptotic (Q2) and necrotic (Q4) cell measured by flow cytometry with the treatment of IC_{50} concentration of noscapine and its 1,3-diynyl-noscapinoids, **20p, 20k** and **20s**.

Viability/ Apoptotic	**Control**	**Noscapine**	**20p**	**20k**	**20s**
Q1	3%	38%	30%	25%	56%
Q2	2%	14%	30%	20%	5%
Q3	94%	47%	40%	40%	29%
Q4	1%	1%	0%	15%	10%

Besides, morphological examination using DAPI, Acridyne orange (AO) and Ethidium bromide (EtBr) staining revealed apoptotic cell death of MDA-MB-231 cancer cells characterized by condensed chromatin, formation of membrane blebs and numerous fragmented nuclei (Figure 13 & 14).

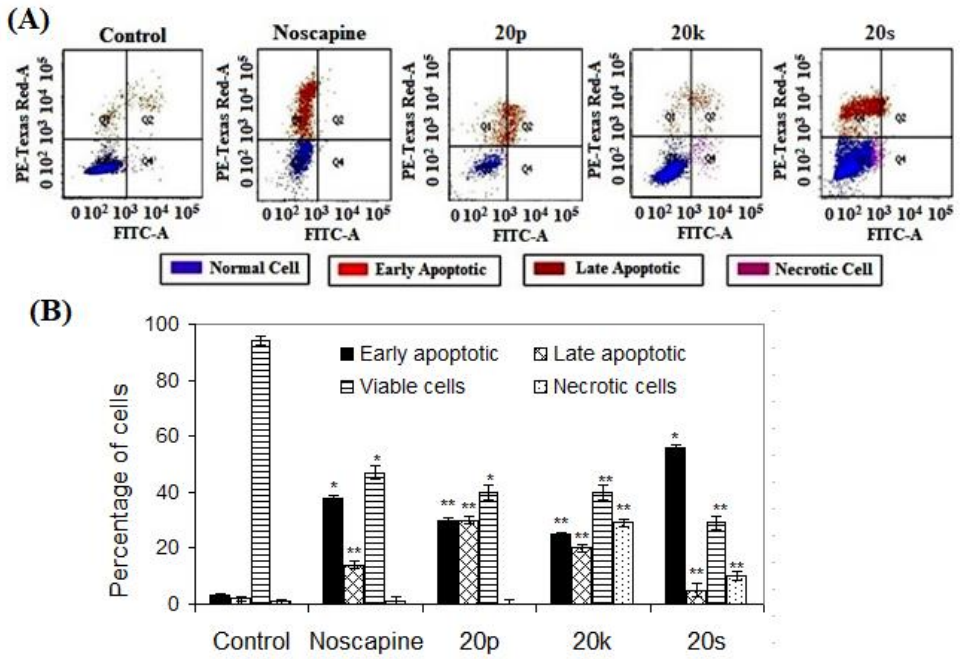

Figure 4.12. Flow cytometry analysis of MDA-MB-231 cells treated with noscapine and its 1,3-diynyl-noscapinoids, **20p, 20k** and **20s** and compared with non treated control cells. Alexa Fluor 488 conjugate of Annexin-V was used, in combination with the non-vital dye propidium iodide (PI), to distinguish among three sub-populations: PI-negative and Alexa Fluor 488-negative viable cells (PI-, Alexa Fluor 488-), PI-negative and Alexa Fluor 488-positive early apoptotic cells (PI-, Alexa Fluor 488+), and PI-positive and Alexa Fluor 488-positive late apoptotic cells (PI+, Alexa Fluor 488+). Results were expressed as mean ± standard deviation of three independent experiments. Noscapine and its 1,3-diynyl derivatives were found to have improved apoptotic activity compared to untreated cells. *$p \leq 0.05$ *and* **$p \leq 0.01$.

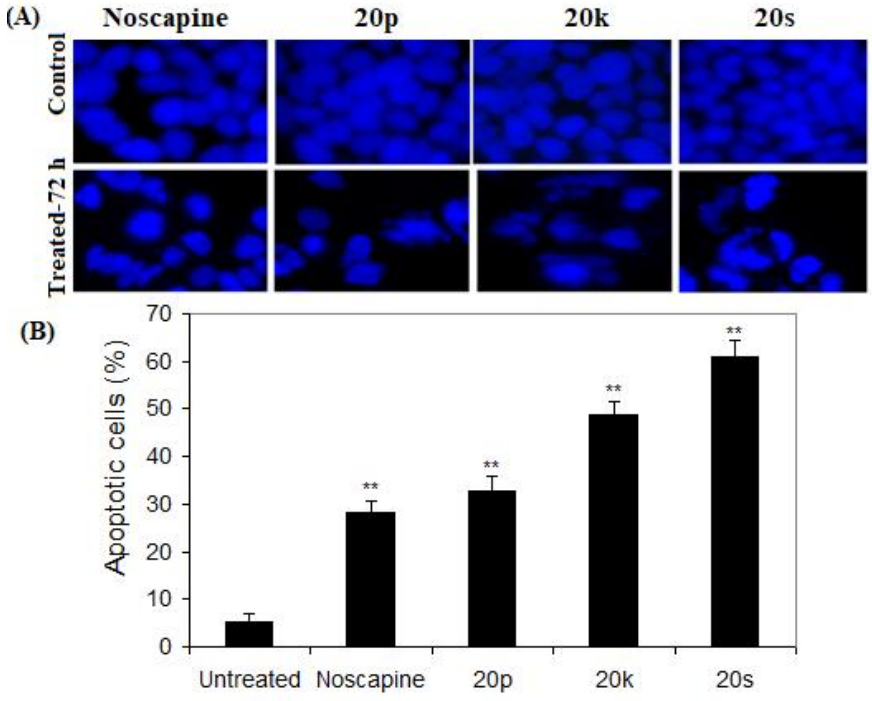

Figure 4.13. Panels show morphological evaluation of nuclei stained with DAPI from control cells (upper panels) and cells treated with IC_{50} concentration of noscapine and its

1,3-diynyl-noscapinoids, **20p, 20k** and **20s** for 72h (lower panels) using fluorescence microscopy. Several typical features of apoptotic cells such as condensed chromosomes, numerous fragmented micronuclei, and apoptotic bodies are evident upon 72h of drug treatment. Results were expressed as mean ± standard deviation of three independent experiments. Noscapine and its 1,3-diynyl derivatives were found to have improved apoptotic activity compared to untreated cells. *$**p \leq 0.01$.*

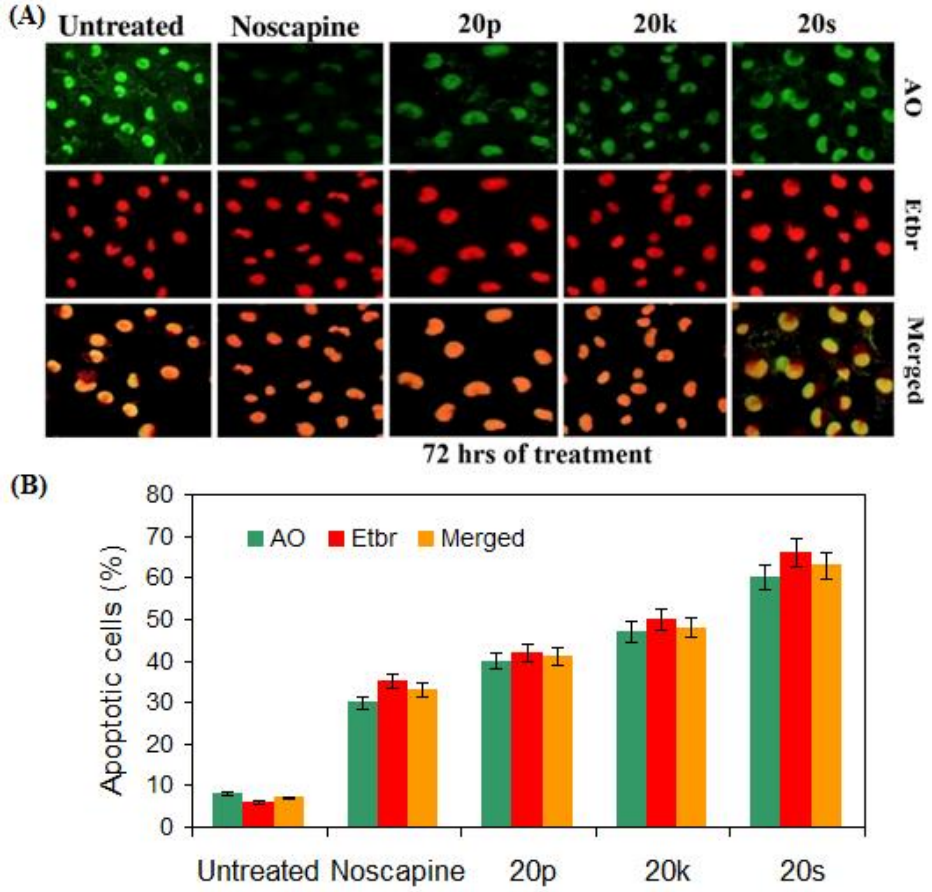

Figure 4.14. The changes in morphological characters such as chromatin condensation, plasma membrane blebbing and appearance of small, apoptotic bodies indicated the apoptotic cells. Panels show morphological features of cells stained with AO, EtBr and merged channel of AO and EtBr. From 0h treatment (upper panels) and cells treated with IC_{50} concentration of noscapine and 1,3-diynyl-noscapinoids, **20p, 20k** and **20s** (lower panels) for 72h using fluorescence microscopy. The apoptotic cancer cells were evident after 72h of drug treatment. Results were expressed as mean ± standard deviation of three independent experiments. Noscapine and its 1,3-diynyl derivatives were found to have improved apoptotic activity compared to untreated cells. *$*p \leq 0.05$ and $**p \leq 0.01$.*

4.3.7. 1,3-diynyl-noscapinoids, 20p, 20k and 20s alter the cell cycle profile and cause mitotic arrest at G_2/M phase

The effect of noscapine and 1,3-diynyl-noscapinoids, **20p, 20k** and **20s** on the cell cycle progression of MDA-MB-231 is based on FACS analysis and represented in Figure 15. Accumulation of fluorescently labelled DNA in presence of noscapinoids, demonstrate the perturbation of cell cycle and cell death. The presence of 2N DNA indicates that the cells are in the G1 phase, while the accumulation of duplicated 4N DNA indicates that the

cells are in G2 and M phases. Accumulation of DNA in between 2N and 4N peaks represents that the cells are in S phase. In contrast, less than 2N DNA indicates the apoptotic cells in which the DNA is degraded to different extents. Treatment of MDA-MB-231 cells for 72h with the noscapine and 1,3-diynyl-noscapinoids, **20p, 20k** and **20s** led to significant inhibition of the cell cycle profile. FACS analysis revealed a high accumulation of cells in the G2/M phase at 72h of treatment with the test compounds (Table 5). In contrast to G2/M block, a hypodiploid DNA content peak (sub-G1) was seen to rise at 72 hours of drug treatment, indicating dying cells.

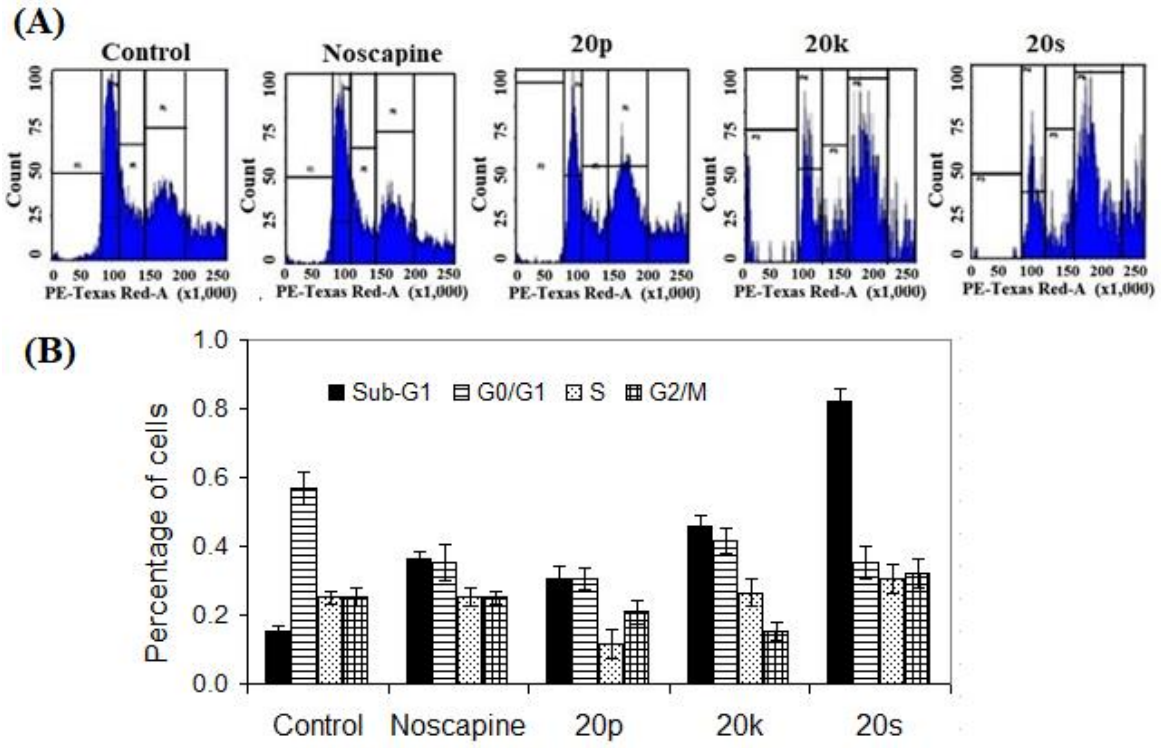

Figure 4.15. Noscapine and its 1,3-diynyl-noscapinoids, **20p, 20k** and **20s** inhibit cell cycle progression at mitosis followed by the appearance of a characteristic hypodiploid (sub-G1) DNA peak, indicative of apoptosis. Panels A-E depict analyses of cell cycle distribution as determined by flow cytometry in MDA-MB-231 cells treated with IC_{50} concentration of noscapine and its 1,3-diynyl-noscapinoids, **20p, 20k** and **20s** at 72h of treatment.

Table 4. 5. Effect of noscapine and its 1,3-diynyl-noscapinoids, **20p, 20k** and **20s** on cell cycle progression of MDA-MB-231 cells treated with IC_{50} concentration for 72 h before being stained with propidium iodide for cell cycle analysis. Noscapine and its 1,3-diynyl derivatives were found to arrest cell cycle progression more effectively compared to untreated cells. Results were expressed as mean ± standard deviation. $^{**}p \leq 0.01$.

	72 h			
	Sub-G_1	G_0/G_1	S	G_2/M
Control	0.7	16.0	21.4	11.2
Noscapine	4.9^{**}	12.5^{**}	13.1^{**}	21.5^{**}
20	5.5^{**}	13.8^{**}	10.3^{**}	27.1^{**}
21	7.9^{**}	14.0^{**}	9.2^{**}	28.7^{**}

22	8.8**	21.0**	10.1**	34.7**

4.3.8. 1,3-diynyl-noscapinoids, 20p, 20k and 20s binds to tubulin at high affinity

Microtubules are autofluorescent by nature due to the presence of aromatic amino acids, tryptophan which can be selectively measured by exciting at 295 nm. Any chemical compounds that bind with tubulin and alter its conformation lead to a decrease in its intrinsic fluorescence (YE et al., 1998). This is a standard assay to test whether a chemical compound binds to tubulin or not (Verma et al., 2021). We have used similar assay to test whether the 1,3-diynyl noscapinoids, **20p, 20k** and **20s** also bind to tubulin or not. It was revealed that the intrinsic fluorescence of tubulin decreased in the presence of 1,3-diynyl noscapinoids, **20p, 20k** and **20s,** which suggests the binding capability of these compounds to tubulin. The relative percentage of decrease in fluorescence intensity was 8.39%, 17.39% and 25.47% respectively in the presence of 25 µM concentration of **20p, 20k** and **20s** (Figure 16), compared to control and were found statistically significant at $p \leq 0.01$ using student t-test.

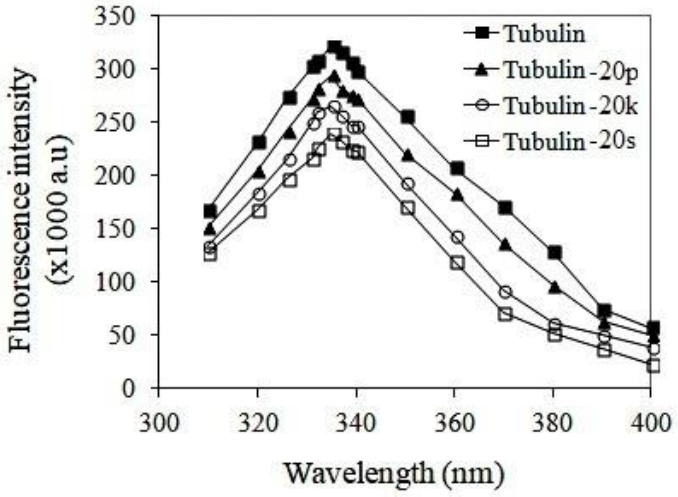

Figure 4.16. Treatment of purified tubulin with 1,3-diynyl noscapinoids, **20p, 20k** and **20s** quenched the intrinsic fluorescence of tubulin significantly compared to untreated tubulin. The relative percentage of decrease in fluorescence intensity was 8.39%, 17.39% and 25.47% respectively in presence of 25 µM concentration of **20p, 20k** and **20s** compared to control. Emission spectra were collected in a range of 310 nm – 400 nm.

4.4. Conclusion

In conclusion, we have strategically developed potent derivatives of the natural lead molecule noscapine in quest of increasing its anticancer activity. We have also provided the simplest methods for direct and regioselective modification of the noscapine scaffold to produce the 1,3-diynyl noscapinoids in high yields. All the three diynyl derivatives screened out based on molecular docking have shown increased predicted

binding affinity with tubulin. Further, it was experimentally demonstrated that these derivatives also bind to tubulin with high affinity. Their anticancer activity was evaluated using two human breast cancer cell lines (MCF-7 and MDA-MB-231) as well as a panel of primary breast tumor cells. All the three diynyl derivatives revealed improved anticancer activity compared to noscapine without affecting the normal healthy cells. Therefore, these novel compounds may prove efficacious not only in the treatment of breast carcinoma but also for other types of cancer. Our results compel us to continue to examine the effects of these novel compounds on in vivo animal experiments with the final goal of taking it to human clinical study.

S1: ^{1}H NMR of compound 20p

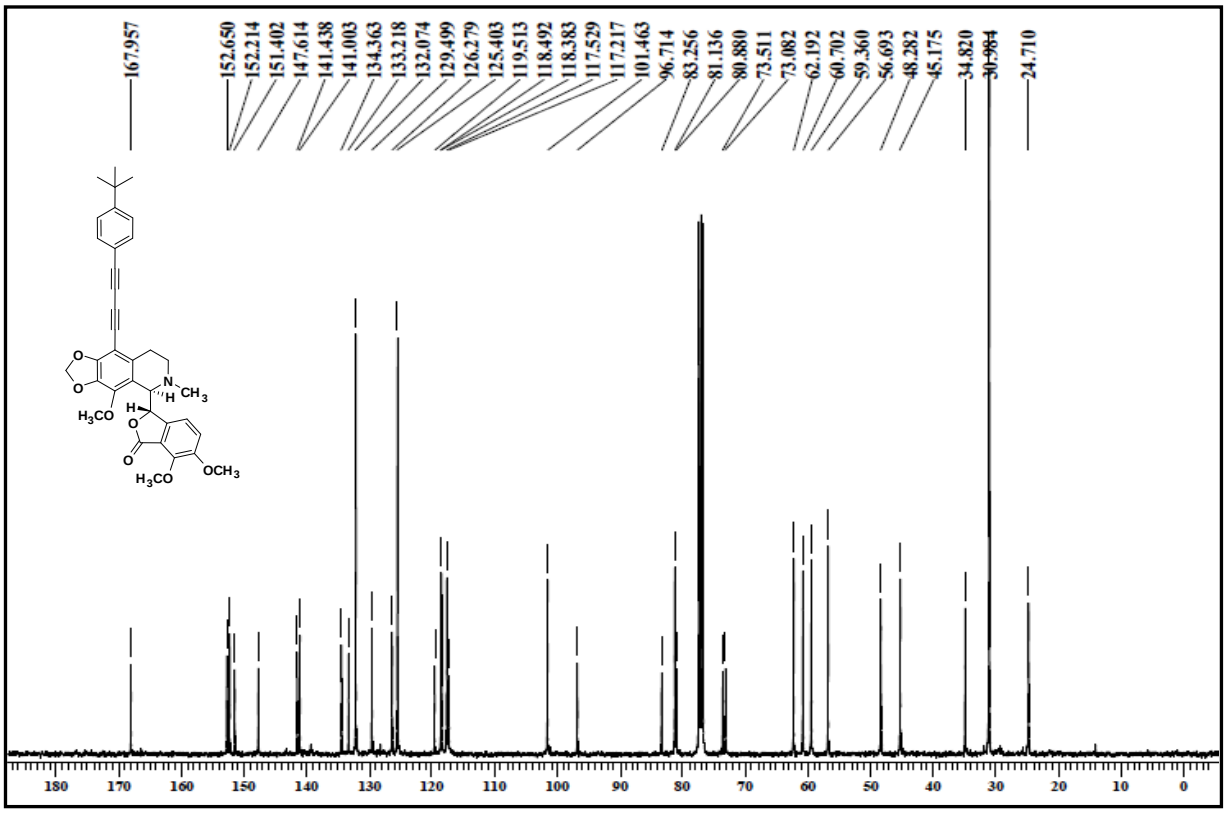

S2: HRMS of compound 20p

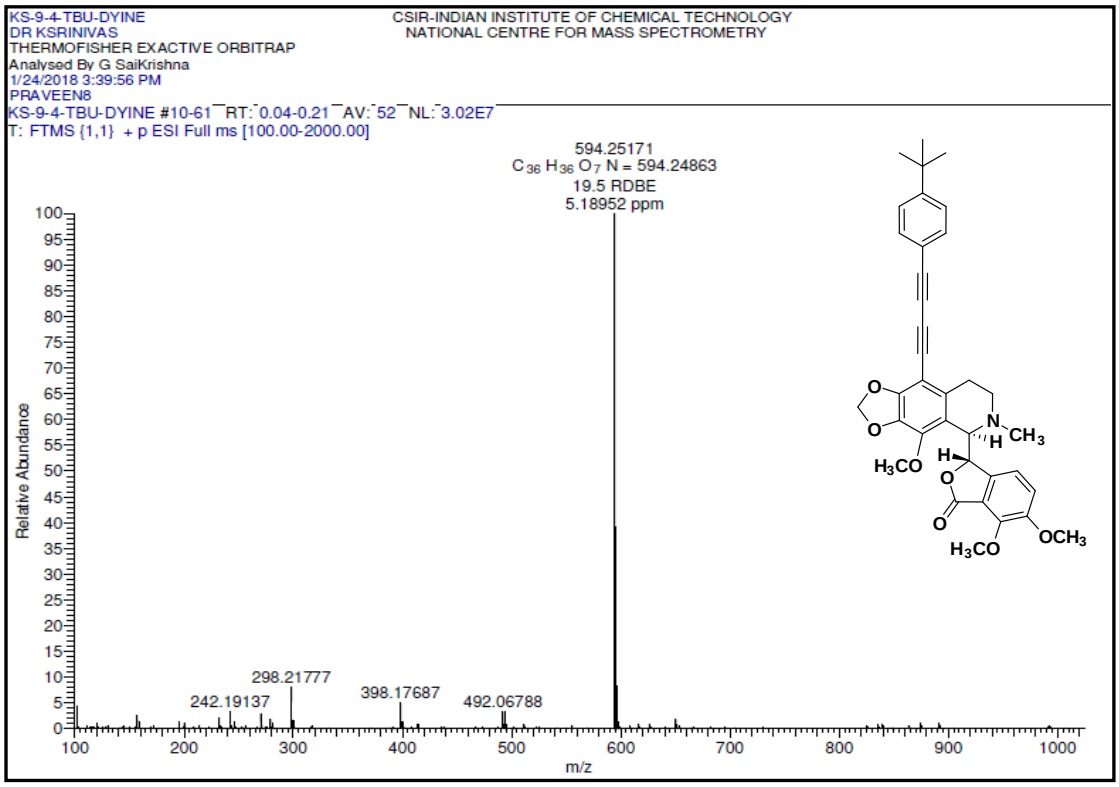

S3: ^{1}H NMR of compound 20k

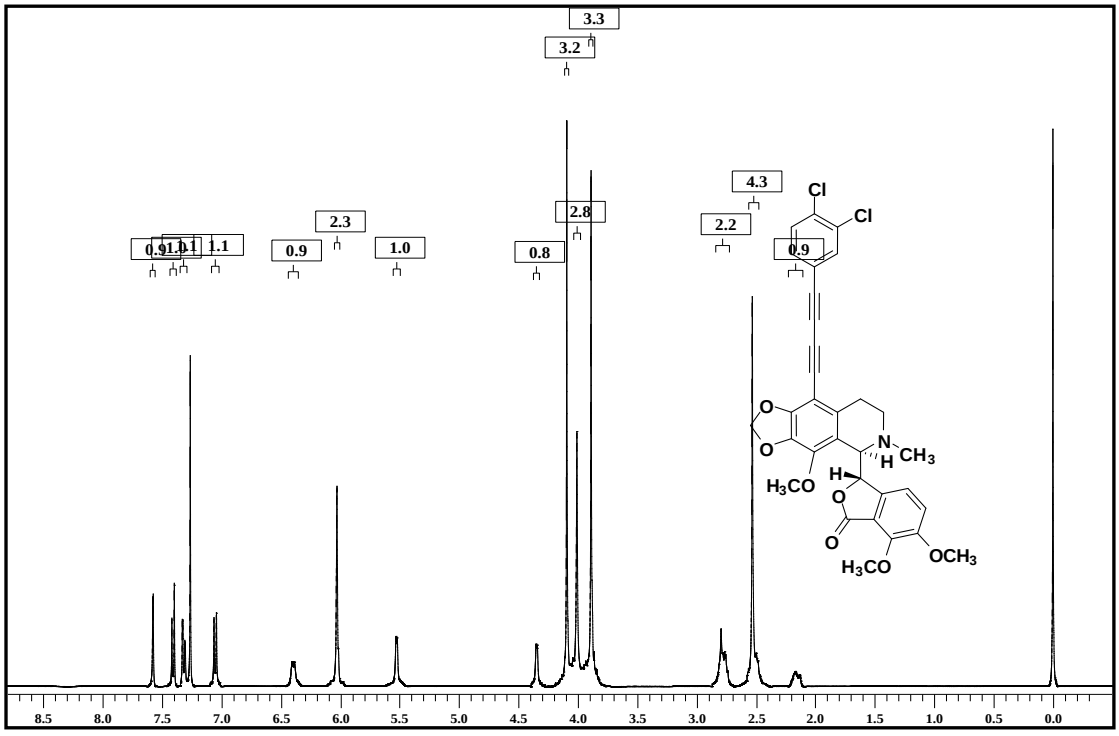

S4: ^{13}C NMR of compound 20k

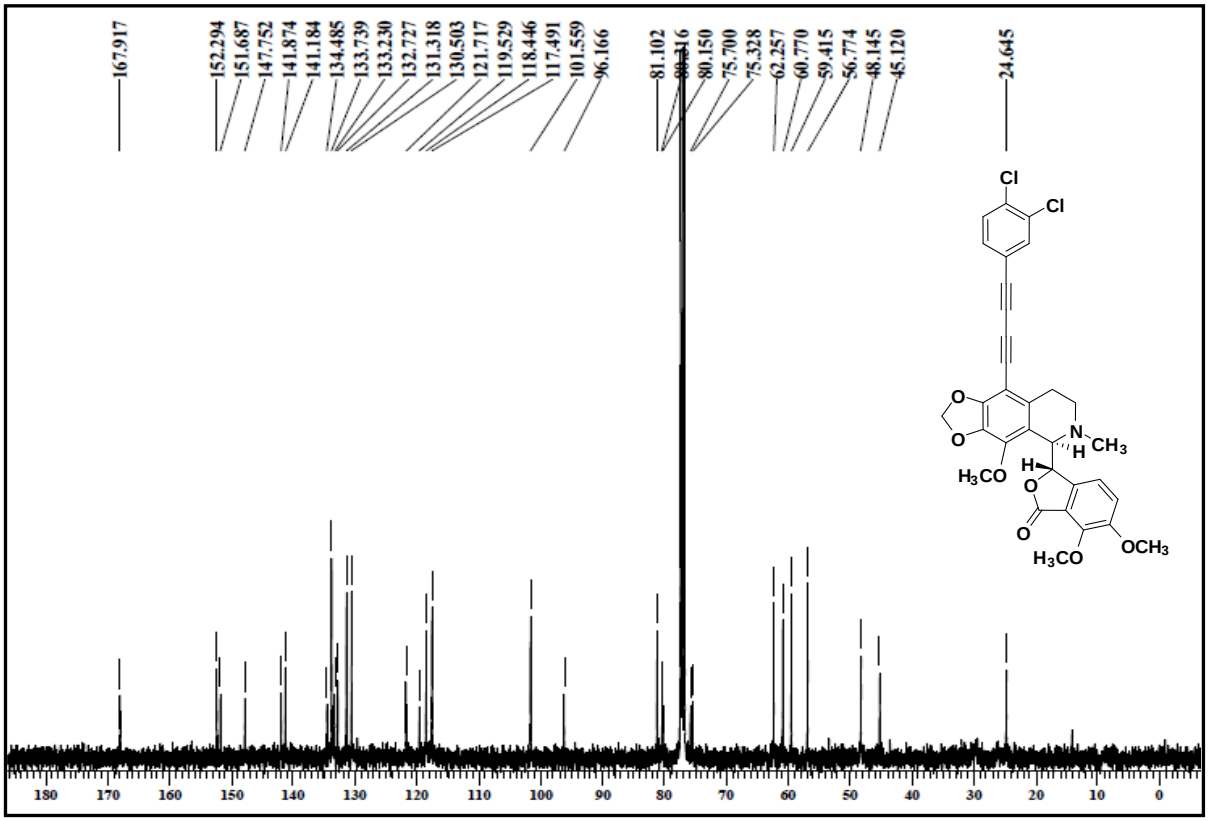

S5: HRMS of compound 20k

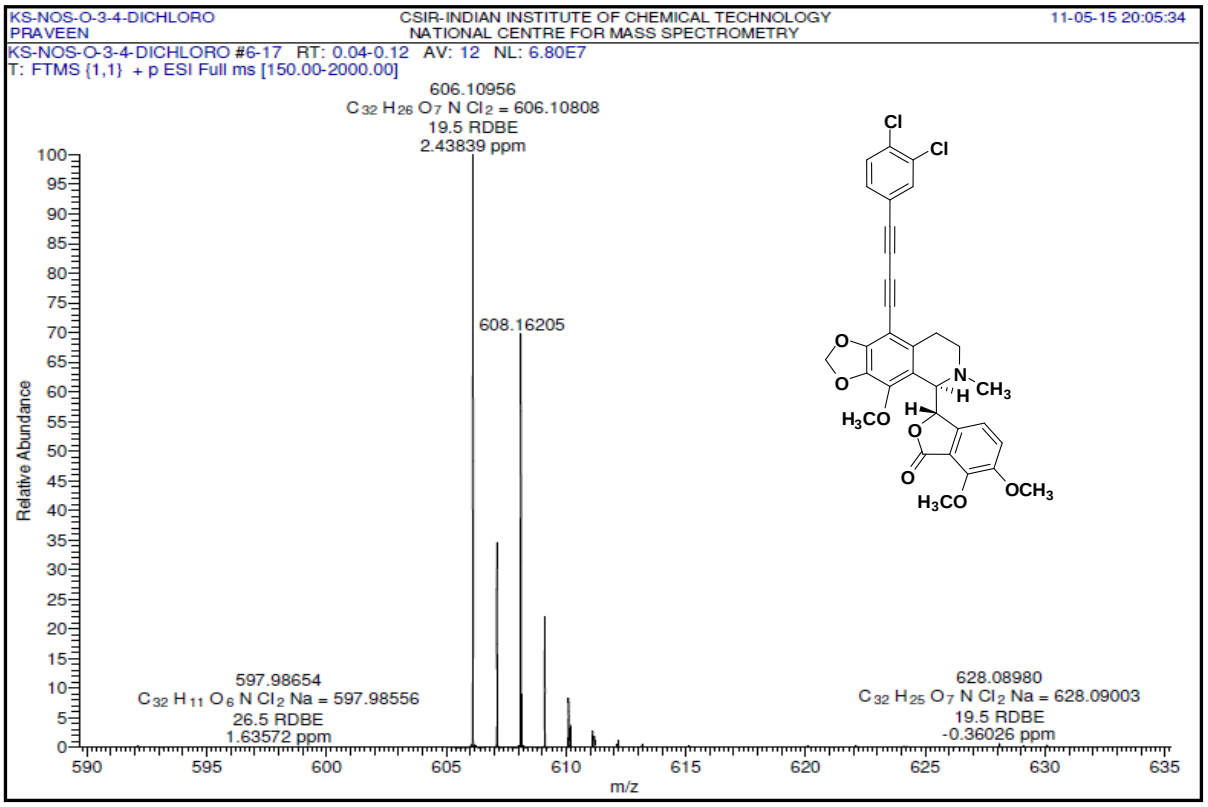

S6: ^{1}H NMR of compound 20s

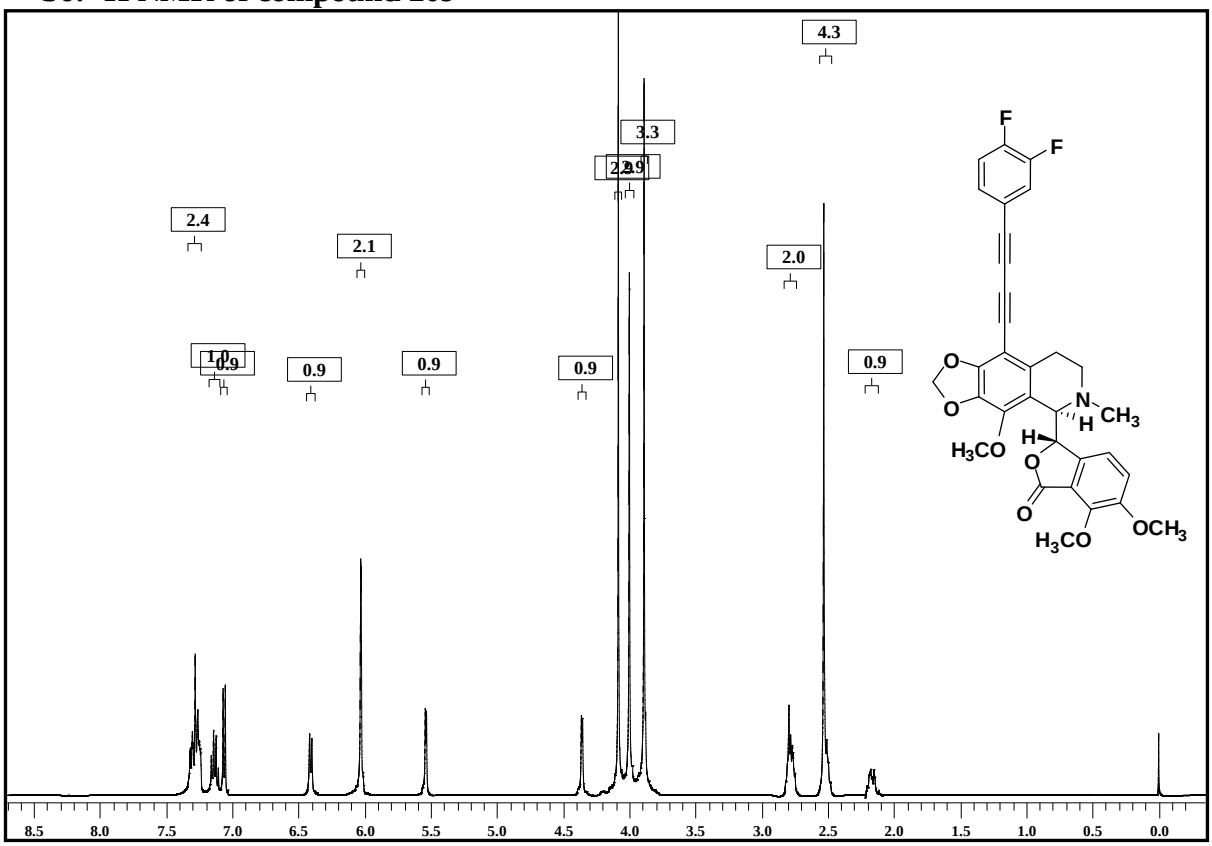

S7: ^{13}C NMR of compound 20s

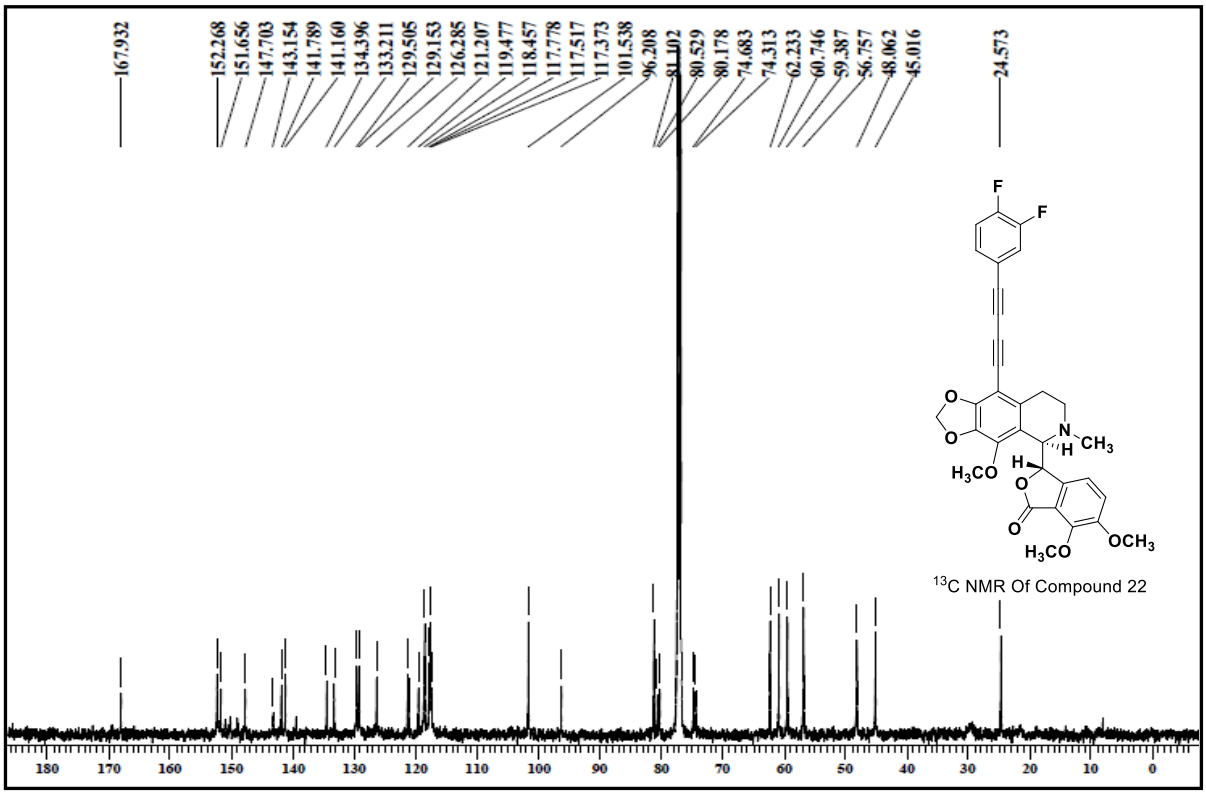

S8: HRMS of compound 20s

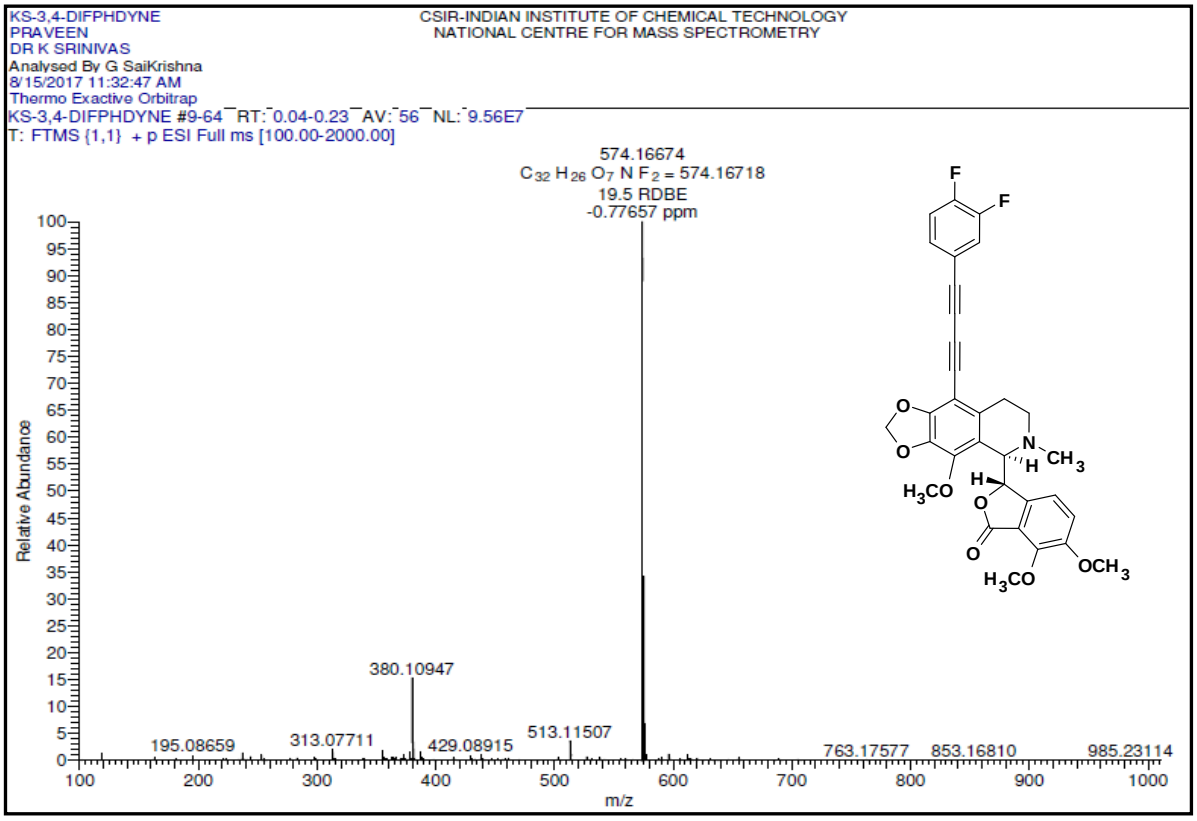

Table S9-S12: Geometry of hydrogen bonds and hydrophobic interaction of 1,3-diynyl-noscapinoids, **20p**-**20s** and the lead molecule, noscapine with the binding site residues of tubulin.

Table S9			**Table S10**		
(a) Noscapine-Tubulin			**(b) 20p-Tubulin**		
Hydrogen bonding			**Hydrogen bonding**		
Hydrogen Donor (D)	**Hydrogen Acceptor (A)**	**Distance (D-A) in Å**	**Hydrogen Donor (D)**	**Hydrogen Acceptor (A)**	**Distance (D-A) in Å**
GLN D 247 NE2	Noscapine O2	3.04	GLN D 247 N	20p O7	4.04
GLU D 47 OE2	Noscapine N1	4.10	20p N1	THR A 225 OG1	4.98
ARG D 48 NH2	Noscapine O5	3.37	TYR A 224 N	20p O5	3.82
			GLN A 15 NE2	20p O2	3.40
Hydrophobic interaction			**Hydrophobic interaction**		
Noscapine	**Tubulin**	**Distance**	**20p**	**Tubulin**	**Distance**
C20	LYS D 254 NZ	3.42	C20	VAL D 355 O	4.27
C16	LYS D 254 NZ	4.9	C10	GLN D 247 OE1	3.64
C20	LYS D 254 CE	3.9	C8	GLN D 247 OE1	4.62
C20	LYS D 254 CD	3.94	C23	GLN D 247 NE2	4.96
C20	LYS D 254 CG	4.95	C19	GLN D 247 NE2	4.87
C20	ASP D 251 OD2	3.2	C18	GLN D 247 NE2	4.61
C17	ASP D 251 OD2	4.65	C17	GLN D 247 NE2	4.27
C20	ASP D 251 CG	4.32	C16	GLN D 247 NE2	4.11
O4	ASP D 251 CG	4.49	C15	GLN D 247 NE2	4.3
C20	ASP D 251 CB	5	C14	GLN D 247 NE2	4.71
O4	ASP D 251 CB	4.73	C13	GLN D 247 NE2	4.89
C20	ALA D 250 CB	3.93	C10	GLN D 247 NE2	2.87
O6	ALA D 250 CB	4.52	C9	GLN D 247 NE2	3.24
O5	ALA D 250 CB	4.8	C8	GLN D 247 NE2	3.01
O4	ALA D 250 CB	3.77	C4	GLN D 247 NE2	4.5
C19	ALA D 250 CB	4.48	C3	GLN D 247 NE2	4.68
C18	ALA D 250 CB	4.05	C2	GLN D 247 NE2	3.75
C17	ALA D 250 CB	3.45	C1	GLN D 247 NE2	4.11
C16	ALA D 250 CB	3.26	O7	GLN D 247 CD	4.79
C15	ALA D 250 CB	3.7	O6	GLN D 247 CD	4.34
C14	ALA D 250 CB	4.32	C17	GLN D 247 CD	4.67
C13	ALA D 250 CB	4.3	C16	GLN D 247 CD	4.41
C18	ALA D 250 O	4.52	C15	GLN D 247 CD	4.89
C17	ALA D 250 O	4.73	O2	GLN D 247 CD	3.52
O4	ALA D 250 C	4.75	C10	GLN D 247 CD	3.68
C18	ALA D 250 C	4.98	O1	GLN D 247 CD	4.27
C17	ALA D 250 C	4.83	C9	GLN D 247 CD	4.51
O4	ALA D 250 CA	4.92	C8	GLN D 247 CD	4.17
C17	ALA D 250 CA	4.76	C2	GLN D 247 CD	4.87
C16	ALA D 250 CA	4.76	C21	GLN D 247 CG	4.04
C13	GLN D 247 OE1	4.68	O7	GLN D 247 CG	3.76
C13	GLN D 247 NE2	4.22	O6	GLN D 247 CG	3.38
C10	GLN D 247 NE2	3.63	C18	GLN D 247 CG	4.93
C9	GLN D 247 NE2	3.91	C17	GLN D 247 CG	3.94
C8	GLN D 247 NE2	3.42	C16	GLN D 247 CG	3.73
C4	GLN D 247 NE2	4.81	C15	GLN D 247 CG	4.6

C2	GLN D 247 NE2	4.78	O2	GLN D 247 CG	4.88
C1	GLN D 247 NE2	3.94	C21	GLN D 247 CB	4.72
O7	GLN D 247 CD	4.87	O7	GLN D 247 CB	4.52
O6	GLN D 247 CD	3.59	O6	GLN D 247 CB	4.47
C13	GLN D 247 CD	4.49	O7	GLN D 247 CA	4.88
O3	GLN D 247 CD	4.71	C20	GLN D 247 N	4.85
O2	GLN D 247 CD	4.24	O7	GLY D 246 C	4.42
C10	GLN D 247 CD	4.85	C20	GLY D 246 CA	4.46
C8	GLN D 247 CD	4.69	O7	GLY D 246 CA	4.29
O6	GLN D 247 CG	4.41	C20	GLY D 246 N	4.59
O6	GLN D 247 CB	4.52	C20	PRO D 245 CB	4.8
O6	GLN D 247 C	4.48	C18	PRO D 245 CB	4.48
O6	GLN D 247 CA	3.65	C20	PRO D 245 O	3.11
C13	GLN D 247 CA	4.39	C18	PRO D 245 O	4.65
O3	GLN D 247 CA	4.82	C17	PRO D 245 O	4.69
C13	GLN D 247 N	4.6	C20	PRO D 245 C	4.01
C16	GLY D 246 O	4.45	O7	PRO D 245 C	4.28
C15	GLY D 246 O	3.74	C18	PRO D 245 C	4.97
C14	GLY D 246 O	4.16	C29	ARG D 48 NE	4.94
C13	GLY D 246 O	3.15	C28	ARG D 48 NE	4.95
C12	GLY D 246 O	4.08	C29	ARG D 48 CD	4.73
O6	GLY D 246 C	4.06	C28	ARG D 48 CD	4.62
C15	GLY D 246 C	4.88	C35	ARG D 48 CG	4.97
C13	GLY D 246 C	4.09	C29	ARG D 48 CG	4.07
O3	GLY D 246 C	4.03	C28	ARG D 48 CG	4.31
C12	GLY D 246 C	4.91	C29	GLU D 47 OE2	4.61
O3	GLY D 246 CA	4.87	C28	GLU D 47 OE2	3.76
C12	GLY D 246 N	4.63	C27	GLU D 47 OE2	4.03
N1	PRO D 245 CB	4.9	C26	GLU D 47 OE2	3.92
C12	PRO D 245 CB	4.89	C25	GLU D 47 OE2	4.22
C7	PRO D 245 CB	3.79	C24	GLU D 47 OE2	4.8
C6	PRO D 245 CB	3.58	C29	GLU D 47 CD	4.9
C3	PRO D 245 CB	4.63	C28	GLU D 47 CD	4.37
C6	PRO D 245 CD	4.92	C27	GLU D 47 CD	4.89
C7	PRO D 245 CG	4.07	C30	GLU D 47 CG	4.92
C6	PRO D 245 CG	3.73	C29	GLU D 47 CG	4.03
C12	PRO D 245 CA	4.74	C28	GLU D 47 CG	3.93
C7	PRO D 245 CA	4.82	C27	GLU D 47 CG	4.73
C6	PRO D 245 CA	4.2	C36	GLU D 47 O	3.43
C21	ARG D 48 NH2	4.66	C35	GLU D 47 O	3.45
C19	ARG D 48 NH2	3.73	C33	GLU D 47 O	3.78
C18	ARG D 48 NH2	3.75	C30	GLU D 47 O	3.88
C17	ARG D 48 NH2	4.76	C29	GLU D 47 O	3.26
C14	ARG D 48 NH2	4.68	C28	GLU D 47 O	4.19
C19	ARG D 48 NH1	4.4	C36	GLU D 47 C	4.48
C18	ARG D 48 NH1	4.94	C35	GLU D 47 C	4.63
C14	ARG D 48 NH1	4.74	C33	GLU D 47 C	4.99
O5	ARG D 48 CZ	4.23	C29	GLU D 47 C	4.32
C19	ARG D 48 CZ	3.85	C36	GLU D 47 CA	4.94
C18	ARG D 48 CZ	4.32	C35	ARG D 2 NH2	4.74
C14	ARG D 48 CZ	4.56	C34	ARG D 2 NH2	3.97
C19	ARG D 48 NE	4.07	C35	ARG D 2 CZ	4.4
C18	ARG D 48 NE	4.78	C34	ARG D 2 CZ	4.31

C14	ARG D 48 NE	4.84	C35	ARG D 2 NE	3.28
C11	ARG D 48 NE	4.33	C34	ARG D 2 NE	3.85
C19	ARG D 48 CD	4.88	C33	ARG D 2 NE	4.26
C11	ARG D 48 CD	4.28	C35	ARG D 2 CD	3.54
C6	ARG D 48 CD	4.62	C34	ARG D 2 CD	4.84
C11	ARG D 48 CG	4.55	C33	ARG D 2 CD	4.86
C11	GLU D 47 OE2	4.56	C35	ARG D 2 CG	4.36
C7	GLU D 47 OE2	3.02	C22	THR A 225 OG1	4.6
C6	GLU D 47 OE2	3.07	C11	THR A 225 OG1	3.82
C3	GLU D 47 OE2	4.47	C5	THR A 225 OG1	4.56
C7	GLU D 47 OE1	4.89	C11	THR A 225 CB	4.96
C6	GLU D 47 OE1	4.95	C11	THR A 225 CA	4.92
C7	GLU D 47 CD	4.17	C11	THR A 225 N	4.31
C6	GLU D 47 CD	4.05	O5	TYR A 224 CE1	4.64
C6	GLU D 47 CG	4.57	O2	TYR A 224 CE1	4.88
C21	MET D 1 CE	3.79	O5	TYR A 224 CD1	3.85
C20	MET D 1 CE	3.31	C13	TYR A 224 CD1	4.68
O5	MET D 1 CE	4.27	C11	TYR A 224 CD1	4.77
O4	MET D 1 CE	3.06	O3	TYR A 224 CD1	4.08
C18	MET D 1 CE	4.78	O2	TYR A 224 CD1	4.35
C17	MET D 1 CE	4.32	C2	TYR A 224 CD1	4.96
C20	MET D 1 SD	4.82	O5	TYR A 224 CG	4.55
O4	MET D 1 SD	4.79	C11	TYR A 224 CG	4.77
C21	MET D 1 O	3.36	O3	TYR A 224 CG	4.49
C18	MET D 1 O	4.95	O5	TYR A 224 CB	4.48
C21	MET D 1 C	4.4	C11	TYR A 224 CB	3.81
O5	MET D 1 C	4.85	O3	TYR A 224 CB	3.89
C21	MET D 1 N	4.37	C11	TYR A 224 C	4.55
C20	ASP A 98 OD2	2.95	O5	TYR A 224 CA	4.75
C20	ASP A 98 OD1	4.3	C11	TYR A 224 CA	4.71
C20	ASP A 98 CG	3.93	O3	TYR A 224 CA	4.9
O4	ASP A 98 CG	4.94	C13	TYR A 224 N	4.78
C10	GLU A 77 OE2	3.79	C13	THR A 223 OG1	4.84
C9	GLU A 77 OE2	3.33	O5	THR A 223 CG2	4.08
C8	GLU A 77 OE2	3.55	C13	THR A 223 CG2	4.58
C4	GLU A 77 OE2	4.39	O4	THR A 223 CG2	4.83
C3	GLU A 77 OE2	4.19	O5	THR A 223 CB	3.55
C2	GLU A 77 OE2	3.67	C13	THR A 223 CB	4.21
C1	GLU A 77 OE2	4.1	O4	THR A 223 CB	4.38
C10	GLU A 77 OE1	4.34	O5	THR A 223 C	4.5
C9	GLU A 77 OE1	4.89	O5	THR A 223 CA	4.16
C8	GLU A 77 OE1	4.73	C25	GLU A 77 OE2	4.08
O2	GLU A 77 CD	4.63	C24	GLU A 77 OE2	3.29
C10	GLU A 77 CD	4.46	C23	GLU A 77 OE2	2.81
O1	GLU A 77 CD	4.65	C9	GLU A 77 OE2	3.61
C9	GLU A 77 CD	4.42	C8	GLU A 77 OE2	4.38
C8	GLU A 77 CD	4.4	C7	GLU A 77 OE2	3.18
C2	GLU A 77 CD	4.89	C6	GLU A 77 OE2	4.38
C1	GLU A 77 CD	4.88	C4	GLU A 77 OE2	4.06
C22	VAL A 74 CG2	3.12	C3	GLU A 77 OE2	3.13
O7	VAL A 74 CG2	3.85	C2	GLU A 77 OE2	4.58
C1	VAL A 74 CG2	4.88	C1	GLU A 77 OE2	2.88
C22	VAL A 74 CB	4.27	C23	GLU A 77 OE1	4.68

O7	VAL A 74 CB	4.93	C9	GLU A 77 OE1	4.48
C22	VAL A 74 CA	4.29	C8	GLU A 77 OE1	4.82
C22	VAL A 74 N	4.03	C3	GLU A 77 OE1	4.64
C22	THR A 73 OG1	2.91	C1	GLU A 77 OE1	4.38
C21	THR A 73 OG1	4.34	C25	GLU A 77 CD	4.92
C19	THR A 73 OG1	3.93	C24	GLU A 77 CD	4.27
C18	THR A 73 OG1	4.17	C23	GLU A 77 CD	3.9
C17	THR A 73 OG1	4.42	O1	GLU A 77 CD	4.88
C16	THR A 73 OG1	4.5	C9	GLU A 77 CD	4.36
C15	THR A 73 OG1	4.32	C8	GLU A 77 CD	4.99
C14	THR A 73 OG1	3.99	C7	GLU A 77 CD	4.36
C12	THR A 73 OG1	4.52	C4	GLU A 77 CD	4.94
C11	THR A 73 OG1	4.25	C3	GLU A 77 CD	4.23
C5	THR A 73 OG1	3.84	C1	GLU A 77 CD	3.93
C4	THR A 73 OG1	4.68	C24	GLU A 77 CG	4.73
C1	THR A 73 OG1	4.76	C23	GLU A 77 CG	4.74
C21	THR A 73 CG2	3.71	C32	ASP A 76 OD2	4.91
O5	THR A 73 CG2	4.51	C31	ASP A 76 OD2	4.67
C19	THR A 73 CG2	4.47	C10	VAL A 74 CG2	4.42
C18	THR A 73 CG2	4.59	O1	VAL A 74 CG2	4.36
C11	THR A 73 CG2	4.2	C32	THR A 73 OG1	4.76
N1	THR A 73 CB	4.51	C27	THR A 73 OG1	4.67
C22	THR A 73 CB	4.08	C26	THR A 73 OG1	4.42
C21	THR A 73 CB	4.68	C25	THR A 73 OG1	4.57
C19	THR A 73 CB	4.66	C32	THR A 73 CG2	3.96
C18	THR A 73 CB	4.98	C31	THR A 73 CG2	4.07
C14	THR A 73 CB	4.94	C30	THR A 73 CG2	4.52
C11	THR A 73 CB	4.15	C29	THR A 73 CG2	4.82
C5	THR A 73 CB	4.42	C28	THR A 73 CG2	4.72
C22	THR A 73 O	4.61	C27	THR A 73 CG2	4.3
C22	THR A 73 C	4.22	C26	THR A 73 CG2	4.82
C22	THR A 73 CA	4.74	C32	THR A 73 CB	3.75
C21	GLU A 71 OE2	2.71	C31	THR A 73 CB	4.34
C20	GLU A 71 OE2	4.28	C28	THR A 73 CB	4.8
C19	GLU A 71 OE2	4.72	C27	THR A 73 CB	4.02
C18	GLU A 71 OE2	3.86	C26	THR A 73 CB	4.11
C17	GLU A 71 OE2	3.76	C25	THR A 73 CB	4.56
C16	GLU A 71 OE2	4.61	C32	THR A 73 O	4.29
C22	GLU A 71 OE1	4.22	C27	THR A 73 O	4.8
C21	GLU A 71 OE1	4.66	C26	THR A 73 O	4.37
C20	GLU A 71 OE1	4.98	C25	THR A 73 O	4.37
C17	GLU A 71 OE1	4.61	C24	THR A 73 O	4.69
C16	GLU A 71 OE1	4.82	C32	THR A 73 C	4.79
C21	GLU A 71 CD	3.88	C26	THR A 73 C	4.93
C20	GLU A 71 CD	4.32	C25	THR A 73 C	4.96
O5	GLU A 71 CD	4.82	C32	THR A 73 CA	4.35
O4	GLU A 71 CD	4	C31	THR A 73 CA	4.91
C18	GLU A 71 CD	4.6	C27	THR A 73 CA	4.96
C17	GLU A 71 CD	4.19	C11	GLN A 15 OE1	3.86
C16	GLU A 71 CD	4.72	C10	GLN A 15 OE1	2.87
C21	GLU A 71 CG	4.81	C9	GLN A 15 OE1	3.47
C20	GLU A 71 CG	4.22	C8	GLN A 15 OE1	3.04
O4	GLU A 71 CG	4.31	C4	GLN A 15 OE1	4.88

C17	GLU A 71 CG	4.9	C2	GLN A 15 OE1	3.86
C10	GLN A 15 OE1	3.24	C1	GLN A 15 OE1	4.55
C9	GLN A 15 OE1	4.95	C11	GLN A 15 NE2	3.57
C8	GLN A 15 OE1	4.15	C10	GLN A 15 NE2	4.09
C1	GLN A 15 OE1	4.93	C8	GLN A 15 NE2	4.07
C10	GLN A 15 NE2	4.39	C2	GLN A 15 NE2	4.48
O2	GLN A 15 CD	4.11	C11	GLN A 15 CD	3.79
C10	GLN A 15 CD	4.08	O3	GLN A 15 CD	4.36
C22	GLN A 11 OE1	4.29	O2	GLN A 15 CD	3.45
C13	GLN A 11 OE1	4.75	C10	GLN A 15 CD	3.85
O7	GLN A 11 CD	4.64	O1	GLN A 15 CD	4.62
O6	GLN A 11 CD	4.79	C9	GLN A 15 CD	4.56
O2	GLN A 11 CD	4.7	C8	GLN A 15 CD	3.89
			C2	GLN A 15 CD	4.44
			C11	GLN A 15 CG	4.68
			O2	GLN A 15 CG	4.94
			C10	GLN A 11 OE1	3.18
			C10	GLN A 11 NE2	3.23
			C8	GLN A 11 NE2	4.78
			O2	GLN A 11 CD	3.73
			C10	GLN A 11 CD	3.08
			O1	GLN A 11 CD	4.3
			O2	GLN A 11 CG	4.22
			C10	GLN A 11 CG	3.69
			O1	GLN A 11 CG	4.84

Table S11			Table S12		
(c) 20k-Tubulin			(d) 20s_Tubulin		
Hydrogen bonding			Hydrogen bonding		
Hydrogen Donor (D)	Hydrogen Acceptor (A)	Distance (D-A) in Å	Hydrogen Donor (D)	Hydrogen Acceptor (A)	Distance (D-A) in Å
GLN D 247 NE2	20k O3	3.01	20s N1	GLY D 246 O	4.33
GLY D 246 N	20k O2	3.03	ARG D 2 NH2	20s O6	4.47
THR A 225 OG1	20k O7	2.75	ARG D 2 NE	20s O6	3.2
THR A 225 N	20k O6	3.46	TYR A 224 N	20s F1	4.05
TYR A 224 N	20k O6	3.66	ARG A 221 NH1	20s F1	3.39
			20s N1	THR A 73 OG1	3.64
Hydrophobic interaction			Hydrophobic interaction		
20k	Tubulin	Distance	20s	Tubulin	Distance
C10	ALA D 250 CB	4.67	C32	MET D 325 CE	4.63
C19	GLN D 247 NE2	4.73	C31	MET D 325 CE	3.62
C15	GLN D 247 NE2	4.09	C30	MET D 325 CE	4.13
C14	GLN D 247 NE2	3.86	C31	MET D 325 SD	4.1
C13	GLN D 247 NE2	3.67	C30	MET D 325 SD	4.34
C12	GLN D 247 NE2	3.2	C31	MET D 325 CG	4.93
C11	GLN D 247 NE2	4.01	C30	MET D 325 CG	4.68
C8	GLN D 247 NE2	4.68	N1	ALA D 250 CB	4.79
C5	GLN D 247 NE2	4.4	C19	ALA D 250 CB	4.84
C4	GLN D 247 NE2	4.46	C6	ALA D 250 CB	4.17
C2	GLN D 247 NE2	3.86	C19	ALA D 250 O	4.76
O5	GLN D 247 CD	4.96	C18	ALA D 250 O	4.96
C13	GLN D 247 CD	4.57	C25	GLN D 247 OE1	4.99
O4	GLN D 247 CD	4.07	C7	GLN D 247 OE1	4.88
C12	GLN D 247 CD	4.5	C28	GLN D 247 NE2	4.95
C11	GLN D 247 CD	4.6	C27	GLN D 247 NE2	4.8
O3	GLN D 247 CD	3.87	C26	GLN D 247 NE2	3.79
C2	GLN D 247 CD	4.85	C25	GLN D 247 NE2	3.22
O5	GLN D 247 CG	4.87	C24	GLN D 247 NE2	3.04
C13	GLN D 247 CG	4.81	C23	GLN D 247 NE2	3.3
O4	GLN D 247 CG	4.37	C7	GLN D 247 NE2	3.68
C11	GLN D 247 CG	4.24	C6	GLN D 247 NE2	4.84
O3	GLN D 247 CG	4	C3	GLN D 247 NE2	4.27
C11	GLN D 247 CA	4.95	C1	GLN D 247 NE2	4.07
O3	GLN D 247 CA	4.9	C28	GLN D 247 CD	4.81
O2	GLN D 247 CA	4.98	C27	GLN D 247 CD	4.74
C11	GLN D 247 N	4.16	C26	GLN D 247 CD	4.02
C11	GLY D 246 O	4.39	C25	GLN D 247 CD	3.76
C10	GLY D 246 O	3.46	C24	GLN D 247 CD	3.87
C8	GLY D 246 O	4.14	C23	GLN D 247 CD	4.3
C2	GLY D 246 O	4.81	C7	GLN D 247 CD	4.26
C11	GLY D 246 C	3.95	C32	GLN D 247 CG	4.56
O3	GLY D 246 C	4.34	C28	GLN D 247 CG	4.05
O2	GLY D 246 C	3.44	C27	GLN D 247 CG	3.75
C10	GLY D 246 C	4.3	C26	GLN D 247 CG	3.26
C8	GLY D 246 C	4.55	C25	GLN D 247 CG	3.31
C2	GLY D 246 C	4.96	C24	GLN D 247 CG	3.76
C11	GLY D 246 CA	3.99	C23	GLN D 247 CG	4.48
O3	GLY D 246 CA	4.8	C7	GLN D 247 CG	4.74
O2	GLY D 246 CA	3.82	C27	GLN D 247 CB	4.79

C10	GLY D 246 CA	4.66	C26	GLN D 247 CB	4.5
C8	GLY D 246 CA	4.91	C25	GLN D 247 CB	4.62
C11	GLY D 246 N	3.6	C7	GLN D 247 CA	4.51
C10	GLY D 246 N	3.77	C6	GLN D 247 CA	4.79
C9	GLY D 246 N	4.9	C25	GLN D 247 N	4.79
C8	GLY D 246 N	4.05	C24	GLN D 247 N	4.86
C2	GLY D 246 N	4.67	C7	GLN D 247 N	4.32
C11	PRO D 245 CB	3.46	C6	GLN D 247 N	4.66
O3	PRO D 245 CB	4.25	C7	GLY D 246 O	3.21
O2	PRO D 245 CB	3.85	C6	GLY D 246 O	2.9
C10	PRO D 245 CB	4.51	C3	GLY D 246 O	4.57
O1	PRO D 245 CB	4.35	C24	GLY D 246 C	4.99
C9	PRO D 245 CB	4.01	C7	GLY D 246 C	3.76
C8	PRO D 245 CB	3.68	C6	GLY D 246 C	3.87
C4	PRO D 245 CB	4.49	C7	GLY D 246 CA	4.58
C3	PRO D 245 CB	4.76	C6	GLY D 246 CA	4.76
C2	PRO D 245 CB	3.91	C23	GLY D 246 N	4.97
C1	PRO D 245 CB	4.53	C7	GLY D 246 N	4.15
C11	PRO D 245 CG	4.91	C6	GLY D 246 N	4.33
O1	PRO D 245 CG	4.87	C3	GLY D 246 N	4.79
C9	PRO D 245 CG	4.65	C24	PRO D 245 CB	4.78
C8	PRO D 245 CG	4.72	C23	PRO D 245 CB	4.25
C1	PRO D 245 CG	4.89	O4	PRO D 245 CB	4.95
C11	PRO D 245 O	3.48	O1	PRO D 245 CB	4.76
C11	PRO D 245 C	3.36	C9	PRO D 245 CB	4.31
O3	PRO D 245 C	4.43	C8	PRO D 245 CB	4.85
O2	PRO D 245 C	3.55	C7	PRO D 245 CB	4.89
C10	PRO D 245 C	4.36	C4	PRO D 245 CB	4.87
O1	PRO D 245 C	4.93	C3	PRO D 245 CB	4.34
C9	PRO D 245 C	4.97	C1	PRO D 245 CB	4.04
C8	PRO D 245 C	4.2	O4	PRO D 245 CG	4.96
C2	PRO D 245 C	4.63	C9	PRO D 245 CG	4.97
C11	PRO D 245 CA	3.9	C24	PRO D 245 O	4.99
O3	PRO D 245 CA	4.75	C24	PRO D 245 C	4.97
O2	PRO D 245 CA	3.53	C23	PRO D 245 C	4.81
C10	PRO D 245 CA	4.02	C7	PRO D 245 C	4.69
O1	PRO D 245 CA	4.17	C3	PRO D 245 C	4.95
C9	PRO D 245 CA	4.27	C23	PRO D 245 CA	4.99
C8	PRO D 245 CA	3.91	O4	PRO D 245 CA	4.95
C2	PRO D 245 CA	4.51	C12	PRO D 245 CA	4.98
C10	ARG D 48 NH2	4.61	C7	PRO D 245 CA	4.84
C10	ARG D 48 NH1	3.88	C3	PRO D 245 CA	4.7
C10	ARG D 48 CZ	4.03	C1	PRO D 245 CA	4.8
O1	ARG D 48 CZ	4.23	C21	VAL D 51 CG2	4.95
C10	ARG D 48 NE	4.23	C19	ARG D 48 NH2	3.22
C10	ARG D 48 CD	4.36	C18	ARG D 48 NH2	3.39
O1	ARG D 48 CD	3.93	C17	ARG D 48 NH2	3.95
C9	ARG D 48 CD	4.92	C16	ARG D 48 NH2	4.28
O1	ARG D 48 CG	4.85	C15	ARG D 48 NH2	4.14
C25	GLU D 47 OE2	4.37	C14	ARG D 48 NH2	3.65
C24	GLU D 47 OE2	3.81	C12	ARG D 48 NH2	4.41
C23	GLU D 47 OE2	3.59	C19	ARG D 48 NH1	4.5
C9	GLU D 47 OE2	4.65	C14	ARG D 48 NH1	4.44

C7	GLU D 47 OE2	4.04	C12	ARG D 48 NH1	4.41
C6	GLU D 47 OE2	4.41	C19	ARG D 48 CZ	3.65
C3	GLU D 47 OE2	4.09	C18	ARG D 48 CZ	4.17
C1	GLU D 47 OE2	3.86	C17	ARG D 48 CZ	4.58
C24	GLU D 47 CD	4.72	C16	ARG D 48 CZ	4.5
C23	GLU D 47 CD	4.66	C15	ARG D 48 CZ	4.03
C1	GLU D 47 CD	4.99	C14	ARG D 48 CZ	3.6
C25	GLU D 47 CG	4.75	C13	ARG D 48 CZ	4.63
C24	GLU D 47 CG	4.67	O4	ARG D 48 CZ	4.46
C23	GLU D 47 CG	4.92	C12	ARG D 48 CZ	3.96
C28	GLU D 47 O	4.46	C21	ARG D 48 NE	4.45
C26	GLU D 47 O	4.97	C19	ARG D 48 NE	3.84
C20	ASN A 228 ND2	3.14	C18	ARG D 48 NE	4.3
C20	ASN A 228 CG	4.3	C17	ARG D 48 NE	4.33
C20	ASN A 228 CB	4.96	C16	ARG D 48 NE	3.86
C21	THR A 225 OG1	2.99	C15	ARG D 48 NE	3.36
C20	THR A 225 OG1	3.82	C14	ARG D 48 NE	3.36
C18	THR A 225 OG1	4.65	C13	ARG D 48 NE	3.7
C17	THR A 225 OG1	3.52	C12	ARG D 48 NE	3.68
C16	THR A 225 OG1	3.71	C21	ARG D 48 CD	4.81
C15	THR A 225 OG1	4.94	O5	ARG D 48 CD	4.22
O7	THR A 225 CG2	4.83	C19	ARG D 48 CD	4.9
C21	THR A 225 CB	3.77	C16	ARG D 48 CD	4.7
C20	THR A 225 CB	4.56	C15	ARG D 48 CD	3.96
O7	THR A 225 CB	3.77	C14	ARG D 48 CD	4.09
O6	THR A 225 CB	4.1	C13	ARG D 48 CD	3.73
C17	THR A 225 CB	4.74	O4	ARG D 48 CD	3.59
C16	THR A 225 CB	4.86	C12	ARG D 48 CD	3.93
C21	THR A 225 CA	4.48	C21	ARG D 48 CG	4.04
C20	THR A 225 CA	3.98	O6	ARG D 48 CG	4.91
O7	THR A 225 CA	3.63	O5	ARG D 48 CG	3.77
O6	THR A 225 CA	4.35	C16	ARG D 48 CG	4.71
C17	THR A 225 CA	4.84	C15	ARG D 48 CG	4.19
C21	THR A 225 N	3.87	C14	ARG D 48 CG	4.77
C20	THR A 225 N	3.66	C13	ARG D 48 CG	3.72
C17	THR A 225 N	4.33	O4	ARG D 48 CG	4
C16	THR A 225 N	4.39	C12	ARG D 48 CG	4.75
O6	TYR A 224 CD1	4.35	C21	ARG D 48 CB	4.7
O5	TYR A 224 CD1	4.91	C21	ARG D 48 CA	4.54
C16	TYR A 224 CD1	4.6	C13	GLU D 47 OE2	4.83
C15	TYR A 224 CD1	4.9	C10	GLU D 47 OE2	3.76
C13	TYR A 224 CD1	4.99	C9	GLU D 47 OE2	4.37
C20	TYR A 224 CG	4.93	C8	GLU D 47 OE2	3.76
O6	TYR A 224 CG	4.47	C2	GLU D 47 OE2	4.21
C16	TYR A 224 CG	4.88	O5	GLU D 47 CD	4.8
C21	TYR A 224 CB	4.83	O2	GLU D 47 CD	4.64
C20	TYR A 224 CB	3.65	C10	GLU D 47 CD	4.85
O7	TYR A 224 CB	3.8	C8	GLU D 47 CD	4.99
O6	TYR A 224 CB	3.58	O5	GLU D 47 CG	4.08
C17	TYR A 224 CB	4.17	C13	GLU D 47 CG	4.85
C16	TYR A 224 CB	4.08	O4	GLU D 47 CG	4.98
C20	TYR A 224 O	3.85	C21	GLU D 47 O	3.49
C21	TYR A 224 C	4.79	C13	GLU D 47 O	4.48

C20	TYR A 224 C	3.62	C21	GLU D 47 C	4.6
O7	TYR A 224 C	3.7	O5	GLU D 47 C	4.56
O6	TYR A 224 C	4.04	C20	ARG D 2 NH2	3.65
C17	TYR A 224 C	4.72	C20	ARG D 2 NH1	4.86
C16	TYR A 224 C	4.86	C21	ARG D 2 CZ	4.77
C21	TYR A 224 CA	4.84	C20	ARG D 2 CZ	3.88
C20	TYR A 224 CA	4.29	O7	ARG D 2 CZ	4.24
O7	TYR A 224 CA	4.31	O6	ARG D 2 CZ	4.27
O6	TYR A 224 CA	3.92	C21	ARG D 2 NE	3.53
C17	TYR A 224 CA	4.96	C20	ARG D 2 NE	3.68
C16	TYR A 224 CA	4.8	C17	ARG D 2 NE	4.47
C21	TYR A 224 N	4.29	C16	ARG D 2 NE	4.32
C16	TYR A 224 N	4.8	C21	ARG D 2 CD	3.6
C21	THR A 223 OG1	3.52	C20	ARG D 2 CD	4.6
C21	THR A 223 CG2	4.48	O7	ARG D 2 CD	4.13
C21	THR A 223 CB	3.7	O6	ARG D 2 CD	3.67
O6	THR A 223 CB	4.15	C17	ARG D 2 CD	4.87
C21	THR A 223 C	4.82	C16	ARG D 2 CD	4.7
O6	THR A 223 C	4.55	C21	ARG D 2 CG	3.93
C21	THR A 223 CA	4.84	C20	ARG D 2 CG	4.32
O6	THR A 223 CA	4.9	O7	ARG D 2 CG	3.49
C22	GLU A 77 OE2	3.74	O6	ARG D 2 CG	3.79
C19	GLU A 77 OE2	3.29	C17	ARG D 2 CG	4.25
C18	GLU A 77 OE2	4.17	C16	ARG D 2 CG	4.42
C14	GLU A 77 OE2	4.08	C20	ARG D 2 CB	3.8
C12	GLU A 77 OE2	4.32	O7	ARG D 2 CB	3.15
C7	GLU A 77 OE2	3.13	O6	ARG D 2 CB	4.46
C6	GLU A 77 OE2	3.21	C17	ARG D 2 CB	4.27
C5	GLU A 77 OE2	3.97	C16	ARG D 2 CB	4.87
C4	GLU A 77 OE2	4.42	C20	ARG D 2 CA	4.47
C3	GLU A 77 OE2	4.09	O7	ARG D 2 CA	3.59
C19	GLU A 77 OE1	3.59	C17	ARG D 2 CA	4.58
C18	GLU A 77 OE1	3.8	C20	ARG D 2 N	4.46
C14	GLU A 77 OE1	4.89	C18	MET D 1 CE	4.82
N1	GLU A 77 CD	4.18	C20	MET D 1 O	3.6
C22	GLU A 77 CD	4.81	C19	MET D 1 O	4.85
C19	GLU A 77 CD	3.83	C18	MET D 1 O	3.55
C18	GLU A 77 CD	4.39	C17	MET D 1 O	3.68
C14	GLU A 77 CD	4.9	C20	MET D 1 C	4.02
C7	GLU A 77 CD	4.23	O7	MET D 1 C	3.58
C6	GLU A 77 CD	4.41	C18	MET D 1 C	4.68
C7	GLU A 77 CG	4.59	C17	MET D 1 C	4.59
C32	ASP A 76 OD2	3.36	C20	MET D 1 CA	4.67
C31	ASP A 76 OD2	3.64	O7	MET D 1 CA	4.64
C27	ASP A 76 OD2	4.63	C20	MET D 1 N	4.07
C32	ASP A 76 CG	4.18	C29	TYR A 224 CE1	4.99
C31	ASP A 76 CG	4.38	C28	TYR A 224 CE1	4.66
C32	ASP A 76 CB	4.35	C29	TYR A 224 CD1	4.92
C31	ASP A 76 CB	4.8	C28	TYR A 224 CD1	4.49
C25	THR A 73 OG1	4.98	C30	THR A 223 CG2	4.68
C24	THR A 73 OG1	4.66	C29	THR A 223 CG2	4.24
C23	THR A 73 OG1	4.62	C28	THR A 223 CG2	4.84
C1	THR A 73 OG1	4.97	C29	THR A 223 CB	4.38

C32	THR A 73 CG2	4.58	C28	THR A 223 CB	4.8
C27	THR A 73 CG2	4.87	C29	THR A 223 CA	4.48
C26	THR A 73 CG2	4.33	C30	ARG A 221 NH2	4.95
C25	THR A 73 CG2	4.24	C30	ARG A 221 NH1	4.17
C24	THR A 73 CG2	4.49	C29	ARG A 221 NH1	4.22
C32	THR A 73 CB	5	C30	ARG A 221 CZ	4.55
C26	THR A 73 CB	4.47	C29	ARG A 221 CZ	4.96
C25	THR A 73 CB	4.13	C11	GLU A 77 OE2	4.04
C24	THR A 73 CB	4.13	C10	GLU A 77 OE2	3.98
C23	THR A 73 CB	4.46	C9	GLU A 77 OE2	4.38
C25	THR A 73 O	4.93	C8	GLU A 77 OE2	4.03
C24	THR A 73 O	4.86	C2	GLU A 77 OE2	4.61
C25	THR A 73 CA	4.96	C11	GLU A 77 CD	4.53
C20	GLN A 15 OE1	4.41	O2	GLU A 77 CD	4.78
C19	GLN A 15 OE1	3.23	C11	GLU A 77 CG	4.21
C18	GLN A 15 OE1	3.22	C22	VAL A 74 CG2	4.33
C17	GLN A 15 OE1	4.16	C11	VAL A 74 N	4.73
C16	GLN A 15 OE1	4.96	C22	THR A 73 OG1	3.21
C15	GLN A 15 OE1	4.95	C19	THR A 73 OG1	4.25
C14	GLN A 15 OE1	4.21	C18	THR A 73 OG1	4.77
C20	GLN A 15 NE2	3.35	C15	THR A 73 OG1	4.56
C19	GLN A 15 NE2	4.4	C14	THR A 73 OG1	4.11
C18	GLN A 15 NE2	3.8	C13	THR A 73 OG1	4.93
C17	GLN A 15 NE2	4.02	C12	THR A 73 OG1	4.27
C16	GLN A 15 NE2	4.81	C11	THR A 73 OG1	4.05
C20	GLN A 15 CD	3.73	C5	THR A 73 OG1	3.4
O7	GLN A 15 CD	4.48	C4	THR A 73 OG1	4.35
C19	GLN A 15 CD	3.94	C2	THR A 73 OG1	4.6
C18	GLN A 15 CD	3.48	C20	THR A 73 CG2	3.64
C17	GLN A 15 CD	4.15	O7	THR A 73 CG2	4.31
C14	GLN A 15 CD	4.93	O6	THR A 73 CG2	4.1
C20	GLN A 15 CG	4.03	O5	THR A 73 CG2	4.67
C19	GLN A 15 CG	4.89	C19	THR A 73 CG2	4.17
C18	GLN A 15 CG	4.23	C18	THR A 73 CG2	4.07
C17	GLN A 15 CG	4.96	C17	THR A 73 CG2	3.78
C20	GLN A 15 CB	3.8	C16	THR A 73 CG2	3.65
C20	GLN A 15 O	4.81	C15	THR A 73 CG2	3.69
C20	GLN A 15 CA	4.88	C14	THR A 73 CG2	3.95
			C13	THR A 73 CG2	4.27
			O4	THR A 73 CG2	4.84
			C12	THR A 73 CG2	4.71
			C11	THR A 73 CG2	4.75
			O3	THR A 73 CG2	4.62
			C5	THR A 73 CG2	4.6
			N1	THR A 73 CB	4.72
			C22	THR A 73 CB	4.51
			C19	THR A 73 CB	4.75
			C16	THR A 73 CB	4.78
			C15	THR A 73 CB	4.4
			C14	THR A 73 CB	4.39
			C13	THR A 73 CB	4.63
			O4	THR A 73 CB	4.84
			C12	THR A 73 CB	4.69

			C11	THR A 73 CB	3.68
			O3	THR A 73 CB	3.83
			C5	THR A 73 CB	4.1
			C4	THR A 73 CB	4.92
			C2	THR A 73 CB	4.79
			C11	THR A 73 O	3.01
			C11	THR A 73 C	3.74
			O3	THR A 73 C	4.66
			C11	THR A 73 CA	4.16
			O3	THR A 73 CA	4.77
			C20	PRO A 72 CD	4.81
			C20	PRO A 72 CG	4.72
			C20	GLU A 71 OE2	4.19
			C19	GLU A 71 OE2	4.34
			C18	GLU A 71 OE2	4.01
			C17	GLU A 71 OE2	4.59
			C22	GLU A 71 OE1	4.43
			C22	GLU A 71 CD	4.97
			C22	GLN A 11 OE1	4.43

CHAPTER-5

Urea congeners of noscapine as potent anticancer agent: chemical synthesis and biological evaluation using *in vitro* breast cancer cells and *in vivo* xenograft animal model

Abstract:

We have rationally designed a panel of urea-noscapine conjugates to increase the anticancer potential of noscapine. These compounds were chemically synthesized and their antiproliferation activity was evaluated using human breast cancer cell lines (MCF-7 and MDA-MB-239), primary breast tumour cells and normal healthy cells using an MTT assay. Inhibition to cell cycle progression and induction of apoptosis to cancer cells with the treatment of one of the most promising urea-noscapine conjugate **7h** were studied using flow cytometry. Further, the apoptosis of cancer cells was visualized using fluorescence imaging and TUNEL assay. Reactive oxygen species (ROS) generation and alteration in mitochondrial membrane potential with the treatment of urea-noscapine conjugate were investigated using the probes, DCFDA, rhodamine-123, and JC-1, respectively. Furthermore, reduction to tumour volume by urea-noscapine conjugate was studied in human breast tumour implanted in nude mice as xenografts of MCF-7. All the urea-noscapine conjugates **7a-h** developed were inhibited the proliferation of breast cancer cell lines (MCF-7 and MDA-MB-231) without affecting the normal healthy cell. The most potent compound **7h** inhibited cell proliferation of MCF-7 (IC_{50} of 4.8 µM), and MDA-MB-231 (IC_{50} of 8.1 µM), primary breast tumour cells from different patients (IC_{50} ranges from 6.2 to 10.9 µM) and colony formation (IC_{50} 1.6 ± 0.35 µM) by arresting the cells at G2/M phase of the cell cycle. Further, it was found to effectively induce apoptosis which is facilitated by the elevated level of ROS. The compound **7h** was also found to significantly reduce the implanted tumour in the xenograft mice model without any toxicity to vital organs. Thus, we conclude that urea-noscapine conjugates have great potential to be a novel therapeutic agent for breast cancers.

Key words: Noscapine, urea-noscapine conjugates, tubulin binding, anticancer agents, breast cancer

5.1. Introduction

Noscapine ($C_{22}H_{23}NO_7$), a benzylisoquinoline alkaloid (413.43 Da) was isolated from the opium plant (*Papaver somniferum*). It is used as a safe anti-tussive drug (Karlsson et al, 1990) in the clinic for several decades. Later on, it has been screened to have anticancer activity (Ye et al., 1998). It was discovered to bind stoichiometrically to tubulin (one noscapine molecule for each αβ-tubulin dimer), modify tubulin compliance, arrest mammalian cells at mitosis phase and induce apoptosis to cancer cells (Ye et al., 1998). Unlike vinca alkaloids and taxanes, however, it does not induce over-polymerization, depolymerization, or any change in the general interphase microtubule (MT) organization. Because of its subtle effect on the kinetic parameters of dynamic instability of MTs, noscapine inhibits mitosis at prometaphase and arrests dividing cancer cells and normal cells in mitosis (Zhou et al, 2002; Landen et al, 2002; Joshi et al 2010). Cancer cells, perhaps due to their mutations that compromise cell cycle checkpoints, often do not sustain arrested mitosis for a long time and undergo apoptosis while the arrested normal cells can resume mitosis after drug removal due to metabolic clearance (Landen et al, 2002; 2004). It is reported previously that, different divergent pathways were found to converge in bringing about apoptosis in cancer cells treated with noscapine and its derivatives. These pathways include the induction of stress-activated jun N-terminal kinase, mitochondrial depolarization, downward regulation of cell survival cascades, and upward regulation of pro-apoptotic signals, and eventually, all converging into caspase 3/7 activation (Heidari et al, 2007; Zhou et al, 2002; Ye et al, 2001; Aneja et al, 2007; Shen et al, 2015; Newcomb et al, 2008; Liu et al, 2011; Sung et al, 2010; Tian et al,2020). In comparison to the other MT binding drugs such as taxanes and vinca alkaloids, noscapine offers various advantages in cancer treatment: (a) noscapine arrests a variety of mammalian cancer cells including drug resistant variants in mitosis and targets them for apoptosis (Karlsson et al, 1990; Jordan et al, 1993) (b) it is a poor substrate for drug pumps (poly glycoproteins and MDR-related proteins) which constitute a major cause of drug resistance (Zhou et al, 2005) (c) it inhibits progression of murine melanoma, lymphoma, glioblastoma and human breast tumors implanted in nude mice without detectable toxicity to the rapidly dividing cells and post mitotic cells such as neurons (Ye et al., 1998; Zhou et al., 2002a; 2002b), (d) it does not hinder primary humoral and cellular responses in mice (Drukman and Kavallaris, 2002) (e) it does not cause measurable immunological and neurological toxicity in mice (Aneja et al, 2007) (f) it is orally administered as opposed to other anti-MT drugs that require peritoneal injections or intravenous infusions with a risk of anaphylactic reactions and infection at the injection

site causing pain, blood vessel thrombosis or embolism (Karlsson et al, 1990; Jordan et al, 1993). However, noscapine has low cytotoxicity to cancer cells of varying tissue origins. The values of IC_{50} remain within the high micromolar ranges (~21.1 to 100 μM) (Ye et al., 1998).

Ever since its discovery as an antitumor agent, several synthetic derivatives (known as noscapinoids) have been developed, having improved therapeutic indices and pharmacological profiles (Anderson et al., 2005; Aneja et al., 2005; Zhou et al., 2005; Zhou et al., 2003; Joshi et al., 2000; Aneja et al, 2006; Naik et al, 2011; Santoshi et al, 2011; Manchukonda et al, 2013; Santoshi et al, 2015). In this study, we approach to develop a novel series of noscapinoids by strategically coupling urea pharmacophore in the scaffold structure of noscapine followed by chemical synthesis and validating their anticancer activity based on a cellular study using two human breast cancer cell lines, MCF-7 and MDA-MB-231, as well as a panel of primary breast cancer cells from patients. The novel derivatives were found to bind tubulin heterodimer with increased binding affinity, effectively inhibit cancer cell proliferation and cause selective G2/M arrest in cancer cells. The mitotic catastrophe in cancer cells is then followed by the induction of apoptosis.

5.2. Materials and methods

5.2.1. Designing of urea congeners of noscapine

Urea derivatives have gained significant interest by chemists and biologists due to their wide range of biological activities, such as anticonvulsant activity, colchicine-binding antagonist, and CXCR3 antagonist (3-5). It was also reported that anticancer drugs with fragments of aryl-urea such as sorafenib (**1**), lenvatinib (**2**), tivozanib (**3**), etc. (Figure 1) are already in the clinic. These anticancer drugs effectively inhibit cell proliferation of human hepatocellular carcinoma, advanced renal cell carcinoma, lung cancer, leukemia, prostate cancer, and other malignant neoplasms (6-9). In addition, the conjugation of urea pharmacophore helps in improving the pharmacological and pharmacokinetic profiles of some drugs (Mounetou et al., 2001; Fortin et al., 2007; Li et al., 2009; Viswas et al., 2019; El-Naggar et al., 2018). Therefore, we strategically coupled the urea pharmacophore at the C-9 position of noscapine scaffold to develop a panel of urea-noscapine conjugates (Figure 2).

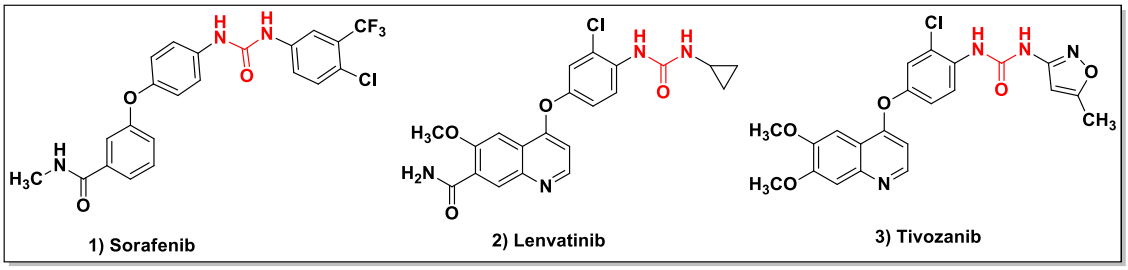

Figure 5.1. Anticancer drugs in the clinic with urea pharmacophore.

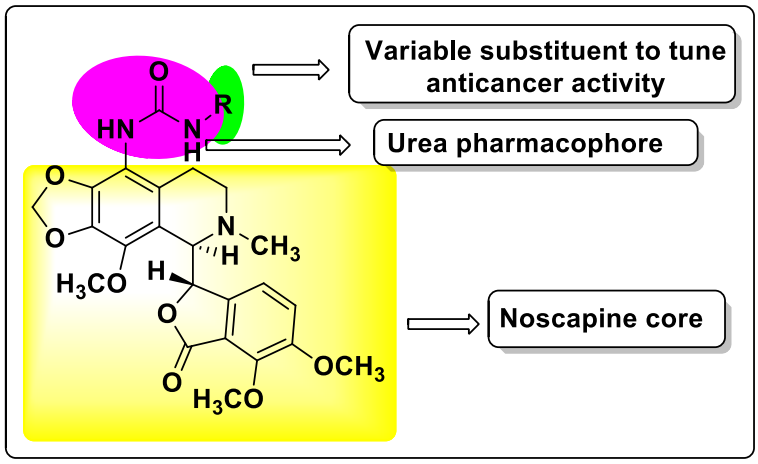

Figure 5.2. General scheme for strategic development of urea-noscapinoids by substitution of various functional groups at C-9 position of the noscapine scaffold.

5.2.2. Chemical synthesis of urea-noscapine conjugates

The selected urea-noscapine conjugates, **7a-h** were chemically synthesized by strategically coupling isocyanates with 9-aminonoscapine. In general chemical synthesis of noscapine derivatives is a bit tricky due to the presence of a highly sensitive C-C bond connecting two heterocyclic phthalide and isoquinoline units in the scaffold. We have optimized the reaction conditions for the synthesis of urea-noscapine conjugates without affecting the sensitive C-C bond. The synthetic scheme is depicted below. Using natural α-noscapine **(4)** as starting material, 9-bromonoscapine **(5)** was synthesized (Scheme 1) in excellent yield (90%) using bromine water (48% aq. HBr) by modifying the reaction conditions described in the literature (16). It was further converted to 9-aminonoscapine **(6)** with CuI, Sodiumazide, L-Proline in DMSO at 135 ^{o}C for 3 h in 62% yield (Scheme 1). The reaction scheme used here is different from our previously reported facile synthesis of 9-aminonoscapine (Manchukonda et al., 2012). The reaction conditions embraced do not influence the sensitive C-C bond. Approximately weighed alkyl/aryl isocyanate (**7a-h**) (1.2 mmol) were added to the solution of 9-aminonoscapine, **6** (1.0 mmol) in DCM (10 mL), and stirred for 12 h at room temperature. After the completion of the reaction (judged by TLC), the contents were washed with brine solution. The organic

layer was collected and passed through a Na_2SO_4 bed and later removed under reduced pressure. The crude residue was chromatographed over a triethylamine silica bed, using pet.ether/ethyl acetate (3:2) as eluents, to give pure compounds **7a-h** as solid products (65-90%, Scheme 2). All the intermediate and final products obtained were structurally characterized by IR, ^{1}H & ^{13}C NMR spectroscopy and mass spectrometry techniques.

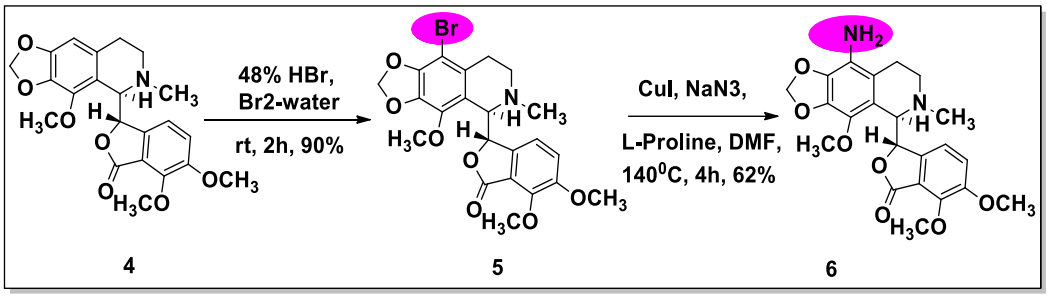

Reaction Scheme 1: Chemical synthesis of 9-bromonoscapine (**3**) and 9-aminonoscapine (**6**) using noscapine as starting material.

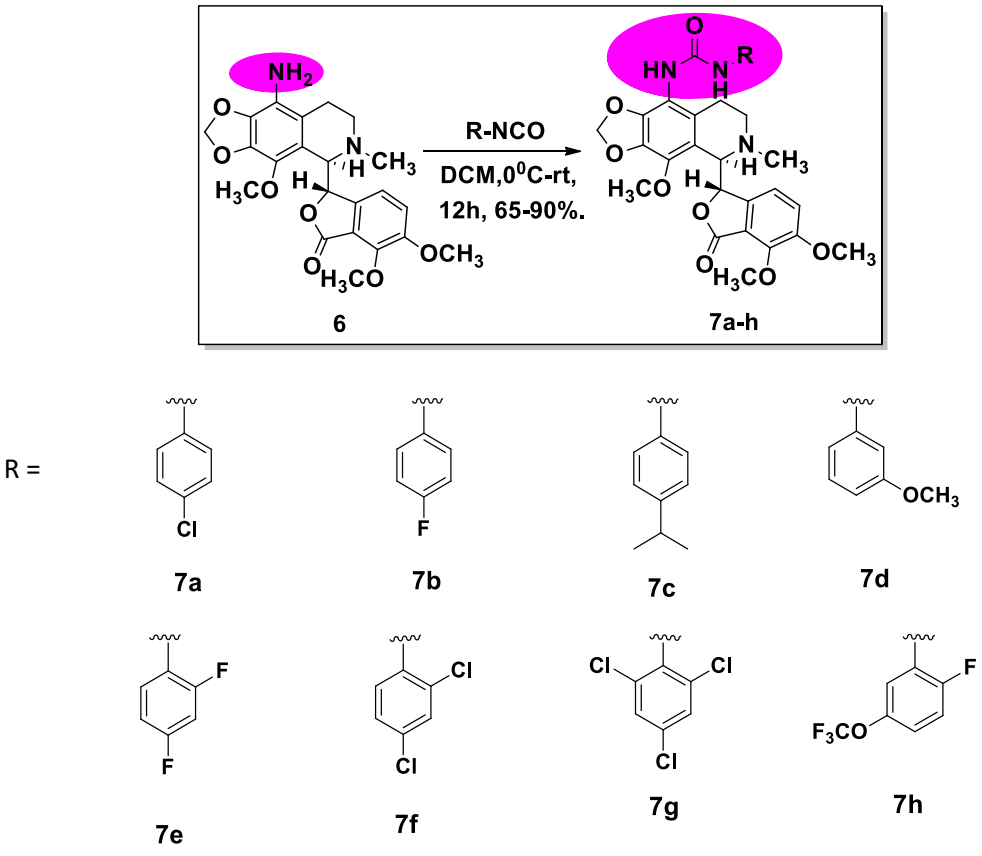

Reaction Scheme 2: Chemical synthesis of urea-noscapinoids: 9-2,4-Di-Cl-Ph-Urea-Nos **(22a)**; 9-2,4,6-Tri-Cl-Ph-Urea-Nos **(22b)** and 9-2F-5OCF3-Ph-Urea-Nos **(22c),** by coupling of alkyl/aryl isocyanates with 9-aminonoscapoine.

1-(4-chlorophenyl)-3-((*R*)-5-((*S*)-4,5-dimethoxy-3-oxo-1,3-dihydroisobenzofuran-1-yl) -4-methoxy-6-methyl-5,6,7,8-tetrahydro-[1,3]dioxolo [4,5-*g*]isoquinolin-9-yl)urea (7a)

Nature: White solid, Mp: 203-205 ^{o}C, IR (KBr): 3290, 2937, 2789, 1758, 1626, 1593, 1557, 1493, 1443, 1394, 1272, 1036, 1008, 970, 820, 753, 647, 507cm^{-1}. ^{1}H NMR (400 MHz, DMSO) : δ 8.82 (bs, 1H, -NH), 7.78 (s, 1H, -NH), 7.50-7.46 (m,2H, Ar-H), 7.32-

7.27 (m, 2H, Ar-H), 7.20 (d, *J* = 8.3 Hz,1H, Ar-H), 6.39 (d, *J* = 8.3 Hz, 1H, Ar-H), 6.04 (dd, *J* = 0.8, 6.7 Hz, 2H, O-CH_2-O), 5.48 (d, *J* = 4.4 Hz, 1H, Ar- CH, (C_3-phthalide)), 4.24 (d, *J* = 4.4 Hz, 1H, Ar-CH, ($C_{5'}$-isoquinoline)), 3.94 (s, 3H, -OCH_3), 3.87 (s, 3H, -OCH_3), 3.79 (s, 3H, -OCH_3), 2.66-2.57 (m, 1H, -C*H*H*N*- CH_3 ($C_{7'}$-isoquinoline)), 2.48-2.40 (m, 4H, -CH*H*-*N*CH_3 ($C_{7'}$-isoquinoline), -*N*-C*H*$_3$), 2.32-2.24 (m, 1H, Ar- C*H*H ($C_{8'}$-isoquinoline)), 1.81-1.72 (m, 1H, Ar-CH*H* ($C_{8'}$-isoquinoline)). ^{13}C NMR (125 MHz, $CDCl_3$ + DMSO) : δ 167.0, 153.0, 151.8, 146.4, 144.1, 140.5, 138.9, 138.4, 134.1, 129.4, 128.4, 125.0, 119.5, 119.1, 118.9, 118.3, 116.5, 112.4, 101.2, 81.0, 61.4, 60.5, 59.2, 56.3, 48.4, 45.3, 22.2. MS (ESI-MS) *m/z*: 582 $[M+H]^+$ HRMS (ESI) : Calcd for $C_{29}H_{29}ClN_3O_8$, $[M+H]^+$: 582.16633, found: 582.16377.

1-((*R*)-5-((*S*)-4,5-dimethoxy-3-oxo-1,3-dihydroisobenzofuran-1-yl)-4-methoxy-6-methyl-5,6,7,8-tetrahydro-[1,3]dioxolo[4,5-*g*]isoquinolin-9-yl)-3-(4-fluorophenyl) urea (7b):

Nature: White solid. mp: 212-214 °C. IR (KBr): 3269, 2944, 2891, 1754, 1617, 1561, 1503, 1441, 1273, 1039, 1015, 971, 793, 661cm^{-1}, ^{1}H NMR (300 MHz, $CDCl_3$) : δ 8.47 (bs, 1H, -NH), 7.69 (bs, 1H, -NH), 7.50-7.38 (m, 2H, Ar-H), 7.13 (d, *J* = 8.2 Hz, 1H, Ar-H), 6.95 (t, *J* = 8.8 Hz, 2H, Ar-H), 6.36 (d, *J* = 8.2 Hz, 1H, Ar-H), 6.01 (s, 2H, O-CH_2-O), 5.50 (d, *J* = 4.1 Hz, 1H, Ar-CH, (C_3- phthalide)), 4.36 (d, *J* = 4.1 Hz, 1H, Ar-CH, ($C_{5'}$-isoquinoline)), 4.02 (s, 6H, 2 x -OCH_3), 3.86 (s, 3H, OCH_3), 2.69-2.56 (m, 1H, -C*H*H-*N*-CH_3 ($C_{7'}$- isoquinoline)), 2.56-2.44 (m, 4H, -CH*H*-*N*-CH_3 ($C_{7'}$- isoquinoline), -*N*-C*H*$_3$), 2.38-2.26 (m, 1H, Ar-C*H*H ($C_{8'}$-isoquinoline)), 1.90-1.75 (m, 1H, Ar-CH*H* ($C_{8'}$-isoquinoline)). ^{13}C NMR (75MHz, $CDCl_3$) : δ 166.9, 158.3, 155.1, 152.7, 150.9, 145.9, 143.1, 139.7, 137.7, 135.0, 133.2, 129.0, 118.8 (d, J_{C-F} = 7.7 Hz), 118.4, 117.9 (d, J_{C-F} = 28.6 Hz), 115.9, 114.1 (d, J_{C-F} = 22.0 Hz), 111.3, 100.1, 80.7, 60.8, 59.8, 58.3,55.5, 48.4, 45.0, 22.1. MS (ESI-MS) *m/z*: 566 $[M+H]^+$, HRMS (ESI): Calcd for $C_{29}H_{29}FN_3O_8$ $[M+H]^+$: 566.19332, found: 566.19552.

1-((*R*)-5-((*S*)-4,5-dimethoxy-3-oxo-1,3-dihydroisobenzofuran-1-yl)-4-methoxy-6-methyl-5,6,7,8-tetrahydro-[1,3]dioxolo[4,5-*g*]isoquinolin-9-yl)-3-(4-isopropylphenyl) urea (7c):

Nature: White solid. Mp: 233-235 ℃. IR (KBr): 3277, 2955, 2793, 1761, 1622, 1557, 1497, 1445, 1272, 1036, 1010, 972, 815, 672 cm^{-1}.^{1}H NMR (400 MHz, $CDCl_3$) : δ 7.25 (d, *J* = 8.4 Hz, 2H, Ar-H), 7.09 (d, *J* = 8.4 Hz, 2H, Ar-H), 7.00 (d, *J* = 8.3 Hz, 1H, Ar-H), 6.56 (bs, 1H, -NH), 6.40 (d, *J* = 8.3 Hz, 1H, Ar-H), 5.90 (s, 2H, OCH_2- O), 5.51 (d, *J* = 4.0 Hz, 1H, Ar-CH, (C_3- phthalide)), 4.35(d, *J* = 4.0 Hz, 1H, Ar-CH, ($C_{5'}$-isoquinoline)), 4.04 (s, 3H, -CH_3), 3.91 (s, 3H, -OCH_3), 3.75 (s, 3H, -OCH_3), 2.88-2.77 (m, 1H, -C*H*(CH_3)$_2$), 2.72-2.62 (m, 1H, -C*H*H-*N*-CH_3 ($C_{7'}$-isoquinoline)), 2.59-2.47 (m, 4H, -CH*H*-*N*-CH_3 ($C_{7'}$-isoquinoline), -*N*C*H*$_3$), 2.39-2.29 (m, 1H, Ar-C*H*H ($C_{8'}$-isoquinoline)), 1.98-1.86 (m, 1H, Ar-CH*H* ($C_{8'}$-isoquinoline)), 1.19 (d, *J* = 6.8 Hz, 6H, -CH(C*H*$_3$)$_2$). ^{13}C NMR (100 MHz,$CDCl_3$) : δ 168.4, 154.4, 152.1, 147.2, 144.6, 143.9, 141.0, 139.3, 136.2, 134.1, 130.0, 126.7, 120.1, 119.4, 118.8, 118.0, 117.1, 111.4, 101.3, 81.9, 62.1, 60.9, 59.2, 56.5, 48.9, 45.6, 33.3, 23.9, 22.6. MS (ESI-MS) *m/z*: 590 $[M+H]^+$, HRMS (ESI) : Calcd for $C_{32}H_{36}N_3O_8$ $[M+H]^+$: 590.24973, found: 590.24969.

1-((*R*)-5-((*S*)-4,5-dimethoxy-3-oxo-1,3-dihydroisobenzofuran-1-yl)-4-methoxy-6-methyl-5,6,7,8-tetrahydro-[1,3]dioxolo[4,5-*g*]isoquinolin-9-yl)-3-(3-methoxyphenyl) urea (7d):

Nature: White solid, Mp : 233-235 °C. IR (KBr) : 3321, 2939, 2244, 1763, 1606, 1561, 1498, 1449, 1279, 1210, 1035, 940, 766, 692 cm^{-1}. ^{1}H NMR (300 MHz, DMSO) : δ 8.29 (s, 1H, -NH), 7.44 (s, 1H, -NH), 7.31 (d, *J* = 10.4 Hz, 2H, Ar-H), 7.13 (d, *J* = 8.2 Hz, 1H, Ar-H), 6.88 (d, *J* = 7.9 Hz, 1H, Ar-H), 6.52 (dd, *J*= 1.9, 7.9 Hz, 1H, Ar- H), 6.37 (d, *J* = 8.2 Hz, 1H, Ar-H), 6.0 (s, 2H, O-CH_2- O), 5.53 (d, *J* = 3.5 Hz, 1H, Ar-CH, (C_3-phthalide)), 4.39 (d, *J* = 3.8 Hz, 1H, Ar-CH, ($C_{5'}$-isoquinoline)), 4.05 (s, 3H, -OCH_3), 4.01 (s, 3H, -OCH_3), 3.86 (s, 3H, - OCH_3), 3.78 (s, 3H, -OCH_3), 2.68-2.57 (m, 1H, -C*H*H*N*-CH_3 ($C_{7'}$-isoquinoline)), 2.56-2.45 (m, 4H, -CH*H*-*N*CH_3($C_{7'}$-isoquinoline), -*N*-C*H*$_3$), 2.39-2.26 (m, 1H, Ar- C*H*H ($C_{8'}$-isoquinoline)), 1.90-1.76 (m, 1H, Ar-CH*H* $C_{8'}$-isoquinoline)). ^{13}C NMR (75 MHz, $CDCl_3$ +DMSO): δ 167.3, 159.4, 153.0, 151.4, 146.3, 143.6, 140.6, 140.1, 138.1, 133.7, 129.6, 128.7, 119.0, 118.4, 118.1, 116.4,111.9, 109.9, 106.6, 103.6, 100.6, 81.2, 61.2, 60.2, 58.8, 55.9, 54.4, 48.9, 45.5, 22.7. MS (ESI-MS) *m/z*: 578 $[M+H]^+$, HRMS (ESI) : Calcd for $C_{30}H_{32}N_3O_9$ $[M+H]^+$: 578.21331, found: 578.21341.

1-(2,4-difluorophenyl)-3-((*R*)-5-((*S*)-4,5-dimethoxy-3-oxo-1,3-dihydroisobenzofuran-1-yl)-4-methoxy-6-methyl-5,6,7,8-tetrahydro-[1,3]dioxolo[4,5-*g*]isoquinolin-9-yl)urea (7e):

Nature: White solid. Mp: 210-211 ^{o}C. IR (KBr) : 3423, 3254, 3065, 2926, 2852, 1751, 1615, 1562, 1497, 1437, 1386, 1273, 1140, 1039, 1014, 970, 929, 885, 695cm^{-1}, ^{1}H NMR (300 MHz, DMSO) : δ 8.39 (bs, 1H, -NH), 8.29-8.17 (m, 1H, Ar-H), 7.89 (s,1H, -NH), 7.11 (d, *J* = 8.2 Hz, 1H, Ar-H), 6.91-6.76 (m,2H, Ar-H), 6.33 (d, *J* = 8.2 Hz, 1H, Ar-H), 6.01 (s, 2H,O-CH$_2$-O), 5.51 (d, *J* = 4.1 Hz, 1H, Ar-CH), 4.37 (d, *J* =4.1 Hz, 1H, Ar-CH), 4.03 (s, 6H, 2 x –OCH$_3$), 3.87 (s, 3H, -OCH$_3$), 2.68-2.57 (m, 1H, -C*H*H-*N*-CH$_3$ (C$_{7'}$-isoquinoline)), 2.56-2.45 (m, 4H, -CH*H*-*N*-CH$_3$ (C$_{7'}$-isoquinoline), -*N*-C*H*$_3$), 2.38-2.27 (m, 1H, Ar-C*H*H (C$_{8'}$- isoquinoline)), 1.88-1.74 (m, 1H, Ar-CH*H* (C$_{8'}$-isoquinoline)). ^{13}C NMR (125 MHz, DMSO) : δ 167.4, 157.9 (d, $J_{C\text{-}F}$ = 10.8 Hz), 156.0 (d, $J_{C\text{-}F}$ = 11.8 Hz), 153.2, 152.1, 151.4 (d, $J_{C\text{-}F}$ = 10.8 Hz), 146.6, 144.2, 140.8, 138.6, 134.3, 129.3, 124.3 (dd, $J_{C\text{-}F}$ = 2.72,10.8 Hz), 119.5, 119.1, 118.5, 116.7, 112.4, 111.1 (dd,$J_{C\text{-}F}$ = 2.7, 21.7 Hz), 103.8 (dd, $J_{C\text{-}F}$ = 23.6, 26.3 Hz),101.4, 81.2, 61.6, 60.8, 59.5, 56.6, 48.4, 45.4, 22.3.
MS (ESI-MS) *m/z*: 584 [M+H]$^{+}$, HRMS (ESI) : Calcd for $C_{29}H_{28}F_2N_3O8$ [M+H]$^{+}$: 584.18390, found: 584.18423.

1-(2,4-dichlorophenyl)-3-((*R*)-5-((*S*)-4,5-dimethoxy-3-oxo-1,3-dihydroisobenzofuran-1-yl)-4-methoxy-6-methyl-5,6,7,8-tetrahydro-[1,3]dioxolo[4,5-*g*]isoquinolin-9-yl)urea (7f):

Nature: White solid, Mp: 109-111 ^{o}C. IR (KBr) : 3339, 2935, 2797, 1746, 1701, 1525, 1444, 1270, 1209, 1043, 1007, 972, 790 cm^{-1}. ^{1}H NMR (500 MHz, CDCl$_3$) : δ 8.21 (d, *J* = 9.0 Hz, 1H, Ar-H), 7.34-7.30 (m, 2H, Ar-H), 7.19 (dd, *J* = 2.4, 9.0 Hz, 1H, Ar-H), 6.99 (d, *J* = 8.2 Hz, 1H, Ar-H), 6.74 (bs, 1H, -NH), 6.43 (d, *J* = 8.2 Hz, 1H, Ar-H), 5.97 (dd, *J* = 1.2, 4.2 Hz, 2H, O-CH$_2$-O), 5.51 (d, *J*= 4.4 Hz, 1H, Ar-CH, (C$_3$-phthalide)), 4.35 (d, *J* = 4.4 Hz, 1H, Ar-CH, (C$_{5'}$-isoquinoline)), 4.06 (s, 3H, -OCH$_3$), 3.99 (s, 3H, -OCH$_3$), 3.80 (s, 3H, -OCH$_3$), 2.77-2.70 (m, 1H, -C*H*H-N-CH$_3$ (C$_{7'}$-isoquinoline)), 2.63-2.55 (m, 1H, -CH*H*-*N*-CH$_3$ (C$_{7'}$-isoquinoline)), 2.51 (s, 3H, *N*-C*H*$_3$), 2.44-2.38 (m, 1H, Ar-C*H*H (C$_{8'}$-isoquinoline)), 1.99-1.92 (m, 1H, Ar-CH*H* (C$_{8'}$-isoquinoline)). ^{13}C NMR (100 MHz, CDCl$_3$) : δ 168.5, 153.5, 152.0, 147.3, 144.5, 141.0, 139.6, 134.3, 134.1, 129.7, 128.4, 127.5, 127.4, 123.0, 121.8, 119.2, 118.7, 117.9, 117.3, 110.8, 101.3, 81.7, 62.0, 60.7, 59.2, 56.4, 48.6, 45.4, 22.2. MS (ESI-MS) *m/z* : 616 [M+H]$^{+}$

1-((R)-5-((S)-4,5-dimethoxy-3-oxo-1,3-dihydroisobenzofuran-1-yl)-4-methoxy-6-methyl-5,6,7,8-tetrahydro-[1,3]dioxolo[4,5-g]isoquinolin-9-yl)-3-(2-fluoro-5-(trifluoromethoxy) phenyl)urea (7g):

Nature: White solid, Mp : 161-163 ^{o}C, IR (KBr) : 3338, 2946, 1746, 1703, 1593, 1539, 1499, 1433, 1333, 1269, 1207, 1127, 1080, 1042, 973, 937, 819, 536 cm^{-1}. ^{1}H NMR (500 MHz, $CDCl_3$) : δ 8.70 (d, *J* = 1.2 Hz, 1H, Ar-H), 7.46 (bs, 1H, -NH), 7.42 (d, *J* = 8.3 Hz, 1H, Ar-H), 7.21 (dd, *J* = 8.3 Hz, 1H, Ar-H), 7.03 (d, *J* = 8.2 Hz, 1H, Ar-H), 6.62 (bs, 1H, -NH), 6.42 (d, *J* = 8.2 Hz, 1H, Ar-H), 5.98 (s, 2H, OCH_2-O), 5.51 (d, *J* = 4.1 Hz, 1H, Ar-CH, (C_3- phthalide)), 4.38 (d, *J* = 4.1 Hz, 1H, Ar-CH, ($C_{5'}$-isoquinoline)), 4.06 (s, 3H, -OCH_3), 4.01 (s, 3H, -OCH_3), 3.81 (s, 3H, -OCH_3), 2.77-2.68 (m, 1H, C*H*H-*N*CH_3 ($C_{7'}$-isoquinoline)), 2.62-2.54 (m, 1H, -CH*H*-*N*-CH_3 ($C_{7'}$-isoquinoline)), 2.52 (s, 3H, *N*-C*H*$_3$), 2.43-2.35 (m, 1H, Ar-C*H*H ($C_{8'}$-isoquinoline)), 1.97-1.88 (m, 1H, Ar-CH*H* ($C_{8'}$-isoquinoline)). ^{13}C NMR (100 MHz, DMSO) : δ 167.1, 152.5, 151.8, 146.3, 143.8, 140.3, 138.4, 137.1, 134.2, 130.2, 129.2, 128.2 (d, $J_{C\text{-}F}$ = 31.5 Hz), 125.1 (d, $J_{C\text{-}F}$ = 31.5 Hz), 122.4, 119.0 x 3, 118.4, 116.6, 116.1, 111.8, 101.3, 81.0, 61.4, 60.5, 59.3, 56.1, 48.8, 45.6, 22.8. MS (ESI-MS) *m/z*: 650 $[M+H]^+$, HRMS (ESI): Calcd for $C_{30}H_{28}F_4N_3O_9$ $[M+H]^+$: 650.17562, found: 650.17289.

1-((*R*)-5-((*S*)-4,5-dimethoxy-3-oxo-1,3-dihydroisobenzofuran-1-yl)-4-methoxy-6-methyl-5,6,7,8-tetrahydro-[1,3]dioxolo[4,5-*g*]isoquinolin-9-yl)-3-(2,4,6-trichlorophenyl)urea (7h):

Nature: White solid. M.P: 125-127 ^{o}C. IR (KBr): 3368, 2925, 2805, 1757, 1713, 1659, 1496, 1441, 1270, 1200, 1034, 789, 747 cm^{-1}. ^{1}H NMR (400 MHz, $CDCl_3$) : δ 7.31 (s, 2H, Ar-H), 6.99 (d, *J* = 8.3 Hz, 1H, Ar-H), 6.47 (d, *J* = 8.3 Hz, 1H, Ar-H), 5.93 (s, 2H, O-CH_2-O), 5.49 (d, *J* = 4.1 Hz, 1H, Ar-CH, (C_3-phthalide)), 4.33 (d, *J* = 4.1 Hz, 1H, Ar-CH, ($C_{5'}$-isoquinoline)), 4.05 (s, 3H, -OCH_3), 3.92 (s, 3H, -OCH_3), 3.79 (s, 3H, -OCH_3), 2.84-2.75 (m, 1H, -C*H*H-*N*-CH_3 ($C_{7'}$-isoquinoline)), 2.70-2.58 (m, 1H, -CH*H*-*N*-CH_3 ($C_{7'}$-isoquinoline)), 2.51 (s, 3H, *N*-C*H*$_3$), 2.48-2.39 (m, 1H, Ar-C*H*H ($C_{8'}$-isoquinoline)), 2.12-2.02 (m, 1H, Ar-CH*H* ($C_{8'}$-isoquinoline)). ^{13}C NMR (100 MHz,$CDCl_3$) : δ 165.3, 160.2, 151.1, 150.0, 144.6, 142.5, 138.6, 136.6, 132.9, 132.3, 131.2, 129.4, 128.2, 126.0, 117.2, 116.6, 114.2, 110.5, 99.3, 79.3, 59.5, 58.7, 57.3, 54.4, 47.0, 43.7, 20.6. MS (ESI-MS) *m/z*: 652$[M+H]^+$, HRMS (ESI): Calcd for $C_{29}H_{27}Cl_3N_3O_8$ $[M+H]^+$: 650.08582, found: 650.08880.

5.2.3. Cell culture and reagents

Noscapine, chemical reagents and media used for cell culture were obtained from Sigma. Human breast cancer cell line, MCF-7 and MDA-MB-231 were obtained from the cell repository of the National Center for Cell Science Pune, Maharashtra, India. Stock solution (100 mM) of the newly synthesized urea-noscapine conjugates, **7a-h** was prepared with dimethyl sulfoxide (DMSO) and stored at 4 ^{o}C until use. The cells were allowed to grow at a temperature of 37 °C in a 5% CO_2 and 95% humidity in Dulbecco's modified Eagle medium (DMEM, Pan Biotech), supplemented with 10% fetal bovine serum (FBS) and antibiotics. Cells with a 70-80 % confluence were sub-cultured for bioassays using trypsin-EDTA (0.25 %).

5.2.4. *In vitro* assessment of cytotoxicity of urea-noscapine conjugates using breast cancer cell lines

Inhibition of cellular proliferation of MCF-7 and MDA-MB-231 cell lines was assessed by 3-(4, 5-dimethylthiazol-2-yl)-2,5, ditetrazolium bromide (MTT). Briefly, MCF-7 and MDA-MB-231 cells (3 X 10^3) were seeded into 96 well plates. After post-attachment, the cells were treated with different concentrations of urea-noscapine conjugates and were maintained in complete medium for 48 h and 72 h. To estimate the viability of cells, we have treated them with 10 µl of MTT (5 mg/ml) for 4 h at 37 ^{o}C and formazan crystals were dissolved in DMSO. Optical density was obtained at 570 nm using a multimode flash reader (Varioskan, Thermo Scientific). The IC_{50} values for the concentration of drugs needed to destroy 50 % of cells have been calculated using the online tool Quest GraphTM IC_{50} Calculator (AAT Bioquest, Inc., Sunnyvale, CA, USA, https://www.aatbio.com/tools/ic50-calculator).

5.2.5. *In vitro* assessment of cytotoxicity of urea-noscapine conjugates using primary breast cancer cells (PBCs)

Primary breast tumor cells were obtained from the patients (8 nos.) of different stages of breast cancer before drug treatment in an aseptic condition. The tumour tissues were treated with 0.25% trypsin and filtered with 70 micron filter followed by centrifugation at 2000 rpm for 3 minutes with serum free medium. The filtered cells were collected and plated in T25 flask and incubated with a complete DMEM medium, supplemented with 10% FBS and 1% penstrip (mixture of penicillin and streptomycin) at 37 °C under 5% CO_2. Fresh media was replaced every 3-4 days, and subsequent passaging was performed under the same conditions as mentioned above. The cultured were maintained for homogeneous cell type at sub-confluence between 3-8 passages. Cells were allowed to reach 80-90% confluence before experimental treatments. After the confluence

reached, the primary cells were plated at 2000 cells/well in 96 wells plates with standard growth media, DMEM (low glucose). The cells were maintained at 37 °C in a humidified atmosphere with 5% CO_2 and were treated with gradient concentrations (5 to 100 µM) of urea-noscapine conjugates for 72 h. Measurement of cell proliferation was performed with a multimode flash reader (Varioskan, Thermo Scientific) by MTT assay as mentioned above. The percentage of cell survival as a function of drug concentration was then plotted to determine the IC_{50} value of the urea-noscapine conjugates.

5.2.6. Flow cytometry analysis of cell cycle progression

In Dulbecco's Modification of Eagle's Medium (DMEM), MDA-MB-231 cells were cultured with 4.5 g/L glucose and L-glutamine, supplemented by 10% bovine fetal serum and 1% penicillin/streptomycin. For cell cycle analysis, cells ($1x10^5$) were seeded in a 6-well culture plate overnight and then were treated with IC_{50} concentration of noscapine (60.9 µM) and its highly promising urea derivative **7h** (8.1 µM). Cells were incubated for 48 hours, harvested using trypsin-EDTA, washed with phosphate-buffered saline (PBS) and fixed in 70% ethanol for 30 minutes. After fixation, the cells were washed and stained with staining solution that included RNase (5 µg/mL), propidium iodide (5 µg/mL) and Triton X (0.1%). The cells were analyzed in a flow cytometer (BD FACS Aria-III) for the effect of drug treatment on different phases of the cell cycle.

5.2.7. Flow cytometry analysis for apoptosis assay:

MDA-MB-231 cells ($5 X 10^4$) were seeded in 35 mm plates. After 24 hours of attachment, cells were treated with IC_{50} concentration of **7h** and were harvested after 48 h of incubation. The cells were then stained with propidium iodide (PI) and Annexin-V-Alexa Fluor 488 (BD Pharmingen, San Diego, CA, USA) according to the manufacturer's protocol. Flow cytometer data with 488 nm excitation for PI and emission at 530 nm were collected using BD FACS Aria-III. Viable cells (Annexin V^- / PI^-), early apoptotic cells (Annexin V^+ / PI^-), late apoptotic/necrotic cells (Annexin V^+ / PI^+) and late necrotic cells (Annexin V^- / PI^+) were identified and determined their percentage.

5.2.8. Cellular observation using Hoechst 33342 & propidium iodide (PI) staining

To detect the change in nuclei morphology of MDA-MB-231 cells after treatment with noscapine and **7h**, Hoechst 33342 staining was performed. MDA-MB-231 cells were grown on poly-L-lysine-coated coverslips in 6-well plates and treated with IC_{50} concentration of **7h** for 72 hours. After incubation, coverslips were fixed in cold methanol, rinsed with PBS, stained with 10 µM Hoechst and 10 µM PI for 15 minutes at room temperature. The stained cells were washed two times with PBS and observed using an

inverted fluorescent microscope (Nikon Eclipse Ts2R-FL) with standard excitation filters. The excitation wavelength was 346 nm and the emission wavelength was 460 nm. Cells that have undergone apoptosis were recognized by characteristics associated with nuclear condensation, formation of membrane blebs, and apoptotic bodies.

5.2.9. Cellular observation using acridine orange (AO) & ethidium bromide (EtBr) staining

MDA-MB-231 cancer cells were cultivated separately on two different culture plates and treated for 72 h with the IC_{50} concentrations of **7h**. Coverslips were removed, then fixed in cold methanol and washed with PBS. It was then stained with acridine orange and ethidium bromide dye separately and placed on slides. An inverted fluorescence microscope was used to obtain these images (Nikon Eclipse Ts2R-FL). Changes in the morphology of apoptotic cells vs untreated cells were identified.

5.2.10. Measurement of mitochondrial membrane potential (ΔΨm)

The effect of the urea-noscapine conjugate on mitochondrial membrane potential was measured by using rhodamine-123 (Sigma-Aldrich Co.; Ex/Em = 485 nm/535 nm), JC-1 (Invitrogen Co.; Ex/Em = 515 nm/529 nm) and DAPI (Sigma-Aldrich Co.; Ex/Em = 358 nm/461 nm) dyes. Briefly, cells were seeded in 12 well plates followed by treatment with **7h** for 48 hours. Cells were washed with PBS and stained with rhodamine-123 (15µg/ml), JC-1 (10 µg/ml) and DAPI (10 µg/ml) for 10 minutes at room temperature. After staining, cells were washed twice with PBS and images were captured using an inverted fluorescence microscope (Nikon Eclipse Ts2R-FL) at 400x magnification. The untreated cells stained with rhodamine-123 appeared light green fluorescence (lower ΔΨm) whereas the treated cells appeared bright green fluorescence (higher ΔΨm). In the case of JC-1 stain, light red fluorescence (lower ΔΨm) was detected in untreated cells whereas bright red fluorescence (higher ΔΨm) was observed in treated cells. Similarly in DAPI stain relatively light blue with no morphological changes was observed in untreated cells, whereas bright blue with changes in morphological features was observed in treated cells. The intensity was measured using image J software.

5.2.11. Intracellular reactive oxygen species (ROS) detection

An increase in intracellular ROS is a quiescent component to damage nucleic acid, cellular lipid membrane as well as organelles, which induces apoptosis in cancer cells. The intracellular ROS concentration was analysed through the oxidative conversion of the sensitive fluorescent probe 2',7'-dichlorofluorescence-diacetate (DCFH-DA) to fluorescent 2',7'-dichlorofluorescein (DCF). Briefly, MDA-MB-231 cells were seeded in 6 well plates containing cover glass and treated with **7h** for 48 hours. The treated cells

were harvested, washed twice with PBS, re-suspended in 500 µL of 10 µM DCFH-DA (purchased from Molecular Probes Inc., Invitrogen) and incubated at room temperature for 30 minutes in the dark. The stained cells were observed under a fluorescent microscope (Nikon Eclipse Ts2R-FL) with standard excitation filters (Nikon). The control untreated cells were observed with low green fluorescence, whereas the treated cells were observed with bright green fluorescence. The results displayed a significant rise in intracellular ROS by **7h.**

5.2.12. Detection of Apoptosis by TUNEL assay

Induction of apoptosis to MDA-MB-231 cells with the treatment of **7h** was studied by the TUNEL assay. DNA fragmentation was studied with the Apo BrdU TUNEL assay kit from Invitrogen (Carlbad, CA,USA), using fluorescence microscopy. Briefly, cells were grown on 12 well plates and treated at an IC_{50} concentration of **7h**. Cells were detached from culture plates, centrifuged and the pellet was collected. Breaks in DNA strands were identified by an Alexa Fluor 488 dye-labeled anti-BrdU antibody. The appearance of fluorescently green cells indicates TUNEL positive cells.

5.2.13. Colony formation assay

A clonogenic experiment was carried out to assess the influence of urea-noscapine conjugate, **7h** on the capacity of the triple-negative breast cancer cell line (MDA-MB-231) to form colonies. Image-J software was used to count the colonies under each setting (National Institute of Health, Bethesda, MD, USA). Briefly, 1000 cells were seeded on 6 well plates and treated with an increasing concentration (1 µM, 10 µM and 20 µM) of **7h** for 10-12 days. Cells were fixed and stained with crystal violet and the number of colonies formed was counted for untreated and treated cells.

5.2.14. *In vivo* antitumor effect against MCF-7 breast tumors

All experimental protocol involved in this study was approved by the Institutional Animal Ethics Committee of National Institute of Pharmaceutical Education and Research (NIPER), Hyderabad (1548/PO/Re/2011/CPCSEA) and followed by the guidelines of "Committee for Control and Supervision of Experiments on Animals" of Govt. of India. About 8 to 10 weeks old female BALB/c athymic nude mice were housed in the Animal Care Facility. Suspensions of $1x10^6$ human epithelial breast adenocarcinoma MCF-7 cells in 0.2 ml of PBS were inoculated subcutaneously into the anterior flank. After 7-10 days when the tumor was palpable, the urea-noscapine conjugate **7h** was administrated by oral gavage. The mice were randomly divided into 2 groups. Group-1 (control) consisted of 5 animals which received daily gavage of vehicle solution (acidified water, pH 4.0) only,

Group-2 consisted of 5 animals were treated with **7h** (50 µM/day), Tumor volumes were estimated on alternate days by measuring tumours in three transverse direction diameters with a vernier calliper and calculated their volume as Π/6 (length x width x height) (Tomayko and Reynolds, 1989). The control group of mice was euthanized at day 30 owing to their large tumor volumes, this served as the endpoint for control animals. Accordingly, this endpoint was used to evaluate tumour size in untreated mice with those administered with **7h**.

5.2.15. Histopathological and haematological analysis

On day 30, tumor-bearing mice treated with **7h** and untreated tumor-bearing mice, received an overdose (0.2 ml) of 3.5 percent chloral hydrate, blood was drawn from the heart, and CBC analysis was conducted using a CBC analyzer (CDC Technologies, Oxford, CT). Following that, the animals were perfused with a 3% paraformaldehyde and 2% glutaraldehyde combination in PBS (pH 7.4). The vital organs like liver, kidney, lung, and heart as well as tumour were extracted and analysed for histological investigation. Tissues were mounted in paraffin, sectioned, and stained with hematoxylin and eosin. The tissues were observed under the microscope for toxicity evaluation.

5.3. Results

5.3.1. Urea derivatives of noscapine inhibited proliferation of cancer cells without affecting the normal cells

The effects of urea derivatives, including the lead molecule, noscapine (0-100 µM) were analyzed for their anti-proliferative activity in two human breast adenocarcinoma cells, MCF-7 (estrogen- and progesterone- receptor positive) and MDA-MB-231 (estrogen- and progesterone- receptor negative) using MTT assay (Figure 3A and 1B). All the urea derivatives **7a-h** exhibited potent cytotoxic activity in comparison to noscapine using both the cell lines. The IC_{50} values for the tested compounds for both the cell lines are collated in Table 1. The IC_{50} value for the urea-noscapine congeners **7a-h** ranges from 35.2 to 4.8 µM was found to be significantly less compared to the lead molecule, noscapine (IC_{50} value is 43.9 µM) for MCF-7 cells. Parenthetically, a similar modest IC_{50} value ranges from 44.3 to 8.1 µM were measured for urea-noscapine congeners, **7a-h** compared to noscapine (IC_{50} value is 60.9 µM) for MDA-MB-231 cells. The IC_{50} value of noscapine and its urea derivatives for both the cancer cell lines was found to be statistically significant compared to untreated cells ($p < 0.001$). Surprisingly noscapine and its urea derivatives **7a-h** inhibited proliferation of normal healthy cells, 293T to a value of < 5% at a concentration of 100 µM, whereas it was found to be above 5% with a concentration above 100 µM (Figure 3C). The compound **7h** was found to be most

promising (IC_{50} value is 4.8 µM and 8.1 µM for the MCF-7 and MDA-MB-231 cell lines, respectively) among the library and was selected for the detailed investigation. We next evaluated the sensitivity of primary cancer cells directly isolated from eight different patients with different stages of breast cancer with the treatment of the most promising urea derivative of noscapine, **7h.** The primary breast cancer cells were treated with increasing concentrations (0-100 µM) of **7h** using MTT assay. The compound significantly inhibited the proliferation of primary tumor cells compared to the untreated cells (Figure 3D). The IC_{50} values range from 2.9±0.4 µM to 9.6±1.1 µM for all the eight primary tumor cells. Further, we examined the effect of the most promising derivative of noscapine **7h** (0-20 µM) on the colony-forming ability of MDA-MB-231 cells. It inhibited colony formation in a concentration-dependent manner. As an example, 10 and 20 µM of **7h** reduced significantly the number of colonies by 60% and 80%, respectively (Figure 3E). The IC_{50} of **7h** was found to be 1.6 ± 0.35 µM for inhibition of colony formation.

Table 5.1. IC_{50} values of novel urea derivatives of noscapine using two human breast adenocarcinoma cell lines, MCF-7 and MDAMB-231 as well as a normal cell line (293T). All the novel derivatives were found to have improved antiproliferative activity compared to noscapine without affecting the normal healthy cell line.

	IC_{50} (µM)		
	MCF-7	**MDAMB-231**	**293T**
Noscapine	43.9±4.6***	60.9±3.8**	312.6±2.2***
7a	35.2 ±2***	44.3 ± 2.4***	337.5±2.1***
7b	31.5± 3.2***	41.4 ± 3.5***	356.3±2.6***
7c	27.2 ±2.7***	38.2 ± 3.1***	332.2±3.7***
7d	22.4±3.4 ***	37.7 ± 2.2***	312.3±2.3***
7e	20.1 ± 2.5***	34.5± 3.5***	310.7± 2.5***
7f	17.6±4.3***	33.2±4.5***	320.5±3.5***
7g	12.5±3.8***	21.6±0.8***	342.3±2.6***
7h	4.8±0.5***	8.1±0.7***	278.4±3.5***

A. MCF-7

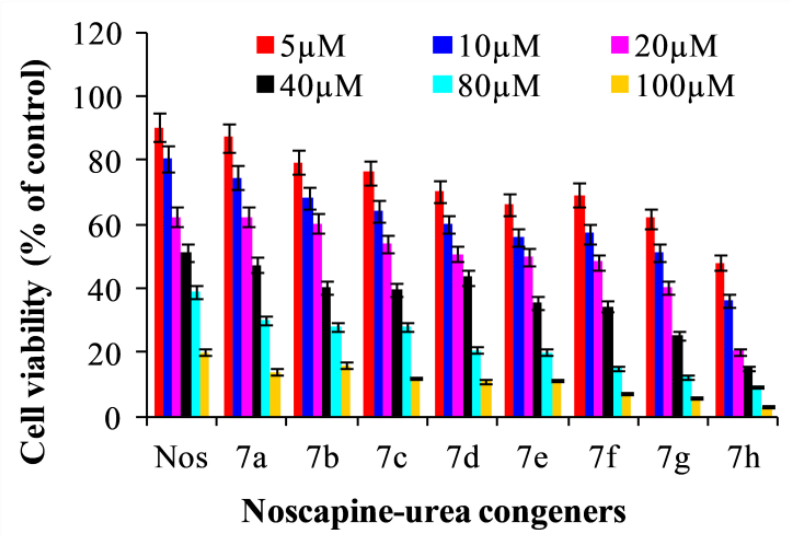

B. MDAMB-231

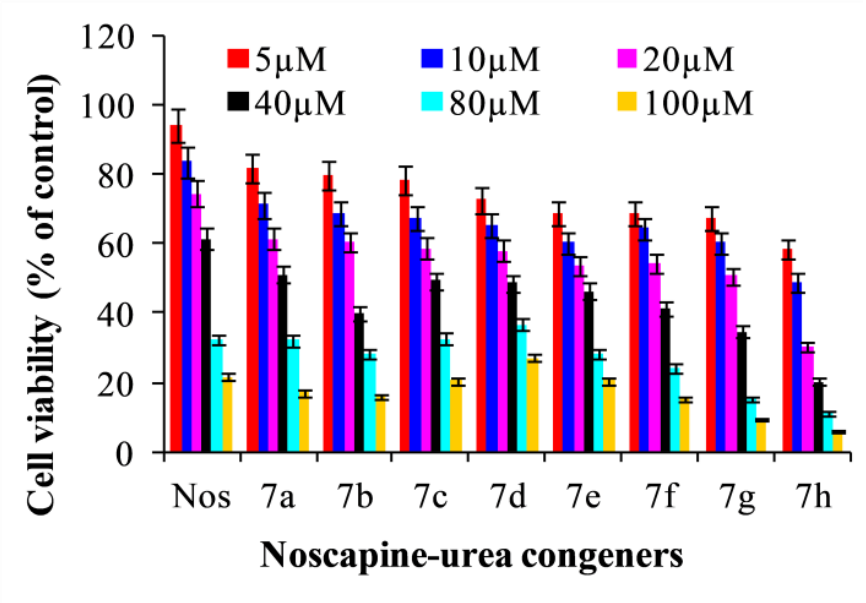

C. Normal healthy cell

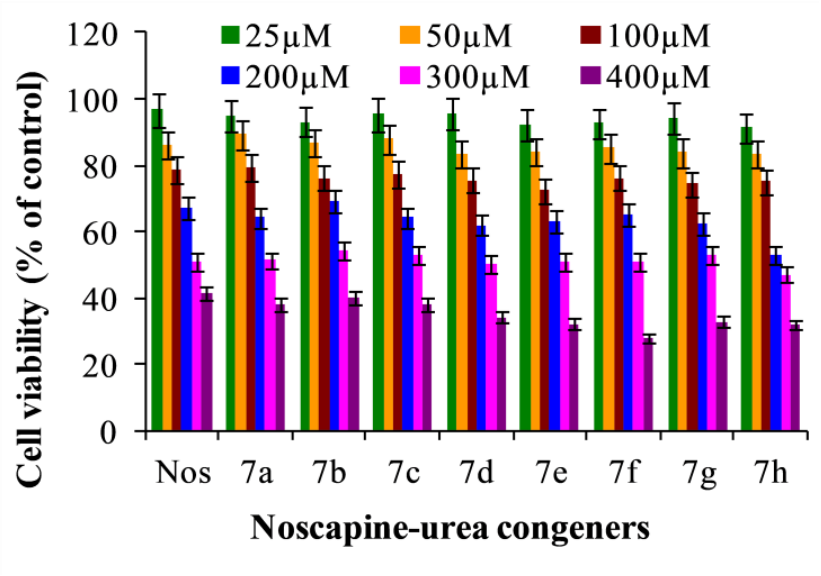

D. Primary tumor cell treated with 7h

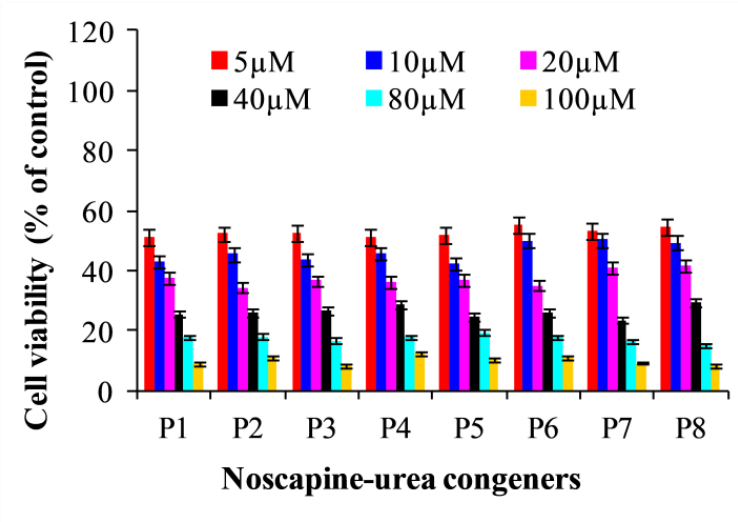

E. Effect of 7h on clonogenicity of MDAMB-231 cells

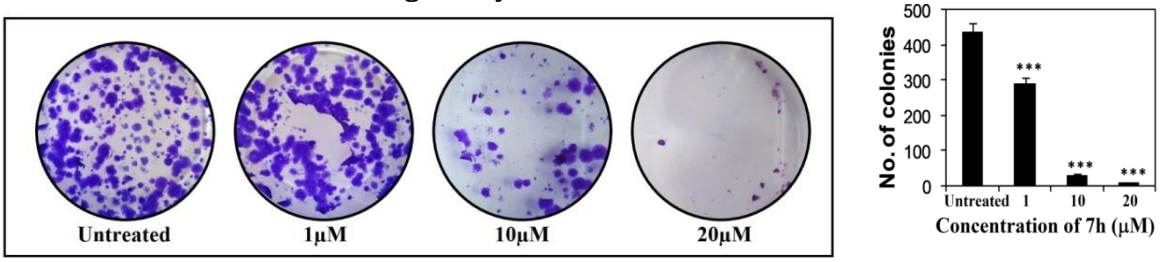

Figure 5.3. Effect of the lead molecule, noscapine and its eight urea derivatives at a gradient of concentration (0–100 µM) on (A) MCF-7 and (b) MDAMB-231 cancer cells viability after a 72-h exposure. Results are shown as mean ± standard deviation, n = 3. (C) Effect of noscapine and its eight urea derivatives (25–400 µM) on the cell viability of normal healthy cell (293T). (D) Effect of the most promising derivative **7h** (0–100 µM) on viability of primary tumor cells obtained from eight patients with different stages of breast cancer (IC50 value ranges from 6.2 ± 0.5 µM to 10.9 ± 1.2 µM) . (E) Effect of **7h** on clonogenicity of MDAMB-231 cells. Images of the colonies and a bar graph showing the

number of colonies under different treatment conditions are presented. Results are shown as mean ± standard deviation, n = 3. ***P < 0.001, compared to the control.

5.3.2. Urea derivatives of noscapine induced cell death in MDA-MB-231 cells

We approached to determine the induction of cell death to MDA-MB-231 cells with the treatment of **7h**. The apoptotic cells were quantified by FACS analysis using Annexin/FITC fluorescent dyes. The percentage of early apoptotic and late apoptotic cells using MDA-MB-231 cells at IC_{50} concentration (8.1 µM) after 72 h is collated in Figure 4A. The control untreated cells contained only very few early apoptotic (2%) and late apoptotic cells (3%), which were considered as the background cell death due to regular trauma during cell culture. In contrast, the percentage of early apoptotic cells of 14% and late apoptotic cells of 70% were noticed with the treatment of **7h** and were found to be significantly high compared to controlled untreated cells.

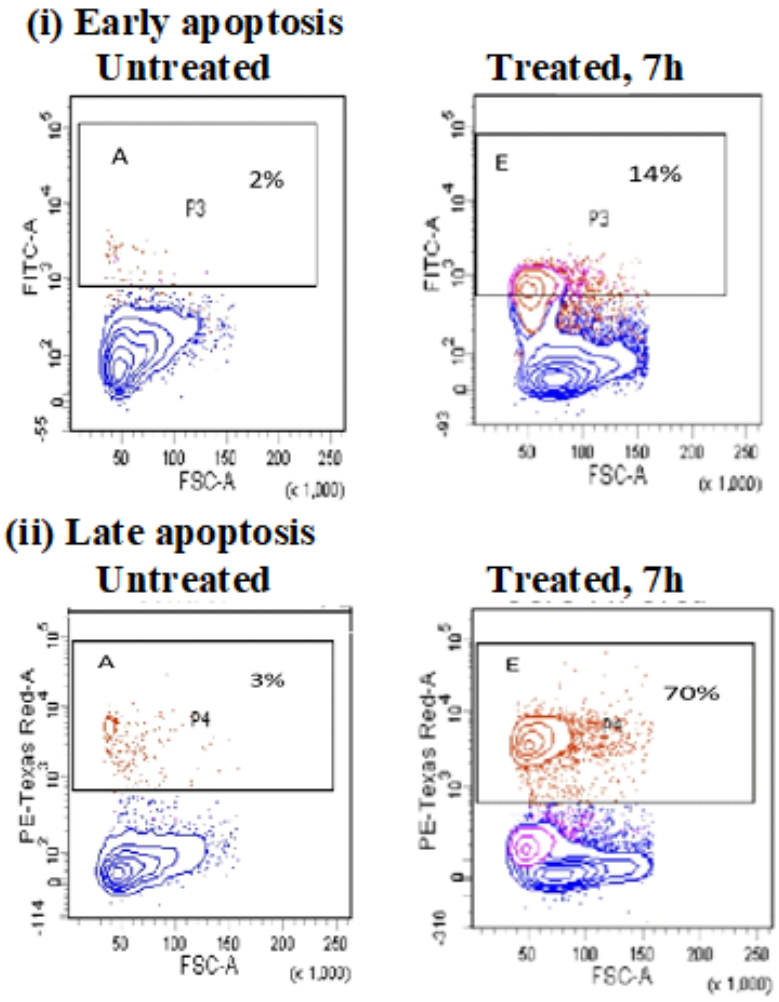

Figure 5.4. Induction of apoptosis by the most promising urea derivative of noscapine, **7h.** Flow cytometry analysis of cells showing increased percentage of early and late apoptosis with the treatment of **7h** for 72 h compared to untreated treated cells.

5.3.3. Detection of apoptosis with the treatment of noscapine and its urea derivatives

Membrane blebbing, cellular shrinkage, chromatin condensation and formation of apoptotic bodies are always the main morphological changes during apoptosis. Therefore, we performed cellular studies using AO, EtBr, HO (Hoechst 33342), and a combination of HO & PI to further confirm the induction of apoptosis by **7h**. MDA-MB-231 treated cells underwent apoptosis as demonstrated by staining of the treated cells with these dyes (Figure 4B). Specifically, the untreated cells were observed to have normal cell morphology, whereas, the treated cells underwent several features of apoptosis such as membrane blebbing, numerous fragmented nuclei, and appearance of apoptotic bodies.

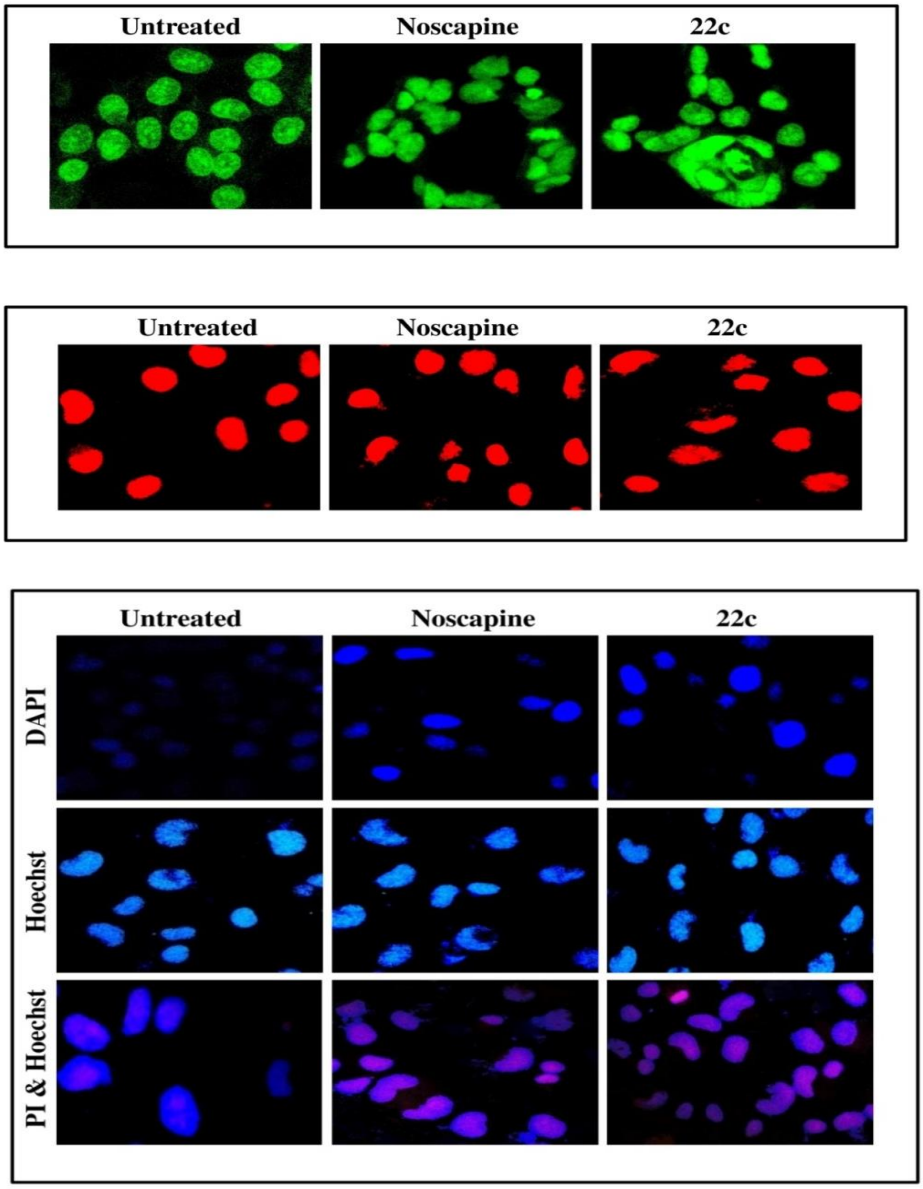

Figure 5.5. Morphological changes of MDAMD-231 cells visualized by staining with AO, EtBr and Hoechst revealed apoptosis with the treatment of **7h** compared to untreated cells.

5.3.4. Effects of noscapine-urea conjugate 7h on ROS accumulation in MDA-MB-231 cells

To further investigate the mechanism of induction of apoptosis to cancer cells, we found that **7h** elevated the levels of ROS. Using DCFDA as the molecular probe, the ROS level was analyzed. When MDA-MB-231 cells were treated with **7h**, the green fluorescence was more intense compared to untreated cells (Figure 4C). We found that **7h** significantly elevated ROS level in MDA-MB-231 cells as measured by fluorescent intensity, indicating that ROS might have a function in the induction of apoptosis (Figure 5D). MDA-MB-231 cells treated with H_2O_2 (10 μM) also showed a substantial amount of ROS inside the cells and were labeled with more intense green fluorescence. Further, TUNEL assay was performed to investigate induction of apoptosis to MDA-MB-231. Results showed that treatment with **7h** increased the number of TUNEL positive nucleus, indicating cell death (Figure 6A).

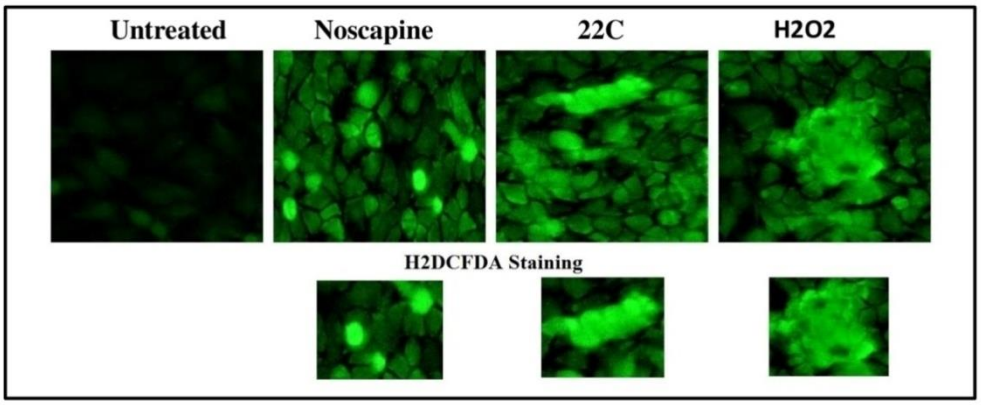

Figure 5.6. Effect of **7h** treatment on intracellular ROS production as imaged and estimated using an oxidation sensitive fluorophore, DCFDA.

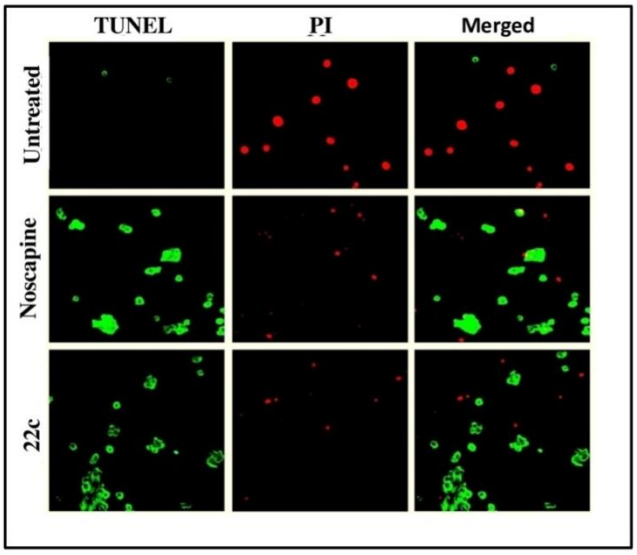

Figure 5.7. Treatment with **7h** increases the number of TUNEL positive cells compared to untreated cells indicating induction of apoptosis to MDAMB-231 cells.

5.3.5. Urea derivative of noscapine alter the cell cycle profile and cause mitotic arrest at G_2/M phase

We examined the effect of **7h** with its IC_{50} concentration (8.1 µM) on the cell cycle profile of MDA-MB-231 based on FACS analysis. Treatment of MDA-MB-231 cells for 72 h led to significant perturbations of the cell cycle profile. FACS analysis revealed a high accumulation of cells in the G2/M phase compared to untreated cells (Figure 6B). In contrast to G2/M block, a characteristic hypodiploid DNA content peak (sub-G1) was seen to rise at 72 h of drug treatment. The progressive generation of cells having hypodiploid DNA content reflects fragmented DNA indicating dying cells.

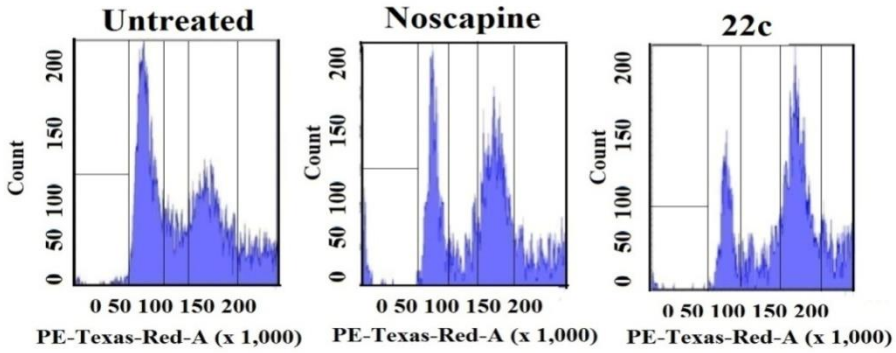

Figure 5.8. Effect of **7h** at IC_{50} concentration (8.1 µM) on MDAMB-231 cell cycle distribution at 72h. The bar graph represents the percentage of cells at the indicated phases of the cell cycle.

5.3.6. Effects of noscapine and its urea derivatives on mitochondrial membrane potential (ΔΨm)

Mitochondria are thought to be the major pathway for apoptosis. The induction of apoptosis is closely related to the collapse of mitochondrial membrane potential (ΔΨm). Thus we have measured the loss of mitochondrial membrane potential (ΔΨm) in MDA-MB-231 cells treated with **7h** using DAPI, JC-1, and Rhodamine 123 dyes. When MDA-MB-231 cells were treated with **7h**, JC-1 red fluorescence, Rhodamine-123 green fluorescence, and DAPI blue fluorescence in treated cells were more intense compared to untreated cells (Figure 5C). The urea derivative of noscapine, **7h** significantly increased the loss of mitochondrial membrane potential (ΔΨm) in MDA-MB-231 cells (Figure 5C) compared to untreated cells.

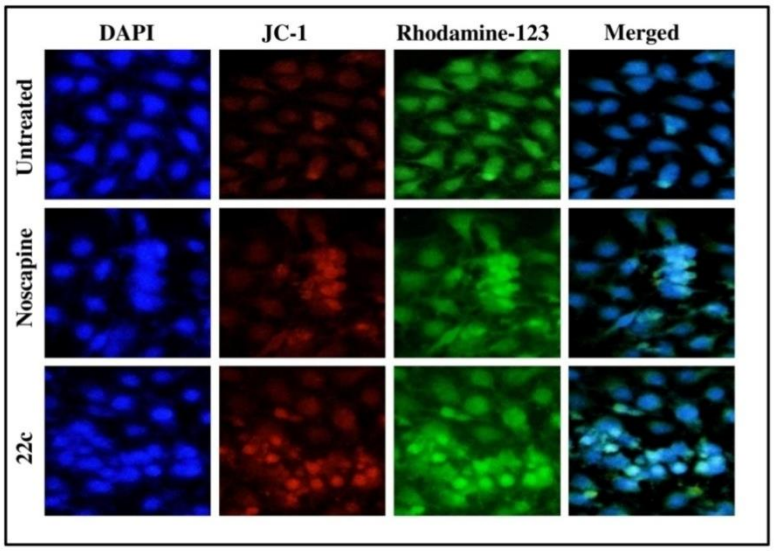

Figure 5.9. Effect of **7h** on mitochondrial membrane potential as visualized using different fluorescent dyes, DAPI, JC-I and Rhodamine 123. The fluorescent intensity was measured using Image J.

5.3.7. Reduction in tumor volume with the treatment of 7h against MCF-7 xenograft model

Treatment with **7h** (150 mg/kg/day) considerably decreased tumor volume in comparison to control ($P < 0.001$) (Figure 6A). Tumor volume was reduced to 809 mm^3 from the tumour size of the untreated control group with tumor volume 1479 mm^3 on day 40 post tumour implantation. On 40^{th} day mice were sacrificed and tumours were removed and weighted. All untreated mice developed solid tumours in sizes ranging from 4.8 to 11.2 g (mean 7.9 ± 2.0 g). Whereas, among the treated groups the tumor size was significantly regressed and showed only small palpable tumors. Compared to untreated control mice, inhibition of tumor growth by **7h** was statistically significant ($p < 0.001$). In addition, we did not observe any apparent weight loss after drug treatment compared to the control group of mice (Fig. 6B).

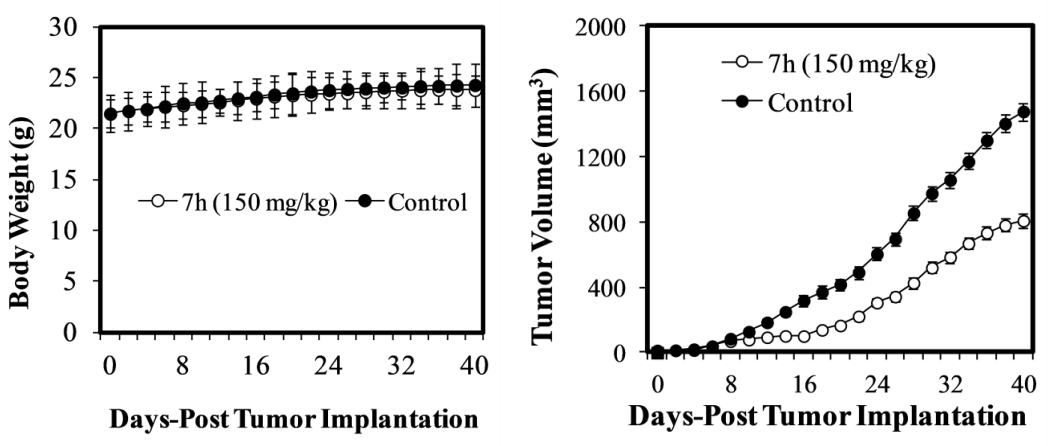

Figure 5.10. Effect of **7h** on the body weight of mice. No difference in body weight was noticed between the treated and untreated mice. (C) Progression in tumor growth on human MCF-7 xenograft mice with the treatment of **7h**. The tumor growth was significantly inhibited by **7h** compared to untreated group.

5.3.8. Treatment of 7h does not cause any detectable toxicity

The severe side effects during chemotherapeutics are a major concern in the treatment of cancer patients. Tubulin binding agents, for example, vinca alkaloids and taxanes, while clinically approved, are known to cause adverse side effects (Rowinsky et al., 1997). As a result, there is a need to identify a drug regimen that is both safe and well-tolerated. We examined the liver, kidney, heart, and lungs of tumor-bearing mice to see if **7h** causes toxicity to normal tissues. Treatment with **7h** fails to reveal any detectable pathological abnormalities in normal tissues involved in normal cell proliferation. H&E staining of paraffin-embedded 5.0 micron-thick sections of the liver, kidney, lung, and heart is shown at 200x magnification in Figure 6A. The hepatic lobular architecture was normal. Normal glomeruli, proximal and distal tubules, interstitium, and blood vessels were found in the kidneys. Among the groups, the heart muscle exhibited normal morphology. Normal alveoli and bronchial airways have been seen in the lung tissue. Furthermore, we observed no differences in hematological parameters between treated and control animals.

Table 5.2. Treated animals with **7h** and vehicle showed no difference in different blood parameters indicating lack of toxicity by the urea derivative of noscapine.

Parameter	Control	Treated (150 mg/kg body weight)
WBC count (10^3/µl)	3.6 ± 1.5	3.8 ± 1.7
Monocytes (%)	0.5 ± 0.03	0.4 ± 0.03
Eosinophils (%)	0.8 ± 0.02	0.7 ± 0.03
RBC count (10^6/µl)	4.9 ± 0.08	5.2 ± 0.2
Hemoglobin (g/dl)	14.2 ± 2.6	15.8 ± 1.5
Hematocrit (%)	42.4 ± 1.8	45.2 ± 1.8
Mean corpuscular volume (fL)	63.4 ± 1.7	65.5 ± 3.6
Mean corpuscular hemoglobin (pg/cell)	28.2 ± 1.5	27.8 ± 1.4
Mean corpuscular hemoglobin concentration (g/dl)	28.4 ± 1.6	32.1 ± 2.3
Platelet (10^3/µl)	93.5 ± 2.4	99.2 ± 4.6

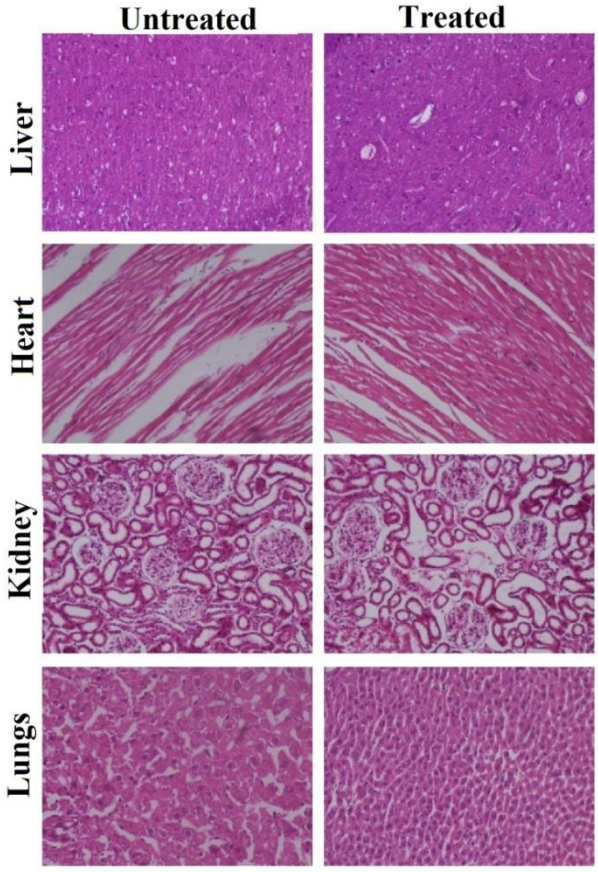

Figure 5.11. Treated animals with **7h** and vehicle fails to reveal any toxicity in vital organs. Panels represent H&E staining of paraffin embedded 5 µ-thick sections of the liver, heart, kidney and lung from **7h**-treated and untreated groups of mice under x200 magnifications.

5.4. Discussion

Urea derivatives have been investigated extensively for their anticancer activities. Many aromatic urea derivatives such as N-aryll-N'-(2-chloroethyl)ureas and benzoylureas show good anticancer activity and were demonstrated to bind tubulin (Mounetou, E et al., 2001). Heterocyclic urea derivatives inhibit receptor tyrosine kinases (RTKs), raf kinases, protein tyrosine kinases (PTKs), and NADH oxidase, which play critical roles in many aspects of tumorigenesis (Li et al., 2009). Thiourea derivatives also revealed diverse anticancer activity against various leukemias and solid tumors (Viswas et al., 2019). Similarly, pyridine-ureas have been reported as potential anticancer agents (El-Naggar et al., 2018). Because of the wide range of pharmacological activity exhibited by the urea scaffold, we envisaged developing a panel of urea-noscapine conjugates in a quest to increase the anticancer activity of noscapine. A library of eight new urea-noscapine conjugates was developed by coupling isocyanates with 9-aminonoscapine (Figure 2). It is always a challenge to synthesize noscapine derivatives due to its sensitive C-C bond. The reaction conditions embraced in this study do not influence the sensitive C-C bond

connecting two heterocyclic phthalide and isoquinoline units (Scheme 1). All the urea-noscapine conjugates were synthesized in good yield and were characterized with NMR, IR and mass spectral data. These molecules were tested *in vitro* for their antiproliferative activity using two human cancer cell lines: MDA-MB-231 (a triple-negative human breast cancer cell line) and MCF-7 (a triple-positive human breast cancer cell line). The wide difference in IC_{50} values obtained using MCF-7 and MDA-MB-231 suggests that these compounds inhibit cellular proliferation of cancer cells and were cell-type dependent. Based on the minimum inhibitory concentration (IC_{50} value), one of the most potent derivatives **7h** having IC_{50} value 4.8 µm and 8.1 µm using MCF-7 and MDA-MB-231 cell lines was selected (Table 1). This potent derivative was further used to investigate more precisely the mechanism of action. Generally, tumour cells propagated to different parts of the body by colonizing. Thus it is useful to investigate the inhibition of colonization ability of tumor cells by the drug molecule. Using colony formation assay, we found that the urea-noscapine conjugate inhibits the colony forming potential of MDA-MB-231 cell (IC_{50} value is 8.1 µM, Figure 3E). It was seen that the inhibition to proliferation of cancer cells was due to the arrest of cell cycle progression at G2/M phase (Figure 5B). This is corroborated from the previous study that many of the noscapine derivatives developed inhibited the cell proliferation by interfering cell cycle progression at G2/M phase (Anderson et al., 2005; Sajadian et al., 2015; Shen et al., 2015; Nagireddy et al., 2021; Devine et al., 2018; Rahmanian-Devin et al., 2021). By arresting the cell cycle the noscapine and its derivatives induced apoptosis to cancer cells (Ye et al., 1998). Therefore, we investigated the induction of cell death by considering the most potent urea derivative of noscapine (**7h**) using three fluorescent dyes, AO, EtBr and Hoechst that discriminate between the live and dead cells. The fluorescent imaging using these dyes demonstrated the induction of cell death more effectively by **7h** (Figure 4B). Also, the proportions of apoptotic cells were quantified using FACS analysis. Biochemically the apoptotic process is characterized by alterations of the lipid composition of cell membrane—phosphatidylserine which is normally on the inner leaflet of the cell membrane, translocates to the outer leaflet and is detected by annexin V binding. In contrast, a cell-impermeant DNA-binding fluorescent dye, propidium iodide can only enter the cells when it is at the stage of late apoptosis when membrane permeability is compromised. The percentage of early apoptotic and late apoptotic cells using MDA-MB-231 cell line with the treatment of IC_{50} concentration of **7h** is 14% and 70% which are much higher compared to untreated cells (Figure 4A). The induction of apoptosis was further confirmed by the appearance of an increased number of TUNEL positive cells with the treatment of **7h** compared to untreated cells (Figure 5A). To illustrate the mechanism of induction of

apoptosis we measured the level of production of reactive oxygen species (ROS) in the cancer cell treated with **7h**. It is well established that elevated levels of ROS disrupt the microtubule network leading to loss of integrity of the mitochondrial membrane and cell death (Nambiar et al., 2020; Tomar et al., 2017). Therefore, we examined the level of production of ROS with the treatment of **7h** using DCFDA as the probe. It was found that the treated cells produced a significantly high amount of ROS compared to untreated cells (Figure 4C) that contributed to the disorganization of cellular microtubules and loss of mitochondrial transmembrane potential (Figure 5C) as a possible mechanism of induction of apoptosis. From a therapeutic point of view, since cancer cells have high levels of ROS compared to normal cells, elevating the ROS level could preferentially kill the cancer cells (Pelicano et al., 2004). Furthermore, the urea derivative of noscapine **7h** significantly inhibits human breast tumour implanted in nude mice as xenografts of MCF-7 cells. Although the founding compound, noscapine, is already in clinical trials, urea derivative of noscapine represents an additional edge over noscapine because of its higher potency, without compromising the nontoxic profile of noscapine.

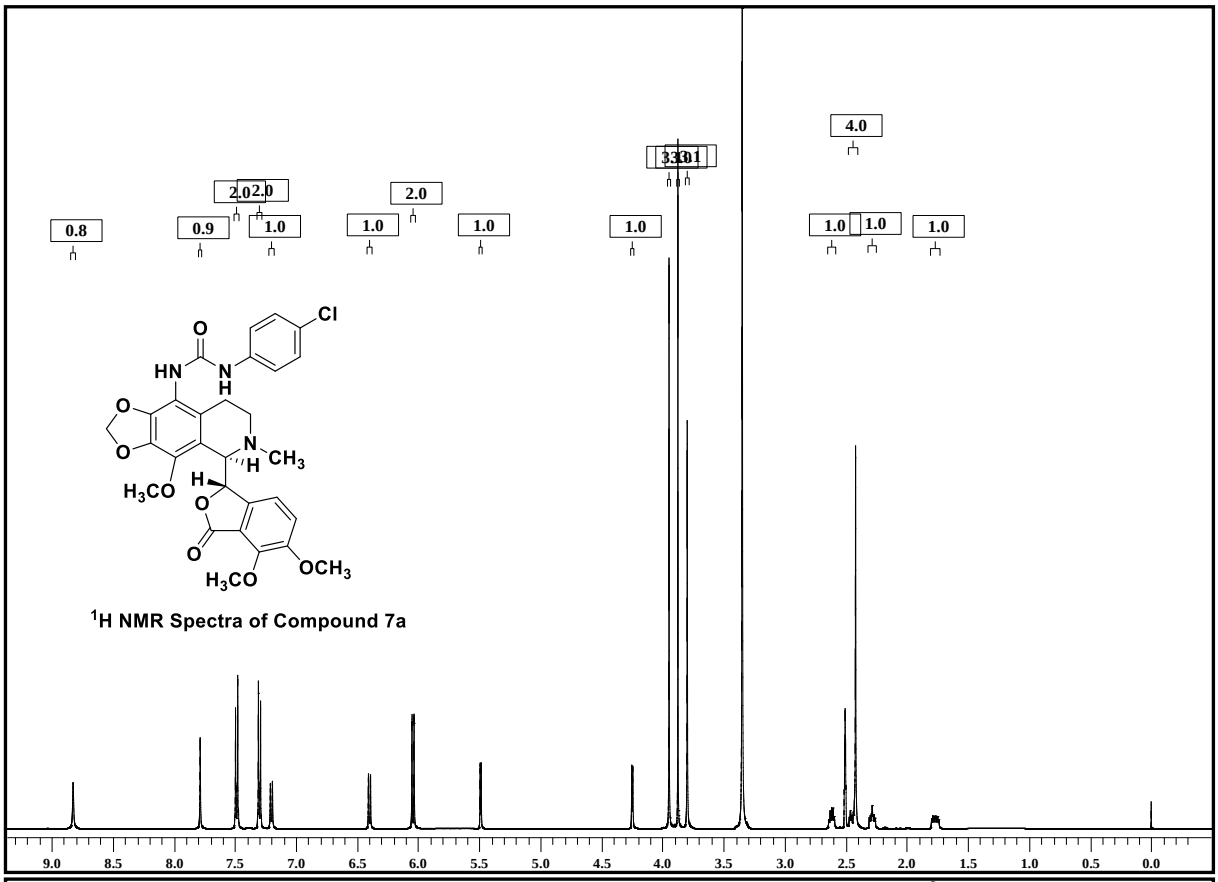

^{1}H NMR Spectra of Compound 7a

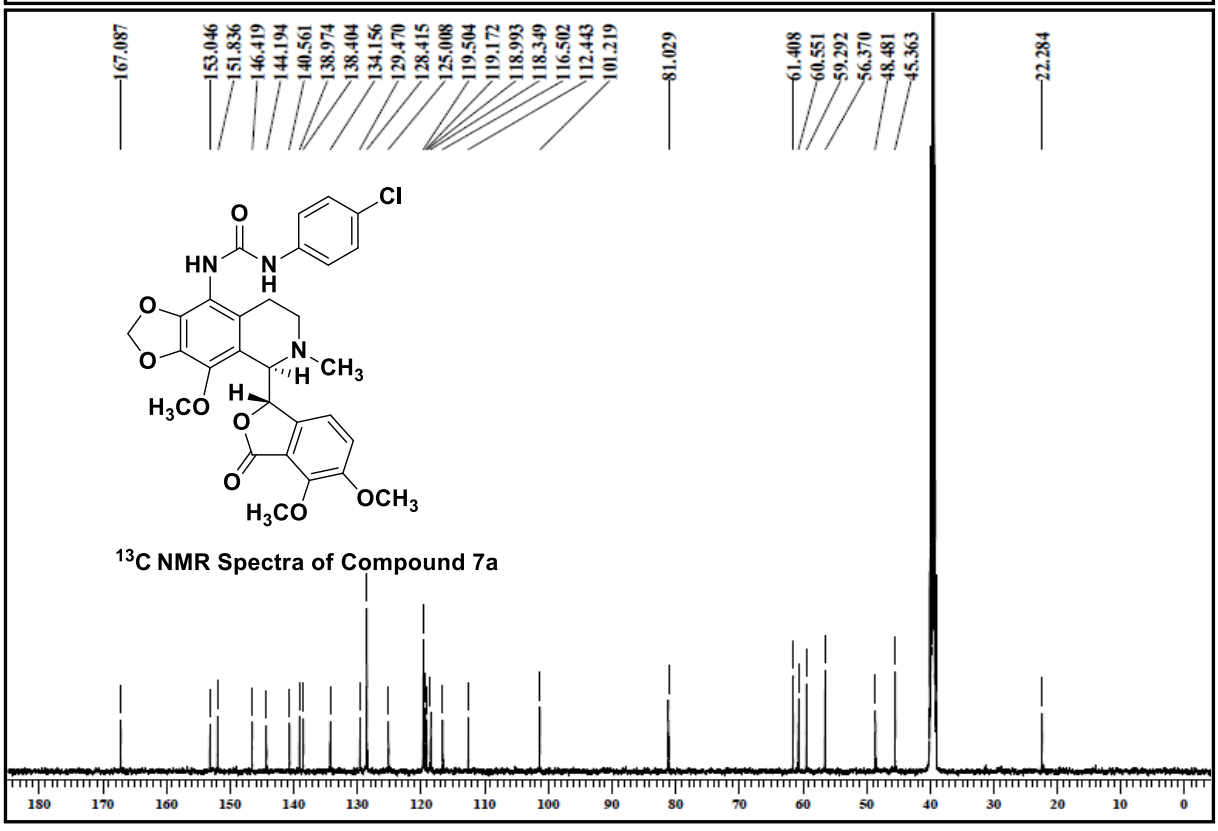

^{13}C NMR Spectra of Compound 7a

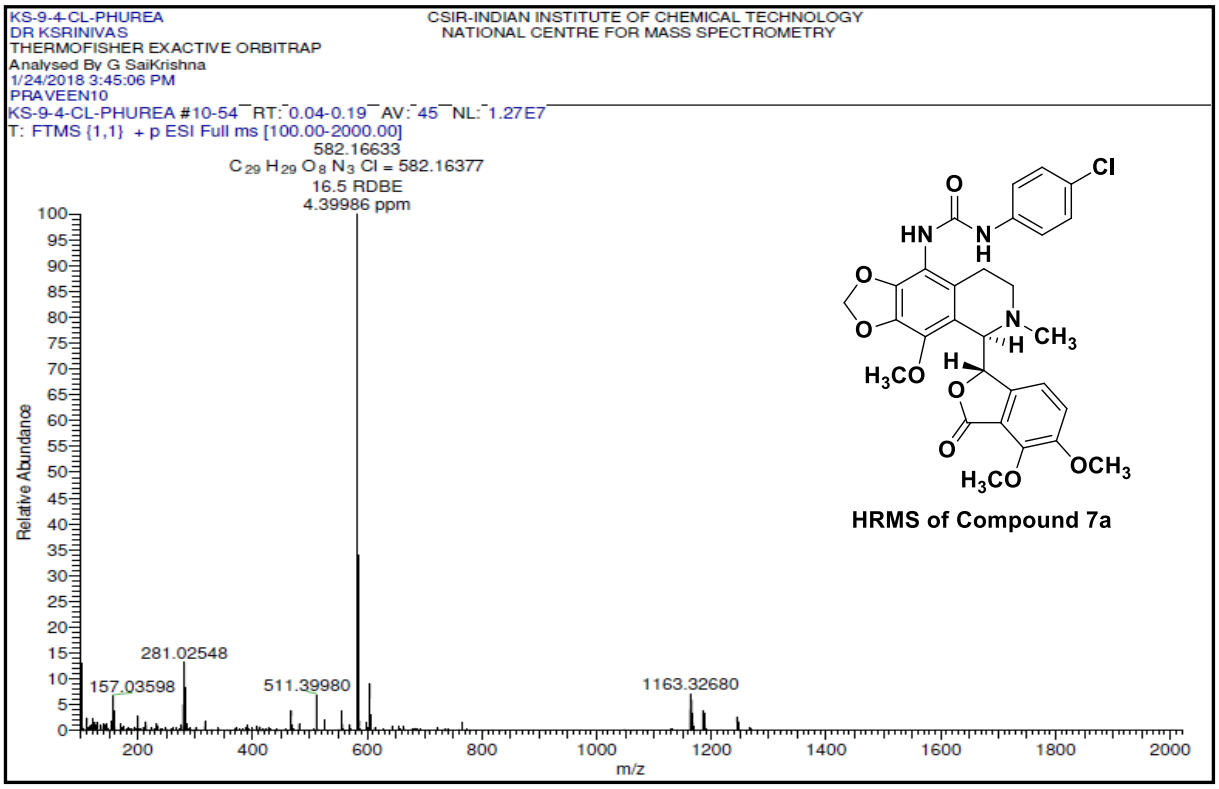
KS-9-4-CL-PHUREA
DR KSRINIVAS
THERMOFISHER EXACTIVE ORBITRAP
Analysed By G SaiKrishna
1/24/2018 3:45:06 PM
PRAVEEN10
CSIR-INDIAN INSTITUTE OF CHEMICAL TECHNOLOGY
NATIONAL CENTRE FOR MASS SPECTROMETRY
KS-9-4-CL-PHUREA #10-54 RT: 0.04-0.19 AV: 45 NL: 1.27E7
T: FTMS {1,1} + p ESI Full ms [100.00-2000.00]
582.16633
C29 H29 O8 N3 Cl = 582.16377
16.5 RDBE
4.39986 ppm
Relative Abundance
m/z
281.02548
157.03598
511.39980
1163.32680
HRMS of Compound 7a

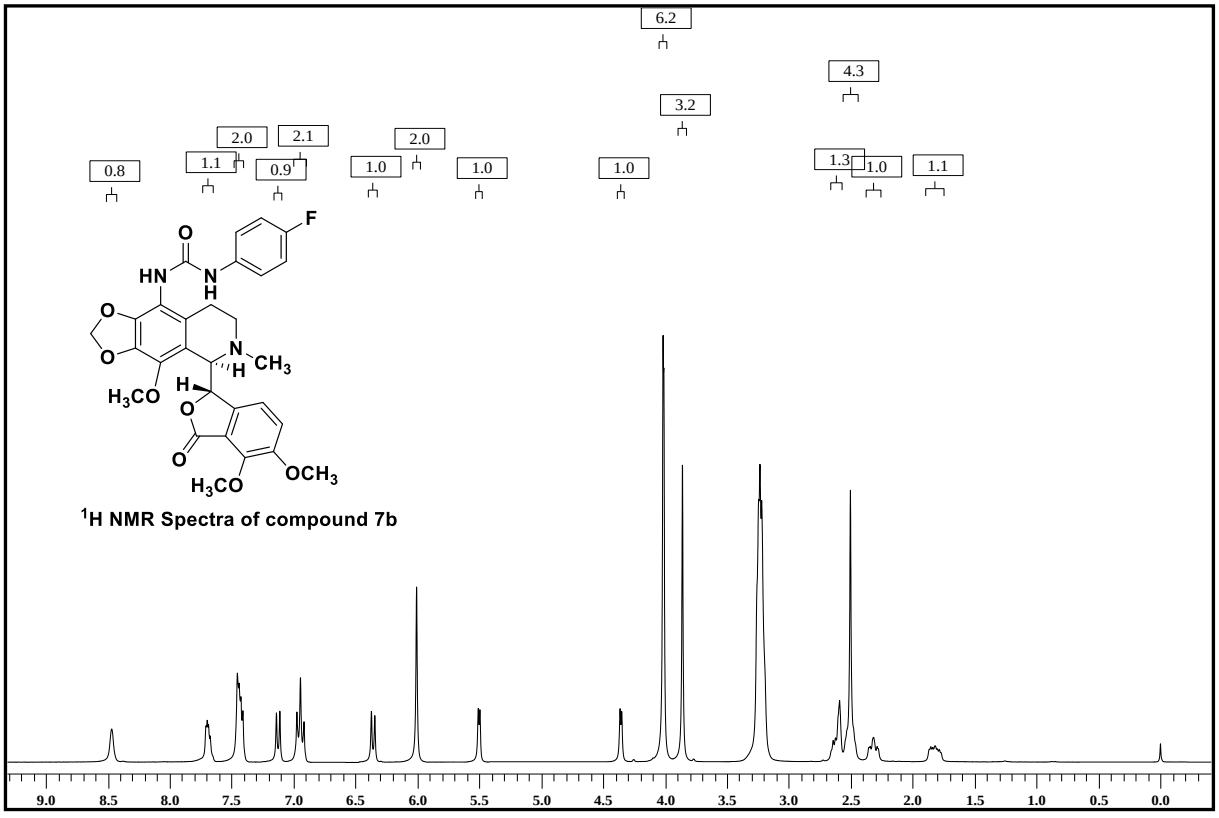
6.2
4.3
3.2
2.0
2.1
2.0
0.8
1.1
0.9
1.0
1.0
1.0
1.3
1.0
1.1
F
1H NMR Spectra of compound 7b

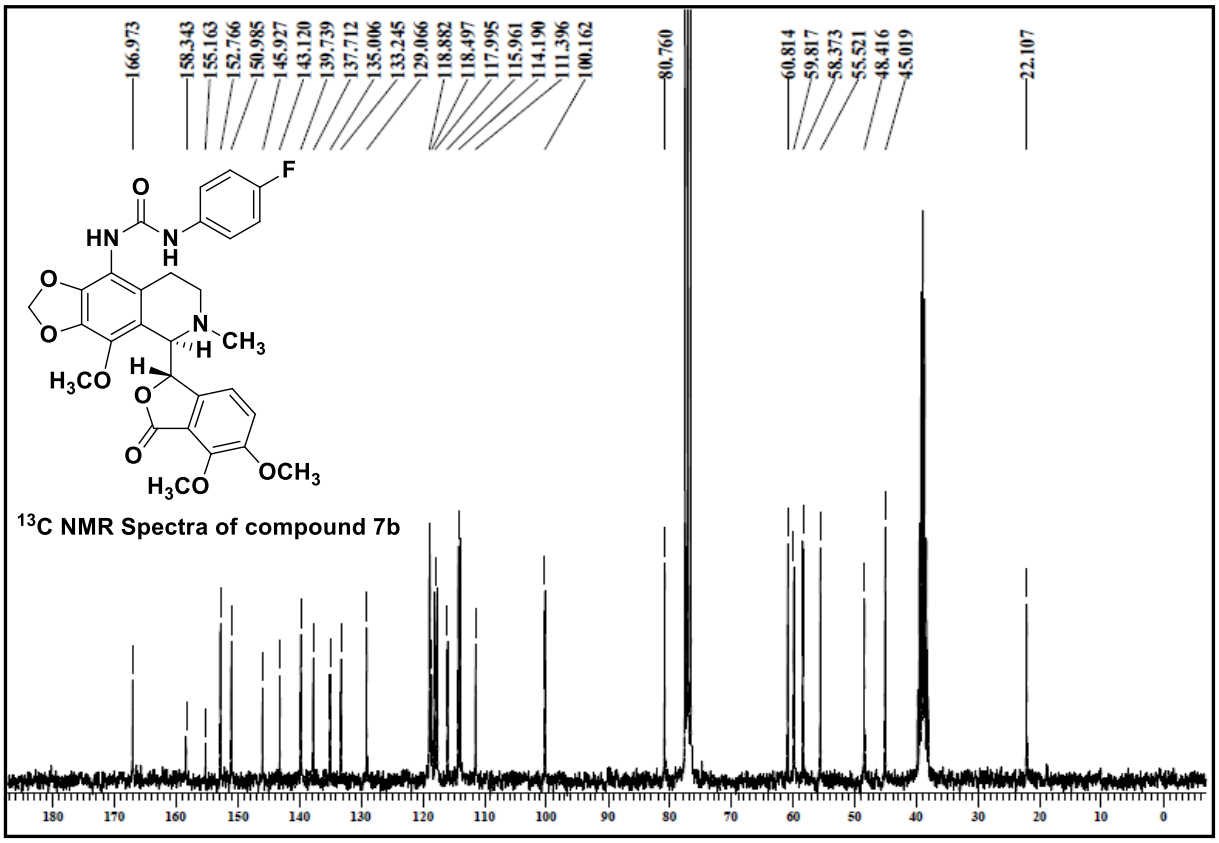

^{13}C NMR Spectra of compound 7b

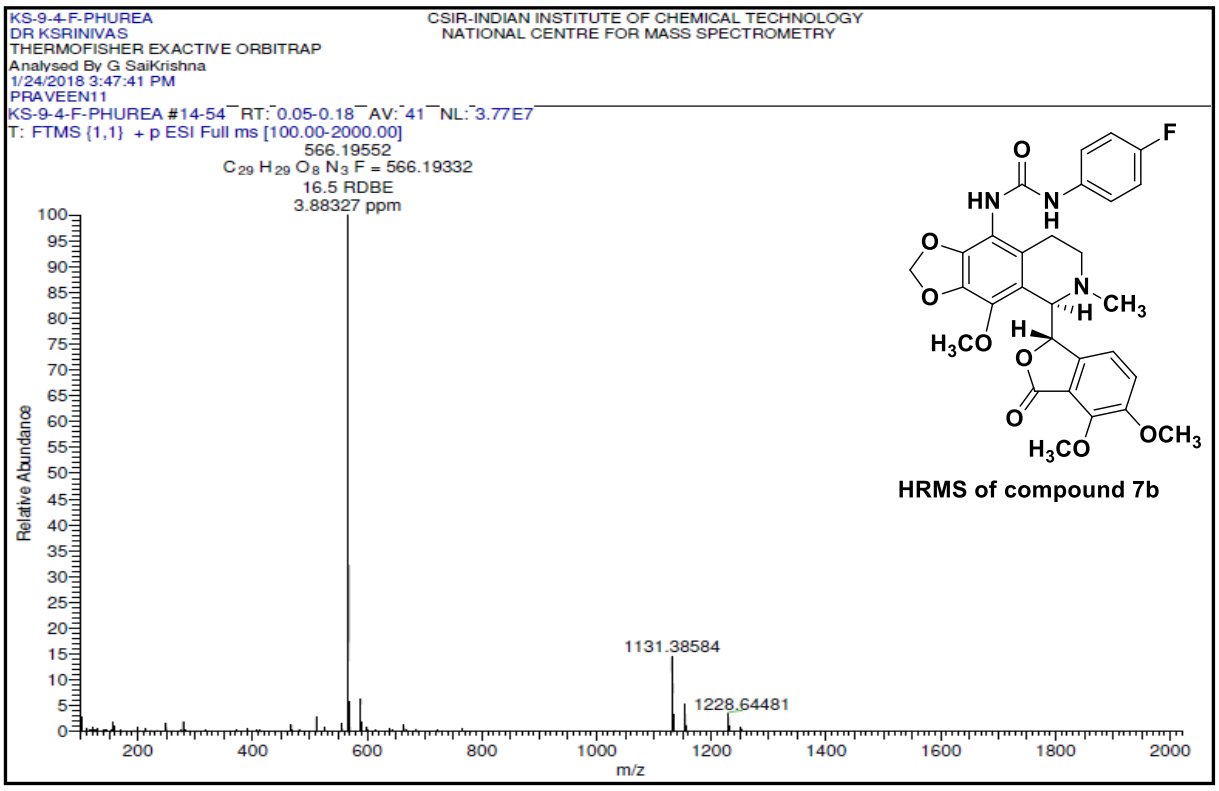

HRMS of compound 7b

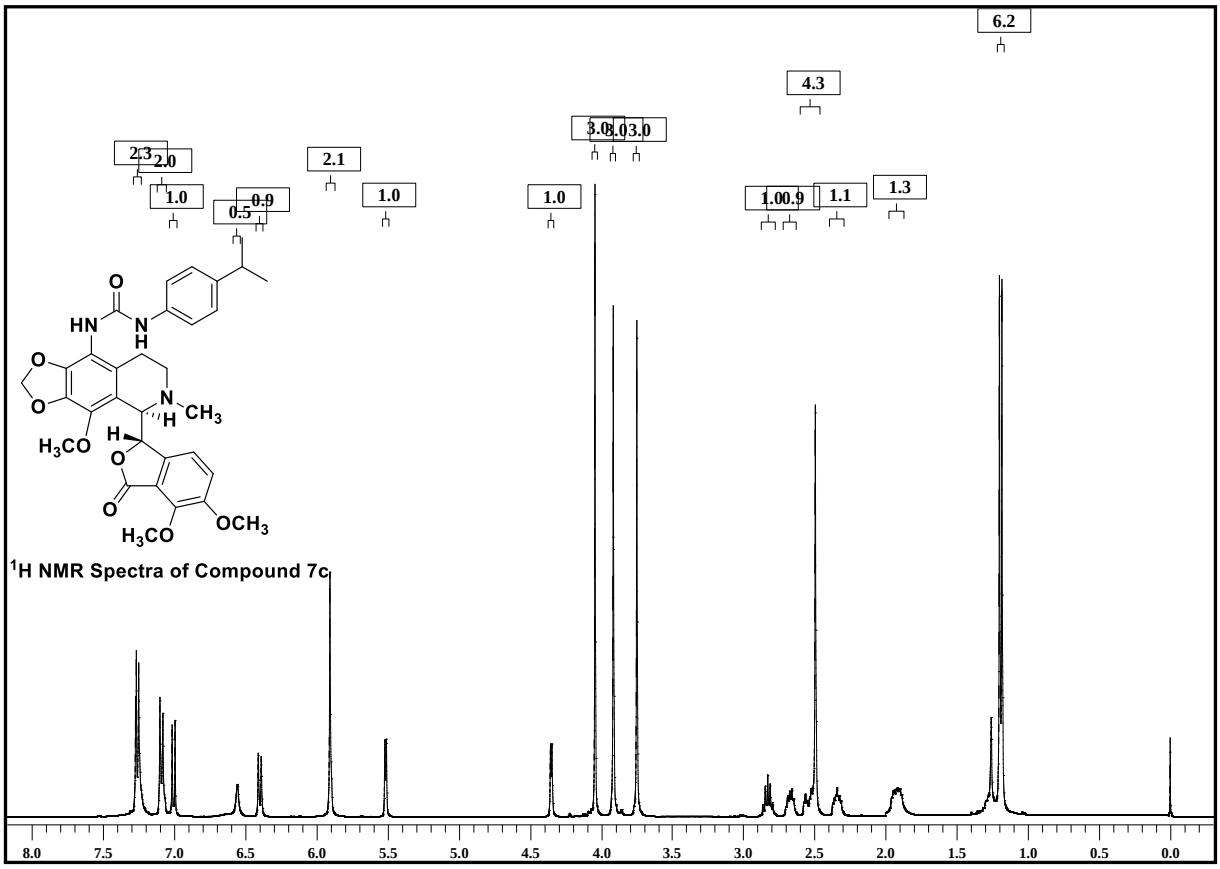

^{1}H NMR Spectra of Compound 7c

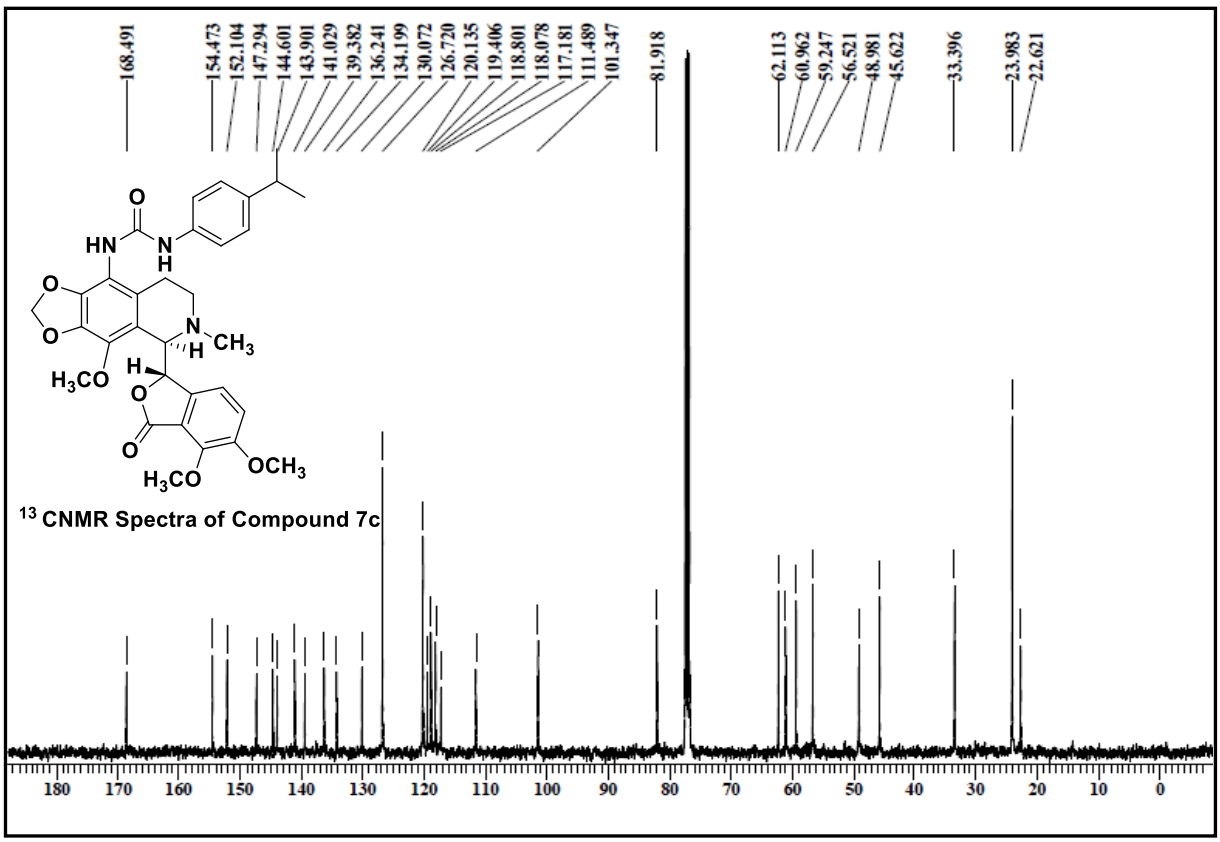

^{13} CNMR Spectra of Compound 7c

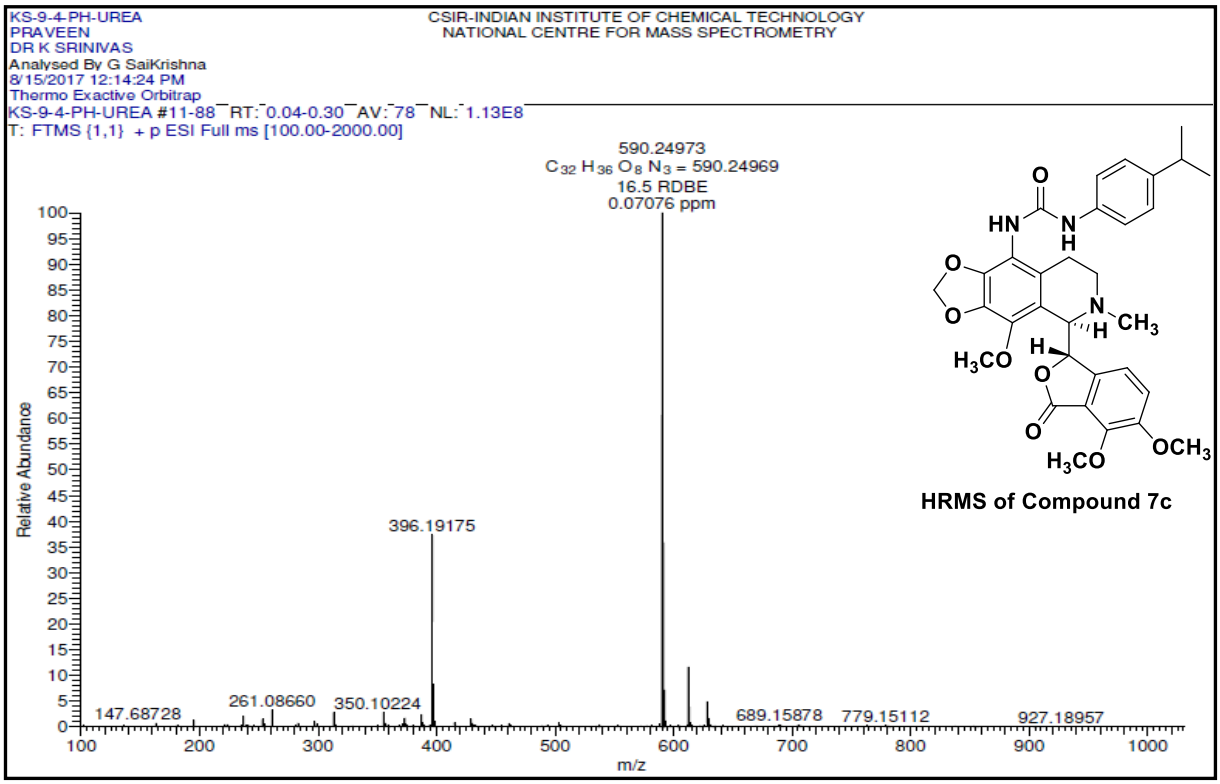

HRMS of Compound 7c

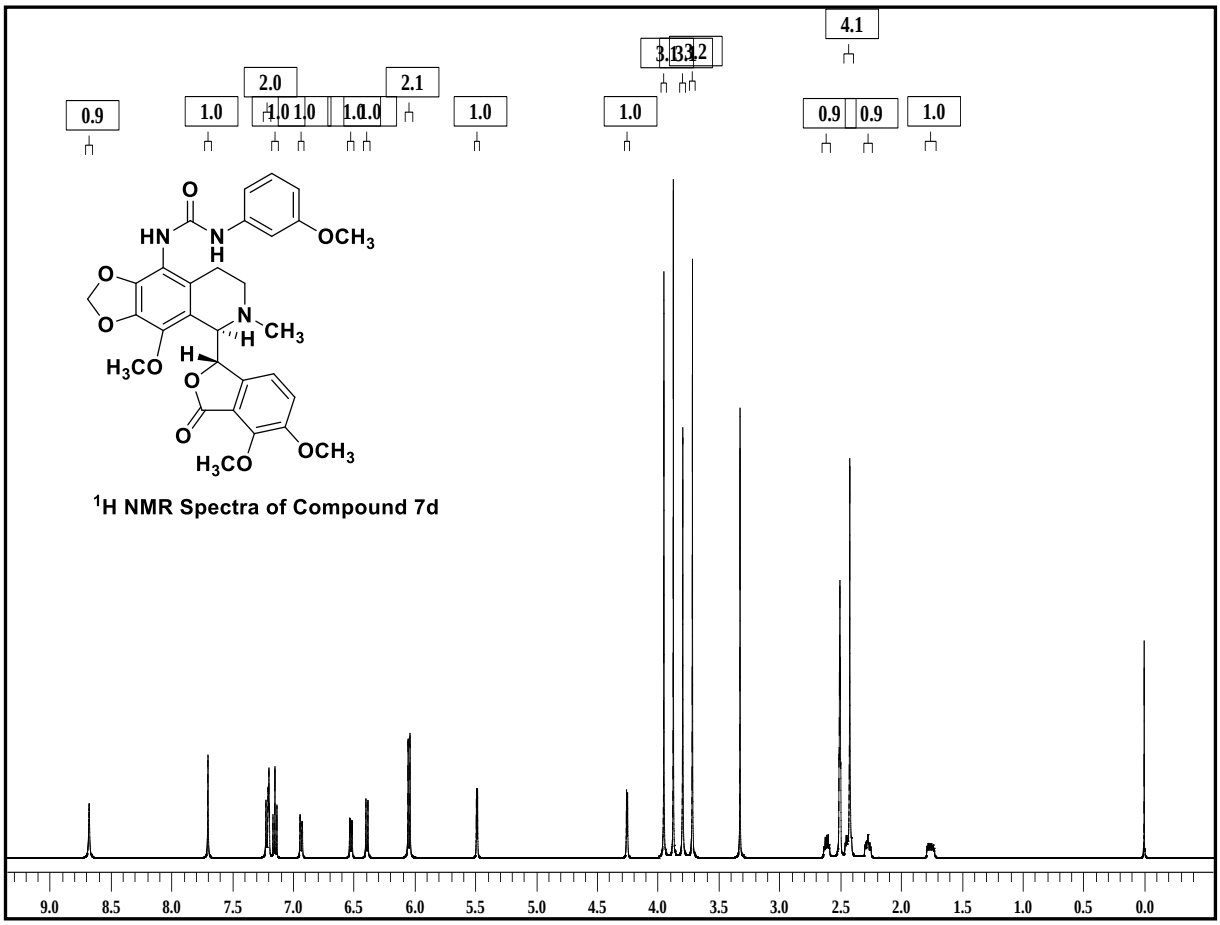

^{1}H NMR Spectra of Compound 7d

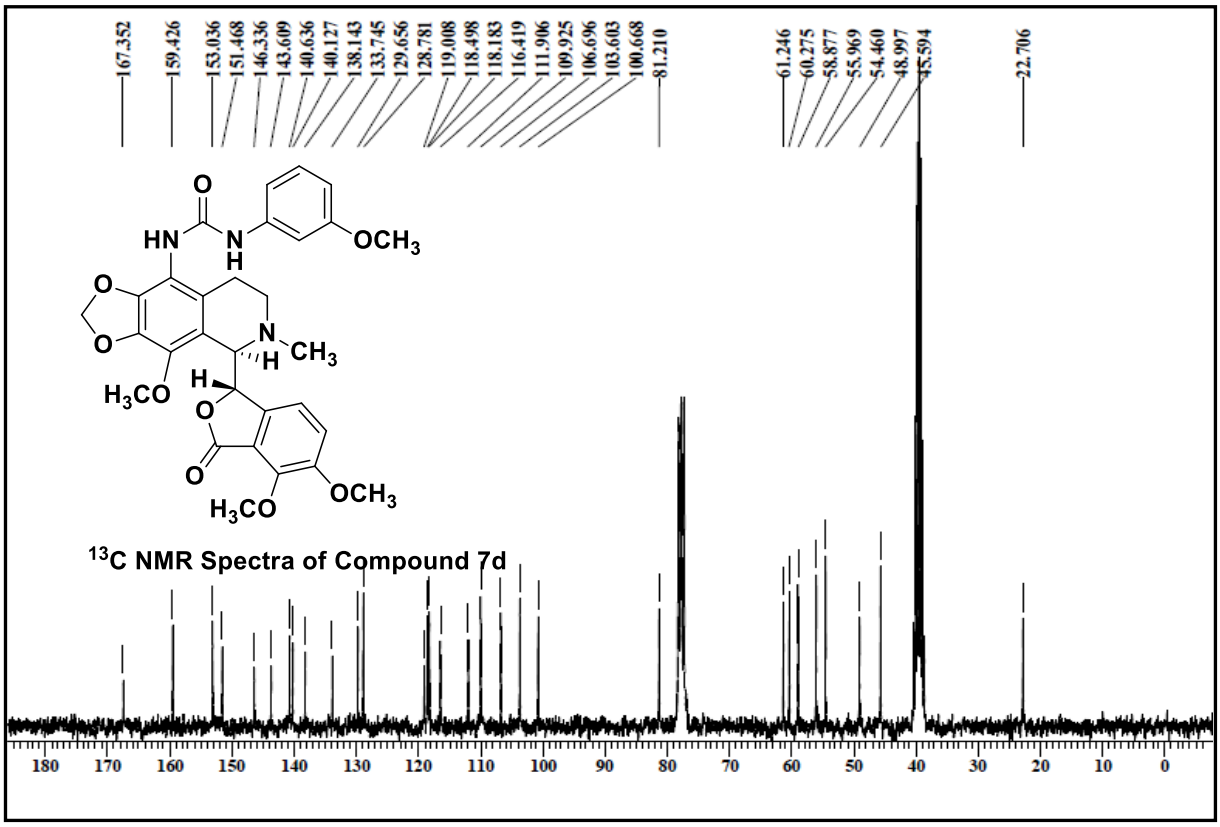

^{13}C NMR Spectra of Compound 7d

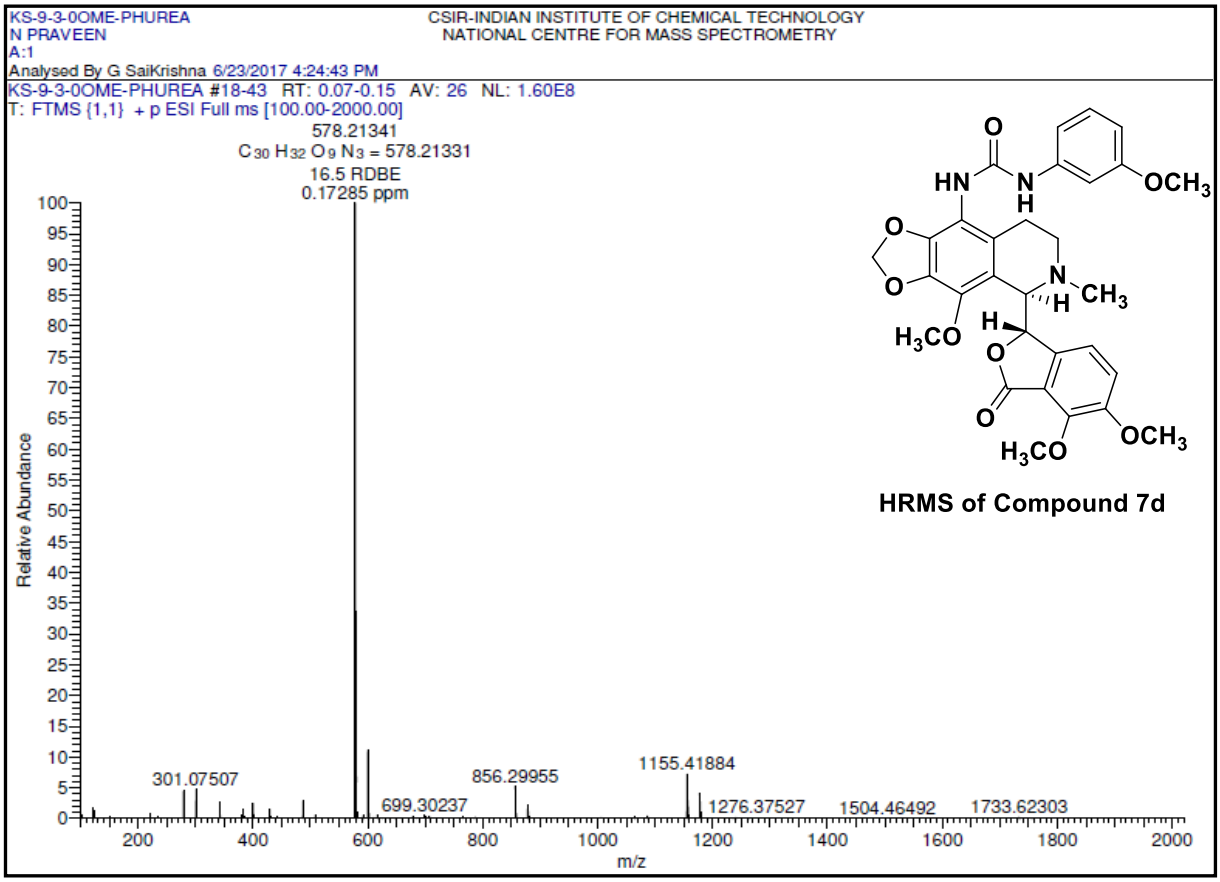

HRMS of Compound 7d

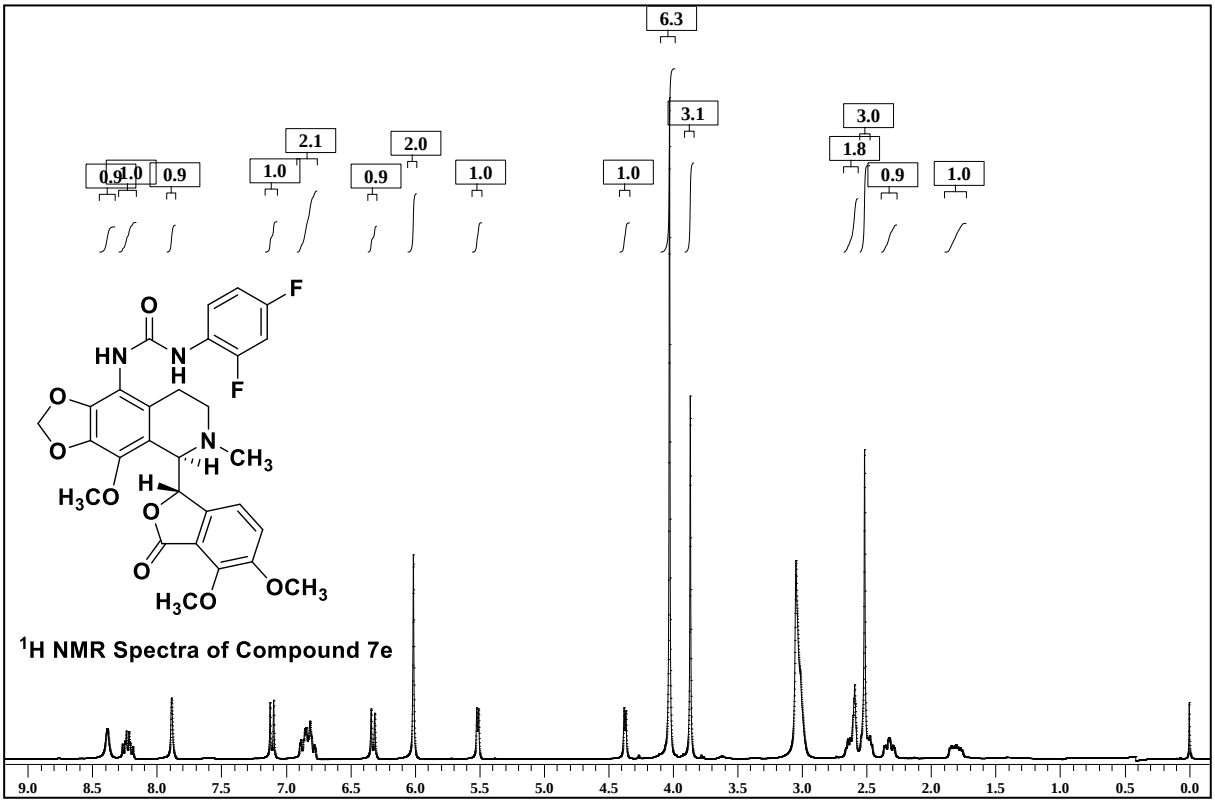

^{1}H NMR Spectra of Compound 7e

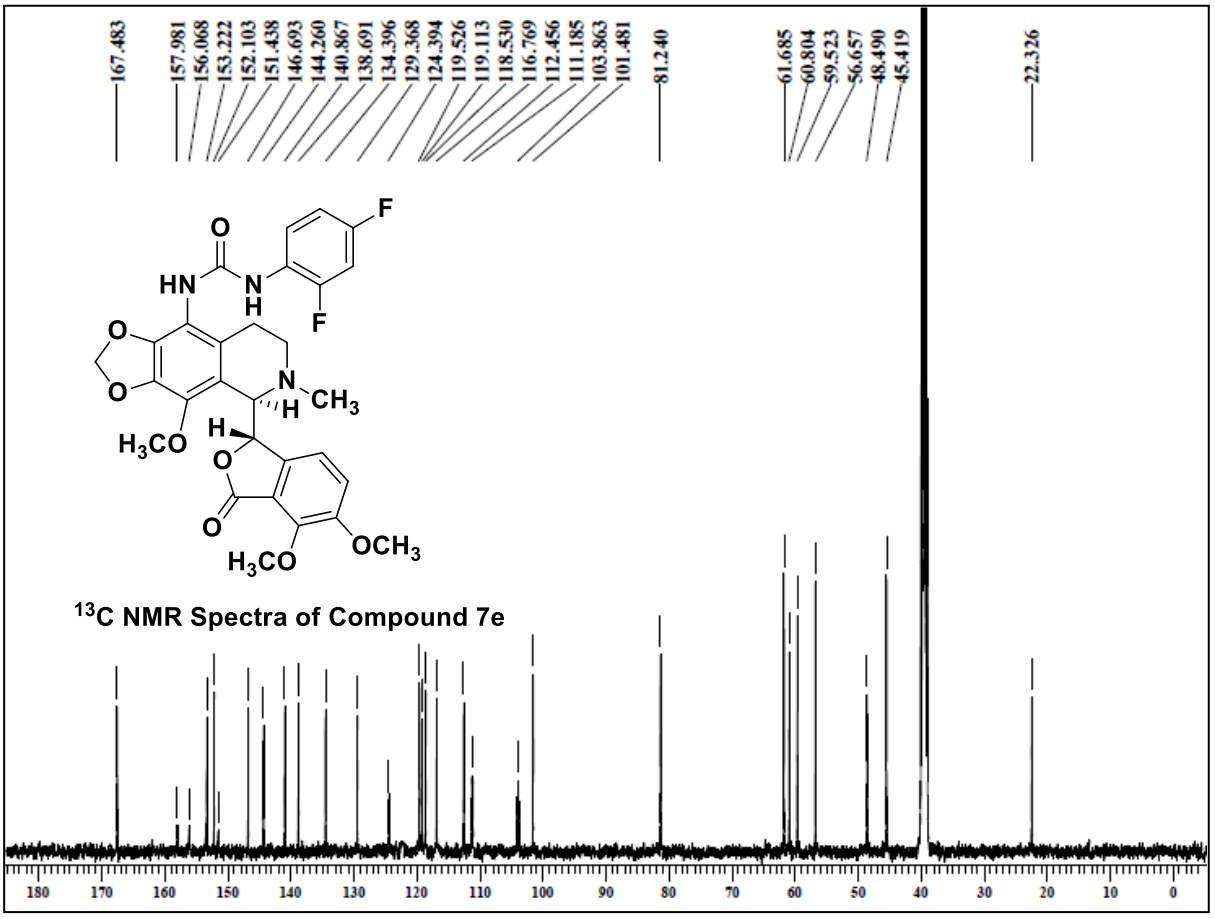

^{13}C NMR Spectra of Compound 7e

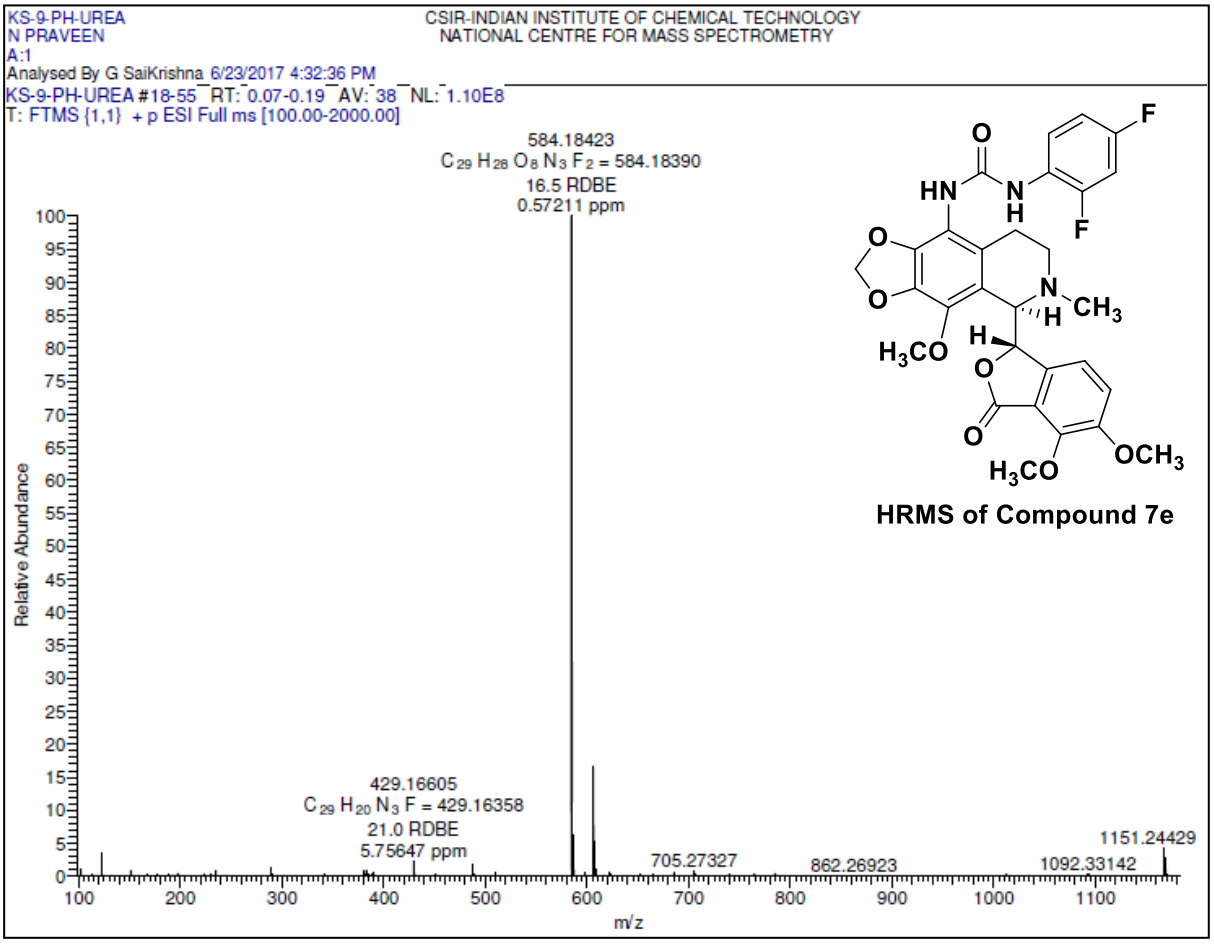

HRMS of Compound 7e

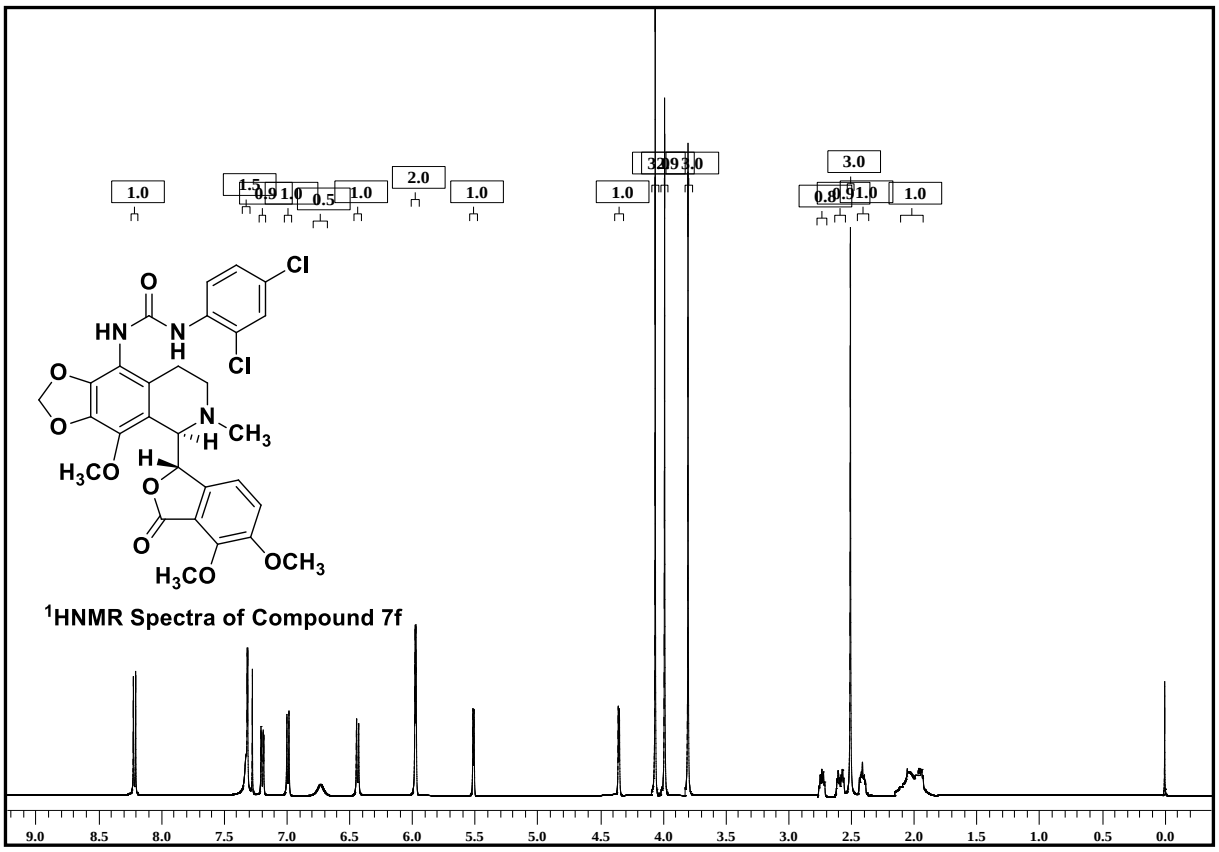

^{1}HNMR Spectra of Compound 7f

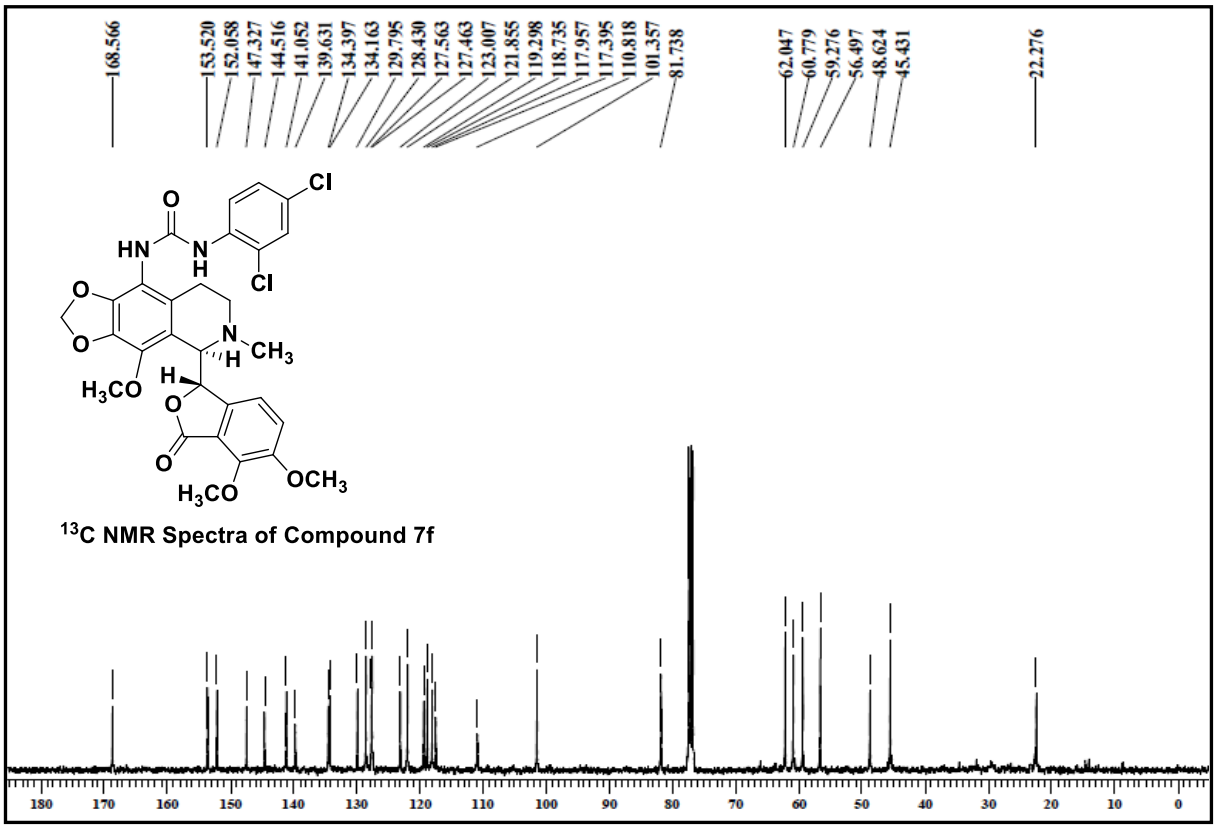

^{13}C NMR Spectra of Compound 7f

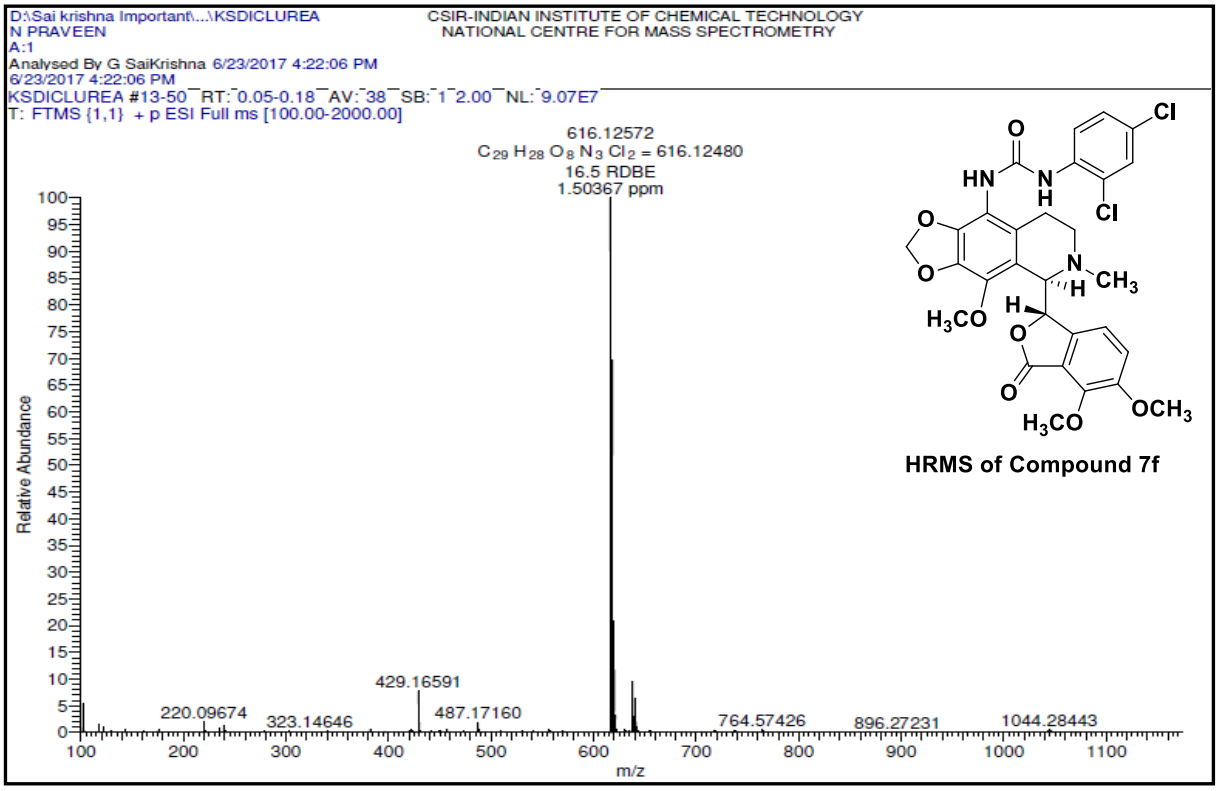

HRMS of Compound 7f

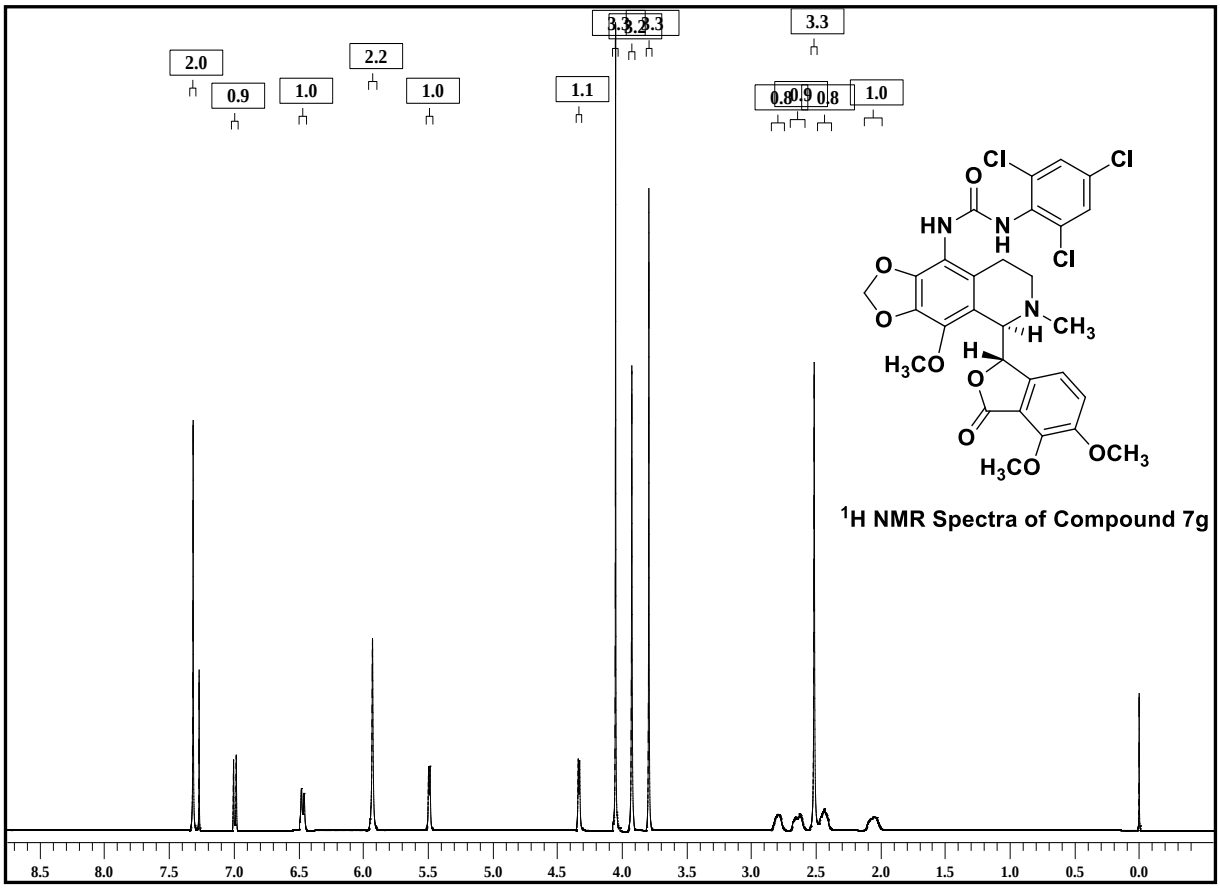

^{1}H NMR Spectra of Compound 7g

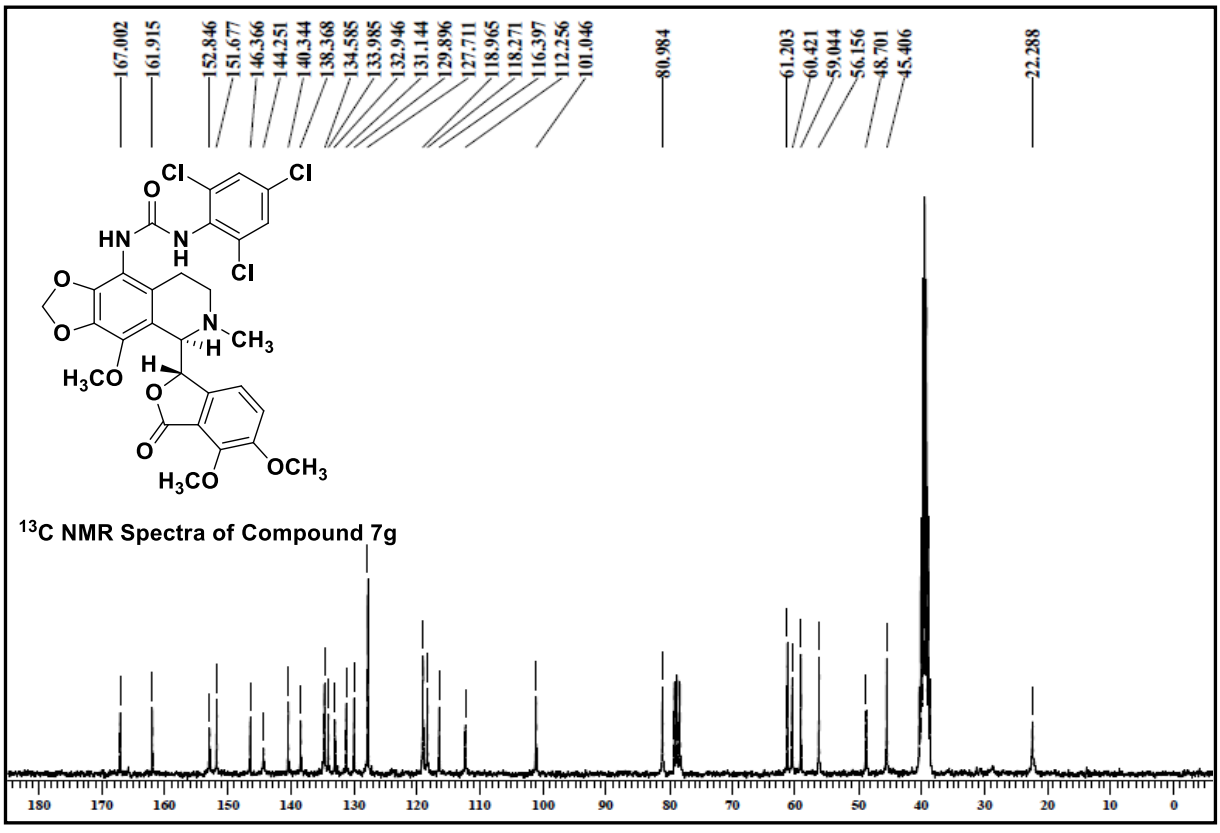

^{13}C NMR Spectra of Compound 7g

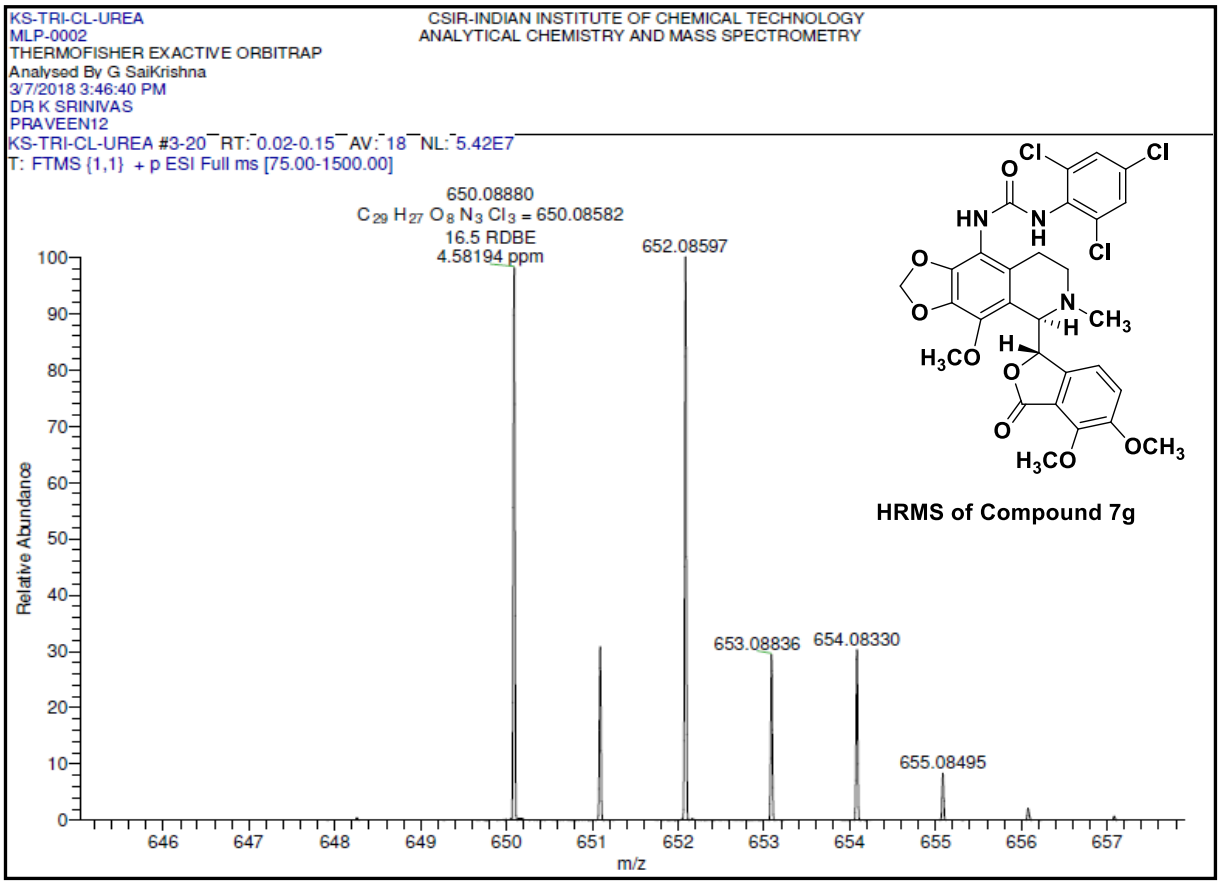
KS-TRI-CL-UREA
MLP-0002
THERMOFISHER EXACTIVE ORBITRAP
Analysed By G SaiKrishna
3/7/2018 3:46:40 PM
DR K SRINIVAS
PRAVEEN12
CSIR-INDIAN INSTITUTE OF CHEMICAL TECHNOLOGY
ANALYTICAL CHEMISTRY AND MASS SPECTROMETRY
KS-TRI-CL-UREA #3-20 RT: 0.02-0.15 AV: 18 NL: 5.42E7
T: FTMS {1,1} + p ESI Full ms [75.00-1500.00]
650.08880
C29 H27 O8 N3 Cl3 = 650.08582
16.5 RDBE
4.58194 ppm
652.08597
653.08836
654.08330
655.08495
Relative Abundance
m/z
HRMS of Compound 7g

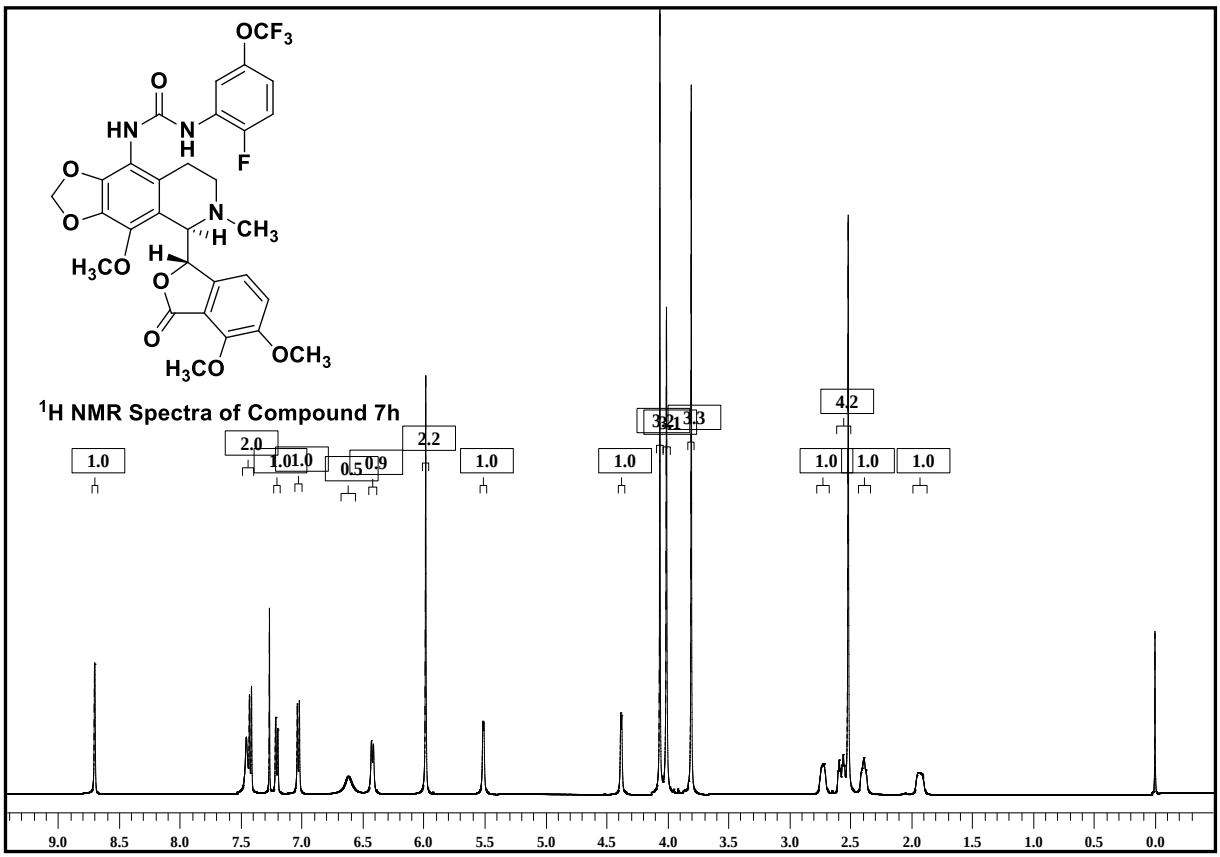
1H NMR Spectra of Compound 7h

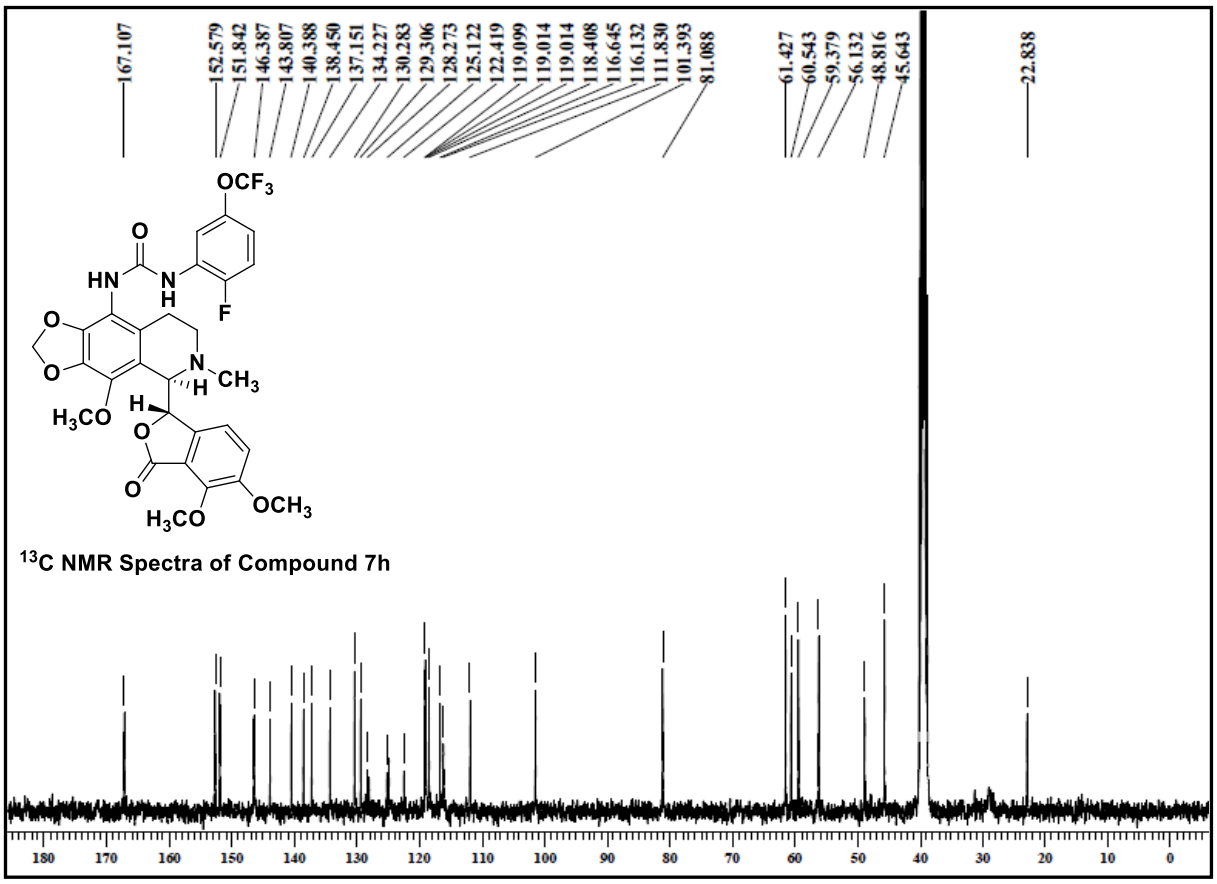

^{13}C NMR Spectra of Compound 7h

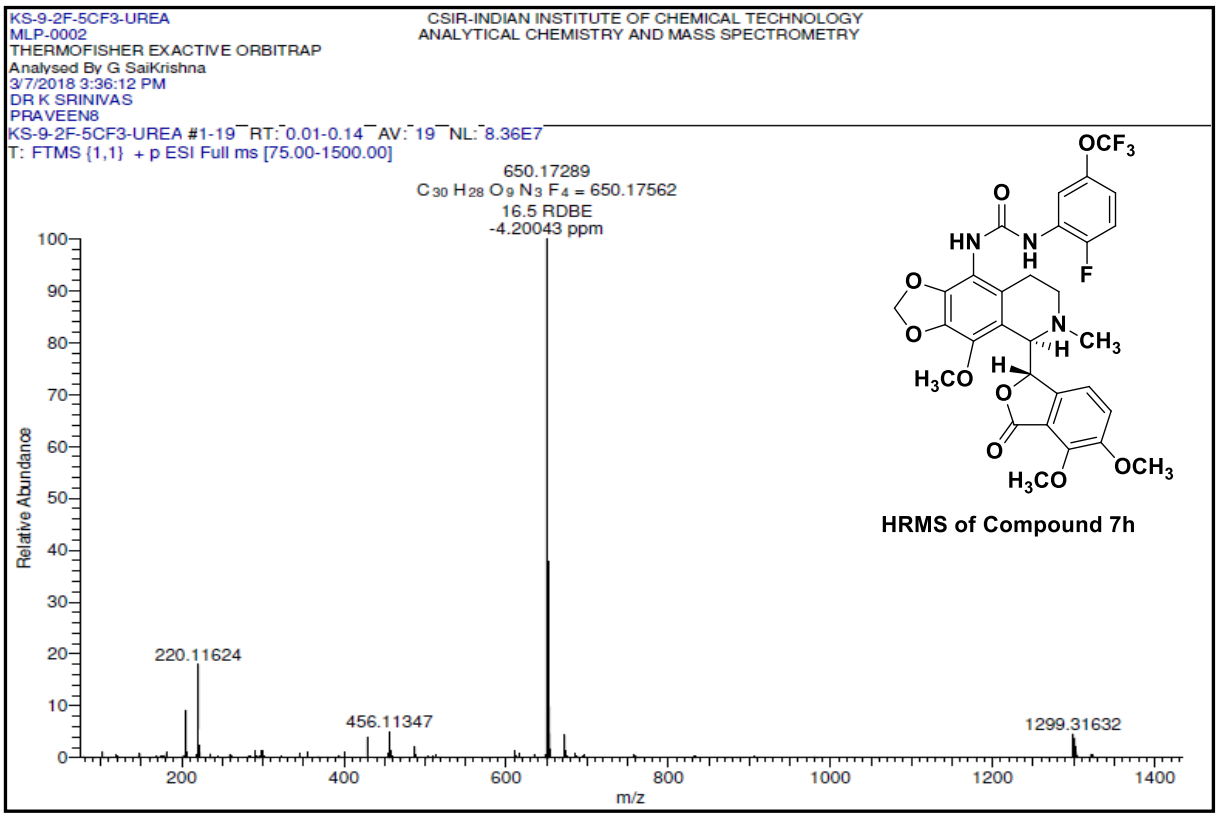

HRMS of Compound 7h

CHAPTER-6

N-imidazopyridine derivatives of noscapine as potent tubulin binding anticancer agents: chemical synthesis and cellular evaluation

Abstract

N-imidazopyridine (Impy) derivatives of noscapine were developed by coupling of imidazo[1,2-*a*]pyridine pharmacophore at the N-atom of the isoquinoline ring of noscapine scaffold and their anticancer activity was evaluated based on a cellular study using two human breast adenocarcinoma, MCF-7 and MDAMB-231, as well as with a panel of primary breast cancer cells isolated from patients. Interestingly, all these derivatives inhibited cellular proliferation in all the cancer cells that ranged between 3.7 to 15.8 μM, which is 11.8 to 2.7 fold lower than that of noscapine. Unlike previously reported derivatives of noscapine that arrest cells in the S-phase, these novel derivatives effectively inhibit proliferation of cancer cells, arrests cell cycle in the G2/M-phase followed by apoptosis and appearance of apoptotic cells. Thus, we conclude that N-imidazopyridine-noscapinoids have great potential to be a novel therapeutic agent for breast cancers.

Key words: Noscapine, N-imidazopyridine-noscapinoids, tubulin binding, anticancer agents, breast cancer,

6.1. Introduction

Microtubules are major cytoskeletal structures responsible for maintaining genetic stability during cell division (Sammak and Borisy, 1987; McIntosh, 1994; Desai and Mitchinson, 1997). The dynamics of these polymers is absolutely crucial for this function that can be described as their growth rate at the plus ends, catastrophic shortening, frequency of transition between the two phases, pause between the two phases, their release from the microtubule organizing center and treadmilling (Margolis and Wilson, 1981; Mitchison and Kirschner, 1984; Kirschner and Mitchison, 1986; Margolis and Wilson, 1998; Jordan and Wilson, 2004). Interference with microtubule dynamics often leads to programmed cell death and thus microtubule-binding drugs are currently used to treat various malignancies in the clinic (Jordan and Wilson, 2004). Although useful, currently used microtubule drugs such as *vincas* and *taxanes* are limited due to their undesirable side effects (Rowinsky, 1997; Pace et al., 1996; Crown and O'Leary, 2000; Theiss and Meller, 2000; Topp et al., 2000). In quest of finding a novel natural compound that is devoid of any side effects, noscapine (an opium alkaloid which is in the clinic as a safe antitussive agent) was discovered that binds tubulin, arrests dividing cells in mitosis and induces apoptosis (Ye et al., 1998). It is well-tolerated in humans and is non-toxic in healthy volunteers including pregnant mothers (Dahlstrom et al., 1982; Karlsson et al., 1990; Jensen et al., 1992). Unlike the other microtubule-targeting drugs, noscapine does not significantly change the microtubule polymer mass even at high concentrations. Instead, it suppresses microtubule dynamics by increasing the time that microtubules spend in an attenuated (pause) state when neither microtubule growth nor shortening is detectable (Landen et al., 2002). Thus noscapine-induced suppression of microtubule dynamics, even though subtle, is sufficient to interfere with the proper attachment of chromosomes to kinetochore microtubules and to suppress the tension across paired kinetochores (Zhou et al., 2002a). This represents an improvement over the *taxanes*, the microtubule-bundling agents or overpolymerizers, and *vincas*, the depolymerizers, that cause toxicities in mitotic and post mitotic neurons at elevated doses. Noscapine thus effectively inhibits the progression of various cancer types both in cultured cells and in animal models with no obvious side effects (Ye et al., 1998; Landen et al., 2002; Zhou et al., 2002b; 2003; Landen et al., 2004). Surprisingly, the apoptosis is much more pronounced in cancer cells compared with normal healthy cells (Landen et al., 2002).

In this study, we approach to develop N-imidazopyridine (impy) derivatives of noscapine and validated their anticancer activity based on a cellular study using two human breast cancer cell lines, MCF-7, MDAMB-231 and primary breast cancer cells from patients.

These derivatives were found to inhibit cancer cell proliferation and cause selective G2/M arrest in cancer cells. The mitotic catastrophe in cancer cells is then followed by the induction of apoptosis.

6.2. Materials and methods

6.2.1. Cell culture and reagents

The natural lead molecule, noscapine was procured from Sigma. All the chemical reagents including media used for cell culture were obtained from Sigma and Invitrogen. MCF-7 and MDAMB-231 human breast cancer cell lines were acquired from the National Center for Cell Science in Pune, Maharashtra, India. The cells were grown in Dulbecco's modified Eagle medium (DMEM, Pan Biotech) supplemented with 10% foetal bovine serum (FBS) and antibiotics at 37 °C in a 5% CO_2 and 95 percent humidity environment. Cells having a confluence of 70-80 percent were subcultured for bioassays with trypsin-EDTA (0.25 percent). A panel of four N-imidazopyridine-noscapinoids were chemically synthesized and dissolved in DMSO to make a working concentration for treatment.

6.2.2. Chemical synthesis of Impy derivatives of noscapine 3-6

The required building block, nornoscapine **2**, was synthesized from natural noscapine **1** using modified nonpolonovski reaction conditions (Figurrre 1). Natural noscapine was treated with *m*-CPBA to give noscapine-*N*-oxide. This *N*-oxide was then treated with 2N HCl to give noscapine-*N*-oxide HCl salt which, upon further reaction with FeSO4.7H2O afforded nornoscapine **2** in 48% overall yield. The reaction of nornoscapine **2** with various substituted 2-(chloromethyl)imidazo[1,2-*a*] pyridines, in presence of K_2CO_3 and KI in acetone at room temperature, for 6 h, afforded *N*-imidazopyridine noscapine congeners **3-6** in 55-72% yields (Scheme 1). To illustrate, the reaction of nornoscapine **2** with 2-(chloromethyl)-7-methylimidazo [1,2-*a*]pyridine **6** and K_2CO_3, KI, in acetone for 6 h at rt, afforded (*S*)-6,7-dimethoxy-3-((*R*)-4-methoxy-6-((7-methylimidazo[1,2-*a*]pyridin-2-yl)methyl)-5,6,7,8-tetrahydro-[1,3]dioxolo[4,5-*g*] isoquinolin 5-yl)isobenzofuran-1(3*H*)-one **6** in 58% yield as crystalline solid (m.p: 92-94 ^oC). Compound **6** was characterized from ^{1}H-NMR spectrum by the appearance of aromatic protons at δ 7.98 (1H) as doublet (J = 6.9 Hz), δ 7.56 (1H), δ 7.25 (1H) as singlet, δ 6.95 (1H) as doublet (J = 8.3 Hz), δ 6.56 (1H) as doublet of doublet (J = 1.4, 6.9 Hz), δ 6.32 (1H) as singlet, and δ 6.14 (1H) as doublet (J = 8.3 Hz). The methylenedioxy protons appeared at δ 5.94 (2H) as doublet (J = 1.3, 4.8 Hz). The chiral protons appeared at δ 5.70 (1H) as doublet (J = 4.1 Hz), and δ 4.69 (1H) as doublet (J = 4.1 Hz) respectively; the *N*methylene protons appeared at δ 4.16 (1H) as doublet (J = 14.3 Hz), and δ 3.90 (1H) as doublet (J = 14.3 Hz) and the three methoxy protons appeared at δ 4.09

(3H), δ 4.02 (3H), and δ 3.85 (3H) as corresponding singlets. The isoquinoline protons appeared at δ 2.54-2.45 (3H), and δ 1.99-1.89 (1H), as multiplet peaks. The aromatic methyl protons on the imidazopyridine core appeared at δ 2.36 (3H) as a singlet. The product was further characterized from ^{13}C-NMR spectrum by the appearance of characteristic aromatic methyl carbon at δ 21.2. In HR-MS (ESI) spectrum, the peak observed at *m/z* 544.20944 for $C_{30}H_{30}N_3O_7$ [M+H]+ confirmed the structure **6** as (*S*)-6,7-dimethoxy-3-((*R*)-4-methoxy-6-((7-methylimidazo [1,2-*a*]pyridin-2-yl)methyl)-5,6,7,8-tetrahydro-[1,3]dioxolo[4,5-*g*]isoquinolin-5-yl)isobenzofuran-1(3*H*)-one. Similarly, the data for all the derivatives were recorded using NMR (^{1}H &^{13}C), IR spectroscopy and mass (HRMS) spectrometry techniques.

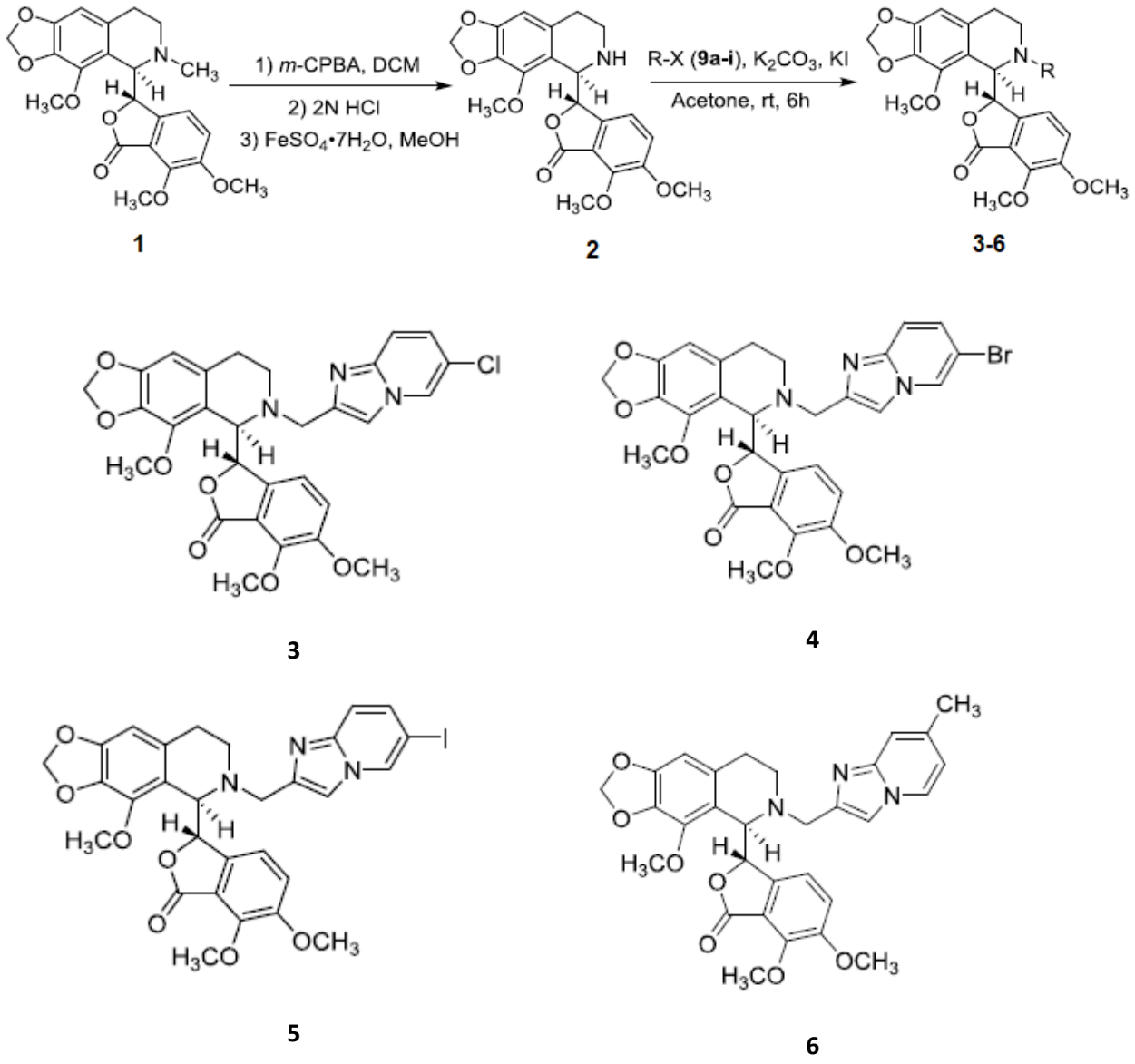

Figure 6.1. Reaction scheme for the synthesis of Impy derivatives of noscapine 3-6.

6.2.3. Structural characterization of Impy derivatives of noscapine 3-6

(*S*)-3-((*R*)-6-((6-chloroimidazo[1,2-*a*]pyridin-2-yl)methyl)-4-methoxy-5,6,7,8-tetrahydro-[1,3]dioxolo[4,5-*g*]isoquinolin-5-yl)-6,7-dimethoxyisobenzofuran-1(3*H*)-one (3):

Nature : White solid. mp : 96-98 °C. IR (KBr) : 3390, 2938, 1755, 1621, 1493, 1268, 1214, 1039, 934, 761, 663, 429 cm^{-1}. ^{1}H NMR (400 MHz, $CDCl_3$) : δ 8.18 (dd, *J* = 0.8, 2.0 Hz, 1H, Ar-H), 7.66 (s, 1H, Ar-H), 7.43 (dt, *J* = 0.8, 9.5 Hz, 1H, Ar-H), 7.06 (dd, *J* = 2.0, 9.5 Hz, 1H, Ar-H), 6.95 (d, *J* = 8.3 Hz, 1H, Ar-H), 6.32 (s, 1H, Ar-H), 6.08 (dd, *J* = 0.4, 8.3 Hz, 1H, Ar-H), 5.94 (dd, *J* = 1.4, 5.9 Hz, 2H, O-CH_2-O), 5.72 (dd, *J* = 0.4, 4.1 Hz, 1H, Ar-CH (C_3-pthalide)), 4.67 (d, *J* = 4.1 Hz, 1H, Ar-CH ($C_{5'}$-isoquinoline)), 4.19 (d, *J* = 14.3 Hz, 1H, -C*H*H-N-CH_2), 4.10 (s, 3H, -OCH_3), 4.04 (s, 3H, -OCH_3), 3.90 (d, *J*= 14.30 Hz, 1H, -CH*H*-*N*-CH_2), 3.86 (s, 3H, -OCH_3), 2.53-2.42 (m, 3H, -C*H*$_2$-*N*-CH_2 ($C_{7'}$-isoquinoline), Ar-C*H*H ($C_{8'}$-isoquinoline)), 1.96-1.86 (m, 1H, Ar-CH*H* ($C_{8'}$-isoquinoline)). ^{13}C NMR (100 MHz, $CDCl_3$) : δ 168.1, 152.2, 148.4, 147.6, 142.8, 140.8, 140.4, 133.9, 131.8, 125.1, 123.6, 119.9, 119.9, 118.0, 117.9, 117.1, 116.4, 111.8, 102.4, 100.7, 81.2, 62.2,59.3, 59.1, 56.6, 55.7, 46.3, 26.4. MS (ESI-MS) *m/z* : 564 $[M+H]^+$ HRMS (ESI) : Calcd for $C_{29}H_{27}ClN_3O_7$ $[M+H]^+$: 564.15320, found: 564.15508.

(*S*)-3-((*R*)-6-((6-bromoimidazo[1,2-*a*]pyridin-2-yl)methyl)-4-methoxy-5,6,7,8-tetrahydro-[1,3]dioxolo[4,5-*g*]isoquinolin-5-yl)-6,7-dimethoxyisobenzofuran-1(3*H*)-one (4):

Nature : White solid. mp : 158-160 °C. IR (KBr) : 3421, 2927, 1759, 1496, 1268, 1214, 1036, 890, 802, 716 cm^{-1}. ^{1}H NMR (400 MHz, $CDCl_3$) : δ 8.29 (s, 1H, Ar-H), 7.65 (s, 1H, Ar-H), 7.40(d, *J* = 9.5 Hz, 1H, Ar-H), 7.16 (d, *J* = 9.5 Hz, 1H, Ar-H), 6.96 (d, *J* = 8.3 Hz, 1H, Ar-H), 6.32 (s, 1H, Ar-H), 6.09 (d, *J* = 8.3 Hz, 1H, Ar-H), 5.94 (d, *J* = 5.2 Hz, 2H, O-CH_2-O), 5.72 (d, *J* = 4.1 Hz, 1H, Ar-CH (C_3-pthalide)), 4.67 (d, *J*= 4.1 Hz, 1H, Ar-CH ($C_{5'}$-isoquinoline)), 4.19 (d, *J* = 14.4 Hz, 1H, -C*H*H-N-CH_2), 4.10 (s, 3H, -OCH_3), 4.04 (s, 3H, -OCH_3), 3.89-3.84 (m, 4H, -OCH_3,-CH*H*-*N*CH_2), 2.54-2.34 (m, 3H, -C*H*$_2$-*N*-CH_2 ($C_{7'}$-isoquinoline), Ar-C*H*H ($C_{8'}$-isoquinoline)), 1.99-1.83 (m, 1H, Ar-CH*H* ($C_{8'}$-isoquinoline)). ^{13}C NMR (100 MHz, $CDCl_3$) : δ 168.4, 152.1, 148.4, 147.6, 146.0, 142.8, 140.8, 140.4, 133.9, 131.7, 127.3, 125.8, 119.9, 118.1, 117.9, 117.5, 116.5, 111.7, 106.5, 102.4, 100.7, 81.2, 62.2, 59.3, 59.1, 56.6, 55.7, 46.2, 26.3. MS (ESI-MS) *m/z* : 608 $[M+H]^+$ HRMS (ESI) : Calcd for $C_{29}H_{27}BrN_3O_7$$[M+H]^+$: 608.10269, found: 608.10558.

(*S*)-3-((*R*)-6-((6-iodoimidazo[1,2-*a*]pyridin-2-yl)methyl)-4-methoxy-5,6,7,8-tetrahydro-[1,3]dioxolo[4,5-*g*]isoquinolin-5-yl)-6,7-dimethoxyisobenzofuran-1(3*H*)-one (5):

Nature : White solid. mp : 99-101°C. IR (KBr) : 3446, 2930, 1755, 1621, 1496, 1268, 1213, 1038, 799, 714, 461cm^{-1}. ^{1}H NMR (400 MHz, $CDCl_3$) : δ 8.40 (dd, *J* = 0.9, 1.4 Hz, 1H, Ar-H), 7.63 (s, 1H, Ar-H), 7.29-7.26 (m, 2H, Ar-H), 6.95 (d, *J* = 8.3 Hz, 1H, Ar H), 6.32 (s, 1H,

Ar-H), 6.09 (dd, *J* = 0.6, 8.3 Hz, 1H, Ar-H), 5.94 (d, *J* = 1.3, 5.9 Hz, 2H, O-CH_2-O), 5.72 (dd, *J* = 0.6, 4.1 Hz, 1H, Ar-CH (C_3-phthalide)), 4.66 (d, *J* = 4.1 Hz, 1H, Ar-CH ($C_{5'}$-isoquinoline)), 4.18 (dd, *J* = 14.4 Hz, 1H, -C*H*H-N-CH_2), 4.10 (s, 3H, -OCH_3), 4.04 (s, 3H, -OCH_3), 3.90 (d, *J* = 14.4 Hz, 1H, -CH*H*-*N*-CH_2), 3.86 (s, 3H, -OCH_3), 2.53-2.41 (m, 3H, -C*H*$_2$-*N*-CH_2 ($C_{7'}$- isoquinoline), Ar-C*H*H ($C_{8'}$-isoquinoline)), 1.97-1.86 (m, 1H, Ar-CH*H* ($C_{8'}$-isoquinoline)). ^{13}C NMR (75 MHz, $CDCl_3$) : δ 168.1, 154.5, 152.0, 147.4, 143.9, 141.2, 139.2, 138.7, 134.4, 131.3, 129.8, 129.1, 127.7, 125.1, 119.7, 118.2, 117.7, 117.6, 100.8, 81.7, 62.1, 60.8, 59.4, 56.6, 49.3, 45.8, 22.5. MS (ESI-MS) *m/z* : 656 $[M+H]^+$ HRMS (ESI) : Calcd for $C_{29}H_{27}IN_3O_7$ $[M+H]^+$: 656.08882, found: 656.09180.

(*S*)-6,7-dimethoxy-3-((*R*)-4-methoxy-6-((7-methylimidazo[1,2-*a*]pyridin-2-yl)methyl)-5,6,7,8-tetrahydro-[1,3]dioxolo[4,5-*g*]isoquinolin-5-yl)isobenzofuran-1(3*H*)-one (6):

Nature : White solid. mp : 92-94°C. IR (KBr) : 3418, 2931, 1756, 1619, 1496, 1386, 1268, 1212, 1037, 892, 787, 711, 603, 439 cm^{-1}. ^{1}H NMR (400 MHz, $CDCl_3$) : δ 7.98 (d, *J* = 6.9 Hz, 1H, Ar-H), 7.56 (s, 1H, Ar-H), 7.25 (s, 1H, Ar-H), 6.95 (d, *J* = 8.3 Hz, 1H, Ar-H), 6.56 (dd, *J* = 1.4, 6.9 Hz, 1H, Ar-H), 6.32 (s, 1H, Ar-H), 6.14 (d, *J* = 8.3 Hz, 1H, Ar-H), 5.94 (dd, *J*= 1.3, 4.8 Hz, 2H, O-CH_2-O), 5.70 (d, *J* = 4.1 Hz, 1H, Ar-CH (C_3-pthalide)), 4.69 (d, *J* = 4.1 Hz, 1H, Ar-CH ($C_{5'}$-isoquinoline)), 4.16 (d, *J* = 14.3 Hz, 1H, -C*H*H-N-CH_2), 4.09 (s, 3H, -OCH_3), 4.02 (s, 3H, -OCH_3), 3.90 (d, *J* = 14.3 Hz, 1H, -CH*H*-*N*-CH_2), 3.85 (s, 3H, -OCH_3), 2.54-2.45 (m, 3H, -C*H*$_2$-*N*-CH_2 ($C_{7'}$-isoquinoline), Ar-C*H*H ($C_{8'}$-isoquinoline)), 2.36 (s, 3H, Ar-CH_3), 1.99-1.89 (m, 1H, Ar-CH*H* ($C_{8'}$-isoquinoline)). ^{13}C NMR (100 MHz, $CDCl_3$) : δ 168.4, 152.1, 148.3, 147.6, 144.8, 144.5, 141.1, 140.4, 134.8, 133.0, 131.8, 124.9, 119.9, 118.1, 117.9, 116.7, 115.5, 114.5, 110.6, 102.4, 100.6, 81.4, 62.2, 59.3, 59.1, 56.6, 55.6, 46.1, 26.4, 21.2. MS (ESI-MS) *m/z* : 544 $[M+H]^+$

HRMS (ESI) : Calcd for$C_{30}H_{30}N_3O_7$ $[M+H]^+$: 544.20783, found: 544.20944.

6.2.4. *In vitro* cell proliferation assay using MCF-7 and MDAMB-231 cell lines

The MCF-7 and MDAMB-231 human breast cancer cell lines were used in the cell proliferation experiment, which was done in 96-well plates as reported before. (Naik et al, 2011). In summary, cells were maintained at 37 °C in a humidified environment with 5% CO_2 in culture media (MEM, DMEM) supplemented with 10% foetal bovine serum, 1% penicillin/streptomycin, and 2 mM l-glutamine. Suspension cells were seeded at a density of 5 x 10^3 cells per well in 96-well plates and treated for 72 hours with a gradient concentration of noscapine and its impy derivatives **3-6** (5 µM to 100 µM). The cells were then stained with 0.4 percent sulforhodamine B solution in 1 percent acetic acid after being fixed with 50 percent trichloroacetic acid. To remove the unbound dye, the cells were rinsed with 1 percent

acetic acid. The protein-bound dye was removed with 10 mM Tris base and estimated using a SPECTRAmax PLUS 384 microplate spectrophotometer 564 nm wavelength. The IC_{50} values, which represent the drug concentration to kill 50% of cells was determined.

6.2.5. Primary breast cancer cells (PBCs) culture and *in vitro* cell proliferation assay

Primary breast cancer cells were acquired in aseptic conditions from eight individuals with various stages of breast cancer before chemotherapy to patients. The tumour tissues were treated with 0.25 percent trypsin and filtered through a 70 micron filter before being centrifuged at 2000 rpm for 3 minutes in serum free media. The filtered cells were collected and plated in T25 flasks, where they were cultured at 37 °C under 5% CO_2 in full DMEM medium supplemented with 10% FBS and 1% pentrip (combination of penicillin and streptomycin). Every 3-4 days, fresh media was replaced, and subsequent passaging was done under the same circumstances as before. Between 3 and 8 passes, the cultures were kept at sub-confluence for homogenous cell types. Before the experimental treatments, the cells were allowed to attain 80-90 percent confluence. The primary cells were plated at 2000 cells/well in a 96-well plate with a normal growth medium, DMEM, once they had attained confluence (low glucose). The cells were treated with gradient concentrations (5 µM to 100 µM) of noscapine and its impy derivatives, **3-6** for 72 hours at 37 °C in a humidified environment with 5% CO_2. Measurement of cell proliferation was performed with a colorimeter by sulforhodamine B (SRB) assay, using the CellTiter96 AQueous One Solution Reagent (Sigma). Cells will be exposed to SRB for 30 minutes followed by washing of unbound dye and adding 1 mM tris and absorbance (optical density) was measured using a microplate reader (Molecular Devices, Sunnyvale, CA) at a wavelength of 564 nm. The percentage of cell survival as a function of drug concentration was then plotted to determine the IC_{50} value.

6.2.6. Flow cytometry analysis of cell cycle progression

MDAMB-231 cells were maintained in Dulbecco's Modification of Eagle's Medium (DMEM) with 4.5 g/L glucose and L-glutamine supplemented with 10% fetal bovine serum and 1% penicillin/streptomycin. Cells were grown at 37 ^{0}C in a 5% CO_2 atmosphere. Cells were treated with noscapine and its impy derivatives, **3-6** dissolve in 1% phosphate buffer saline (PBS). Cells were sampled after 72h of treatment, followed by analysis using flow cytometry. Briefly, 2 x 10^6 cells was centrifuged, washed twice with ice-cold phosphate-buffered saline (PBS), and fixed in 70% ethanol. Tubes containing the cell pellets were stored at -20 ^{o}C for 24h. After this, the cells were centrifuged at 1000 x g for 10 min and the supernatant was discarded. The pellet was resuspended in 30 µl of phosphate/citrate buffer (0.2 M Na_2HPO_4/0.1 M citric acid, pH 7.5) at room temperature for 30 min. Cells were then

washed with 5 ml of PBS and incubated with 0.5 ml of propidium iodide (20 µg/ml in 0.6% Triton-X in PBS) and 0.5 ml of RNase A (20 µg/ml in PBS) for 45 min. in dark. Samples were analysed on a flow cytometer (BD FACS Aria-III) and the progress in the cell cycle was determined.

6.2.7. Flow cytometry analysis for apoptosis assay

The Annexin-V-FITC apoptosis detection method was used to detect apoptosis in cancer cells using an apoptosis detection kit (Sigma–Aldrich, USA) according to the manufacturer's instructions. For the experiment, $3x10^4$ cells per well were planted on a 12 well culture plate and cultured with full media for 24 hours. After 48 hours of treatment with IC_{50} concentrations of noscapine and its impy derivatives, **3-6**, the cells were collected. Surface marker antibodies (biotin-conjugated Annexin V, FITC-conjugated streptavidin) and propiumdium iodide were used to stain the cells (PI). The cells were suspended in 1X binding buffer and treated with Annexin V FITC conjugate for 20 minutes at room temperature in the dark. Data was acquired using a flow cytometer with PI excitation at 488 nm and emission at 530 nm. The percentages of viable cells (Annexin V / PI), early apoptotic cells (Annexin V+ / PI), late apoptotic/necrotic cells (Annexin V+ / PI+), and late necrotic cells (Annexin V / PI+) were calculated.

6.2.8. Cellular observation using DAPI, Acridyne Orange and Ethidium bromide staining

4',6-diamidino-2-phenylindole (DAPI) staining was used to identify changes in nuclei morphology in MDAMB-231 cells after 7 hours of treatment with noscapine and its impy derivatives, **3-6**. MDAMB-231 cells were cultivated in 6-well plates on poly-L-lysine-coated coverslips and treated with the IC_{50} concentration of noscapine and its derivatives for 72 hours. After incubation, coverslips were fixed in cold methanol, washed with PBS, and stained for 15 minutes at room temperature with 10 µM DAPI, 15 µM, AO and 15 µM EtBr. The stained cells were washed twice in PBS and viewed using a Nikon Eclipse Ts2R-FL inverted fluorescent microscope with standard excitation filters. The wavelengths of excitation and emission were 346 nm and 460 nm, respectively. Characteristics linked with nuclear condensation, membrane bleb development, and apoptotic bodies were used to identify cells that had experienced apoptosis.

6.2.9. Measurement of mitochondrial membrane potential ($\Delta\Psi m$)

The effect of noscapine and its impy derivative, **6** on mitochondrial membrane potential was measured by using rhodamine-123 (Sigma-Aldrich Co.; Ex/Em = 485 nm/535 nm), JC-1

(Invitrogen Co.; Ex/Em = 515 nm/529 nm) and DAPI (Sigma-Aldrich Co.; Ex/Em = 358 nm/461 nm) dyes. Briefly, cells were seeded in 12 well plate followed by treatment with noscapine and its impy derivative, **6** for 48 hours. Cells were washed with PBS and stained with rhodamine-123 (15µg/ml), JC-1 (10 µg/ml) and DAPI (10 µg/ml) for 10 minutes at room temperature. After staining, cells were washed twice with PBS and images were captured using an inverted fluorescence microscope (Nikon Eclipse Ts2R-FL) at 400x magnification. The untreated cells stained with rhodamine-123 appeared light green fluorescence (lower $\Delta\Psi m$) whereas the treated cells appeared bright green fluorescence (higher $\Delta\Psi m$). In the case of JC-1 stain, light red fluorescence (lower $\Delta\Psi m$) was detected in untreated cells whereas bright red fluorescence (higher $\Delta\Psi m$) was observed in treated cells. Similarly in DAPI stain relatively light blue with no morphological changes was observed in untreated cells, whereas bright blue with changes in morphological features was observed in treated cells. The intensity was measured using image J software.

6.2.10. Intracellular reactive oxygen species (ROS) detection

Increased intracellular ROS is a dormant component that damages nucleic acid, cellular lipid membranes, and organelles, causing cancer cells to die. The oxidative conversion of the sensitive fluorescent probe 2',7'-dichlorofluorescence-diacetate (DCFH-DA) to fluorescent 2',7'-dichlorofluorescein was used to determine the intracellular ROS levels (DCF). MDAMB-231 cells were sown in a 6 well plate with cover glass and treated for 48 hours with noscapine and its impy derivative, **6**. The treated cells were collected, washed twice in PBS, re-suspended in 10 mM DCFH-DA (bought from Molecular Probes Inc., Invitrogen), and incubated in the dark for 30 minutes at room temperature. The stained cells were examined with conventional excitation filters using a fluorescent microscope (Nikon Eclipse Ts2R-FL) (Nikon). The untreated control cells fluoresced dimly, but the treated cells fluoresced brightly. Both noscapine and its impy derivative, **6**, produced a considerable increase in intracellular ROS.

6.2.11. Detection of Apoptosis by TUNEL assay

The TUNEL assay was used to investigate the induction of apoptosis in MDAMB-231 cells after treatment with noscapine for 7 hours. The Apo BrdU TUNEL test kit from Invitrogen (Carlbad, CA, USA) was used to investigate DNA fragmentation using fluoroscence microscopy. Cells were cultivated on a 12 well plate for 7 hours after being treated with the IC_{50} concentration of noscapine and its impy derivative, **6**. An Alexa Fluor 488 dye-labelled anti-BrdU antibody was used to identify DNA strand breaks after cells were

removed from culture plates and pellets were collected. In contrast to the red fluorescence created by nuclear staining with PI, the outcome appears as green nuclear fluorescence.

6.2.12. Colony formation Assay

The effect of impy derivative, **6** on the ability of the triple negative breast cancer cell line (MDAMB-231) to form colonies was investigated in a clonogenic experiment. The colonies were counted using Image-J software in each setting (National Institute of Health, Bethesda, MD, USA). Specifically, 1000 cells were sown on a 6 well plate and incubated overnight before being treated with imidazothiazole derivative **6** and incubated for 10-12 days, after which the cells were fixed and stained with crystal violet, and colonies were counted for both untreated and treated cells.

6.3. Results

6.3.1. Impy derivatives, 3-6 inhibited proliferation of cancer cells without affecting the normal cells

Impy derivatives, including the lead compound, noscapine (0-100 µM), were tested for anti-proliferative activity in MCF-7 (estrogen- and progesterone- receptor positive) and MDAMB-231 (estrogen- and progesterone- receptor negative) human breast cancer cells using the sulforhodamine B assay (Figure 6.2A and B). All of the impy derivatives of noscapine **3-6** demonstrated a considerable cytotoxic effect in both cell lines when compared to noscapine. Table 1 summarises the IC_{50} values for the test compounds using both the cell lines. For MCF-7 cells, the IC_{50} value for the impy derivatives of noscapine, **3-6** varies from 35.7. to 3.7 µM, which is much smaller than the lead molecule, noscapine (IC_{50} value is 43.9 µM). For MDAMB-231 cells, impy derivatives of noscapine, **3-6** showed an IC_{50} value of 45.2 to 5.1 µM, which was comparable to noscapine (IC_{50} value of 60.9 µM). When compared to untreated cells, both cancer cell lines displayed statistically significant IC_{50} values for noscapine and its derivatives ($p \leq 0.001$). Surprisingly, noscapine and its impy derivatives **3-6** suppressed normal healthy cell 293T proliferation to a value of 5% at a concentration of 100 µM, but it was shown to be greater than 5% at concentrations greater than 100 µM. (Figure 6.2C). Among the library, the impy derivative, **6** was determined to be the most promising (IC_{50} values of 3.7 µM and 5.6 µM for MCF-7 and MDAMB-231 cell lines, respectively) and was chosen for further research. We next evaluated the sensitivity of primary cancer cells with the treatment of the most promising impy derivative of noscapine, **6.** The primary breast cancer cells were treated for 72 hours with escalating concentrations (0-100 µM). When compared to untreated cells, the chemical greatly slowed the multiplication of primary tumour cells (Figure 6.2D). For the panel of primary tumour cells,

the IC_{50} values vary from 12.3 µM to 3.7 µM (Table 6.2). We also looked at the effect of the most promising impy derivative of noscapine **6** (1.5 µM) on MDAMB-231 cells' colony-forming abilities. It has a concentration-dependent inhibitory effect on colony development. For example, 1, 10 and 20 µM of **6** considerably reduced the number of colonies by 70% and 90%, respectively (Figure 6.2E). The IC_{50} of **6** was found to be 1.5 µM for inhibition of colony formation.

Table 6.1. IC_{50} values of noscapine and its impy derivatives **3-6** using two human breast adenocarcinoma cell lines, MCF-7 and MDAMB-231 as well as a normal cell line (293T). All the novel derivatives were found to have improved antiproliferative activity compared to noscapine without affecting the normal healthy cell line.

	IC_{50} (µM)		
	MCF-7	**MDAMB-231**	**293T**
Noscapine	44.1±4.3***	57.4±5.2***	310.4±3.2***
3	25.5± 3.2***	43.4 ± 3.5***	330.2±3.6***
4	7.5 ±1.8***	15.8 ± 2.4***	337.4±2.7***
5	6.5±2.1 ***	13.4 ± 2.3***	340.2±3.3***
6	3.7 ± 1.8***	5.6± 1.2***	330.5± 3.5***

Table 6.2. IC_{50} values of noscapine and its impy derivative **3-6** on primary breast tumor cells. All the novel derivatives were found to have improved antiproliferative activity compared to noscapine without affecting the normal healthy cell line.

	IC_{50} (µM)				
Patients No.	**Noscapine**	**3**	**4**	**5**	**6**
1	59.8±4.3***	8.2±2.3***	17.2±2.5***	4.9±0.6***	3.9±1.8***
2	61.4±4.5***	12.3±1.9***	8.6±1.5***	4.8±0.8***	3.6±2.6***
3	44.3±3.8***	8.6±1.6***	14.6±2.4***	5.0±0.5***	5.8±3.3***
4	41.2±3.5***	5.2±1.3***	14.9±2.6***	4.6±0.7***	3.9±1.7***
5	50.3±4.6***	5.0±1.8***	8.2±1.4***	3.7±0.4***	3.2±2.4***
6	49.8±4.8***	8.5±2.2***	11.4±1.8***	4.9±0.6***	4.8±3.6***
7	47.6±3.6***	9.2±1.5***	8.5±1.7***	5.0±0.5***	5.8±1.9***
8	58.7±4.2***	10.6±1.7***	18.2±2.4***	4.8±0.7***	3.8±2.3***

(A) MCF-7

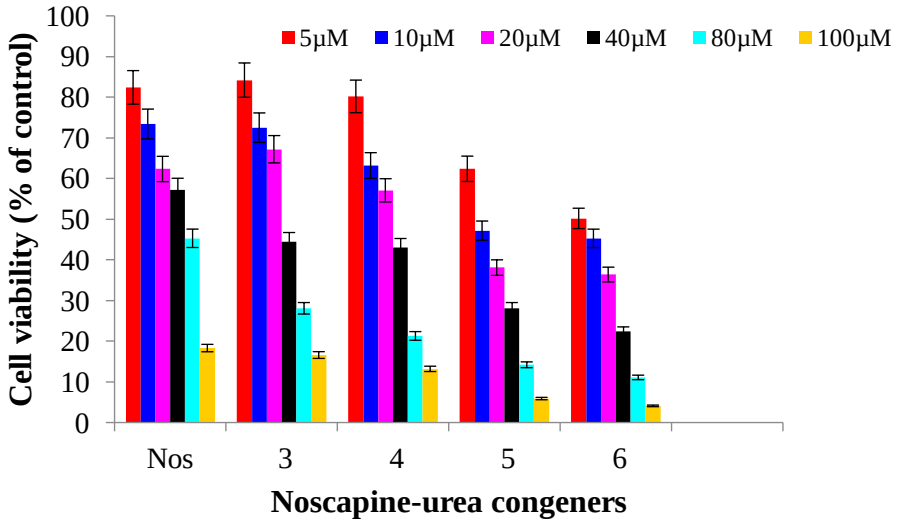

(B) MD-AMB-231

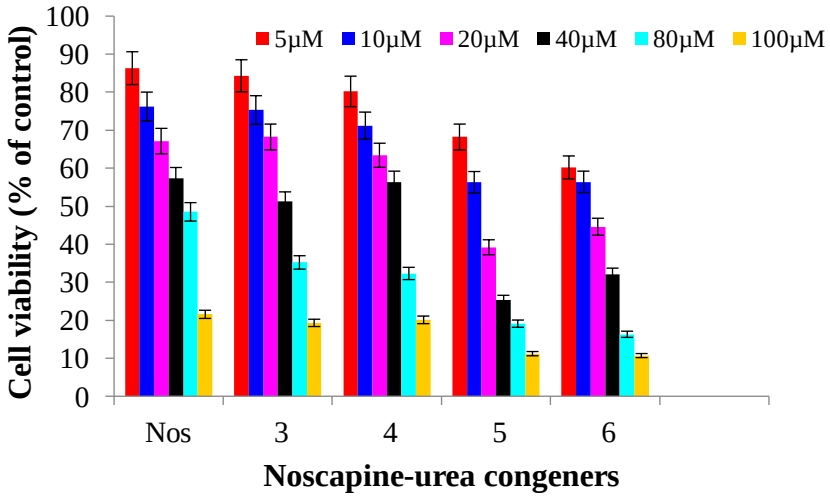

(C) Normal cell (293-T)

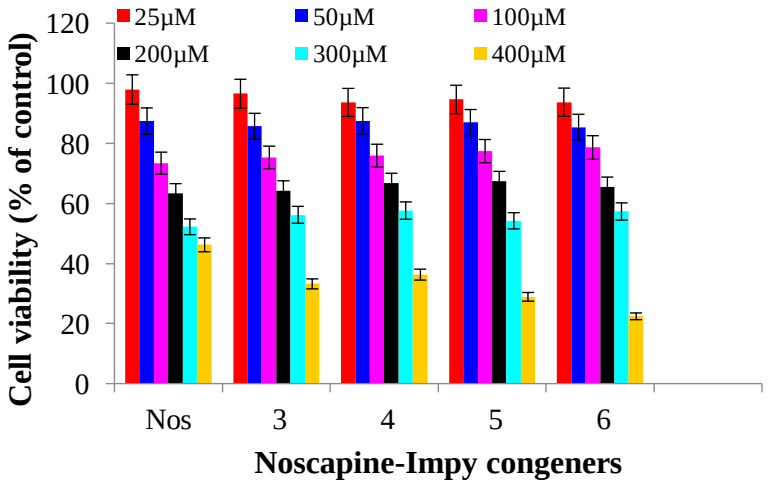

Primary breast cancer cell

(D) **(E)**

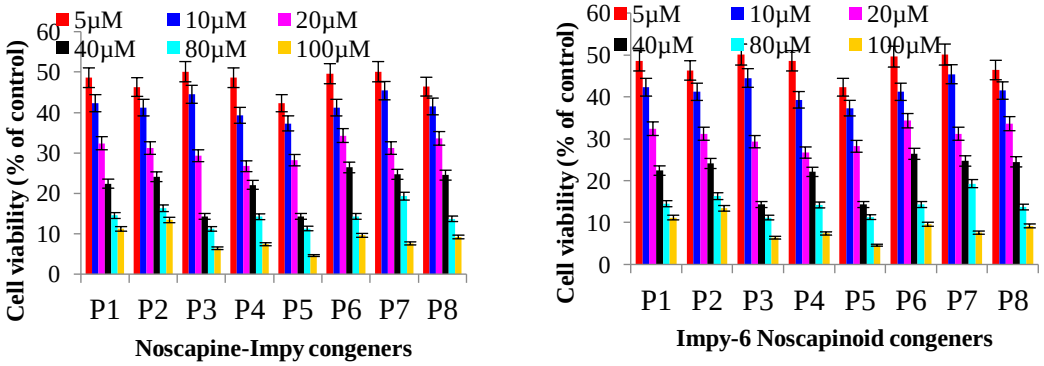

(F)

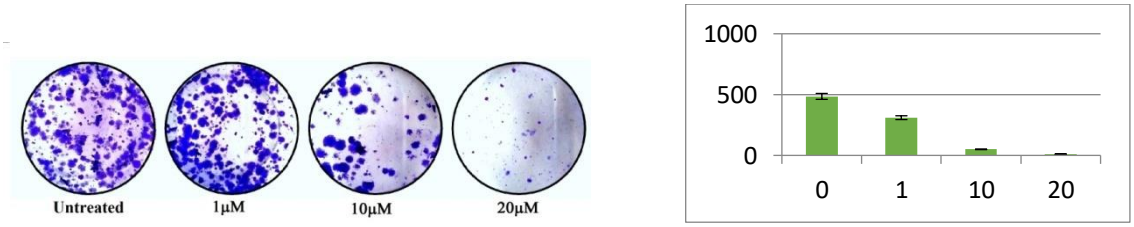

Figure 6.2. Effect of the lead molecule, noscapine and its impy derivatives **3-6** at a gradient of concentration (0–100 µM) on (A) MCF-7 and (B) MDAMB-231 cancer cells viability after a 72-h exposure. Results are shown as mean ± standard deviation, n = 3. (C) Effect of noscapine and its five imidazothiazole derivatives (25–400 µM) on the cell viability of normal healthy cell (293T). (D) Effect of Noscapine (0–100 µM) on viability of primary tumor cells obtained from eight patients with different stages of breast cancer (IC_{50} value ranges from 3.7 ± 0.4 µM to 5.0 ± 0.5 µM . (E) Effect of the most promising derivative **6**(0–100 µM) on viability of primary tumor cells obtained from eight patients with different stages of breast cancer (IC_{50} value ranges from 3.7 ± 0.4 µM to 5.0 ± 0.5 µM . (F) Effect of **6** on clonogenicity of MDAMB-231 cells. Images of the colonies and a bar graph showing the number of colonies under different treatment conditions are presented. Results are shown as mean ± standard deviation, n = 3. ***P < 0.001, compared to the control.

6.3.2. Impy derivatives of noscapine induced cell death in MDAMB-231 cells

The goal of this study was to see if the treatment with impy derivative, **6** induce cell death in MDAMB-231 cells. Figure 6.2 revealed the proportion of early and late apoptotic cells after 72 hours using MDAMB-231 cells treated with IC_{50} concentration (5.6 µM). The control untreated cells contained only very few early apoptotic (2%) and late apoptotic cells (3%), which were considered as the background cell death due to regular trauma during cell culture. In contrast, the percentage of early apoptotic cells of 45% and late apoptotic cells of

35% were noticed with the treatment of **6** and were found to be significantly high compared to controlled untreated cells.

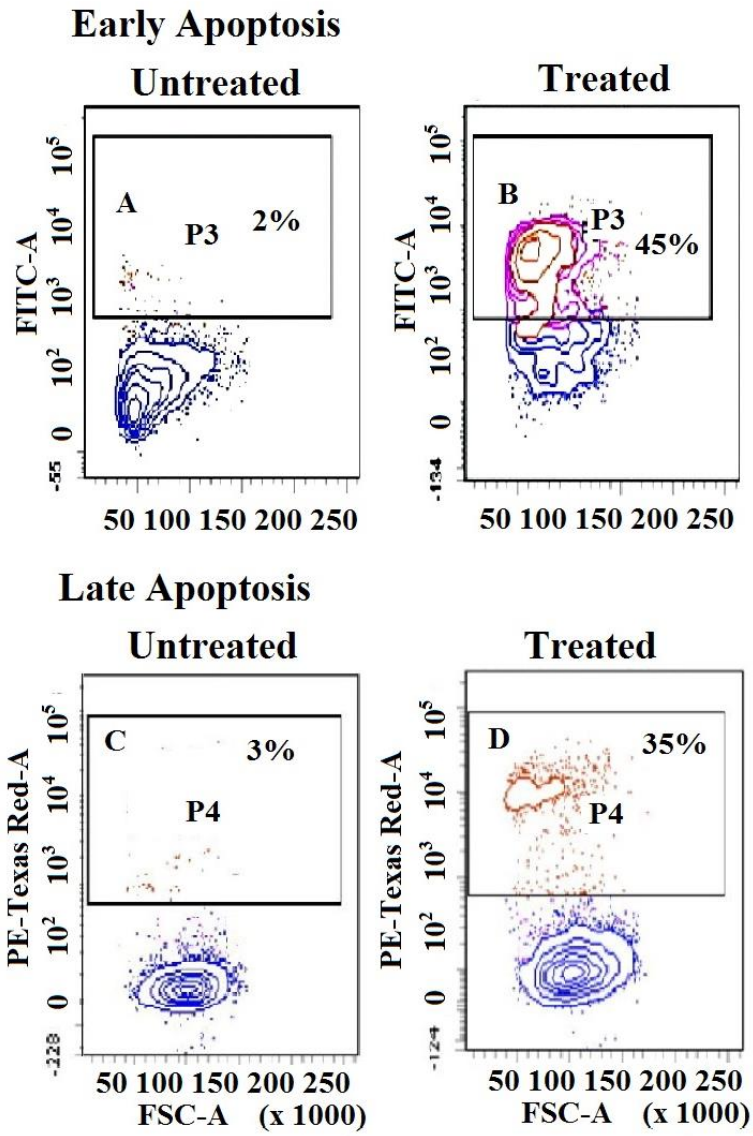

Figure 6.3. Induction of apoptosis by the most promising impy derivative of noscapine, **6.** Flow cytometry analysis of cells showing increased percentage of early and late apoptosis with the treatment of **6** for 72 h compared to untreated treated cells.

6.3.3. Detection of apoptosis with the treatment of noscapine and its impy derivative

The key morphological changes during apoptosis include membrane blebbing, cellular shrinkage, chromatin condensation, and the production of apoptotic bodies. To confirm the induction of apoptosis by impy derivative **6**, we used AO, EtBr, HO (Hoechst 33342). Apoptosis occurred in MDAMB-231 treated cells, as indicated by staining the treated cells with these colours (Figure 6.3). The untreated cells had normal cell shape, but the treated cells had multiple apoptotic characteristics such as membrane blebbing, numerous shattered nuclei, and the presence of apoptotic bodies.

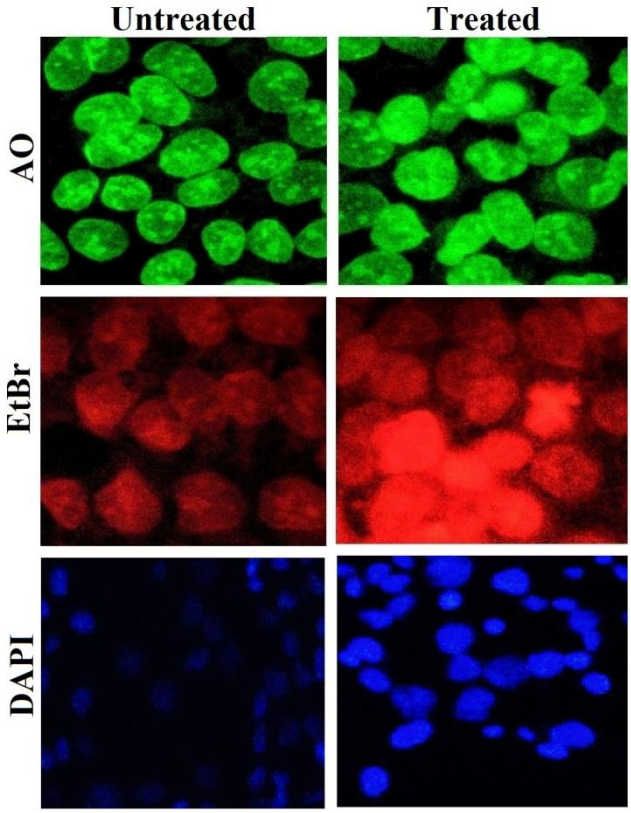

Figure 6.4. Morphological changes of MDAMD-231 cells visualized by staining with AO, EtBr and DAPI revealed apoptosis with the treatment of **6** compared to untreated cells.

6.3.4. Effects of noscapine-urea congener 10f on ROS accumulation in MDAMB-231 cells

To learn more about the mechanism of induction of apoptosis in cancer cells, we discovered that impy derivative of noscapine **6** increased the amounts of reactive oxygen species (ROS). The ROS level was measured using DCFDA as a molecular probe. When MDAMB-231 cells were treated for 72 hours, the green fluorescence was more bright than when the cells were not treated (Figure 6.4). We discovered that impy derivative **6** dramatically increased ROS levels in MDAMB-231 cells as evaluated by fluorescence intensity, indicating that ROS may play a role in apoptosis induction (Figure 6.4). MDAMB-231 cells treated with H_2O_2 (10 µM) produced a significant quantity of ROS and were labelled with a more intense green fluorescence. A TUNEL test was also used to look at the induction of apoptosis in MDAMB-231 cells. The number of TUNEL positive nuclei increased after 72 hours of treatment, indicating cell death (Figure 6.5).

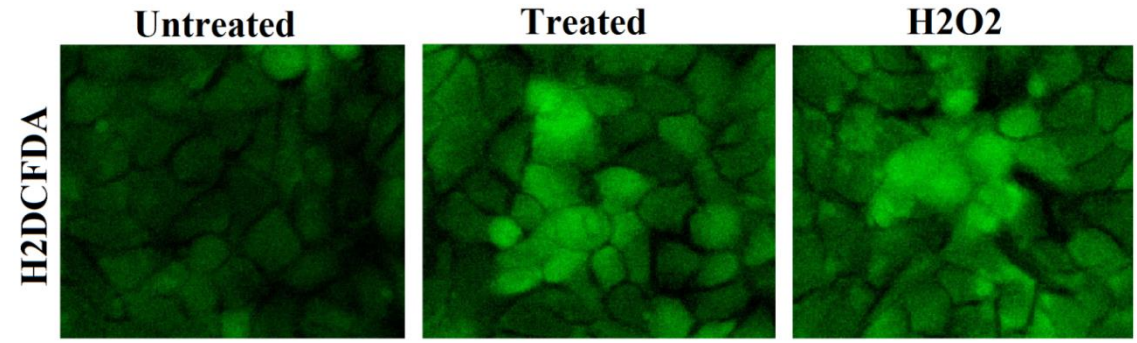

Figure 6.4. Effect of **10f** treatment on intracellular ROS production as imaged and estimated using an oxidation sensitive fluorophore, DCFDA.

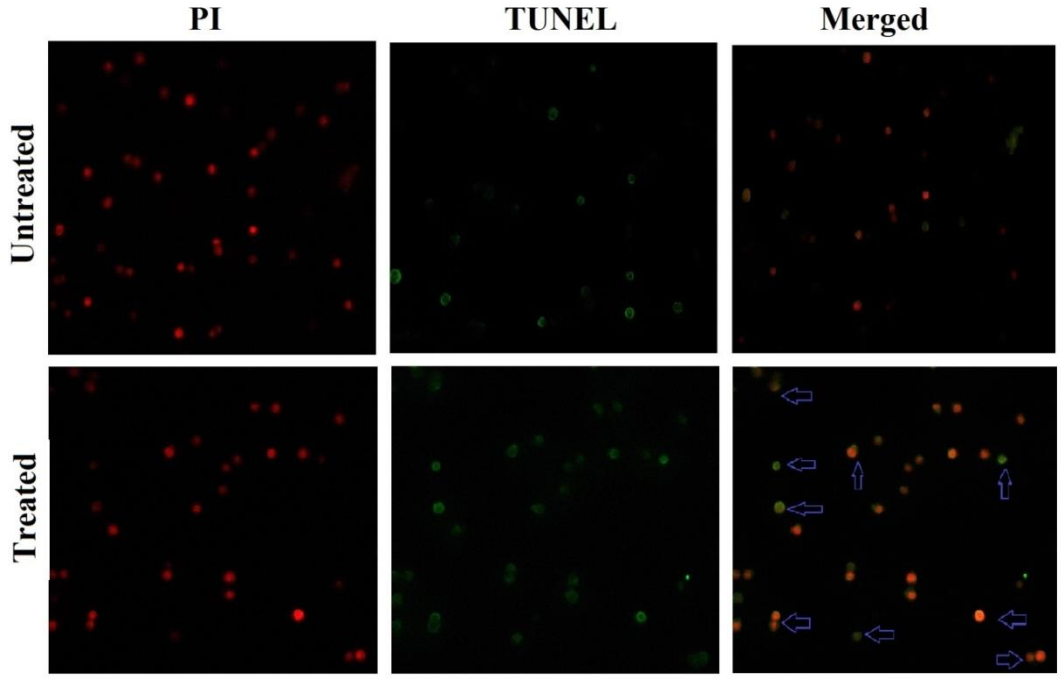

Figure 6.6. Treatment with impy derivative **6** increases the number of TUNEL positive cells compared to untreated cells indicating induction of apoptosis to MDAMB-231 cells.

6.3.5. Impy derivative of noscapine alter the cell cycle profile and cause mitotic arrest at G_2/M phase

Using FACS analysis, we investigated the effect of impy derivative **6** at its IC_{50} concentration (5.6 µM) on the cell cycle profile of MDAMB-231. The cell cycle profile of MDAMB-231 cells was significantly altered after 72 hours of treatment. In comparison to untreated cells, FACS analysis demonstrated a large concentration of cells in the G2/M phase (Figure 6.6). At 72 hours after drug treatment, a distinctive hypodiploid DNA content peak (sub-G1) was seen, in contrast to G2/M block. The gradual creation of cells with hypodiploid DNA reflects fragmented DNA, which indicates that the cells are dying.

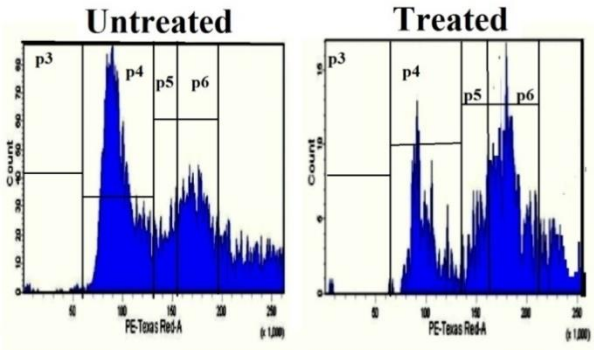

Figure 6.7. Effect of impy derivative **6** at IC_{50} concentration (5.6 μM) on MDAMB-231 cell cycle distribution at 72h. The bar graph represents the percentage of cells at the indicated phases of the cell cycle.

6.3.6. Effects of noscapine and its impy derivative on mitochondrial membrane potential (ΔΨm)

Apoptosis is assumed to be primarily mediated by mitochondria. The collapse of mitochondrial membrane potential ($\Delta\Psi_m$) is linked to the induction of apoptosis. Using DAPI, JC-1, and Rhodamine 123 dyes, we assessed the decrease of mitochondrial membrane potential ($\Delta\Psi_m$) in MDAMB-231 cells treated for 7 hours. When MDAMB-231 cells were treated for 7 hours, the intensity of JC-1 red fluorescence, Rhodamine-123 green fluorescence, and DAPI blue fluorescence was higher in treated cells compared to untreated cells (Figure 6.7).

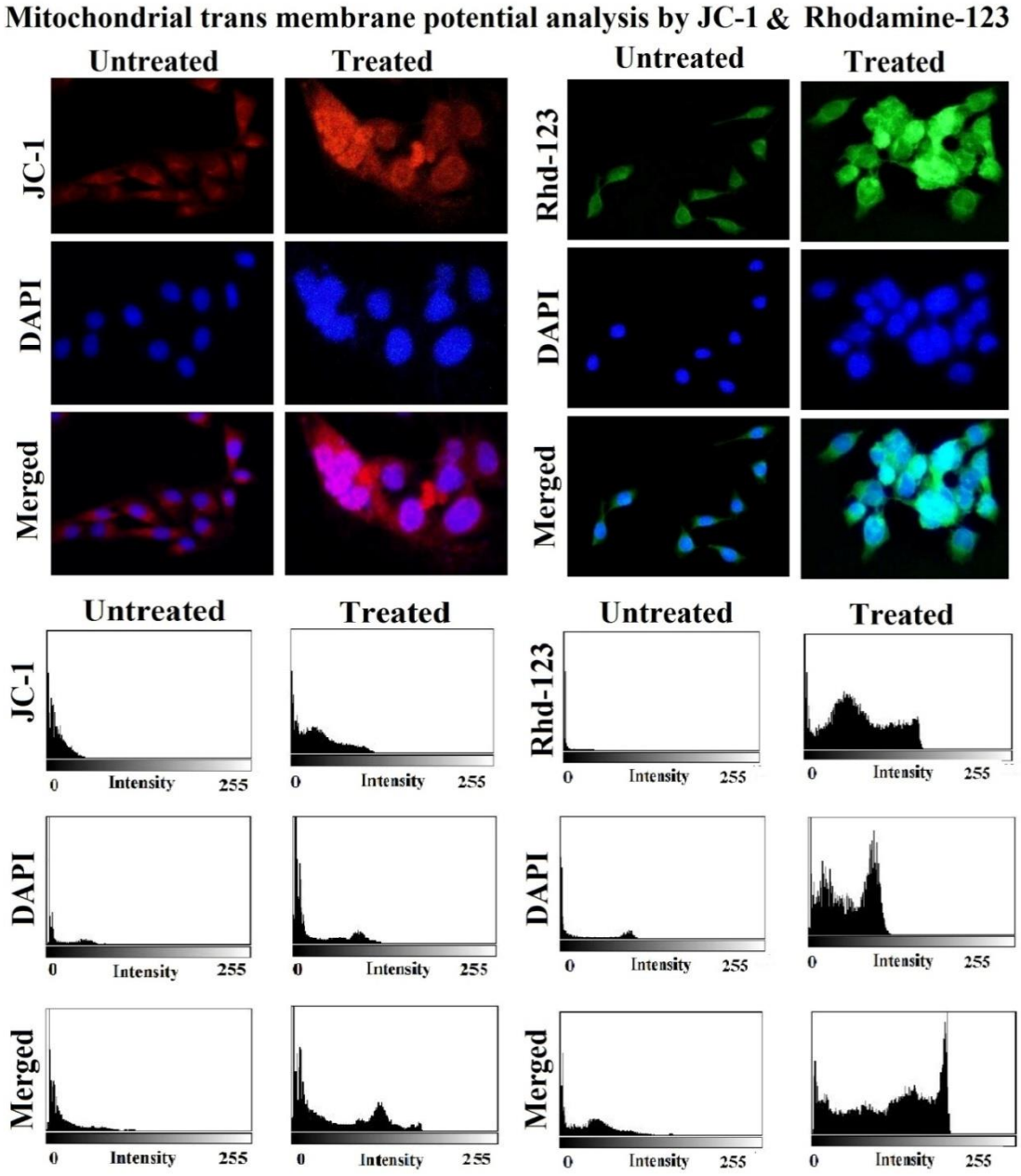

Figure 6.8 Effect of **6** on mitochondrial membrane potential as visualized using different fluorescent dyes, DAPI, JC-I and Rhodamine 123. The fluorescent intensity was measured using Image J.

6.4. Discussion

The anticancer properties of imidazopyridine compounds have been widely studied. Many derivatives of the compounds have been analysed against various cancer types and showed potent antiproliferative activity. As an example, imidazo[2,1-b]pyridine/pyrimidine chalcone derivatives showed anticancer activity against MCF-7 cell line by down regulating procaspase-9 (Kamal et al., 2010). Similarly, benzimidazole conjugates of imidazopyridine/imidazopyrimidine have been studied against cervical, prostate, lungs as well as melanoma and found to be a potent antiproliferative agent, which arrests cell cycle at

G_2/M phase and induce apoptosis by activating caspase-3. These derivatives have also been studied as microtubule inhibitors against cervical cancer at the cellular and molecular level (Kamal et al., 2015). Bis-imidazoles and bis-imidazo 1,2-a pyridines have been studied for antimitotic effects against cervical, breast and renal cancer (Meenakshisundaram et al., 2019). A library of these compounds has been synthesized and screened for their anticancer activity against breast carcinoma, lungs carcinoma as well as prostate carcinoma, which display potent activity against all these cancer cell lines (Suma et al., 2020). Sulphonamide derivatives of benzofuron imidazopyridine have been evaluated for anticancer potential against breast cancer, ovarian cancer and colon cancer (Murthy et al., 2021). Similar studies have been carried out by using the compounds against various cancer types (Güçlü et al., 2018; Ramesh et al., 2019; Bakherad et al 2019). Because of the wide range of pharmacological action demonstrated by imidazo-pyridine scaffold, we sought to develop a panel of noscapine imidazo-pyridine derivatives to increase the anticancer activity of noscapine. These congeners were chemically synthesised in high yield and experimentally evaluated their anticancer activity. Two human breast adenocarcinoma cell lines, MDAMB-231 and MCF-7, were used to test their antiproliferative efficacy *in vitro*. The large variation in IC_{50} values between MCF-7 and MDAMB-231 suggests that these test chemicals suppress cancer cell growth and are cell type-dependent. One of the most powerful derivative, **6** with IC_{50} values of 3.7 µM and 5.6µM respectively against MCF-7 and MDAMB-231, was selected and employed to elucidate the mechanism of action in greater detail. Generally, tumour cells colonize and spread to different regions of the body. As a result, it is important to look at the potential of the drug molecule to prevent tumour cells from colonizing. Using a colony formation assay, we observed that the N-imidazo pyridine congeners of noscapine inhibited the capacity of MDAMB-231 cancer cells to form colonies (IC_{50} value of 1.5 µM) (Figure 6.1). The inhibition of cell cycle progression in G2/M phase was shown to be the cause of the cancer cell's inability to proliferate (Figure 5B). This is supported by a recent study in which several of the synthesized noscapine derivatives suppressed cell growth by interfering with cell cycle progression during the G2/M phase (Anderson et al., 2005; Sajadian et al., 2015; Shen et al., 2015; Nagireddy et al., 2021; Devine et al., 2018; Rahmanian-Devin et al., 2021). Interfering with cell cycle progression, noscapine and its derivatives lead to apoptosis in cancer cells (Ye *et al*., 1998). The induction of apoptosis by 7h has been studied by imaging using three fluorescent dyes, AO, EtBr, and Hoechst (Figure 4B). FACS analysis was also used to determine the percentage of apoptotic cells. The apoptotic process is defined biochemically by changes in cell membrane lipid composition, phosphatidylserine which is typically found on the inner leaflet of the cell membrane

translocates to the outer leaflet and is recognized by annexin V binding. Propidium iodide, a cell-impermeant DNA-binding fluorescent dye, can only enter cells when they are in the late stages of apoptosis, when membrane permeability is weakened. When the MDAMB-231 cell line was treated with IC_{50} concentration for 72 hours, the percentage of early and late apoptotic cells were 45 and 35%, respectively, which is significantly greater than untreated cells (Figure 6.2). The induction of apoptosis was further validated by the appearance of an increased number of TUNEL positive cells after 72 hours of treatment (Figure 6.5). We assessed the degree of formation of reactive oxygen species (ROS) in cancer cells to highlight the mechanism of apoptosis induction. It is widely known that high levels of ROS damage the microtubule network, resulting in the loss of mitochondrial membrane integrity and cell death. (Nambiar et al., 2020; Tomar et al., 2017). It was discovered that treated cells generated much more ROS compared to untreated cells (Figure 6.4), which contributed to cellular microtubule instability and loss of mitochondrial transmembrane potential (Figure 6.7) as a potential apoptosis-inducing mechanism. On a therapeutic level, because cancer cells have higher amounts of ROS than normal cells, increasing the ROS level might selectively kill cancer cells (Pelicano et al., 2004). Although the parent molecule, noscapine, is currently in clinical trials, the N-imidazo pyridine derivative of noscapine offers a competitive advantage over noscapine due to its increased potency without compromising the nontoxic profile of noscapine.

Conclusion

Microtubules have long been considered a promising target for anticancer drugs, because of their critical function in mitosis, where they form the dynamic spindle machinery. As a result, a large range of antimitotic agents that modify microtubule dynamics are now in the clinics such as paclitaxel, docetaxel, and the vinca alkaloids to treat a variety of cancers. However, because of their non-selective action and extreme overpolymerizing (by taxanes) or depolymerizing (by vincas) effects on microtubules, these chemotherapy drugs are associated with serious toxicity (particularly peripheral neuropathies, gastrointestinal toxicity, myelosuppression, and immunosuppression). As a result, new tubulin-binding compounds that are much more effective and less hazardous than currently existing medications for the treatment of human tumours are urgently needed. Noscapine and its derivatives (collectively known as noscapinoids) have been discovered to influence microtubule dynamics at stoichiometric doses without changing tubulin polymer mass. This distinct feature of noscapinoids is bringing it to the forefront of research. Interfering with microtubule dynamics typically results in programmed cell death, and because noscapinoids are less toxic than currently used tubulin-binding medicines, they show tremendous promise as a chemotherapeutic agent for the treatment of human cancer in the clinic. Even though noscapine is a potent chemotherapeutic agent, it only works at high micromolar concentrations, hence analogues of noscapine have been produced in the search for novel therapies that work at lower concentrations without affecting normal cells. As a result, the primary objective is to use structural alterations to create a more powerful derivative of noscapine. To improve the activity of noscapine, we developed a series of derivatives and investigated their activity as effective tubulin-binding anticancer drugs, as well as additional mechanisms of action that lead to programme cell death in cancer cells.

A series of new noscapine derivative called 9-arylimino–noscapine was developed, using computational methods, chemically synthesised, and tested its biological function experimentally. The current work highlights the value of LIE-SGB calculations in directing this endeavour in the context of structure-based drug design and offering insights into the sources of activity variations. The imine-series of noscapinoids were found to increased the anticancer activity of noscapine to many folds using MCF-7 and MDA-MB-231 breast cancer cell line as well as a panel of human breast cancer primary cells derived from the patient.

In the quest to discover a new set of noscapinoids, we have designed and chemically synthesised N-alkyl amine series of noscapine and analysed their biological activity in the

hopes of producing newer noscapinoids with superior activity. The ability of these compounds to bind tubulin revealed that they may be used as tubulin-binding anti-cancer medicines. In certain human breast cancer cell lines, it was also shown that this class of noscapinoids are substantially more effective than noscapine at arresting mitosis and inhibiting cell growth. In cancer cells as well as primary cells derived from patients, these derivatives disrupted DNA synthesis, slowed cell cycle development in the S and G2M phases, and caused apoptosis.

Further, we have computationally developed a new series of noscapinoids called 1,3-diynyl noscapinoids, chemically synthesized and studied their anticancer potential against breast cancer cell lines with primary cells derived from patients. These derivatives were found to bind tubulin more effectively which suggests that they might be employed as tubulin-binding anticancer drugs. This series of noscapinoids was also proven to be significantly more effective than noscapine at arresting mitosis and suppressing cell proliferation in human breast cancer cell lines. These compounds inhibited DNA synthesis, retarded cell cycle progression in the S and G2M phases, and induced death in cancer cells and primary cells obtained from patients without affecting normal cells and tissues.

A new class of noscapine derivatives was developed by conjugating urea pharmacophore with noscapine, followed by chemical synthesis and experimental evaluation as strong anticancer agents. Anticancer potential of the novel derivatives was studied against breast cancer cell lines and patient derived primary cells. All the experiments for anticancer evaluation retained outstanding activities against the cell lines. Their apoptotic activity, arrest of cell cycle progression at S and G2/M phase as well as ROS activation, DNA breakage, and loss of mitochondrial transmembrane potential with tumour regression ability in mice xerograph model without toxicity to normal human cells and tissues of mice prove that Urea-noscapine might be used as a chemotherapeutic drug to treat human breast cancer.

To uncover a novel class of noscapinoids with great anticancer potential, we used rational design followed by chemical synthesis strategy to create a new series of molecules called N-imidazopyridine noscapinoids. Breast cancer cell lines and patient-derived primary cells were used to test the new derivatives for anticancer potential. All of the anticancer tests revealed that the cell lines had remarkable anticancer activity. Their apoptotic activity, cell cycle arrest at S and G2/M phases, as well as ROS activation, DNA breakage, and loss of mitochondrial transmembrane potential with tumour regression ability in mice xerograph model without toxicity to normal human cells and tissues of mice, demonstrates that the derives are the most potent and safe anticancer agents.

In the conclusion, our findings provide persuasive evidence that these analogues have a high potential for additional preclinical and clinical testing. Thus, the future offers promise in terms of additional clinical assessment of newly developed noscapinoids in this study, as well as more efficient and precise targeting of tumours of varied tissue origin by leveraging the interaction mechanism of noscapinoids with tubulin.

References

1. Abraham, M..J., Murtola, T., Schulz, R., Pall, S., Smith, J.C., Hess, B., & Lindahl, E. (2015). GROMACS: high performance molecular simulations through multi-level parallelism from laptops to supercomputers. *Sofware X* 1, 19–25.
2. Ali, I., Haque, A., Saleem, K., & Hsieh, M. F. (2013). Curcumin-I Knoevenagel's condensates and their Schiff's bases as anticancer agents: synthesis, pharmacological and simulation studies. *Bioorganic & medicinal chemistry*, *21*(13), 3808–3820.
3. Almirante, L.; Polo, L.; Mugnaini, A.; Provinciali, E.; Rugarli, P.; Biancotti, A.; Gamba, A.; Murmann, W. (1965). *J. Med. Chem*. *8*, 305.
4. Anderson, J. T.; Ting, A. E.; Boozer, S.; Brunden, K. R.; Crumrine, C.; Danzig, J.; Dent, T. Faga, L.; Harrington, J. J.; Hodnick, W. F.; Murphy, S. M.; Pawlowski, G.; Perry, R.; Raber, A.; Rundlett, S. E.; Stricker-Krongrad, A.; Wang, J.; Bennani, Y. L.(2005). dentification of novel and improved antimitotic agents derived from noscapine. *Journal of medicinal chemistry*, *48*(23), 7096-7098.
5. André, N., & Meille, C. (2006). Taxanes in paediatric oncology: and now?. *Cancer treatment reviews*, *32*(2), 65-73**.**
6. Aneja, R., Vangapandu, S. N., Lopus, M., Chandra, R., Panda, D., & Joshi, H. C. (2006). Development of a novel nitro-derivative of noscapine for the potential treatment of drug-resistant ovarian cancer and T-cell lymphoma. *Molecular pharmacology*, *69*(6), 1801-1809.
7. Aneja, R., Vangapandu, S. N., Lopus, M., Viswesarappa, V. G., Dhiman, N., Verma, A., ... & Joshi, H. C. (2006). Synthesis of microtubule-interfering halogenated noscapine analogs that perturb mitosis in cancer cells followed by cell death. *Biochemical pharmacology*, *72*(4), 415-426..
8. Aneja, R., Dhiman, N., Idnani, J., Awasthi, A., Arora, S.K., Chandra, R., & Joshi, H.C. (2007). Preclinical pharmacokinetics and bioavailability of noscapine, a tubulin-binding anticancer agent. *Cancer Chemotherapy and Pharmacology*, 60, 831-839.
9. Aneja, R., Ghaleb, A. M., Zhou, J., Yang, V. W., & Joshi, H. C. (2007).Determine the sensitivity of noscapine-induced apoptosis in colon cancer cells. *Cancer research*, *67*(8), 3862-3870.

10. Aneja, R., Katyal, A., & Chandra, R. (2004). Modulatory influence of noscapine on the ethanol-altered hepatic biotransformation system enzymes, glutathione content and lipid peroxidation in vivo in rats. *European journal of drug metabolism and pharmacokinetics*, *29*(3), 157-162.

11. Aneja, R., Liu, M., Yates, C., Gao, J., Dong, X., Zhou, B., Vangapandu, S.N., Zhou, J., Joshi, H.C. (2008). Multidrug resistance-associated protein overexpressing teniposide-resistant human lymphomas undergo apoptosis by a tubulin-binding agent. *Cancer Research*, 68, 1495–1503.

12. Aneja, R., Lopus, M., Zhou, J., Vangapandu, S.N., Ghaleb, A., Yao, J., Nettles, J.H., Zhou, B., Gupta, M., Panda, D., Chandra, R., Joshi, H.C. (2006c). Rational design of the microtubule-targeting anti-breast cancer drug EM015. *Cancer Ressearch*, 66, 3782–3791.

13. Aneja, R., Vangapandu, S. N., Lopus, M., Chandra, R., Panda, D., & Joshi, H. C. (2006a). Development of a novel nitro-derivative of noscapine for the potential treatment of drug-resistant ovarian cancer and T-cell lymphoma. *Molecular pharmacology*, *69*(6), 1801-1809.

14. Aneja, R., Vangapandu, S. N., Lopus, M., Viswesarappa, V. G., Dhiman, N., Verma, A., & Joshi, H. C. (2006b). Synthesis of microtubule-interfering halogenated noscapine analogs that perturb mitosis in cancer cells followed by cell death. *Biochemical pharmacology*, *72*(4), 415-426.

15. Aneja, R., Vangapandu, S.N., Joshi, H.C. (2006d). Synthesis and biological evaluation of a cyclic ether fluorinated noscapine analog. *Bioorganic & Medicinal Chemistry*, 14, 8352–8358.

16. Aneja, R., Zhou, J., Zhou, B., Chandra, R., & Joshi, H. C. (2006e). Treatment of hormone-refractory breast cancer: apoptosis and regression of human tumors implanted in mice. *Molecular cancer therapeutics*, *5*(9), 2366-2377.

17. Asai, T., Liu, Y., Bae, N., & Nimer, S. D. (2011). The p53 tumor suppressor protein regulates hematopoietic stem cell fate. *Journal of cellular physiology*, *226*(9), 2215-2221.

18. Bakherad, Z., Safavi, M., Sepehri, S., Fassihi, A., Sadeghi-Aliabadi, H., Bakherad, M., & Mahdavi, M. (2019). Preparation of some novel imidazopyridine derivatives of indole as anticancer agents: one-pot multicomponent synthesis, biological evaluation and docking studies. *Research on Chemical Intermediates*, *45*(10), 5261-5290.

19. Bardelmeijer, H. A., Ouwehand, M., Beijnen, J. H., Schellens, J. H., & van Tellingen, O. (2004). Efficacy of novel P-glycoprotein inhibitors to increase the oral uptake of paclitaxel in mice. *Investigational new drugs*, *22*(3), 219-229.

20. Becke, A. D. (1993). A new mixing of Hartree–Fock and local density-functional theories. *The Journal of chemical physics*, *98*(2), 1372-1377.

21. Beigoli, S., Sharifi Rad, A., Askari, A., Assaran Darban, R., & Chamani, J. (2019). Isothermal titration calorimetry and stopped flow circular dichroism investigations of the interaction between lomefloxacin and human serum albumin in the presence of amino acids. *Journal of biomolecular structure & dynamics*, *37*(9), 2265–2282.

22. Berendsen, H. J., van der Spoel, D., & van Drunen, R. (1995). GROMACS: a message-passing parallel molecular dynamics implementation. *Computer physics communications*, *91*(1-3), 43-56.

23. Bhattacharyya, B., Panda, D., Gupta, S., & Banerjee, M. (2008). Anti-mitotic activity of colchicine and the structural basis for its interaction with tubulin. *Medicinal research reviews*, *28*(1), 155-183.

24. Binet, S., Chaineau, E., Fellous, A., Lataste, H., Krikorian, A., Couzinier, J. P., & Meininger, V. (1990). Immunofluorescence study of the action of navelbine, vincristine and vinblastine on mitotic and axonal microtubules. *International journal of cancer*, *46*(2), 262-266.

25. Binkley, J. S., Pople, J. A., & Hehre, W. J. (1980). Self-consistent molecular orbital methods. 21. Small split-valence basis sets for first-row elements. *Journal of the American Chemical Society*, *102*(3), 939-947.

26. Boerner, R. J.; Moller, H. J. *Psychopharmacother.* **1997**, *4*, 145.

27. Bollag, D. M., McQueney, P. A., Zhu, J., Hensens, O., Koupal, L., Liesch, J., ... & Woods, C. M. (1995). Epothilones, a new class of microtubule-stabilizing agents with a taxol-like mechanism of action. *Cancer research*, *55*(11), 2325-2333.

28. Bradford M. M. (1976). A rapid and sensitive method for the quantitation of microgram quantities of protein utilizing the principle of protein-dye binding. *Analytical biochemistry*, *72*, 248–254.

29. Bray, F., Laversanne, M., Weiderpass, E., & Soerjomataram, I. (2021). The ever-increasing importance of cancer as a leading cause of premature death worldwide. *Cancer*, *127*(16), 3029-3030.

30. Bruce, J. L., Hurford Jr, R. K., Classon, M., Koh, J., & Dyson, N. (2000). Requirements for cell cycle arrest by p16INK4a. *Molecular cell*, *6*(3), 737-742.

31. Burkhart, C.A., Kavallaris, M., Band Horwitz S. (2001). The role of beta-tubulin isotypes in resistance to antimitotic drugs. *Biochim Biophysica Acta*, 1471, O1–O9.

32. Cabral, F., Abraham, I., & Gottesman, M. M. (1982). Revertants of a Chinese hamster ovary cell mutant with an altered β-tubulin: Evidence that the altered tubulin confers both colcemid resistance and temperature sensitivity on the cell. *Molecular and Cellular Biology*, *2*(6), 720-729.

33. Cahill, D. P., Lengauer, C., Yu, J., Riggins, G. J., Willson, J. K., Markowitz, S. D.,& Vogelstein, B. (1998). Mutations of mitotic checkpoint genes in human cancers. *Nature*, *392*(6673), 300-303.

34. Calabrese, E. J., & Baldwin, L. A. (2002). Defining hormesis. *Human & experimental toxicology*, *21*(2), 91–97.

35. Cassimeris, L., Pryer, N. K., & Salmon, E. D. (1988). Real-time observations of microtubule dynamic instability in living cells. *The Journal of cell biology*, *107*(6), 2223-2231.

36. Chamani, J., Moosavi-Movahedi, A. A., Saboury, A. A., Gharanfoli, M., & Hakimelahi, G. H. (2003). Calorimetric indication of the molten globule-like state of cytochrome c induced by n-alkyl sulfates at low concentrations. *The Journal of Chemical Thermodynamics*, *35*(2), 199-207.

37. Chen, J., Lu, L., Feng, Y., Wang, H., Dai, L., Li, Y., & Zhang, P. (2011). PKD2 mediates multi-drug resistance in breast cancer cells through modulation of P-glycoprotein expression. *Cancer letters*, *300*(1), 48–56.

38. Chougule, M. B., Patel, A. R., Jackson, T., & Singh, M. (2011). Antitumor activity of Noscapine in combination with Doxorubicin in triple negative breast cancer. *PloS one*, *6*(3), e17733.

39. Couty, F.; Evano, G.; Katritzky, A. R.; Ramsden, C. A.; Scriven E. F. V.; Taylor, R. J. K(2008). *11*, 409-499.

40. Crown, J., & O'Leary, M. (2000). The taxanes: an update. *Lancet (London, England)*, *355*(9210), 1176–1178.

41. Da Silva, A.W.S., & Vranken, W.F. (2012). ACPYPE-Antechamber python parser interface. *BMC Research Notes*, 5, 1-8.

42. Dahlström, B., Mellstrand, T., Löfdahl, C. G., & Johansson, M. (1982). Pharmakokinetic properties of noscapine. *European journal of clinical pharmacology*, *22*(6), 535-539.

43. Darden, T., York, D., & Pedersen, L. (1993). Particle mesh ewald: An N· log (N) method for ewald sums in large Systems. *Journal of Chemical Physics*, 98, 10089-10092.

44. Derry, W. B., Wilson, L., & Jordan, M. A. (1995). Substoichiometric binding of taxol suppresses microtubule dynamics. *Biochemistry*, *34*(7), 2203-2211.

45. Desai A and Mitchinson TJ (1997) Microtubule polymerization dynamics. *Annu Rev Cell Dev Biol* 13:83-117.

46. Dhamodharan, R. A. M. A., Jordan, M. A., Thrower, D., Wilson, L., & Wadsworth, P. (1995). Vinblastine suppresses dynamics of individual microtubules in living interphase cells. *Molecular biology of the cell*, *6*(9), 1215-1229.

47. Dobbelstein, M., & Moll, U. (2014). Targeting tumour-supportive cellular machineries in anticancer drug development. *Nature reviews Drug discovery*, *13*(3), 179-196.

48. Drukman, S., & Kavallaris, M. (2002). Microtubule alterations and resistance to tubulin-binding agents. *International journal of oncology*, *21*(3), 621-628.

49. Dustin, P. (1984). Microtubule poisons. In *Microtubules* .Springer, Berlin, Heidelberg. (pp. 171-233).

50. Erwin A. L. (2016). Antibacterial Drug Discovery Targeting the Lipopolysaccharide Biosynthetic Enzyme LpxC. *Cold Spring Harbor perspectives in medicine*, *6*(7), a025304.

51. Essmann, U., Perera, L., Berkowitz, M.L., Darden, T., Lee, H., & Pedersen, L.G. (1995). A smooth particle mesh ewald method. *Journal of Chemical Physics*, 103, 8577-8593.

52. Falck, J., Mailand, N., Syljuåsen, R. G., Bartek, J., & Lukas, J. (2001). The ATM–Chk2–Cdc25A checkpoint pathway guards against radioresistant DNA synthesis. *Nature*, *410*(6830), 842-847.

53. Fang, Z. Z., Krausz, K. W., Li, F., Cheng, J., Tanaka, N., & Gonzalez, F. J. (2012). Metabolic map and bioactivation of the anti-tumour drug noscapine. *British journal of pharmacology*, *167*(6), 1271-1286.

54. Fekete, G. L., & Fekete, L. (2019). Cutaneous leukocytoclastic vasculitis associated with erlotinib treatment: A case report and review of the literature. *Experimental and therapeutic medicine*, *17*(2), 1128–1131.

55. Fisher, B., Costantino, J. P., Wickerham, D. L., Redmond, C. K., Kavanah, M., Cronin, W. M., Vogel, V., Robidoux, A., Dimitrov, N., Atkins, J., Daly, M., Wieand, S., Tan-Chiu, E., Ford, L., & Wolmark, N. (1998). Tamoxifen for prevention of breast cancer: report of the National Surgical Adjuvant Breast and Bowel Project P-1 Study. *Journal of the National Cancer Institute*, *90*(18), 1371–1388.

56. Fisher, M. H.; Lusi, A. *J. Med. Chem.* **1972**, *15*, 982.

57. Friesner, R. A., Banks, J. L., Murphy, R. B., Halgren, T. A., Klicic, J. J., Mainz, D. T., Repasky, M. P., Knoll, E. H., Shelly, M., Perry, J. K., Shaw, D. E., Francis, P., & Shenkin, P. S. (2004). Glide: a new approach for rapid, accurate docking and scoring. Method and assessment of docking accuracy. *Journal of medicinal chemistry*, *47*(7), 1739-1749.

58. Gelfand, V. I., & Bershadsky, A. D. (1991). Microtubule dynamics: mechanism, regulation, and function. *Annual review of cell biology*, *7*(1), 93-116.

59. Gerber, D.E. and Chan, T.A.(2008). *Recent advances in radiation therapy.* Am Fam Physician, 78:1254-62.

60. Gjerdrum, C., Tiron, C., Høiby, T., Stefansson, I., Haugen, H., Sandal, T., Collett, K., Li, S., McCormack, E., Gjertsen, B. T., Micklem, D. R., Akslen, L. A., Glackin, C., & Lorens, J. B. (2010). Axl is an essential epithelial-to-mesenchymal transition-induced regulator of breast cancer metastasis and patient survival. *Proceedings of the National Academy of Sciences of the United States of America*, *107*(3).

61. Goodin, S., Kane, M. P., & Rubin, E. H. (2004). Epothilones: mechanism of action and biologic activity. *Journal of clinical oncology*, *22*(10), 2015-2025.

62. Gorbsky, G. J., & Borisy, G. G. (1989). Microtubules of the kinetochore fiber turn over in metaphase but not in anaphase. *The Journal of cell biology*, *109*(2), 653-662.

63. Gordon, M. S., Binkley, J. S., Pople, J. A., Pietro, W. J., & Hehre, W. J. (1982). Self-consistent molecular-orbital methods. 22. Small split-valence basis sets for second-row elements. *Journal of the American Chemical Society*, *104*(10), 2797-2803.

64. Graña, X., & Reddy, E. P. (1995). Cell cycle control in mammalian cells: role of cyclins, cyclin dependent kinases (CDKs), growth suppressor genes and cyclin-dependent kinase inhibitors (CKIs). *Oncogene*, *11*(2), 211-220.

65. Greene, M. H. (1999). The genetics of hereditary melanoma and nevi: 1998 update. *Cancer: Interdisciplinary International Journal of the American Cancer Society*, *86*(S11), 2464-2477.

66. Gubaidullin, R. R., Khalitova, R. R., Nedopekina, D. A., & Spivak, A. Y. (2018). Homo-and Cross Coupling of C-2 Propargyl Substituted Triterpenoic Acids: Synthesis of Novel Symmetrical and Unsymmetrical Triterpene 1, 3-Diynes. *ChemistrySelect*, *3*(47), 13526-13529.

67. Güçlü, D., Kuzu, B., Tozlu, İ., Taşpınar, F., Canpınar, H., Taşpınar, M., & Menges, N. (2018). Synthesis of novel imidazopyridines and their biological evaluation as potent anticancer agents: a promising candidate for glioblastoma. *Bioorganic & medicinal chemistry letters*, *28*(15), 2647-2651.

68. Gudmundsson, K.; Boggs, S. D. *PCT Int. Appl.* (**2006)**, WO 2006026703.

69. Halachmi, S., & Gilchrest, B. A. (2001). Update on genetic events in the pathogenesis of melanoma. *Current opinion in oncology*, *13*(2), 129-136.

70. Halgren, T. A., Murphy, R. B., Friesner, R. A., Beard, H. S., Frye, L. L., Pollard, W. T., & Banks, J. L. (2004). Glide: a new approach for rapid, accurate docking and scoring. 2. Enrichment factors in database screening. *Journal of medicinal chemistry*, *47*(7), 1750-1759.

71. Hamdouchi, C., de Blas, J., del Prado, M., Gruber, J., Heinz, B. A., & Vance, L. (1999). 2-Amino-3-substituted-6-[(E)-1-phenyl-2-(N-methylcarbamoyl) vinyl] imidazo [1, 2-a] pyridines as a novel class of inhibitors of human rhinovirus: stereospecific synthesis and antiviral activity. *Journal of medicinal chemistry*, *42*(1), 50-59.

72. Hamel, E., & Lin, C. M. (1981). Glutamate-induced polymerization of tubulin: characteristics of the reaction and application to the large-scale purification of tubulin. *Archives of biochemistry and biophysics*, *209*(1), 29–40.

73. Hartwell, L. H., & Kastan, M. B. (1994). Cell cycle control and cancer. *Science*, *266*(5192), 1821-1828.

74. Heidari, N., Goliaei, B., Moghaddam, P. R., Rahbar-Roshandel, N., & Mahmoudian, M. (2007). Apoptotic pathway induced by noscapine in human myelogenous leukemic cells. *Anti-cancer drugs*, *18*(10), 1139-1147.

75. Hornak, V., Abel, R., Okur, A., Strockbine, B., Roitberg, A., & Simmerling, C. (2006). Comparison of multiple amber force fields and development of improved protein backbone parameters. *Proteins: Structure, Function and Bioinformatics*, 65, 712–725.

76. Horwitz, S. B., Cohen, D., Rao, S., Ringel, I., Shen, H. J., & Yang, C. P. (1992). Taxol: mechanisms of action and resistance. *J. Natl. Cancer Inst. Monogr*, 55-61.

77. Institute MR. Noscapine: A Safe Cough Suppressant with Newly Discovered Effects in Treating Cancer and Stroke. 2007. http://www.pcref.org.

78. Ishii, N., Maier, D., Merlo, A., Tada, M., Sawamura, Y., Diserens, A. C., & Van Meir, E. G. (1999). Frequent Co-Alterations of TP53, p16/CDKN2A, p14ARF, PTEN Tumor Suppressor Genes in Human Glioma Cell Lines. *Brain pathology*, *9*(3), 469-479.

79. Jackson, T., Chougule, M.B., Ichite, N., Patlolla, R.R., Singh, M. (2008). Antitumor activity of noscapine in human non-small cell lung cancer xenograft model. *Cancer Chemotherapy Pharmacology*, 63, 117–126.

80. Jain, N., Yada, D., Shaik, T. B., Vasantha, G., Reddy, P. S., Kalivendi, S. V., & Sreedhar, B. (2011). Synthesis and antitumor evaluation of nitrovinyl biphenyls: anticancer agents based on allocolchicines. *ChemMedChem 6*(5), 859-868.

81. Jakalian, A., Bush, B.L., Jack, D.B., & Bayly, C.I. (2000). Fast, efficient generation of high-quality atomic charges. am1-bcc model: I. Method. *Journal of Computational Chemistry*, 21, 132–146.

82. Jakalian, A., Jack, D.B., & Bayly, C.I. (2002). Fast, efficient generation of high-quality atomic charges. am1-bcc model: ii. parameterization and validation. *Journal of Computational Chemistry*, 23, 1623–1641.

83. Jensen, L. N., Christrup, L. L., Jacobsen, L., Bonde, J., & Bundgaard, H. (1992). Relative bioavailability in man of noscapine administered in lozenges and mixture. *Acta pharmaceutica Nordica*, *4*(4), 309–312.

84. Johnson, I. S., Armstrong, J. G., Gorman, M., & Burnett, J. P. (1963). The vinca alkaloids: a new class of oncolytic agents. *Cancer research*, *23*(8 Part 1), 1390-1427.

85. Jordan, M. A., & Wilson, L. (1998). Microtubules and actin filaments: dynamic targets for cancer chemotherapy. *Current opinion in cell biology*, *10*(1), 123-130.

86. Jordan, M. A., & Wilson, L. (2004). Microtubules as a target for anticancer drugs. *Nature Reviews Cancer*, *4*(4), 253-265.

87. Jordan, M. A., Thrower, D., & Wilson, L. (1991). Mechanism of inhibition of cell proliferation by Vinca alkaloids. *Cancer research*, *51*(8), 2212-2222.

88. Jordan, M. A., Thrower, D., & Wilson, L. (1992). Effects of vinblastine, podophyllotoxin and nocodazole on mitotic spindles. Implications for the role of microtubule dynamics in mitosis. *Journal of cell science*, *102*(3), 401-416.

89. Jordan, M. A., Toso, R. J., Thrower, D., & Wilson, L. (1993). Mechanism of mitotic block and inhibition of cell proliferation by taxol at low concentrations. *Proceedings of the National Academy of Sciences*, *90*(20), 9552-9556.

90. Joshi, H. C., Salil, A., Bughani, U., & Naik, P. (2010). Noscapinoids: A new class of anticancer drugs demand biotechnological intervention. *Medicinal Plant Biotechnology*, 303-320.

91. Kach, J., Sandbo, N., La, J., Denner, D., Reed, E. B., Akimova, O., ... & Dulin, N. O. (2014). Antifibrotic effects of noscapine through activation of prostaglandin E2 receptors and protein kinase A. *Journal of Biological Chemistry*, *289*(11), 7505-7513.

92. Kamal, A., Kumar, G. B., Nayak, V. L., Reddy, V. S., Shaik, A. B., & Reddy, M. K. (2015). Design, synthesis and biological evaluation of

imidazopyridine/imidazopyrimidine-benzimidazole conjugates as potential anticancer agents. *MedChemComm*, *6*(4), 606-612.

93. Kamal, A., Reddy, J. S., Ramaiah, M. J., Dastagiri, D., Bharathi, E. V., Sagar, M. V. P., ... & Pal-Bhadra, M. (2010). Design, synthesis and biological evaluation of imidazopyridine/pyrimidine-chalcone derivatives as potential anticancer agents. *MedChemComm*, *1*(5), 355-360.

94. Kaminsky, J. J.; Doweyko, A. M. *J. Med. Chem*. **1999**, *40*, 427.

95. Karlsson, M. O., Dahlström, B., Eckernäs, S. A., Johansson, M., & Alm, A. T. (1990). Pharmacokinetics of oral noscapine. *European journal of clinical pharmacology*, *39*(3), 275–279.

96. Karna, P., Rida, P.C., Pannu, V., Gupta, K.K., Dalton, W.B., Joshi, H., Yang, V.W., Zhou, J., Aneja, R. (2011). A novel microtubulemodulating noscapinoid triggers apoptosis by inducing spindle multipolarity via centrosome amplification and declustering. *Cell Death & Differentiation*, 18, 632–644.

97. Karna, P., Sharp, S.M., Yates, C., Prakash, S., Aneja, R. (2009). EM011 activates a survivin-dependent apoptotic program in human non-small cell lung cancer cells. *Molecular Cancer*, 8, 93.

98. Kasibhatla, S., Amarante-Mendes, G. P., Finucane, D., Brunner, T., Bossy-Wetzel, E., & Green, D. R. (2006). Acridine Orange/Ethidium Bromide (AO/EB) Staining to Detect Apoptosis. *CSH protocols*, *2006*(3), pdb.prot4493.

100. Kavanagh, J. J., & Kudelka, A. P. (1993). Systemic therapy for gynecologic cancer. *Current opinion in oncology*, *5*(5), 891-899.

101. Ke, Y., Ye, K., Grossniklaus, H. E., Archer, D. R., Joshi, H. C., & Kapp, J. A. (2000). Noscapine inhibits tumor growth with little toxicity to normal tissues or inhibition of immune responses. *Cancer Immunology, Immunotherapy*, *49*(4), 217-225.

102. Kirschner M and Mitchison TJ (1986). Beyond self-assembly: From microtubules to morphogenesis. *Cell* 45:329-342.

103. Knapp, F. F., & Dash, A. (2016). *Radiopharmaceuticals for therapy* (pp. 3-23). New Delhi, India:: Springer.

104. Kollman, P.A., Massova, I., Reyes, C., Kuhn, B., Huo, S., Chong, L., Lee, M., Lee, T., Duan, Y., Wang, W., & Donini, O. (2000). Calculating structures and free

energies of complex molecules: combining molecular mechanics and continuum models. *Accounts of Chemical Research*, 33, 889-897.

105. Kruczynski, A., Barret, J. M., Etiévant, C., Colpaert, F., Fahy, J., & Hill, B. T. (1998). Antimitotic and tubulin-interacting properties of vinflunine, a novel fluorinated Vinca alkaloid. *Biochemical pharmacology*, *55*(5), 635-648.

106. Kumar, V. K., swamy Puli, V., Prasad, K. R. S., & Sridhar, G. (2021). Synthesis and biological evaluation of chalcone linked structural Modified benzothizaole-imidazopyridine derivatives as anticancer agents. *Chemical Data Collections*, *33*, 100696.

107. Labuhn, M., Jones, G., Speel, E. J., Maier, D., Zweifel, C., Gratzl, O., ... & Merlo, A. (2001). Quantitative real-time PCR does not show selective targeting of p14 ARF but concomitant inactivation of both p16 INK4A and p14 ARF in 105 human primary gliomas. *Oncogene*, *20*(9), 1103-1109.

108. Landen, J. W., Hau, V., Wang, M., Davis, T., Ciliax, B., Wainer, B. H., & Archer, D. R. (2004). Noscapine crosses the blood-brain barrier and inhibits glioblastoma growth. *Clinical cancer research*, *10*(15), 5187-5201.

109. Landen JW, Lang R, McMahon SJ, Rusan NM, Yvon AM, Adams AW, Sorcinelli MD, Campbell R, Bonaccorsi P, Ansel JC, Archer DR, Wadsworth P, Armstrong CA and Joshi H.C. (2002). Noscapine alters microtubule dynamics in living cells and inhibits the progression of melanoma. *Cancer research*, *62*(14), 4109-4114.

110. Langer, S. Z.; Arbilla, S.; Benavides, J.; Scatton, B. *Adv. Biochem. Psychopharmacol*. **1990**, *46*, 61.

111. Lanni, J. S., & Jacks, T. (1998). Characterization of the p53-dependent postmitotic checkpoint following spindle disruption. *Molecular and cellular biology*, *18*(2), 1055-1064.

112. Larkin, J. M., & Kaye, S. B. (2006). Epothilones in the treatment of cancer. *Expert opinion on investigational drugs*, *15*(6), 691-702.

113. Lasagna, L., Owens Jr, A. H., Shnider, B. I., & Gold, G. L. (1961). Toxicity after large doses of noscapine. *Cancer chemotherapy reports*, *15*, 33-34.

114. Lee, C. J., Liang, X., Wu, Q., Najeeb, J., Zhao, J., Gopalaswamy, R., Titecat, M., Sebbane, F., Lemaitre, N., Toone, E. J., & Zhou, P. (2016). Drug design from the cryptic inhibitor envelope. *Nature communications*, *7*, 10638.

115. Lee, C., Yang, W., & Parr, R. G. (1988). Development of the Colle-Salvetti correlation-energy formula into a functional of the electron density. *Physical review. B, Condensed matter*, *37*(2), 785–789.

116. Lehmann, J., Wright, M. H., & Sieber, S. A. (2016). Making a Long Journey Short: Alkyne Functionalization of Natural Product Scaffolds. *Chemistry (Weinheim an der Bergstrasse, Germany)*, *22*(14), 4666–4678.

117.LETTRE H. (1954). Synergists and antagonists of mitotic poisons. *Annals of the New York Academy of Sciences*, *58*(7), 1264–1275.

118. Li, S., Yuan, W., Yang, P., Antoun, M., Balick, M., & Cragg, G. (2010). Pharmaceutical crops: An overview.

119. Liang, X., Gopalaswamy, R., Navas, F., 3rd, Toone, E. J., & Zhou, P. (2016). A Scalable Synthesis of the Difluoromethyl-allo-threonyl Hydroxamate-Based LpxC Inhibitor LPC-058. *The Journal of organic chemistry*, *81*(10), 4393–4398.

120. Liu, B., Staren, E.D., Iwamura, T., Appert, H.E., Howard, J.M. (2001). Mechanisms of taxotere-related drug resistance in pancreatic carcinoma. *Journal of Surgical Research*, 99, 179–186.

121. Liu, J.; Chen, Q. *HuaxueJinzhan*, **2010**, *22*, 631.

122. Liu, M., Luo, X. J., Liao, F., Lei, X. F., & Dong, W. G. (2011). Noscapine induces mitochondria-mediated apoptosis in gastric cancer cells in vitro and in vivo. *Cancer chemotherapy and pharmacology*, *67*(3), 605-612.

123. Luh, S. P., & Liu, H. P. (2006). Video-assisted thoracic surgery—the past, present status and the future. *Journal of Zhejiang University Science B*, *7*(2), 118-128.

124. Ma, K. Q., Miao, Y. H., Li, X., Zhou, Y. Z., Gao, X. X., Zhang, X., & Qin, X. M. (2017). Discovery of 1, 3-diyne compounds as novel and potent antidepressant agents: synthesis, cell-based assay and behavioral studies. *RSC advances*, *7*(26), 16005-16014.

125. Mahaddalkar, T., Naik, P. K., Choudhary, S., Manchukonda, N., Kantevari, S., & Lopus, M. (2017). Structural investigations into the binding mode of a novel noscapine analogue, 9-(4-vinylphenyl) noscapine, with tubulin by biochemical analyses and molecular dynamic simulations. *Journal of biomolecular structure & dynamics*, *35*(11), 2475–2484.

126. Mahmoudian, M., & Rahimi-Moghaddam, P. (2009). The anti-cancer activity of noscapine: a review. *Recent patents on anti-cancer drug discovery*, *4*(1), 92–97.

127. Manchukonda NK, Naik PK, Santoshi S, Lopus M, Joseph S, Sridhar B, Kantevari S (2013). Rational design, synthesis and biological evaluation of third generation a-noscapine analogues as potent tubulin binding anti-cancer agents. *PLoS One* 8(10):e77970.

128. Manchukonda, N. K., Naik, P. K., Sridhar, B., & Kantevari, S. (2014). Synthesis and biological evaluation of novel biaryl type α-noscapine congeners. *Bioorganic & medicinal chemistry letters*, *24*(24), 5752–5757.

129. Manchukonda, N. K., Sridhar, B., Naik, P. K., Joshi, H. C., & Kantevari, S. (2012). Copper (I) mediated facile synthesis of potent tubulin polymerization inhibitor, 9-amino-α-noscapine from natural α-noscapine. *Bioorganic & medicinal chemistry letters*, *22*(8), 2983-2987.

130. Manchukonda, N.K., Naik, P.K., Santoshi, S., Lopus, M., Joseph, S., Sridhar, B., & Kantevari, S. (2013). Rational design, synthesis, and biological evaluation of third generation α-noscapine analogues as potent tubulin binding anti-cancer agents. *PLoS One*, 8, e77970.

131. Manchukonda, N.K., Naik, P.K., Sridhar, B., & Katevari, S. (2014). Synthesis and biological evaluation of novel biaryl type α-noscapine congeners. *Bioorganic Medicinal Chemistry Letter*, 24, 5752-5757.

132. Margolis RL and Wilson L (1981). Microtubule treadmills-possible molecular machinery. *Nature* 293:705-711.

133. Margolis, R. L., & Wilson, L. (1998). Microtubule treadmilling: what goes around comes around. *Bioessays*, *20*(10), 830-836.

134. Martindale P., (1977). The Extra Pharmacopeia, A Wade (ed) 27th edn. The Pharmaceutical Press, London, p 1250.

135. Mattson, M. P., & Cheng, A. (2006). Neurohormetic phytochemicals: Low-dose toxins that induce adaptive neuronal stress responses. *Trends in neurosciences*, *29*(11), 632–639.

136. McIntosh J.R (1994) The role of microtubules in chromosome movement, in *Microtubules* (Hyams JS and Lloyd CW eds) pp 413-434, Wiley-Liss, New York.

137. McKeon V. A. (1999). The breast cancer prevention trial: should women at risk take tamoxifen?. *Journal of obstetric, gynecologic, and neonatal nursing : JOGNN*, *28*(6 Suppl 1), 34–38.

138. Medeiros, L. R., Rosa, D. D., Bozzetti, M. C., Fachel, J. M., Furness, S., Garry, R., ... & Stein, A. T. (2009). Laparoscopy versus laparotomy for benign ovarian tumour. *Cochrane Database of Systematic Reviews*, (2).

139. Meenakshisundaram, S., Manickam, M., & Pillaiyar, T. (2019). Exploration of imidazole and imidazopyridine dimers as anticancer agents: Design, synthesis,

and structure–activity relationship study. *Archiv der Pharmazie*, *352*(12), 1900011.

140. Meher, R.K., Nagireddy, P.K.R., Pragyandipta, P., Kantevari, S., Singh, S.K., Kumar, V., Naik, P.K. (2021). In silico design of novel tubulin binding 9-arylimino derivatives of noscapine, their chemical synthesis and cellular activity as potent anticancer agents against breast cancer.*Journal of Biomolecular Structure and Dynamics*, 25, 1-12.

141. Mishra, R.C., Karna, P., Gundala, S.R., Pannu, V., Stanton, R.A., Gupta, K.K., Robinson, M.H., Lopus, M., Wilson, L., Henary, M., & Aneja, R. (2011). Second generation benzofuranone ring substituted noscapine analogs: synthesis and biological evaluation. *Biochemical Pharmacology*, 82, 110-121.

142. Mitchison, T., & Kirschner, M. (1984). Dynamic instability of microtubule growth. *nature*, *312*(5991), 237-242.

143. Mooraki, A., Jenabi, A., Jabbari, M., Zolfaghari, M. I., Javanmardi, S. Z., Mahmoudian, M., & Bastani, B. (2005). Noscapine suppresses angiotensin converting enzyme inhibitors-induced cough. *Nephrology*, *10*(4), 348-350.

144. Murthy, I. S., Sireesha, R., Deepti, K., Rao, P. S., & Raju, R. R. (2021). Design, synthesis and biological evaluation of sulphonamide derivatives of benzofuran-imidazopyridines as anticancer agents. *Chemical Data Collections*, *31*, 100608.

145. Nagireddy, P. K., Sridhar, B., & Kantevari, S. (2019). Copper-Catalyzed Glaser-Hey-Type Cross Coupling of 9-Ethynyl-α-Noscapine Leading to Unsymmetrical 1, 3-Diynyl Noscapinoids. *Asian Journal of Organic Chemistry*, *8*(8), 1495-1500.

146. Naik PK, Chatterji BP, Vangapandu SN, Aneja R, Chandra R, Kanteveri S, Joshi HC (2011).Rational design, synthesis and biological evaluations of amino-noscapine: a high affinity tubulin-binding noscapinoid. J Comput Aided Mol Des 25:443–454

147. Naik PK, Lopus M, Aneja R, Vangapandu SN, Joshi HC (2012). In silico inspired design and synthesis of a novel tubulin-binding anti-cancer drug: folate conjugated noscapine (Targetin). J Comput Aided Mol Des 26:233–247

148. Naik PK, Santoshi S, Rai A, Joshi HC (2011). Molecular modelling and competition binding study of Br-noscapine and colchicine provide insight into noscapinoid-tubulin binding site. J Mol Graph Model 29:947–955

149. Naik, P. K., Chatterji, B. P., Vangapandu, S. N., Aneja, R., Chandra, R., Kanteveri, S., & Joshi, H. C. (2011). Rational design, synthesis and biological

evaluations of amino-noscapine: a high affinity tubulin-binding noscapinoid. *Journal of computer-aided molecular design*, *25*(5), 443-454.

150. Naik, P. K., Lopus, M., Aneja, R., Vangapandu, S. N., & Joshi, H. C. (2012). In silico inspired design and synthesis of a novel tubulin-binding anti-cancer drug: folate conjugated noscapine (Targetin). *Journal of computer-aided molecular design*, *26*(2), 233-247.

151. Naik, P. K., Santoshi, S., Rai, A., & Joshi, H. C. (2011). Molecular modelling and competition binding study of Br-noscapine and colchicine provide insight into noscapinoid–tubulin binding site. *Journal of Molecular Graphics and Modelling*, *29*(7), 947-955.

152. Newcomb, E. W., Lukyanov, Y., Smirnova, I., Schnee, T., & Zagzag, D. (2008). Noscapine induces apoptosis in human glioma cells by an apoptosis-inducing factor-dependent pathway. *Anti-cancer drugs*, *19*(6), 553-563.

153. Ngan, V. K., Bellman, K., Panda, D., Hill, B. T., Jordan, M. A., & Wilson, L. (2000). Novel actions of the antitumor drugs vinflunine and vinorelbine on microtubules. *Cancer research*, *60*(18), 5045-5051.

154. Nogales, E. (2001). Structural insights into microtubule function. *Annual review of biophysics and biomolecular structure*, *30*(1), 397-420.

155. Norbury, C., & Nurse, P. (1992). Animal cell cycles and their control. *Annual review of biochemistry*, *61*(1), 441-468.

156. Nushtaeva, A. A., Karpushina, A. A., Ermakov, M. S., Gulyaeva, L. F., Gerasimov, A. V., Sidorov, S. V., Gayner, T. A., Yunusova, A. Y., Tkachenko, A. V., Richter, V. A., & Koval, O. A. (2019). Establishment of primary human breast cancer cell lines using "pulsed hypoxia" method and development of metastatic tumor model in immunodeficient mice. *Cancer cell international*, *19*, 46.

157. Oliva, M. A., Prota, A. E., Rodríguez S. J., Bennani, Y. L., Jiménez B. J., Bargsten, K., Canales, A., Steinmetz, M. O., & Díaz, J. F. (2020). Structural basis of noscapine activation for tubulin binding. *Journal of Medicinal Chemistry*, *63*(15), 8495-8501.

158. Osborne C. K. (1998). Tamoxifen in the treatment of breast cancer. *The New England journal of medicine*, *339*(22), 1609–1618.

159. Pace, A., Bove, L., Nisticò, C., Ranuzzi, M., Innocenti, P., Pietrangeli, A., Terzoli, E., & Jandolo, B. (1996). Vinorelbine neurotoxicity: clinical and

neurophysiological findings in 23 patients. *Journal of neurology, neurosurgery, and psychiatry*, *61*(4), 409–411.

160. Panda, D., Chakrabarti, G., Hudson, J., Pigg, K., Miller, H. P., Wilson, L., & Himes, R. H. (2000). Suppression of microtubule dynamic instability and treadmilling by deuterium oxide. *Biochemistry*, *39*(17), 5075–5081.

161. Patel, A. K., Meher, R. K., Reddy, P. K., Pedapati, R. K., Pragyandipta, P., Kantevari, S., Naik, M. R., & Naik, P. K. (2021). Rational design, chemical synthesis and cellular evaluation of novel 1,3-diynyl derivatives of noscapine as potent tubulin binding anticancer agents. *Journal of molecular graphics & modelling*, *106*, 107933.

162. Perez, E. A. (2009). Microtubule inhibitors: Differentiating tubulin-inhibiting agents based on mechanisms of action, clinical activity, and resistance. *Molecular cancer therapeutics*, *8*(8), 2086-2095.

163. Pettit, G. R. (1996). Progress in the discovery of biosynthetic anticancer drugs. *Journal of natural products*, *59*(8), 812-821.

164. Pietro, W. J., Francl, M. M., Hehre, W. J., DeFrees, D. J., Pople, J. A., & Binkley, J. S. (1982). Self-consistent molecular orbital methods. 24. Supplemented small split-valence basis sets for second-row elements. *Journal of the American Chemical Society*, *104*(19), 5039-5048.

165. Polak, E., & Ribiere, G. (1969). Revue Francaise Inf Rech Oper. *Serie Rouge*, *16*, 35-43.

166. Rahbar Saadat, Y., Saeidi, N., Zununi Vahed, S., Barzegari, A., & Barar, J. (2015). An update to DNA ladder assay for apoptosis detection. *BioImpacts : BI*, *5*(1), 25–28.

167. Rai, S. S., & Wolff, J. (1996). Localization of the vinblastine-binding site on β-tubulin. *Journal of Biological Chemistry*, *271*(25), 14707-14711.

168. Rai, S. S., & Wolff, J. (1998). Localization of critical histidyl residues required for vinblastine-induced tubulin polymerization and for microtubule assembly. *Journal of Biological Chemistry*, *273*(47), 31131-31137.

169. Ramesh, V., Rao, G. P. C., Ramachandran, D., & Chakravarthy, A. K. (2019). Synthesis and Biological Evaluation of Amide Derivatives of Imidazopyridine as Anticancer Agents. *Russian Journal of General Chemistry*, *89*(7), 1491-1495.

170. Reed, J. A., Loganzo, F., Shea, C. R., Walker, G. J., Flores, J. F., Glendening, J. M., & Albino, A. P. (1995). Loss of expression of the p16/cyclin-dependent kinase inhibitor 2 tumor suppressor gene in melanocytic lesions correlates with invasive stage of tumor progression. *Cancer research*, *55*(13), 2713-2718.

171. Rida, P. C., LiVecche, D., Ogden, A., Zhou, J., & Aneja, R. (2015). The noscapine chronicle: a pharmaco-historic biography of the opiate alkaloid family and its clinical applications. *Medicinal research reviews*, *35*(5), 1072-1096.

172. Rieder, C. L., & Salmon, E. D. (1994). Motile kinetochores and polar ejection forces dictate chromosome position on the vertebrate mitotic spindle. *The Journal of cell biology*, *124*(3), 223-233.

173. Rieger, A. M., Nelson, K. L., Konowalchuk, J. D., & Barreda, D. R. (2011). Modified annexin V/propidium iodide apoptosis assay for accurate assessment of cell death. *Journal of visualized experiments: JoVE*, (50), 2597.

174. Rival, Y.; Grassy, G.; Michel, G. *Chem. Pharm.Bull*. **1992**, *40*, 1170.

175. Rival, Y.; Grassy, G.; Taudou, A.; Calle, R. E. *Eur. J. Med. Chem*. **1991**, *26*, 13.

176. Rowinsky, MD, E. K. (1997). The development and clinical utility of the taxane class of antimicrotubule chemotherapy agents. *Annual review of medicine*, *48*(1), 353-374.

177. Rowinsky, E. K., & Donehower, R. C. (1991). The clinical pharmacology and use of antimicrotubule agents in cancer chemotherapeutics. *Pharmacology & therapeutics*, *52*(1), 35-84.

178. Rowinsky, E. K., Eisenhauer, E. A., Chaudhry, V., Arbuck, S. G., & Donehower, R. C. (1993). Clinical toxicities encountered with paclitaxel (Taxol). In *Seminars in oncology*, 20(4),1-15.

179. Sammak PJ and Borisy GG (1987). Direct observation of microtubule dynamics in living cells.*Nature* 332:724-726.

180. Sampath, D., & Plunkett, W. (2001). Design of new anticancer therapies targeting cell cycle checkpoint pathways. *Current opinion in oncology*, *13*(6), 484-490.

181. Santoshi S and Naik PK (2014). Molecular insight of isotypes specific β-tublin interaction of tubulin heterodimer with noscapinoids. J Comput Aided Mol Des28: 751-763.

182. Santoshi S, Manchukonda NK, Suri C, Sharma M, Sridhar B, Joseph S, Lopus M, Kantevari S, Baitharu I, Naik PK (2015). Rational design of biaryl pharmacophore inserted noscapine derivatives as potent tubulin binding anticancer agents. J. comput Aided Mol Des(full name) 29: 249-270.

183. Santoshi, S., & Naik, P. K. (2014). Molecular insight of isotypes specific β-tubulin interaction of tubulin heterodimer with noscapinoids. *Journal of computer-aided molecular design*, *28*(7), 751-763.

184. Santoshi, S., Naik, P. K., & Joshi, H. C. (2011). Rational design of novel anti-microtubule agent (9-azido-noscapine) from quantitative structure activity relationship (QSAR) evaluation of noscapinoids. *Journal of biomolecular screening*, *16*(9), 1047–1058.

185. Sertel, S., Eichhorn, T., Plinkert, P. K., & Efferth, T. (2011). Cytotoxicity of Thymus vulgaris essential oil towards human oral cavity squamous cell carcinoma. *Anticancer research*, *31*(1), 81–87.

186. Shapiro, G. I., & Harper, J. W. (1999). Anticancer drug targets: cell cycle and checkpoint control. *The Journal of clinical investigation*, *104*(12), 1645-1653.

187. Shen, W., Liang, B., Yin, J., Li, X., & Cheng, J. (2015). Noscapine increases the sensitivity of drug-resistant ovarian cancer cell line SKOV3/DDP to cisplatin by regulating cell cycle and activating apoptotic pathways. *Cell biochemistry and biophysics*, *72*(1), 203-213.

188. Sherr, C. J. (1996). Cancer cell cycles. *Science*, *274*(5293), 1672-1677.

189. Shi, W., & Lei, A. (2014). 1, 3-Diyne chemistry: synthesis and derivations. *Tetrahedron Letters*, *55*(17), 2763-2772.

190. Sondhi, S. M., Arya, S., Rani, R., Kumar, N., & Roy, P. (2012). Synthesis, anti-inflammatory and anticancer activity evaluation of some mono-and bis-Schiff's bases. *Medicinal Chemistry Research*, *21*(11), 3620-3628.

191. Straume, O., Sviland, L., & Akslen, L. A. (2000). Loss of nuclear p16 protein expression correlates with increased tumor cell proliferation (Ki-67) and poor prognosis in patients with vertical growth phase melanoma. *Clinical Cancer Research*, *6*(5), 1845-1853.

192. Suma, V. R., Sreenivasulu, R., Rao, M. V. B., Subramanyam, M., Ahsan, M. J., Alluri, R., & Rao, K. R. M. (2020). Design, synthesis, and biological evaluation of chalcone-linked thiazole-imidazopyridine derivatives as anticancer agents. *Medicinal Chemistry Research*, *29*(9), 1643-1654.

193. Sung, B., Ahn, K. S., & Aggarwal, B. B. (2010). Noscapine, a benzylisoquinoline alkaloid, sensitizes leukemic cells to chemotherapeutic agents and cytokines by modulating the NF-κB signaling pathway. *Cancer research*, *70*(8), 3259-3268.

194. Sung, Hyuna, Jacques Ferlay, Rebecca L. Siegel, Mathieu Laversanne, Isabelle Soerjomataram, Ahmedin Jemal, and Freddie Bray. "Global cancer statistics 2020: GLOBOCAN estimates of incidence and mortality worldwide for 36 cancers in 185 countries." *CA: a cancer journal for clinicians* 71, no. 3 (2021): 209-249.

195. Theiss C and Meller K (2000). Taxol impairs anterograde axonal transport of microinjected horseradish peroxidase in dorsal root ganglia neurons in vitro. *Cell Tissue Res* 299:213-224.

196. Tian, X., Liu, M., Huang, X., Zhu, Q., Liu, W., Chen, W., ... & Tan, J. (2020). Noscapine induces apoptosis in human colon cancer cells by regulating mitochondrial damage and warburg effect via PTEN/PI3K/mTOR signaling pathway. *OncoTargets and therapy*, *13*, 5419.

197. Topp, K. S., Tanner, K. D., & Levine, J. D. (2000). Damage to the cytoskeleton of large diameter sensory neurons and myelinated axons in vincristine-induced painful peripheral neuropathy in the rat. *The Journal of comparative neurology*, *424*(4), 563–576.

198. Valiron, O., Caudron, N., & Job, D. (2001). Microtubule dynamics. *Cellular and Molecular Life Sciences CMLS*, *58*(14), 2069-2084.

199. Van Meir, E. G., Kikuchi, T., Tada, M., Li, H., Diserens, A. C., Wojcik, B. E., ... & Cavenee, W. K. (1994). Analysis of the p53 gene and its expression in human glioblastoma cells. *Cancer research*, *54*(3), 649-652.

200. Verma, P., Manchukonda, N. K., Kantevari, S., & Lopus, M. (2021). Induction of microtubule hyper stabilization and robust G_2 /M arrest by N-4-CN in human breast carcinoma MDA-MB-231 cells. *Fundamental & clinical pharmacology*, 10.1111/fcp.12660. Advance online publication.

201. Verma, P., Nagireddy, P., Prassanawar, S. S., Nirmala, J. G., Gupta, A., Kantevari, S., & Lopus, M. (2020). 9-PAN promotes tubulin- and ROS-mediated cell death in human triple-negative breast cancer cells. *The Journal of pharmacy and pharmacology*, *72*(11), 1585–1594.

202. Vidal, A., & Koff, A. (2000). Cell-cycle inhibitors: three families united by a common cause. *Gene*, *247*(1-2), 1-15.

203. Waldman, T., Zhang, Y., Dillehay, L., Yu, J., Kinzler, K., Vogelstein, B., & Williams, J. (1997). Cell-cycle arrest versus cell death in cancer therapy. *Nature medicine*, *3*(9), 1034-1036.

204. Walker, G. J., Gabrielli, B. G., Castellano, M., & Hayward, N. K. (1999). Functional reassessment of P16 variants using a transfection-based assay. *International journal of cancer*, *82*(2), 305-312.

205. Wang, J., Wolf, R.M., Caldwell, J.W., Kollman, P.A., & Case, D.A. (2004). Development and testing of a general amber force field. *Journal of Computational Chemistry*, 25, 1157–1174.

206. Wang, Y., O'Brate, A., Zhou, W., & Giannakakou, P. (2005). Resistance to microtubule-stabilizing drugs involves two events: beta-tubulin mutation in one allele followed by loss of the second allele. *Cell cycle (Georgetown, Tex.)*, *4*(12), 1847–1853.

207. Wang, Y., Schmid-Bindert, G., & Zhou, C. (2012). Erlotinib in the treatment of advanced non-small cell lung cancer: an update for clinicians. *Therapeutic advances in medical oncology*, *4*(1), 19–29.

208. Warolin C. (1999). Pierre-Jean Robiquet: (Rennes, 14 janvier 1780 - Paris, 29 avril 1840) [Pierre-Jean Robiquet]. *Revue d'histoire de la pharmacie*, *47*(321), 97–110.

209. Wassmann, K., & Benezra, R. (2001). Mitotic checkpoints: from yeast to cancer. *Current opinion in genetics & development*, *11*(1), 83-90.

210. Wilson, L., & Jordan, M. A. (1995). Microtubule dynamics: taking aim at a moving target. *Chemistry & biology*, *2*(9), 569-573.

211. Wilson, L., Miller, H. P., Farrell, K. W., Snyder, K. B., Thompson, W. C., & Purich, D. L. (1985). Taxol stabilization of microtubules in vitro: dynamics of tubulin addition and loss at opposite microtubule ends. *Biochemistry*, *24*(19), 5254-5262.

212. Wilson, L., Panda, D., & Jordan, M. A. (1999). Modulation of microtubule dynamics by drugs: a paradigm for the actions of cellular regulators. *Cell structure and function*, *24*(5), 329-335.

213. World Health Organization (WHO). (2020). Global Health Estimates 2020: Deaths by Cause, Age, Sex, by Country and by Region, 2000-2019. *World Health Organization*.

214. Ye K, Ke Y, Keshava N, Shanks J, Kapp JA, Tekmal RR, Petros J and Joshi HC (1998). Opium alkaloid noscapine is an antitumor agent that arrests metaphase and induces apoptosis in dividing cells. *Proc Natl Acad Sci USA*95:1601-1606.

215. Ye, K., Zhou, J., Landen, J. W., Bradbury, E. M., & Joshi, H. C. (2001). Sustained activation of p34 cdc2 is required for noscapine-induced apoptosis. *Journal of Biological Chemistry*, *276*(50), 46697-46700.

216. Ye, X. S., Xu, G. A. N. G., Pu, R. T., Fincher, R. R., McGuire, S. L., Osmani, A. H., & Osmani, S. A. (1995). The NIMA protein kinase is hyperphosphorylated and activated downstream of p34cdc2/cyclin B: coordination of two mitosis promoting kinases. *The EMBO Journal*, *14*(5), 986-994.

217. Yoo, H. D., & Gerwick, W. H. (1995). Curacins B and C, new antimitotic natural products from the marine cyanobacterium Lyngbya majuscula. *Journal of natural products*, *58*(12), 1961-1965.

218. Zhou J, Gupta K, Aggarwal S, Aneja R, Chandra R, Panda D and Joshi HC (2003). Brominated derivatives of noscapine are potent microtubule-interfering agents that perturb mitosis and inhibit cell proliferation. *Mol Pharmaco l* 63:799–807.

219. Zhou J, Gupta K, Yao J, Ye K, Panda D, Giannakakou P and Joshi HC (2002b). Paclitaxel-resistant human ovarian cancer cells undergo c-Jun NH_2-terminal kinase-mediated apoptosis in response to noscapine. *J Biol Chem* 277:39777-39785.

220. Zhou J, Panda D, Landen JW, Wilson L and Joshi HC (2002a). Minor alteration of microtubule dynamics causes loss of tension across kinetochore pairs and activates the spindle checkpoint. *J Biol Chem* 277:17200–17208.

221. Zhou, R., Friesner, R. A., Ghosh, A., Rizzo, R. C., Jorgensen, W. L., & Levy, R. M. (2001). New linear interaction method for binding affinity calculations using a continuum solvent model. *The Journal of Physical Chemistry B*, *105*(42), 10388-10397.

222. Zhou, J., Gupta, K., Aggarwal, S., Aneja, R., Chandra, R., Panda, D., & Joshi, H. C. (2003). Brominated derivatives of noscapine are potent microtubule-interfering agents that perturb mitosis and inhibit cell proliferation. *Molecular pharmacology*, *63*(4), 799-807.

223. Zhou, J., Gupta, K., Yao, J., Ye, K., Panda, D., Giannakakou, P., & Joshi, H. C. (2002). Paclitaxel-resistant human ovarian cancer cells undergo c-Jun NH2-terminal kinase-mediated apoptosis in response to noscapine. *Journal of Biological Chemistry*, *277*(42), 39777-39785.

224. Zhou, J., Liu, M., Aneja, R., Chandra, R., Lage, H., & Joshi, H. C. (2006). Reversal of P-glycoprotein-mediated multidrug resistance in cancer cells by the c-Jun NH2-terminal kinase. *Cancer research*, *66*(1), 445–452.

225. Zhou, J., Panda, D., Landen, J.W., Wilson, L., & Joshi, H.C. (2002b). Minor alteration of microtubule dynamics causes loss of tension across kinetochore pairs and activates the spindle checkpoint. *Journal of Biological Chemistry*, 277, 17200-17208.

226. Zhou, J.; Liu, J.; Chen, Q. *YoujiHuaxue*, **2009**, *29*, 1708.

227. Zhou, J., Liu, M., Luthra, R., Jones, J., Aneja, R., Chandra, R., ... & Joshi, H. C. (2005). EM012, a microtubule-interfering agent, inhibits the progression of multidrug-resistant human ovarian cancer both in cultured cells and in athymic nude mice. *Cancer chemotherapy and pharmacology*, *55*(5), 461-465.

228. Zhou, R., Friesner, R. A., Ghosh, A., Rizzo, R. C., Jorgensen, W. L., & Levy, R. M. (2001). New linear interaction method for binding affinity calculations using a continuum solvent model. *The Journal of Physical Chemistry B*, *105*(42), 10388-10397.

229. Zorn, K. C., Gofrit, O. N., Steinberg, G. D., & Shalhav, A. L. (2007). Evolution of robotic surgery in the treatment of localized prostate cancer. *Current treatment options in oncology*, *8*(3), 197-210.

230. Zou JI, Huang YU, Chen Q, Wang N, Cao KE, Hsieh TC, Wu JM. (1999). Suppression of mitogenesis and regulation of cell cycle traverse by resveratrol in cultured smooth muscle cells. *International journal of oncology*, *15*(4), 647-698.

LIST OF PUBLICATION

1. **Meher, R. K**., Naik, M. R., Bastia, B., & Naik, P. K. (2018). Comparative evaluation of anti-angiogenic effects of noscapine derivatives. *Bioinformation*, *14*(5), 236.

2. **Meher, R. K**., Nagireddy, P. K. R., Pragyandipta, P., Kantevari, S., Singh, S. K., Kumar, V., & Naik, P. K. (2021). In silico design of novel tubulin binding 9-arylimino derivatives of noscapine, their chemical synthesis and cellular activity as potent anticancer agents against breast cancer. *Journal of Biomolecular Structure and Dynamics*, 1-12.

3. **Meher, R. K**., Pragyandipta, P., Reddy, P. K., Pedaparti, R., Kantevari, S., & Naik, P. K. (2021). Development of 1, 3-diynyl derivatives of noscapine as potent tubulin binding anticancer agents for the management of breast cancer. *Journal of Biomolecular Structure and Dynamics*, 1-18.

4. **Meher, R. K**., Pragyandipta, P., Pedapati, R. K., Nagireddy, P. K., Kantevari, S., Nayek, A. K., & Naik, P. K. (2021). Rational design of novel N-alkyl amine analogues of noscapine, their chemical synthesis and cellular activity as potent anticancer agents. *Chemical Biology & Drug Design*, *98*(3), 445-465.

5. Patel, A. K., **Meher, R. K**., Reddy, P. K., Pedapati, R. K., Pragyandipta, P., Kantevari, S., ... & Naik, P. K. (2021). Rational design, chemical synthesis and cellular evaluation of novel 1, 3-diynyl derivatives of noscapine as potent tubulin binding anticancer agents. *Journal of Molecular Graphics and Modelling*, *106*, 107933.

6. Patel, A. K., **Meher, R. K**., Nagireddy, P. K., Pragyandipta, P., Pedapati, R. K., Kantevari, S., & Naik, P. K. (2021). 9-Arylimino noscapinoids as potent tubulin binding anticancer agent: chemical synthesis and cellular evaluation against breast tumour cells. *SAR and QSAR in Environmental Research*, *32*(4), 269-291.

7. Pragyandipta, P., **Meher, R. K**., Naik, M. R., Nagireddy, P. K., Pedapati, R. K., Kantevari, S., & Naik, P. K. (2021). In-Silico-Inspired Design of 1, 3-Diynyl Congeners of Noscapine as Promising Tubulin-Binding Anticancer Agent: Chemical Synthesis and Cellular Activity with Breast Cancer Cell Lines. *ChemistrySelect*, *6*(14), 3500-3511.

8. Pragyandipta, P., **Meher, R. K**., Reddy, P. K., Pedaparti, R., Kantevari, S., & Naik, P. K. (2022). Structure Based Design of Tubulin Binding 9-Arylimino Noscapinoids: Chemical Synthesis and Experimental Validation Against Breast Cancer Cell Lines. *Analytical Chemistry Letters*, *12*(1), 29-43.

CONFERENCE PRESENTATION

1. Rajesh Kumar Meher and Pradeep Kumar Naik. "Development of most potent analogues of noscapine and their preclinical validation for management of human breast cancer" at CRTBBI, Department of Biotechnology and Bioinformatics, Sambalpur University, Jyoti Vihar, Burla, Sambalpur , Odisha, held on 3rd to 4th March, 2020.

2. Rajesh Kumar Meher and Pradeep Kumar Naik "Rational design of novel tubulin binding anticancer agents based on chemoinformatics evaluation of noscapinoids ,their chemical synthesis and experimental validation' at DST INSPIRE review meet ,KIIT, Bhubaneswar, Odisha, held on 6th -8th June 2019.

3. Rajesh Kumar Meher and Pradeep Kumar Naik "Recent advances on molecule of chemical and biological importance" organized by Municipal college Rourkela, Odisha, held on 6th - 7th February 2018.